



## **Phase I Report**

DOE Award: DE-EE0002777

AltaRock Energy Inc

August 26, 2011

## **Contributing Authors**

### **AltaRock Energy**

Susan Petty, William L. Osborn, Trenton T. Cladouhos, Joe L. Iovenitti, Laura L. Nofziger, Owen Callahan, Daniel Bour, Maisie L. Nichols, Yini Nordin, Matthew Clyne and Jon Sainsbury

### **Davenport Newberry**

Doug Perry and Todd Jaffe

### **Consultants and Subrecipients**

Paul Stern (PLS Environmental)

Eric Sonnenthal and Nicholas Spycher (LBNL)

Nicholas Davtzes (Temple)

Ahmad Ghassemi (Texas A&M)

Steve Hickman (USGS)

Amelia Letvin and Drew Fetterman (The School for Renewable Energy Science)

Gillian Foulger and Bruce Julian (Foulger Consulting)

*Acknowledgment:* This material is based upon work supported by the Department of Energy under Award Number DE-EE0002777.

*Disclaimer:* This report was prepared as an account of work sponsored by an agency of the United States Government. Neither the United States Government nor any agency thereof, nor any of their employees, makes any warranty, express or implied, or assumes any legal liability or responsibility for the accuracy, completeness, or usefulness of any information, apparatus, product, or process disclosed, or represents that its use would not infringe privately owned rights. Reference herein to any specific commercial product, process, or service by trade name, trademark, manufacturer, or otherwise does not necessarily constitute or imply its endorsement, recommendation, or favoring by the United States Government or any agency thereof. The views and opinions of authors expressed herein do not necessarily state or reflect those of the United States Government or any agency thereof.

# Table of Contents

1	INTRODUCTION.....	1
1.1	Project Description.....	1
1.2	Goals and Purpose .....	2
1.3	Site Characterization.....	2
1.4	Site Selection.....	5
2	GEOLOGIC MODEL .....	11
2.1	Geography.....	11
2.2	Regional Setting .....	11
2.3	Local Geology .....	16
2.4	Hydrology.....	28
2.5	Geophysics .....	36
2.6	Geothermal Exploration Activity.....	40
2.7	Conceptual Geologic Model.....	43
3	CONCEPTUAL RESOURCE MODEL .....	46
3.1	Geophysical Conditions Around Well .....	46
3.2	Wellbore Conditions .....	46
3.3	NWG 55-29 Conceptual Resource Model .....	110
4	SEISMICITY .....	113
4.1	Historical Seismicity .....	113
4.2	Background Seismicity Monitoring .....	113
4.3	Evaluation of Proximal Faults.....	116
4.4	Final MSA Deployment Plan.....	116
4.5	Seismicity Analysis Plan.....	118
4.6	Geomechanical Predictive Modeling .....	118
4.7	Lessons Learned From Other Projects .....	119
4.8	Maximum Magnitude Predictions .....	120
4.9	Local Induced Seismicity During Injection .....	120
4.10	Assessment of Induced Seismicity and Seismic Hazards and Risk .....	122
4.11	Induced Seismicity Mitigation Protocol and Proposed Controls .....	122
4.12	Summary .....	122
5	IN SITU STRESS .....	123
5.1	Regional Stress Indicators.....	123
5.2	Stress Indicators from Nearby Wells and Temperature Coreholes .....	126
5.3	Stress from Local Background Seismicity.....	128

5.4	Borehole Stress Indicators in NWG 55-29.....	128
5.5	Stress Magnitude Model for Open Hole of NWG 55-29 .....	131
5.6	Contingency and Risk Mitigation .....	156
6	PERMITTING .....	158
6.1	Existing Permits.....	158
6.2	Outstanding Permits .....	158
6.3	NEPA-Related Items and Determination .....	159
7	STIMULATION PLAN .....	163
7.1	Introduction .....	163
7.2	Historical Data – Review of Worldwide EGS Stimulation.....	164
7.3	Pre-Stimulation Conditions at NWG 55-29 .....	171
7.4	AltaStim Modeling .....	174
7.5	Temperature Modeling.....	189
7.6	Diverter Technology.....	194
7.7	Field Operations and Monitoring.....	198
7.8	Operating Procedures .....	208
7.9	EGS Reservoir Characterization .....	216
7.10	Production Well Stimulation.....	217
7.11	Contingency and Risk Mitigation .....	218
8	EGS RESERVOIR CHARACTERIZATION .....	223
8.1	Analysis of Induced Microseismicity .....	223
8.2	Geomechanical Response Model.....	226
8.3	Tracer Modeling.....	228
8.4	Updated THMC Model .....	230
8.5	Production Well Targets .....	231
9	DRILLING PROGRAM .....	233
9.1	Introduction .....	233
9.2	Drilling Schedule .....	235
9.3	Drilling and Casing Plan.....	235
9.4	Cementing Plan .....	251
9.5	Logging Plan .....	254
9.6	Risk Mitigation and Contingencies.....	255
10	WELL TESTING .....	261
10.1	Single-Well Test.....	261
10.2	Connectivity Testing.....	264



10.3	Circulation Testing .....	265
10.4	Hydrogen Sulfide Abatement.....	266
10.5	Schedule.....	266
10.6	Data Collection.....	267
10.7	Contingency and Mitigation Plan.....	270
11	RISK MITIGATION .....	273
11.1	Financing and Liability.....	273
11.2	Schedule and Budget .....	273
11.3	Permitting .....	273
11.4	Technical Risks .....	274
12	REPORTING .....	276
12.1	Ongoing Activities .....	276
12.2	Stimulation and Flow Test Reports.....	276
12.3	Drilling Reports .....	277
12.4	DOE Reporting.....	277
12.5	DOE National Geothermal Database Repository.....	278
12.6	Related Projects .....	278
13	REFERENCES.....	279
	APPENDIX A-1 – Induced Seismicity Mitigation Plan.....	Attached
	APPENDIX A-2 – EGS Site Selection Matrix .....	Attached
	APPENDIX B-1 – <b><u>Confidential</u></b> Analysis of NWG 55-29 Drill Cuttings (Letvin, 2011).....	Attached
	APPENDIX B-2 – Porosity Evolution in Newberry System (Fetterman, 2011).....	Attached
	APPENDIX B-3 – Evaluation of Water Usage for Newberry EGS Demonstration.....	Attached
	APPENDIX B-4 – Newberry Water Monitoring.....	Attached
	APPENDIX B-5 – Independent Hydrologist Review (Kleinfelder, 2011).....	Attached
	APPENDIX B-6 – <b><u>Confidential</u></b> Bouguer Gravity Data .....	Attached
	APPENDIX B-7 – <b><u>Confidential</u></b> Davenport Magnetotelluric Data .....	Attached
	APPENDIX C-1 – <b><u>Confidential</u></b> Trouble-time Summary .....	Attached
	APPENDIX C-2 – Full Borehole Televiwer Image Log .....	Attached
	APPENDIX C-3 – X-Ray Diffraction Analysis Results .....	Attached
	APPENDIX C-4 – Petrophysical and Rock Mechanical Properties from GEO N-2.....	Attached
	APPENDIX C-5 – Acoustic Image Log Description .....	Attached
	APPENDIX D-1 – Newberry Calibration Shot Project (Foulger, 2010).....	Attached
	APPENDIX D-2 – Moment Tensors, Sensor Selection and Array Geometry (Foulger, 2011).....	Attached
	APPENDIX E-1 – Porosity and Strength Background.....	Attached
	APPENDIX F-1 – Surface Permits.....	Attached
	APPENDIX F-2 – Subsurface Permits.....	Attached

APPENDIX F-3 – Scenic Resources Inventory and Assessment (RSE Services, 2011)..... Attached  
APPENDIX F-4 – Impact of EGS-Induced Seismicity on Paulina Lake Dam (Wong, 2011)..... Attached  
APPENDIX G-1 – ***Confidential*** Diverter Materials and Expected Degradation Products ..... Attached  
APPENDIX G-2 – Newberry Well Testing Piping And Instrumentation Diagrams ..... Attached  
APPENDIX I-1 – Directional Drilling Plan for 55A-29 ..... Attached  
APPENDIX I-2 – Directional Drilling Plan for 55B-29 ..... Attached  
APPENDIX I-3 – Mini-frac Test Procedure ..... Attached  
APPENDIX L-1 – Newberry Daily Drilling Report ..... Attached

## Table of Figures

Figure 1-1. Location map for the EGS Demonstration at Newberry Volcano.....	1
Figure 2-1. Tectonic boundaries and geological provinces of the Pacific Northwest.....	12
Figure 2-2. Block motions for Cascadia forearc .....	13
Figure 2-3. Regional structure map .....	15
Figure 2-4. LiDAR coverage with scarps, vents, and fissures .....	15
Figure 2-5. Outline of the Newberry Volcano massif.....	16
Figure 2-6. Cross-section location map.....	20
Figure 2-7. West-east cross-section A-A' .....	21
Figure 2-8. North-south cross-section B-B' .....	21
Figure 2-9. Deschutes Basin in central Oregon.....	28
Figure 2-10. Upper Deschutes Basin generalized geology .....	29
Figure 2-11. Digital elevation map with surface hydrologic features.....	30
Figure 2-12. Deschutes Basin precipitation and recharge.....	33
Figure 2-13. Groundwater equipotential contours and inferred flow direction .....	34
Figure 2-14. Sensitive aquifers in the Deschutes Basin. ....	35
Figure 2-15. Cross section A-A' (west-east) showing groundwater aquifer. ....	36
Figure 2-16. Cross section B-B' (north-south) showing groundwater aquifer.....	37
Figure 2-17. Residual gravity anomaly map.....	38
Figure 2-18. Newberry Volcano structural interpretation based on gravity modeling .....	38
Figure 2-19. Geoelectric structure at Newberry Volcano.....	39
Figure 2-20. Location of temperature coreholes and geothermal exploration wells.....	41
Figure 2-21. Equilibrated temperatures of coreholes and exploration wells.....	42
Figure 2-22. Conceptual model of the Newberry caldera geothermal system. ....	43
Figure 2-23. Numerical model of the thermal conditions at Newberry Volcano .....	44
Figure 3-1. Newberry NWG 55-29 well bore and casing profile.....	48
Figure 3-2. NWG 55-29 temperature profiles.....	51
Figure 3-3. NWG 55-29 pressure surveys .....	51
Figure 3-4. Rock-forming minerals, natural radioactivity, bulk density, porosity and mud losses.....	52
Figure 3-5. Correlation of breakout width and constraints on rock strength.....	54
Figure 3-6. Paragenetic sequence and fluid inclusions.....	57
Figure 3-7. Fluid inclusion homogenization temperatures.....	58
Figure 3-8. Drill core showing lithologic changes. ....	59
Figure 3-9. Vein compositions .....	60
Figure 3-10. Evidence of zoning in veins or pores. ....	60
Figure 3-11. Photomicrographs showing secondary minerals in pores and cracks.....	61
Figure 3-12. Indications of structural deformation in slickenside texture on several grains. ....	61
Figure 3-13. Pyrite occurring within rock mass.....	62
Figure 3-14. Evidence of chlorite growing authigenically.....	62

Figure 3-15. Summary of rock types and cuttings analysis.....	63
Figure 3-16. Cores representing skeletal and open porosity in GEO N-2 .....	65
Figure 3-17. Measurements of skeletal and open porosity.....	66
Figure 3-18. Model for evolution of porosity in the absence of clay in core GEO N-2.....	67
Figure 3-19. Core sample from Well GEO N-2 .....	68
Figure 3-20. X-ray CT image of welded tuff from vertical plugs. ....	69
Figure 3-21. Thin section image from GEO N-2 welded tuff.....	69
Figure 3-22. Mohr Coulomb envelope for Newberry welded tuff.....	70
Figure 3-23. THC model boundaries superimposed on cross-section C-C' .....	72
Figure 3-24. Approximate location of the THC model boundaries on E-W cross-section .....	73
Figure 3-25. Numerical mesh corner nodes and centers superimposed on digitized geologic contacts ...	73
Figure 3-26. THC model numerical mesh and refined gridding along a cross-cutting fracture zone. ....	74
Figure 3-27. Numerical mesh showing model parameters.....	75
Figure 3-28. Initial estimate of temperature distribution.....	76
Figure 3-29. Simulated steady-state pressure distribution. ....	77
Figure 3-30. Simulated steady-state temperature distribution.....	77
Figure 3-31. Simulated steady-state temperature distribution, including the supercritical region.....	78
Figure 3-32. Computed mineral saturation indices, assuming equilibrium with kaolinite.....	82
Figure 3-33. Computed mineral saturation indices, assuming equilibrium with muscovite.....	82
Figure 3-34. Simulated distribution of mineral dissolution after 1000 years.....	85
Figure 3-35. Simulated distribution of mineral precipitation after 1000 years.....	86
Figure 3-36. Simulated change in permeability after 1000 years.....	87
Figure 3-37. Time evolution of precipitating alteration minerals in rock.....	88
Figure 3-38. Single-shot azimuth and direction compared with BHTV telemetry.....	90
Figure 3-39. Unwrapped images of the BHTV travel time and amplitude signals.....	92
Figure 3-40. Examples of interpreted BHTV log from two depth intervals .....	93
Figure 3-41. Number of fractures in 50-foot intervals and definition of boundaries of Zones A-D. ....	95
Figure 3-42. Equal area stereogram of the poles to layers identified in the BHTV image .....	96
Figure 3-43. Rose diagrams of LiDAR scarp trends. ....	96
Figure 3-44. Modified tadpole plot showing distribution of fractures and primary layering.....	97
Figure 3-45. Equal area stereogram of poles to BHTV-identified natural fractures.....	98
Figure 3-46. Contoured fracture poles for Zone B and Zone C.....	98
Figure 3-47. Results of fracture orientation forward modeling.....	101
Figure 3-48. Cumulative fracture thickness with depth and log-log plot of apertures. ....	102
Figure 3-49. Temperature logs during injection .....	103
Figure 3-50. Top of first granodiorite dike at 2625 m.....	104
Figure 3-51. Focused view of the PT survey data .....	108
Figure 4-1. Calibration shot arrivals.....	114
Figure 4-2. Seismic energy recorded on 16 of 21 components of the local MSA.....	115

Figure 4-3. AltaRock final MSA as currently planned.....	117
Figure 4-4. Focal coverage map showing final MSA geometry as planned .....	117
Figure 4-5. Hypothetical Gutenberg-Richter Law .....	121
Figure 5-1. Earthquake focal mechanisms used to invert for principal stress directions.....	123
Figure 5-2. Rose diagram summarizing strike of mapped fault scarps and other structures.....	124
Figure 5-3. LiDAR image from the west flank of Newberry Volcano .....	125
Figure 5-4. Rose diagrams of LiDAR scarps and fissures mapped in Figure 5-3.....	125
Figure 5-5. Locations of exploratory holes on western flank of Newberry. ....	127
Figures 5-6. Contoured stereonet plots of interpretations from BHTV in CEE 76-15 TCH. ....	127
Figure 5-7. Unwrapped BHTV images of the travel time and amplitude signals.....	129
Figure 5-8. Amplitude and two-way travel time images from the NWG 55-29 BHTV log .....	130
Figure 5-9. Statistics of breakout occurrence in NWG 55-29 .....	131
Figure 5-10. Circumferential variation of tangential normal stress.....	132
Figure 5-11. Initial evaluation of the correspondence of breakout width .....	134
Figure 5-12. High resolution X-ray CT scan of core sample from Newberry well GEO N-2 .....	136
Figure 5-13. <i>In situ</i> model showing estimates of the uniaxial compressive strength (UCS).....	137
Figure 5-14. Static coefficient of friction of key mineral phases. ....	138
Figure 5-15. Analysis of stresses versus depth for NWG 55-29, assuming a constant UCS.....	139
Figure 5-16. Summary of minimum and maximum fluid pressures measured in NWG 55-29.....	142
Figure 5-17. Example of stress polygons mapping the range of principal stress ratios. ....	143
Figure 5-18. Analysis of stresses versus depth for NWG 55-29, assuming a variable UCS.....	146
Figure 5-19. Stress polygon showing bounds on principal stress ratios.....	148
Figure 5-20. Mohr Circle analysis and slip tendency versus depth.....	151
Figure 5-21. Mohr Circle analysis of ambient stress and fluid pressures .....	152
Figure 5-22. End cap model illustrating dependence of fracture dilatancy on stress. ....	154
Figure 5-23. Temperature logs acquired during the inject-to-cool operation in Sept.-Oct. 2010.....	155
Figure 7-1. Injectivity comparison for several EGS projects worldwide. ....	165
Figure 7-2. The 2000 stimulation of GPK2 .....	170
Figure 7-3. GPK2 hydraulic stimulation parameters.....	171
Figure 7-4. Stress profile for NWG 55-29 based on average rock density.....	180
Figure 7-5. Total fracture volume for five different wellhead pressures in Zones A-E.....	185
Figure 7-6. Mohr circle plots for Zone C .....	186
Figure 7-7. Modeled cloud of microseismicity for one model realization of Zone C.....	187
Figure 7-8. View looking north through modeled microseismicity for Zone D.....	187
Figure 7-9. Combined microseismicity for all five zones .....	188
Figure 7-10. Modeled temperatures, showing cooling after one month of water injection .....	190
Figure 7-11. Modeled thermal recovery at 9600 ft after injecting for one month .....	191
Figure 7-12. Modeled temperature profiles after injecting 40 gpm for 0, 1, 2, 3 and 8 days .....	191
Figure 7-13. Modeled temperature profiles after injecting 120 gpm for 0, 1, 2, 3 and 8 days .....	192

Figure 7-14. Comparison of measured and modeled downhole temperatures in NWG 55-29 .....	192
Figure 7-15. Comparison of measured and modeled downhole temperatures after 3 days injection. ....	193
Figure 7-16. Stimulation of fracture with diverter application.....	194
Figure 7-17. Estimated stimulation pump output pressure and flow rate for NWG 55-29.....	202
Figure 7-18. Picture of skid-mounted triplex injection pump.....	202
Figure 7-19. Existing wellhead on NWG 55-29. ....	203
Figure 7-20. Modeled heat-up of NWG 55-29 after injecting 31 L/s (500 gpm) for 21 days.....	205
Figure 7-21. Equipment used in geothermal well flow test.....	207
Figure 8-1. Microseismic hypocenters determined conventionally and with relative relocation.....	224
Figure 8-2. Example of confidence region for source type of a microearthquake .....	225
Figure 8-3. Moment tensors for six microseismic events from a hydraulic injection at Coso.....	226
Figure 8-4. Mean residence time of tracers at various temperatures.....	228
Figure 8-5. $R_f-1$ for Safranin T as a function of temperature.....	229
Figure 8-6. Tracer sorption in fractures and matrix.....	230
Figure 8-7. Possible well trajectories for NWG 55A-29 and NWG 55B-29.....	232
Figure 9-1. Well Pad S-29, showing existing well NWG 55-29 and proposed wells.....	233
Figure 9-2. 21-1/4 in BOPE stack configuration .....	242
Figure 9-3. 13-5/8 in BOPE stack configuration .....	245
Figure 9-4. 16-3/4 in BOPE stack for Case 5.....	246
Figure 9-5. Temperature simulation of cooling and thermal recovery .....	250
Figure 10-1. Approximate timeline of a 3-day flow test.....	262
Figure 10-2. Tracer data showing the results of a typical injection and backflow experiment.....	264
Figure 10-3. Example of connectivity test data between an injector and a producer .....	265
Figure 10-4. Newberry NWG 55-29 Phase II stimulation, drilling and well testing timeline.....	267
Figure 10-5. Sampling and monitoring sites around the Newberry project area .....	269

## Table of Tables

Table 1-1. EGS demonstration site selection criteria.....	6
Table 2-1. Depth to base of formation in various wells and coreholes.....	19
Table 2-2. Well data and injectivity test results.....	24
Table 2-3. Base of upper loss zone. ....	26
Table 2-4. Identified loss zones in surrounding wells and temperature coreholes.....	27
Table 2-5. Fluid compositions for project area features.....	31
Table 3-1. Newberry NWG 55-29 survey history. ....	50
Table 3-2. Multistage test results for GEO N-2 welded tuff .....	70
Table 3-3. Hydrological and transport properties. ....	74
Table 3-4. Thermal Properties .....	76
Table 3-5. Gas analyses from NWG 55-29 .....	79
Table 3-6. Chemical composition of groundwater and geofluid used in geochemical modeling.....	80
Table 3-7. Geothermometry of gas samples from well NWG 55-29 (from Geologica, 2010). ....	80
Table 3-8. List of Primary and Potential Secondary Minerals in the THC model. ....	83
Table 3-9. Structure types distinguished by BHTV image log. ....	91
Table 3-10. Image Log Quality Ranking.....	94
Table 3-11. Quality ranking of fracture interpretation and number of observed fractures.....	94
Table 3-12. Fracture orientation sets identified by ISIS analysis of 351 fractures measured in BHTV.....	99
Table 3-13. FracMan forward model inputs. ....	100
Table 3-14. Dikes identified in mud log. ....	104
Table 3-15. Zone summary. ....	105
Table 3-16. NWG 55-29 injection test results.....	107
Table 3-17. Injectivity data from nearby Newberry wells and temperature coreholes .....	109
Table 4-1. 1-D velocity model .....	114
Table 4-2. One regional and six global earthquakes identified on the local MSA network.....	115
Table 4-3. Projects involving injection-induced seismicity studied for this Demonstration. ....	120
Table 5-1. Injectivity in NWG 55-29 measured immediately before BHTV logging. ....	140
Table 5-2. Characteristics of permissible stress regimes. ....	149
Table 7-1. Summary parameters of other EGS development efforts .....	165
Table 7-2. Analysis of mud log for possible stimulation targets.....	172
Table 7-3. Summary of AltaStim modeled zones based on parameters observed in NWG 55-29.....	177
Table 7-4. Inputs for deterministic dikes. ....	177
Table 7-5. Stress inputs to AltaStim models. ....	179
Table 7-6. AltaStim model realizations .....	184
Table 7-7. AltaStim total volume for combined model of all zones. ....	188
Table 7-8. Temperature recovery after 120 gpm injection at 2530 m .....	193
Table 7-9. Typical stimulation treatment for O&G application .....	195
Table 7-10. Baseline injection test flow rates and pressures. ....	200

Table 7-11. Step-Rate test flow rates and estimated pressures.....	200
Table 7-12. Responsibilities and contact information.....	210
Table 7-13. Step-Rate test flow rates and estimated pressures.....	213
Table 7-14. Flow-back test sampling schedule.....	216
Table 8-1. Newberry Volcano model parameters.....	227
Table 8-2. Distribution coefficients of Safranin T on fractions of Ottawa sand.....	229
Table 9-1. Long-lead time items prior to drilling.....	235
Table 9-2. Drilling stage durations.....	235
Table 9-3. Production well casing designs.....	236
Table 9-4. Production well casing size, weight, grade and connection.....	237
Table 9-5. High temperature tool options for open-hole logging.....	255
Table 9-6. High-temperature tools and insurance availability.....	260
Table 10-1. Flow-back test sampling schedule.....	268
Table 10-2. Connectivity test sampling schedule.....	268
Table 10-3. Circulation test sampling schedule.....	268

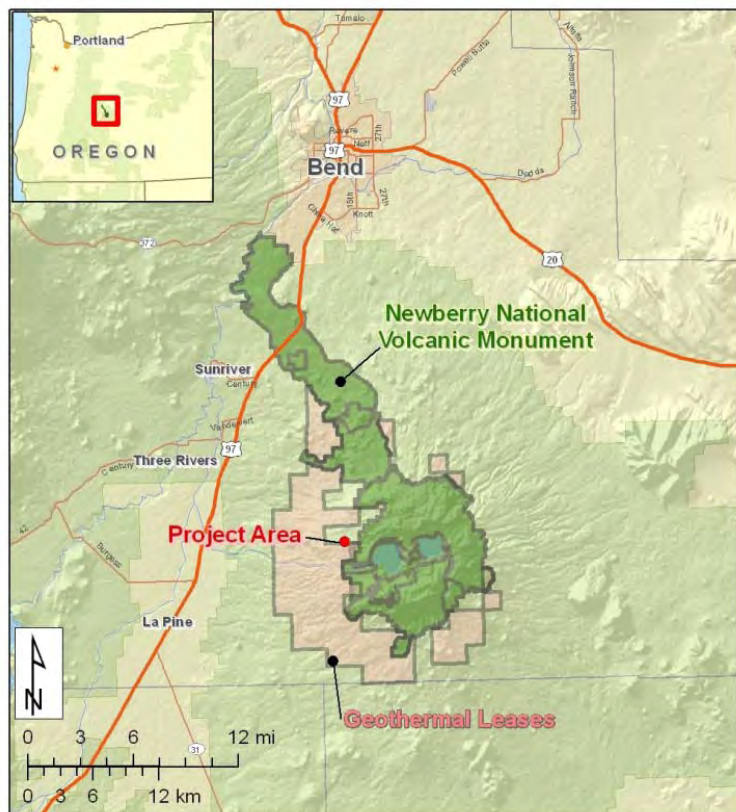


# 1 INTRODUCTION

## 1.1 PROJECT DESCRIPTION

The Newberry EGS Demonstration will develop an Enhanced Geothermal System (EGS) reservoir in the high temperature, low permeability resource present in volcanic formations on the northwest flank of the Newberry Volcano. The project team will quantitatively demonstrate stimulation techniques to successfully induce and sustain fluid flow and heat extraction from one injection well and two production wells, culminating in the conceptual design of a commercial-scale wellfield and power plant.

The project is located about 37 km (23 miles) south of Bend, Oregon, with the nearest small community about 11 km (7 miles) away at Newberry Estates, and the nearest town of La Pine about 16 km (10 miles) away (Figure 1-1). The project site is on land leased from the Bureau of Land Management (BLM) with the surface controlled by the BLM and the US Forest Service (FS). The leased land lies adjacent to the Newberry National Volcano Monument (NNVM), which was created in 1990 to preserve the scenic beauty and the volcanic features inside the Newberry Volcano caldera while providing for geothermal development and other uses on adjacent lands. Land that had been leased for geothermal development inside the caldera was exchanged for land outside the NNVM boundaries with the proviso that the presence of the NNVM would not preclude development of projects suitable to the site outside the NNVM.



The Newberry site is extremely favorable for demonstration of an EGS reservoir. Four deep, high temperature production wells have been drilled in the area, along with a number of temperature gradient and core holes. All of the wells have identified a large, high temperature, very low permeability geothermal resource at depths ranging from 2 to 3.5 km (1.2-2.2 mi).

In 2009, AltaRock Energy Inc (AltaRock) and Davenport Newberry Holdings LLC (Davenport) concluded a Memorandum of Understanding (MOU) regarding the use of the two wells drilled by Davenport in the northeastern part of their leased area for the purpose of demonstrating EGS technology developed by AltaRock. Both wells exhibit maximum temperatures of over 300°C (572°F) and very low permeability.

Figure 1-1. Location map for the EGS Demonstration at Newberry Volcano, showing Newberry National Volcanic Monument, geothermal leases, and the communities of Bend, Sunriver, Three Rivers and La Pine.

## 1.2 GOALS AND PURPOSE

The project is being executed in three phases. This report summarizes Phase I, wherein the primary objectives were to obtain necessary permits and comply with all regulations, including NEPA, communicate with the public, regulators and other stakeholders, develop a geologic model by evaluating current geoscience data and characterizing existing wells, supplemented by additional injection test and wellbore survey information, and formulate a detailed stimulation plan for Phase II.

In Phase I, the project site has been characterized in detail, and reports, plans, permits, licenses, and other items required by governmental regulatory agencies, including NEPA determination and documentation, have been submitted for approval of Phase I and initial Phase II operations. All available and relevant historic data has been compiled and thoroughly reviewed to build a comprehensive model of the geothermal resource previously identified on the northwest flank of the Newberry Volcano. The condition of the two candidate wells was evaluated and the best well was selected for stimulation. The resulting geologic model and site characterization is used herein to document a detailed Phase II stimulation plan. Aided by the output from a temporary seismic array, a study of induced seismicity and seismic hazards was completed by an independent consultant, URS Corporation, and followed by additional, increasingly detailed studies by 1) Fugro Consultants, 2) Simpson, Gumpertz & Heger, and 3) Treadwell & Rollo. These detailed stimulation plans and seismic risk analysis documents will serve as a basis for the DOE stage gate review to proceed with Phase II.

In Phase II, the primary objectives are to stimulate the existing fracture network around one of the Davenport injection wells, then drill two production wells into the resulting EGS reservoir. After detailed seismic mapping, the first production well will be drilled into one flank of the EGS fracture network created around the injection well. A connectivity flow test will be conducted after completion of the first production well, followed by similar completion and testing of the second production well into the opposite flank of the fracture network. If necessary, additional stimulation activities will be conducted to enhance connectivity between the injection and production wells. Closing out Phase II, a 30 to 60-day flow test involving all three wells will demonstrate the capability of the EGS reservoir and wells to support long-term power generation. The objective of Phase III is to refine numerical models, forecast long-term reservoir performance, and develop a conceptual model of a complete EGS power plant and wellfield system.

## 1.3 SITE CHARACTERIZATION

The Newberry Volcano KGRA (Known Geothermal Resource Area) has been an area of ongoing geothermal energy interest since the 1970s. Extensive exploration activities have been conducted in the area by public and private entities, including various geoscience surveys, and the drilling of thermal gradient, slimholes, and deep, large-bore wells.

AltaRock has access to the project site and to data collected by Davenport, based on a MOU with Davenport, the owner of the BLM geothermal site leases.

Davenport completed the drilling of two deep wells, NWG 55-29 and NWG 46-16, in July and November of 2008, respectively. Davenport and AltaRock have entered into a development agreement that will provide AltaRock with the right to use these wells, to drill additional wells on existing pads, and use the surrounding leases for testing and monitoring. Each of the existing wells is located on a five-acre pad (Pads S-16 and S-29). These well pads have been permitted to allow the drilling of at least three wells on each pad. The pads are surfaced with crushed rock and are contoured to channel all runoff into large, on-site sumps. The sumps are double-lined with bentonite and HDPE, with a capacity of about 5300 m<sup>3</sup> (1.4 million gallons) each. A similar Davenport well pad, S-17, is also located nearby, but no drilling has

been conducted there and the sump is presently unlined. Groundwater wells located on each of the first two well pads are each capable of producing about 22 to 57 L/s (350-900 gpm). Access roads to the site are FS roads that have been upgraded to facilitate the passage of large drill rigs and other heavy equipment, and have been recently maintained.

After a detailed evaluation of existing data (wireline logs, well cuttings, drilling history and injectivity tests), NWG 55-29 was selected as the best candidate for EGS stimulation. NWG 55-29 is completed to 3066 m (10060 ft), with a 8.5 in open hole from 1790 m (6462 ft) to total depth. This well was open to total depth during injection testing and other baseline surveys during the summer of 2010. NWG 46-16 is completed to 3553 m (11599 ft), with 12-1/4 in open hole to 2100m (6888 ft) and 10-5/8 in open hole to total depth. NWG 55-29 was selected as the target EGS well because NWG 46-16 has a formation collapse and bridge at 1448 m (4736 ft) which would likely require a drilling rig to remove, making the use of NWG 46-16 more risky and expensive. NWG 46-16 will be used for seismic monitoring. The wells, located two miles apart, are too far apart to be used as an EGS injection-production pair or for pressure monitoring.

### ***1.3.1 PERMITTING AND REGULATORY COMPLIANCE***

Task 1.3 in the Phase I schedule includes the dissemination of project development plans to affected parties and the procurement of the necessary permits and other regulatory approvals to conduct Phase I and Phase II operations. Public outreach meetings and informational forums were conducted prior to commencement of site activities. These meetings allowed us to communicate directly with local stakeholders that might be affected by the Demonstration, and helped us identify concerns and issues that needed to be addressed through additional public outreach and the permitting process.

In 1994, an Environmental Impact Statement (EIS) was completed for CE Newberry (CalEnergy) for the “Newberry Geothermal Pilot Project.” In June 1994, the Deschutes National Forest and the Prineville District BLM issued a joint Record of Decision to implement the Newberry Geothermal Pilot Project. The decision was based on the environmental analysis and Final Environmental Impact Statement (EIS), and included mitigation measures and an extensive monitoring program. In October 1994, the Bonneville Power Administration released their Record of Decision adopting the same alternative as the FS and BLM. The approved project included exploration, development, and production operations for 14 well pads, a 33-megawatt power plant, a 115-kV transmission line, and supporting facilities on the west flank of Newberry Volcano, outside the NNVM. Approval from all three federal agencies allowed the operator, CE Exploration Company, to begin implementation. By the end of 1995, the exploration phase of the project was underway. The Deschutes National Forest and the Prineville District of the BLM jointly administered the project. Implementation was carried out in full compliance with the EIS. Two small-diameter temperature core holes were drilled in 1995, providing new information on the geology and subsurface structure. One of these holes was developed by CE Exploration in partnership with the DOE Sandia Laboratories as a research project to improve the technology and application of slim-hole exploratory drilling. Two deeper and larger-diameter production-size holes were also drilled, to a depth of about 2743 m (9,000 feet). These deep wells were aimed to tap into the underground geothermal heat source. Testing of the wells and a thorough review of the data collected was completed during the winter of 1995-1996.

In 2007, an Environmental Assessment (EA) was completed for Davenport for the “Newberry Geothermal Exploration Project” in response to an application to construct three well pads and drill up to three 3048 m (10000 ft) geothermal exploration wells at each well pad. The purpose of the project was to assess the geothermal resource potential of the area for the generation of electricity.

Subsequently, Davenport drilled wells NWG 55-29 and NWG 46-16 with geothermal drilling permits issued by the BLM and State of Oregon Department of Geology and Mineral Industries (DOGAMI).

In 2010, an Environmental Assessment (EA) was completed for Davenport for the “Drilling, Testing, and Monitoring of up to 12 Temperature Gradient/Passive Seismic Geothermal Exploratory Wells.” This exploration program, currently in progress as DOE Grant EE0002833, seeks to identify a hydrothermal resource around the Newberry Volcano using innovative exploration techniques.

Also in 2010, a sundry notice was filed with the BLM for the Phase I baseline injection test conducted by AltaRock at well NWG 55-29. An exploration permit for the deployment of a temporary microseismic array, used for Phase I baseline monitoring of natural seismicity, was issued by the FS. The two new production wells planned for Phase II will require geothermal drilling permits from BLM and DOGAMI. An EA is being conducted to address environmental concerns associated with the microseismic array and well stimulation activities. An Underground Injection Control (UIC) permit will be obtained from the Oregon Department of Environmental Quality (DEQ) for the injection of geothermal fluids. Davenport currently possesses an Oregon DEQ Simple Air Contaminant Discharge Permit (ACDP), allowing atmospheric emissions during testing and the drilling of additional wells. This permit will be used for the EGS demonstration project.

Davenport has two existing groundwater wells, and possesses permits to complete two additional wells, if necessary. In addition, the water well originally drilled by CalEnergy in 1995 may be available for water production. The groundwater limited water use license allows temporary industrial water usage, including drilling. Davenport has obtained a new limited water use license to allow water production sufficient for stimulation and injection, well flow testing and additional drilling. To mitigate regional water consumption, temporary water mitigation credits will be purchased from the Deschutes Water Conservancy.

### ***1.3.2 DEVELOPMENT OF STIMULATION PLAN***

As an initial step in development of the stimulation plan, a temporary microseismic array (MSA) was installed around the target well. Seven surface stations were deployed to facilitate precise event detection for seismic events with magnitudes as low as about M 0.5. Data from the array has been periodically downloaded and evaluated since the summer of 2010. The resulting datasets were included in the Induced Seismicity and Seismic Hazards and Risk Analysis conducted by URS Corporation.

The project team has compiled all available information for the Newberry Volcano EGS target site, integrating regional and local geology for the area of the northwestern flank of the volcano, including: (1) structure and stratigraphy; (2) permeability of the existing wells, including surface and subsurface fractures; (3) petrology and mineralogy of the existing wells at the depths of interest, from about 1500-3000 m (5000-10000 ft); (4) geophysical data; (5) seismicity data; (6) in-situ stress; (7) geochemistry; and (8) regional heat flow and wellbore temperature profiles.

To fully characterize the target well for stimulation, a conventional injection test, temperature surveys and a high-temperature borehole televiewer survey (BHTV) were conducted. The temperature and pressure survey data, BHTV data and geophysical log data, which includes caliper, natural gamma ray, induction, density and neutron porosity logs, were extensively analyzed to identify the depth, concentration and direction of naturally-occurring fractures to identify probable stimulation targets and aid in the development of a stress model.

Following collection and analysis of the various data sets, a conceptual model of lithology, temperature and stress at depth was created. The schematic cross section of Fitterman (1988), based upon a suite of geophysical measurements, provided a starting point for the conceptual model that now includes

structural, lithological, geomechanical, and thermal components. The model includes a seismo-tectonic framework that predicts principal stress directions and relative magnitudes, and a geological fracture and faulting model with predictions of open, sealed and closed orientations.

The resulting geologic model provided the initial inputs to a 3D numerical reservoir model constructed by Lawrence Berkeley National Laboratory (LBNL) using TOUGHREACT, and a stimulation model constructed by AltaRock. The stimulation has been modeled using AltaStim, AltaRock's software for predicting the geometry of the resulting EGS reservoir volume. AltaStim output will be used to iteratively modify and optimize the stimulation plan.

### **1.3.3 PUBLIC OUTREACH AND EDUCATION**

Public outreach and education is being accomplished through three primary mechanisms: public outreach meetings, reports and publications, and various social media.

Reporting and publications completed in Phase I include quarterly and annual project updates to the DOE (quarterly and annual Financial and Technical Reports, Annual Operating Plan, and annual Peer and Program Review Report), an Induced Seismicity and Seismic Hazards and Risk Analysis, an evaluation of water usage and evolution, publication and presentation of peer-reviewed reports to the geothermal industry, and this Phase I report. This report includes a geologic model generated using historical data, augmented with Phase I baseline surveys, and a detailed plan for stimulation of the selected injection well. The *Induced Seismicity Mitigation Plan (ISMP)* prepared by AltaRock has been reviewed and approved by DOE (attached as Appendix A-1). The ISMP includes detailed reports by independent consultants, including the *Induced Seismicity and Seismic Hazards and Risk Analysis* report by URS Corporation. The ISMP and its appendices will serve as the basis for the DOE Stage-Gate Review to proceed with Phase II and stimulation of the injection well.

All data collected and analyzed during Phase I, as well as the overall project technical plan, will be published in various geothermal industry and scientific forums, as appropriate. Papers and presentations have already been made at the annual meetings of the Geothermal Resources Council, Stanford Geothermal Workshop, and the American Geophysical Union and are planned for the upcoming meetings in the fall of 2011.

## **1.4 SITE SELECTION**

AltaRock began the process of selecting a site for a possible demonstration project in the summer of 2007. The process was initiated by identifying the critical characteristics needed for a suitable site and incorporating these into a Site Selection Matrix (SSM). The starting point for the SSM was one developed by Black Mountain Technology as part of a DOE study of the potential for EGS development. This original matrix was altered somewhat for this project because AltaRock was contemplating testing technology as well as developing the site commercially. The criteria used for site selection are shown in Table 1-1.

The site selection matrix uses criteria that are additive for all options except Seismic Hazard Susceptibility, which is multiplicative. In general, each criterion is ranked with a value of 5 (high) to 1 (low) and then the values are summed. Criteria with less impact have a lower scale, from 3 to 1. If Seismic Hazard Susceptibility has a zero value (i.e., a high risk of induced seismicity hazard), the site is assigned a total value of zero and eliminated from further assessment. When there is no data available to determine a value for a criterion, it is given a zero. This emphasizes the impact of poor data, since there is an entire additional category of criteria related to data value. Economic criteria are calculated using Geothermal Electricity Technology Evaluation Model (GETEM)<sup>1</sup> with well costs determined using

---

<sup>1</sup> <http://www1.eere.energy.gov/geothermal/getem.html>



WellCost Lite (Mansure et al., 2005). The completed site selection matrix for Newberry is included as Appendix A-2.

A site with a high temperature of about 250°C (482°F) at a relatively shallow depth of 4 km (2.5 mi) or less was desirable. A well of opportunity that could be stimulated without workover was very desirable. Because most work has been done on stimulating EGS wells in crystalline rock, and so the most data is available for this process, the target would be crystalline rock with either shear or normal faulting tectonic stress regime and some pre-existing jointing or fracturing, even if sealed. An existing power plant with spare capacity and existing transmission and water supply to take the produced fluid without construction of a power plant would be optimal. Data availability and data quality were also important considerations. Image logs, temperature surveys, both static and injecting, as well as geophysical data would help to determine if the site could be expanded into a commercial size project.

As each site was considered, we contacted the respective owner or operator to discuss the potential for testing. Some sites could not be pursued due to an inability to negotiate with site owner or due to a change in ownership that was still in progress. A total of ten sites, summarized below, were considered for the demonstration project.

**Table 1-1. EGS demonstration site selection criteria.**

<b>Resource Characteristics</b>		
Temperature at depth	Tectonic stress	Geology and fracture spacing
<b>Existing Resource Information</b>		
Temperature data	Shallow wells	Wells of opportunity
In situ fluid	Fracture data in wells	Undisturbed permeability
Geologic mapping	Aerial photos and remote sensing data	
<b>Geophysics Data Availability</b>		
Gravity	Seismic monitoring	Magnetics and aeromagnetics
Seismic survey	Resistivity, SP, MT or other electrical methods	
<b>Social, Political, and Economic Factors</b>		
Environmental impact	Seismic hazard susceptibility	Water availability
Site access	Operating power plant	Power transmission
Power market	Land ownership and availability	Political climate
<b>Economic Viability</b>		
Total acreage	Calculated IRR - demo project	Calculated IRR - 100 MW project
Condition of wells of opportunity	Cost of power - demo project	Cost of power - 100 MW project

### **1.4.1 THE GEYSERS (NCPA), CALIFORNIA**

At the time of this DOE funding opportunity and proposal writing, AltaRock was actively working on a demonstration of EGS technology at NCPA Geysers. NCPA well E-7 was being deepened to serve as an injection well in an EGS doublet. Due to drilling difficulties, the well and EGS project were abandoned.

The major components of the local infrastructure needed to support demonstration operations are in place at the Geysers. The nearby NCPA facilities were available including office space, a steam gathering system, an unlimited water supply 34000 m<sup>3</sup> (9 million gallons) per day via the Southeast Geysers Effluent Pipeline. Power lines traverse the lease, and two NCPA power plants located less than 1.6 km (1 mile) from the demonstration site provide immediate access to the local 230 KV transmission line that connects to the PG&E system that delivers Geysers power to the Fulton Substation in Santa Rosa and the Lakeville Substation in Petaluma. About 20 years ago, NCPA generated as much as 240 MW<sub>e</sub> from

these two plants. However, generation has gradually declined to about half that level, leaving unused transmission capacity available for new development. NCPA Geysers remains a strong candidate for site selection, especially if wells of opportunity are not required for funding and new wells can be drilled.

#### **1.4.2 DIXIE VALLEY, NEVADA**

This site is located in the Dixie Valley area south of the current Terra-Gen Power plant and wellfield. Two wells on the lease, held by Dixie Valley Power Partners (DVPP), were drilled by Caithness in 1993. Well 62A-23 is a high temperature, low permeability well of opportunity that did not intersect any faults or major fractures. Dixie Valley is one of the highest ranked prospects according to our site selection matrix and criteria. The area has an operating power plant with associated infrastructure. However, the plant is at capacity and is about 4.8 km (3 miles) from Well 62A-23.

Dixie Valley has been the site of several major earthquakes ( $M > 7$ ), including the most recent in 1954. However, there is little seismicity in the area around Well 62A-23, and the area is largely uninhabited except for the power plant and a few ranches. There are two seismic stations fairly close to the power plant, with a total of 6 stations within a 80 km (50 mile) radius of Well 62A-23. The USArray<sup>2</sup> was installed in the Basin and Range for a period of time, and the respective data is available. The well is not drilled into any fault and, in fact, is over 2.5 km (1.5 mi) from the basin-bounding fault. The well does lie in close proximity (~1 km, 3280 ft) to the geophysical inferred trace of a major piedmont fault that shows no surface expression and trends parallel to the basin-bounding fault. So, while the site does present a significant natural seismic hazard, the possibility of the stimulation or operation of an EGS causing significant induced seismicity is currently unknown. However, because the area is remote and relatively uninhabited, risks are low for hazards from induced seismicity.

During the time that Well 62A-23 was being considered for an EGS demonstration, the Caithness geothermal projects were being acquired by ArcLight. Later, Terra-Gen was formed to operate these projects. At the time of the initiation of discussion, Terra-Gen had not acquired the DVPP leases south of the operating power plant and so negotiations were conducted with Caithness. Eventually, Caithness decided on another plan for the leases, which have since been acquired by Terra-Gen. Negotiation for use of Well 62A-23 for a demonstration site was hampered by the coinciding change of ownership.

#### **1.4.3 MEAGER CREEK, BRITISH COLUMBIA**

The Meager Creek area presented a significant potential for a demonstration site for EGS technology. A great deal of data exists from six very deep, high temperature wells drilled in the area. Three were drilled in the early 1980s by BC Hydro, and three more were drilled by Western GeoPower in 2004 and 2005. None of these wells achieved commercial production, but all exhibited high bottom-hole temperatures. Well MC-8, drilled by Western GeoPower, had some permeability. This well presented an excellent opportunity for testing AltaRock's technology. The area is a typical Cascades volcanic setting with recent andesitic volcanics overlying metamorphic rocks. The stress regime is complex with some indication of shear to the west of the volcanic edifice.

Poor site access makes this location undesirable. There is no transmission or transmission access in the area. The roads are maintained for logging, but are not accessible in winter and spring due to avalanches and landslides. The area has no support services available within reasonable distance. In addition, when DOE funding was considered, the site was not eligible due to its location outside the U.S.

---

<sup>2</sup> <http://www.usarray.org/>

#### ***1.4.4 ROOSEVELT HOT SPRINGS, UTAH***

Roosevelt Hot Springs has a great deal of data available, high temperatures at shallow depth and an operating power plant and wellfield. The area is in the Basin and Range, with tensional stresses favorable for EGS. Geology is also favorable, with recent sediments and metamorphics over granitic intrusives. Drilling has not been particularly difficult in this area, with loss of circulation and high temperatures being the major problem.

The site is now owned entirely by PacifiCorp (a MidAmerican company). The plant was previously owned by Utah Power and Light (a PacifiCorp company), while the wellfield was owned by CalEnergy, and operated with a prepaid steam sale agreement with UPL that made new development difficult. After the field and plant had the same owner, expansion of the project was feasible. However, the plant is generating at design capacity and has recently installed a binary bottoming cycle, with no capacity for additional steam or high temperature geofluid. No usable wells of opportunity exist at the site; wells not currently in use were drilled long ago and would be unacceptable due to poor mechanical condition. Yet, areas of low permeability exist at the site, so this location might be a feasible if new drilling was acceptable.

#### ***1.4.5 PUNA, HAWAII***

Low permeability wells with high temperatures have been drilled in the Puna area. Stresses in this volcanic rift area are shear or tensional, which are favorable for EGS. However, there are no wells of opportunity and the current owner was not interested in discussions of an EGS demonstration. In addition, drilling problems abound, with extreme loss of circulation, very high temperatures at unexpectedly shallow depths that have caused a serious blowout, and hard abrasive basalt that causes high bit wear and low rate of penetration. In addition, this area is the site of frequent low level seismicity, with an unfriendly population nearby that is sensitive to potentially negative impacts from geothermal development.

#### ***1.4.6 SODA LAKE, NEVADA***

At the time that AltaRock looked at Soda Lake as an EGS site there were no wells of opportunity. Since that time, two deep, high temperature wells with low permeability have been drilled. The site does have high temperatures at relatively shallow depths, and a favorable tensional stress regime with typical Basin and Range geology of sediments and volcanics overlying intrusive rocks. There is an existing power plant that is not operating at design capacity and so could use additional production fluids with little or no additional infrastructure. Water is available from the power plant, but storage facilities would be needed to cool and store enough for stimulation.

The site is located in a remote area with very low population density. There is little seismic activity, but there are also very few seismic monitoring stations. The recent faults mapped in the area are not long, making larger seismic events unlikely and, therefore, reducing seismic hazards and risk.

A great deal of geologic and well data is available for Soda Lake. While the geology is somewhat more complex than typical Basin and Range geothermal areas, the large amount of data should be possible to interpret. The area with a significant temperature anomaly is large, which could lead to a large scale EGS project.

#### ***1.4.7 COVE FORT, UTAH***

The Cove Fort-Sulphurdale geothermal system is located about 300 km (186 mi) south of Salt Lake City, within one of the largest thermal anomalies in the western U.S. (Moore et al., 2000). Geothermal well drilling commenced here in 1975 and power generation from a shallow steam cap and an underlying



liquid reservoir started in 1985. The power plant and well field are currently owned by Enel Green Power. The production is from very permeable dolomite and limestone, with open fractures and solution permeability. There have been some low permeability wells drilled, but these generally did not have high temperatures. The stress regime is favorable, with tensional and shear stresses at the edge of the Basin and Range and the Colorado Plateau. Cove Fort is a remote area with low population density. However, the fault system bounding the edge of the Colorado Plateau runs through this area, controlling permeability for the geothermal area. There have been larger earthquakes to the south and north of Cove Fort, but none in the immediate area. It would be difficult to assess the seismic hazard in this area because there are few seismic monitoring stations.

#### ***1.4.8 CLEARLAKE, CALIFORNIA***

This site has very high temperatures and a high potential for EGS development, with significant existing resource data. Leases available for development are on private land and negotiations with the leaseholders were proceeding when the lease term expired, and the landowners did not wish to continue the lease arrangement under the old terms. In addition, the possible project location is in a Superfund area due to the presence of an old mercury mining site<sup>3</sup>. Thus, permitting would be difficult and potentially problematic. A fairly large population exists close to the potential project site. The area exhibits high natural seismicity. Water is available from the old mercury mine and the potential for injecting it to aid in mitigation of the flow of mercury contaminated water into Clear Lake was a possibility. The Lake County sewage treatment plant is next to the possible project area and the County would consider leasing the geothermal rights for drilling below the land set aside for the treatment plant. There is no nearby power plant, but transmission access is close.

Geology and stresses are favorable, with volcanics overlying intrusive crystalline rock and favorable stress conditions. Data from several wells drilled in the past is also available. This site might be feasible in the future if the land owners are amenable to a new lease agreement.

#### ***1.4.9 SUMMER LAKE, OREGON***

This site is on land leased from Weyerhaeuser by AltaRock, with favorable temperatures at depth and favorable stress regime. However, there is little existing geology or resource data. The geology would present drilling difficulties because thick volcanic flows overlay unknown basement rocks. There is transmission access and a possible agreement with the Surprise Valley Electrification Corp for power purchase or wheeling. There are no wells of opportunity or power plants near this site. This site was considered largely due to the land position held by AltaRock and might be favorable for a future EGS demonstration because it appears likely that a large body of high temperature intrusive rock underlies the volcanic rocks.

#### ***1.4.10 NEWBERRY VOLCANO – OREGON***

During our initial search for a demonstration site, two deep wells existed in the Newberry area, both drilled by CalEnergy Exploration in 1995. Both were dry holes and had been abandoned, one with a casing problem. AltaRock considered opening one of the abandoned CalEnergy wells and recompleting it for stimulation, but this was considered too risky. Two additional wells were drilled by Davenport in 2008, bringing this site back into consideration.

The CalEnergy wells showed very high temperatures (over 600°F at 9200 ft), but extremely low permeability and were not productive (Spielman and Finger, 1998). The geology is a series of layered volcanics overlying igneous intrusives likely to be related to the Newberry Volcano. The upper volcanic

---

<sup>3</sup> <http://www.epa.gov/superfund/sites/nplfs/fs0902228.pdf>

layers have created significant drilling challenges due to major lost circulation zones. A seismic monitoring station, maintained by the Pacific Northwest Seismic Network, is located east of the caldera. The USArray was installed in the Cascades and included this area, so this data is available. The location is not expected to have a significant induced seismicity hazard because there are no large, active faults in the vicinity of the potential site. In addition, there are few inhabitants in the area and no large communities or towns. La Pine, Oregon, is about 10 miles from the well field.

While this area has high potential for EGS development, very little stress information is available and some issues surround the determination of stress in volcanic calderas. The stress regime is unknown because the wells are inside the ring fracture structures of the caldera margin and, hence, may be disassociated from the regional tectonic stresses. Other EGS projects on the edge of calderas have experienced dramatic changes in stress conditions with both depth and horizontal distance. Varying stresses along the borehole can be an issue for both creating an EGS reservoir and stimulating multiple fracture zones.

## 2 GEOLOGIC MODEL

### 2.1 GEOGRAPHY

The Newberry EGS Demonstration is located in Deschutes County, OR, on the west flank of Newberry Volcano, which lies approximately 65 km (40 miles) from the crest of the Cascade Range (Figure 2-1). The nearest major city is Bend, located about 35 kilometers (22 miles) north of the volcano. [Bend](#) (pop. 77000), at an elevation of 1104 m (3622 ft), has a semi-arid, high desert climate. Tourism is a major source of revenue for the city, as Bend provides close access to many recreational activities including skiing, hiking, biking, and rock climbing. Other populations near Newberry include [Three Rivers](#) (pop. 2353) and [La Pine](#) (pop. 1653), and the resort community of [Sunriver](#) (pop. 1300).

### 2.2 REGIONAL SETTING

#### 2.2.1 GEOLOGICAL AND TECTONIC PROVINCES

Newberry Volcano is situated near the juncture of several geologic provinces in central Oregon: the Cascade Range and volcanic arc to the west, the Columbia Plateau to the northeast, and the Basin and Range to the southeast (Figure 2-1). The Cascade Arc is a long-lived feature with a magmatic history including several prominent eruptive periods, Western Cascades from 35-17 Ma, the early High Cascades from 7.4 to 4.0 Ma, and the late High Cascades from 3.9 Ma to present (Priest, 1990). According to Wilson (1993), the formation of the Cascades results from the subduction of the Juan de Fuca plate beneath the North America, occurring at a rate of 3.0-4.5 cm/year. Modern volcanic features include large stratovolcanoes such as Mount Hood at 3429 m (11250 ft), Mount Jefferson at 3199 m (10495 ft), Mount Bachelor at 2764 m (9068 ft) and the Three Sisters at 3062-3159 m (10046-10364 ft), as well as many smaller domes and mafic vents. The Columbia Plateau is one of the largest flood basalt plateaus on earth, extending between the Cascade Range and the Rocky Mountains and covering about 160000 km<sup>2</sup> (61776 mi<sup>2</sup>) of the Pacific Northwest ([Columbia Plateau, 2011](#)). The Basin and Range Province is a broad physiographic and geologic region characterized by alternating narrow faulted mountain ranges (horsts) and flat arid valleys or basins (grabens) that developed as a result of crustal extensional that began in Early Miocene time ([Basin and Range Province, 2011](#)).

#### 2.2.2 NEOTECTONICS

Oblique subduction of the Juan de Fuca plate beneath North America has produced a complex tectonic setting for the Pacific Northwest (Figure 2-2). Neogene deformation, paleomagnetic rotations, and geodetic data suggest the Cascadia fore arc (defined as the area between the plate boundary and volcanic arc) is migrating northward along the coast and breaking up into large rotating blocks (Wells et al., 1998). Deformation occurs mostly around the margins of a large, relatively aseismic Oregon coastal block composed of thick, accreted seamount crust. This 400-km (249 mi) long block is rotating clockwise with respect to North America about an Euler pole in eastern Washington, thus increasing convergence rates along its leading edge near Cape Blanco, Oregon, and creating an extensional volcanic arc (which includes Newberry Volcano) on its trailing edge. Northward movement of the block breaks western Washington into smaller, seismically active blocks and compresses them against the Canadian Coast Mountains restraining bend (Wells et al., 1998).

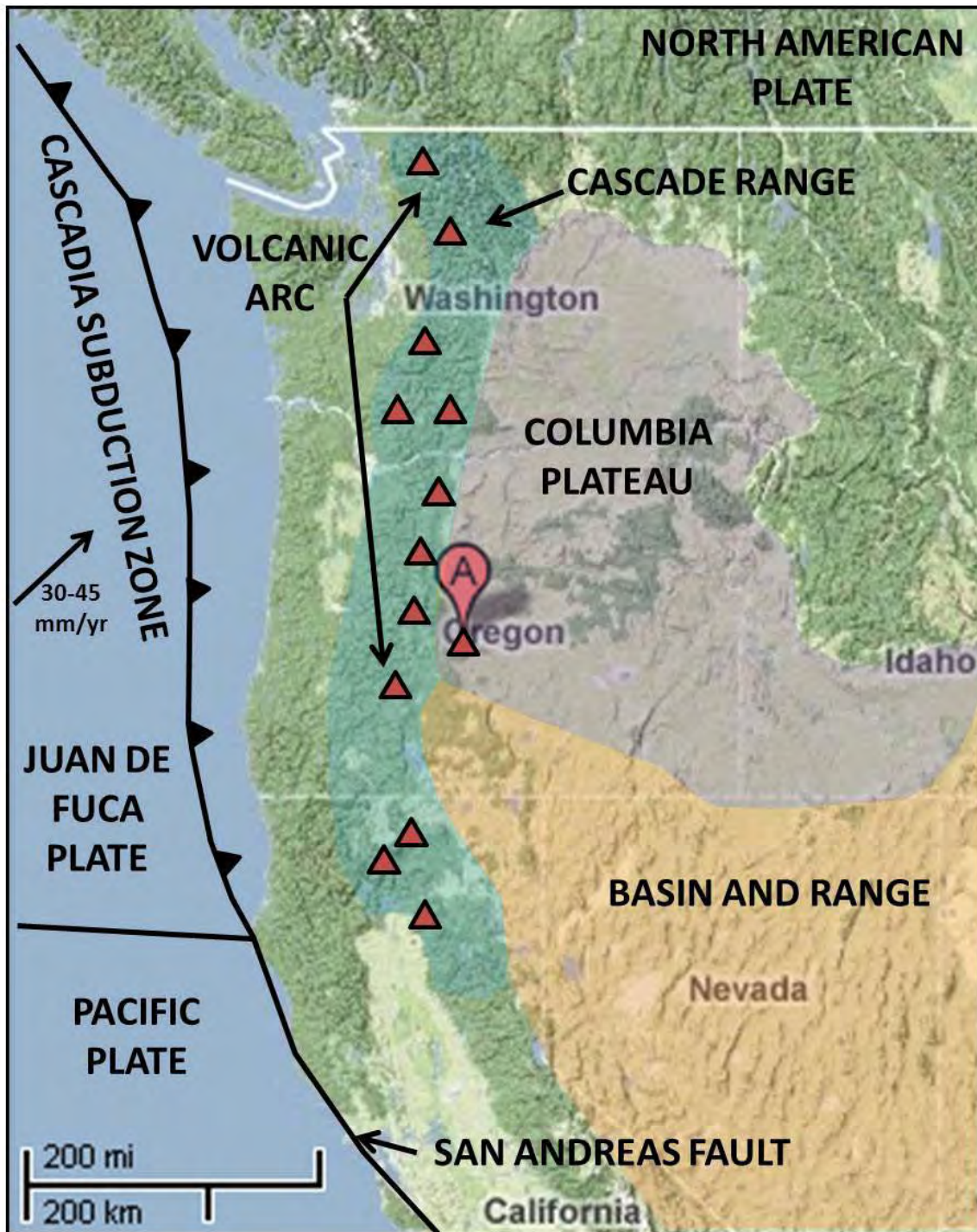


Figure 2-1. Tectonic boundaries and geological provinces of the Pacific Northwest. Red triangles represent major volcanic centers of the Cascade Arc ('A' is Newberry Volcano). Blue, purple, and orange regions represent the Cascade Range, Columbia Plateau, and Basin and Range provinces, respectively (regional boundaries estimated from Geologic Provinces of the United States, 2004). The bold black lines represent tectonic plate boundaries: the Cascadia Subduction Zone to the north and the San Andreas Fault to the south, and the east-west Mendocino Transform Fault separating the Pacific and Juan de Fuca plates (plate boundaries estimated from Cascadia Subduction Zone 2009).



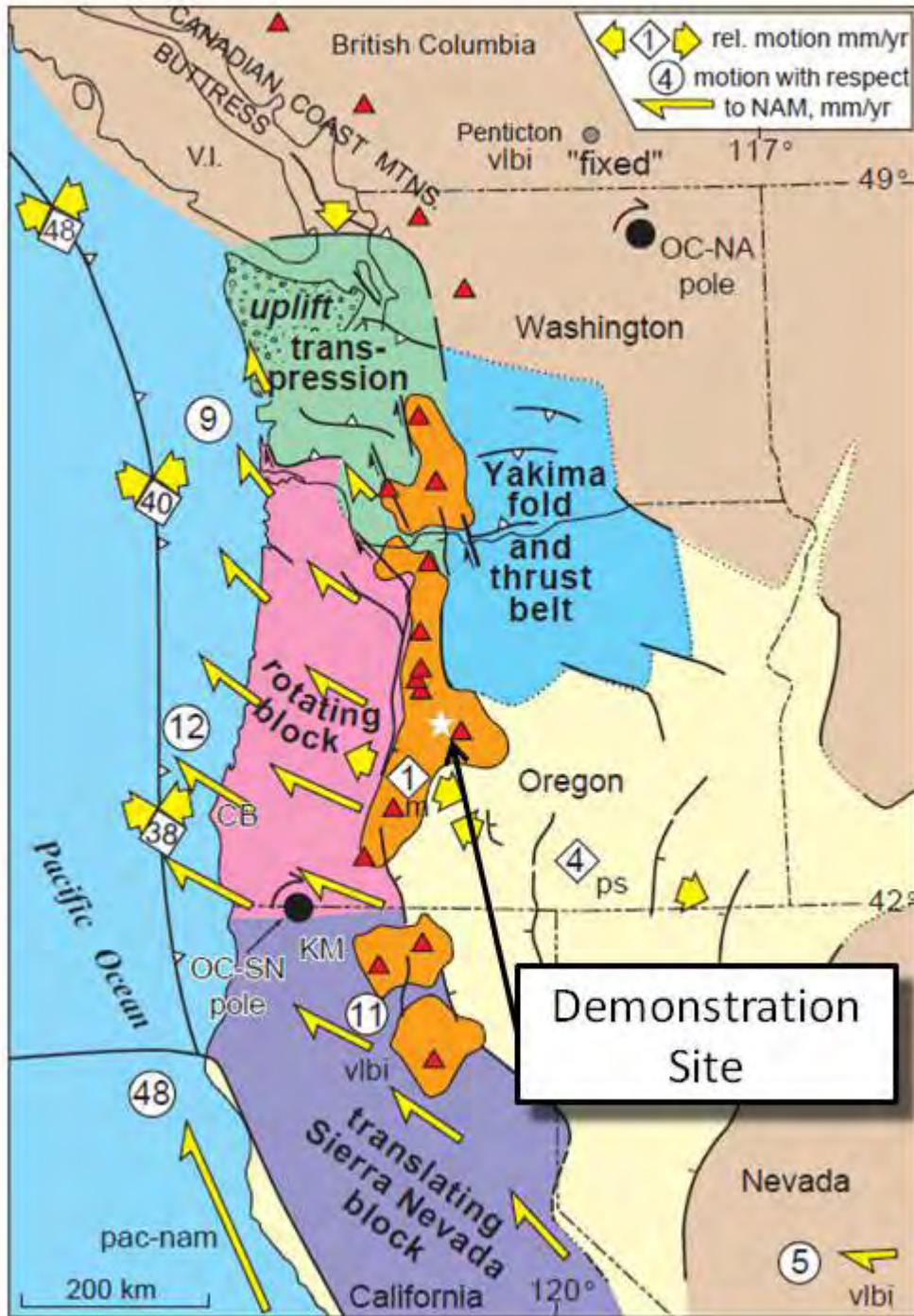


Figure 2-2. Block motions for Cascadia forearc proposed by Wells et al. (1998). The Oregon forearc block (pink) is rotating clockwise due to northwest translation of Sierra Nevada block causing extension in the Cascade Volcanic Arc (orange) along the trailing (east) edge of the Oregon forearc. The north end of Oregon block deforms Washington forearc (green) against Canadian buttress, causing north-south compression, uplift, thrust faulting, and earthquakes. Rates from vlbi; paleoseismology (ps); magmatic spreading (m); Pacific– North America motion (PAC-NAM); other symbols as in Figure 2-1. Figure and caption after Wells et al. (1998); see this paper for further explanation of this figure and Cascadia neotectonics.

Two structural patterns dominate the Newberry Volcano area. The first are the volcanic and caldera-related structures of the volcano itself, including arcuate vents and ring fractures in its central portion. Four caldera ring fractures have been mapped on the NW flank of Newberry (Sherrod et al., 2004). In the USGS database (Personius, 2002b), the ring fractures are classified as Class B: “Geologic evidence demonstrates the existence of Quaternary deformation, but either (1) the fault might not extend deeply enough to be a potential source of significant earthquakes, or (2) the currently available geologic evidence is too strong to confidently assign the feature to Class C but not strong enough to assign it to Class A.”<sup>4</sup> In the entry for these faults (Personius, 2002b) states “these faults are everywhere concealed, and have been mapped on the basis of the topographic expression of these escarpments.”

The second group of structural features is the set of regional northwest- and northeast-trending faults that are found beyond, and in places cross cut, the volcanic massif, such as the Walker Rim, Brothers and Tumalo fault zones. Southwest of Newberry, is the northeast-trending Walker Rim Fault Zone, which is likely transitional between Cascade Arc Central Graben and Basin and Range extension. The Cascades Graben, defined by various sets of N-trending normal faults, is an important structural feature of the Cascades volcanic arc of central Oregon. Faults associated with the Walker Rim fault zone cut early Newberry rocks. The northwest-trending Brothers Fault Zone, located northeast of Newberry Volcano, forms the northern boundary of the Basin and Range. The Brothers Fault Zone cuts Miocene and Pliocene lavas, and does not cut Quaternary Newberry Volcano lavas (MacLeod and Sherrod, 1988). To the north-northwest of Newberry is the Tumalo Fault Zone, which approaches the boundary of the Cascade Range and has a north-northwest orientation. The Sisters Fault Zone (of which the Tumalo fault is part) shows normal offset, with local minor oblique strike-slip. Undeformed alluvium overlying this fault zone is dated at between 25000 BP and 50000 BP (Sherrod et al., 2004). These three sets of fault orientations, all classified as Quaternary in the USGS database (Personius, 2002a), are mapped in the region surrounding Newberry Volcano (Figure 2-3).

AltaRock joined the Oregon LiDAR consortium to add La Pine, the community nearest the Demonstration, to the 2010 LiDAR survey of Newberry Volcano and the Deschutes National Forest. In particular, we were interested in better characterizing the La Pine Graben faults shown in the USGS fault and fold database at the western edge of the valley (Personius, 2002a), the ring fractures (Personius, 2002b), and checking for evidence of faults or fractures in the Demonstration area. Our analysis of the 880 km<sup>2</sup> (340 mi<sup>2</sup>) of new LiDAR data is shown in Figure 2-4 and discussed in detail in Cladouhos et al. (2011). On the west side of the LiDAR image we mapped a swarm of short, <6 km (<3.7 mi), discontinuous normal faults that occur in nested grabens and are often related to volcanic flows and cones. The USGS fault and fold database includes many of these faults, but in less detail. The USGS database also includes two long, 30 km and 35 km (19 and 22 mi), NNE-trending faults in the La Pine Graben fault set (see long yellow lines on Figure 2-3 west of 55-29). However, no evidence of these longer faults can be seen in the LiDAR. This is not surprising, as the notes in the USGS database for these faults (Personius, 2002a) are “the graben margin faults inferred from the gravity data by Ake et al. (2001) have no topographic expression or demonstrated offset in Quaternary deposits.” Our examination of the maps and figures in Ake et al. (2001) confirms that these faults are drawn on the basis of inflections in gravity profiles. Nevertheless, the seismic risk caused by faults is included in the URS seismic hazards

---

<sup>4</sup> [USGS Earthquake Glossary](#), Class A faults: Geologic evidence demonstrates the existence of a Quaternary fault of tectonic origin, whether the fault is exposed by mapping or inferred from liquefaction or other deformational features. Class C faults: Geologic evidence is insufficient to demonstrate the existence of tectonic faulting, or Quaternary slip or deformation associated with the feature.



report (Wong et al., 2010). This document makes no comment on whether these faults, which are 15 km (9 mi) away from the Project site, do or do not exist at depth.



Figure 2-3. Regional structure map showing location of the Newberry EGS Demonstration, indicated by the EGS injection well NWG 55-29. Newberry Volcano lies at the intersection of three structural trends in central Oregon (see Figure 2-1 for geographic reference). Colored lines are faults from the USGS Quaternary fold and fault database. The fault ages are coded by color, from oldest to youngest: blue, younger than 1.6 million years; green, younger than 750000 years; yellow, younger than 130000 years; and orange, younger than 15000 years.

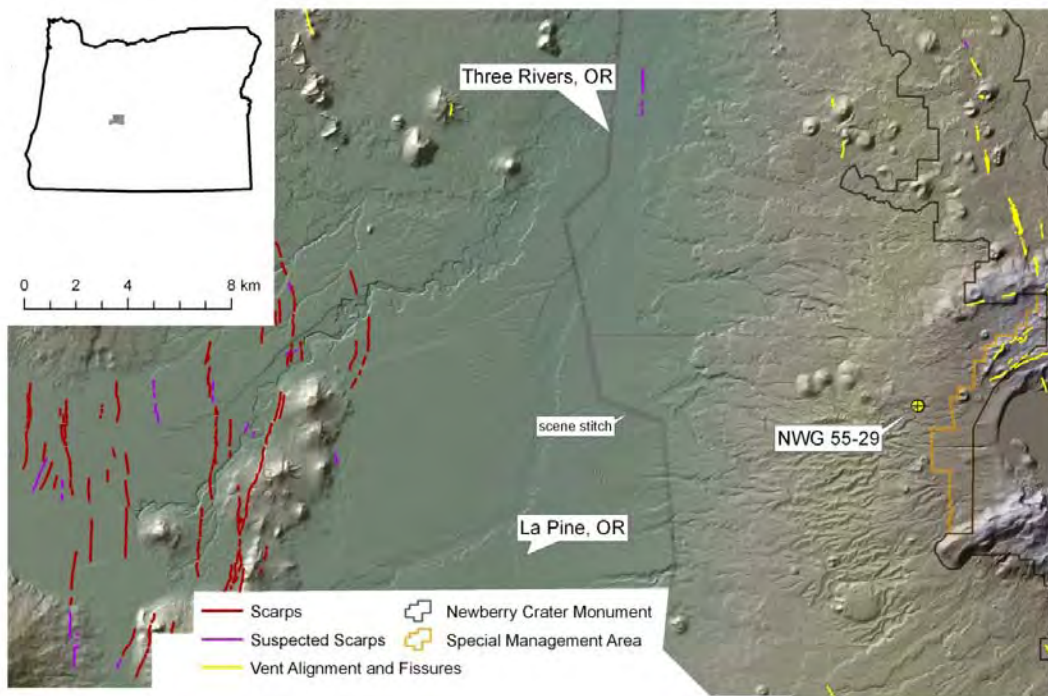


Figure 2-4. LiDAR coverage with scarps, vents, and fissures mapped by AltaRock (Cladouhos et al., 2011).

## 2.3 LOCAL GEOLOGY

Sections below describe geologic features particular to the western flank of Newberry Volcano. Information on the subsurface conditions are derived from the numerous temperature coreholes (TCH) and geothermal exploration wells that have been drilled at Newberry since the 1970s by both the private and public sectors (Figure 2-20). Early work was conducted by Occidental Petroleum (Santa Fe Geothermal), Phillips Petroleum, Sunedco, USGS, Sandia National Laboratory (Sandia), Geothermal Resources International (GEO), Union Oil, and CalEnergy Exploration (CEE).

### 2.3.1 GEOMORPHOLOGY

Newberry Volcano is a broad eruptive center active for approximately the last 600000 years (MacLeod et al., 1982; Jensen, 2006). The volcano has built up an elliptical shaped massif approximately 50 km by 30 km (31 mi by 19 mi), with some lava flows reaching more than 64 km (40 mi) north of the caldera (Figure 2-5). The more gently sloped lower flanks are composed of ash and lahar deposits, basaltic lava,

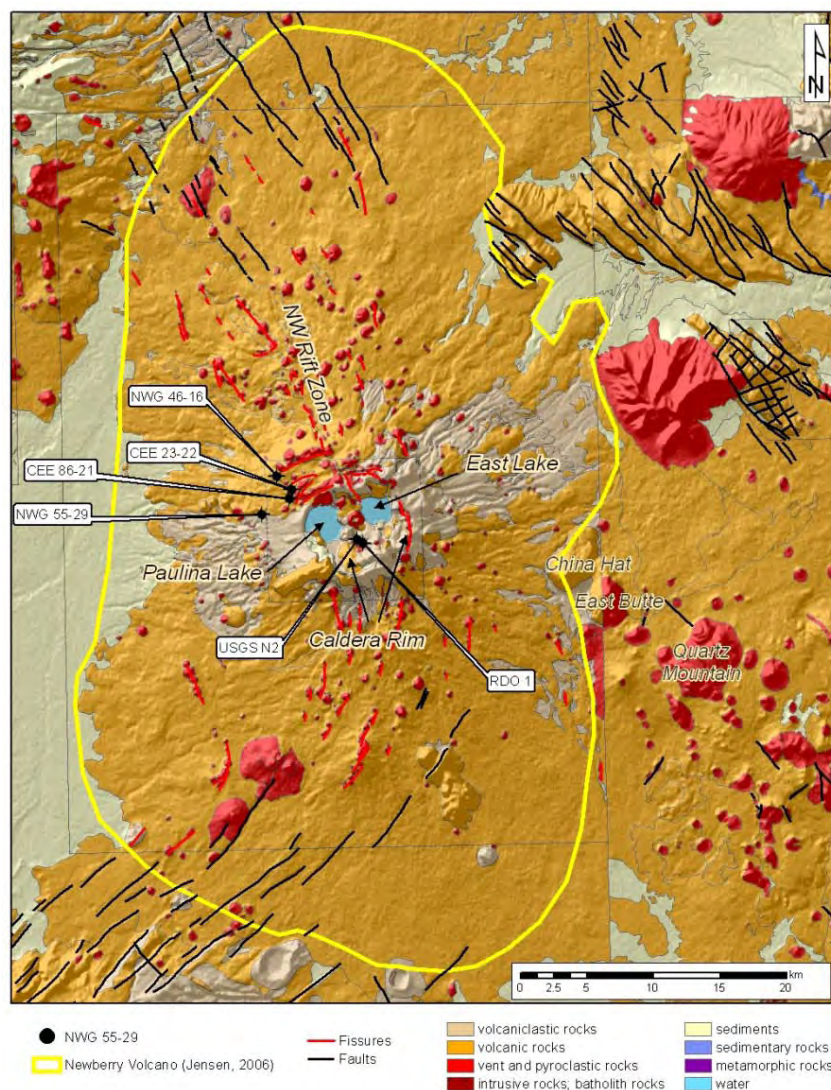


Figure 2-5. Outline of the Newberry Volcano massif (in yellow), showing caldera, rim, extent of flows, and locations of some geothermal exploration wells.



cinder cones, and minor silicic domes. Several basalt flows sourced from rifts in the NW flank of the edifice are younger than 7000 years, the age of the regionally extensive Mazama ash. The more steeply sloped upper flanks of the volcano are composed predominantly of overlapping silicic domes and subordinate basaltic rock. The central caldera is about 8 km by 5 km (5 mi by 3 mi) and is a nested composite of craters and vents, and contains two lakes: Paulina Lake on the west at an elevation of 1930 m (6332 ft) and East Lake on the east at an elevation of 1941 m (6365 ft). Paulina Lake is drained by the west-flowing Paulina Creek, the only perennial surface water found on the flanks of the edifice. Paulina Creek is a losing stream for most of its reach. Within the caldera are resurgent obsidian flows, cinder cones and maars, with the most recent eruptions occurring between 1.6 ka and 1.3 ka. The elevation of the rim of the caldera ranges from 2133-2408 m (6998-7900 ft), except along the breached western side, where the elevation is 1929 m (6329 ft).

The conventional wisdom on the glaciation of Newberry Volcano has changed in recent years. Early investigations concluded that there was no evidence for major glaciations of the edifice (Russel, 1905). MacLeod et al. (1995) reported small moraines at the base of the steep north face of Paulina Peak. Donnelly-Nolan and Jensen (2009) conclude that there is substantial evidence for glaciation of the edifice of Newberry Volcano. Their evidence includes cone morphology influenced by flowing ice, glacial erratics down to elevations of 1735 m (5692 ft), deeply incised channels (average depth 20-30 m [64-96 ft], maximum depth of 60 m [192 ft]) with no modern streams, polished outcrops, and landforms suggestive of small constructive moraines and poorly developed cirques. Whether or not all of these features are truly glacial landforms may be somewhat debatable, given the likelihood that past eruptions could have been accompanied by rapid melting of snow pack or destabilization of summit crater lakes. However, the elevation of Newberry volcano (>2000 m [>6562 ft]) and evidence for glaciation at similar elevations in the Cascades and Medicine Lake Caldera would make an 'ice-free' Newberry during glacial periods particularly anomalous (Donnelly-Nolan and Jensen, 2009).

Due to the porous nature of the surface material on the flanks of Newberry, little modern fluvial erosion or deposition occurs except at Paulina Creek or after heavy rainfall or melt events (Donnelly-Nolan and Jensen, 2009). Soil development is fairly limited in the 1-3 m (3.3-9.8 ft) of ~7 ka Mazama ash that blankets the edifice, and does not play a fundamental role in understanding the geothermal aspect of the project area.

### **2.3.2 STRATIGRAPHY**

Analyses of surface rock samples show a wide range of igneous rock compositions, dominated by a bimodal concentration of basaltic andesite and rhyodacite. Hundreds of volcanic vents and fissures are located on and adjacent to the volcano, some of which pre-date Newberry. Data from MacLeod et al. (1982), and from deeper temperature coreholes, suggest that the early eruptive history of the edifice was dominated by mafic lava. Over time, the magmatic character changed to the current bimodal basaltic andesite and rhyodacite. The Newberry flows are deposited on older volcanic and clastic sequences, most of which do not outcrop locally.

The descriptions of the geologic formations, presented below in order from youngest (shallowest) to oldest (deepest), are extracted from the Site Characterization report presented in AltaRock (2009). Table 2-1 presents a description of the correlations determined by AltaRock (2009) and used to generate the cross sections (Figure 2-6, Figure 2-7 and Figure 2-8). Formation dates described below are derived from various reports from around the region. Downhole geochronology is currently being conducted as part of Davenport's exploration and formation correlation efforts. No existing downhole geochronology is available for the Newberry edifice. Whole rock geochemistry from borehole cuttings on the western flank of the edifice will be acquired as part of Davenport's exploration efforts as well.

- *Recent Pleistocene-Holocene Newberry Volcanics* (~700 ka to 1.3 ka) – The volcano is a bimodal construct of intermediate to mafic lava flows, cinder cones, silicic lava flows, and domes, tuffs, lahars, and debris flows. Xenoliths, and cuttings from wells drilled by Calenergy and Davenport provide evidence for intrusive rocks related to the Newberry volcanics. The potassium feldspars in the silicic igneous rocks of Newberry Volcano are dominated by albite, with an absence of sanidine. This potentially could be used to distinguish the felsic intrusive of the Newberry Volcanics from older felsic units observed in the Deschutes, Mascall and John Day Formations. The subvolcanic rocks include granodiorite, dikes of felsic rocks, and fresh olivine basalt. Radiometric age dates from across the edifice reveal multiple episodes of volcanic activity. The youngest flows are found within the central caldera, including the Big Obsidian Flow. Carbon-14 ages obtained from material beneath the preceding ash flows range in age from 2045 ±230 to 1270 ±60 years (reported in MacLeod et al., 1981). K-Ar dates from rhyolite domes around the edifice range from 400 ka to 700 ka (MacLeod et al., 1981). Rhyolite at Paulina Peak has not been dated, but is believed to be around 400 ka based on the age of rhyolite flows down slope. Numerous basalt flows along the northwest rift are less than 7 ka, as they overlie the Mazama ash erupted from Mount Mazama (Crater Lake) between 6600 and 6700 carbon-14 years BP (MacLeod et al., 1981).
- *Pliocene-Pleistocene Lavas and Sediments* (~5.3 Ma to 126 ka) – Broad olivine basalt shield volcanoes and volcanic sediments are mapped off the flanks of Newberry Volcano. Much of the detailed mapping of these rocks has been done to the north and west of the volcano. Pre-Newberry silicic volcanic centers of East Butte, China Hat and Quartz Mountain are on the periphery of Newberry Volcano (Figure 2-5).
- *Pliocene Deschutes Formation* (>7-4 Ma) – The upper portion is composed of olivine basalt flows, andesite flows, basaltic ash, debris flows, eroded, and re-worked basaltic and andesitic volcanic sediments, and debris flows dating from about 6 Ma to 4 Ma (Smith, 1986). These are underlain by ash-flow tuffs, ignimbrites, rhyolites and rhyodacites, and black-pumice dacite pyroclastics, dating to about 7.4 Ma (Smith, 1986). Pyroclastic and debris units are observed to contain a mix of andesite, scoria, dacite, and pumice fragments, all within a single flow (Smith, 1986; Sherrod et al., 2004). Ferns and McClaughry (2006) identify Deschutes Formation members that are older than 7 Ma as indicated by their position beneath the 7.05 Ma Rattlesnake ash-flow tuff observed to the northeast of Newberry Volcano.
- *Miocene Mascall (Simtustus) Formation* (14.7-16.0 Ma) – The Mascall Formation is composed of white- to light-gray sanidine crystal lithic tuff, tuffaceous sandstone and siltstone, lacustrine sediments and conglomerates (Ferns and McClaughry, 2006; Sherrod et al., 2004). Draus (2002) reports magnetic chronology ages of 14.7 to 16.0 Ma, consistent with reported K-Ar ages of 16.6 (±1.4 Ma) for the basal tuff, 16.0 Ma for an interbedded Columbia Basalt flow, and a Ar/Ar age of 15.8 Ma for included tuff beds.
- *Un-Named Basalt Flows* (19-16 Ma) – Filling the 2 million year unconformity between the Mascall and John Day Formations; temporal correlatives of the widespread Steens and Columbia River Basalt Group.
- *Oligocene John Day Formation* (37-19 Ma) – The John Day Formation is composed of silicic, intermediate and basaltic volcanic lava flows, rhyolite ash-flow tuff, and dacite to rhyodacite tuffs and alluvial deposits, dated at 19 Ma to 37 Ma (Robinson et al., 1984). The western exposures show welded and cemented tuff, volcanoclastic deposits, rhyolite domes and flows, and basalt to andesitic basalt flows. The rhyolite flows and tuffs are sanidine-normative.

**Table 2-1. Depth to base of formation in various wells and coreholes (meters above sea level).**

Temperature Corehole or Well	Newberry	Deschutes	Mascall	John Day	Intrusives
NWG 55-29 <sup>1</sup>	309 (1014 ft)		Not present?	-746 (-2447 ft)	<-1294 (-4244 ft)
GEO N-2	<443 (1453 ft)				
GEO N-5	<744 (2440 ft)				
Santa Fe NC-01	<603 (1978 ft)				
CEE 76-15 TCH	1015 (3329 ft)	878 (2880 ft)	<437 (1433 ft)		
CEE NB4	<693 (2273 ft)				

<sup>1</sup>Geothermal exploration well

Stratigraphic correlation in an area with millions of years of volcanic activity emanating from multiple eruptive centers is problematic. The geometry of flows from any given eruptive center is unpredictable in width, depth, or length because of compositional and viscosity variations, preexisting topography, erosion and re-deposition of volcanic materials, intrusion and associated contact metamorphism, lithologic similarities between formations, and other factors. Because of the extreme compositional variability in both time and space, subsurface stratigraphic correlation, even with geophysical borehole logs, is very difficult (A. Waibel, pers. comm., 2009). However, ‘lumping’ of lava flows, tuffs and debris flows can result in broad correlations, as indicated in Table 2-1 where lumping between several of the main formations (Newberry-Deschutes, Deschutes-Mascall, and Mascall-John Day) is presented.

Two cross-sections across the project area have been prepared along the lines shown in Figure 2-6. The two sections, a west-east line (Figure 2-7) and a north-south line (Figure Figure 2-8), use the formation lumping described above. However, for the purposes of geothermal resource evaluation and drilling considerations, formation identification is of only marginal interest; the composition of the rocks is more important with respect to the tendency to fracture. Debris flows, cemented tuffs, and volcanoclastic sediments typically have a clay matrix, are poorly consolidated as deposited, and undergo plastic deformation when stressed. Lava flows, welded tuffs, and intrusive rock tend to be brittle, and will mechanically fail (fracture) when stressed. Rock intruded by magma has the potential to be recrystallized by high heat and become more brittle, and be fractured by the pressure and mechanical movement of the intruding magma. Post-intrusive cooling fractures can occur in both the crystallizing magma and adjacent rock. These characteristics and processes are not formation-specific. Even in the absence of detailed geologic correlations, the combination of brittle rock, regional tectonic strain and faulting, intrusive-related fracturing, and high temperatures present an attractive combination for EGS development.

The isotherms shown in the cross sections of Figure 2-7 and Figure 2-8 were drawn by interpolating the temperatures measured in wells assuming conductive gradients. Away from the control points at the wells, the isotherms can be considered speculative.



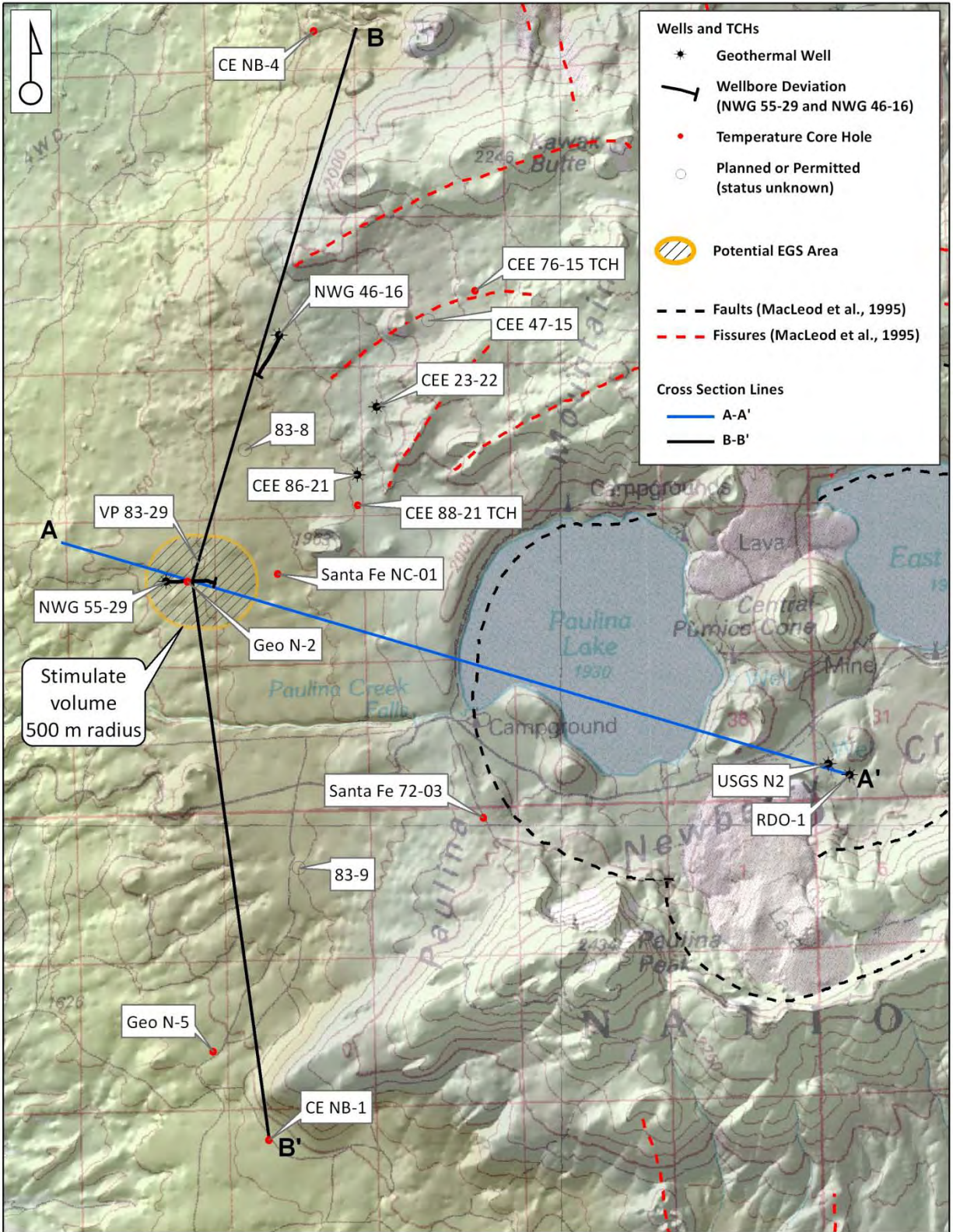


Figure 2-6. Cross-section location map.



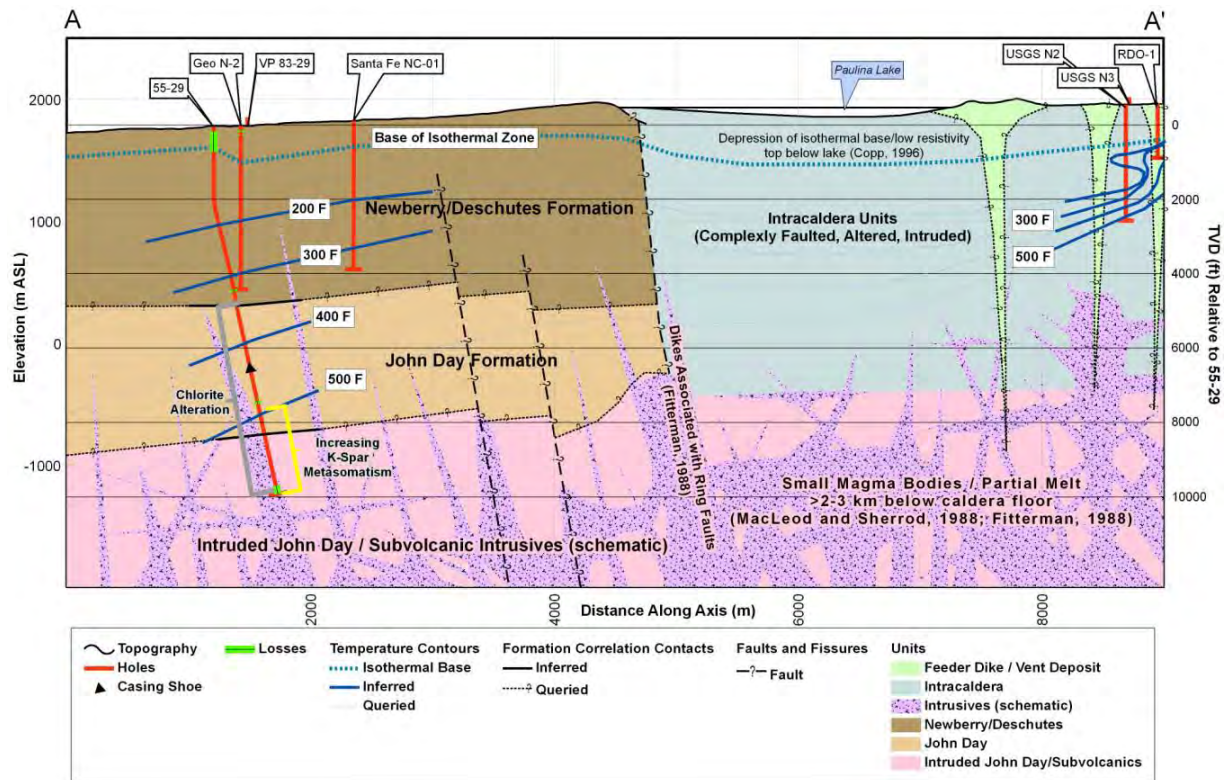


Figure 2-7. West-east cross-section A-A' showing formation correlations and speculative isotherms.

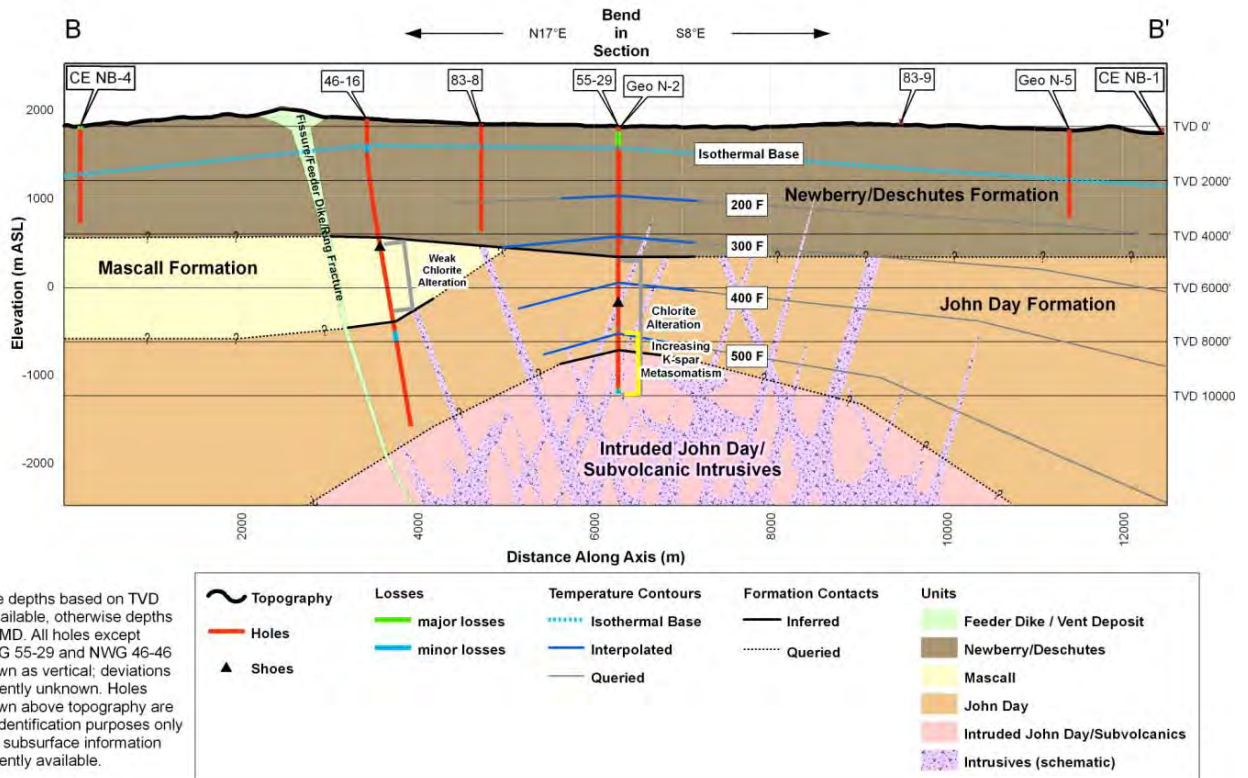


Figure 2-8. North-south cross-section B-B' showing formation correlations and speculative isotherms.

### 2.3.3 MINERAL ALTERATION

In general, the grade and degree of alteration increases with depth in the Newberry geothermal exploration wells with some heterogeneity related to local conditions. Deeper, older units may have experienced multiple episodes of intrusion during the past tens of millions of years, unrelated to Newberry volcanism. Younger, less permeable dikes might be relatively unaltered, but surrounded by small contact aureoles. Fracture zones and zones that contained primary permeability, such as autobreccia and scoria zones, and have hosted hydrothermal fluids in the past show a greater degree of alteration than less permeable host units. The following general characteristics of the alteration in the area, based on various reports (e.g., Epoch, 2008a, 2008b; Bargar and Keith, 1999) and AltaRock's interpretation to follow, are worth highlighting up-front:

- The mineral assemblages observed in various wells and coreholes from around the edifice are often consistent with temperatures recorded in those holes, not retrograde conditions, suggesting the modern heat input to the region is near its maximum value. However, mineral inclusions often show hotter conditions did exist in the past (Bargar and Keith, 1999).
- Mud logs for the wells 55-29 and 46-16 show a general lack of permeability, and limited fluid flow during alteration (Epoch, 2008a, 2008b).
- In the vicinity of NWG 55-29, there appears to be minimal mineralogical evidence for a hydrothermal system (Epoch, 2008a, 2008b; Bargar and Keith, 1999).
- Low permeability, due in part to clay alteration below ~300 m (1000 ft), seems to be a defining characteristic of the western flank of the edifice. Above this point, lack of alteration is associated with major loss zones, while within the lower altered zone, decreased permeability and high conductive gradients have resulted in attractive EGS targets.

#### 2.3.3.1 ALTERATION IN NWG 55-29

Alteration in NWG 55-29, a 3066 m (10060 ft) deep well, is predominantly diagenetic overprinted by thermal contact metamorphism, with very minor amounts of hydrothermal alteration associated with past fluid flow in fractures and joints. The upper portion of the hole (0 to 951 m [3120 ft]) is described as unaltered volcanic sequences, but mud log notes and reports (Epoch, 2008b) show minor alteration to 'green clays', zeolites (e.g., natrolite), and kaolinite in some zones below about 274 m (900 ft). Smectite becomes more common in cutting descriptions by about 360 m (1181 ft). Calcite first appears in veins below 506 m (1660 ft). By 870 m (2855 ft) the dominant type of alteration is calcite and smectite in veins and vugs. Silica and pyrite veining is noted below about 1096 m (3595 ft), along with minor silicification. Chlorite becomes more dominant by about 1341 m (4400 ft), but is heterogeneous, increasing intensity below 1524 m (5000 ft). Low-grade greenschist facies alteration (albite-chlorite-calcite) is apparent below 1829 m to 1951 m (6000-6400 ft), with epidote noted in increasing abundance below 1768 m (5800 ft). There is increasingly complex and abundant alteration products below 2134 m [7000 ft] (chlorite-epidote-calcite-pyrite), with minor silicification noted at 2201 m (7220 ft); however, mud loggers note a general lack of permeability. Strong chloritization exists below 2187 m (7175 ft), and an altered zone is found at 2262 m (7420 ft). Higher greenschist facies alteration (chlorite-actinolite-albite-epidote) is encountered below 2591 m (8500 ft). Below 2865 m (9400 ft) evidence of dikes and sills, ranging in composition from basaltic to felsic, are more abundant, and there appears to be an associated increase in contact metamorphism. The cuttings from NWG 55-29 were analyzed in detail for a graduate research thesis completed at The School for Renewable Energy Science at the Universities of Iceland & Akureyri. The thesis (Letvin, 2011), not made public due to a non-disclosure agreement and proprietary data, is included as a confidential appendix (Appendix B-1) and summarized in Section 3.2.5.

Bargar and Keith (1999) reviewed the alteration present in cuttings from GEO N-2, a temperature corehole with a total depth of 1341 m (4398 ft) located 230 m (755 ft) east of NWG 55-29. The limited and minor alteration described in GEO N-2 is similar to that observed in NWG 55-29. They note that primary and secondary voids (autobreccias, vesicles, joints, and fractures) are usually partly to completely filled with hydrothermal alteration minerals below approximately 400 m (1312 ft). They note smectite of various colors in voids and after volcanic glass in lithic tuffs, and mixed green chlorite-smectite in core. In general, alteration is fairly minor, and fluid inclusion studies suggest temperatures were only 20-40°C (68°-104°F) warmer than current conditions (BHT = 167°C [333°F]). In CalEnergy records reviewed, “continuous smectite alteration” is noted in GEO N-2, below 219 m (720 ft) near the transition from the isothermal, upper aquifer and the impermeable lower, conductive zone as indicated in Figure 2-7. See Appendix B-2 for additional details on Fetterman (2011) work on fractures, alteration, and mineralogy in GEO N-2.

### 2.3.3.2 ALTERATION IN NWG 46-16

Drill cuttings show the same gradational weathering and diagenesis, grading to thermal metamorphism, as observed in well NWG 55-29. Low-grade greenschist facies occurs below 1829 m (6000 ft). Below 2438 m (8000 ft), greenschist facies metamorphism increases to chlorite-albite-epidote. Evidence of hydrothermal activity is observed in the cuttings from this well. At 1310 m (4300 ft), silica cementing in a microbreccia is observed. At 2255 m (7300 ft), fragments of drusy epidote and quartz vein minerals are observed. Intermittent traces of quartz and epidote vein minerals are observed occasionally through the rest of the hole, with an increase in the vicinity of 3383 m (11100 ft).

### 2.3.4 POROSITY AND PERMEABILITY

The bulk permeability and injectivity for the open-hole section of several CalEnergy and Sandia National Laboratory wells and TCHs is described in Spielman and Finger (1998) and summarized in Table 2-2, along with comparable data for NWG 55-29. These wells, located on the northwestern flank of the Newberry volcanic edifice in close proximity to EGS target injection well NWG 55-29, had bottom hole temperatures ranging from 177°C at 1634 m (351°F at 5360 ft), to 317°C at 2804 m (603°F at 9200 ft), and very low permeability.

Attempts to flow the three geothermal exploration wells were unsuccessful. Spielman and Finger (1998) noted that the flow test results for these two geothermal exploration wells were typical of hot, low permeability wells. The injected water boils and flows out of the borehole and, because no formation fluids replace the boiling water, flow stops when the well is empty. The flow tests are described below:

- A flow test for CEE 86-21 was conducted between 27 November 1995 and 2 December 1995, during which time water was injected at 5.4 L/s (85 gpm) and 0.34 MPa (50 psi) at the wellhead, and then on 12 Dec 1995 nitrogen was pumped to 2134 m (7000 ft) through coiled tubing. The well unloaded but stopped flowing after 4 hours. After attempting to repair casing damage a second injection test was conducted at 3.1 L/s (49 gpm) at a pressure of 5.5 MPa (800 psig) for 5 hours, with similar results.
- Water was injected into CEE 23-22 between 31 December 1995 and 8 January 1996 at 7.6 L/s (120 gpm) with wellhead pressure of 1.4 MPa (200 psig). After injecting 15 m<sup>3</sup> (4000 gallons) of 15% HCl on 9 Jan 1996, a second injection test at 5.0 L/s (80 gpm) and a 9.31 MPa (1350 psig) wellhead pressure was conducted until 21 January 1996. On 20 Apr 1996 an attempt to flow the well by injecting nitrogen at 2530 m (8300 ft) was unsuccessful.
- Attempts to flow NWG 55-29 were made from 16-19 July 2008, while the rig was still on the hole. The well was air-lifted several times, in stages with increasing depth, but would not flow unassisted.



It only unloaded water and small amounts of noncondensable gas that had accumulated inside the wellbore. At the end of the test, CO<sub>2</sub> gas readings were in excess of 30000 ppm without air assist. On 19 July 2008, an injection test was conducted. The test continued for 30 minutes, with no indication that the formation was capable of accepting injection water at a surface pressure of 6.7 MPa (970 psig). In September and October 2010, two injection tests were conducted in order to cool the wellbore for BHTV logging and establish baseline injectivity. The injection rates were 5000 lb/hr (0.63 kg/s) and 10500 lb/hr (1.32 kg/s), respectively. The calculated injectivities were 0.007 kph/psi, and 0.014 kph/psi, respectively. These results were similar to the results from the offset wells analyzed by CalEnergy.

**Table 2-2. Well Data and Injectivity Test Results (AltaRock, 2009).**

Well		Total Depth (m)	Max Static Temp (°C)	Bottomhole Gradient (°C/km)	Injection Rate (kph)	WHP (psig)	Injectivity (kph/psi)
CEE 76-15 TCH		1634	177	NA	1-2	300	0.0015-0.0031
CEE 88-21 TCH		1486	211	NA	NA	NA	NA
CEE 23-22		2927	294	86-98	40-60	1350-2000 <sup>†</sup>	0.024-0.026
CEE 86-21		2804	317	86-98	25-42.5	50-800 <sup>†</sup>	0.022-0.026
NWG 55-29*	08/2008	3066	331	~93 <sup>‡</sup>	NA	970	NA
	09/2010	"	"	"	5	751	0.007
	10/2010	"	"	"	10.5	1153	0.014

\* NWG 55-29 injection test from July 2008, and September and October 2010. Results of the later two test periods are presented.

<sup>†</sup> Liquid head at zero wellhead pressure (WHP) was assumed to be 2.3 MPa (333 psi) based on water levels of 236 m (775 ft) in the wells (Spielman and Finger, 1998).

<sup>‡</sup> Average gradient from 2966 m to TD (bottom 100 m).

NA = not available

Results of the injection tests for CEE 23-22, CEE 86-21, CEE 76-15 TCH, and NWG 55-29 reveal injectivity several orders of magnitude lower than the lowest permeability geothermal producers. Spielman and Finger (1998) note that injectivity in geothermal wells typically range from a high of 1000 kph/psi, to a low of 1 kph/psi for low permeability wells. The injectivities for wells 23-22 and 86-15 were 0.024-0.026 kph/psi and 0.022 kph/psi, respectively. Injectivity for CEE 76-15 TCH and NWG 55-29 are even lower at 0.0015-0.0031 kph/psi and 0.007-0.014 kph/psi, respectively<sup>5</sup>. Bulk permeability for CEE 23-22 was determined to be 0.26 mD. By comparison, permeability in geothermal fields such as Coso and the Salton Sea range from 25-300 mD (Spielman and Finger, 1998).

Based on the results of the four exploration wells drilled on the northwestern flanks of the volcano in 1995, Spielman and Finger (1998) concluded that while the area had adequate temperature, it did not have the permeability necessary to host a viable hydrothermal resource at economic depths with then-current drilling technology. The authors note that the injectivity measured in two CEE wells closely

<sup>5</sup> Spielman and Finger (1998) provided well injectivities in kph/psi. The original papers cited below used a variety of metric volume units. Since the injectivities provided here are primarily for comparison purpose, we present them in the units used by Spielman and Finger (1998). Elsewhere, we use gpm/psi for English unit injectivities and L/s/MPa for metric unit injectivities. This is consistent with international EGS projects which always use volume rates (i.e. L/s/MPa or L/min/MPa) to quantify injectivities of EGS wells. Injected fluid density is at standard surface pressure and temperature.



resembles those found at 'hot dry rock' (HDR) projects worldwide. In Japan, HDR wells had an average injectivity of 0.002 kph/psi (Kaieda et al., 1990), the Tirniauz HDR well in Russia had an injectivity of 0.04 kph/psi (Kruger, 1992), and the Soultz-sous-Forêts (Soultz) well in France had an injectivity of 0.1 kph/psi (Jung, 1992). Spielman and Finger (1998) specifically note that the low permeability and high temperatures "qualify this area for a hot-dry-rock project."

While the CEE and NWG 55-29 wells have demonstrated low permeability in the immediate vicinity of these wells, the data provided by the deep wells are not capable of addressing permeability elsewhere on the volcano or below the total depth of the wells (>3000 m [>10000 ft]). Davenport and others are of the opinion that there is a reasonable probability that permeable areas occur on Newberry's flanks, a theory currently being investigated by Davenport as part of DOE Grant EE0002833.

### **2.3.5 LOCAL STRUCTURE**

Newberry Volcano is located at the intersection of structural trends as evidenced by the varying fault orientations between the Tumalo, Walker Rim, and Brothers fault zones (see Section 2.2). In addition, the central portion of the elliptical-shaped edifice (Figure 2-5) has experienced multiple caldera forming collapses, at least one at ~300 ka and another around ~80 ka (Donnelly-Nolan, 2004). The associated ring faults and fracture/fissure zones have been the target of multiple geothermal wells (including the exploration wells drilled by CalEnergy). However, no geothermal fluids were encountered at the targeted depths.

NWG 55-29 was drilled on a portion of the western flank of the edifice with no clear surface expression of the ring fractures mapped elsewhere around the central caldera. LiDAR analysis of the mapped ring fractures northeast of NWG 55-29 reveals curved vent fissures and tentatively correlated vent alignments that end more than 3 km (1.9 miles) from the wellhead. Dip-slip fault offset along the ring fractures is not observed in the LiDAR surfaces. In addition, there is only limited evidence of potential faults in the NWG 55-29 well bore from drilling logs, mud logs, BHTV data (see Sections 3.2 and 5.4), or cuttings analysis (Section 3.2.5). Potential fault and fracture zones in NWG 55-29 from the end of drilling report and mud log (Epoch, 2008a, 2008b) are detailed below:

- 805 m (2640 ft) = ..."loc abundant subrounded cuttings and sand sized particles – bit action?"
- 1822 – 1826 m (5977-5990 ft) = veining, increased torque, drusy qtz (open fractures), lost 1.4 m<sup>3</sup> (9 barrels)
- 2045 – 2051 m (6710-6730 ft) "bleaching at 6710' -6730' mélange, altered epidote-chlorite + hem...; coincident with drill break possible fracture zone."
- 2765 – 2768 m (9070-9080 ft) "Note: Sample 9070' to 9080' has diverse mixture of lithology and alteration styles may be a rubble zone/contact." Lost 7.2 m<sup>3</sup> (450 barrels) on return trip around 50 m (164 ft) deeper.
- 2856 m (9370 ft)= brecciation w/ epidote veins

Data on lost circulation encountered while drilling, which could be used to identify permeable fault or fracture zones, among other things, were compiled for several wells and temperature coreholes around the project area. In general, the upper, permeable and isothermal zone, for almost all wells and TCHs, showed significant problems with lost circulation. The depth of this zone varies, but upper level losses usually decreased around 200 m (656 ft) depth. The depth to the base of upper zone losses is summarized in Table 2-3, where all of the upper zone losses in resulted in either complete losses, or losses at a rate greater than 53 L/min (20 barrels per hour [bbl/hr]).

Of additional interest are losses that occurred at greater depths (Table 2-4). Mud logs and drilling reports were reviewed for common lithologies or conditions that coincided with loss zones at depth. In summary, loss zones might be related to lithologic contacts (e.g., porous scoria deposits, autobreccias, fractured volcanic flow tops/bases), but these are not predictive (losses would occur prior to recognition of the lithology changes), and changes in lithology were too chaotic to be anticipated. Areas of alteration and silicification might be precursors to loss zones; much of the alteration is limited to zones that at one time had enhanced secondary permeability. However, not all zones of alteration were coincident with loss zones, and not all loss zones showed signs of alteration.

**Table 2-3. Base of upper loss zone.**

Well/TCH ID	Depth of Last Major Shallow Loss Zone m (ft)
NWG 55-29	342 (1122)
NWG 46-16	72 (235)
GEO N-2	151 (495)
CE88-21 TCH	158 (517)
CEE 86-21	277 (908)
CEE 23-22	171 (560)
CE76-21 TCH	228 (747)
CE NB4	166 (544)

Table 2-4. Identified loss zones in surrounding wells and temperature coreholes (TCH). Blank cells in table indicate no losses.

NWG 55-29		NWG 46-16		GEO N-2		CEE 86-21		CEE 23-22		CEE 88-21 TCH		CEE 76-15 TCH		CE NB4	
Depth m (ft)	Description	Depth m (ft)	Description	Depth m (ft)	Description	Depth m (ft)	Description	Depth m (ft)	Description	Depth m (ft)	Description	Depth m (ft)	Description	Depth m (ft)	Description
41-342 (135-1122)	complete to partial losses	69-73 (228-239)	180 bbls lost	37-41 (122-133)	partial losses	103-107 (337-352)	complete losses	16 (54)	Complete losses, LCM did not work	15-158 (50-517)	battled full to partial losses	9-18 (31-58)	minor losses controlled with plug	0-166 (0-544)	battled complete losses for >10 days
1336 (4384)	lost 35 bbl 11 bbl/hr	305-383 (1002-1233)	lost 5-10 bbls for 6 hours	46-47 (150-155)	partial losses	183 (600)	lost 100 bbl/hr	43-45 (142-146)	Full to partial losses 120 bbl/hr	219 (720)	partial losses	18-52 (58-170)	minor losses controlled by lcm		
1497 (4910)	lost 10 bbl	2419-2525 (7937-8285)	lost 20 bbls/hr, 120 bbls	76-78 (250-255)	partial losses	277 (908)	lost 30 bbl/hr	62 (202)	lost 20 bbl	320 (1050)	partial losses	52-53 (170-174)	30 bbl/hr set 3 plugs		
2093-2097 (6868-6880)	lost 22 bbl			495 (151)	complete losses	1623 (5324)	lost 20 bbl	107-171 (352-560)	lost 60 bbl/hr	469 (1540)	partial losses	53-84 (174-274)	lost returns set 3 plugs		
2224 (7295-7297)	lost 25 bbl					2264 (7427)	lost 43 bbl on survey	1116 (3660)	lost 70 bbl,	476 (1561)	lost 10 bbl, total losses	123 (404)	lost returns set 3 plugs		
2256-2263 (7400-7425)	lost 30 bbl					2663-2676 (8738-8778)	lost 22 bbl/hr 163 bbl total	1346 (4417)	lost 115 bbl	518 (1698)	lost 40 bbl, total losses	173-178 (566-583)	5-12 bbl/hr lcm		
2265-2272 (7432-7454)	lost 26 bbl							2063-2073 (6770-6801)	lost 45 bbl	1103 (3619)	minor losses	184 (604)	partial returns hole sloughing		
2564-2565 (8411-8415)	lost 15 bbl											216 (709)	full loss set plug		
2950-2968 (9678-9736)	lost 95 bbl											219 (719)	full loss set plug		
2968-3066 (9736-10060)	lost 12 bbl/hr											228 (747)	full loss lcm		
3005-3056 (9860-10026)	lost 470 bbls/24hr											274-838 (900-2748)	partial returns lcm		
3056-3066 (10026-10060)	lost 90 bbl											317 (1040)	minor losses when opening hole		

## 2.4 HYDROLOGY

AltaRock drafted water consumption (Appendix B-3) and groundwater monitoring (Appendix B-4) plans which were reviewed in Kleinfelder (2011)(Appendix B-5). Background information regarding surface and groundwater conditions around the Demonstration is presented below.

The Newberry EGS Demonstration is located in the southern edge of the Upper Deschutes Basin (Figure 2-9). The groundwater hydrology of the upper Deschutes Basin (Figure 2-10) was the subject of a USGS water resources investigations report (Gannett et al., 2001). In this report the upper Deschutes Basin was defined as bounded on the west by the Cascades and on the east by an artificial boundary based on low data availability and on the low likelihood of significant groundwater exchange between this east boundary and the Deschutes Basin. The geology of the upper Deschutes Basin is dominated by a long history of bimodal arc and back-arc volcanism.

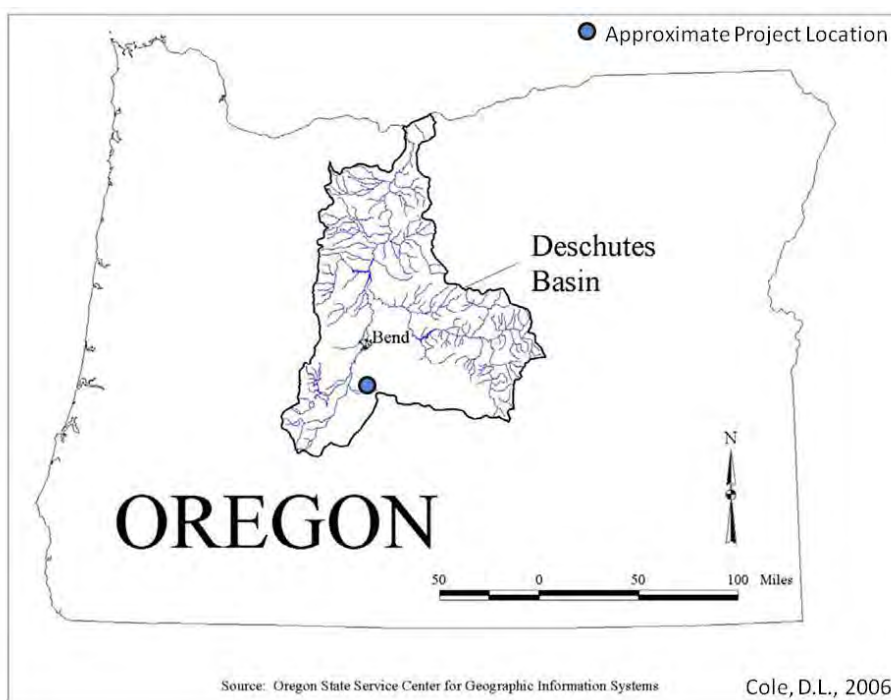


**Figure 2-9. Deschutes Basin in central Oregon and Newberry EGS Demonstration area (from Cole, 2006).**

Newberry Volcano rises to 2408 m (7900 ft) on the southeastern side of the Deschutes Basin. Newberry volcanic rocks are built upon the regionally extensive Pliocene Deschutes Formation (>7-4 Ma), which includes basalt flows, andesite flows, debris flows, ash-flow tuffs, ignimbrites, rhyolite and rhyodacite, and eroded and re-worked basaltic and andesitic volcanic sediments (Smith, 1986; Sherrod et al., 2004). Beneath the Deschutes Formation older volcanic, sedimentary and tuffaceous rocks of the John Day, Mescal, and Clarno formations are either encountered or inferred. See Sections 2.2 and 2.3 for a detailed discussion of the geologic setting.

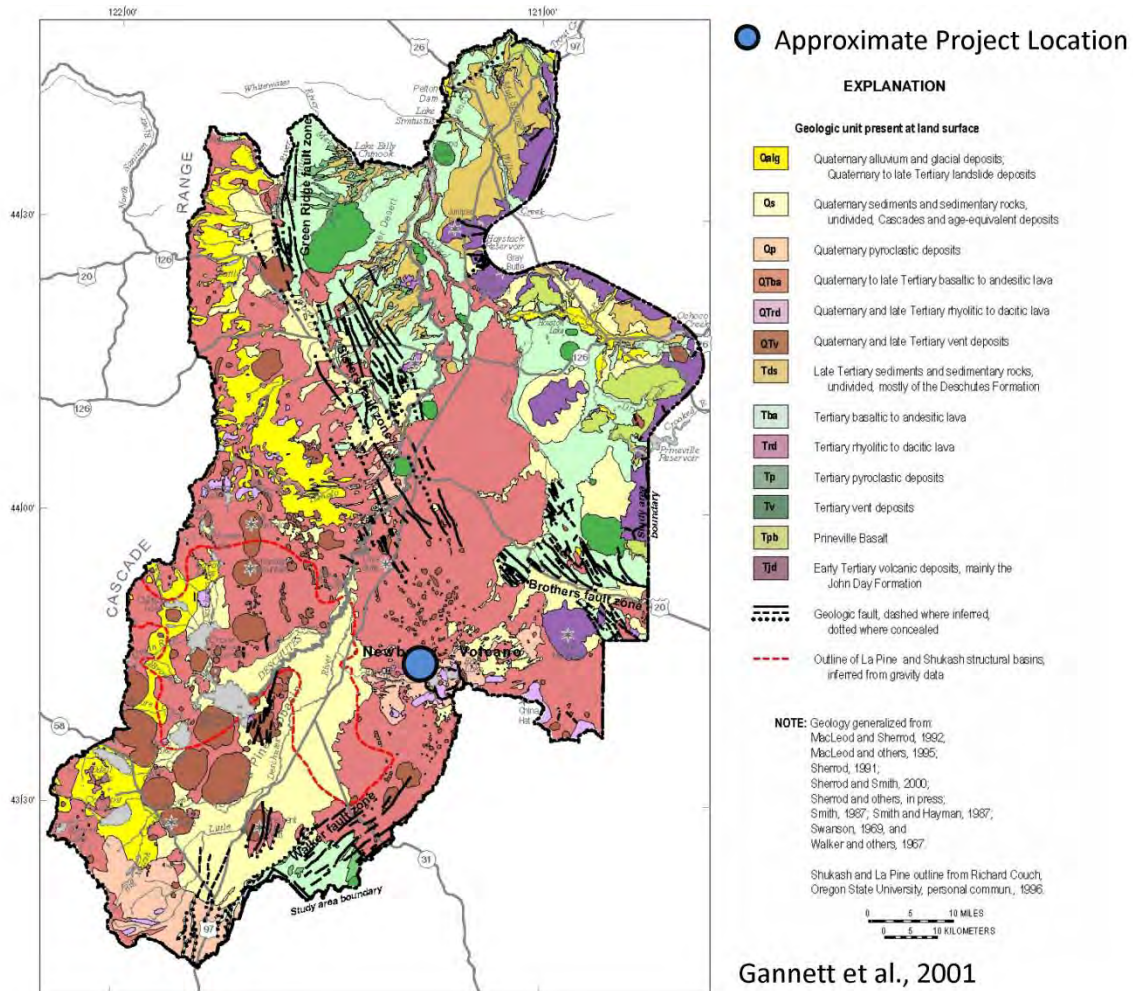


**Figure 2-10. Upper Deschutes Basin generalized geology. All of the units except Q<sub>alg</sub> and Q<sub>s</sub> are volcanic. Surface Water**

Figure 2-11 presents the surface hydrologic features. The most prominent surface hydrologic features in the project area are East Lake (69600 acre-feet or  $8.5 \times 10^7 \text{ m}^3$ ), Paulina Lake (249800 acre-feet or  $3.1 \times 10^8 \text{ m}^3$ ) and Paulina Creek, a net losing stream with a net leak-off rate of  $0.17 \text{ m}^3/\text{s}$  (6.1 cfs) for the 13 km (8 mi) stretch of creek from Paulina Lake to USFS Road 21 (Sammel and Craig, 1983; Morgan et al., 1997). Both Paulina and East lakes are found within the central caldera at Newberry Volcano. East Lake, at an elevation of 1941 m (6368 ft), drains through the subsurface of the central vent complex to the lower Paulina Lake, elevation 1930 m (6332 ft). Paulina Lake is drained by Paulina Creek, which is partially controlled at the outflow of the lake by a small diversion structure to moderate flows for downstream irrigation. Paulina Creek is the only surface water found on the flanks of the edifice. Results of geochemical analysis from surface waters, as well as ground and thermal waters, are presented in Table 2-5.



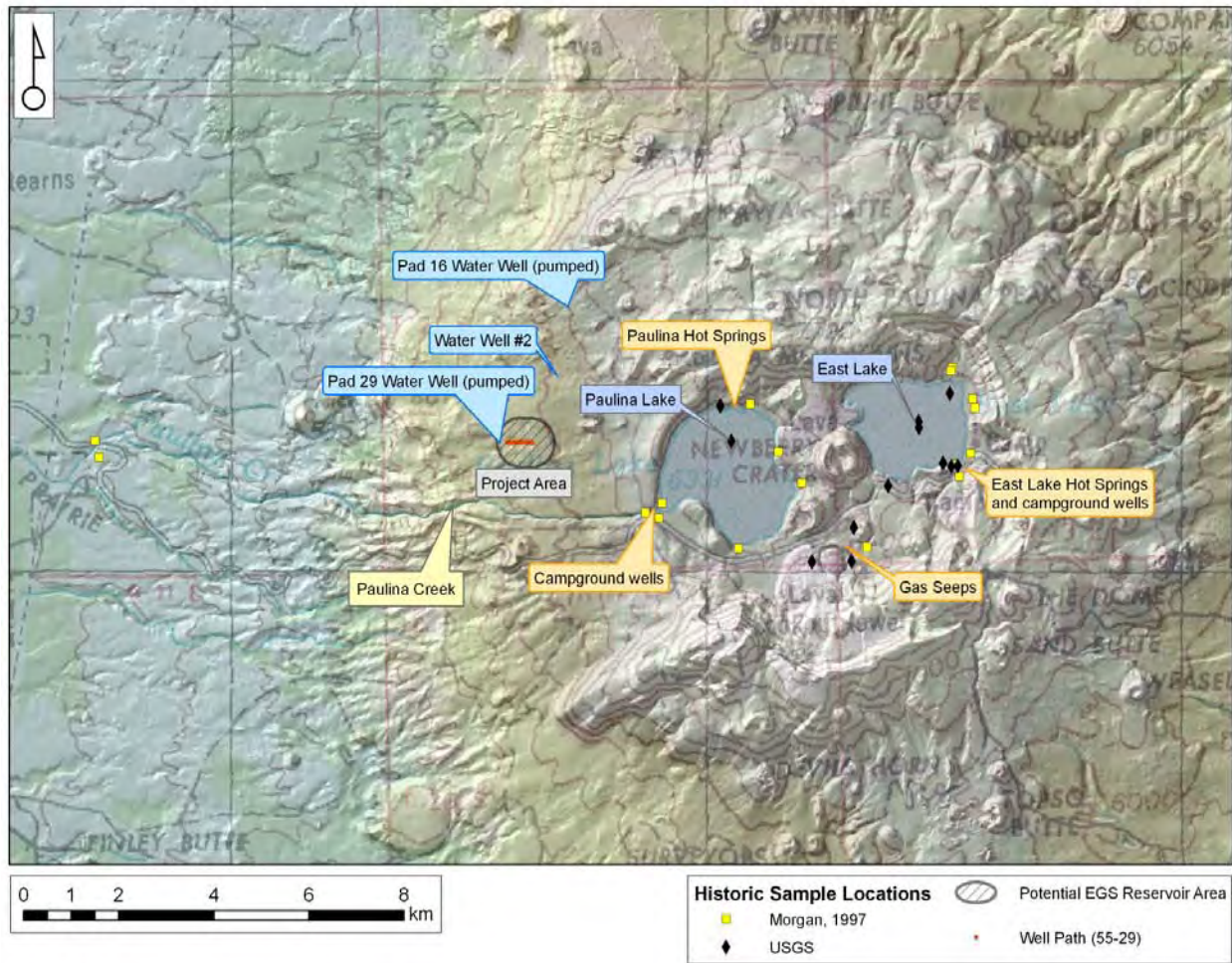


Figure 2-11. Digital elevation map with surface hydrologic features.

Table 2-5. Fluid compositions for project area features, and EPA drinking water standards for reference. Values shown in red are above EPA maximum contamination levels for drinking water. Data are from Davenport records and Morgan et al. (1997). Units in mg/L unless otherwise specified. Values from Morgan et al. (1997) are median values.

Sample Site or Standard	Parameter	Analyte (median values in mg/L)																
		Temp (°F)	Alkalinity	As*	B	Ca	Cl	Fe	Li	Mg	Hg* (ng/L)	pH	K	SiO <sub>2</sub>	Na	Cond. (µS/cm)	Sr	SO <sub>4</sub>
East Lake Hot Springs No. 5B (29CDD06)†	146	450	<0.001	1.2	72	1	0.004	0.033	34	<10	6.3	8.3	220	54	814	360	10	654
Paulina Hot Springs No. 2B (26AAB03)†	133	632	0.012	0.95	55	5	0.01	0.21	45	<10	6.4	16	210	130	1145	200	3.6	822
East Lake†	51.4	101	0.002	0.96	25	0.4	0.003	0.011	12	<10	7.2	3.8	9.9	24	330	98	65	212
Paulina Lake†	50.4	342	0.015	0.89	28	2.3	0.01	0.071	38	<10	8.3	5.6	43	48	590	84	3.1	358
Paulina Creek†	54.3	38	0.014	0.002	27	2.4	0.006	0.07	38	<10	8.8	5.4	40	46	566	83	3.2	350
Pad 29 Water Well (3/08)‡	53	255	0.027	n/a	19	3	0.06	n/a	n/a	bdl	7.5	n/a	n/a	38	420	n/a	2.8	256
Pad 29 Water Well (9/10)‡	53	230	0.026	0.55	19	3	<0.1	<0.1	24	n/a	7.8	5.0	60	42	n/a	0.08	2.5	270
La Pine High School (15AAA)†	48	56	<0.001	0.0025	5.2	2	0.057	<0.004	5.2	< 10	8.2	1.8	30	9.5	106	22	1.2	80
EPA Drinking Water Standards*			0.010			250	0.3			2000	6.5-8.5						250	500

\*As and Hg = primary MCLs, all others = secondary MCLs. Oregon regulations are the same as the EPA for As and Hg.

† Morgan et al. (1997).

‡Data from Davenport records.

### 2.4.1 GROUNDWATER

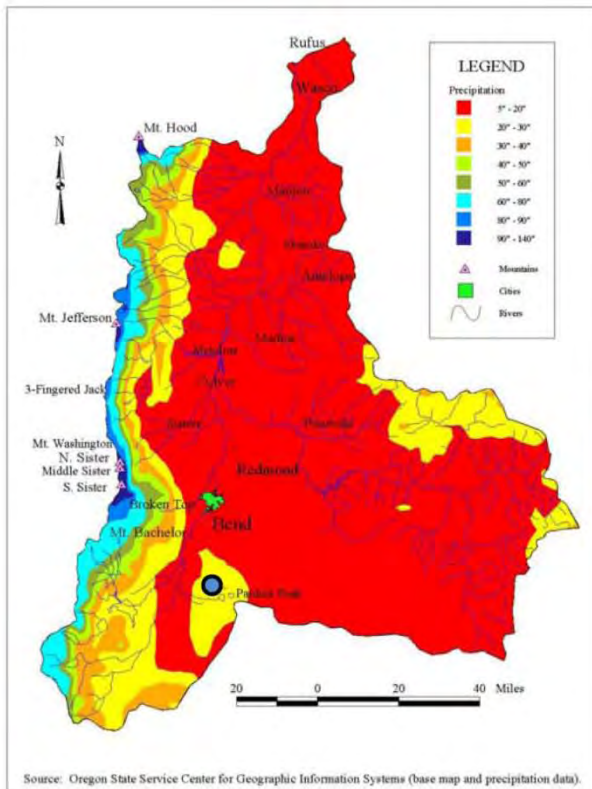
Several studies have attempted to quantify or estimate groundwater recharge across the Deschutes Basin, although these rates obviously vary from year to year and precise values are particularly elusive. Dames and Moore (1994) report that annual groundwater recharge was estimated at  $1.4 \times 10^9 \text{ m}^3$  (1.1 million acre feet) in the upper Deschutes Basin based on spring discharge in the lower portions of the basin. Gannett et al. (2001) place the estimated annual rate of groundwater recharge for the upper Deschutes Basin at  $137 \text{ m}^3/\text{sec}$  (3.5 million acre-feet/year). Sammel and Craig (1983) conducted a more focused assessment of the hydrologic system within Newberry Caldera proper. They estimated groundwater recharge within the caldera to be  $3.1\text{-}8.0 \times 10^6 \text{ m}^3$  (2500-6500 acre-feet/year), or approximately 19-50% of the 79 cm (31 in) or  $1.6 \times 10^7 \text{ m}^3$  (13000 acre feet) of precipitation that falls within the caldera annually. Bauer and Vaccaro (1987) estimated recharge rates in the project area, based on their deep percolation model, at 18-64 cm/yr (7-25 in/yr) (23-81% of precipitation). Regardless of the discrepancies between recharge estimates, and potentially between recharge in various years, all researchers would likely agree that infiltration of precipitation is the dominate source of groundwater recharge in the basin. Precipitation is heterogeneous across the basin, and is heavily influenced by topography. Figure 2-12A shows precipitation around the Deschutes basin (ranging from 13-356 cm/yr [5-140 in/yr]), and Figure 2-12B shows estimated groundwater recharge (between 0-356 cm/yr [0-140 in/yr]) after Gannett et al. (2001). The Cascade Arc, and to a lesser extent Newberry Volcano, are clearly discernible in both graphics as precipitation and recharge highs.

Regionally, groundwater is hosted in Quaternary alluvial valley fill, and late Cenozoic volcanic and volcanoclastic units with significant primary permeability (e.g., scoria, cinder) and secondary permeability (e.g., faults and joints). Volcanic and sedimentary units of the extensive Deschutes formation host many prolific aquifers across the entire basin, and unconfined to partially confined aquifers are also encountered in younger deposits on the flanks of Newberry Volcano. Devitrified tuffs and altered sedimentary and volcanic deposits of the older (Oligocene) John Day, Mescall, and Clarno formation found below the Deschutes formation form a regional aquiclude (Gannett et al., 2001).

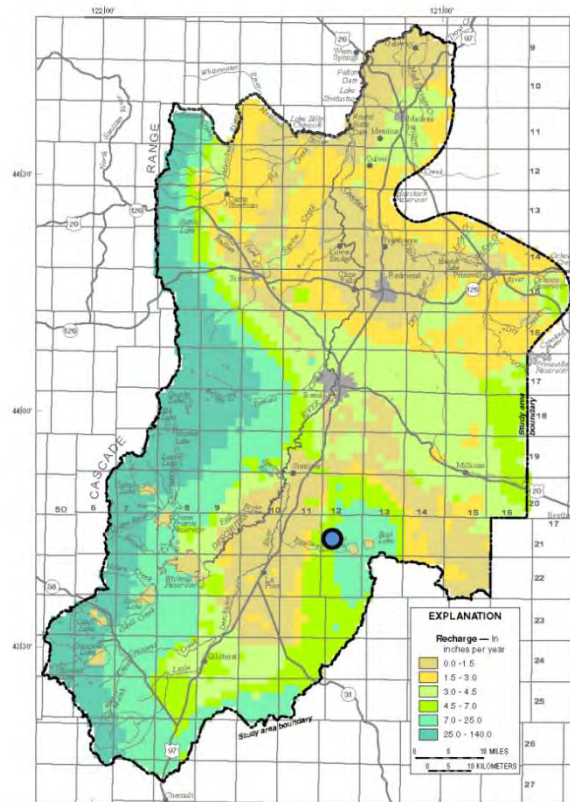
Groundwater flows eastward from the Cascades, and west to northwest from Newberry Volcano towards the La Pine sub-basin (Figure 2-13), where groundwater is hosted in shallow (0-100 m [328 ft]) permeable units within young alluvium. Groundwater then flows north to the confluence of the Deschutes, Crooked and Metolius River. A shallowing of the John Day formation forces the groundwater to discharge around the confluence of the three rivers. Groundwater also discharges into streams that originate in the Cascades, as well as other points along the Deschutes River. Absolute paths are unknown, and are likely complicated by faults and variable lithology along the way. Discharge is from fractured lava flows and interflow sedimentary units that are part of the Deschutes formation. The elevation of discharge near La Pine is about 1290 m (4232 ft) above sea level, with decreasing elevations to the north.

One of the most heavily used aquifers near the project area is the La Pine aquifer (Figure 2-14). The La Pine aquifer is a shallow, unconfined aquifer hosted in Quaternary alluvium and interspersed lava flows in the La Pine sub-basin of the Deschutes valley. The La Pine aquifer is underlain by low permeability clay-rich marsh and lacustrine, low energy fluvial deposits created when lava flows from Newberry Volcano dammed the ancestral Deschutes River (Morgan et al., 2007). Water table depth varies geographically and temporally, but is often less than 6 m (20 ft), with permeable units extending to only about 100 m (328 ft) (Gannett et al., 2001).





● Approximate Project Location



Cole, D.L., 2006; Gannett et al., 2001

**Figure 2-12. Deschutes Basin precipitation and recharge. The topographic influence of the Cascade range (western border) and Newberry Volcano on precipitation (A) and groundwater recharge (B) is evident.**

Groundwater on the flanks of Newberry volcano around the project area is hosted in young volcanic flows and interspersed sedimentary deposits, with occasional and discontinuous impermeable lithologies. Figure 2-6 (above) shows a plan view of the project area and cross section lines A-A' and B-B'. Cross sections A-A' (Figure 2-15) and B-B' (Figure 2-16) show the shallow unconfined aquifer on the flanks of Newberry Volcano. Based on loss zones encountered while drilling, isothermal temperature profiles, and alteration described in mud logs, the shallow, mostly unconfined aquifer intersected by the water wells on pads S-16 and S-29 (well numbers DESC 58649 and DESC 58395, respectively) only extends to depths of about 300 m (984 ft) across the project area, with some spatial variability (Dames and Moore, 1994). Below this depth, decreasing permeability caused by increase clay content forms a basal aquiclude. The top of the aquifer likely fluctuates several meters or more depending on seasonal precipitation, and represents the base of the vadose zone in this area. A drawdown test conducted at the S-29 water well indicated a specific capacity of 3.3 L/s per meter (16 gpm per foot) of drawdown. Transmissivity and conductivity were estimated, respectively, at 602 m<sup>2</sup>/day (6485 ft<sup>2</sup>/day) and 49 m/day (162 ft/day) for a 12.2 m (40-ft) thick aquifer. Transmissivity estimates from the drawdown test are 5-10 times higher than results from Gannett et al. (2001). However, this is not unexpected given the heterogeneous nature of aquifer lithologies across the basin. A second drawdown test is planned for the S-16 water well in summer 2011.

**Approximate Project Location**

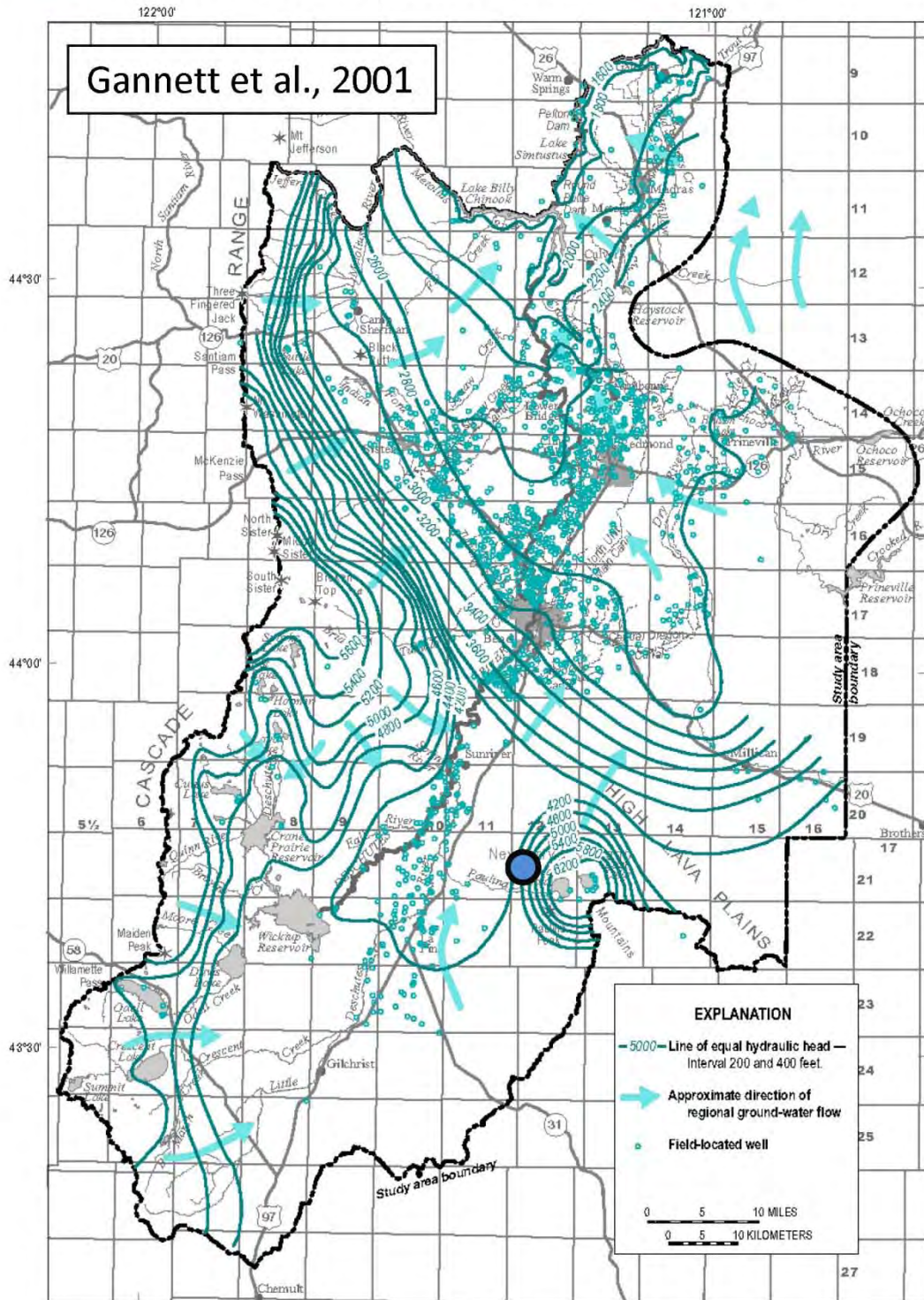
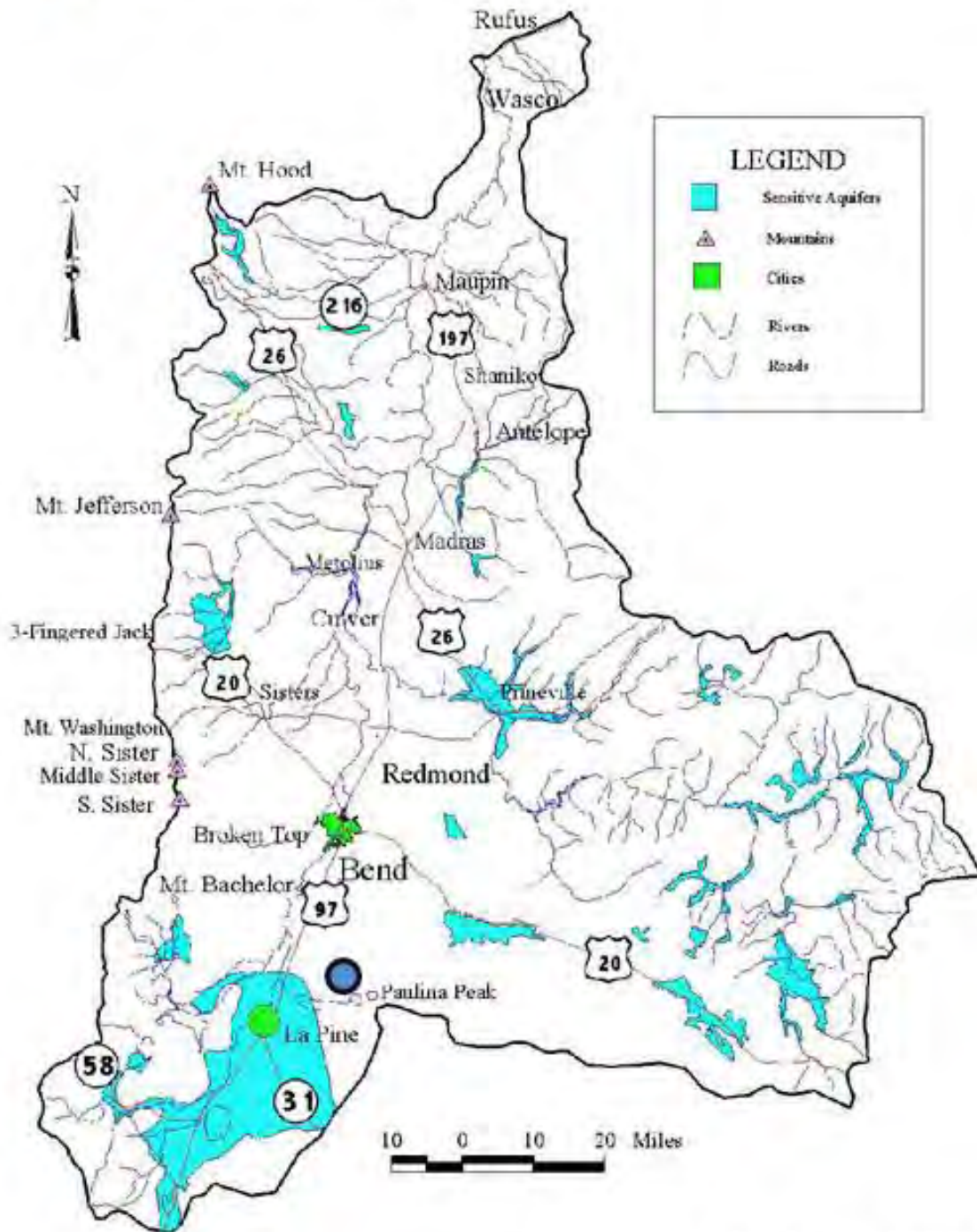


Figure 2-13. Groundwater equipotential contours and inferred flow direction. Groundwater around the project area flows west and north into the La Pine sub-basin.



● Approximate Project Location



Cole, D.L., 2006

Source: Oregon State Service Center for Geographic Information Systems (base map and sensitive aquifer data)

Figure 2-14. Sensitive aquifers in the Deschutes Basin.

## 2.4.2 THERMAL SPRINGS

Thermal features within Newberry caldera, including Paulina Hot Springs 52°C (126°F) and East Lake Hot Springs 62°C (144°F), are believed to result from the circulation and steam heating of meteoric water, with no significant contribution of geothermal liquid (Sammel and Craig, 1983). Gas seeps are also found in the central part of the caldera, near the younger rhyolite domes (Figure 2-11). Geochemical analyses of the springs are listed in Table 2-5.

## 2.4.3 GEOTHERMAL SYSTEM

At depths between 200 m and 330 m (656 and 1083 ft) beneath NWG 55-29, increased smectite and green clay alteration forms an impermeable base in the host rock, and at greater depths (approximately 1500 m [4921 ft]) the altered tuffs of the John Day Formation result in extremely low permeability. The results of injection tests for wells CEE 23-22, CEE 86-21, and CEE 76-15 TCH, all located on the western flank of Newberry Volcano in the vicinity of the Demonstration site, reveal injectivity several orders of magnitude lower than the lowest permeability geothermal wells found in other hydrothermal fields (Section 2.3.4 above). Unlike hydrothermal projects, the very low permeability found at depth on the flanks of Newberry Volcano is a desirable feature for EGS development, allowing development of a closed hydraulic circuit.

## 2.5 GEOPHYSICS

The USGS published a special issue on the geophysics of the Newberry Volcano in the Journal of Geophysical Research in 1988 (Vol. 93, No. B9). Presented below are the salient features of their geothermal resource findings, other public domain data and the results of a proprietary study by Davenport.

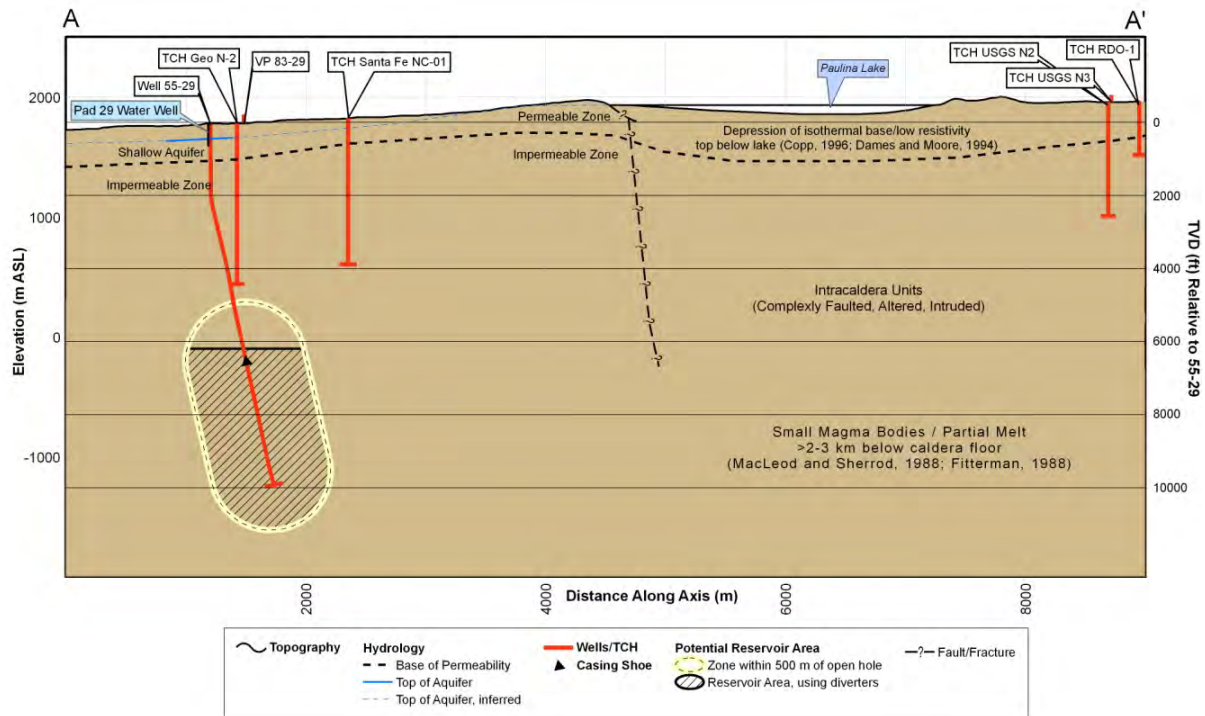


Figure 2-15. Cross section A-A' (west-east) showing groundwater aquifer.

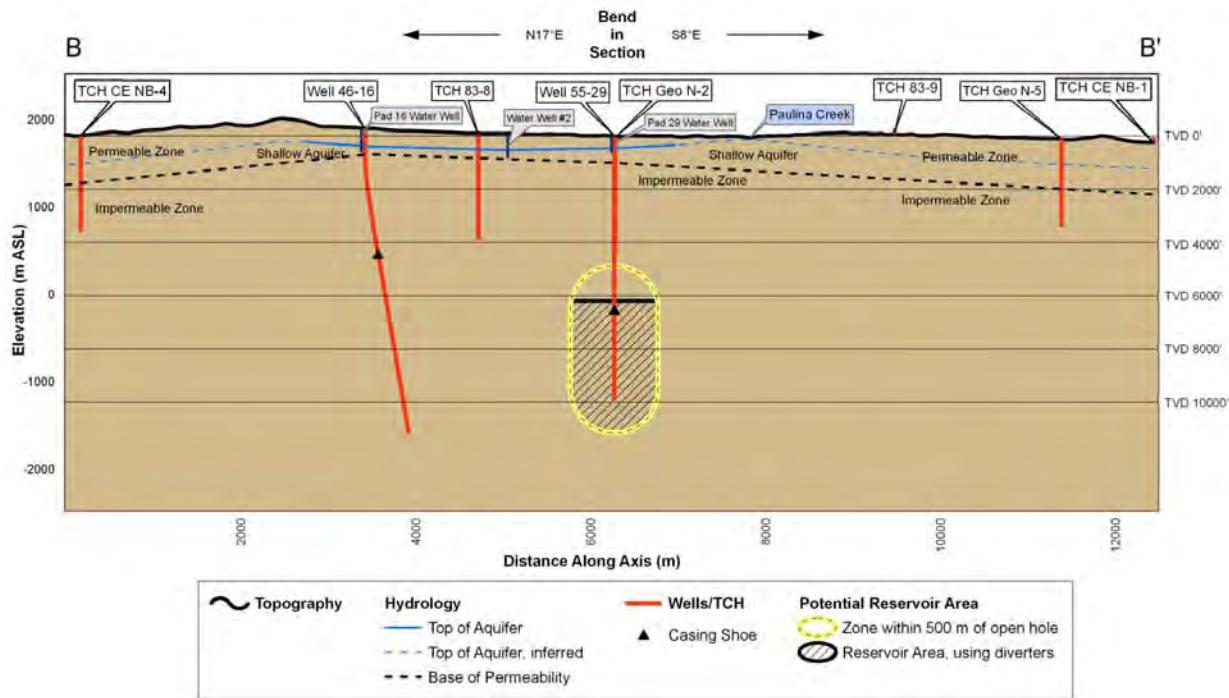


Figure 2-16. Cross section B-B' (north-south) showing groundwater aquifer.

### 2.5.1 GRAVITY

Based on detailed gravity modeling and other data, Gettings and Griscom (1988) concluded that “Newberry Volcano...has a coincident positive residual gravity anomaly of about 12 mGals. Model calculations of the gravity anomaly field suggest that the volcano is underlain by an intrusive complex of mafic composition of about 20 km (12.4-mi) diameter and 2 km (1.2 mi) thickness, at depths above 4 km (2.5 mi) below sea level....Significant amounts of felsic intrusive material may exist above the mafic intrusive zone but cannot be resolved by the gravity data.” Figure 2-17 presents the residual gravity map of Newberry Volcano with station locations (Gettings and Griscom, 1988), including data from 397 stations (A. Waibel, pers. comm., 2009). Figure 2-18 is a diagrammatic illustration by Gettings and Griscom (1988) summarizing the “generalized structure of Newberry Volcano inferred from the gravity model studies and for the most part consistent with seismic, electrical, and drill hole data” available at that time.

Davenport, in its exploration efforts at Newberry, collected gravity data from approximately 400 additional stations. This data is considered confidential (Appendix B-6) and presents the variation in observed gravity as a function of Bouguer reduction density of 2.2 g/cm<sup>3</sup> and 2.67 g/cm<sup>3</sup>, respectively, based on the combined USGS and Davenport data. The principal feature of this detailed gravity survey relative to the Newberry EGS Demonstration is a gravity high on the western flank of the volcano, most likely reflecting a granitic pluton at depth as reported by Gettings and Griscom (1988), and shown in Figure 2-18.



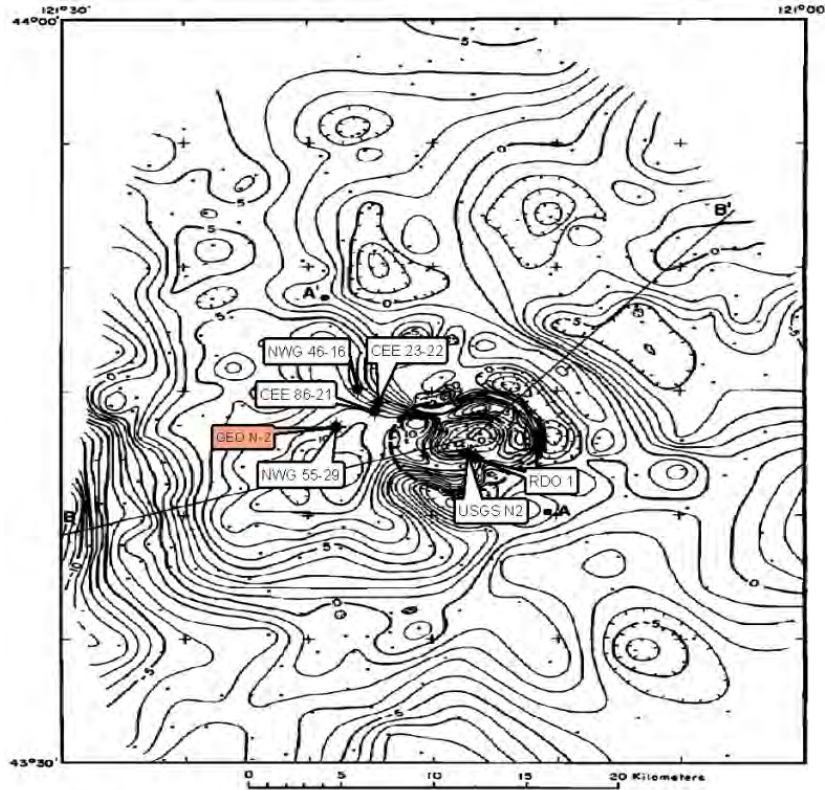


Figure 2-17. Residual gravity anomaly map (mGal) of Newberry Volcano showing the location of EGS Demonstration well NWG 55-29 (from Gettings and Griscom, 1988).

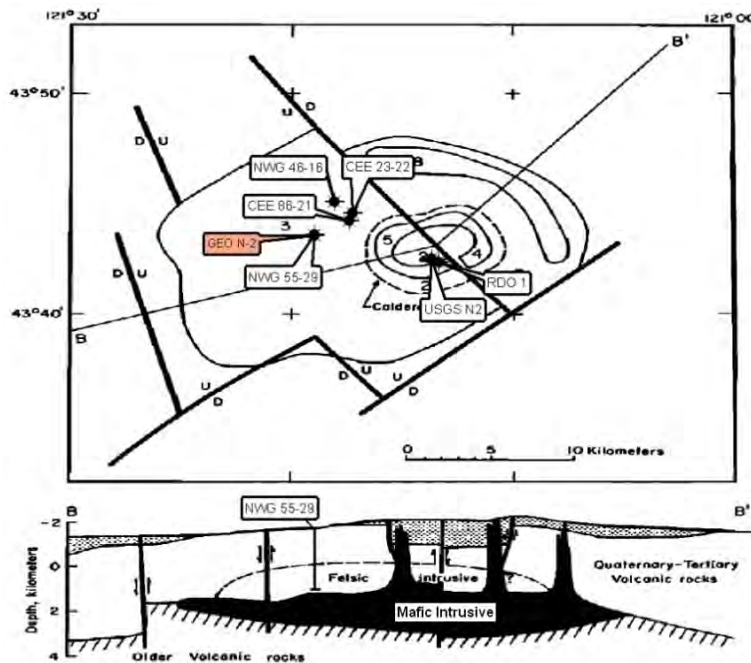


Figure 2-18. Diagrammatic illustration of Newberry Volcano structural interpretation based on gravity modeling by Gettings and Griscom (1988). The six geothermal exploration wells drilled at Newberry Volcano are shown along with GEO N-2, a temperature corehole discussed in Section 3.

## 2.5.2 ELECTRICAL

From 1979 to 1983, the USGS conducted geophysical surveys at Newberry using three different electrical methods; magnetotelluric, transient electromagnetic, and Schlumberger resistivity. Fitterman et al. (1988) interpreted the three data sets to develop a four layer electrical structure model of Newberry Volcano. From the surface downward (Figure 2-19), the geoelectrical units are: (1) unaltered and young, very resistive volcanic rocks; (2) older altered tuff forming a conductive layer; (3) an intrusive rock layer which is very resistive; and (4) a lower crustal conductor (>10 km, not shown in Figure 2-19).

Inside the caldera, Layer 2 corresponds to the steep temperature gradient and alteration minerals observed in the USGS Newberry 2 test hole. Drill hole information on the south and north flanks of the volcano (test holes GEO N-1 and GEO N-3, respectively) indicates that outside the caldera Layer 2 is due to alteration minerals (primarily smectite) and not high-temperature pore fluids. On the flanks of Newberry the conductive Layer 2 is generally deeper than inside the caldera, and it deepens with distance from the summit. A notable exception to this pattern is seen just west of the caldera rim, where the conductive Layer 2 is shallower than at other flank locations.

The volcano sits atop a rise in the resistive Layer 3 (Figure 2-19) interpreted to be due to intrusive rocks. The intrusive material has served as a heat source to produce the hydrothermal alteration and associated geothermal system within the caldera and hot, dry conditions on the west-flank. This deep resistive zone correlates with the region of subvolcanic intrusive identified in Figure 2-7 and Figure 2-8. Fitterman et al. (1988) reported that, “while no public drill hole information is available to confirm this hypothesis, the west flank anomaly appears to be a good geothermal target.” This prediction proved correct ten years later when exploration wells drilled by CalEnergy encountered high temperatures in the area.

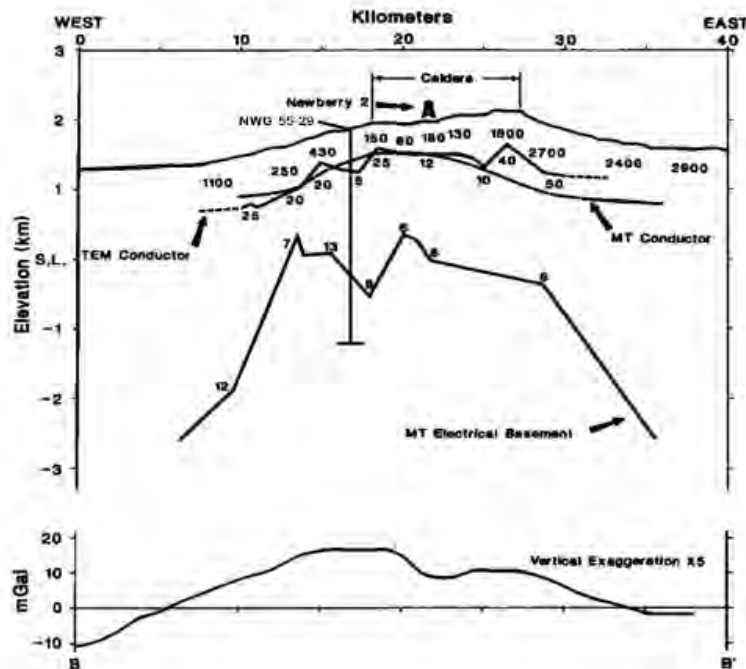


Figure 2-19. Geoelectric structure at Newberry Volcano as defined by Fitterman et al. (1988), with location of EGS Demonstration well NWG 55-29. The open-hole interval of NWG 55-29 is coincident with a lower resistivity zone, and the felsic intrusion interpreted from gravity data (Figure 2-18). The conductive Layer 4 discussed in the text occurs below 10 km below surface and is not illustrated.

### **2.5.2.1 MT RESISTIVITY**

Appendix B-7 presents confidential MT resistivity data collected on the western flank of Newberry Volcano by Davenport. This study did not identify any anomalies that could be interpreted as conduits for hydrothermal fluids.

## **2.6 GEOTHERMAL EXPLORATION ACTIVITY**

### **2.6.1 GEOLOGY**

The regional and local geology of Newberry Volcano and its western flank are described in Sections 2.2 and 2.3. Deep drilling on the northwestern flank of Newberry Volcano has encountered low permeability volcanic and subvolcanic intrusives.

### **2.6.2 SOIL MERCURY SURVEY**

The results of a soil mercury survey at Newberry Volcano were reported by Hadden et al. (1983). A total of 1641 soil samples were collected at Newberry over an area approximating 1000 km<sup>2</sup> (372 mi<sup>2</sup>). A probability plot of the data evidenced two populations, one background and one anomalous. According to Priest et al. (1983), anomalous high mercury concentrations occur: (1) on the north and northwestern caldera ring fractures; (2) on the east flank; (3) in a broad northeast-trending zone approximately coincident with northeast-trending faults and volcanic cone alignments on the southern flank; and (4) in small areas on the western flank. The authors speculate that the northwest-trending mercury anomalies on the south flank may continue to the southwest, possibly merging with similar (but undefined) anomalies on the Walker Rim fault zone. They also concluded that the mercury anomalies on the caldera ring faults, eastern and southern [Walker Rim trend] flanks show “highly favorable indications of high vertical permeability and possible hydrothermal circulation. The latter two anomalies indicate that the south and east flanks of Newberry volcano probably have high potential for geothermal resources.”

### **2.6.3 THERMAL SETTING AND EXPLORATION WELLS**

Public-domain equilibrated temperature depth profiles are available for some of the temperature coreholes and geothermal exploration wells (Figure 2-20 and Figure 2-21). Two coreholes and two relatively shallow geothermal exploratory wells were drilled in the caldera. The shallow exploratory wells were drilled by the USGS (N-2) and Sandia (RDO-1). A maximum temperature of 265°C (509°F) was measured in USGS N-2 at its total depth of 932 m (2990 ft). A maximum temperature of 160°C (320°F) at a total depth of 411 m (1320 ft) was encountered in RDO-1. Temperatures encountered in RDO-1 were significantly higher than those at comparable depths in USGS N-2 (Figure 2-21).

Four deep exploratory wells have been drilled on the northwestern flank of the volcano (Figure 2-20), two by CalEnergy (CEE 86-21 and CEE 23-22) and two by Davenport (NWG 55-29 and NWG 46-16). The temperature profile for NWG 55-29 (Figure 2-21) indicates a conductive regime from an elevation of about +1700 m to total depth at -1300 m. While the temperature profiles for the other three wells remain confidential, Spielman and Finger (1998) reported that the two CalEnergy wells encountered temperatures in excess of 315°C (600°F) below 2740 m (9000 ft). They concluded, based on the two CEE wells and two temperature coreholes, that while adequate temperatures are present, the permeability in the area investigated was too low for a commercial geothermal resource.



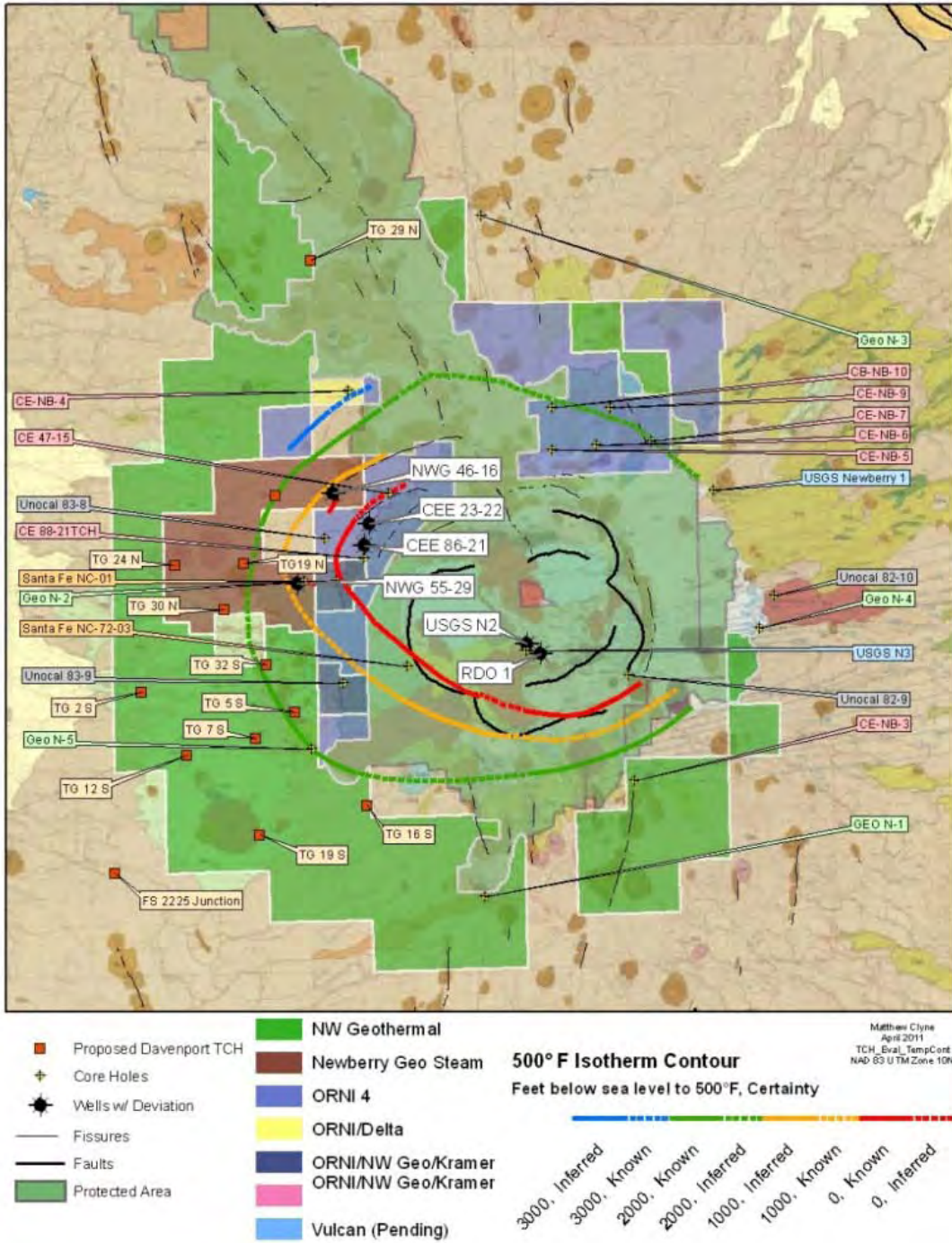


Figure 2-20. Location of temperature coreholes and geothermal exploration wells at Newberry Volcano with inferred contours showing the depth to the 260°C (500°F) isotherm from an internal CalEnergy report.

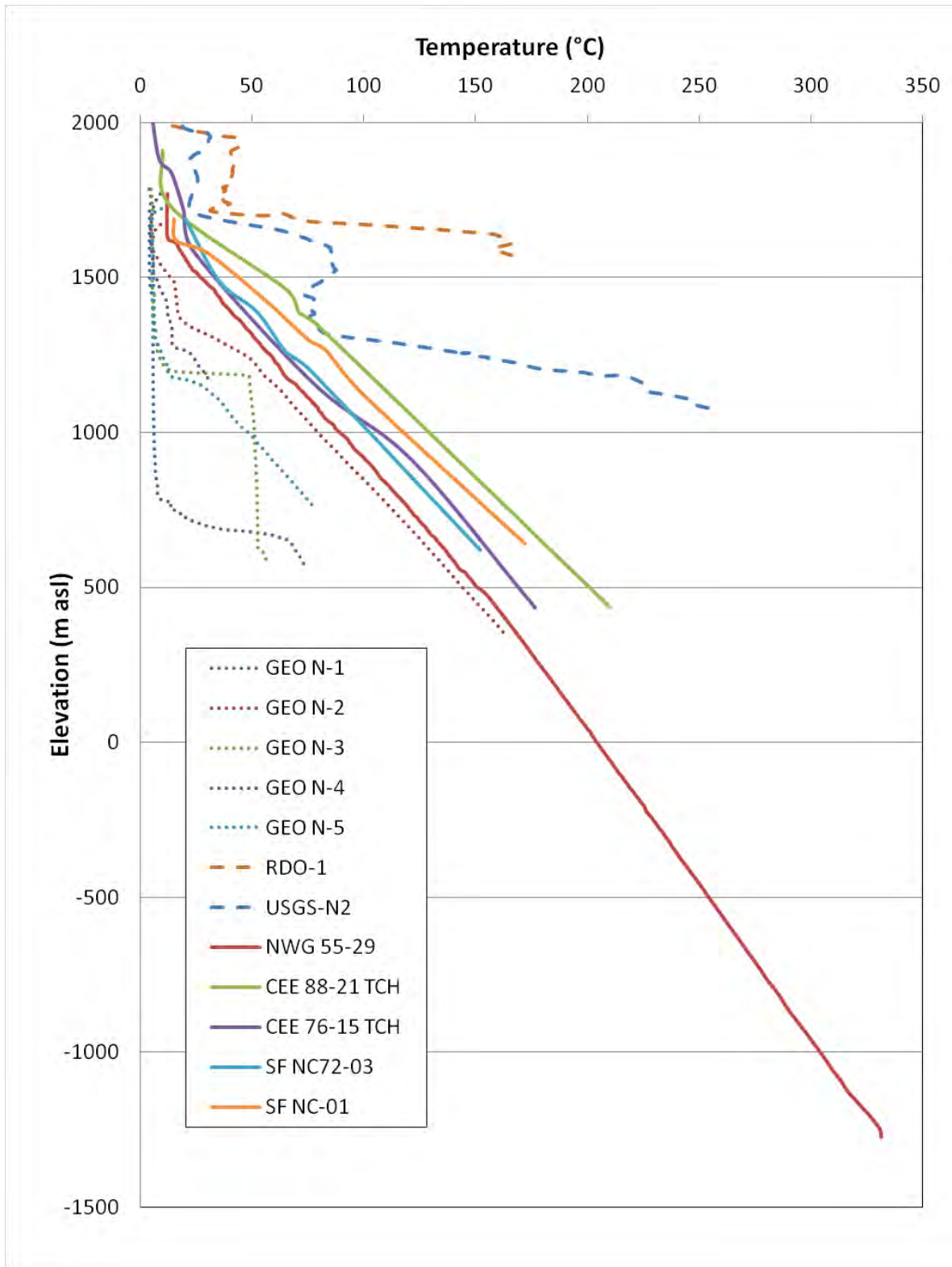


Figure 2-21. Equilibrated temperatures of coreholes and exploration wells at Newberry Volcano. Depth is relative to mean sea level.



## 2.7 CONCEPTUAL GEOLOGIC MODEL

All available geothermal exploration data at Newberry Volcano indicates that there is a hydrothermal resource within the caldera and an EGS resource on the northwestern flank. Insufficient data is available to fully assess the northern, eastern, and southern flanks of the volcano.

### 2.7.1 CALDERA HYDROTHERMAL SYSTEM

Sammel (1983) presented a comprehensive conceptual model for the caldera hydrothermal system at Newberry Volcano (Figure 2-22). He postulated that minor amounts of steam and gas are rising from a deep reservoir through poorly permeable faults and fractures within the caldera. Meteoric water infiltrating the caldera is heated and chemically altered by the rising steam and gas. This is supported by chemical and isotopic data that indicate that a near-surface, low temperature origin for the thermal waters. Some of this thermally heated meteoric water discharges locally within the caldera along the ring fractures or recent vents. The rest of the thermal water was considered to infiltrate deeper into the volcano and to disperse to its flanks. Horizontal permeability is considered high enough to make vertical infiltration into the deep reservoir unlikely. A small, silicic magma body was postulated to be present at depth and to also be the heat source for the caldera hydrothermal system.

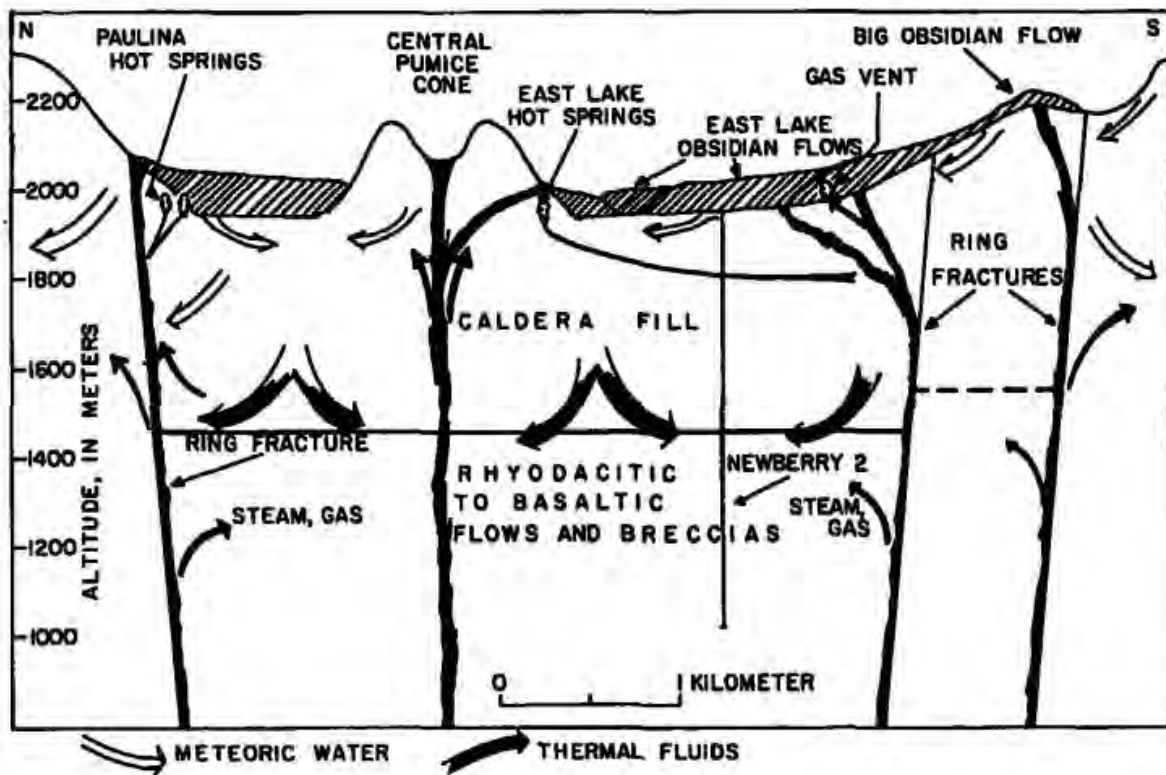


Figure 2-22. Conceptual model of the Newberry caldera geothermal system (from Sammel, 1983).

This model was updated and numerically simulated by Sammel et al. (1988) integrating the results from additional USGS geological and geophysical investigations (MacLeod and Sherrod, 1988; Stauber et al., 1988; Keith and Barger, 1988; Gettings and Griscom, 1988; Fitterman et al., 1988; Fitterman, 1988; Catchings and Mooney, 1988; Achauer and Evans, 1988). These numerical simulations were based on the emplacement of a small, silicic magma body, flow patterns, and thermal histories for three sets of hypothetical permeability values taken from previous drilled wells (Figure 2-23).

The original model runs north-south through the caldera but is radially symmetric, so can also be representative of the conditions on the western flank of the volcano. It is assumed that the presence of a small silicic magma body under the caldera gave rise to a hydrothermal system in the caldera and a conductive thermal regime outside the caldera. The model accounted for the elevated thermal conditions in the caldera and a conductive regime on the northern and southern flank. This model is consistent with the known and suspected results from the four deep geothermal wells drilled on the northwestern flank of the volcano.

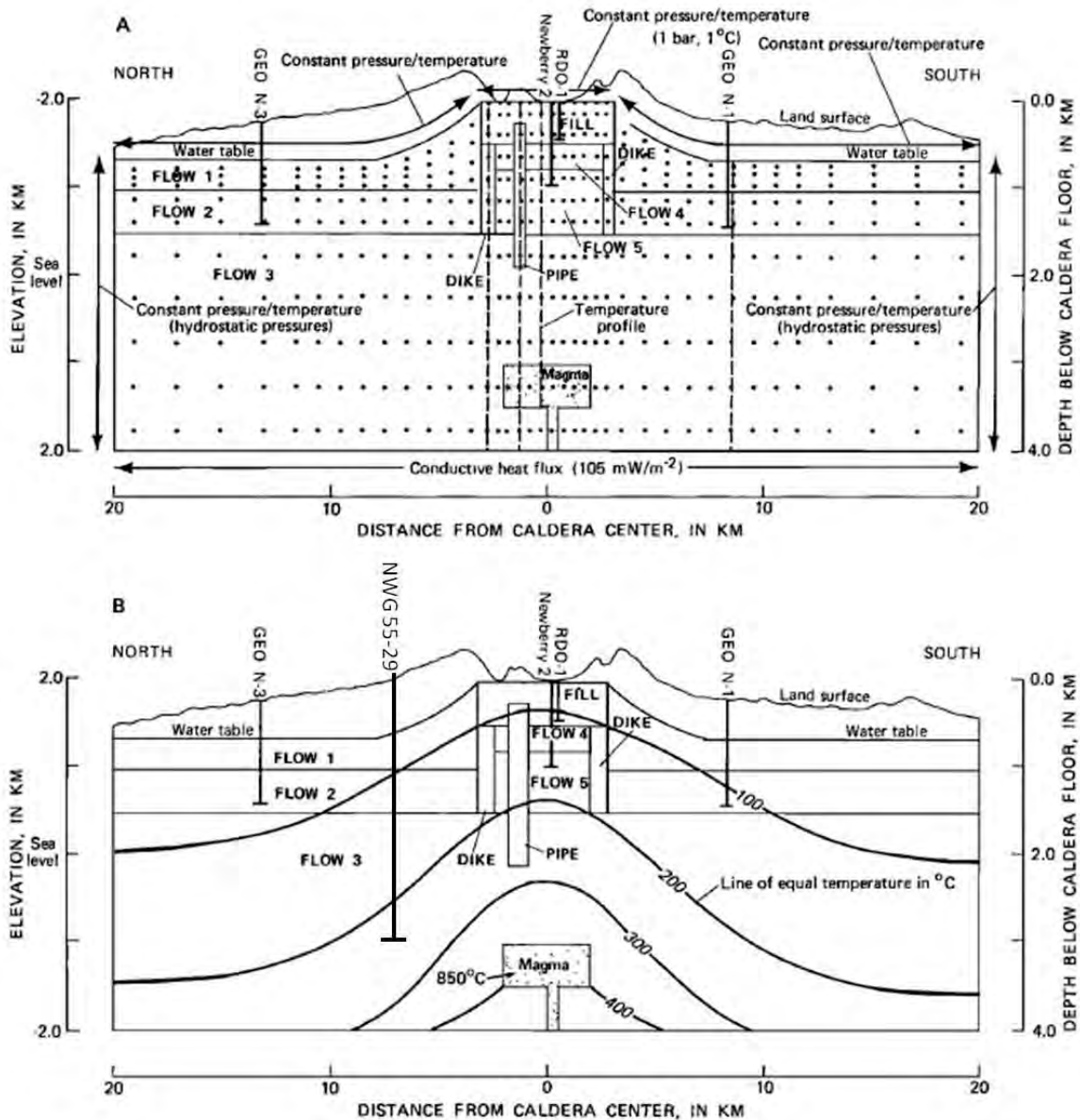


Figure 2-23. Numerical model of the thermal conditions at Newberry Volcano. Section runs north-south through the volcano. The model is considered representative of the thermal conditions on the western flank of the volcano. NWG 55-29 has been diagrammatically superimposed on this model in its correct topographic location assuming that the model is radially symmetric. Figure is after Sammel et al. (1988).

### **2.7.2 WESTERN FLANK GEOTHERMAL SYSTEM**

Four deep, non-productive geothermal exploration wells drilled on the northwestern flank of Newberry Volcano all show elevated bottomhole temperatures of >300°C (572°F), lack of significant hydrothermal alteration and very low permeability. The lack of permeability at depth is consistent with the results of Davenport's proprietary MT survey (Appendix B-7) and numerical modeling results (Sammel et al., 1988). Lithologies at depths greater than 2000 m (6562 ft), where high temperatures occur, consist of brittle volcanic and subvolcanic rocks with small, discontinuous fractures (based on the NWG 55-29 mud log and drilling records).

All available geoscience evidence indicates that the northwestern flank of Newberry Volcano represents an excellent EGS resource area. Available thermal, lithologic, and hydrologic data from four geothermal exploration wells and numerous temperature coreholes drilled here indicate an area of proven EGS reserves<sup>6</sup> of 21 km<sup>2</sup> (8 mi<sup>2</sup>), and an additional area of 36 km<sup>2</sup> (14 mi<sup>2</sup>) of probable EGS reserves.

### **2.7.3 PROPOSED DEMONSTRATION WELL SITE**

Given the excellent resource base, AltaRock evaluated the potential wells of opportunity for an EGS demonstration project. Davenport drilled two exploratory geothermal wells in 2008 at Newberry (NWG 55-29 and NWG 46-16), and was very interested in participating in an EGS demonstration so AltaRock evaluated the wells.

NWG 55-29 has been determined to: (1) be mechanically sound (Section 3.2.3); (2) have an appropriate temperature range in the open-hole interval, with temperatures ranging from the 228°C at 1969 m (442°F at 6461 ft), to 331°C at 3041 m (628°F at 9977 ft); (3) have volcanic and subvolcanic lithology in the open-hole interval suitable for hydroshearing; (4) have discontinuous fractures in the open-hole interval; and (5) have a stress field conducive to EGS.

NWG 46-16 has a formation collapse and bridge at 1448 m (4736 ft) in the upper part of the open hole. A drilling rig would have been required to remove the bridge just to run the additional open hole logs required to determine the suitability of NWG 46-16 for EGS. Therefore, AltaRock determined that making use of NWG 46-16 in the EGS Demonstration would add unnecessary risk and expensive. A borehole seismometer will be installed in the cased part of the well as part of the microseismic monitoring array.

---

<sup>6</sup> Defined for the Newberry Volcano region as having a temperature of greater than 260°C (500°F) at -2000 ft msl.

## 3 CONCEPTUAL RESOURCE MODEL

### 3.1 GEOPHYSICAL CONDITIONS AROUND WELL

The Newberry EGS Demonstration will conduct hydroshearing stimulation of the target well NWG 55-29. It is located on the edge of a gravity high anomaly identified by Gettings and Griscom (1988) (Figure 2-17). According to the Gettings and Griscom (1988) geologic model based on gravity data (Figure 2-18), NWG 55-29 bottomhole location is within the felsite west of the caldera. This interpretation is consistent with the geologic interpretation of drill cuttings from this well. Additionally, the well also penetrates the geoelectric units defined by Fitterman (1988) illustrated in Figure 2-19. The open-hole interval in this well runs from 1903 m (6242 ft) to 3066 m (10060 ft) total measured depth (TMD<sup>7</sup>).

### 3.2 WELLBORE CONDITIONS

#### 3.2.1 DRILLING HISTORY

Geothermal exploration well NWG 55-29 began drilling on 13 April 2008 and was completed at 3066 m (10060 ft) TMD on 22 July 22 2008. The upper zone of the well from the surface to approximately 305 m (1000 ft) had significant lost circulation and borehole stability issues due to the rubble zones, cinder and unaltered tuffs encountered while drilling. Highly viscous lost circulation mud pills and cement plugs were used with varying degrees of success. Mud losses were inevitable and were managed with excess mud volume in the drilling of the upper part of the hole. When drilling reached the altered volcanic layer containing smectite, chlorite and kaolinite in the 305 m (1000 ft) interval, the permeability decreased rapidly and major loss zones ceased.

Below the surface casing shoe at 338 m (1108 ft), the wellbore is characterized by a conductive gradient of 109°-128°C/km (6°-7°F/100 ft). At these conditions, mud coolers and high temperature tools were necessary during drilling. In NWG 55-29, the mud cooler was turned on at a depth of 1540 m (5050 ft). The loss zones encountered in the deeper part of the well were large, but intermittent and less problematic than the upper 305 m (1000 ft) intervals. Also, rapid changes in lithology may have led to minor stuck pipe problems. The rate of penetration was highly variable and dependent on lithology and the presence of fractured intervals. A summary of trouble-time is presented in the confidential Appendix C-1.

Lessons learned from drilling NWG 55-29 include better preparation for addressing lost circulation and hole swelling problems to a depth of 308 m (1110 ft). Additionally, several times the shale shakers were bypassed to build weight and viscosity of the drilling mud. However, this resulted in damage to the mud pumps and lost rig time while waiting on equipment repair or replacement. As a result, it is recommended that drill cuttings not bypass the shale shaker.

#### 3.2.2 MUD LOGS

Drill cuttings were collected at ten-foot intervals from NWG 55-29 during drilling operations from April through July of 2008 by Epoch Well Services, Inc. They were collected directly from the shale shaker and washed. In NWG 55-29 the drilling fluid was a high temperature, water-polymer gel, composed of gels of water and montmorillonite.

---

<sup>7</sup> Measured depth (MD) with respect to NWG 55-29 refers to the depth in the deviated borehole relative to the kelly bushing (KB) which was ~9.45 m (31 ft) above ground level (GL). Unless otherwise identified, all depths reported are relative to MD. Unknown datums are noted.

The lithologies described in NWG 55-29 include a wide variety of volcanic, volcanoclastic and hypabyssal units, ranging from ash flows and debris flows, to silicic domes, mafic flows, and mafic and felsic dikes (Epoch, 2008a). The lithology is heterogeneous, but is grouped into the following general categories in the report:

- Unaltered Volcanic Sequence, 42.7-951.0 m (140-3120 ft)
- Intercalated Bleached Ash Tuff, Lava and Crystal Lithic Tuff, 951-1463 m (3120-4800 ft)
- Chloritized Tuffs, 1463-1722 m (4800-5650 ft)
- Chloritized Volcanic Sequence (tuffs, basalts, andesites), 1722-2627 m (5650-8620 ft)
- Dacite Intrusive and Basalt Subvolcanic, 2627-2956 m (8620-9700 ft)
- Basalt, Altered Basalt, Dikes, and Granite, 2956-3066 m (9700-10060 ft)

Alteration in the well predominantly reflects diagenetic overprinting by thermal contact metamorphism, with very minor amounts of hydrothermal alteration associated with past fluid flow in fractures and joints. The upper portion of the hole (0 to 951 m [3120 ft]) consists of unaltered volcanic sequences, but mud logs report (Epoch, 2008a) minor alteration to “green clays”, zeolite (e.g., natrolite), and kaolinite in some zones below about 274 m (900 ft). Smectite becomes more common by about 360 m (1181 ft). Calcite first appears in veins below 506 m (1660 ft). By 870 m (2855 ft) the dominant type of alteration is calcite and smectite in veins and vugs. Silica and pyrite veining occurs below about 1096 m (3595 ft), along with minor silicification. Chlorite becomes more dominant by about 1341 m (4400 ft), but is heterogeneous, with increasing intensity below 1524 m (5000 ft). Low-grade greenschist facies alteration (albite-chlorite-calcite) is apparent below 1829-1951 m (6000-6400 ft), with epidote in increasing abundance below 1768 m (5800 ft). There is increasingly complex and abundant alteration products below 2134 m [7000 ft] (chlorite-epidote-calcite-pyrite), with minor silicification noted at 2201 m (7220 ft). However, Epoch (2008b) reports a general lack of permeability. Strong chloritization exists below 2187 m (7175 ft), and an altered zone is found at 2262 m (7420 ft). Higher greenschist facies alteration (chlorite-actinolite-albite-epidote) is encountered below 2591 m (8500 ft). Below 2865 m (9400 ft) evidence of dikes and sills, ranging in composition from basaltic to felsic, are more abundant, and there appears to be an associated increase in contact metamorphism. No mineralogical evidence of a significant hydrothermal system is observed in the drill cuttings from this well. The cuttings from NWG 55-29 were analyzed for a Master’s thesis done at The School for Renewable Energy Science at the Universities of Iceland & Akureyri. The thesis (Letvin, 2011) has not been made public due to a non-disclosure agreement and proprietary data, is summarized in Section 3.2.5 and attached as confidential Appendix B-1.

Drilling breaks in geothermal drilling are often associated with zones of increased permeability. A review of the mud log does not show evidence of any distinct drilling breaks encountered in the well. Higher than normal concentrations of CO<sub>2</sub> and H<sub>2</sub>S were encountered while drilling through several intervals. However, the source of these gases is unclear because the increases are not coincident with drilling breaks or other indications of increased permeability.

### **3.2.3 CASING PROFILE AND INTEGRITY**

The casing profile in NWG 55-29 (Figure 3-1) begins with a 30 in conductor casing set to 40 m (130 ft), followed by 20 in surface casing set at 338 m (1108 ft), and 13-3/8 in, 72 lb/ft L-80 rating casing set at 1339 m (4391 ft). The 9-5/8 in production casing is set from 1277-1970 m (4189-6462 ft). The 8-1/2 in open-hole section extends from 1970-3066 m (6462-10060 ft). Below 854 m (2800 ft), well inclination builds over 10° due east to a maximum deviation of 20° at TD. The total easterly drift from the wellhead to TD is 530 m (1740 ft).



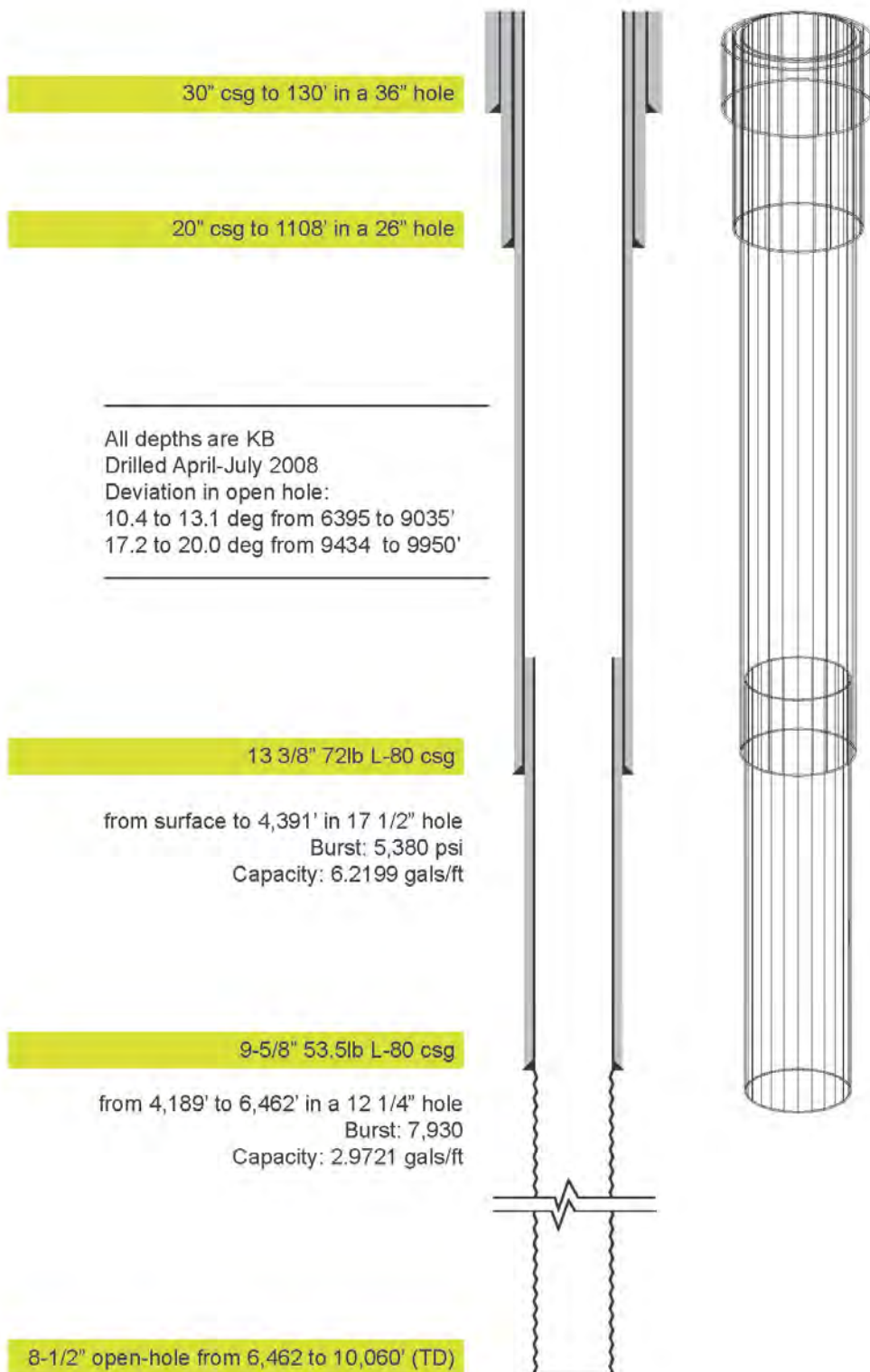


Figure 3-1. Newberry NWG 55-29 well bore and casing profile.

The 13-3/8 in, 72lb/ft, L-80 surface casing is cemented from the casing shot at 1339 m (4391 ft) to the surface to protect local groundwater aquifers. The 13-3/8 in casing has a burst pressure of 37.1 MPa (5380 psi). Assuming a cold freshwater fluid density of 9.8 MPa/km (0.433 psi/ft), a surface pressure of 24.6 MPa (3566 psi) would result in a fluid pressure less than the casing burst pressure at the shoe depth of 1277 m (4189 ft). The burst pressures for casing are calculated using 87.5% minimum yield strength for steel, according to API standards, and, hence, incorporate a 1.14 safety margin. Further, burst pressure testing is conducted on un-cemented, free-hanging pipe, so the cement sheath also provides additional, but unquantified, strength to the casing in the wellbore. The relatively young age of the well, the positive casing integrity test conducted in 2008, the caliper survey in 2008, the temperature surveys in 2008 and 2010, and the maximum pressure profile achieved during the inject-to-cool operation in 2010 indicate the casing has retained its integrity.

### **3.2.4 WELLBORE GEOPHYSICAL LOGS**

Geophysical logs are primarily used to distinguish the lithologic units intersected by a well, locate lithologic boundaries, and provide physical property measurements (e.g., bulk density and porosity) to aid in the interpretation of borehole televiewer (BHTV) image logs, as well as aiding in rock strength determination to constrain stress models. High-resolution induction, spectral density, dual-spaced neutron, temperature, spontaneous potential, natural gamma ray, and caliper logs were obtained in NWG 55-29 by Halliburton during the drilling operation in the summer of 2008 using their high temperature, high pressure, hostile slimhole logging (HEAT) suite. A sonic log was not included in the original log suite because equilibrium wellbore temperatures preclude running this log without substantial cooling of the well, which could only be achieved immediately after borehole completion. Detailed discussion of the use of the available logs in the derivation of porosity and strength is provided in Section 5.5.1.

Geophysical logs were run three times during drilling operations, on 4 June, 22 June, and 13 July 2008, each covering a different depth range: 338-1340 m (1109-4396 ft), 1338-1971 m (4390-6466 ft), and 1970-3066 m (6462-10058 ft), respectively. In addition to the open-hole log suite, both static and injecting pressure-temperature (PT) surveys were conducted after drilling operations, and again in the fall of 2010. A BHTV survey was conducted in October 2010. A list of the type of logs run, and their respective logging interval is provided in Table 3-1. This table also summarizes the maximum tool-head temperature that was encountered during each logging run. A basic description of each geophysical log is given below, with additional details in the sections in which the data collected by the logs is interpreted and modelled (e.g., porosity and fracture model - Section 3.2.4, *in situ* strength model - Section 5.5.1, stress model - Section 5.5.2).

#### **3.2.4.1 PRESSURE, TEMPERATURE AND SPINNER SURVEYS**

Pressure, temperature and spinner tools measure fluid pressure, temperature and velocity in the borehole. Temperature data aids in identifying thermodynamic conditions in the well, zones of fluid loss and production, designing the cement program, and designing the diverter product strategy for stimulation. A temperature survey conducted on 17 June 2008, approximately 12 hours after circulating the hole with cold water, and 5 days after completion of the well, measured a maximum bottom hole static temperature of 229°C (445°F; Figure 3-2), and identified a zone at approximately 2957 m (9700 ft) that exhibited minor, localized cooling, most likely associated with a 0.5 L/s (12 bph) mud loss at this depth during drilling. Except for this minor zone of fluid loss, the temperature profile measured was essentially linear, indicating a conductive temperature gradient. Subsequent static surveys in October 2008 and September 2010 exhibited essentially identical temperature profiles, with a maximum

temperature of 331°C (628°F) at 3046 m (9993 ft)<sup>8</sup> and 331°C (628°F) at 3044 m (9986 ft), respectively. The pressure gradient observed under static conditions during the 2008 survey was 8.4 MPa/km (0.37 psi/ft), while the under injection in 2010 was 8.6 MPa/km (0.38 psi/ft; Figure 3-3). A spinner tool was run with the PT tool, but the results were not reliable. Section 3.2.9 presents a more detailed discussion of injection testing and related survey results.

**Table 3-1. Newberry NWG 55-29 survey history.**

<b>Log Type</b>	<b>Date of Log</b>	<b>Maximum Depth Logged m (ft)</b>	<b>Maximum Measured Temperature °C (°F)</b>	<b>Maximum Rated Tool Temperature °C (°F)</b>
Pressure	7/16/2008 7/19/2008 10/3/2008 9/22/2010 9/27/2010 10/20/2010	3066 (10060)	331.4° (628.6°)	350° (662°)
Temperature	7/16/2008 7/19/2008 10/3/2008 9/22/2010 9/27/2010 10/20/2010	3066 (10060)	331.4° (628.6°)	350° (662°)
Natural Gamma	06/04/2008- 07/13/2008	3062 (10048)	247° (476°)	260° (500°)
Caliper	06/04/2008- 07/13/2008	3062 (10048)	247° (476°)	260° (500°)
High Resolution Induction	06/04/2008- 07/13/2008	3062 (10048)	247° (476°)	260° (500°)
Spectral Density	06/04/2008- 07/13/2008	3062 (10048)	247° (476°)	260 (500°)
Dual-spaced Neutron	06/04/2008- 07/13/2008	3062 (10048)	247° (476°)	260° (500°)
Borehole Televiwer	10/22/2010	2701 ( 8864)	277° (531°)	285° (545°)

<sup>8</sup> Datum for October 2008 PTS survey is unknown. Total depth indicated on survey is 3046 m (9993 ft).

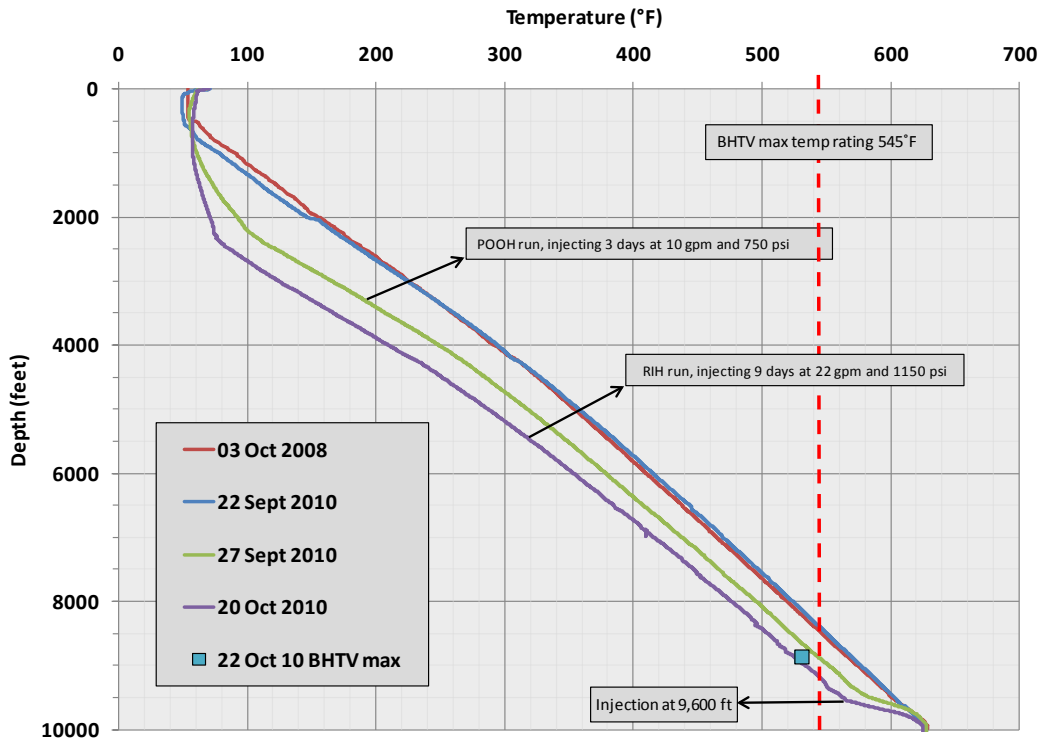


Figure 3-2. NWG 55-29 temperature profiles. Original well completion date is 12 June 2008. Inject-to-cool operation performed Sept-Oct 2010 to cool well for BHTV survey.

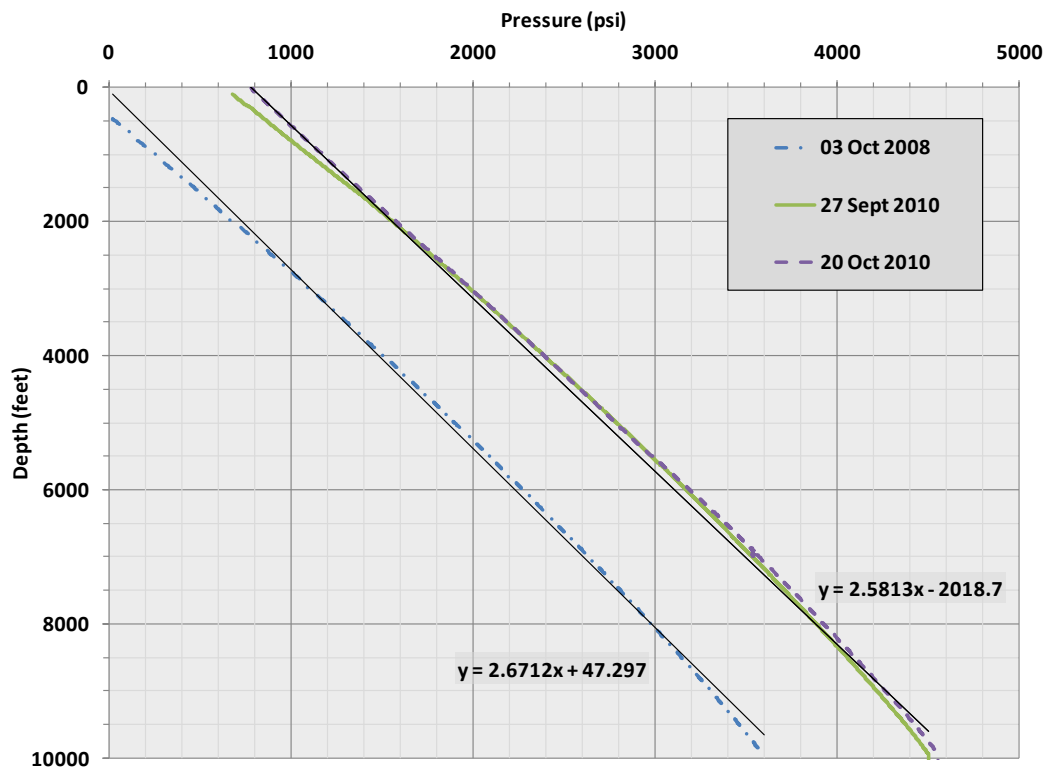


Figure 3-3. NWG 55-29 pressure surveys, showing best-fit pressure gradient curves.



### 3.2.4.2 NATURAL GAMMA

The natural gamma ray (GR) tool measures the presence of naturally-occurring gamma radiation, generally associated with potassium, thorium, or uranium in minerals in the exposed very near-borehole environment. It is typically sensitive to the presence of clays in sedimentary formations or in the clay-rich caps associated with many geothermal systems, felsic intrusions rich in potassium, select metals, and radioactive scales precipitated on well casing. It also provides depth correlation between geophysical logging runs and can be used to correlate formations or intrusions. The application of gamma ray logs rely on the fact that in a volcanic environment the concentration of radioactive isotopes varies from one rock type to another. The gamma ray log is reviewed in conjunction with other geophysical and mud logs, and analysis of cuttings mineralogy, to correlate areas of natural radioactivity with potassium-rich fracture-filling minerals such as illite-muscovite (Figure 3-4). This information aids in the development of a velocity model and in identifying hydrothermal alteration or anomalous porosity associated with fractured zones.

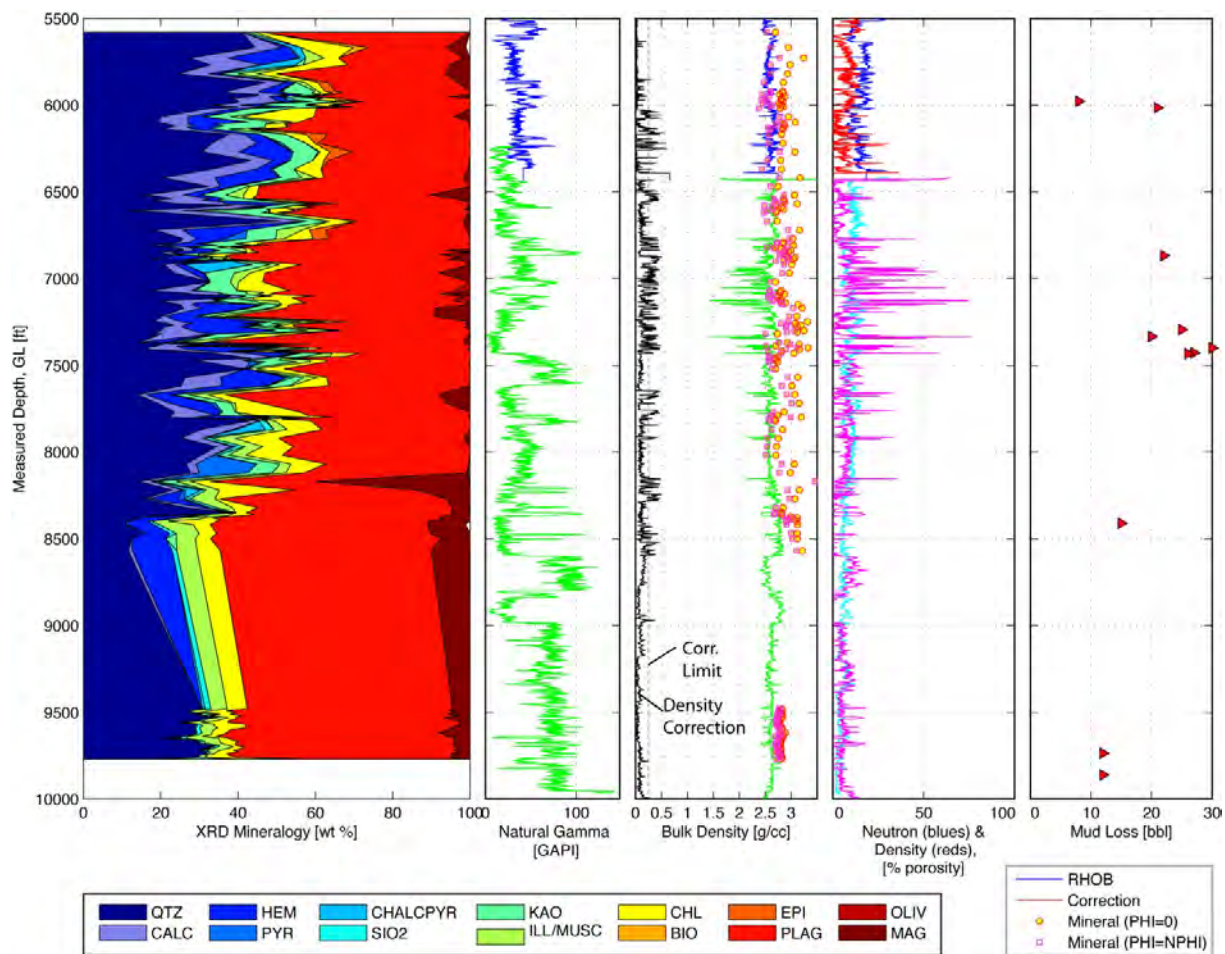


Figure 3-4. From left to right: (1) distribution of rock-forming minerals with depth; (2) correlated natural radioactivity measured by the natural gamma ray log; (3) bulk density measured by borehole compensated litho-density log and estimated from mineralogy; (4) porosity as measured by the borehole compensated neutron porosity log and lithodensity log; and (5) mud losses summarized from the mud log. QTZ = quartz, CALC = calcite, HEM = hematite, PYR = pyrite, CHALCPYR = chalcopyrite, SIO<sub>2</sub> = silica, KAO = kaolinite, ILL/MUSC = illite/muscovite, CHL = chlorite, BIO = biotite, EPI = epidote, PLAG = plagioclase, OLIV = olivine, MAG = magnetite. At the time of this report, analysis of cuttings from 2637-2896 m (8650-9500 ft) was incomplete.

In the NWG 55-29 borehole, mineralogy by XRD analysis and examination of thin sections at 1000x magnification revealed that expandable clays in the smectite group are essentially absent in the open-hole interval across all rock types. Minor amounts of illite-muscovite are found in the shallow tuffs below the casing shoe but are absent in deeper intrusive rock and also in basalt and andesite flows. Chlorite is present throughout, but is most developed in the volcanics, with lesser development in the intrusive bodies at greater depth. Initial comparison to natural fractures studied in similar clay-poor rock types in shallower core from the nearby GEO N-2 borehole (Fetterman, 2011; Fetterman and Davatzes, 2011) suggests fractures in these rock types will tend to dilate and self-prop during shearing.

#### *3.2.4.3 CALIPER*

A one-arm caliper log conducted in NWG 55-29 was used to make a continuous recording of the gauge and rugosity of the wellbore. The caliper is a mechanical tool that measures diameter at a specific chord across the well. The caliper data correlated well with the BHTV data, both showing breakouts and gauge hole in the same locations (Figure 3-5). The caliper showed a small, but consistent shift in measurement of the borehole diameter. The caliper data was used to constrain the borehole radius to calculate apparent fracture dip. An adjusted caliper measurement was calculated and used in the dip calculations. The caliper also aided in determining the usefulness of the geophysical log data. Because data quality declines with stand-off from the borehole wall, in areas in which the caliper showed a significantly enlarged borehole diameter the geophysical log data was deemed to be unreliable.

#### *3.2.4.4 BOREHOLE COMPENSATED ARRAY INDUCTION*

The induction log is used to measure flushed zone resistivity, invaded zone resistivity, and true formation resistivity. The induction log shows shallow and deep resistivity generally similar across the entire open-hole interval, indicating no fluid-bearing intervals and a lack of permeability, because the mud filtrate was unable to penetrate the host rocks. Geothermal activity influences the formation resistivity through hydrothermal alteration of the rocks where the alteration minerals may have different resistivity than the host rock, and fluid content and salinity in permeable hot zones. Smectite and mixed-layer clays are relatively conductive due to associated bound water and exchangeable cations, but their occurrence in geothermal systems is highly temperature sensitive, with the most common smectite persisting to temperatures of 200°C (392°F) and mixed-layer clays persisting to temperatures 200°-230°C (392°-446°F). Minerals that are formed at high reservoir temperature (>230°C [416°F]), on the other hand, generally have higher resistivity. The general resistivity structure on a larger depth scale can also be compared to results of surface resistivity soundings (e.g., magneto-tellurics) and resulting resistivity depth models, although it must be kept in mind that the volumes sampled by these methods are very different. The most prevalent alteration minerals in the NWG 55-29 borehole, according to cuttings analysis, are quartz and calcite with minor amounts of chlorite (Figure 3-4), which, along with the low porosity, should tend to keep the rock relatively resistive as compared to the clay-rich shallower intervals indicated by the NWG 55-29 mud log and by fractures in nearby coreholes such as GEO N-2.

#### *3.2.4.5 BOREHOLE COMPENSATED SPECTRAL DENSITY*

The density tool indirectly measures the electron density of a given formation by emitting a beam of gamma rays and measuring the backscatter. Litho-density tools measure the bulk density of the rock mass by the interaction of gamma rays with the electrons orbiting atoms between a source and a detector. This measurement is highly sensitive to the number of atoms in the path of the gamma ray and the atomic number of those atoms. Thus, electron density relates directly to mass density. The density tool helps to determine rock physical properties, such as density (and conversely constrains

porosity if a reference rock type or mineralogy is available) and, combined with the neutron porosity log, can be used to constrain the strength and static elastic moduli. Estimates of density from weighted average mineral density agrees well with the bulk density log (Figure 3-4), both over-predicting density if zero porosity is considered, and largely overlying the bulk density curve once adjusted for fluid-filled porosity based on the neutron porosity log. In locations of high pyrite, chalcopyrite and magnetite concentration, the bulk density log clearly underestimates density.

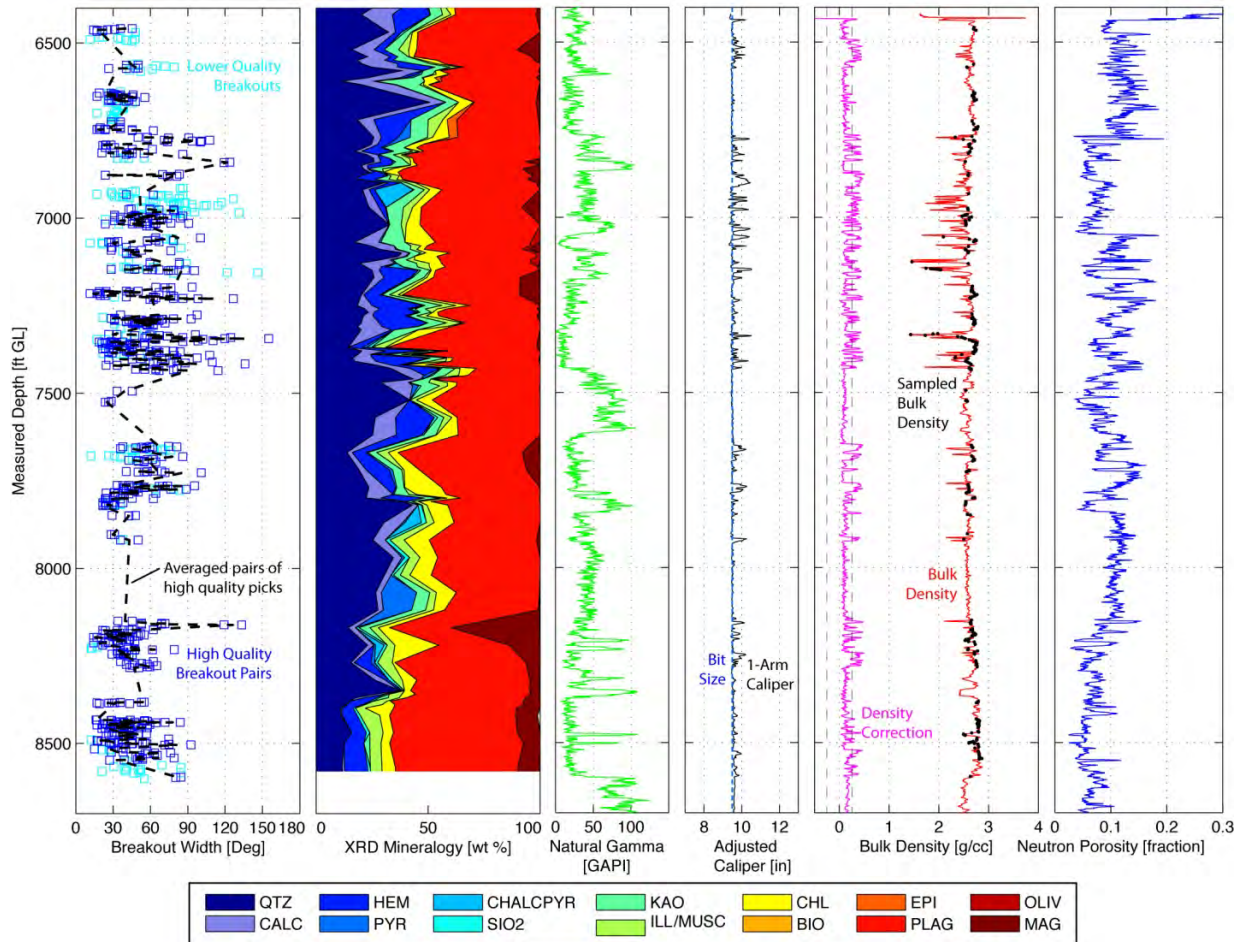


Figure 3-5. Correlation of breakout width and geologic and geophysical constraints on rock strength. From left to right: (1) measured breakout width (wBO); (2) minerals in cuttings from XRD; (3) natural gamma (4) adjusted caliper; (5) bulk density; and (6) neutron porosity.

### 3.2.4.6 DUAL-SPACED BOREHOLE COMPENSATED NEUTRON

In NWG 55-29, the borehole compensated neutron porosity and litho-density logs are strongly affected by the total porosity. In contrast to the lithodensity log previously described, the neutron porosity log measures the total porosity of the rock by direct interaction of neutrons with hydrogen atoms primarily associated with water molecules between a source and a detector. It is insensitive to the shape of the pore containing the fluid and to whether the water is structured in minerals such as clay or zeolite, or present as a free (mobile) fluid. This log will underestimate porosity in steam zones.

Figure 3-5 shows a comparison of the neutron and density logs within the interval logged by the BHTV where breakout width has been measured. Both of these logs have depth resolutions commensurate with the distribution of breakouts (Hearst et al., 2001) of about 0.08-0.40 m (0.25-1.3 ft) along the



borehole. Although mineralogy is available from XRD and thin section analysis of cuttings, the vertical distribution is in 3 m (10 ft) increments, and often less, making it less suitable for application to a detailed breakout analysis. Figure 3-5 shows first order correlations between breakout width and the key physical properties of mineralogy, density, and porosity. Regions characterized by high plagioclase content (low quartz) and high kaolinite, chlorite, and illite/muscovite content tend to show larger breakout width. The relative natural radioactivity of the rock measured in the gamma ray log does not show a simple correlation to breakout width, although low breakout width or the absence of breakouts does occur in several intervals of high gAPI<sup>9</sup> such as 2265-2321 m (7430-7612 ft), 2373-2390 m (7785-7840 ft), and 2623 m (8602 ft) to the end of the BHTV log. Depth intervals in which the borehole is enlarged by breakout are also revealed in the caliper log, and as intervals of anomalously low bulk density and relatively high neutron porosity.

### 3.2.4.7 BOREHOLE TELEVIEWER

On 22 October 2010, a high-resolution BHTV log was acquired using the ALT ABI85 BHTV tool in the slightly deviated NWG 55-29. Prior to logging, an inject-to-cool program was initiated to cool the borehole to extend the potential depth of the interval to be logged. The resulting BHTV log spans the upper 739 m (2425 ft) portion of the 1106 m (3629 ft) open-hole interval from the casing shoe at 1970 m (6462 ft) to 2701 m (8860 ft). The motor that directs the acoustic pulse in the BHTV tool stopped working at 2701 m (8860 ft) at a temperature of 277°C (531°F), so the remainder of the open-hole interval could not be logged.

The BHTV images the borehole wall with an acoustic pulse that reveals the presence of fractures from their impact on the shape of the borehole wall. See Section 5 for the detailed BHTV log analysis and Appendix C-2 for the full BHTV log. The BHTV log identified 351 fractures in the open-hole section of the well from 1963-2701 m (6439-8860 ft), most of which have an apparent aperture greater than zero at the wellbore interface. These fractures represent stimulation targets because they are weak points in the rock matrix but, as indicated by all previous logging and testing, they are currently incapable of flow and lack significant permeability. Interpretation of the BHTV images indicated that the zone immediately above the first granodiorite intrusion, 2553-2591 m (8375-8500 ft), contained the highest concentration of natural fractures. The dominant fracture sets strike roughly NNE-SSW and dip approximately 50° to the east and west, as expected for conjugate normal faults.

### 3.2.5 PETROLOGIC AND PETROGRAPHIC ANALYSIS

Mineralogy is a primary control on the frictional strength ( $\mu_s$ ) (Lockner and Beeler, 2002; Tembe et al., 2010) and permeability ( $\kappa$ ) of fractures and fault zones (e.g., Crawford et al., 2003). Recent quantitative studies on the impact of mineral mixtures such as quartz, illite, and smectite (and other phyllosilicates) on these properties generally show behaviors intermediate between monolithic mineral end-members (Crawford et al., 2003; Tembe et al., 2010; Davatzes et al., 2010). In geothermal systems, minerals and their textures also record the history of heating and hydrothermal rejuvenation (e.g., Lutz et al., 2009; Bargar and Keith, 1999). Heat transport and fluid flow are typically controlled by fractures and faults, which concentrate hydrothermal alteration within narrow zones. Complex thermal histories and localized alteration produce highly variable physical properties in the subsurface, making it difficult to predict the performance of geothermal wells or the impact of hydraulic stimulation to enhance natural permeability in an EGS reservoir. Thus, determining the *in situ* type and distribution of minerals in a

---

<sup>9</sup> The gAPI unit (Gamma-ray American Petroleum Institute) is based on a measurement made in a calibration pit at the University of Houston.



geothermal well is critical to successful EGS stimulation planning and to post-stimulation evaluation of EGS procedures. Cuttings collected during drilling can provide this key constraint.

Crawford et al. (2003) suggests that there should be a negative correlation between permeability and clay content but that clay content, especially expandable smectite, weakens faults making them more susceptible to slip. Other phyllosilicates such as illite-muscovite or chlorite will have similar, but less extreme impacts. In fact, the potential for a long-lived increase in permeability resulting from hydraulic stimulation strongly depends on reactivation of self-propping natural fractures in shear (Davatzes and Hickman, 2009; Lutz et al., 2010). Thus, the association of faults and types of alteration will significantly impact stimulation potential either by limiting the flow of fluid into fractures, and thereby preventing reactivation by normal stress reduction, or by minimizing porosity production associated with slip. These properties will similarly impact the usefulness of alternate methods such as chemical stimulation through dissolution, which primarily exploit vein-filling minerals, such as calcite and quartz. Thus, the correlation of geophysical estimates of *in situ* porosity and permeability with the type of alteration from cuttings mineralogy could help identify potential targets for stimulation.

Therefore, the analysis of cuttings has three distinct goals: (1) establish independent evidence for fractures, veins and localized hydrothermal alteration; (2) define the distribution of minerals comprising the open-hole interval; and (3) establish the number, relative timing and characteristics of alteration events. Additional details on the XRD portion of this work are provided in Appendix C-3.

#### 3.2.5.1 GEOLOGIC CONTEXT

Three distinct formations are generally recognized in the vicinity of the NWG 55-29, including the Deschutes Formation, the John Day Formation, and granodiorite which intrudes into the lower John Day Formation. The Deschutes Formation consists of lava flows, volcanoclastic deposits, and fluvial deposits from the ancient Deschutes River. Lava flows are mostly pahoehoe with rare interbedded a'a lava flows, and some scoria. O'Connor et al. (2009) report that Newberry deposits vary in age from 8-4 Ma to geologically modern (<100 ka). The John Day Formation consists largely of dacitic and rhyolitic ash flow and air-fall tuffs with minor rhyolite flows and domes and alkali basalts. Most of the ash-flow tuffs occur in the western facies of the formation between the Blue Mountain uplift and the Cascade Range. Six major ash flow sheets are present in this area; ash-flow tuffs are largely rhyolitic and typically contain abundant phenocrysts of quartz, sanidine, and plagioclase (Robinson, 2007). Below the John Day Formation are subvolcanic intrusions, which are generally poorly characterized (due to a lack of nearby outcrops or samples from wells), but are comprised of dacite to granodiorite. This zone is often referred to as "highly intruded John Day", or simply as Subvolcanic. All formations contain layers of mafic to silicic lava flows and tuffs along with their feeder pipes and dikes, which have been documented by surface mapping or in drill cuttings (Fitterman et al., 1988).

Surface geophysical surveys of resistivity and density suggest that the interior of Newberry Volcano consists of three distinct zones (Fitterman et al., 1988). The upper zone is low in density and high in electrical resistivity, suggesting only mild alteration. The intermediate zone is characterized by moderate density and low resistivity, suggesting that hydrothermal alteration has caused development clays. This conclusion is consistent with shallow core studies in the nearby GEO N-2 corehole (Bargar and Keith, 1999) that show some development clays. The lower zone is characterized by high density and high electrical resistivity, suggesting the presence of subvolcanic intrusives and more resistive alteration mineralogy.

Bargar and Keith (1999) investigated the hydrothermal mineralogy in core from geothermal drill holes at Newberry. Their work suggests that shallow hydrothermal alteration on the flanks of the volcano where NWG 55-29 is located is confined to fractured and vuggy zones. In GEO N-2, alteration is

characterized by a suite of minerals including analcime, aragonite, siderite, rhodochrosite, calcite, smectite, chlorite, quartz, mordenite, pyrite, pyrrhotite and hematite. The paragenetic sequence of this nearby shallow corehole is summarized in Figure 3-6a. Fluid inclusions in quartz and calcite from GEO N-2 (Figure 3-6b) and SF NC-01, both located on the western flank of the volcano, yield homogenization temperatures that generally match present measured temperatures, or possibly slightly hotter (~20°-40°C [68°-104°F]). Homogenization temperatures from inclusions in the deeper portions of the caldera wells (USGS-N2 and RDO-1) fall about the boiling point curve and are elevated above the current measured temperatures, by about 80°C in RDO-1 and about 100°C in USGS N2 (Figure 3-7). Homogenization temperatures in SF NC 72-03, located at the caldera edge, appear transitional between flank and caldera systems; homogenization temperature ranges are broad, and fall between the hydrostatic boiling point and present measured temperatures (Figure 3-7). These results suggest a boiling, perhaps vapor-dominated, geothermal system exists within the caldera, while past conditions on the flanks of the edifice were dominated by a conductive regime, similar to present conditions.

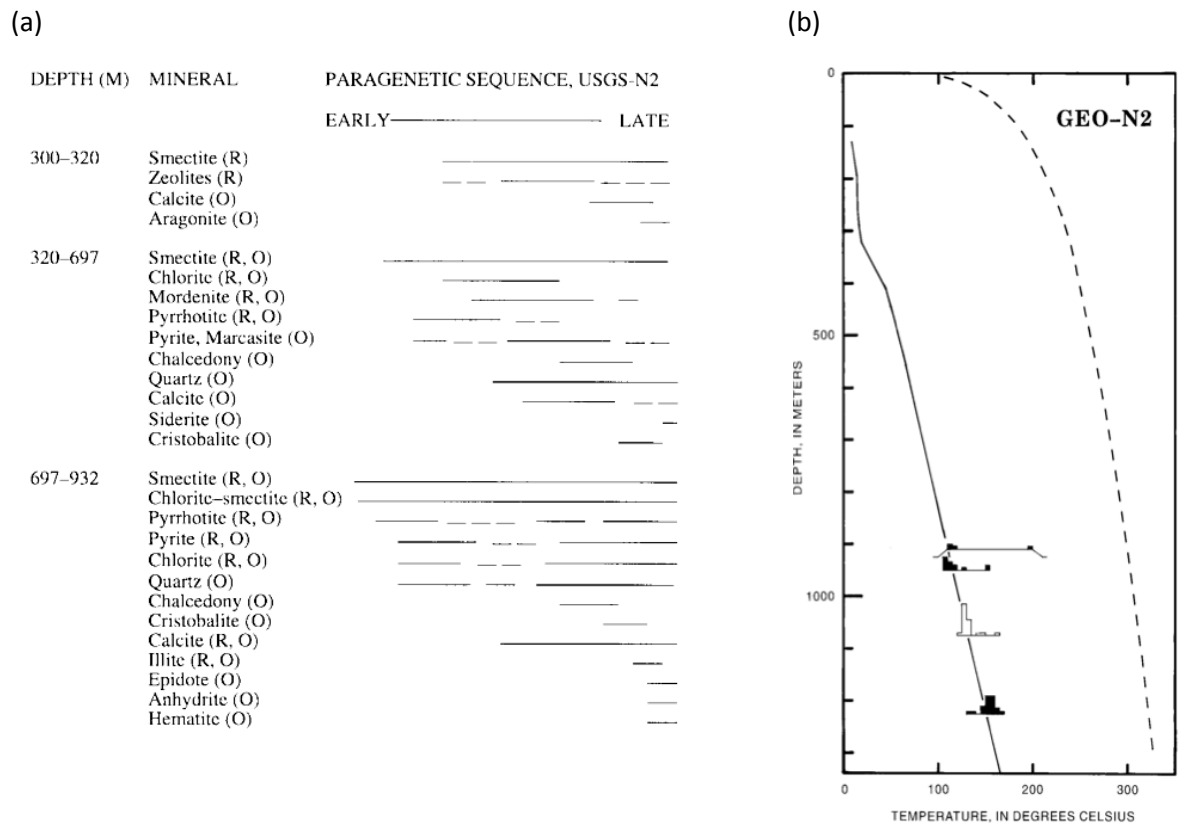


Figure 3-6. (a) paragenetic sequence and (b) comparison of modern measured temperatures (solid line), homogenization temperatures of fluid inclusions in calcite and quartz (embedded histograms), and the hydrostatic boiling point for pure water (dashed line) in GEO N-2 (Bargar and Keith, 1999), located about 1 km (3280 ft) from NWG 55-29. Homogenization temperatures are shown by filled squares for quartz and open squares for calcite.

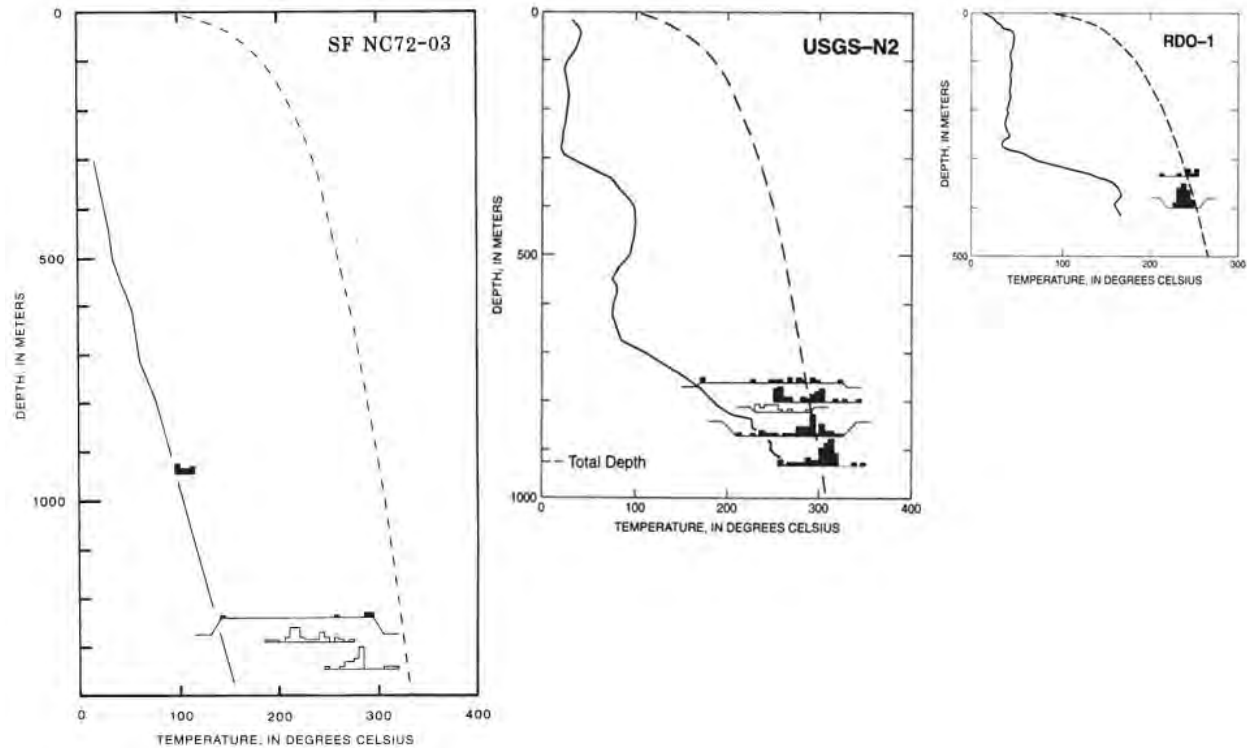


Figure 3-7. Fluid inclusion homogenization temperatures in SF NC72-03, USGS N2 and RDO-1 reveal hotter conditions than the modern temperature profile, including boiling reservoir conditions in the caldera wells.

### 3.2.5.2 CUTTINGS SAMPLE PREPARATION

Cuttings from NWG 55-29 were collected for analysis over an interval from 1707-2620 m (5600-8600 ft). This depth range spans the upper open-hole interval and extends above the casing shoe at 1970 m (6462 ft) in which stimulation must have an impact. Background sampling at intervals of 15.2 m (50 ft) was chosen to provide sufficient context but keep the number of samples small enough to complete the analysis in a timely fashion. In addition to the context provided by these samples, additional targeted sampling was conducted based on initial review of the mud log, temperature logs, and geophysical logs with a focus on the neutron porosity and density logs. These samples targeted regions of mud loss during drilling, initial identification of euhedral crystals in the mud log, anomalously high or low temperatures relative to the background gradient, and high porosity zones and low density zones. The cuttings samples were split using a micro-splitter to ensure unbiased sampling. Half of the cuttings were retained as an archive by Davenport and the remaining half was shipped to Temple University for analysis.

To provide context for the analysis of cuttings, intact core stored at the core library maintained by EGI at the University of Utah in Salt Lake City was examined (Figure 3-8). We focused on samples from the neighboring GEO N-2 corehole extending to a depth of 1225 m (4020 ft), which is well short of the open-hole interval of NWG 55-29, but nevertheless provides some insight into the rock types present at Newberry. In the extrusive volcanics, we noted enhanced hematite alteration associated with the top of basaltic and rhyolitic flows, bleaching, a relatively low number of fractures, and the abundance of vesicles that ranged from completely open to completely filled by quartz, amorphous silica, calcite, and often possessed thin layers of chlorite.

Cuttings from NWG 55-29 were analyzed at the macroscopic length-scale using a binocular stereoscope. These samples were thin sectioned and analyzed using a polarized petrographic microscope to determine textural relationships among secondary minerals including mineral associations, recrystallization, and relative ages of mineral formation from cross-cutting or replacement relationships. Determining which minerals crystallized at the same time and are part of the same mineral assemblage helps establish the history of geothermal activity in the rocks pierced by the borehole. In this borehole, cuttings are several millimeters in diameter or smaller and are comprised of both single grains and multiple sub-millimeter grains.

Bulk rock mineralogy was quantified using XRD of powdered samples using the Rigaku powder XRD verified by thin section analysis and will be discussed in detail below.



**Figure 3-8. Drill core from the University of Utah core library showing that lithologic changes can be both abrupt (A), as with a dike (from well 72-3 at 1363 m (4469 ft), or gradual (B), as with hydrothermal bleaching (from GEO N-2 corehole at 1101-1104 m [3610-3620 ft]). Cores are approximately 7.6 cm (3 in) in diameter.**

### **3.2.5.3 RESULTS: EVIDENCE FOR FRACTURES, VEINS AND LOCALIZED ALTERATION**

Veins are identified by the precipitation of secondary minerals on a discontinuity that otherwise cross-cuts the primary rock texture and mineralogy. They often show a coarsening-inward layering of mineral coatings with the finest grain size along the fracture margin and larger grain sizes towards the interior. Euhedral crystals within the veins are used as an indicator of open-space porosity associated with veins. However, these criteria require relatively large cuttings that provide both samples of vein material and wall-rock for unambiguous identification.

The most common pore-filling minerals in the cuttings from NWG 55-29 include calcite, quartz, hematite, and chlorite, with trace amounts of pyrite and epidote. Although these minerals often occur in veins (Figure 3-9), nearly all of these minerals can also be found filling primary vesicles throughout the full section of core analyzed (Figure 3-10). The occurrence of these minerals in both pore types suggests the same fluid chemistry accessed all open spaces, resulting in consistent mineral assemblages. The exception is opaline silica, which is associated with vesicles and not veins.

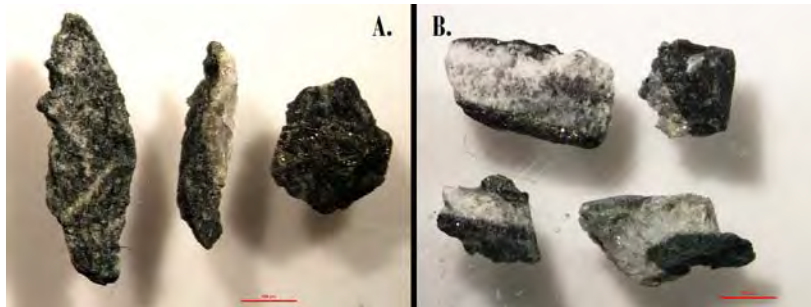


Figure 3-9. Veinlets from (A) 2164 m (7100 ft) and (B) 1859 m (6100 ft) showing varying compositions, including calcite, epidote, pyrite, and quartz. In (A) the first grains show calcite veins cross-cutting, while the pyrite veins have braided distribution. In (B) the two on the left show layers of pyrite and quartz, while the two on the right show euhedral crystals indicative of precipitation in open pores.

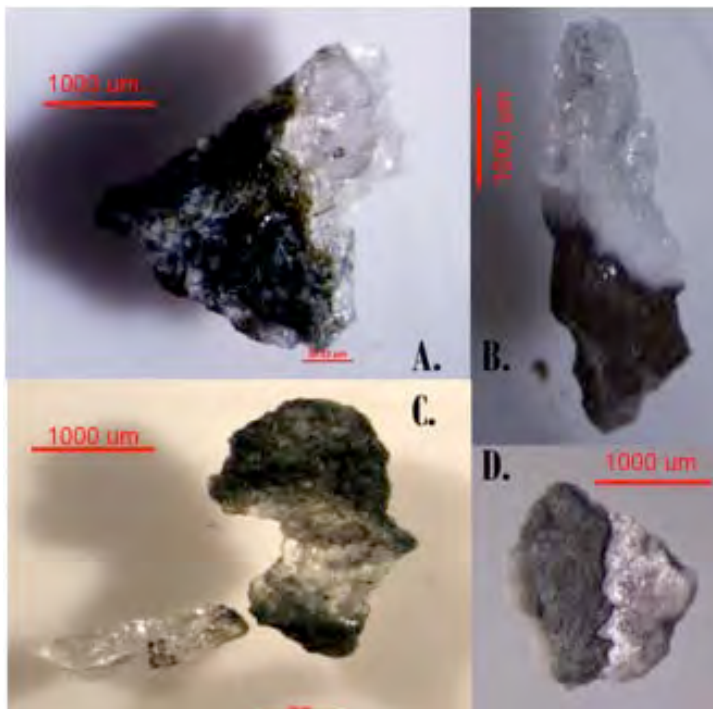


Figure 3-10. Evidence of zoning in veins or pores at: (A) 2225 m (7300 ft), (B) 1823 m (5980 ft), (C) 2164 m (7100 ft), and (D) 1981 m (6500 ft). Crystals grown in open space of either a vug or fault with evidence of layered mineralization textures and euhedral crystal form. Note that in (A) and (C) crystals show signs of a yellow-green rind that could be chlorite or epidote (often found with quartz in open geothermal pores). In (B) the precipitate shows a very fine grained coating of amorphous silica formed on a smooth, curving surface common in vesicles of core samples. In (D) the jagged interface of the vein and wall-rock is more typical of a brittle discontinuity.

Most pores exhibit a fine-grained coating of either chlorite or quartz. Pore-filling chlorite occurs as thin, <100 µm-thick coating that conforms to the shape of the pore in both fractures and vesicles, and generally coats their entire surfaces (Figure 3-11). Grain size in the coatings is typically <10 µm. The location adjacent to the host rock is consistent with formation by the interaction of a hydrothermal fluid with a host rock. Thin, 10-25 µm-thick veneers of microcrystalline quartz also coat many fracture and vesicle surfaces. Superposed on these base layers are coarser-grained cements including quartz, calcite, and hematite. In these subsequent, more massive layers of pore-filling minerals, there is no consistent sequence to the layering of quartz and calcite, although in vesicles quartz filling is most common. In addition, both veins and filled vesicles show growth bands indicating multiple cycles of mineral precipitation and changing fluid chemistry.

Veins uniquely identified by the preservation of host rock on both sides of the vein material (Figure 3-9) also show cross-cutting relationships that indicate that: (1) fractures undergo reactivation and recovery of porosity; (2) the most common fracture healing minerals are coarse-grained calcite and quartz; and (3) there is no consistent sequence of fracture-healing minerals. In addition to the precipitation of



minerals to form veins, fractures are associated with rinds of altered host rock indicated by dissolution textures in plagioclase. Note that the frequency of these uniquely identified veins is limited by the small size of the cuttings and, therefore, the distribution of veins should be considered an underestimate.

Micro-faults that accommodate shearing can be recognized in cuttings by the occurrence of angular cataclasites, slickensided and polished surfaces, or slickenfibers (Figure 3-12). As a quality control, we required that slickensided grains must be flat or coated by a secondary mineral to help rule out apparent slicks, or simply striated surfaces that might result from drill bit wear. Slickensides were identified on grains throughout the entire borehole. However, the most developed zone of slicks is associated with mud losses between 2210 m (7250 ft) and 2271 m (7450 ft).

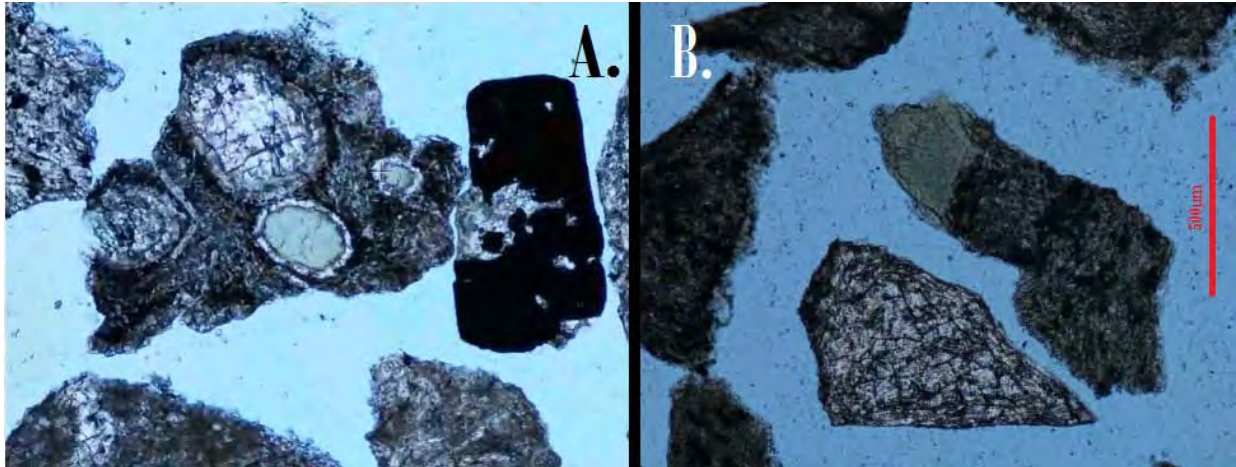


Figure 3-11. Photomicrographs in plane polarized light showing the growth of secondary minerals in (A) pores and (B) cracks. (A) Example from 1920 m (6300 ft) showing growth rings visible in a vesicle in the grain in the center of the image, and calcite filling a crack visible in the grain on the right. (B) Example from 2222 m (7290 ft) showing chlorite crystal occurring on the fine-grained host rock in an open pore.

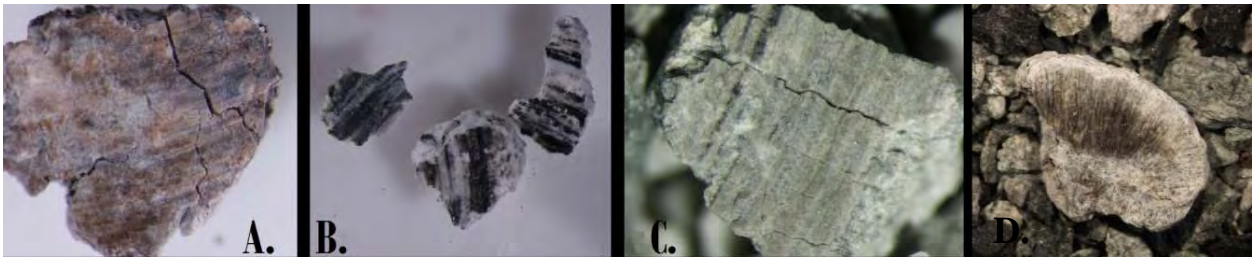


Figure 3-12. Indications of structural deformation at (A) 1823 m (5980 ft), (B) 2094 m (6870 ft), (C) 2387 m (7830 ft) and (D) 2557 m (8390 ft) are evident in slickenside texture on several grains.

As noted earlier, in addition to the precipitation of minerals in vesicles and fractures, several of the secondary minerals are distributed throughout the host rock. These minerals include pyrite (Figure 3-13), chlorite (Figure 3-14), and hematite. Chlorite occurs interstitially at grain boundaries and as a replacement of primary minerals. Pyrite is generally located at grain boundaries. In addition to chlorite, other replacement phyllosilicates identified by XRD analysis include illite/muscovite and kaolinite (see discussion below).

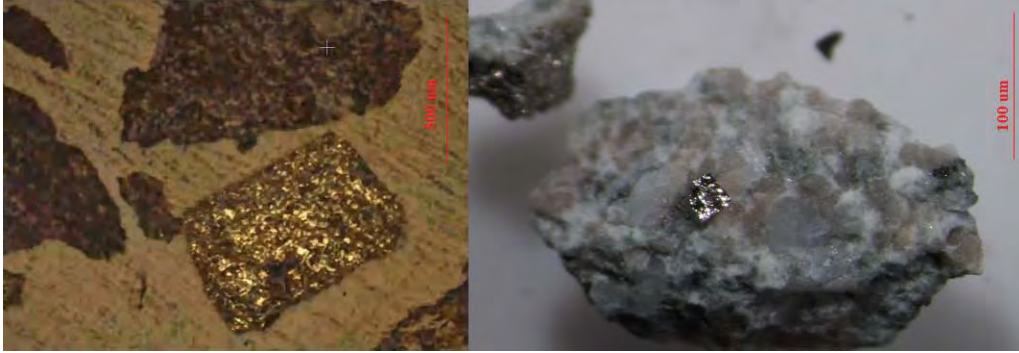


Figure 3-13. Pyrite occurring within the rock mass at a microscopic grain size visible under reflected light in thin section (left, from 2222 m [7290 ft]) and within cataclasite (right, from 2387 m [7830 ft]). Red scale bars represent 500 and 100  $\mu\text{m}$ , respectively.

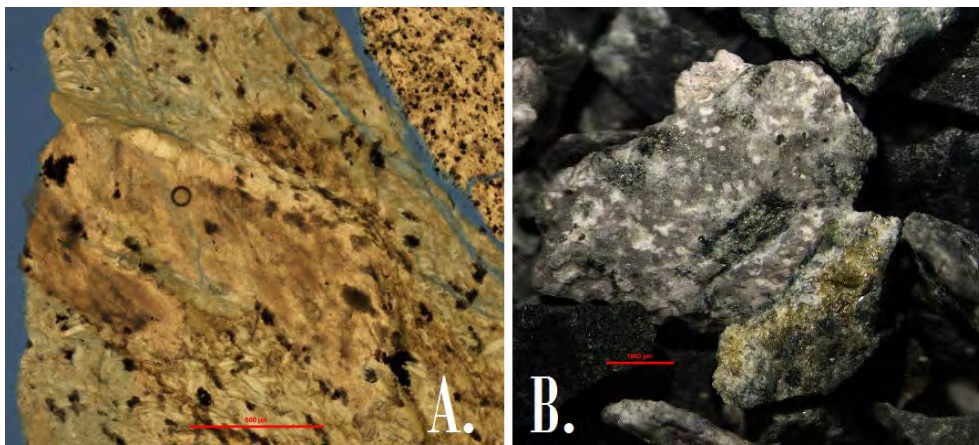


Figure 3-14. (A) Microscopic and (B) macroscopic evidence of chlorite growing authigenically between grains from the 2545 m (8350 ft) depth interval. Red scale bars represents 500 and 1000  $\mu\text{m}$ , respectively.

Figure 3-15 summarizes the rock types, distribution and relative abundance of structural indicators including veins, pores, slickensides and mineral alteration through the formation of the secondary minerals, including chlorite and pyrite revealed by macroscopic analysis of cuttings. Volcanic flows dominate the shallow rock types, whereas the felsic intrusives predominantly comprised of dacite are more prevalent at depth. Rhyolite is interspersed throughout. The cuttings indicate that fractures are prevalent throughout the open-hole. Similarly, chlorite forms the primary alteration mineral except at the bottom of the analyzed interval, whereas the abundance of pyrite increases slightly with increasing depth. The variation in mineralogy was quantified through analysis of bulk X-ray; see Appendix C-3 for a summary of the analytical methods.

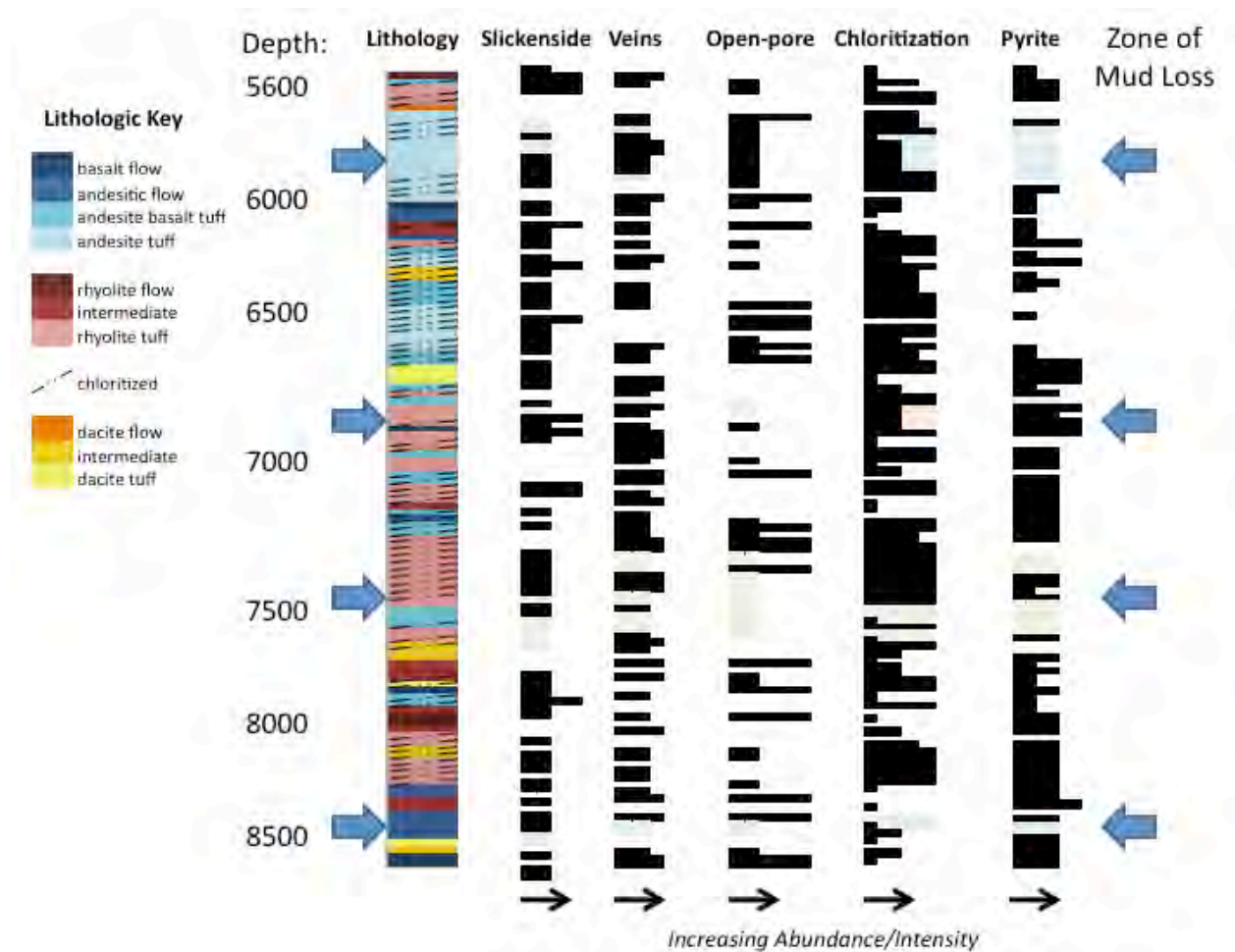


Figure 3-15. Summary of rock types and cuttings analysis documenting the occurrence of fractures indicated by slickensided grains, veins, and open porosity in cuttings as well as alteration indicated by the presence of chlorite both as vein coatings and replacement of primary minerals and pyrite (Letvin, 2011).

#### 3.2.5.4 RESULTS: MINERALOGY

The overall distribution of rock forming minerals and alteration minerals with depth is summarized in Figure 3-15. Generally, alteration is most extensive in the volcanic extrusive units overlying intrusives above 2633 m (8640 ft). The assemblage of vein-filling and replacement minerals in this shallower interval include calcite, hematite, chlorite and minor epidote. Phyllosilicates include kaolinite, illite/muscovite and chlorite. However, kaolinite is absent inside the underlying intrusive bodies, and illite/muscovite and chlorite are less abundant. In addition, calcite is not present in the underlying intrusives, whereas it is prevalent in the overlying volcanics as a vein forming mineral. Pyrite and chalcopyrite are extensively present throughout all rock types, most commonly as interstitial minerals, but are also present in veins. There is also a general trend toward increasing plagioclase content with increasing depth.

Estimates of density from the weighted average of mineral densities is in good agreement with the bulk density log (Figure 3-4), both over-predicting density if zero porosity is considered, and largely overlying the bulk density curve if adjusted for fluid-filled porosity based on the neutron porosity log. This comparison also reveals that in locations of high pyrite, chalcopyrite and magnetite concentration, the bulk density log clearly underestimates density.



It is worth noting here that the clay-sized fraction is particularly susceptible to being lost in the mud shakers and by washing of cuttings during cuttings collection. However, expandable clays are completely absent despite the presence of other clay-sized phases such as illite. We also note that in a single fracture in core from GEO N-2, serpentine and talc were detected. Examination of XRD-spectra from the cuttings of NWG 55-29 did not detect these minerals, although it is possible that trace concentrations occur at depth.

### 3.2.5.5 Paragenesis

Cutting and thin section analysis indicates that volcanic extrusives were initially altered by early chlorite replacement and quartz precipitation in both vesicles and fractures. At shallow depths, the analysis of Bargar and Keith (1999) documented well-developed clay alteration in fractured zones, which has also been supported by fracture studies by Fetterman (2011) and Fetterman and Davatzes (2011). However, in the stimulation interval, expandable clays such as smectite or mixed layer phases such as chlorite-smectite or illite-smectite are absent, and phyllosilicates are limited to chlorite, illite/muscovite and kaolinite. Thus, the geothermal system has a clay-enriched cap, and the current stimulation interval lies well below this cap, as evidenced by the lack of expandable clays, consistent with surface resistivity measurements (Fitterman, 1988). We also see layering of these mineral phases in pores. The most common vein-filling minerals are calcite and quartz, but chlorite and hematite are also common. Veins show repeated opening, regardless of mineral filling. The lack of a consistent pattern to the layering or to cross-cutting relationship in veins by these minerals indicates repeated pulses of precipitation. The presence of quartz and calcite in many veins suggests precipitation associated with up-welling and down-welling fluids because of the relative impact of temperature on their solubility given the large temperature gradients in this borehole. However, calcite is primarily confined to units overlying the granodiorite or dacite intrusions, which might indicate that such a relatively open system predates the intrusions or was associated with the intrusion into the overlying volcanics.

Formation of illite/muscovite is consistent with potassium metasomatism and, in conjunction with abundant chlorite and minor epidote, suggests greenschist metamorphism throughout the stimulation volume. These minerals are distributed within fractures, but also as a penetrative alteration of the host rock adjacent to fractures. The lack of a clear set of relative ages among the alteration minerals suggests the alteration results from a single persistent episode of geothermal activity, with episodic fluid flow in a variety of directions. The vertical extent of the fluid flow is uncertain, but there is no clear evidence of an extensive hydrothermal system. Local rejuvenation or long term maintenance of the geothermal system is also indicated by the presence of the intrusive bodies, which clearly show less greenschist alteration than overlying volcanic flows. This model is consistent with the analysis of fluid inclusion homogenization temperatures by Bargar and Keith (1999) that shows that modern temperatures are not significantly different than ancient temperatures in the west flank of the Newberry volcano. Future work could use the chlorite chemistry resolved by microprobe analysis to estimate formation temperature for comparison to modern temperatures (e.g., Cathelineau and Nieva, 1985; Cathelineau, 1988; Xie et al., 1997), and is currently being investigated.

## 3.2.6 CORE ANALYSIS

### 3.2.6.1 GEOLOGIC CHARACTERISTICS OF NATURAL FRACTURES IN CORE

A key to success of EGS at Newberry is whether fracture-generated permeability remains high or returns to pre-fracturing levels (or even lower) after stimulation stops and fluid pressure dissipates. High permeability is a function of high porosity, which can be maintained where slip across naturally rough fracture surfaces causes mismatched asperities to prop them apart, a process called hydroshear dilation.

Key controls on this potential for dilation are: (1) the geometry and survival of asperities during slip; (2) the initial porosity; (3) the type of mineral present along the surfaces of the fracture; and (4) the role of fluid flux and dissolution/precipitation in the pores along fractures. In natural systems that ubiquitously contain fractures, the surfaces of the fractures and any pulverized rock are subject to chemical interaction with *in situ* waters, leading to precipitation of new minerals and alteration of primary minerals. In addition, the protolith clearly plays an important role, which at Newberry includes various forms of basalt, andesite, dacite and rhyolite, deposited as flows, tuffs, and intrusives. For the purpose of this study, the analysis was confined to fractures in basalt or andesite.

The role of mineralogy and fault rock texture on the potential for production of connected porosity during hydroshear stimulation in EGS is quantified by examining natural fractures at different stages of development (Figure 3-16). The evolution of porosity in natural fractures, in particular its regeneration after healing, also lays the groundwork for determining the role of deformation in the life-cycle of geothermal systems through the generation of fracture porosity that can increase fluid flow and storage volume. Thus, we quantify the relationship between: (1) secondary fracture porosity; (2) deformation; and (3) healing through mineral precipitation and hydrothermal alteration in crystalline basaltic rock of core obtained from the GEO N-2 temperature corehole at depths up to ~1219 m (4000 ft).

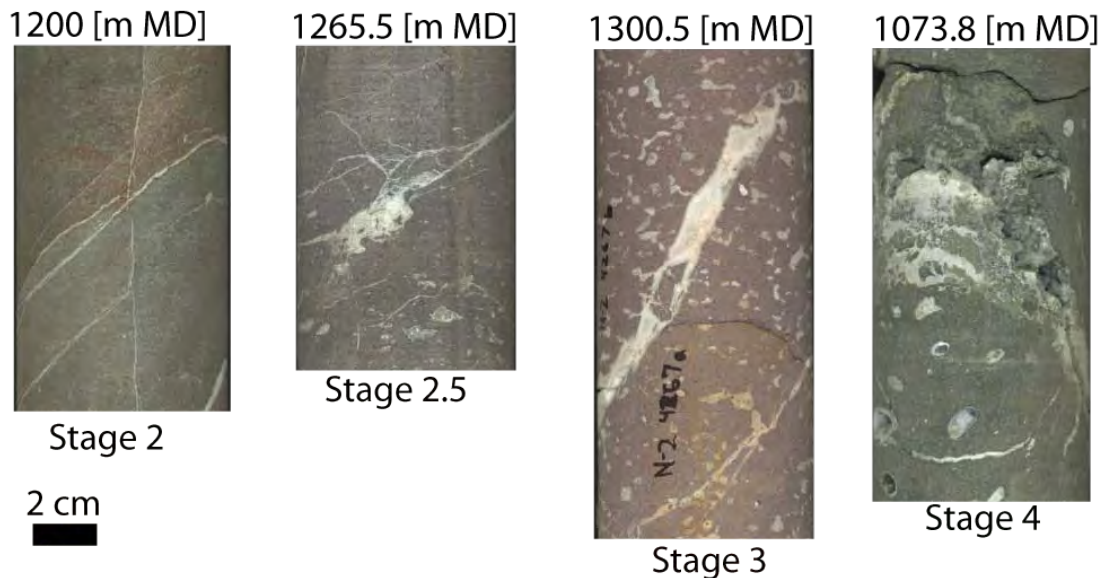
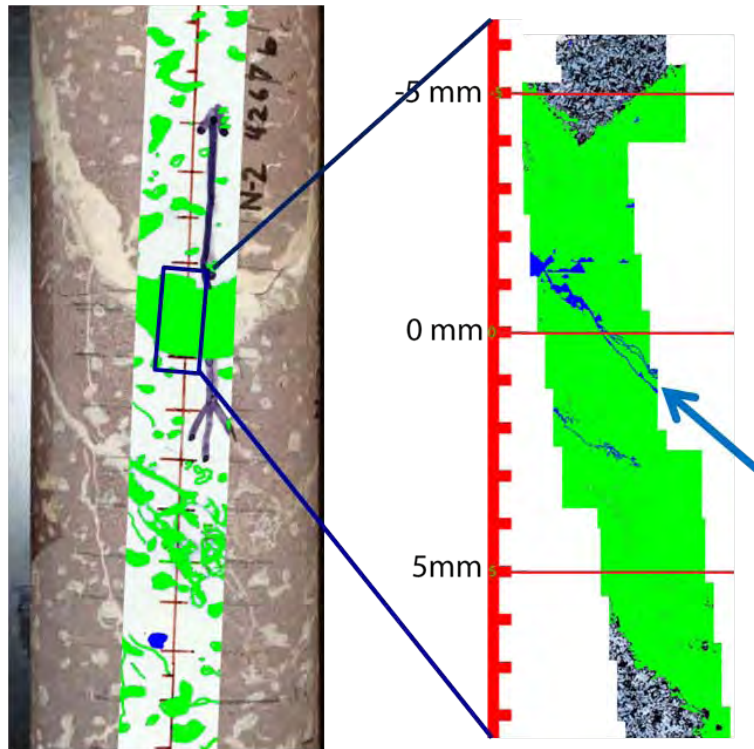


**Figure 3-16. Four cores representing skeletal (healed) and open porosity in clay-poor faults of the GEO N-2 borehole (from Fetterman, 2011).**

The distribution and geometry of open pores, pore-filling minerals, and skeletal porosity (the combination of open and healed pores) are mapped at the decimeter to 25 micron scale (Figure 3-17). The associated mineralogy of the host rock and the secondary minerals are mapped from core and thin sections, and quantitative estimates of the mineral phases and their relative weight percents are obtained through Rietveld refinement of XRD spectra. In addition, mapping of elemental chemistry at a length-scale of approximately 0.5 cm (0.197 in) across faults is accomplished through the use of the hand-held Niton XI2t XRF. This mapping allows a comparison of the bulk chemistry of the host and fault rocks to determine if the fault rocks evolve via: (1) in-place alteration, in which case the host and fault rocks have equivalent chemistry; or (2) extensive fluid flux, in which case differences in elemental chemistry are expected.





### Non-clay stage 3

**Figure 3-17. Measurements of skeletal (green) and open (blue) porosity in hand sample and thin section used to quantify effect of mineralogy on fracture dilatancy (from Fetterman, 2011).**

The generation of porosity through dilation is explored in two end-member fracture types, non-clay and clay-dominated, typical of fractures captured in cores in basalt from Newberry (Figure 3-18). Both fracture types appear to have a common origin as dilated, brittle shear fractures. The fracture is a zone of dilation, generally healed by high-strength minerals such as quartz and calcite along with weaker clay minerals. At this stage, the porosity is confined close to the fracture zone. The elemental chemistry of the fracture-filling minerals is distinct from the host rock, especially in terms of relatively immobile elements including titanium and zirconium. More developed fractures are characterized by broken cement documenting repeated healing and slip, and by multiple connected fractures and breccia. In each stage, the skeletal porosity increases, with significant increases in open porosity limited to the later stages of fracture development. With each re-fracturing event, the porosity generated allows an inflow of new exotic material revealed by a different elemental chemistry than the host rock. In advanced stages, small fractures in the volume adjacent to the primary fracture zone are also well developed and the exotic material flowing into the system has seeped into these cracks, creating a damage zone. This damage zone has a chemical signature falling between the fracture and the host rock.

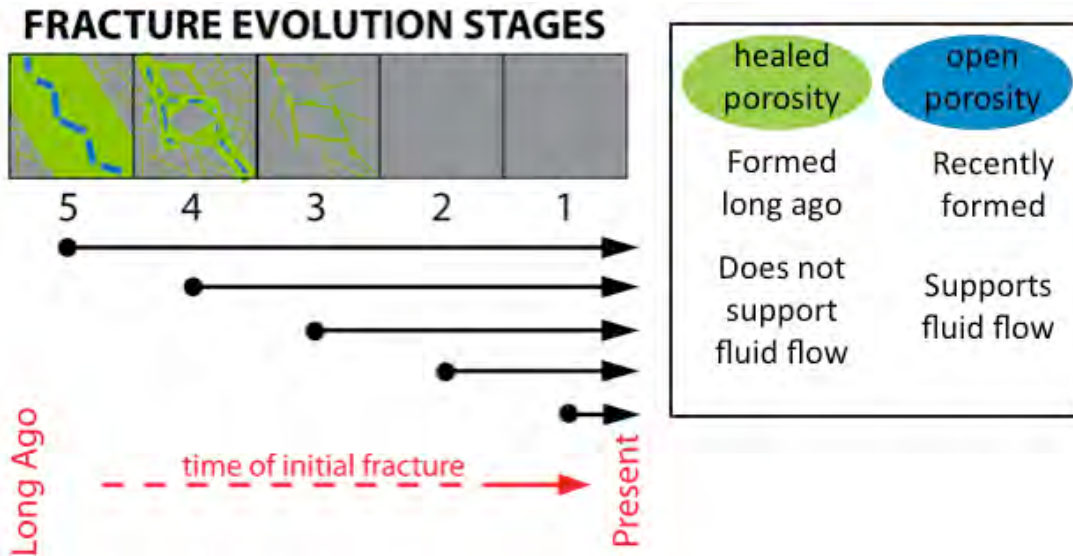


Figure 3-18. Model for evolution of porosity in the absence of clay in core GEO N-2 (from Fetterman, 2011).

However, once increased concentrations of clay develop in the fracture, its porosity evolves along a different path. As the clay fraction increases, repeated slip ceases to cause dilation in the fault rock, although dilation continues in the adjacent volume of fractured host rock and healing in this region continues to be dominated by quartz and calcite. With continued development, the clay-rich fault rock is characterized by chemistry similar to the host rock. At this point, the driving mechanism behind the widening of the clay-rich fractures is a combination of fracture-induced dilation in the adjacent host rock and alteration that advances into this fracture zone. In the most developed examples in the core, evidence of dilation in the adjacent volume is minimal to absent, with much lower amounts of open porosity compared to the equivalent examples in the non-clay fractures. The threshold for the transition from non-clay to clay-dominated behavior might be as low as 10-20%, as indicated by initial mineralogical examination of these geologic samples and studies of synthetic gouges comprised of various mixing ratios of smectite, illite, and quartz (Tembe et al., 2010).

This analysis indicates that porosity due to dilation in fractures occurs most prevalently in late-stage, non-clay dominated fractures. The measureable open porosity is also highest in the late stage non-clay fractures. Open porosity is an indication of recent fracturing because precipitating minerals have not yet filled the open space. The large amounts of open porosity found in late-stage non-clay fractures suggests that porosity caused by dilation in such fractures may be occurring at a rate faster than the rate of secondary mineral deposition. This kind of fracture system has mineralogical and structural characteristics that support fluid flow sustainable on production time-scales. Therefore, fracture systems dominated by non-clay mineral filling and with later stage development should be ideal candidates for EGS hydroshearing.

In the NWG 55-29 borehole, XRD analysis, and the examination of thin sections at magnifications up to 1000x, reveals that clay is essentially absent in the open-hole interval across all rock types. Minor amounts of illite-muscovite and chlorite are found in the shallow tuffs below the casing shoe, but are absent in deeper intrusive rock and also in basalt/andesite flows. Initial comparison to geophysical logs, including natural gamma, litho-density, and neutron porosity, suggest the non-clay faults in core studied here are representative of the materials that occur from the casing shoe to a depth of approximately 2621 m (8600 ft). Thus, these initial results suggest that, during slip, fractures will tend to dilate and self-prop consistent with the behavior of the clay-poor rock described above.

In addition to the geologic characterization of naturally-occurring fractures in two boreholes at Newberry, rock mechanics experiments to determine the mechanical properties of these rocks under controlled conditions have been undertaken, see discussion below. These tests, in combination with a compilation of the attributes of similar rock types from the literature, form the basis of an *in situ* strength model that is necessary for predicting the behavior of natural fractures during stimulation and for deriving a complete stress model from observations of borehole deformation (see discussion below).

### 3.2.6.2 ROCK MECHANICS TESTING OF CORE

This section summarizes the petrophysical and rock mechanical properties of welded tuff from GEO N-2. The methodology, laboratory calibration, and full results of this analysis are attached as Appendix C-4. The GEO N-2 core samples were taken from 1305 m (4281 ft; Figure 3-19). The core mechanically tested can be categorized as Stage 2.5-Stage 3 non-clay, as described above (Figure 3-16).

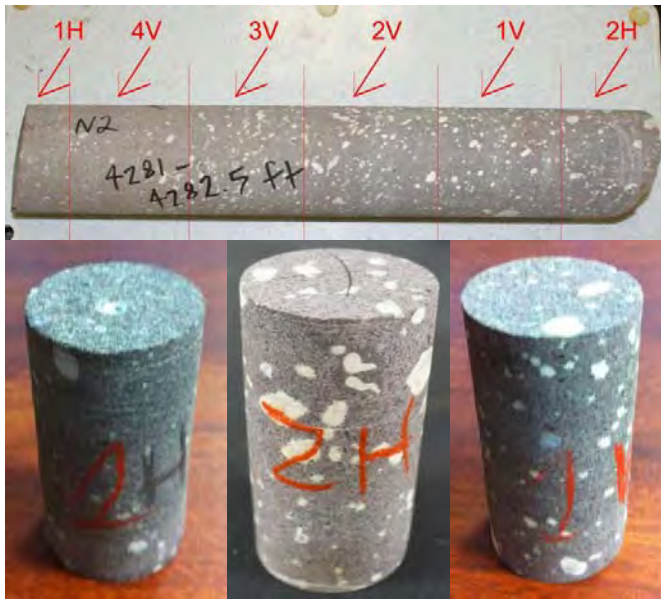


Figure 3-19. Core sample from Well GEO N-2 from 4281-4282.5 ft MD (top), and three of six plugs used for mechanical testing.

The rocks from this depth in GEO N-2 range from basaltic to andesitic, with basalt being distinguished from rhyolite layers by <52 wt.% SiO<sub>2</sub> (Bargar and Keith, 1999). Petrographic thin sections of welded tuff were used to describe rock texture and mineralogy. An X-ray CT (computed tomography) scanner was also used to provide images of the rock pore structure, constructing a 3-D montage of the 2D images from each section of the core plug. Rock permeability was measured using a pulse permeameter, and triaxial compression tests were performed to determine Young's modulus, Poisson's ratio, and failure envelope.

Welded tuff is a pyroclastic igneous rock that is composed mainly of lithified volcanic ash. During the lithification process, interaction with hydrothermal fluids (water, steam, and volcanic gases) can result in mineral deposition in vesicles and deformation-induced cracks. Some of these cracks remain open because the matrix permeability is too low to allow fluid flow. Evidence of such open pores can be seen (Figure 3-20) in an X-ray CT-scan image of GEO N-2 plug 1V. Thin sections from this core also show evidence of such open vesicles (Figure 3-21).

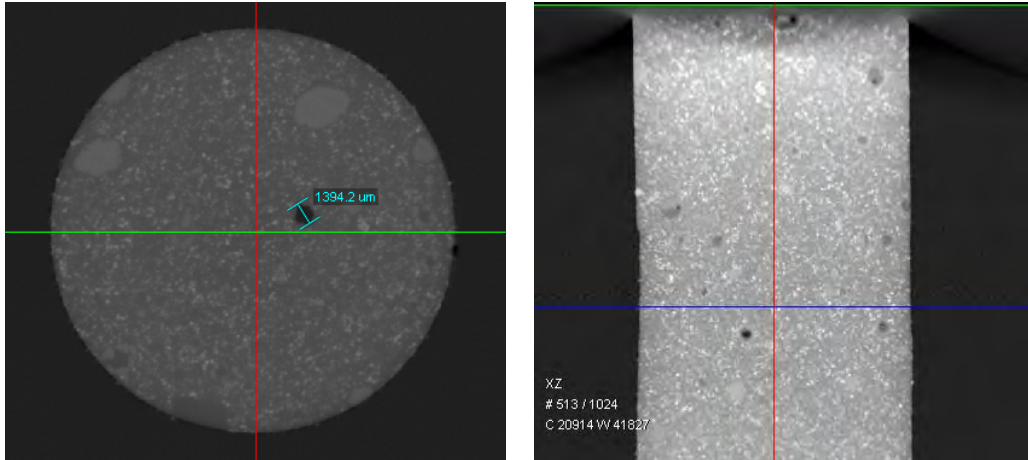


Figure 3-20. An X-ray CT scanner image of welded tuff from vertical plugs (not tested at this time). One of the vesicles is 1394.2  $\mu\text{m}$  in diameter. Left image is XY view; right is XZ view.

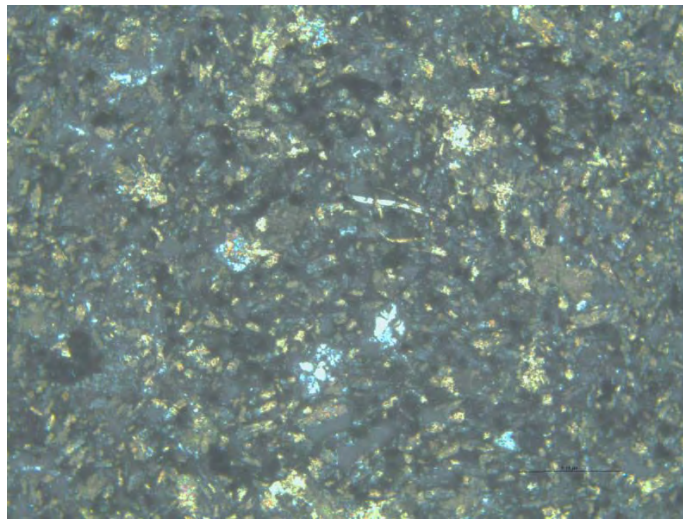


Figure 3-21. Thin section image from GEO N-2 welded tuff sample N2-4281-2H. The blue colors are pore spaces, which are mostly intercrystalline, and are disconnected in a fine-grained volcanic ash solid matrix. Matrix porosity is too small to be measured using conventional methods. Several opaque minerals exist and are not identified. View is under crossed polarization. Image is about 0.1 mm (0.04 in) across.

Two Newberry core samples were tested to measure the mechanical and failure properties. The tests were performed on a multistage triaxial testing machine at Texas A&M University. The Mohr Coulomb envelope for the tuff, based on failure tests at five confining pressures, was determined to have a cohesion (intercept) of 31.3 MPa (4357 psi) and a friction angle (slope) of  $18.85^\circ$  (Figure 3-22). Compared to other volcanic rocks, the 1305 m (4281 ft) welded tuff sample from GEO N-2 has a relatively low strength (see Section 5 and Appendix E-1 for comparison). The test results for sample N2-4281-2H are shown in Table 3-2. Equipment calibration results and other Newberry sample results are included as Appendix C-4.

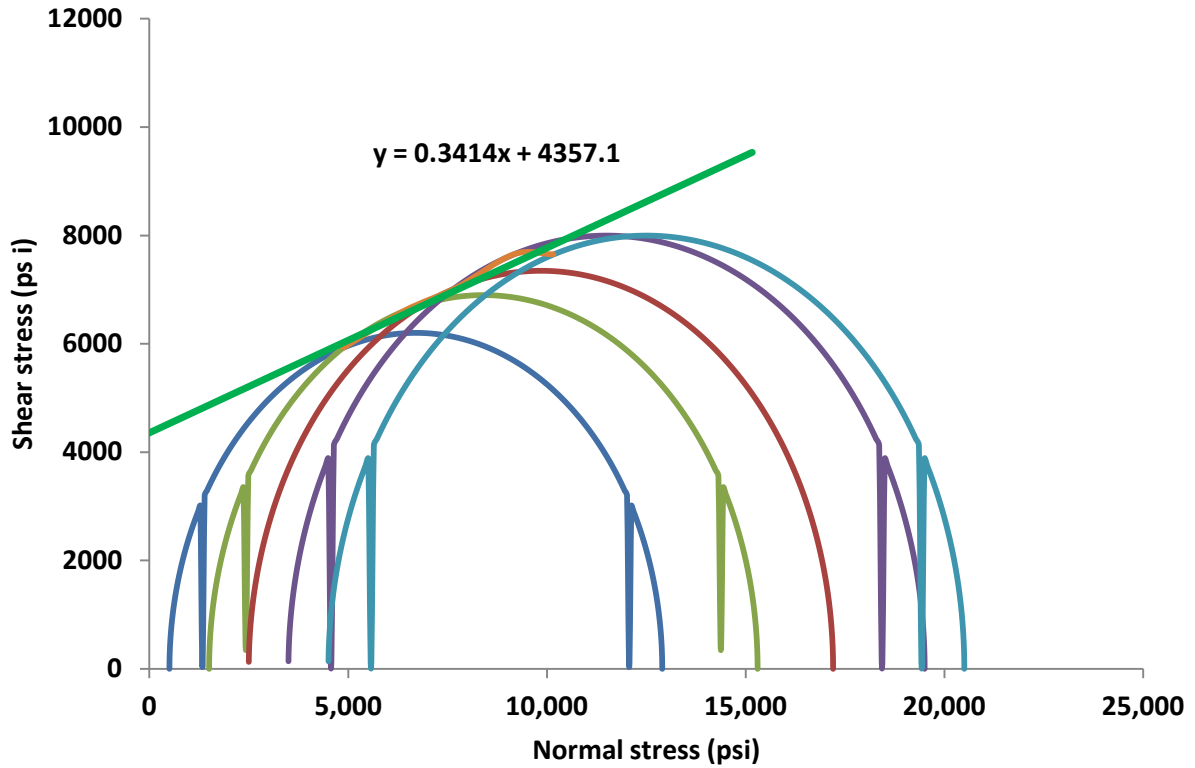


Figure 3-22. Mohr Coulomb envelope for Newberry welded tuff at confining pressures of 500, 1500, 2500, 3500, and 4500 psi.

Table 3-2. Multistage test results for GEO N-2 welded tuff (sample N2-4281-2H).

Test Parameter	Test Results			
Confining pressure (psi)	1500	2500	3500	4500
Young's modulus (psi)	2.50E+6	2.43E+6	2.36E+6	2.30E+6
Poisson's ratio	0.163	0.107	0.079	0.035
Friction angle	18.85°			
Cohesion (psi)	4357			
Uniaxial compressive strength (psi)	12183			
Permeability, mD (before triaxial test)	3.2x10 <sup>-6</sup>			
Permeability, mD (after triaxial test)	0.93x10 <sup>-6</sup>			
Porosity (lab)	2.5±0.5 %			
Porosity (CT)				
Porosity (NPHI)	6%			
Density (lab) (g/cc)	2.6			
Density (RHOB) (g/cc)	2.78			



### **3.2.7 NEWBERRY THERMAL-HYDROLOGICAL-CHEMICAL MODEL**

#### **3.2.7.1 INTRODUCTION**

This section discusses the fluid and gas geochemistry at Newberry Volcano using measured groundwater geochemistry, high-temperature gas chemistry, and information gained from prior studies of mineral alteration, fluid inclusions, and hydrothermal modeling of Newberry Volcano. These data are the basis for the native state thermal-hydrological-chemical (THC) model of mineral-water-gas reactions for the west flank of Newberry Volcano, including NWG 55-29. A well-tested and in some cases calibrated native state THC model then provides a strong foundation for THC and THMC models of stimulation. A mechanical model is under development for analysis of the THMC effects of stimulation, but is not yet available. Prior modeling of the hydrothermal system (fluid flow and temperature) at Newberry Volcano was presented by Sammel et al. (1988), and provides a useful basis for the set-up and evaluation of the THC model.

In addition to the primary rock lithology, the subvolcanic temperature distribution strongly controls the character of the mineral alteration seen in boreholes, including NWG 55-29. However, the availability of fluids and the permeability distribution govern the localization and extent of alteration (Bargar & Keith, 1999). Therefore, a native state model of water-gas-rock interaction must necessarily capture the thermal and hydrological character of the system. Thus, before discussing the geochemical system, the development and analysis of the thermal-hydrological system is presented.

#### **3.2.7.2 NATIVE-STATE MODEL BOUNDARIES AND NUMERICAL GRID**

A model boundary was chosen that was large enough to encompass the stimulation, injection, and production zones of the EGS reservoir around NWG 55-29. The eastern boundary extends to one of the ring faults outside the caldera rim and the west boundary extends approximately to the edge of the C-C' cross-section (Figure 3-23). It might seem reasonable to set the eastern boundary at the caldera-bounding fault, but the temperatures at the lower part of the domain would exceed 500°C and, thus, would be well outside the range of the thermodynamic properties of the flow module and the mineral-water-gas equilibrium constant database. Owing to the slope of the volcano, groundwater tends to flow laterally away from the rim (as observed in the simulations by Sammel et al., 1988), and thus the western boundary of the model could be set further to the west. As the geologic model is developed, and production holes are planned, a reevaluation of the model boundaries will be made.

The model boundary is also shown superimposed on the cross-section of Sammel et al. (1988), with their temperature contours generated by conductive cooling of a rhyolitic magma body initially at 850°C (Figure 3-24). They defined three hydrologic units on the western flank, denoted as Flows 1-3. These layer units do not correspond directly to the units shown in Figure 3-23. Note that the temperatures in Flow 3 of Figure 3-24 are somewhat lower than those in the new cross-section, based on more recent deeper drilling on the flank of the volcano. A more complex cross-section depicting potential locations of numerous moderate-sized rhyolitic and basaltic magma chambers is given in Fitterman (1988). However, the overall conceptual model for the hydrothermal system in Sammel et al. (1988) appears to be a good starting point for the THC model.

A numerical mesh was developed with the attributes that it could serve to evaluate the native state hydrothermal system and also to be used for modeling near-well processes such as injection and stimulation (Figure 3-25). Therefore, the gridding was made progressively finer towards the well. The two-dimensional mesh is composed of 7070 grid blocks, and will eventually be extended to three dimensions. A pseudo-three-dimensional mesh for use in flow test simulations was also generated by modification of the volumes of the grid blocks by radial symmetry around the well. The orientation of

the well was taken from the cross-section and has not been updated to reflect the actual trajectory of the well, which is more nearly vertical for the first kilometer, and then progressively changes its angle to about 20 degrees from vertical. Another zone of very fine gridding was placed at the postulated fracture zone where fluid losses were indicated during the flow tests and wireline surveys (see Figure 3-26). Once the locations and orientations of fractures are known, the gridding will likely be modified. Because the mesh may be changed many times during the project, a computer code was developed to automatically generate the mesh, assign geologic and geochemical properties according to the geologic contacts, and generate initial and boundary conditions. The mesh was also constructed such that it would be a good basis for the finite element model incorporated in the new THMC code under development through another DOE-funded project.

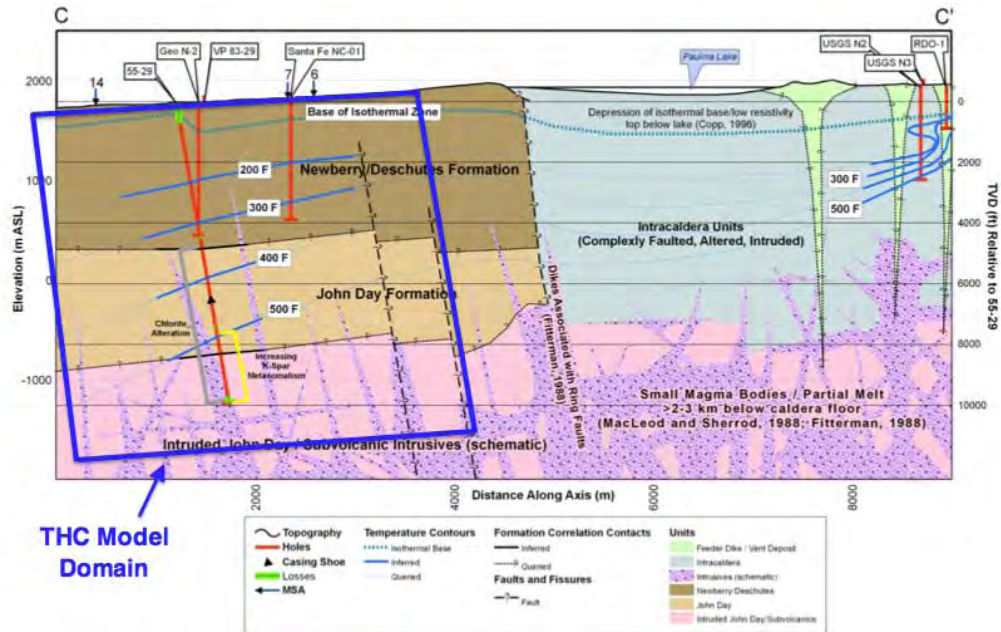


Figure 3-23. THC model boundaries superimposed on cross-section C-C' (roughly E-NE to W-SW) (see plan view of Newberry Volcano – Figure 2-6).

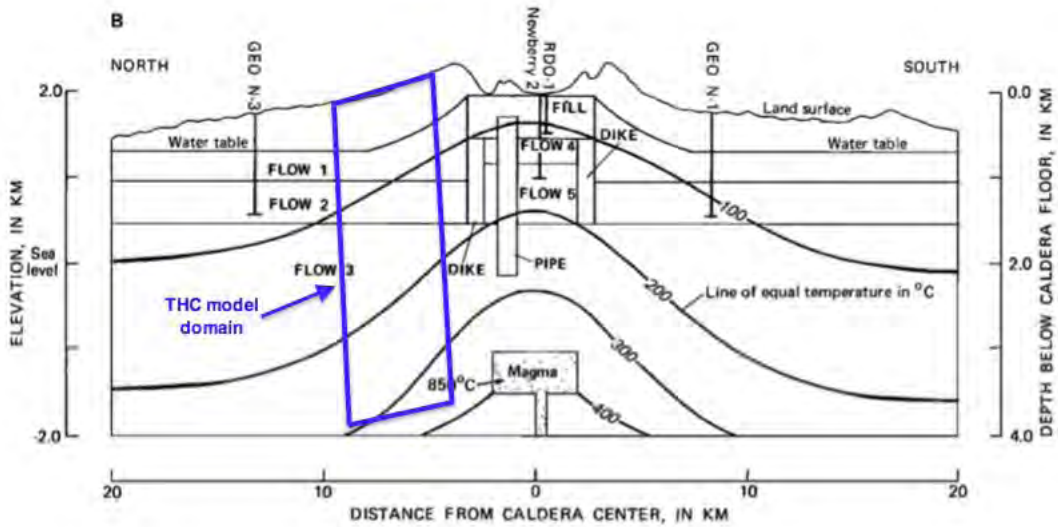


Figure 3-24. Approximate location of the THC model boundaries (in blue) superimposed on E-W cross-section from Sammel et al. (1988). A conductive cooling model assuming intrusion of an 850°C rhyolitic magma body was used to generate the isotherms.

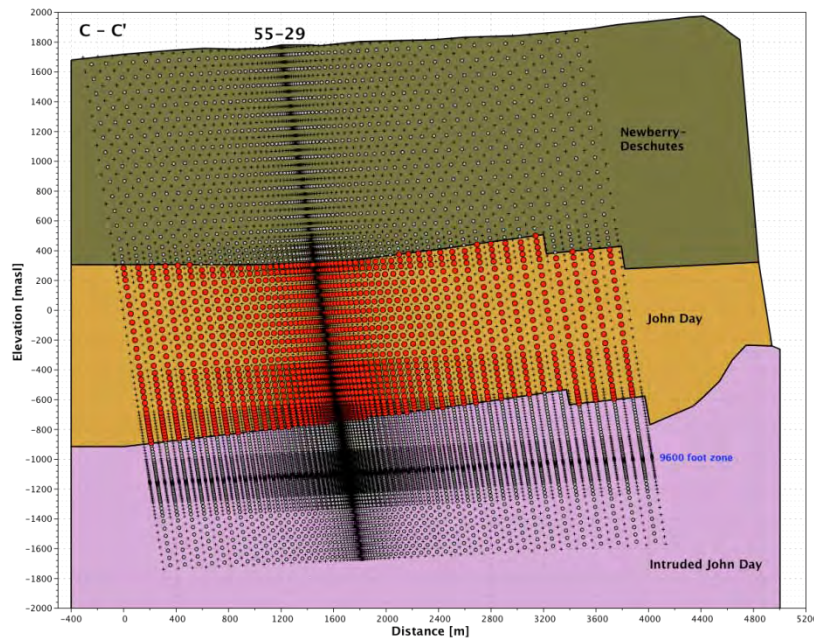


Figure 3-25. Numerical mesh corner nodes and centers superimposed on digitized geologic contacts. Red points show how the mesh generation code effectively assigns geologic properties from a digitized database of geologic contacts.

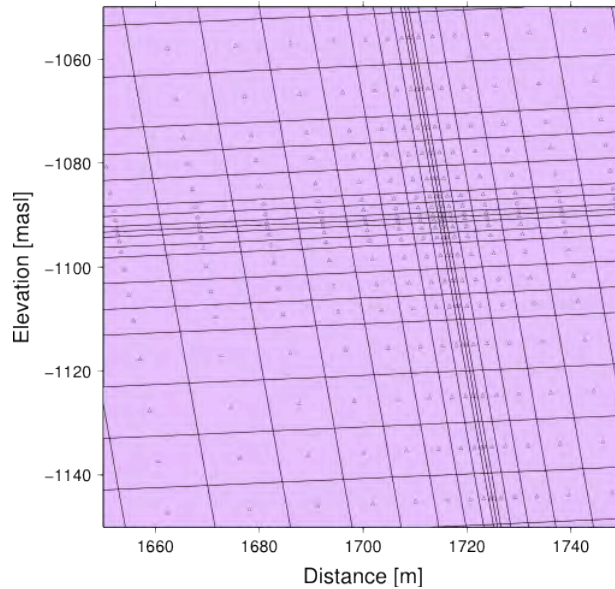


Figure 3-26. THC model numerical mesh showing blow-up of well and refined gridding along a cross-cutting fracture zone.

### 3.2.7.3 HYDROLOGICAL AND TRANSPORT PROPERTIES

Hydrological properties were, for the most part, estimated for the major units shown in Figure 3-23, with some additions at the top and bottom of the domain. A bulk permeability value for the John Day unit of  $2.6 \times 10^{-16} \text{ m}^2$  was measured by Spielman and Finger (1998) in the CEE 23-22 wellbore (about 3 km NE of NWG 55-29) for the slotted portion of the well over the depth interval from 6488 to 9577 ft. Although the lower 920 feet of the well penetrated "granitic" bedrock, much of the water loss contributing to the bulk permeability was likely at the 6770 foot level. A value of  $1.5 \times 10^{-12} \text{ m}^2$  for the near-surface permeability was estimated from groundwater velocity measurements. The Newberry-Deschutes permeability ( $1 \times 10^{-17} \text{ m}^2$ ) was based on discussions with Dave Blackwell (SMU). Neither field or core-scale permeabilities are available for the site; however, porosities were measured on numerous samples. The values are quite scattered and will need to be considered once a detailed geological model is developed. Some permeability values were measured in other drill holes or derived from flow data. If data were not available they were estimated. The hydrological data used in the model simulations are given in Table 3-3 and shown in Figure 3-27.

Table 3-3. Hydrological and transport properties.

Hydrogeologic Unit	Porosity	Permeability ( $\text{m}^2$ )	Compressibility (1/Pa)	Tortuosity
Newberry-Deschutes (top 300 m)	0.20	$1.5 \times 10^{-12}$	$3.20 \times 10^{-9}$	0.20
Newberry-Deschutes	0.10	$1.0 \times 10^{-17}$	$3.20 \times 10^{-9}$	0.20
John Day	0.05	$2.6 \times 10^{-16}$	$3.20 \times 10^{-9}$	0.20
Intruded John Day	0.03	$5.0 \times 10^{-18}$	$3.20 \times 10^{-9}$	0.20
Intruded John Day (lowest 100m)	0.01	$1.0 \times 10^{-18}$	$3.20 \times 10^{-9}$	0.20



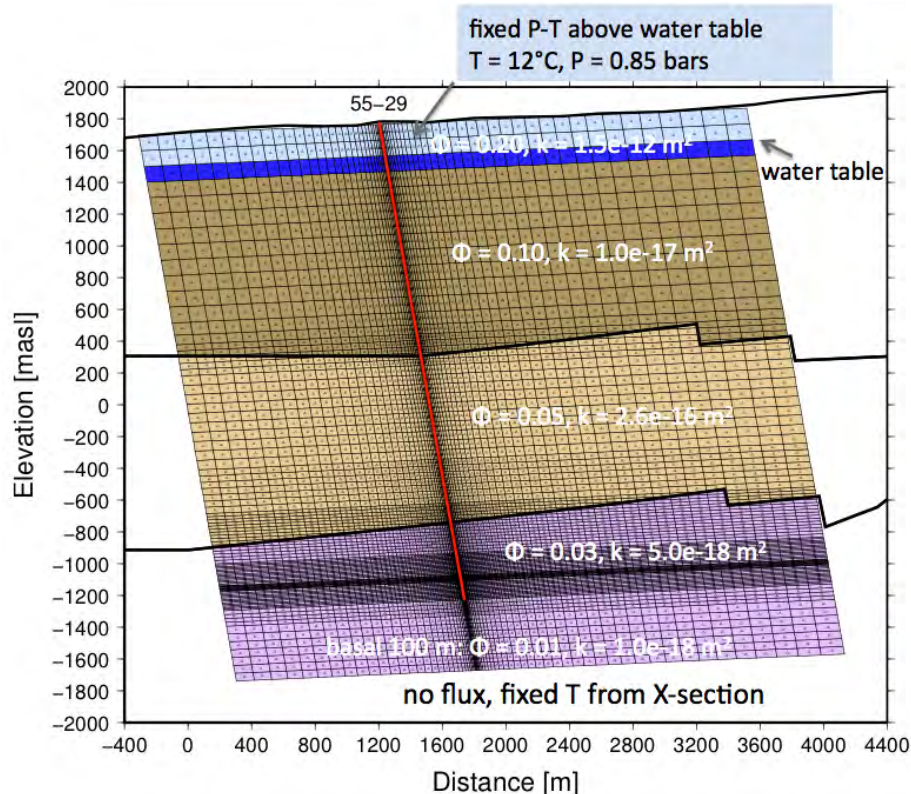


Figure 3-27. Numerical mesh showing hydrogeologic units, assigned porosity and permeability values, and thermal and hydrological boundary conditions.

The initial boundary conditions for the modeling are also shown in Figure 3-27. The base was assumed as a no-flux boundary for flow, and assumes a fixed temperature. A top zone of 300 meters was assigned a fixed pressure and temperature to approximate the constant temperature region above the water table. The side boundaries were initially considered as hydrostatic; however, the no-flux boundary behaved better for temperature in the steady state simulations, so the latter was used. Likely, the model will be extended to the east and west with coarser gridding to allow implementation of a hydrostatic boundary.

For this first phase of the model simulations, without having measurements on core samples, thermal conductivities for the THC model were calibrated by trial-and-error adjustment to approximate downhole temperature measurements. The initial starting value was estimated at  $2.00 \text{ W m}^{-1} \text{ K}^{-1}$ . Results of the calibration are given in the following section.

#### 3.2.7.4 SIMULATED STEADY-STATE PRESSURE AND TEMPERATURE DISTRIBUTION

The fluid temperature and pressure in the current system were modeled assuming a fully water-saturated rock mass. Simulations were performed using the most recent update of TOUGHREACT V2 (Xu et al., in press; Xu et al., 2006). A comparison simulation was also performed using a supercritical version of TOUGH2, known as AU-TOUGH2 (Croucher and O'Sullivan, 2008).

An initial temperature distribution (Figure 3-28) was developed from the contours shown in Figure 3-23 and used to make a first estimate of the hydrostatic pressure distribution. Temperatures above  $365^\circ\text{C}$  were fixed to  $365^\circ\text{C}$ , because TOUGHREACT cannot handle supercritical water.

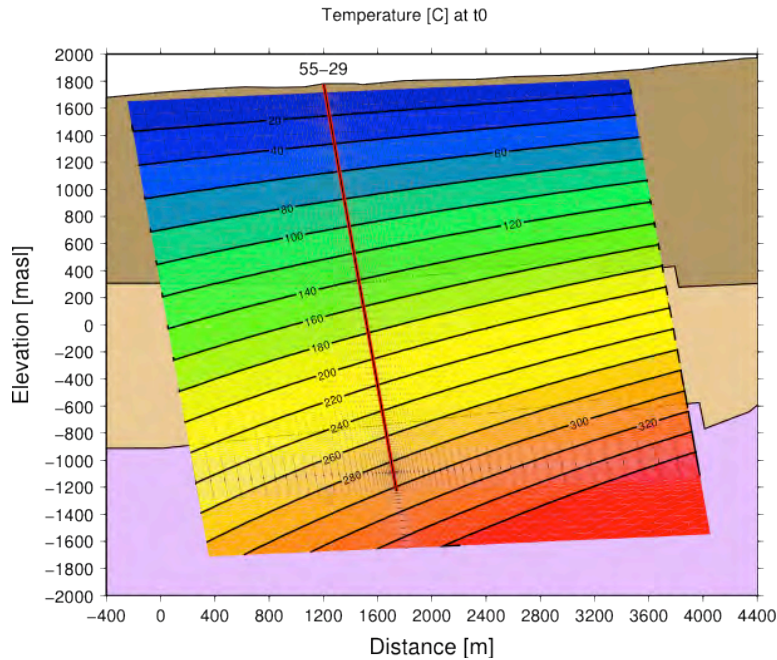


**Figure 3-28. Initial estimate of temperature distribution derived from approximate mean temperature gradients at the model boundaries in Figure 3-23. The maximum temperature was fixed to 365°C (solid red region in lower right corner). Lithology is shown underlying the model domain.**

Once the first approximation of the steady-pressure distribution was obtained, the temperature was fixed at the top and bottom boundaries and allowed to reach steady-state concurrently with pressure. A 100000-year simulation time was found to result in a close approach to steady-state. Thermal conductivities were then modified by trial-and-error so that the temperature profile better matched the October 2008 measured temperature. Starting from the initial thermal conductivity of 2.0 W/m K, it was only necessary to modify the values by about 10% in each direction. The resulting steady-state pressure and temperature distributions and profiles, compared to the measured data, are shown in Figure 3-29 and Figure 3-30. The simulated pressure profile closely matched the hydrostatic distribution in the well. Temperatures were also matched quite closely with modest changes in the thermal conductivities of the units.

Calibrated thermal conductivities (liquid-saturated) are given in Table 3-4. Thermal properties, in addition to the other fixed properties (porosity, solid grain density, and solid grain heat capacity) that are included in the conservation of energy equation. The solid (grain) density and the heat capacity are assumed to be the same for all rock units with the same values as in Sammel et al. (1988).

**Table 3-4. Thermal properties.**

Hydrogeologic Unit	Porosity	Solid Dens (kg/m <sup>3</sup> )	Solid Heat Cap (J/kg °C)	Sat Thermal Cond (W/m K)
Newberry-Deschutes (upper 300 m)	0.20	2700	1000	1.70
Newberry-Deschutes	0.10	2700	1000	1.80
John Day	0.05	2700	1000	2.15
Intruded John Day	0.03	2700	1000	2.20
Intruded John Day (lowest 100m)	0.01	2700	1000	2.20

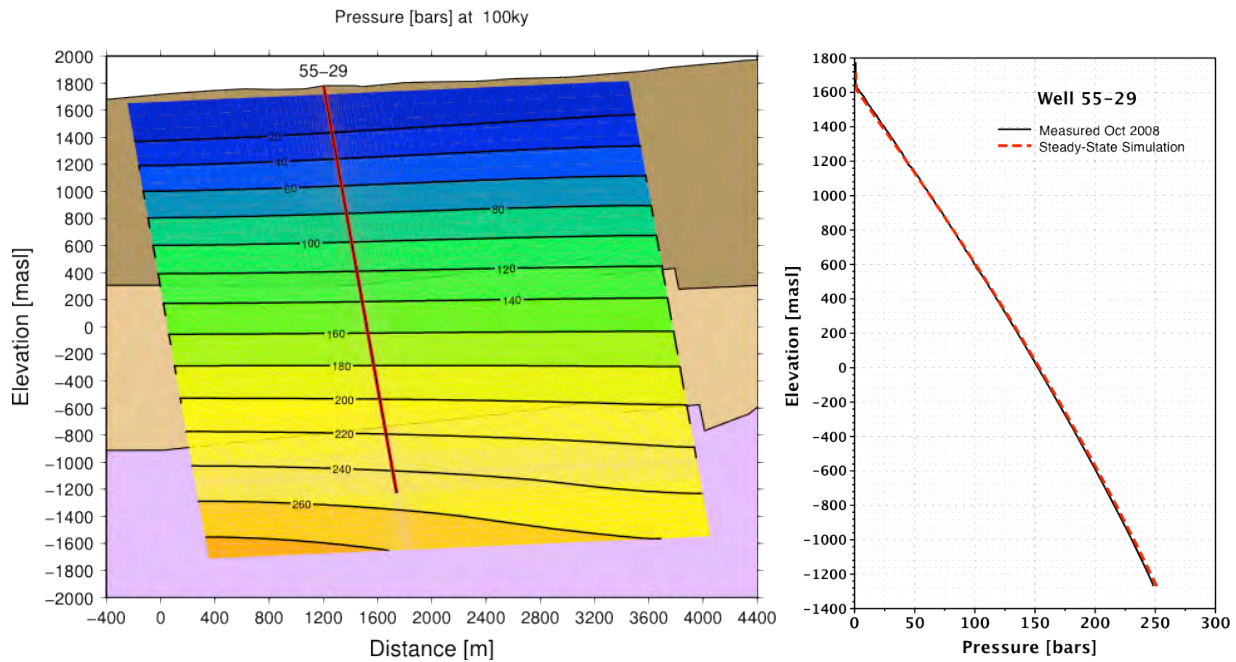


Figure 3-29. Simulated steady-state pressure distribution, assuming region of fixed temperature above 365°C (left), and comparison of simulated and measured pressure profile (right).

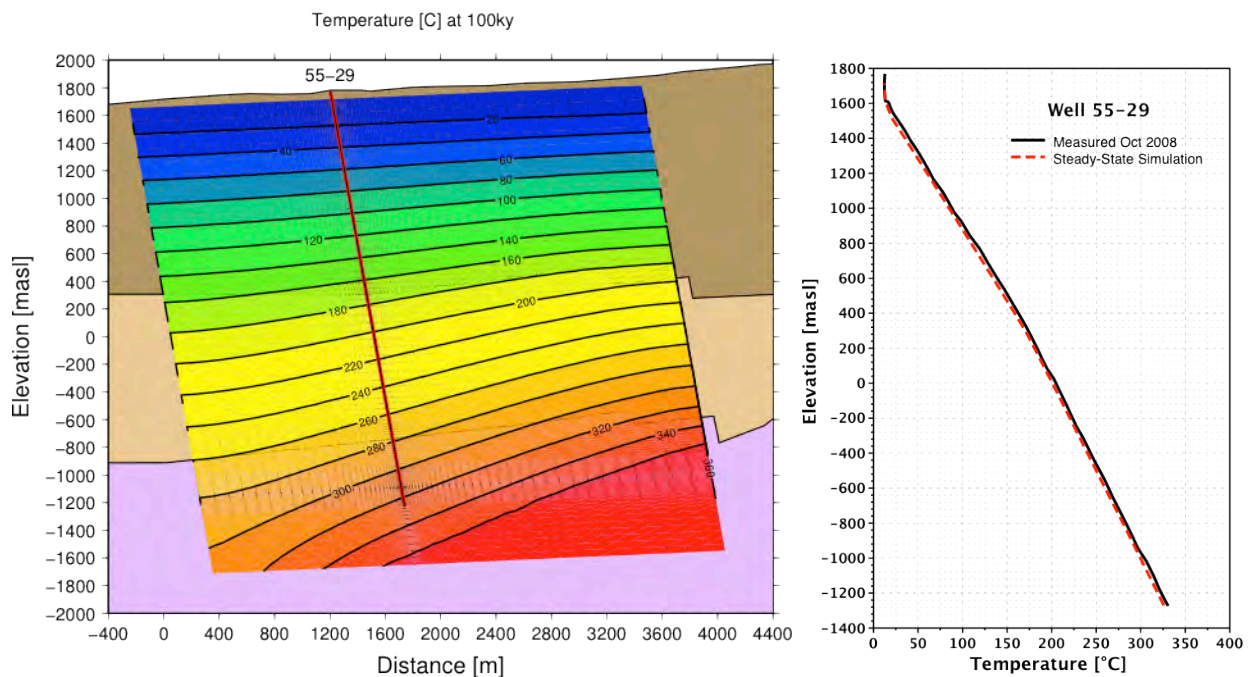


Figure 3-30. Simulated steady-state temperature distribution, with region of fixed temperature at 365°C (left), and comparison of simulated and measured temperature profile (right).

Some support for the calibrated thermal conductivities can be given by comparison to measured values on cores from other drill holes. Swanberg et al. (1988) reported thermal conductivity measurements on cores from lavas taken at depths of 1164 to 1219 m in drill hole GEO N-1. Measurements were made on twelve samples from three intervals, giving average values of 1.76, 2.01, and 2.00  $\text{Wm}^{-1}\text{K}^{-1}$ . These samples are likely correlative to lavas encountered near the lower part of the Newberry-Deschutes Formation in NWG 55-29. Another series of nine samples from drillhole N-3 at about the same depth



range gave an average value of  $1.59 \text{ W m}^{-1} \text{ K}^{-1}$ . Because lithologies and porosities vary considerably within these units there is no way to correlate any single set of samples between these drill holes and NWG 55-29, at least 10 km away. Another complicating factor is that measurements were likely performed at room temperature, whereas the calibrations reflect the conductivity at the *in situ* temperature. Acknowledging these uncertainties, though, the calibrated thermal conductivity ( $1.80 \text{ W m}^{-1} \text{ K}^{-1}$ ) of the Newberry-Deschutes unit is within the range observed in the sample measurements.

The entire pressure-temperature regime, including the supercritical region, was simulated using a recently developed supercritical version of TOUGH2 (AU-TOUGH2; Croucher and O'Sullivan, 2008). While the supercritical region was successfully simulated (Figure 3-31), the temperatures in the subcritical region along the drill hole were not modified substantially. Therefore, thermal conductivities calibrated to the new temperature field would not change significantly, assuming a fixed subcritical temperature for the supercritical region. However, this will be something to evaluate in future work.

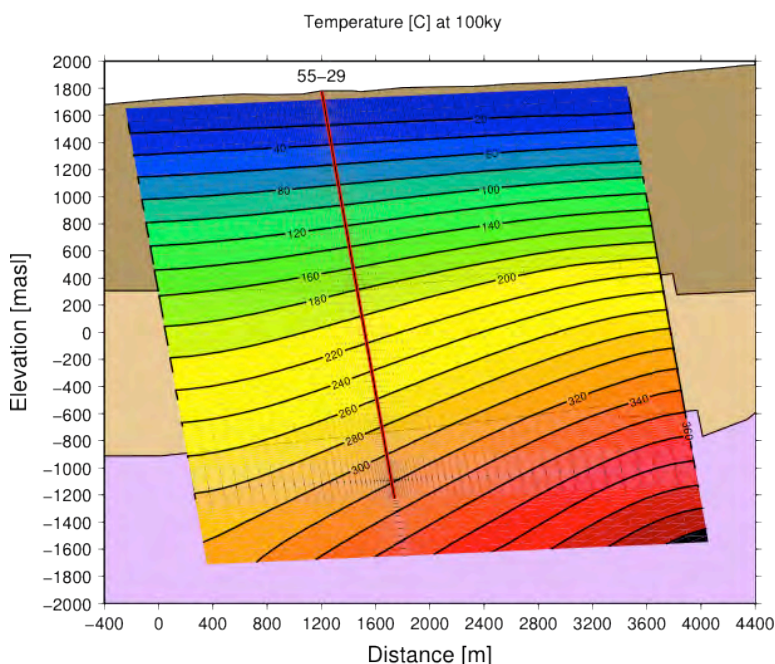


**Figure 3-31. Simulated steady-state temperature distribution, including the supercritical region, using AU-TOUGH2 (Croucher and O'Sullivan, 2008). Highest temperatures in the black region (lower right corner) are about 470°C.**

### 3.2.7.5 WATER GEOCHEMISTRY

Meteoric water is thought to be the principal source of recharge to the subsurface hydrothermal system, with magmatic volatiles and water-rock interaction as important modifiers to the groundwater geochemistry (as implied by groundwater analyses compiled by the USGS<sup>10</sup>). Groundwater was pumped from the water well on Pad S-29 (Oregon Water Resources Department number DESC 58395), and analyzed in 2008, shortly after completing NWG 55-29, and again in 2010. Analyses of these waters are given in Table 3-6.

The waters were speciated and chemical geothermometry attempted using the newly developed Geo-T geothermometry code (Spycher et al., 2010) funded through another DOE project. The Pad S-29

<sup>10</sup> <http://hot.springchem.wr.usgs.gov/imgquery.php?rlon=-121&lat=44>



groundwater was chosen for the first series of reaction-transport simulations using TOUGHREACT described below.

### 3.2.7.6 GEOCHEMICAL MODELING OF GAS AND WATER SAMPLES FROM NWG 55-29

Geologica (2008) reported analyses of noncondensable gas (NCG) for two samples collected directly from the two-phase flow line of NWG 55-29 during a rig flow test conducted 16 July 2008 (Table 3-5). The well was induced to flow with compressed air. These samples were collected about two hours after air-assist was terminated. Line pressure was too low to drive the sample through the sample line, so a vacuum pump was used to fill the evacuated sample bottles. Very little water, dark grey to brown in color, was produced during the test. Geologica reported analysis of a sample of this liquid collected from the weir box, and a water sample from the Pad S-29 water well (Table 3-6). The well flow produced no apparent steam condensate (i.e., water vapor). The weir box water sample is similar in composition to evaporated local groundwater, the source of water used for drilling, and is possibly partially equilibrated with calcite and other minerals, whereas the noncondensable gas composition is consistent with a geothermal source.

Geologica (2010) used the gas analyses to calculate equilibrium temperatures based on various gas geothermometers (Table 3-7). The absence of condensate in the gas samples precluded the determination of NCG to water vapor ratios. Because four of the seven applied gas geothermometers required such data, various assumptions were made to constrain gas to liquid ratios at various values, yielding temperatures widely ranging from 117°-321°C (242°-609°F), and averaging 258°C (496°F). Calculations independent of the gas/water ratio yielded a higher temperature range of 279°-310°C (534°-590°F), averaging 293°C (559°F).

**Table 3-5. Gas analyses from NWG 55-29 (Geologica, 2008).**

Sample ID. No.	2	3
Date/Time	19 July 2008 0:00	19 July 2008 0:36
H <sub>2</sub> O	ND	ND
CO <sub>2</sub>	99.2	99.2
H <sub>2</sub> S	0.0589	0.0601
NH <sub>3</sub>	<.0274	<.0144
Ar	0.00138	0.00151
O <sub>2</sub>	0.0234	0.0028
N <sub>2</sub>	0.622	0.562
CH <sub>4</sub>	0.042	0.0408
H <sub>2</sub>	0.113	0.106
Air	0.117	0.014

Concentrations are vol.% in dry gas.

An attempt was made to reconstitute the composition of the downhole fluid (liquid plus gas) and derive, from these analyses, possible equilibration temperatures of formation minerals with that fluid. The method is essentially that described previously by Reed and Spycher (1984), whereby gas amounts are stoichiometrically titrated back into liquid samples, and multi-component speciation calculations with the resulting fluid are carried out over a wide temperature range to assess the saturation indices of minerals likely to have equilibrated with the reconstituted (deep) fluid. The clustering of saturation indices near zero ( $\log(Q/K) = 0$ , the value at equilibrium) for multiple minerals at any given temperature can then be inferred as a possible temperature of the deep fluid.

Table 3-6. Chemical composition of groundwater and geofluid used in geochemical modeling effort.

Component	Pad 29 Water Well	Pad 29 Water Well	NWG 55-29	East Lake Hot Spr. 5B <sup>s</sup>
Date	15 Oct 2010	2008	2008	1997
pH (lab)	7.97	7.85	8.3	6.3
Na	42	45.7	1360	54
K	5	4.72	120	8.3
Ca	19	20	15.3	72
Mg	24	24.9	3.36	34
Li	ND	< 0.1	ND	0.033
Sr	0.08	< 0.1	ND	0.36
Ba	0.008	0.064	2.62	0.004
Rb	0.012	ND	ND	NA
B	0.55	0.57	247	1.2
Al	ND	ND	ND	ND
Fe	ND	<0.05	7.98	0.004
Mn	ND	0.0089	1.14	1
F	0.5	0.582	7.75	NA
Cl	3.0	13.8	646	0.8
SO <sub>4</sub>	2.5	2.58	233	10
P	0.2	ND	ND	NA
SiO <sub>2</sub>	60	54.7	99.4	220
As	0.026	0.034	3.96	ND
Alkalinity	230	296	2930	450
CO <sub>3</sub> <sup>-2</sup>	ND	< 2.00	235	NA
HCO <sub>3</sub> <sup>-</sup>	230	296	1350	NA
NH <sub>3</sub>	ND	< 0.255	12	0.96

Concentrations mg/L except where noted. ND = not detected, NA = not analyzed  
<sup>s</sup>Morgan et al., 1997 (median values reported where applicable)

Table 3-7. Geothermometry of gas samples from well NWG 55-29 (from Geologica, 2010).

Geothermometry Method	Calculated Temperature (°C/°F)				
	Ptot = PCO2 by D'Am-P = 10 bar	PCO = Ptot = by mineral equilibria	Max WHP = 600 psig = 42 bar	Sat water @ 550°F = 72 bar	BHP- hydrostatic @ 550°F = 139 bar
Estimated Total Pressure					
Empirical (D'Amore & Panichi 1980)	225/438	229/445	248/479	265/509	321/609
Pyrite-Magnetite (Giggenbach 1980)	223/434	226/439	256/492	269/516	286/547
Pyrite-Pyrhotite (Giggenbach 1980)*	279/535	279/535	279/535	279/535	279/535
H <sub>2</sub> S (Giggenbach 1997)	209/408	213/415	248/479	265/509	286/548
Ammonia Breakdown (Giggenbach 1991)*	117/242	120/248	155/311	172/341	194/381
H <sub>2</sub> /Ar (Giggenbach 1991)*	291/556	291/556	291/556	291/556	291/556
H <sub>2</sub> /Ar-CO <sub>2</sub> /Ar grid (Powell 2000)	310/590	310/590	310/590	310/590	310/590
Average of Select Geothermometers*	293/560	---	---	---	---
Average of All Geothermometers	258/496	---	---	---	---

\*independent of gas/water considerations

These computations require knowledge of the amount of water vapor in the gas phase, as well as the relative proportion of liquid and gas in the discharge (the steam weight fraction). In the absence of these data, the steam weight fraction was inferred from the ratio of the chloride concentration reported in the earlier water sample from the Pad S-29 water well (13.8 ppm) to the chloride concentration in the fluid collected in the weir box (646 ppm). This assumes conservative behavior of chloride and a negligible contribution of chloride from a magmatic source. This approach yields a steam fraction of 0.9787. It should be noted that later groundwater samples from the Pad S-29 water well appear to have essentially the same composition as at the nearby Water Well #2 (Oregon Water Resources Department number DESC 10060), but a lower chloride concentration of about 3 ppm (Table 3-6). Therefore, we also performed computations using the lower chloride concentration, yielding a steam weight fraction of 0.9954. The application of these steam weight fractions thus assumes that the difference in the chloride concentrations in groundwater relative to the liquid from the weir box results from evaporative concentration (boiling) of local groundwater.

Using the steam weight fractions calculated in this manner, and recognizing associated assumptions and their uncertainty, the amount of water vapor in the gas phase was estimated by varying this parameter until the best clustering of mineral saturation indices near zero was achieved anywhere in the temperature range 150°-350°C (302°-662°F). The computations were carried out using a fluid-reconstitution and speciation code in development, designed specifically for geothermometry calculations, and derived from the TOUGHREACT code (Xu et al., 2006 and 2011). Thermodynamic data were taken from the database compiled by Reed and Palandri (2006).

Computations were first run using the lower steam fraction representing evaporative concentration of water from earlier samples of the Pad S-29 water well. In the absence of measured aluminum concentrations, computations were conducted assuming concentrations fixed by equilibrium with muscovite (Figure 3-32) or with kaolinite (Figure 3-33). In the first case, forced equilibration with muscovite, two groups of potential minerals are observed to loosely cluster at  $\log(Q/K)=0$  near 260°C (500°F) for the mineral assemblage chlorite-muscovite-paragonite-kaolinite-pyrrhotite-pyrite, with another loose clustering near 320°C (609°F) for epidote-anorthite-muscovite-paragonite-kaolinite-pyrrhotite. Note that each group separately (not both together) can be used to infer near-equilibration temperatures of the reconstituted fluid. In the second case, forced equilibration with kaolinite, one relatively good cluster is observed near 320°C (609°F) for the group epidote-siderite-anorthite-muscovite-paragonite-kaolinite.

Computations conducted using the higher steam fraction, derived from groundwater chloride concentrations of about 3 ppm, yielded a more dilute fluid that remained undersaturated with respect to essentially all potential formation minerals in the temperature range 150°-350°C (302°-662°F). This, and the fact that the steam weight fraction in the discharge and amount of water vapor in the wet gas were unknown and had to be estimated, emphasizes the uncertainty of the computation results shown here, and emphasize the need for very careful interpretation. Furthermore, computation results are quite sensitive to the assumed amount of water vapor in the wet gas, and the manual optimization of this value is likely to be non-unique. Nevertheless, it is interesting to note that potential equilibration temperatures inferred by Figure 3-32 and Figure 3-33 appear in line with the range of temperatures previously derived from gas geothermometers. If valid, these results would infer some degree of equilibration of the Pad S-29 well water used for drilling with the faster-reacting formation minerals, but undersaturation with slower-reacting formation minerals.

In summary, the well flow was not sustainable, and thus did not reach equilibrium flow conditions. Because of this, gas/steam and vapor/liquid ratios could not be measured accurately, so total mass flow fluid compositions are poorly constrained. Analysis of samples of the produced water indicates that it is

slightly modified groundwater introduced during drilling of NWG 55-29 and, thus, is not representative of deep, native fluids. In contrast, geothermometers based on the components of the gas samples results in calculated temperatures consistent with a geothermal gas in equilibrium with the hot rock in the well. In any case, the geochemical analysis above provides a methodology and baseline against which to compare water and gas samples produced during flowback at the end of EGS stimulation.

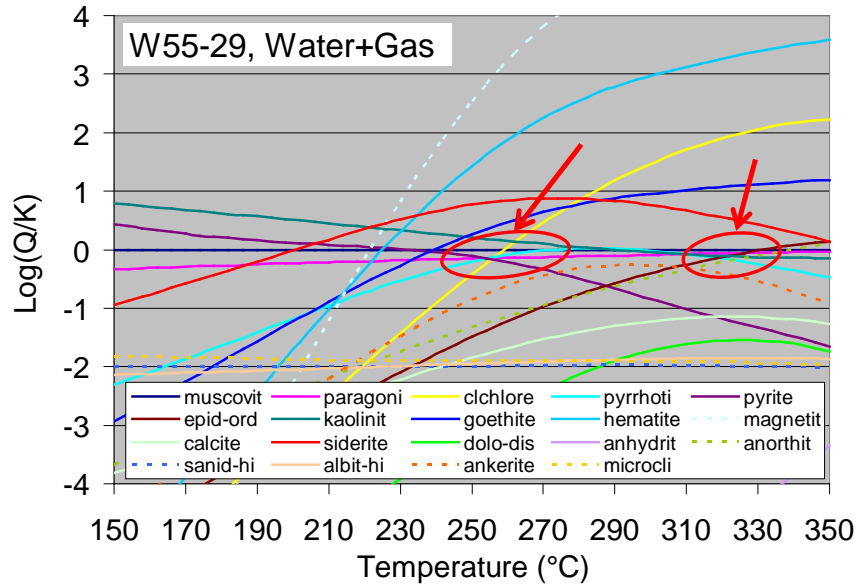


Figure 3-32. Computed mineral saturation indices, assuming equilibrium with kaolinite at all temperatures, and assuming a steam weight fraction of 0.9787 (see text). The mole fraction of water vapor in the (wet) gas is optimized to 0.9973 for maximum clustering of saturation indices near zero in the temperature interval shown. Arrows indicate clustering areas representing potential near-equilibration temperatures.

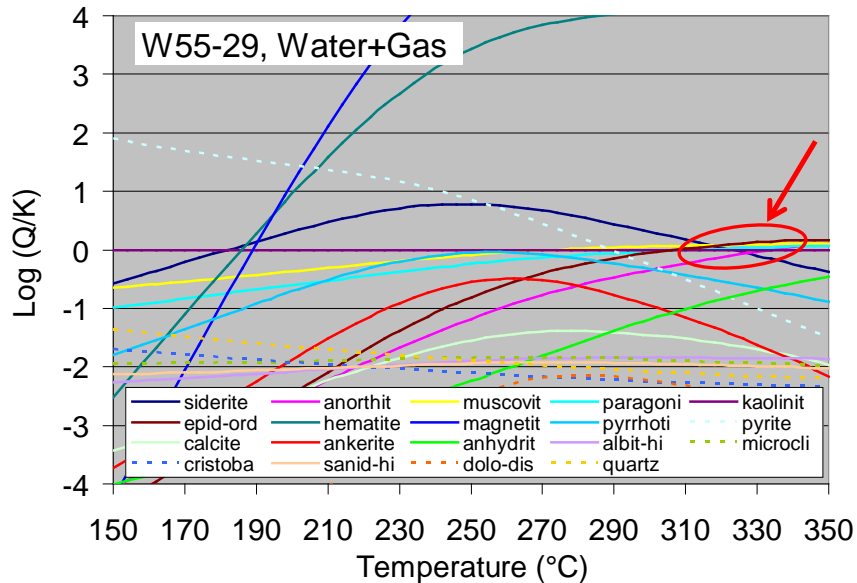


Figure 3-33. Computed mineral saturation indices, assuming equilibrium with muscovite at all temperatures, and assuming a steam weight fraction of 0.9787 (see text). The mole fraction of H<sub>2</sub>O vapor in the (wet) gas is optimized to 0.9990 for maximum clustering of saturation indices near zero in the temperature interval shown. Arrow indicates clustering area representing potential near-equilibration temperatures.



### 3.2.7.7 PRIMARY AND ALTERATION MINERALOGY

Mineral assemblages are characterized according to their origin as either those that were present at the time of emplacement of the lavas, intrusion, pyroclastics, etc (i.e., primary) or those that formed during subsequent hydrothermal alteration or other effects of burial or groundwater interaction. The minerals chosen for the THC model simulations (Table 3-8) are based primarily on detailed studies of hydrothermal alteration by Keith and Bargar (1988) and Bargar and Keith (1999), and on recent mud log descriptions from drill hole NWG 55-29. However, availability of thermodynamic data for minerals or their endmembers dictate which minerals can be included in the analysis, and substitutions may be made of similar minerals. The list evolves over time as the applicability of the thermodynamic data for certain minerals is tested by simulation and comparison to well-constrained field and laboratory data. Also, as more data is gained from field studies of fracture mineralogy the list may also change, especially with respect to minor phases that may control certain isotopic systems, or changes induced by stimulation/injection that result in effects unlike that of the natural system.

In the current mineral description, the solid solution phases are represented as their endmembers (e.g., chlorite is represented as clinocllore and daphnite). This is usually easier numerically than treating minerals as solid solutions, but potentially leads to unrealistic mineral assemblages.

Distributions of minerals were not tied to specific flows or intrusives and were just assigned to roughly approximate the average bulk composition of the units. The units with more basaltic rocks were given larger proportions of pyroxenes, plagioclase, and magnetite, whereas tuffs and rhyolitic rocks assigned more sanidine and cristobalite with fewer mafic minerals. The "Intruded John Day", having extensive intrusion of granodiorites, was assigned more quartz, microcline, and muscovite with less mafic minerals because of the fewer basaltic rocks in this unit. This will be updated as the model is refined, but for the first set of simulations the goal was just to capture the overall behavior of the system.

**Table 3-8. List of Primary and Potential Secondary Minerals in the THC model.**

Primary Minerals		Potential Secondary Minerals			
Albite	Phlogopite	Calcite	Quartz	Kaolinite	Analcite
Anorthite	Annite	Siderite	Microcline	Epidote	Magnetite
Microcline	Muscovite	Ankerite	Muscovite	Daphnite	Hematite
Sanidine	Quartz	Dolomite	Paragonite	Clinocllore	Goethite
Diopside	Cristobalite	Anhydrite	Illite	Heulandite	Pyrite
Hedenbergite	Magnetite	Chalcedony	Ca, Mg, Na & K Nontronite	Laumontite	Pyrrhotite

### 3.2.7.8 THERMODYNAMIC AND KINETIC DATA FOR REACTIONS

Thermodynamic data for THC simulations was derived from the SOLTHERM database (Reed and Palandri, 2006). This database has been specifically developed for the study of hydrothermal alteration over more than 30 years, and was used for the geothermometry calculations presented in Section 3.2.7.6. Other thermodynamic databases were also evaluated (e.g., THERMODDEM, Blanc et al., 2007), but were not as complete for these mineral assemblages and temperatures.

Kinetic data were derived from various sources (e.g., Palandri and Kharaka, 2004) or assumed to be the same as similar minerals. Reactive surface areas were estimated to be in the range of 1-20 cm<sup>2</sup>/g mineral, typically less for primary minerals and greater for secondary minerals. These data will be updated once fracture spacings and surface areas are measured or estimated, in addition to having a more detailed geologic model.

### 3.2.7.9 *SIMULATED FLUID AND GAS GEOCHEMISTRY AND MINERAL ALTERATION*

Several types of simulations were performed to evaluate the thermal, hydrological, and chemical factors leading to the observed mineral alteration distribution. The simulations are in their early stages and the results shown here can only be considered as preliminary.

Two-dimensional reaction transport simulations were performed assuming an initial unaltered mineral assemblage, steady-state fluid flow (Figure 3-29), and the fixed steady-state temperature distribution (Figure 3-30). Thus, only the primary minerals in Table 3-8 were present at the initiation of the simulation.

For this first set of 2-D simulations it was assumed that there is no flux of magma-derived fluids or gases. A parallel set of simulations was performed in 1-D to evaluate the effect of different CO<sub>2</sub> and SO<sub>2</sub> fluxes on the fluid geochemistry and mineral alteration distribution as a function of temperature and depth.

As all the minerals are described by kinetic rates of reaction, the mineral distributions and assemblages change significantly over time. The 2-D simulation discussed in this report was run for 1000 years, but from other 1-D simulations it was found that the mineral distributions change significantly over several thousands of years. However, after 1000 years, the mineral assemblages and their locations tend to stabilize compared to the first few hundred years where minerals disappear and reappear at different depths.

Dissolution of plagioclase, sanidine, cristobalite, and pyroxenes (diopside and hedenbergite) dominate at the depths of the planned EGS reservoir (Figure 3-34). Plagioclase (albite and anorthite) alteration (as changes from the initial volume %) is particularly intense in the temperature range of 240° to 290°C. Cristobalite is generally unstable in the rhyolitic/tuffaceous rocks and is replaced by the more stable silica polymorph, quartz. In contrast to the other primary minerals, sanidine becomes unstable at the higher temperatures and depths, above about 260°C. The alteration regions are clearly controlled primarily by temperature, but the extent of dissolution is governed by the lithology. Thus, it will be important to add the detailed lithology into the model domain in order to evaluate the native state and to make predictions on the effects of stimulation and eventually injection/production.

Now that the effects on primary mineral dissolution have been shown, the secondary mineral alteration assemblage is described. Within the granodiorite-intruded lavas and tuffs at the depths of the proposed EGS reservoir there is considerable precipitation of quartz, epidote, chlorite (clinochlore and daphnite), and heulandite (Figure 3-35). In the mud log from the NWG 55-29 drill hole quartz, epidote, and chlorite are the most commonly observed fracture filling and alteration phases at temperatures over 230°C. On the plot of epidote distributions, the observed epidote locations in NWG 55-29 are plotted along the borehole in green. Except for a minor occurrence at a temperature of 207°C, the epidote is distributed from about the 230°C isotherm to the base of the well, as in the simulated distribution. There is another band of epidote that appears in the 120°-140°C region in the model, but this appears to be an early "metastable" region, since this band was in the process of disappearing by the time the simulation reached 1000 years. Chlorite is a widely seen alteration mineral as in the drill holes and described as interlayered chlorite-smectite at shallower depths and chlorite at temperatures exceeding about 140°C (Bargar and Keith, 1999). The simulated chlorite distribution is primarily clinochlore and is distributed over nearly the entire domain, with the greatest abundances in the basaltic rocks at the base of the Newberry-Deschutes where temperatures are highest. Overall, temperature and primary lithology are the overall controls on the alteration mineral distribution.

Abundant heulandite is seen in the simulation, where little is observed in the drill hole studies. This discrepancy is likely the result of the low PCO<sub>2</sub> developed in the system and the destabilization of calcite relative to heulandite. After 1000 years, calcite precipitation is localized in the uppermost kilometer, yet

earlier in the simulation had precipitated at much greater depths and temperatures and then redissolved as the  $\text{PCO}_2$  declined.

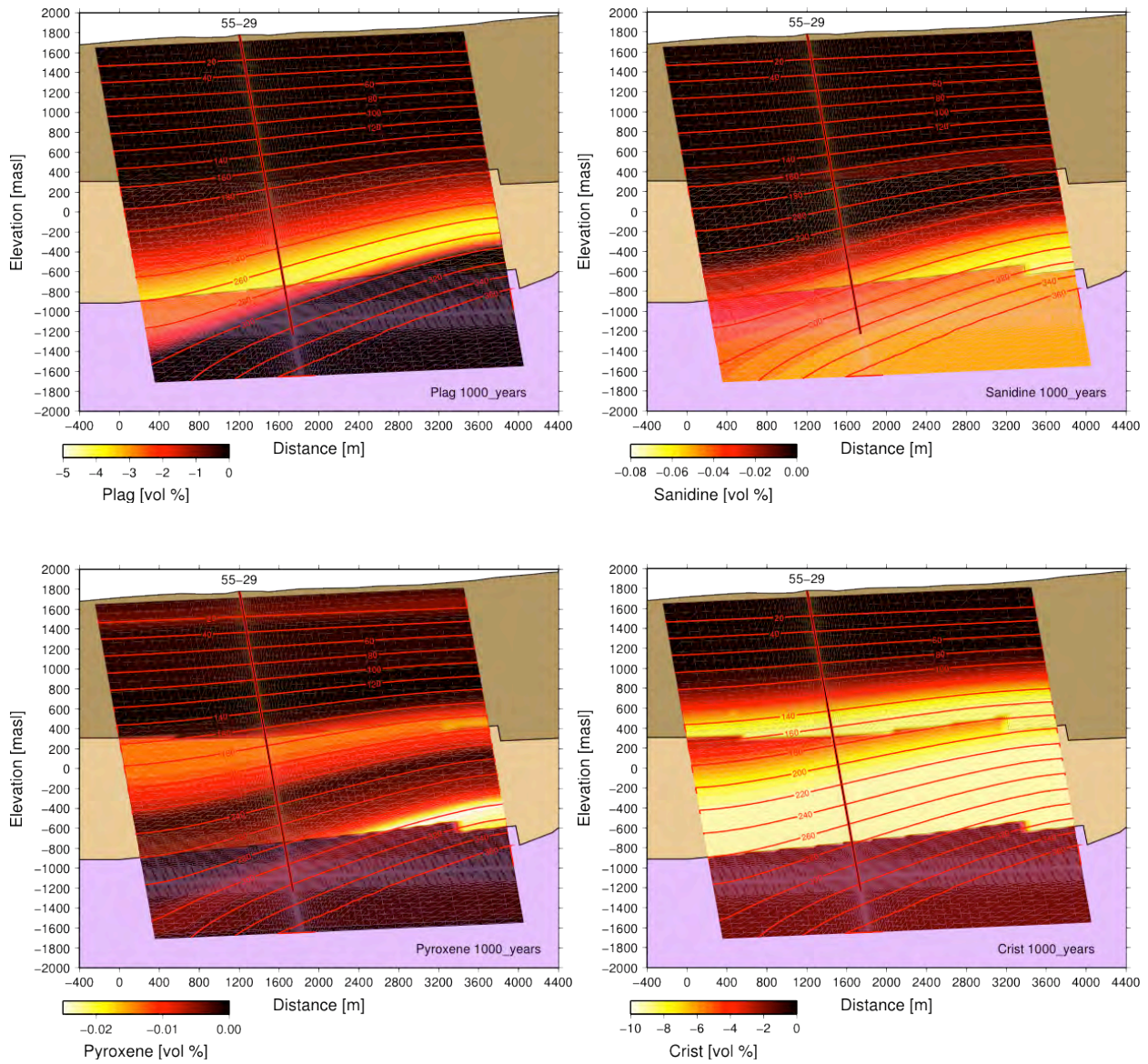


**Figure 3-34.** Simulated distribution of mineral dissolution (volume % change) after 1000 years. Temperature contours are overlain and lithology is shown underlying the model domain. Upper left - plagioclase (albite + anorthite), upper right - sanidine, lower left - clinopyroxene (diopside + hedenbergite), and lower right - cristobalite.



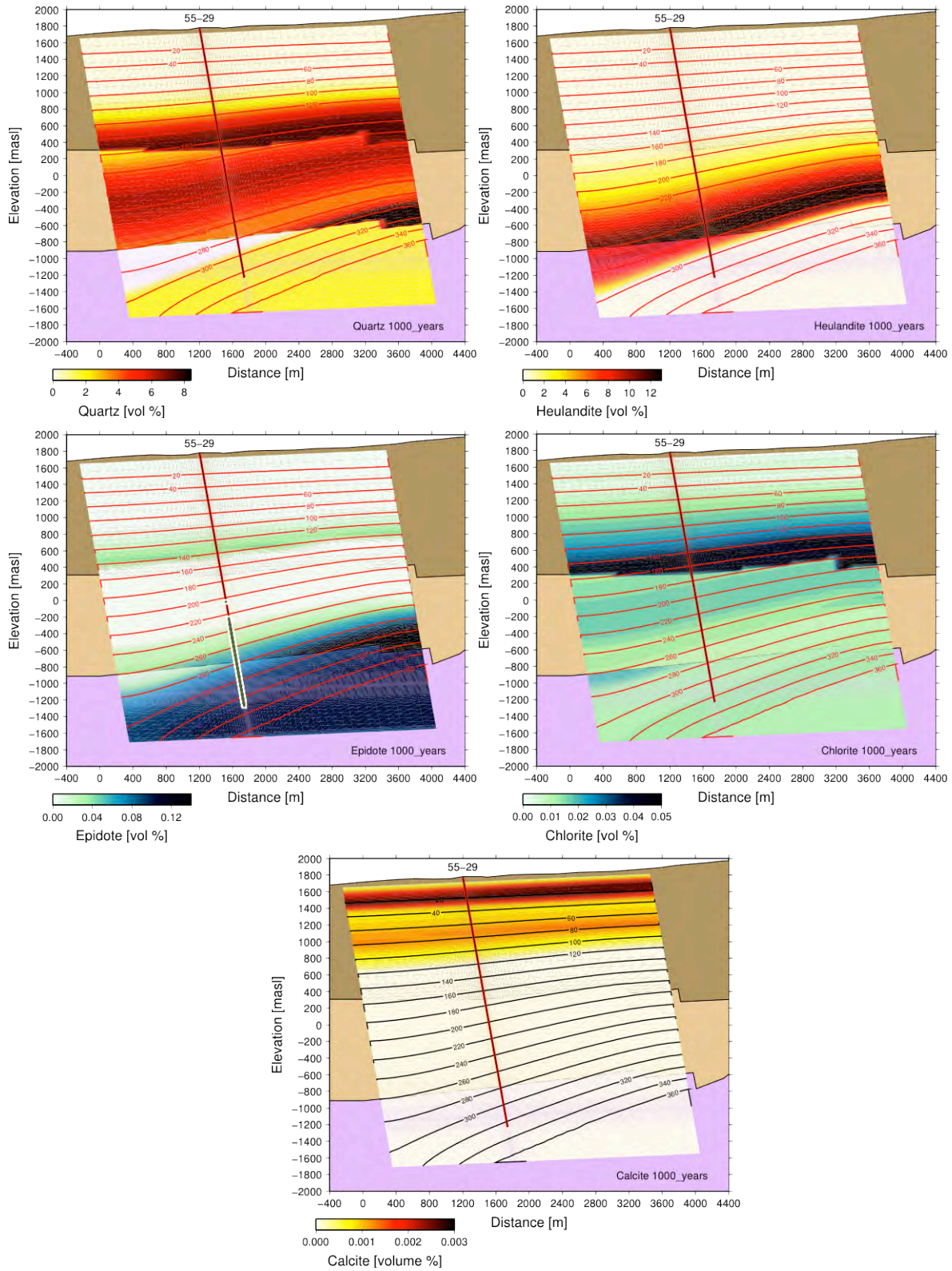


Figure 3-35. Simulated distribution of mineral precipitation (volume %) after 1000 years. Temperature contours are overlain and lithology is shown underlying the model domain. Upper left – quartz, upper right – heulandites, middle left – epidote, middle right – chlorite, and bottom - calcite.



The potential regions of permeability changes by hydrothermal alteration was evaluated using the Carman-Kozeny model for permeability as a function of porosity change (Xu et al. 2005), as follows:

**Equation 3-1**

$$k = k_i \frac{(1 - \phi_i)^2}{(1 - \phi)^2} \left( \frac{\phi}{\phi_i} \right)^3$$

where  $k_i$  and  $\phi_i$  are the initial permeability and porosity, and  $k$  and  $\phi$  are the values at the current time.

Since we do not have details of the mineral surfaces in rock fractures and the rock matrix yet, and the time frame for mineral alteration is unconstrained, the absolute changes are not meaningful. However, the locations of significant permeability changes may be useful as an indicator of the permeability distribution in the hydrothermal system (Figure 3-36). The largest change in permeability is in the temperature range of 230° to 290°C, with reductions of about 2.5 orders of magnitude (blue region). This permeability reduction is due to the primarily to the combined effects of quartz, epidote, chlorite, and heulandite precipitation.

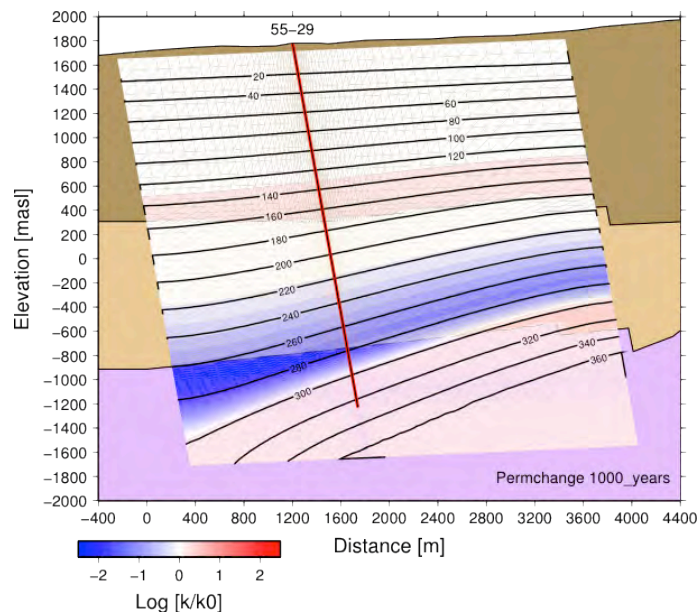


**Figure 3-36. Simulated change in permeability ( $\log k/k_0$ ) after 1000 years.**

Permeability increases are much smaller, with a maximum of only a factor of two, and are located in the regions of 130°-180°C and for greater than 300°C. These small increases are due primarily to K-feldspar (sanidine and microcline) and pyroxene dissolution.

As was noted earlier, whereas the silicate mineral alteration assemblage roughly captures the observed alteration phases at depth (quartz + epidote + chlorite) some inconsistencies in the modeled mineral assemblages include the lack of calcite and pyrite and the addition of substantial heulandite not observed at these depths. The lack of calcite at depth is clearly due to the strong reduction in the partial pressure of  $\text{CO}_2$  over time, as there is no external source of  $\text{CO}_2$ , except from groundwater near the surface. The lack of pyrite is also likely due to the lack of volcanic gas added to the system (i.e.,  $\text{SO}_2$  and  $\text{H}_2\text{S}$ ). As a simple evaluation of the fluid composition necessary to result in the appearance of calcite and pyrite along with the effects on the entire mineral assemblage, the lower boundary water was modified by successively effectively equilibrating it with  $\text{CO}_2$  and  $\text{SO}_2$  gas. This boundary fluid then was allowed to interact by aqueous diffusion with a single basal grid block (Intruded John Day) set at 327°C, so that the fluid chemistry could change slowly and the mineral assemblage change owing to the increasing flux of  $\text{CO}_2$  (as  $\text{HCO}_3^-$ ) and  $\text{SO}_2$  (as a reaction involving  $\text{SO}_4^{2-}$  and  $\text{HS}^-$ ). Eventually, pyrite and calcite form, in

addition to muscovite, quartz, epidote, clinochlore, daphnite, analcite, and minor hematite (Figure 3-37).

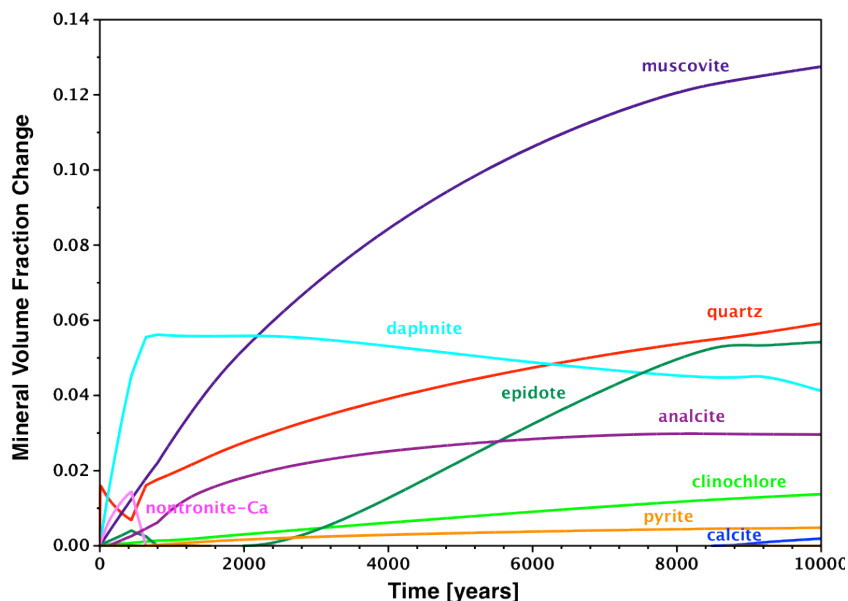


Figure 3-37. Time evolution of precipitating alteration minerals in rock (Intruded John Day) at 327°C as CO<sub>2</sub>- and SO<sub>2</sub>-equilibrated fluid diffuses into it.

When a better estimate of the gas-water ratio in the system is known and the model can be set up as a multiphase system with contribution of the magmatic gas component, the model will be better constrained in terms of the overall reaction rate of the system (including knowing the fracture-matrix surface area). From this and other scoping simulations, a magmatic gas component is clearly necessary to obtain the mineral assemblages observed in the high-temperature regions.

### 3.2.7.10 PLANNED THC MODEL ENHANCEMENTS

For the thermal-hydrological basis of the THC model, dual-continuum and discrete fracture modeling approaches will be employed once a model of fracture densities and orientations become available. The model will also be extended to consider multiphase flow owing to the likely vapor-dominant character of the geothermal system. Consideration will be made to extending TOUGHREACT to consider supercritical water if funding from other projects becomes available.

It will be important to refine the initial lithologic distribution, porosities, and mineralogical variations particularly for permeable zones and fractures. With the dual-permeability formulation, mineralogical data can then be assigned to the rock matrix and the fracture fillings and coatings as in Sonnenthal et al. (2005). In concert with the improved mineralogical description all thermodynamic and kinetic data will be reevaluated and tested against field and laboratory data. Once details of the fracture distribution are known, then apertures can be estimated and the permeability law using effective hydraulic aperture in TOUGHREACT can be utilized.

Following the extension of the flow model to multiphase water-water vapor, then gas species transport will be added for the important noncondensable and reactive gases (i.e., Ar, N<sub>2</sub>, CO<sub>2</sub>, SO<sub>2</sub>, HCl, HF, and H<sub>2</sub>). For analysis of stimulation, injection and production, other gas species, tracers, and isotopic systems will be added, such as <sup>3</sup>He/<sup>4</sup>He, <sup>18</sup>O/<sup>16</sup>O, D/H, and <sup>13</sup>C/<sup>12</sup>C (as in Dobson et al., 2006). In the aqueous phase and minerals, oxygen isotopes will be incorporated to further refine the model to use the calculated extent of reaction from Carothers et al. (1987) as another constraint to the effective reaction rates at

differing temperatures, fluid compositions, and lithologies. Sr isotopic studies of primary volcanic lithologies from Newberry Volcano (Goles and Lambert, 1990) and alteration mineralogy can also be used to provide constraints on rates of water-rock interaction especially for stimulation predictions.

### 3.2.8 FRACTURE ANALYSIS

#### 3.2.8.1 BOREHOLE IMAGE LOGGING

Natural fractures play a critical role in developing an EGS reservoir in low permeability rock because the combination of slightly greater than background permeability and inherent rock weakness enhances interaction with the stimulation fluid. Hydroshearing takes advantage of these properties, with water invading the fracture, reducing effective normal stress, and inducing slip. If slip is accompanied by dilation, permeability will be enhanced in the near-field environment along the stimulated fracture, facilitating flow of fluid into the far-field and stimulating the natural fracture network at depth. This process can provide a positive feedback, diverting fluid into the extending permeable network as resistance to flow is decreased. This tendency can be controlled, using carefully selected diverter products, to engineer multiple stimulated volumes in a single well bore.

The behavior of natural fractures and the likelihood of slip and dilation during stimulation strongly depend on properties of the natural fracture population, such as geometry (i.e., orientation, hydraulic aperture, and connectivity), minerals occurring within and around the fractures, the combination of the pressure applied, and the *in situ* stress state driving deformation. To evaluate the potential for stimulation and develop a robust stimulation strategy we must establish several characteristics of the fracture population intersecting the NWG 55-29 borehole including:

- the distribution of natural fractures or other planar discontinuities in the rock mass
- the attitude of natural fractures with respect to the stress state (which will control their propensity for shear failure)
- the mineralogy of the intervals containing the natural fractures, which strongly correlates with their frictional resistance to shearing (Lockner and Beeler, 2002) and the potential for dilation (Paterson and Wong, 2005; Davatzes and Hickman, 2009)
- geometric characteristics which might indicate the relative importance of individual fractures
- *in situ* permeability that will provide access for stimulation fluids to enter fractures, reduce the effective normal stress, and induce slip

To accomplish these tasks, analysis of cuttings and physical property logs are combined with a BHTV log which is capable of both determining the depth and attitude of natural fractures. Details of the BHTV logging operation in NWG 55-29 are provided in Section 3.2.4.7 and Appendix C-5. The complete mud log for NWG 55-29 is provided in Appendix C-6. We note here that field calibration of the tool revealed that the BHTV accelerometer used to orient the acoustic images of the borehole wall was inadvertently installed upside down on the electronics board prior to logging, resulting in a uniform error in the log. Formulas to correct this error are also provided in Appendix C-5. Comparison of the corrected BHTV deviation and the single-shot deviation log (Figure 3-38), confirms that the correction was successfully applied to the BHTV data allowing proper orientation of the image log and recovery of fracture attitudes.

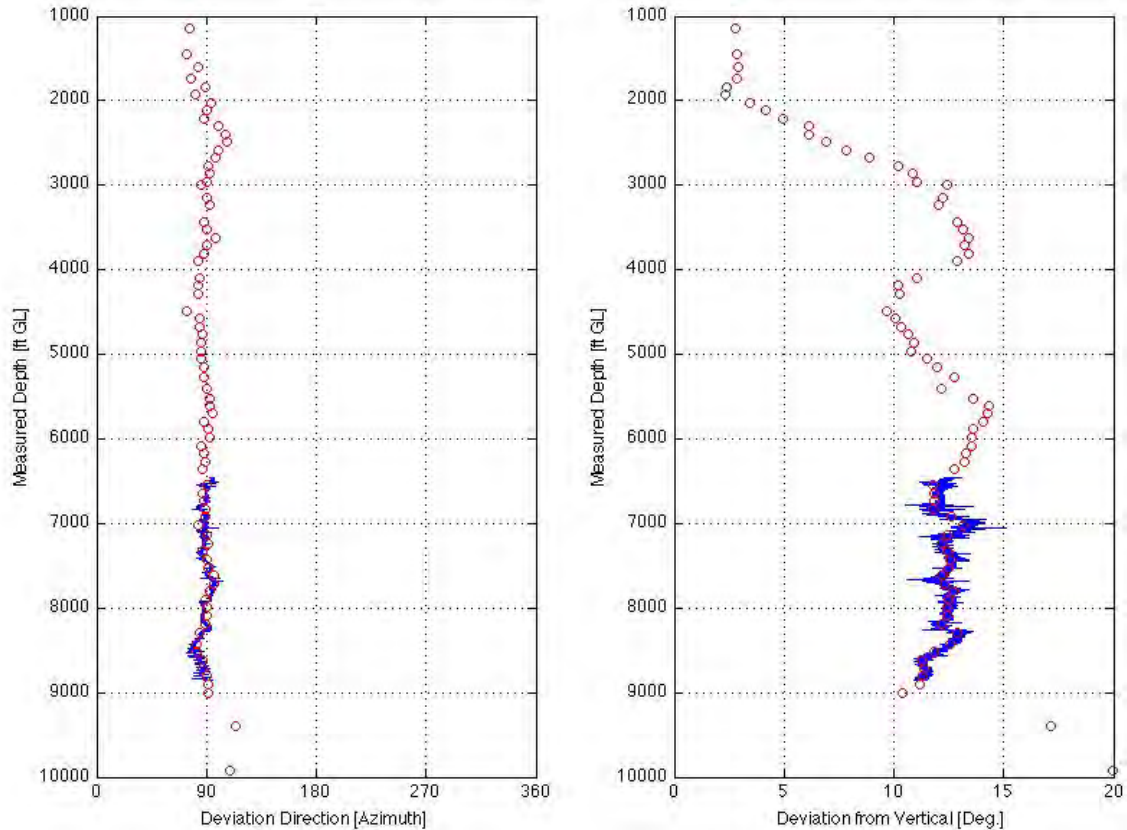


Figure 3-38. Single-shot deviation azimuth (left) and deviation direction (right), shown by open circles, compared with the corrected borehole televiewer telemetry, shown in blue.

Prior to logging, an inject-to-cool program was initiated to extend the maximum depth of the BHTV log because the equilibrated (pre-cooled) bottom-hole temperature is above the rated tool capability. The inject-to-cool operation, which was conducted at moderate wellhead pressures, was initiated 22 September 2010 and ran intermittently until 22 October 2010. Injection of cold groundwater continued during the logging operation to maintain the lower temperature that was achieved.

### 3.2.8.2 FRACTURE IDENTIFICATION

In BHTV images, fractures are revealed by the roughness they impart on the borehole wall. Although an image log can reveal hairline fractures, the relative density of fractures, roughness of the adjacent borehole surface, mineral filling, and overlap among different types of planar structures (e.g., fractures versus bedding) can impact whether a fracture is visible in the acoustic image. Previous studies have shown that the total number of fractures identified in image logs is smaller than are visible in core from the imaged interval (Genter et al., 1997). This bias in detection is toward relatively open fractures, or fractures with strength significantly different than the surrounding rock. However, although every fracture might not be detected, the relative density, and a sampling of fracture attitudes, can be determined.

The image log obtained in NWG 55-29 reveals extensive, shallowly dipping layers corresponding to volcanic flow boundaries, foliation and lithologic transitions. Petrographic analysis of cuttings from this borehole, and core from the nearby GEO N-2 borehole, indicate that these layers consist of extrusive volcanic basalt, andesite, rhyolite and dacite, and related tuffs as well as intrusive felsic dikes. At approximately 2624 m (8610 ft) there is a sharp transition to massive granodiorite that continues to the



total depth of the BHTV log at 2609 m (8860 ft). The mud log shows that granodiorite is not continuous to the total depth of the well. In the log, the volcanic layers are cut by natural fractures, with dips consistent with normal faulting, and similar to dips observed in core from the nearby GEO N-2 (total depth 1337 m [4386 ft]). A smaller number of natural fractures occur in the underlying granodiorite.

Planar structures intersecting the borehole were assigned attributes of type, measured depth, dip direction, dip angle, and thickness. Eight categories of natural geologic structures are distinguished by interpretation of the image log (Table 3-9). These structures provide a qualitative designation of the significance of each planar structure, roughly falling into either primary structures, such as bedding/banding/foliation (Figure 3-39 and green traces in Figure 3-40), lithologic contacts (Figure 3-39 and blue traces in Figure 3-40), dikes (dark gray traces in Figure 3-40), and fractures (Figure 3-39 and magenta (A) and gray (C) traces in Figure 3-40). In addition, the depth, attitude and apparent thickness of all structures are measured during log interpretation.

In addition to the interpretation of the geologic significance of planar structures intersecting the borehole, two quality control criteria were used in evaluating the image log. First the quality of the image log is assessed as high, medium, low, or unusable (Table 3-10). The image log quality provides a tool for assessing whether low fracture density is geologically significant or simply an artifact of poor data quality. Reduced image quality can result from a rough borehole surface, enlargement of the borehole, and decentralization of the BHTV. Second, the certainty in both the type of structure identified and the precision of the measured attitude are assessed and assigned values of A - unequivocal, B - interpretive, and C - poor (Table 3-11).

**Table 3-9. Structure types distinguished by BHTV image log.**

ID No.	Name	Description	Count
0	Undifferentiated	undifferentiated fracture	229
1	Major Joint/Fracture: Amplitude plus travel time	well-developed fracture with apparent aperture/thickness, often with clustered damage; visible in amplitude and travel time logs	8
2	Minor Joint/Fracture: Amplitude plus travel time	minor fracture with significant apparent aperture; visible in amplitude and travel time logs	114
3	Broken/Rubble/Breccia	---	0
4	Fracture/Joint: Amplitude	minor fracture or joint; only visible in amplitude log	0
5	Bedding/Banding/Foliation	planar structures within lithologic unit (bedding, foliation, flow structure, etc.)	111
6	Lithologic Contact	boundary between units (gradational contacts not picked)	44
7	Igneous Dike	boundary of igneous dike, most dikes will be identified twice - top and bottom	26

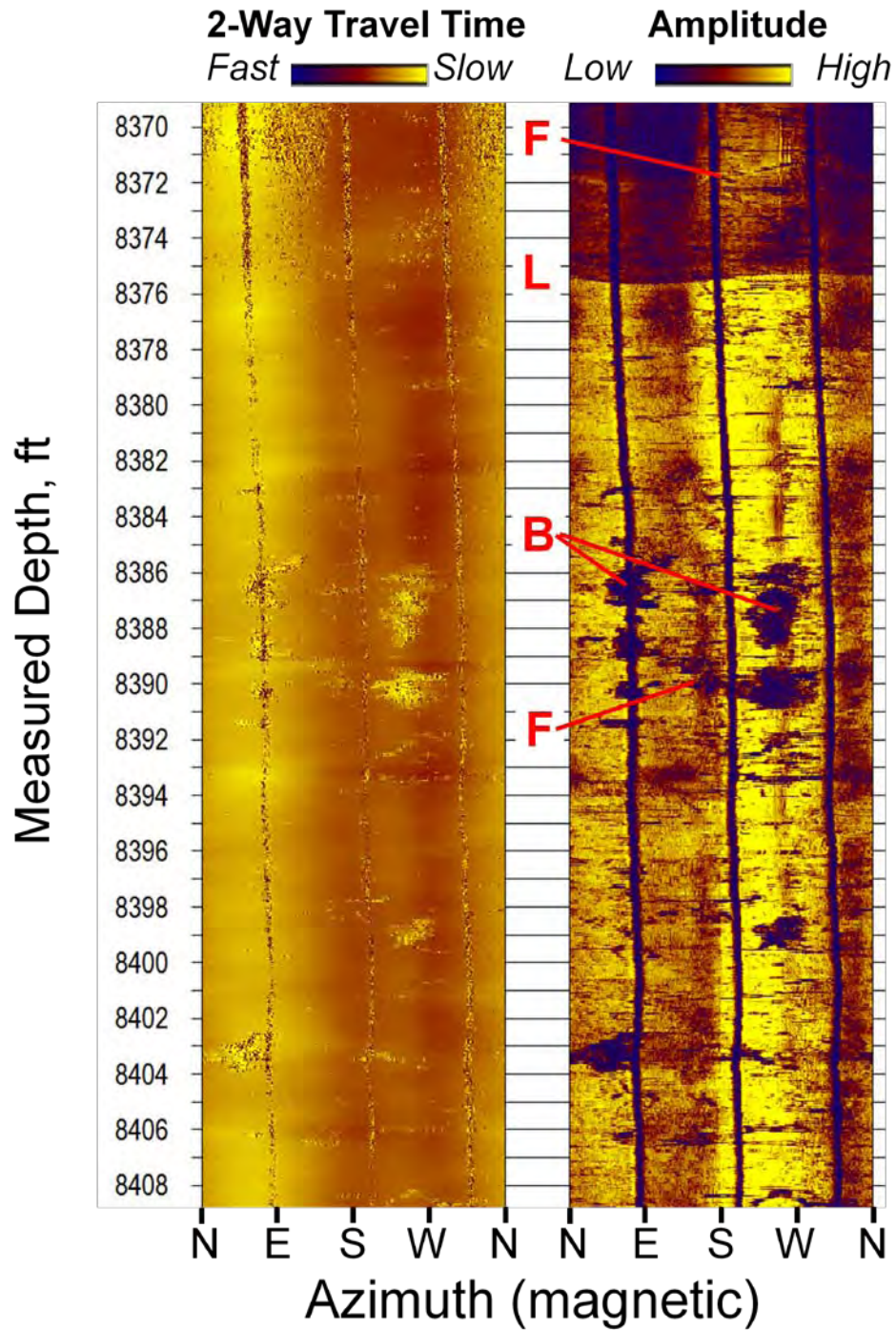


Figure 3-39. Unwrapped images of the travel time and amplitude signals recovered from NWG 55-29. Sinusoidal Natural Fractures (F) are generally subtle, the Lithologic Boundary (L) is indicated by an abrupt transition in amplitude, and breakouts (B) occur as patches of low amplitude (see discussion below). The three dark bands at 120° increments are from the harness that helps secure the piston assembly at the bottom of the tool, below the acoustic window, to the rest of the tool.

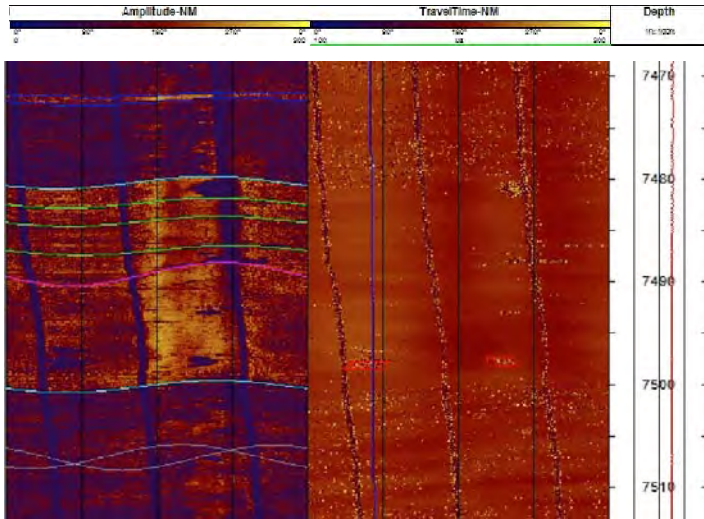
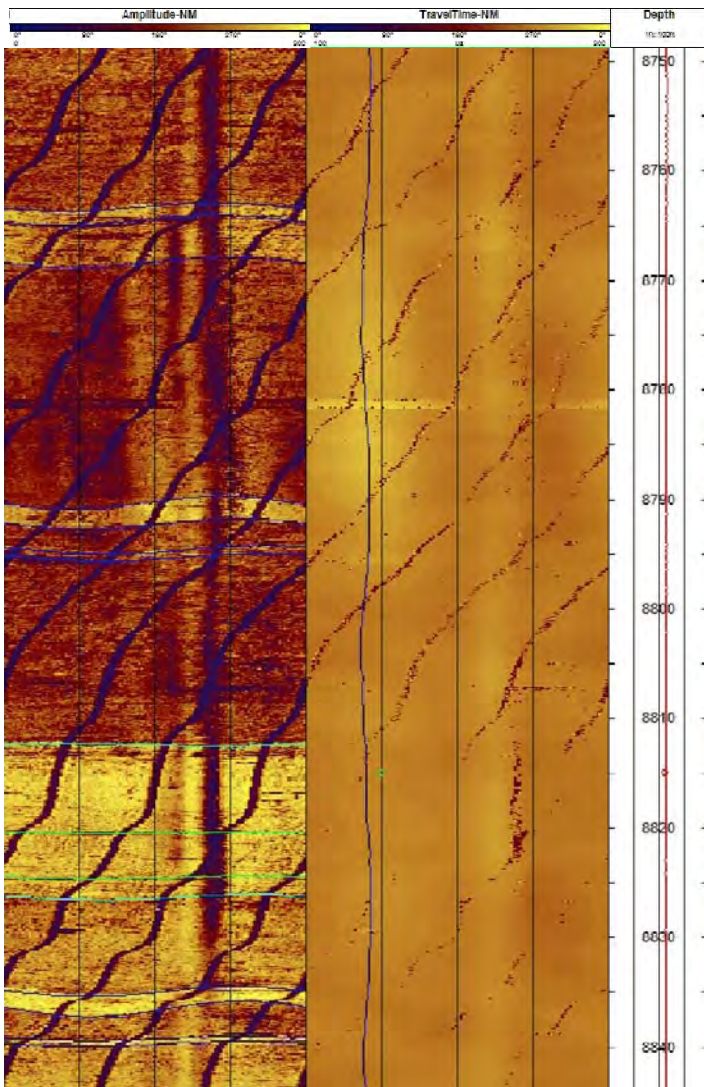


Figure 3-40. (top) Examples of interpreted logs from two depth intervals including: natural fractures (magenta) revealed by locations of data loss; lithologic transitions (blue) revealed as differences in relative amplitude and 'roughness' of the borehole wall as revealed both by amplitude and data drop-out; and, layering within lithologic units (green) traces.



(bottom) Image corresponding to the transition to crystalline intrusives including a series of shallowly dipping dikes. Depths are measured depth from 1.2 m (4 ft) above ground level (GL) and azimuthal orientation is relative to Magnetic North.



**Table 3-10. Image log quality ranking.**

Quality	Description
High	Can pick fractures reliably even if closely spaced, breakouts and tensile fractures evident
Medium	Can pick fracture attitudes accurately and identify breakout pairs
Low	Fractures missed or difficult to interpret, breakout might be evident, but only on one side of the hole
Unusable	Image quality is too poor/noisy to interpret structures

Notes: In all cases, extensive breakout can cause a degradation of the image, reducing the ability to identify natural fractures, thus lowering the quality level. In all cases, well-developed fracture zones can cause a degradation of the image, reducing the ability to identify breakouts and also discern the attitude of the zone, thus lowering the quality level.

**Table 3-11. Quality ranking of fracture interpretation, and number of observed fractures identified in each rank.**

Rank	Description	Count
A	Unequivocal interpretation and attitude: complete trace in at least travel time or amplitude	42
B	Requires some interpretation, traces extend over > 50% of borehole and include at least the peak or trough of the sinusoid	155
C	Requires extensive interpretation, sinusoidal trace extends over < 50% of borehole	335

### 3.2.8.3 FRACTURE ANALYSIS

In this subsection, the data set of 351 fractures in the 739 m (2425 ft) logged interval is analyzed by a methodology designed to provide the inputs to a discrete fracture network (DFN) model. To build a DFN model, the geologist must provide models or statistical descriptions of fracture density, zonation, attitude, size and aperture. In addition, because there is evidence that dikes and intrusives in the lower portion of the borehole were the sites of mud losses during drilling and injected water loss, the characteristics of dikes are also analyzed.

### 3.2.8.4 FRACTURE DENSITY

The 351 natural fractures identified in the BHTV log are distributed throughout the logged interval. Lower fracture densities occur just below the casing shoe and in the deep granodiorite intrusive at the base of the image log, whereas the volume immediately above the granodiorite shows the highest fracture and dike density. The fracture density is divided into four zones with distinct density characteristics (Figure 3-41). The boundaries between these zones are also based on geologic and drilling characteristics of the zones, which are summarized at the end of this section.

In the first 91 m (300 ft) of the open hole (Zone A – 1966-2057 m [6450-6750 ft]), only five fractures were identified on the BHTV log, a remarkably low fracture density. The typical well completion goal of installing the casing shoe in competent rock seems to have been well-achieved. The apparent lack of fracturing near the casing shoe will also be an advantage during the stimulation as hydroshearing will be unlikely to occur in a zone with so few fractures.

The fracture density in the next 381 m (1250 ft) of the open hole (Zone B – 2057-2423 m [6750-7950 ft]) is moderate, averaging 14.8 fractures/100 ft, but highly variable from 2 fractures/100 ft to 28 fractures/100 ft. Between 2423-2590 m (Zone C – 7950-8500 ft), the fracture density is consistently higher (average 28.2 fractures/100 ft), with one 100 ft zone with 53 fractures identified. Below 2590 m (Zone D – >8500 ft), the fracture density drops to an average of just 9.3 fractures/100 ft.



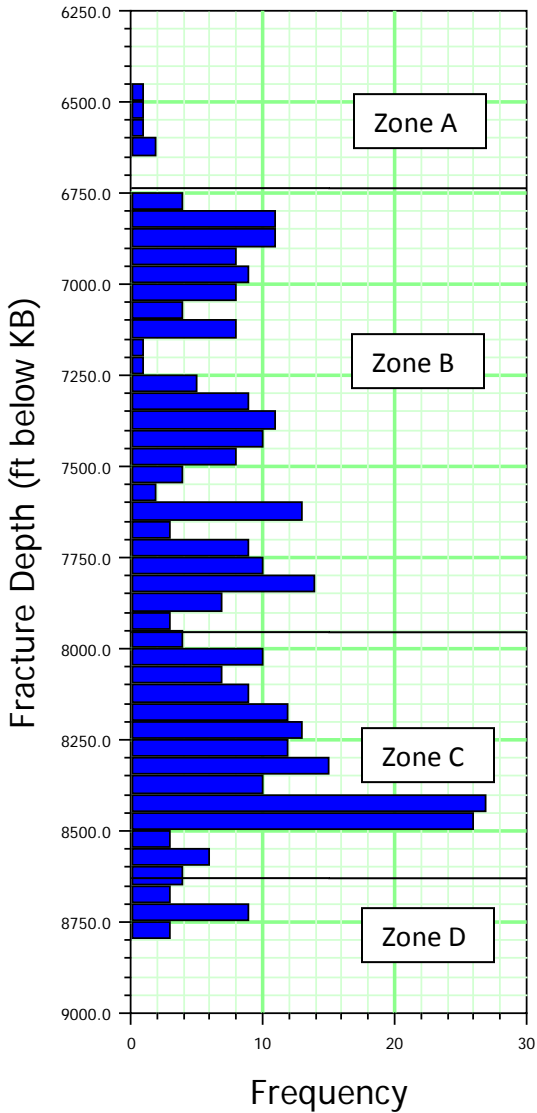


Figure 3-41. Number of fractures in 50-foot bins (intervals) and definition of boundaries of Zones A-D.

### 3.2.8.5 FRACTURE ORIENTATION

The volcanic and igneous layers identified in the BHTV dip up to 50° to the east and west, with more dips to the east than west (Figure 3-42). The volcanic rocks at this depth, pre-date the current Newberry edifice. The relatively steep dips of the layers could be explained by deposition on steep cinder cones, or rotation of the volcanic strata by pre-Newberry volcanic or tectonic activity, or Newberry related caldera collapse. Similar dips have been identified in other wells including CEE 76-15 TCH and were interpreted as deposition on cinder cones.

The fractures identified in the BHTV have a wide variety of strikes and dips. The dominant strike direction is NNE, which is within 15° of the average trend of regional normal faults, and consistent with the direction of horizontal stresses from regional normal faults (Figure 3-43; Cladouhos et al., 2011a) and from borehole analysis (see Section 5.4). The median dip is 60°, also consistent with a normal faulting regime. There are more east-dipping (toward-the-caldera) fractures (40%), than west-dipping

fractures (30%), observed in the well bore (Figure 3-44), with the remaining 30% of fractures poorly oriented for normal faulting in the current stress regime.

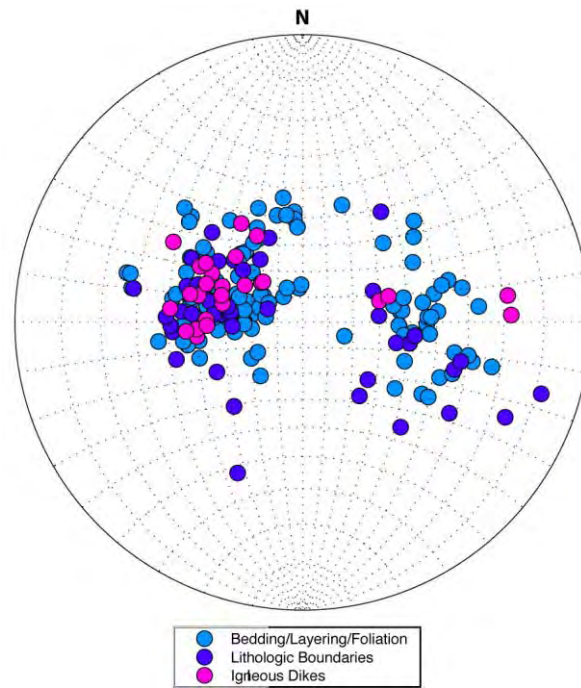


Figure 3-42. Equal area stereogram of the poles to layers identified in the BHTV image

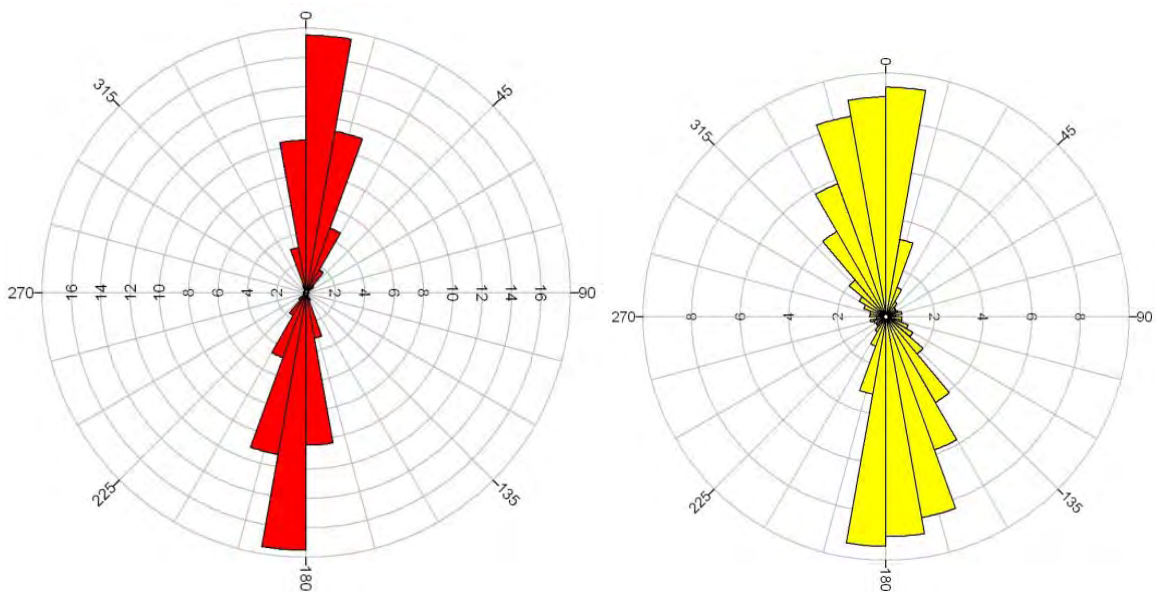
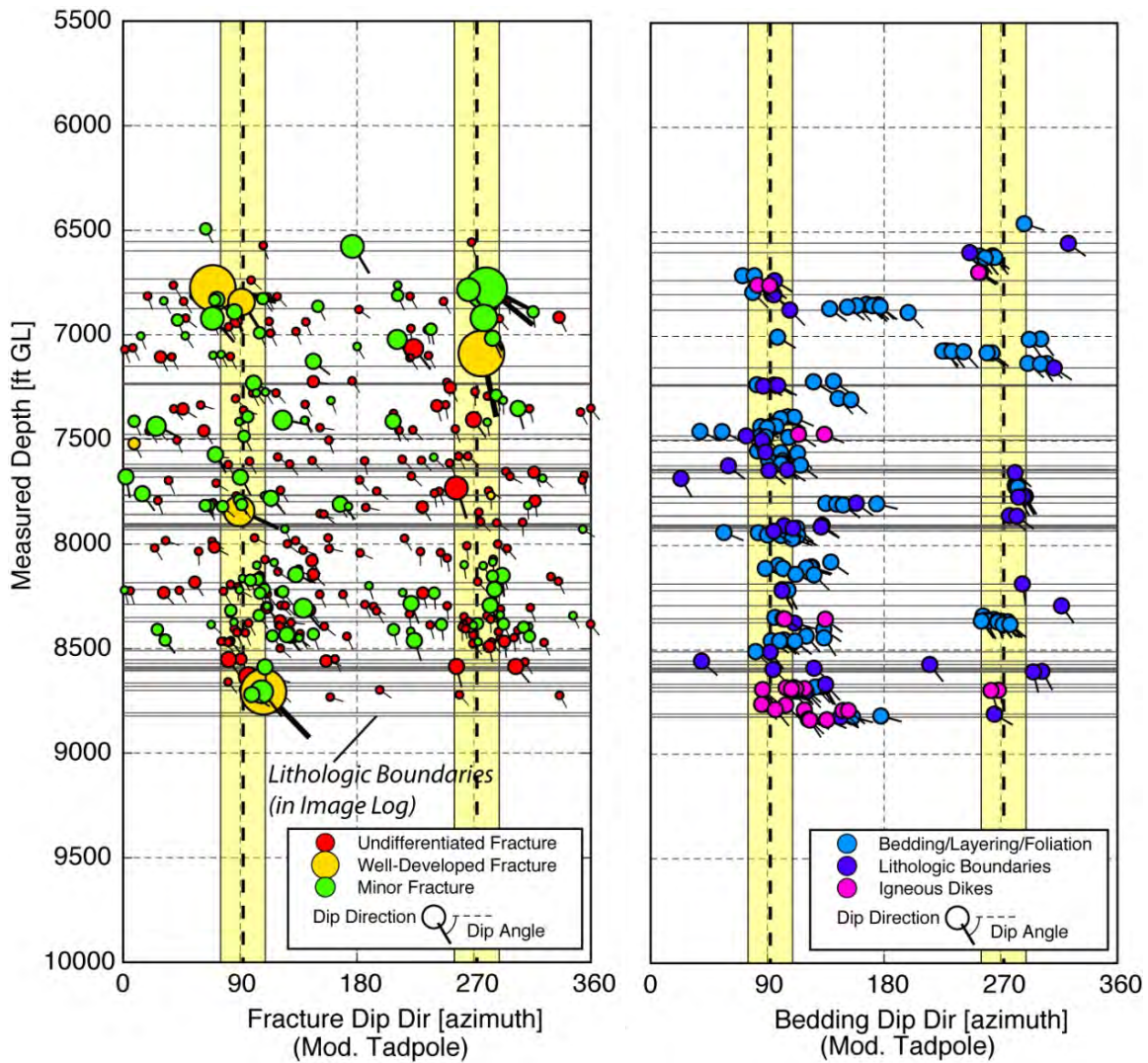


Figure 3-43. Rose diagrams of LiDAR scarp trends west of La Pine (left), and vents and fissures on the west flank of Newberry Volcano (right). Features interpreted by AltaRock on Oregon LiDAR Consortium image (Cladouhos et al., 2011a). See additional details in Section 5.1. Concentric circles show percent of total measurements.



**Figure 3-44. Modified tadpole plot showing depth distribution of natural fractures (left) and primary layering (right) attitude. In this plot, the azimuth of dip direction is given along the x-axis and the tail of the tadpole indicates the dip relative to horizontal. Left: modified tadpole plot of natural fractures distinguishing undifferentiated fractures, major fractures and minor fractures (Table 3-9). Right: modified tadpole plot of layering including bedding/banding/foliation, lithologic transitions, and dikes.**

The thickest fractures are strongly aligned with these average attitudes, whereas thinner fractures have a wider distribution of attitudes. That is, the biggest tadpoles on Figure 3-44 cluster at dip azimuths of 90° and 270° (yellow bands). However, many of these large fractures are characterized by either very steep or relatively shallow dips that would not be consistent with normal faults. The attitudes of primary layering groups trend in a fashion similar to natural fractures, except their dips are generally lower. Dikes have a similar attitude to natural fractures. Fracture and bedding attitudes do not appear to vary systematically with depth.

Figure 3-45 shows a scatter stereogram of the poles (downward normal vectors) of the full BHTV fracture population on the left, and a contour plot of the poles on the right. Fracture poles are generally used to analyze fracture attitudes because it is straightforward to contour, evaluate clustering denoting a population of similarly oriented fractures, and thus develop statistical models of fracture attitude. The colored contour plot reveals that the highest concentration of fracture poles (the region in red) occurs at

a trend of  $282^\circ$  and plunge of  $34^\circ$ , corresponding to a mean strike of  $12^\circ$  and dip of  $60^\circ$  to the east. Figure 3-46 shows the contoured poles for the two zones (B and C) with sufficient fractures to consider separate orientation analysis. As suggested by the depth plot of fracture orientation, there does not appear to be a significant difference between the fracture orientations in the two zones. Therefore, the statistical analysis of fracture orientations is done for all fractures grouped together, rather than by zone.

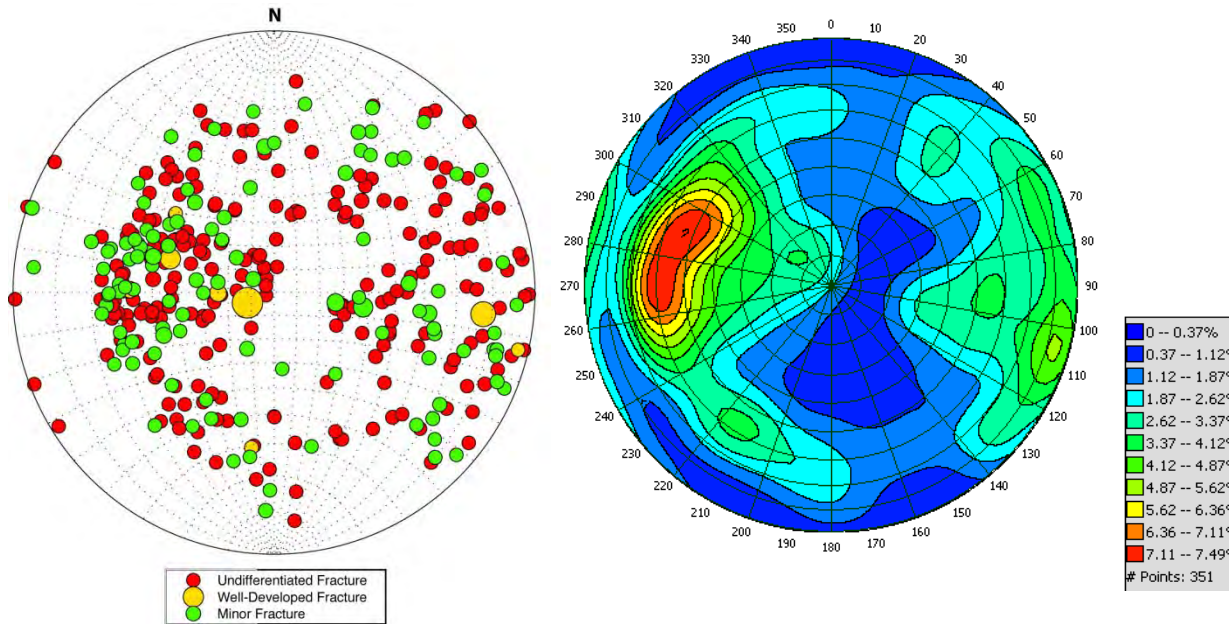


Figure 3-45. Equal area stereogram of the poles to the BHTV-identified natural fractures in NWG 55-29 (left) and the contoured fracture poles (right). Diagrams show data for all 351 fractures identified.

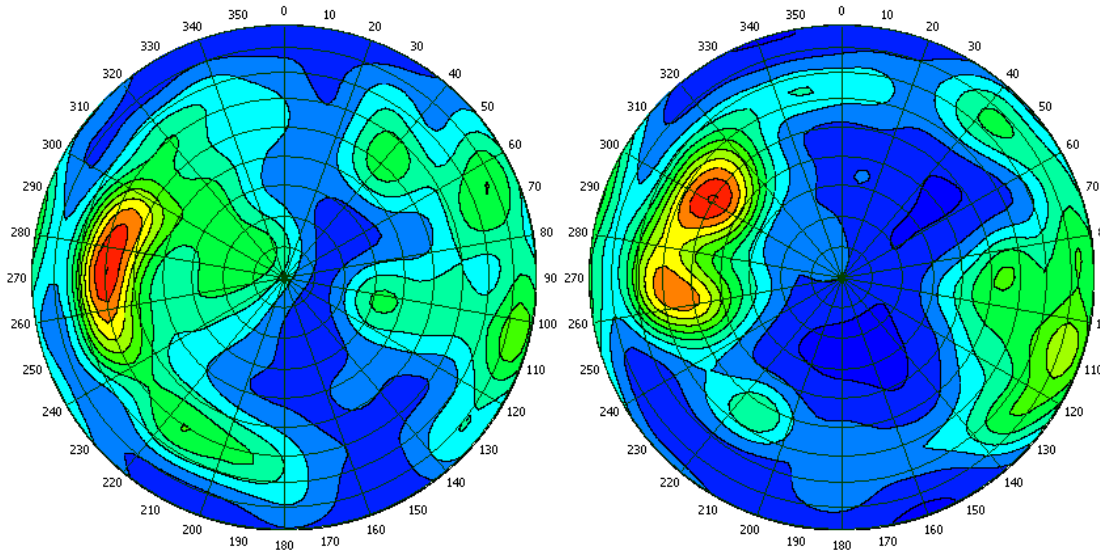


Figure 3-46. Contoured fracture poles for Zone B [N=215] (left) and Zone C [N=116] (right). Zone A [N=5] and Zone D [N=15] have too few fractures for contouring or separate statistical analysis.



Closer examination of the contour plot also reveals orientation bias (Figure 3-45). The blue band (denoting lower density) to the left of the red region (high density) represents fractures that dip 75°-85° to the east. Fractures in this orientation would be less likely to be intersected by the well, which deviates about 15° from vertical to the east, because these fractures and the well are nearly parallel. That is, fractures that dip 75°-85° to the east are undersampled and are likely to exist at a density that would fill-in the apparent gap between shallower (65°-75°) and steeper (85°-90°), east dipping fractures.

Further analysis of the orientations is best accomplished by using orientation statistics software. The ISIS (Interactive Set Identification System) module of FracMan<sup>11</sup> can distinguish portions of the total fracture population that represent sets (i.e., clustered orientations), determine orientation and density statistics for each set, and account for sampling bias. At a minimum, an orientation model consists of a mean pole (defined by a trend and plunge), a dispersion coefficient which can vary from 0 (no discernible mean) to infinity (all orientations are exactly the same), and a fit probability that indicates the goodness of fit between the data and the model. ISIS can use a variety of orientation distribution models including spherical, elliptical, or cylindrical variation about the mean pole. After statistical fitting of the orientations (Table 3-12), using the forward modeling capability of FracMan, a synthetic discrete fracture model can be created using the derived statistics. To confirm that this model accurately reproduces the borehole data, it is sub-sampled using a synthetic borehole with the same geometry as the original well.

The results of the ISIS analysis (Table 3-12) reveal two dominant fracture sets in NWG 55-29 fit by an elliptical Fisher orientation model (Dershowitz and Einstein, 1978). As the name implies, an elliptical orientation model can quantify anisotropy in the dispersion about the mean pole by two orthogonal dispersion coefficients corresponding to axes of the elliptical distribution and specifying the trend and plunge of the major axis, rather than just as a single dispersion coefficient characteristic of the traditional circular Fisher orientation model (Mardia and Jupp, 2000). The fit probabilities to elliptical Fisher orientation models for the two sets are 96% and 86%, while the fit probabilities for the circular Fisher orientation models are 79% and 1% (Table 3-12).

**Table 3-12. Fracture orientation sets identified by ISIS analysis of 351 fractures measured in BHTV.**

<b>Fracture Set</b>	<b>Fisher distribution</b>	<b>Elliptical Fisher distribution</b>
<b>Set 1: ESE dipping</b>		
Fracture Count	62	79
Relative Density	17.7%	22.5%
Mean Pole (trend, plunge)	276°, 35°	296°, 70°
Major Axis (trend, plunge)		191°, 13°
Dispersion Coefficients (K1 / K2)	23.7	10.0 / 1.0
Fit Probability	79.4%	95.6%
<b>Set 2: Subvertical</b>		
Fracture Count	289	272
Relative Density	82.3%	77.5%
Mean Pole (trend, plunge)	079°, 73°	267°, 4°
Major Axis (trend, plunge)		167°, 71°
Dispersion Coefficients (K1 / K2)	1.9	2.8 / 1.2
Fit Probability	1.4%	85.5%

<sup>11</sup> ©2010, Golder Associates Inc, <http://www.fracman.com/>

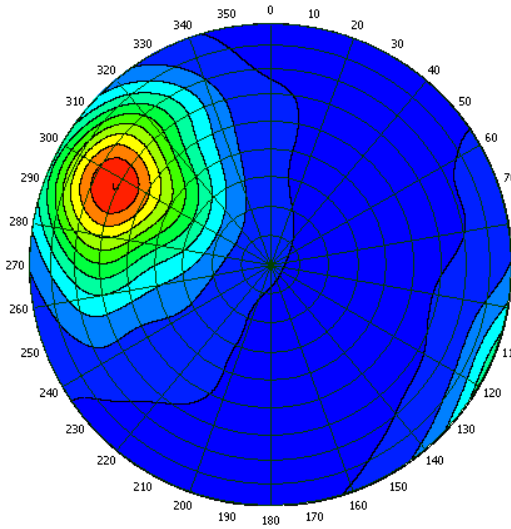
Fracture Set 1, with 22.5% of the fractures in the BHTV image, has a mean pole of with a trend of 296° and plunge of 50° (mean strike 026°, dip 40° E). The orientations of fractures in this set are relatively tightly clustered and represent the highest density of poles in Figure 3-45. This fracture set parallels the nearest portion of the caldera rim, and dips towards the caldera, suggesting that these fractures could have formed to accommodate extension and normal slip related to caldera collapse. It will be shown in Section 7.4 that the attitudes of many of the fractures in this set are likely to slip during hydroshearing stimulation.

Fracture Set 2, representing the remaining 77.5% of the fractures in the BHTV image, has a mean pole with a trend of 267° and a plunge of 4° (mean strike 357°, dip 86° east). On average, fractures in this set are N-S trending, sub-vertical fractures that dip both east and west. The steep average dips suggest that these fractures formed as tensile fractures or cooling joints, not shear fractures. In this circumstance the fractures in extrusive volcanic rocks would form very early after deposition at shallow burial, resulting in a wide range of strike. This fracture set has far more dispersion than Set 1 and some fractures in this set can have quite shallow dips, and still fit within the ‘tail’ of the statistical distribution.

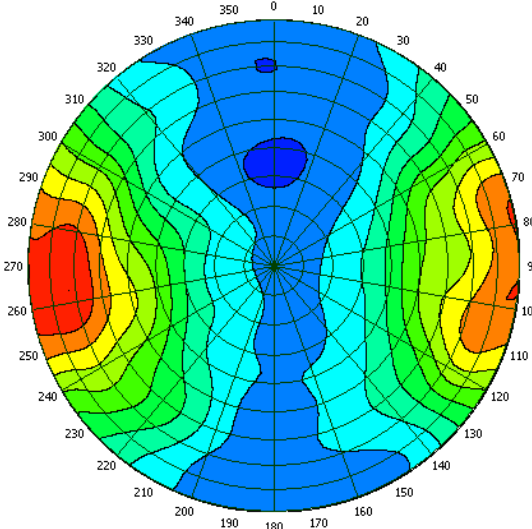
From this statistical characterization of the fracture densities and attitudes revealed by the BHTV log in NWG 55-29, a synthetic population was generated in FracMan. The modeled volume was a cylinder with a radius of 200 m (656 ft) centered on the wellbore and with a height equivalent to the depth interval logged by the BHTV. However, in this model the fracture density is expressed as the fracture area per model volume to accommodate the three-dimensionality of the problem. This measure of fracture density retains the same dimensions as the earlier characterization from the borehole and has the advantage that it is independent of borehole or fracture orientations. Figure 3-47 shows the results of the forward modeling. Comparing Figure 3-47c and Figure 3-47d confirms that the orientation model in is a reasonable description of the fractures observed on the BHTV image. This orientation fit is not critical. In the DFN model developed in Section 7.4, the modeled fracture orientations are chosen from the list of actual fracture orientations (sometimes called bootstrapping), rather than using a statistical model to generate the modeled fracture orientations. The orientation fit is presented here for possible use in other future modeling efforts.

**Table 3-13. FracMan forward model inputs.**

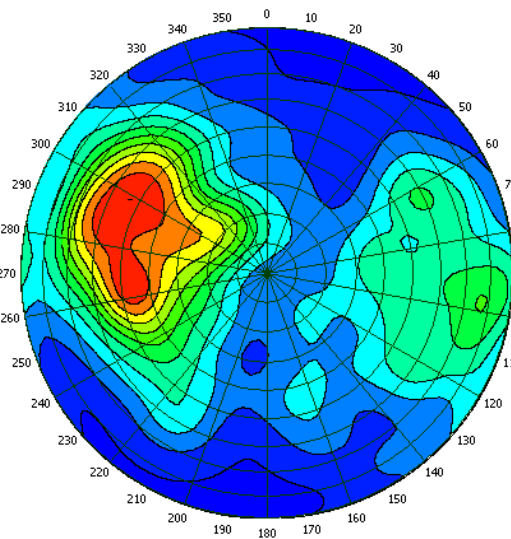
<b>Parameter</b>	<b>Set 1: ESE dipping set</b>	<b>Set 2: Subvertical set</b>
Mean Pole (trend, plunge)	296°, 30°	267°, 4°
Dispersion Coefficients (K1/K2)	10.0 / 1.0	2.8 / 1.2
Density (fracture area/model volume)	0.005 m <sup>2</sup> /m <sup>3</sup>	0.008 m <sup>2</sup> /m <sup>3</sup>
Spacing (perpendicular to mean pole)	1.45 m	1.40 m
Count	3200	4800



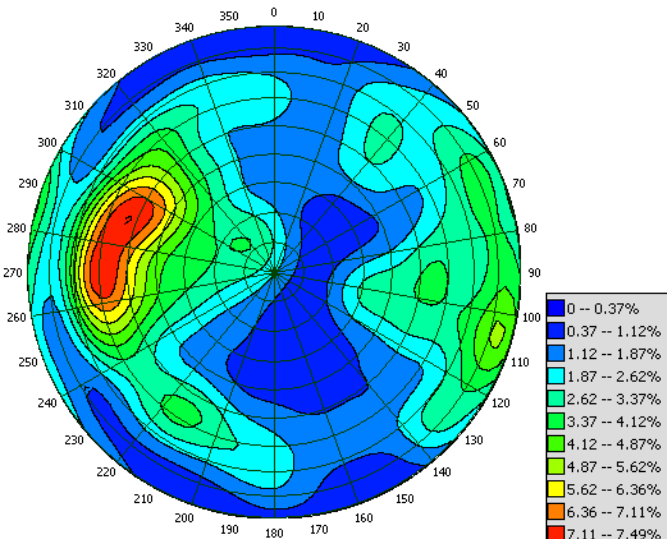
a) Set 1: 3200 modeled fractures



b) Set 2: 4800 modeled fractures



c) Synthetic sample using NWG 55-29 well course



d) Actual BHTV fractures for comparison

Figure 3-47. Results of fracture orientation forward modeling. The contour interval legend, shown at bottom right, is the same for all four figures.

### 3.2.8.6 FRACTURE THICKNESS

The thickness of fractures measured in the BHTV image (sometimes misleadingly called the ‘apparent aperture’) and the hydraulic aperture, which controls the flow of fluid along a fracture from the borehole into the surrounding formation, are not equivalent. However, the thickness is the best measure of relative fracture size available. Of the 351 fractures identified, it was possible to measure the thickness of 111 fractures (Figure 3-48), with a range of thicknesses from 250 mm (9.8 in) down to 1.49 mm (0.06 in). Most of the thicker fractures are in the shallower part of the BHTV log. Like many quantitative measures of magnitude versus frequency (e.g, the Gutenberg-Richter law for earthquakes, or fault length or maximum slip versus frequency; i.e., Turcotte, 1992; Cowie and Scholz, 1992; Cladouhos and Marrett, 1996), the frequency of measured fracture thickness follows a power-law size distribution. That means that they can be fit by a line on a log N vs. log aperture plot (Figure 3-48b). The

power-law distribution equation shown on Figure 3-48b can be used to generate apertures in the DFN model developed in Section 7.4. However, like the orientations, modeled apertures are also bootstrapped from a list of actual fracture thickness. Again, the statistical distribution of fracture thickness is presented here for possible use in other future modeling efforts.

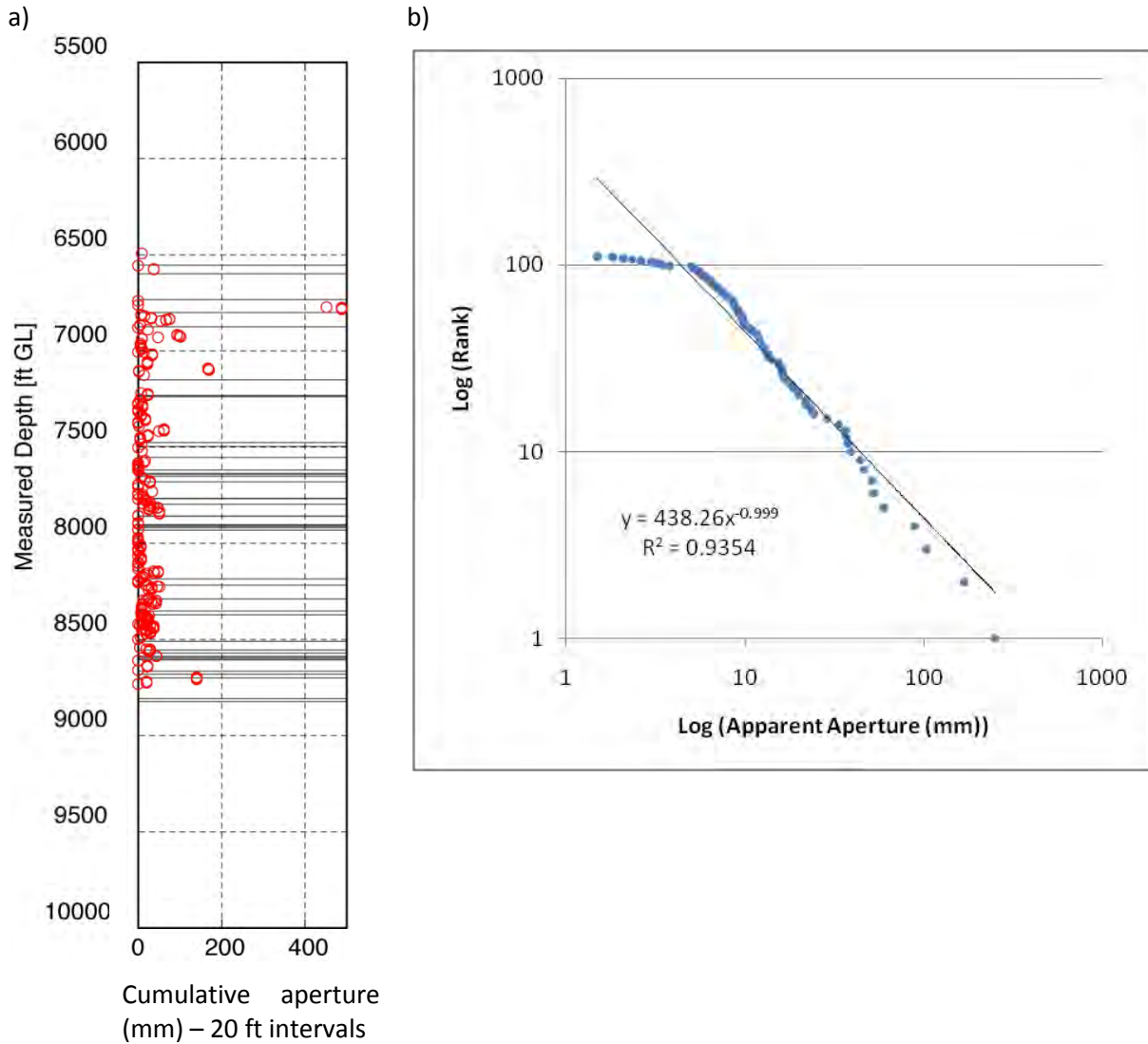


Figure 3-48. Cumulative fracture thickness (aperture) with depth (a) and log-log plot of apertures (b).

### 3.2.8.7 DIKES

A comparison of the distribution of dikes identified in the mud log and BHTV log to the distribution of mud losses and local temperature anomalies revealed during injection indicates that dikes might also play a critical role in the permeability structure in the volume penetrated by NWG 55-29 (Figure 3-49). In particular, the temperature log that was performed after injection at 1.4 L/s (22 gpm) shows several inflections, suggesting permeable zones in the borehole. These inflections, which only occur deeper than 2622 m (8600 ft), can be correlated to dike margins. Locally enhanced permeability at the margin of dikes is consistent with cracking caused by thermal stresses induced when the magma that becomes the solid dike is intruded into the country rock. In addition, analysis of cuttings shows less developed alteration of these intrusive rocks (e.g., less abundant chlorite and calcite) suggesting that late fractures



formed in these dikes might be relatively open or have somewhat greater capacity for self-propping. In fact, one of the densest zones of fracturing (Zone C) occurs immediately above intruded granodiorite, at the bottom of the interval logged by the BHTV. The distribution and thickness of dikes is documented by two independent data sets in NWG 55-29, the mud logs and the BHTV image.

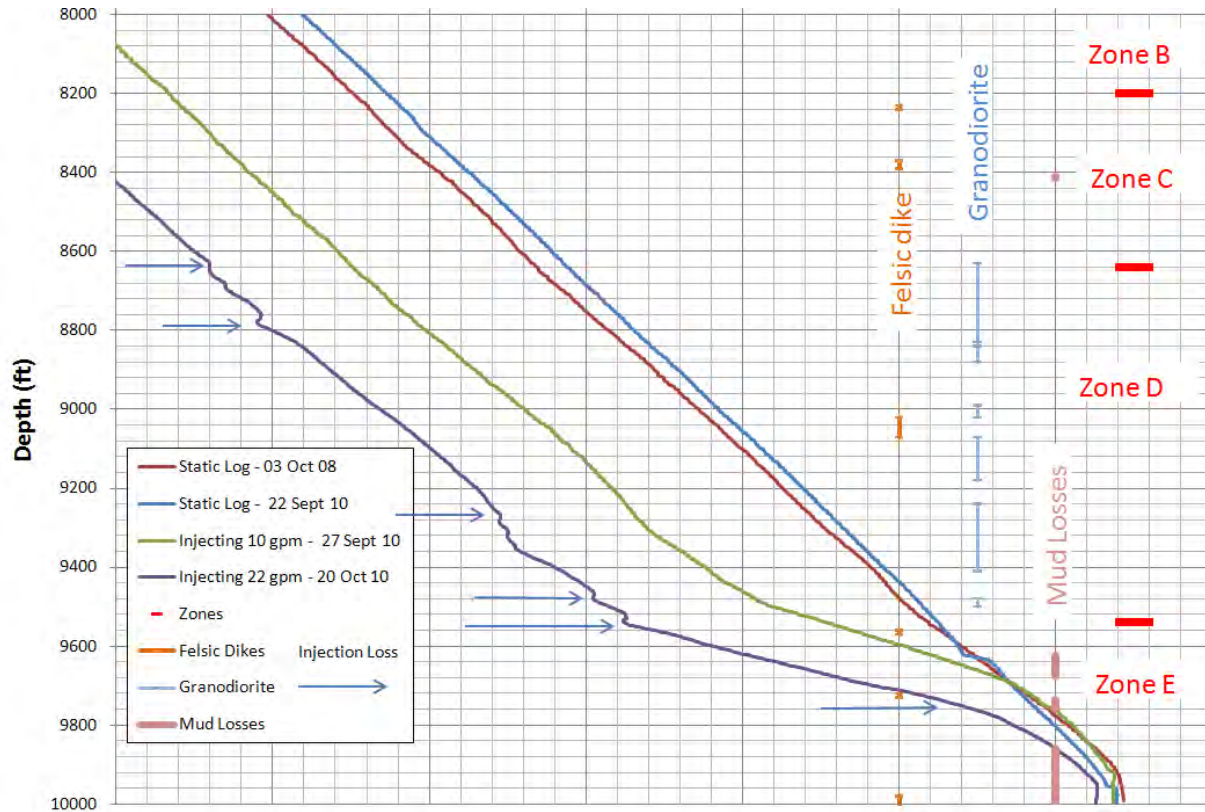


Figure 3-49. Temperature logs during injection, annotated with geologic and drilling data and zone definitions.

Six felsic dikes with thicknesses from 3 to 24 m (10 to 80 ft) are identified in the mud logs (Table 3-14). Due to the 3 m (10 ft) sampling frequency of cuttings used to create mud logs, the precision in the depth of a dike and its thickness are greater than 3 m (10 ft); therefore the ~3 m (10 ft) minimum dike thickness should be considered a limit on the precision, not an actual minimum thickness for felsic dikes. Six granodiorite or microcrystalline granodiorite units are also identified in the mud logs. Although much thicker than the felsic dikes, the granodiorite units include basal contacts with extrusive country rock (basalt), and can be considered dikes. Three of the granodiorite dikes are more than about 30 m (100 ft) thick.

**Table 3-14. Dikes identified in mud log.**

Mud Log Depth (ft KB)	Thickness (ft) <sup>1</sup>	Dike Lithology
8230	10	Felsic Dike
8370	20	Felsic Dike
8630	200	Granodiorite
8840	40	Granodiorite
8990	30	Granodiorite
9020	50	Felsic Dike
9070	110	Granodiorite
9240	170	Granodiorite
9480	20	Granodiorite
9560	10	Felsic Dike
9720	10	Felsic Dike
9980	80	Felsic Dike
Average	30	Felsic Dike
Average	95	Granodiorite

<sup>1</sup>Because the mud log does not constrain the margins of these dikes, no attempt was made to determine the true thickness perpendicular to the dike margins.

Igneous dikes are also identified in the BHTV. In these images, the dikes are typically <60 cm (2 ft) thick, much thinner than indicated in the mud logs. This is reasonable because drilling fluid circulation tends to mix cuttings across a greater apparent depth interval, and each sample in the mud log represents a composite of cuttings over a 3 m (10 ft) interval. Three thin dikes were identified in the interval 2043-2287 m (6700-7500 ft), and eleven within the first granodiorite unit, the only granodiorite unit logged by the BHTV. The attitudes of the dikes in the BHTV images (Figure 3-42) are concordant with the adjacent layers, indicating that they may be sills intruded between the volcanic layers.

Unlike the dikes identified in the mud log, dikes visible in the BHTV images are too thin to warrant consideration as separate units. However, the BHTV image does reveal the attitude of the contact between the volcanics and the first extensive granodiorite dike (Figure 3-50). Lithologic contacts at 2631 m (8630 ft) and 2632 m (8634 ft) have a strike and dip of 212°, 62° W and 205°, 76° W, respectively. Rather than choose between the two attitudes, both are used to define deterministic fractures and granodiorite dike margins in the stimulation model discussed in Section 7.4.

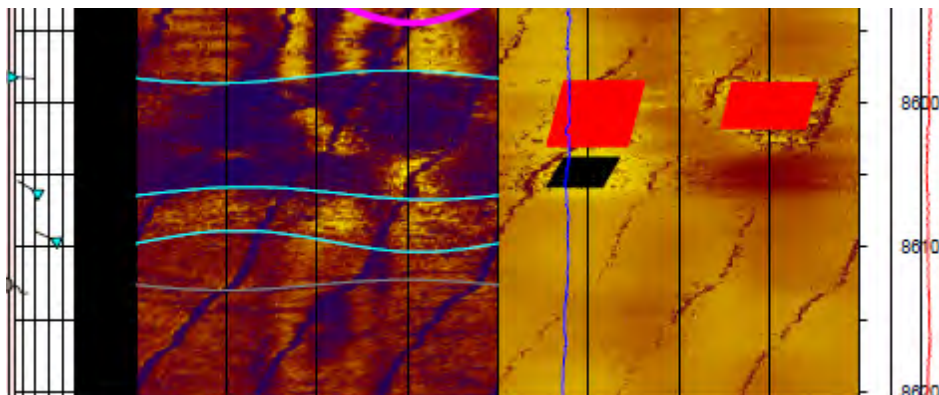


**Figure 3-50. Top of first granodiorite dike at 2625 m (8610 ft). The deepest breakout recorded in the BHTV log (red quadrilaterals) occurs in the basalt, immediately above the granodiorite, at 2622 m (8600 ft).**

### 3.2.8.8 MODEL STRATEGY AND ZONES

The primary purpose of the fracture analysis presented above is to build AltaStim models (Section 7.4), which are used to develop plausible parameters for stimulation, including the fluid pressure necessary to hydroshear and estimates of the injected volume, as constrained by a conceptual model of the fractures, geology, and quantitative data on the statistics of fracture distribution and attitudes. For the purpose of modeling, the well bore geology has been divided into five zones. Identification of the zones is based on the analysis of the mud logs and drilling logs, the fractures, and the temperature logs. Table 3-15 summarizes the depths of each zone and its characteristics. For simplicity, depths given below are in feet TMD only. In Section 7.4, all depths are given in true vertical depth (TVD) from the ground level (GL) to account for borehole deviation.

Like any model, AltaStim requires that the geology and fracturing be simplified to a tractable problem. One simplification is the total number of modeled fractures must be kept under 32000 in each stimulation model run. For a model region with horizontal dimensions of 700 x 1100 m (2296 x 3608 ft), and the fracture densities observed in NWG 55-29, model heights less than about 300 m (around 1000 ft) are required. Practically, this is not an issue, because the geology and fracturing support evaluation of zones with heights less than this limit.

**Table 3-15. Zone summary.**

Zone	Depth Range (ft)	Thickness (ft)	Lithology	Fluid Loss (-) and Gain (+)
A	6450-6750	300	Primary: welded lithic tuff Secondary: other tuff	None
B	6750-8000	1250	Primary: tuffs Secondary: basalt, dacite, andesite	-22 bbl @ 6868-6880 ft -25 bbl @ 7296 ft +20 bbl @ 7335 ft -30 bbl @ 7400-25 ft +27 bbls @ 7428-31 ft -26 bbl @ 7432-54 ft
C	8000-8640	640	Primary: basalt, basaltic andesite Secondary: two felsic dikes	-15 bbl @ 8411-15 ft
D	8640-9540	900	Primary: microcrystalline granodiorite (5 dikes, 570 ft total) Secondary: basalt, one large (50) felsic dike	None
E	9540-10060	520	Primary: basalt Secondary: three felsic dikes	-91 bbl @ 9626-76 ft -98 bbl @ 9750 ft -12 bbl/hr @ 9736-60 ft -12 bbl/hr @ 9860-10060 ft (seeping)

### 3.2.8.9 ZONE A – LIGHTLY FRACTURED WELDED TUFF

The shallowest zone, a 91 m (300 ft) interval below the casing shoe (1963 m [6439 ft]), is characterized by a low fracture density in the BHTV log, and no mud losses. The lithology is dominated by welded, lithic tuffs of various compositions, with minor unwelded tuffs. This zone showed a smooth conductive thermal gradient during the inject-to-cool operation.

### *3.2.8.10 ZONE B – MODERATELY FRACTURED VARIETY OF VOLCANIC EXTRUSIVES*

At 2058 m (6750 ft), the fracture intensity increases about tenfold, relative to Zone A, to 14.8 fractures per 30 m (100 ft). Compared to the zone above, there is a wider variety of extrusive volcanics, with interbedded tuff, basalt, dacite and andesite. During drilling of this zone, there were minor and temporary mud losses (<4.8 m<sup>3</sup>, 30 bbl); the lost mud was apparently regained 0.9-30 m (3-100 ft) deeper than the original loss. This zone showed a smooth conductive thermal gradient during the inject-to-cool operation.

### *3.2.8.11 ZONE C – MINOR DIKES AND INCREASE IN FRACTURING*

At about 2439 m (8000 ft), the fracture density increases to consistently more than 20 fractures per 30 m (100 ft), with an average fracture density of 26.4 fractures/30 m (100 ft), nearly double Zone B. Below 2500 m (8200 ft) on the mud log, the tuffs are not present and the lithology is basalt and basaltic andesite. At 2509 m (8230 ft) is a 3 m (10 ft) thick felsic dike, which is the first indication of intrusives in the mud log. Another felsic dike is tentatively identified at 2552 m (8370 ft). Both dikes are identified as lithology changes in the BHTV, the first with a dip azimuth of 083° and dip of 49° (i.e., approximately north-striking with dip to the east).

The increased fracture density and number of dikes at this depth are likely related to the much larger intrusions in Zone D. Despite the increase in fracture density and dikes, the mud log indicates that this zone only had a single, small mud loss and showed a smooth conductive thermal gradient during the inject-to-cool operation.

### *3.2.8.12 ZONE D – GRANODIORITE INTRUSIONS*

Zone D is defined by five major granodiorite intrusions with an average thickness of 29 m (95 ft) described in the mud log, and one large felsic dike. Together, these intrusions comprise 189 m (620 ft) of the 274 m (900 ft) thick zone (69%), with the remainder comprised of basalt. The top of Zone D (2634 m (8640 ft)) is visible in the BHTV images as an east-dipping contact. Only the top 67 m (220 ft) of this zone was imaged by the BHTV due to the upper temperature limit of the tool being reached at 2701 m (8860 ft). The fracture density from the BHTV images of this zone is significantly less than Zone C, 6.8/100 ft vs. 26.4/200 ft, respectively. Borehole breakouts are also absent in the portion of this zone imaged by the BHTV, indicating relatively strong rock. Throughout the interval, no mud losses are recorded in the mud log. Together, these three observations suggest that the granodiorite itself is not a suitable stimulation target. However, the contacts between the granodiorite and the basaltic rock do represent likely stimulation targets. The mud log describes the bottom of the first granodiorite body, at about 2869 m (9410 ft), as having strong alteration intensity and abundant epidote. During the inject-to-cool operation, several temperature profile inflections not present at the lower injection rate of 0.6 L/s (10 gpm) were apparent at an injection rate of 1.4 L/s (22 gpm; compare green and purple profiles in Figure 3-49). This suggests incipient stimulation of fractures or lithologic contacts in Zone D at a WHP of 7.95 MPa (1153 psi; Section 3.2.9). To account for the potential relevance of the margins of the granodiorite for EGS stimulation, five deterministic fractures were added to Zone D, in addition to background fracturing, in the stimulation model discussed in Section 7.4.

### *3.2.8.13 ZONE E – BASALTS WITH MINOR DIKES*

The deepest part of NWG 55-29 extends below the thicker granodiorite bodies and into the same lithologies encountered in Zone C, characterized by basalts intruded by felsic dikes. There is no BHTV data in this zone, so the character of the fractures is unknown. For the purpose of modeling, the statistical characteristics of fractures in Zone C are used. Both zones are adjacent to large granodiorite



bodies and contain felsic dikes and dikelets, according to the mud logs, as well as similar volcanic components.

Zone E contains the largest loss zones 14.3 to 15.6 m<sup>3</sup> (90-98 bbls; instantaneous losses plus 0.53 L/s (12 bbl/hr seeping losses) in the well. While it is possible that these zones may have been at least partially sealed or damaged by lost drilling mud, localized temperature anomalies detected during the October 2010 inject-to-cool operation suggest significant fluid may have slowly exited the well, providing a potential target for stimulation of natural fractures.

### 3.2.9 INJECTION AND FLOW TESTING

Upon completion of NWG 55-29 in 2008, Davenport attempted to flow test and inject into NWG 55-29. The well flowed back about one well bore volume of fluid and then died. Multiple attempts to initiate flow using compressed air through coil tubing were unsuccessful. These results are a clear indication of a lack of permeability in the well. In an attempt to inject, Davenport pressured up the well to 6.7 MPa (970 psig) with the rig pumps, but the injection rate was too low to measure with rig instrumentation. These injection testing results also indicate a lack of permeability. The conductive temperature gradient in the well (Figure 3-2), inability to sustain flow, and low of injectivity at a wellhead pressure of 6.7 MPa (970 psig), indicate that a hydrothermal resource is not connected to the well.

AltaRock conducted a baseline injectivity test for this Demonstration using low-rate, high-pressure pumping equipment, and measured flow with sensitive instrumentation (Table 3-16). Prior to initiating injection, on 22 September 2010, AltaRock conducted a static survey to measure temperature and pressure, identify fluid level, and ensure that the well was open to total depth. That same week, injectivity testing began using untreated groundwater produced from the onsite water well. Water was injected at a rate of about 0.6 L/s (10 gpm) and a wellhead pressure of 5.2 MPa (750 psig) for three days. On 27 September, after three days of constant-rate injection, another injecting pressure-temperature (PT) survey was conducted to determine if injection was indeed cooling the wellbore. The PT survey results are shown in Figure 3-2 and Figure 3-3. Inflections in the temperature profile indicate that water was exiting the well bore from 2829 m to 2914 m (9280 to 9560 ft). The mud log identifies several dikes and an altered zone in this interval containing “abundant epidote”, as well as several transitions between basalt and granodiorite. These contact surfaces all represent prime stimulation targets because they are areas where we would expect to find high natural fracture density.

**Table 3-16. NWG 55-29 injection test results.**

Average WHP (psig)	Injection Rate (gpm)	Injectivity (gpm/psi)
751	14	0.019
821	17	0.021
1153	21	0.018

After the injecting PT survey on 27 September, injection was discontinued until 18 October, when injection was re-started at a higher injection rate to cool the well bore in preparation for BHTV logging. From 18-20 October groundwater was injected at a rate of 1.4 L/s (22 gpm) and wellhead pressure of 7.9 MPa (1150 psig). On 20 October, a third PT survey was conducted just prior to BHTV logging to ensure that the well was cool enough for tool deployment. The injection rate and pressure was reduced during the PT survey to accommodate wireline lubricator limitations. The measured temperature profile indicates that fluid was entering the formation from 2633 m to 2682 m (8640 to 8800 ft) and from 2828 m to 2914 m (9280 ft to 9560 ft; Figure 3-51). The green and purple curves in Figure 3-2 represent the two most recent injecting PT surveys. The zone from 2366 m to 2682 m (8640 ft to 8800 ft) does not appear to be taking flow during the September survey when water was being injected at 5.2 MPa (750

psi) and 0.6 L/s (10 gpm). Just prior to the October 20 survey, water was being injected at 7.95 MPa (1153 psig) and 1.4 L/s (22 gpm). A comparison of these temperature profiles suggests that, because the zone from 2366-2682 m (8640-8800 ft) did not show any cooling during the September injection, a surface pressure of 5.2 MPa (750 psi) is not enough pressure to shear and dilate existing fractures in that section of the open hole, but that 7.9 MPa (1153 psig) is approaching shear failure.

A maximum temperature of 329°C (625°F) was recorded a depth of 3059 m (10036 ft). Injectivity at wellhead pressures of 5.2 to 7.9 MPa (751 to 1153 psig) are calculated to be 0.2 and 0.5 L/s per MPa (0.02 and 0.05 gpm/psi), which is comparable to injectivity measured in surrounding Newberry wells and temperature coreholes (Table 3-17).

Injection continued during televiewer deployment to keep the wellbore cool and allow more of the open-hole interval to be visualized. On 22 October, BHTV image logging commenced. After 15 hours of logging, a depth of 2701 m (8860 ft) was reached in granodiorite. At an external temperature of 277°C (531°F) the tool motor stopped functioning, logging was terminated, and the well was shut in.

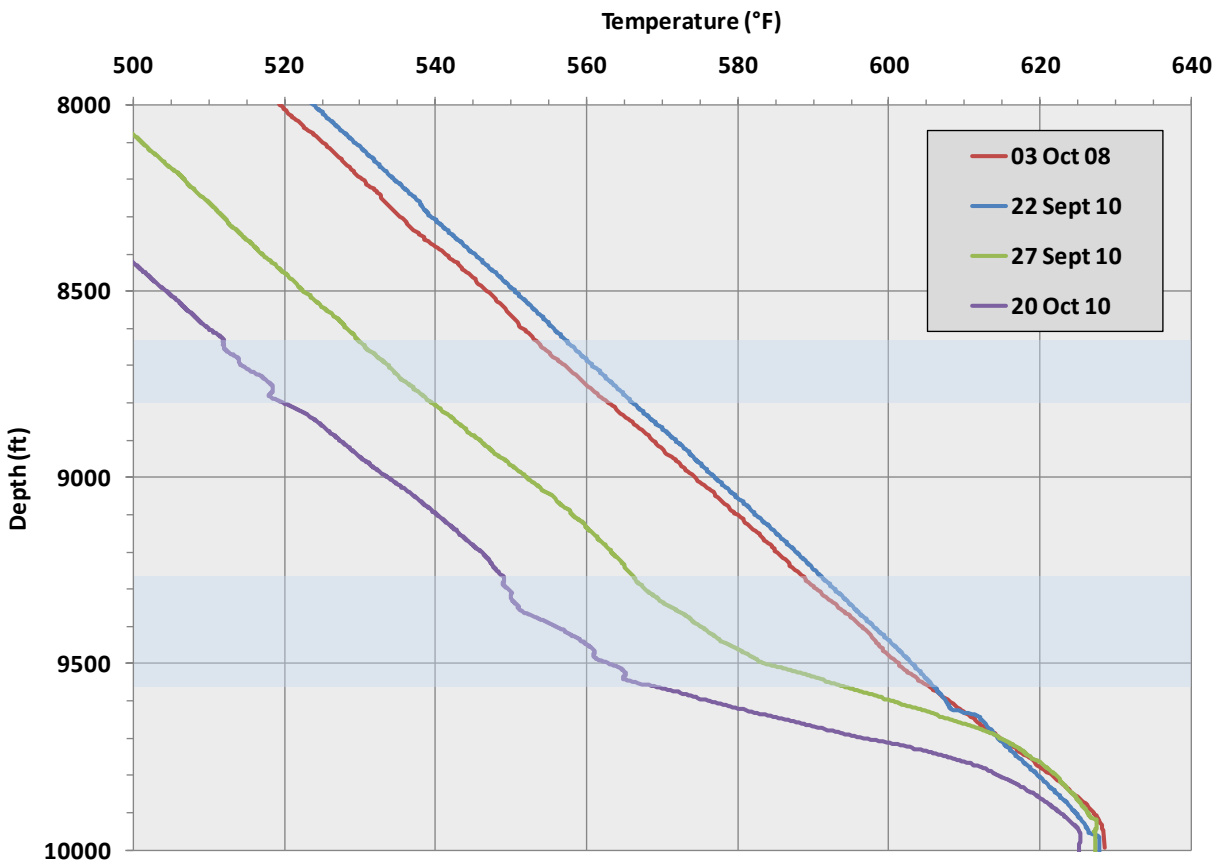


Figure 3-51. Focused view of the PT survey data, highlighting inflow zones from 8640-8800 ft (2633-2682 m) and 9280-9560 ft (2828-2914m).

**Table 3-17. Injectivity data from nearby Newberry wells and temperature coreholes (from Spielman and Finger, 1999).**

Well	Date	Open Hole (feet KB)	Injection Rate (kph)	WHP (psig)	Injectivity (kph/psig)	Injectivity <sup>1</sup> (gpm/psig)
CEE 76-15 TCH	11/18/95	5116-5360	1	300	0.0015	0.0030
CEE 76-15 TCH	11/18/95	2748-4800	2	300	0.0031	0.0062
CEE 86-21 <sup>2</sup>	12/02/95	4199-9020	42.5	50	0.11	0.2196
CEE 86-21	04/18/96	5701-9185	25	800	0.022	0.0439
CEE 23-22	01/08/96	4418-9602	60	200	0.026	0.0519
CEE 23-22	01/21/96	4418-9602	40	1350	0.024	0.0479

<sup>1</sup>Water level was approximately 775 ft in all the wells, therefore liquid head at zero WHP was assumed to be 333 psi. This is added to WHP to calculate injectivity.

<sup>2</sup>According to Spielman and Finger (1999), holes were discovered in the 13-3/8 in casing after this test. The second test on CEE 86-21 was after casing repair.

### **3.2.10 POWER GENERATION POTENTIAL OF NWG 55-29**

The EGS Demonstration well NWG 55-29 has no significant permeability below the casing shoe at 1970 m (6462 ft) and it is not connected to a hydrothermal system. As such, the well in its current state is considered a dry hole (i.e., it does not have any power generation capability), but is ideal for EGS stimulation. This well is our planned injection well for the proposed EGS triplet.

After stimulation, the injected water will be allowed to flow to the surface by exposing the well to atmospheric pressure. The well will flow up the casing unassisted and will most likely flash somewhere between the 9-5/8 in casing shoe at 1979 m and 1219 m (6462 ft and 4000 ft). We assume that the well will produce no more than 50 kg/s (400 kph), or approximately 50 L/s (800 gpm), the maximum planned injection rate to stimulate NWG 55-29. Assuming a single-phase reservoir production temperature of 177°C (350°F), the flowing steam fraction will be 16% at atmospheric pressure; that is, 42 L/s (665 gpm) of liquid flow and 8.2 kg/s (65 kph) of steam flow. The flow-back will be the first indication that the native state surrounding NWG 55-29 has been altered.

In the next phase of the demonstration, two production wells will be drilled into EGS reservoir. The power generation potential of the two planned production wells, NWG 55A-29 and NWG 55B-29, can be estimated by making assumptions about flow rate and the enthalpy of produced fluid. The enthalpy of the total mass flow will determine the steam fraction at the surface. There are many unknowns at this time regarding the enthalpy of production from the EGS-generated fracture system including, but not limited to:

1. Residence time – the time that water takes to travel between the injection and production wells is a function of permeability and tortuosity in the created fracture network. Longer residence time leads to hotter production because the water has more time to exchange heat with the rock matrix.
2. Surface area of the reservoir – the area of rock that is contacted by water as it travels between the injection and production wells. The more surface area that is encountered, the hotter the water.
3. Mass-weighted average temperature in the production well – the average temperature that can be expected in the production wells during circulation.

These unknowns contribute to the wide range of enthalpies that are investigated below. The open-hole interval in NWG 55-29 has a static temperature range of 210°C (410°F) at 1829 m (6000 ft), to over 316°C (600°F) at the total well depth of 3066 m (10060 ft). The 10°C (50°F) water injected during circulation testing into NWG 55-29 is expected to heat through the EGS fracture network length of

500 m (1640 ft) to a temperature of 177°-279°C (350°-535°F). The fluid will be completely liquid at depth in the production well since it will be under hydrostatic pressure. A typical flash power plant separation pressure of 0.7 MPa (100 psi) will result in a steam fractions of 0.026-0.259. Assuming that each production well produces a total mass flow of 75 kg/s (585 kph), the steam production rate will be 1.95-19.4 kg/s (15.2-151 kph). Further assuming a steam to power conversion efficiency of 1.9 kg/s per MW (15 kph/MW), the resulting power output is expected to range from 1.0-10.0 MW<sub>e</sub> per well. Binary power generation may be more cost-effective and environmentally desirable. Phase III of the Newberry EGS Demonstration will fully explore and document the potential power generation based on Phase III test results.

### 3.3 NWG 55-29 CONCEPTUAL RESOURCE MODEL

A geothermal well suitable for demonstration of multi-zonal EGS stimulation technology has, at a minimum, the following qualitative mechanical and geological characteristics:

1. It must be drilled into a large volume of hot, relatively impermeable rock.
2. The borehole must have cemented casing to the depth of the stimulation target to protect shallow aquifers and isolate the target formation. The casing must be strong enough to support the hydraulic pressures necessary for stimulation.
3. The open-hole section should be sufficiently long to allow for multiple stimulation zones.
4. The open-hole section of the borehole should be in strong, impermeable, hot rock. Usually, this will mean that the borehole does not intersect an existing hydrothermal system.
5. The open-hole section should contain stimulation targets such as pre-existing natural fractures and/or lithological contacts that are relatively weak and well-oriented for slip in the current stress regime.
6. The walls of the fractures or contacts should be composed of hard rock capable of self-propping so that hydroshear-generated permeability remains high at fluid pressures lower than that required for hydroshear. Fractures filled with clay minerals or wall rock with significant clay alteration will not be suitable because hydroshear dilation is suppressed in clay-rich materials. Soft rocks like unwelded tuffs or unconsolidated sediments would also not be suitable for stimulation.
7. In order to have a successful demonstration, the improvement attributable to the applied technology should be quantifiable. That is, baseline values of injectivity and geothermal resource should be determined to compare to post demonstration values.

The above list is not exhaustive, but focused on the EGS resource and the potential to exploit it. Additional technical and non-technical requirements are discussed in other sections of this report. As discussed in detail in this section, the EGS resource surrounding NWG 55-29 meets all of the necessary characteristics listed above, as summarized below.

- **Large thermal anomaly** - Four deep exploration wells drilled on the northwestern flank of Newberry Volcano including NWG 55-29 indicate that the well lies within a large thermal anomaly (21 km<sup>2</sup>, 8 mi<sup>2</sup>) sufficient for many more well than the three planned for the demonstration.
- **Low permeability wells** – Where intersected by exploration wells, the natural reservoir permeability is very low, as evidenced by the lack of production flow. The measured injectivities in CEE 86-21, CEE 23-22 and NWG 55-29 were, respectively, 0.04 gpm/psi, 0.05 gpm/psi, and



0.02 gpm/psi, which are several orders of magnitude lower than typical geothermal production wells.

- **Sound well casing** – The upper portion of the well has multiple, cemented casing strings. The casing shoe is in strong rock with few fractures. The weakest portion of the casing can safely withstand a surface (wellhead) pressure of up to 24.6 MPa (3566 psi), which will be shown to be more than sufficient to create an EGS reservoir in sections to follow.
- **Long open hole** – The 8-1/2 in open-hole section is over 1000 m (3500 feet) long, extending from the casing shoe at 1969 m (6462 ft) to the TD at 3066 m (10060 ft).
- **Very high temperature in open hole** – In the open-hole interval, the temperature ranges from 228°C (442°F) up to 331°C (628°F).
- **Conductive temperature gradient in Well** – NWG 55-29 is characterized by an equilibrated conductive temperature gradient of 109°-128°C/km (6°-7°F/100 ft) from the surface casing at 338 m (1108 ft) to TD.
- **Low well injectivity** – Injection tests have been performed on NWG 55-29 at three different peak flow rates and wellhead injection pressures. All tests indicated injectivity of about 0.02 gpm/psi, which is more than an order of magnitude lower than needed for an EGS injection well. The low measured natural injectivity means that the water injected will be efficiently focused on generating new permeability, and that any injectivity improvement will be straightforward to measure.
- **Strong rock in open hole** – The lithologies in NWG 55-29 include a wide variety of volcanic, volcanoclastic and hypabyssal units, ranging from ash flows and debris flows, to silicic domes, mafic flows, and mafic and felsic dikes. The BHTV image did not reveal any irregularities in the borehole that would indicate weak zones.
- **No evidence of past hydrothermal system** – Mineralogical alteration in the well predominantly reflects diagenetic overprinting by thermal contact metamorphism, with very minor and localized hydrothermal alteration associated with past fluid flow in fractures and joints. No mineralogical evidence of a significant hydrothermal system is observed in the drill cuttings from this well. XRD analysis of drill cuttings and core indicates good correlation between modern temperatures and the borehole mineral assemblage.
- **No clay alteration of host rock or in fractures** – In the open-hole interval in NWG 55-29, expandable clays such as smectite or mixed layer phases such as chlorite-smectite or illite-smectite are absent. Phyllosilicates are limited to chlorite, illite/muscovite, and kaolinite. Formation of illite/muscovite, in conjunction with abundant chlorite and minor epidote, suggests a greenschist grade metamorphism throughout the open-hole interval. These minerals are distributed within fractures, but also as a penetrative alteration of the host rock adjacent to fractures. The lack of a clear set of relative ages among the metamorphic minerals suggests a single persistent episode of metamorphism.
- **Analogous core suggest that fractures will dilate and self-prop** – Geophysical logs indicate that the Geo N-2 core that was studied is representative of the materials that occur in NWG 55-29 from the casing shoe to a depth of approximately 2622 m (8600 ft). Thus, petrologic evidence that sheared fractures in clay-poor rock of Geo N-2 had dilated during slip, suggests that fractures in NWG 55-29 will behave in the same way.

- **Stimulation targets, fractures** – The BHTV log identified 351 fractures in the open-hole section of the well from 1970-2707 m (6462-8882 ft), most of which have an apparent aperture greater than zero at the wellbore interface. These fractures represent stimulation targets because they are weak points in the rock matrix, but, as indicated by all previous logging and testing, they are currently incapable of flow and lack significant permeability. The fractures identified in the BHTV have a wide variety of strikes and dips. A significant set of fractures with a mean strike of NNE and 60° E dip are likely to slip during EGS stimulation.
- **Stimulation targets, dike margins** – Felsic and granodiorite dike margins are likely to play a critical role in the permeability structure in NWG 55-29. The temperature log that was performed after injection at 1.39 l/s (22 gpm), showed several inflections near dike margins suggesting permeable zones in the borehole wall. In the BHTV image, the depths with felsic dikes immediately above the largest of the granodiorite intrusions contained the highest density of fractures.
- **Dike margin permeability** – Locally enhanced permeability at the margin of dikes is consistent with cracking caused by thermal stresses. In addition, analysis of cuttings shows less developed alteration of these intrusive rocks (e.g., less abundant chlorite and calcite) suggesting that late fractures formed in these dikes might be relatively open or have somewhat greater capacity for self-propping. The mud log identifies several dikes and an altered zone containing “abundant epidote” as well as several transitions between basalt and granodiorite below 2622 m (8600 ft). These contact surfaces all represent prime stimulation targets since they are areas where we would expect to find high natural fracture density.
- **Native and post-stimulation flow** – NWG 55-29 is a dry hole. It has no significant permeability below the casing shoe and is not connected to a hydrothermal system. A successful stimulation will create an EGS reservoir that will flow steam and water back to the surface at up to 800 gpm, indicating that the reservoir is ready to be tapped by production wells.
- **Power generation potential of producers** – The power generation potential of the two production wells is expected to range from 1.0-10.0 MW<sub>e</sub> per well.

To conclude, NWG 55-28 is a very high temperature, dry hole with resource characteristics that make it an ideal candidate for a demonstration of EGS technology. Sections below cover other important characteristics including seismicity (Section 4), stress orientations and magnitudes (Section 5), and stimulation planning and modeling (Section 7).

## 4 SEISMICITY

An Enhanced Geothermal System (EGS) reservoir is created by inducing shear slip on existing fractures by injecting water at high pressure (hydroshearing) into a rock formation. The shear slip increases fracture permeability and generates seismic vibrations, termed induced seismicity, that can be detected by seismometers and used to map EGS reservoir growth. Most induced seismic events have a magnitude less than M 2.0 and are not felt at the surface. However, some EGS projects have generated events large enough to be felt and cause minor damage. Thus, it is critical that EGS projects follow procedures to evaluate, monitor, and mitigate the risk of felt or potentially damaging induced seismicity.

The International Energy Agency (IEA) developed a protocol for addressing induced seismicity during geothermal projects that was adopted by the DOE for EGS demonstration projects (Majer et al., 2008). AltaRock has adapted this protocol to the geologic and environmental conditions at the Newberry EGS Demonstration and developed site-specific controls and mitigation procedures. A recent update to the IEA protocol, now available in draft form, (Majer et al., 2011) has also been incorporated into AltaRock's plan to mitigate induced seismicity.

An Induced Seismicity Mitigation Plan (ISMP) prepared by AltaRock has been reviewed and approved by DOE. The DOE-approved ISMP is attached as Appendix A-1 which includes 14 appendices of its own. As part of the ISMP preparation, AltaRock contracted with URS Corporation (URS) to conduct a thorough independent Induced Seismicity and Seismic Hazards and Risk Analysis for the Demonstration (ISMP Appendix F). This section summarizes details on Newberry Volcano seismicity that are discussed in detail within the ISMP and URS reports, and also incorporates additional details not included in those reports. Both documents must be reviewed as essential prefaces to this section.

### 4.1 HISTORICAL SEISMICITY

A review of historic earthquake data demonstrates that Newberry Volcano is essentially aseismic (Wong et al., 2010). In the pre-instrumental period, between 1891 and 1980, no earthquakes greater than M 5.0 are known to have occurred within 100 km (62 mi) of Newberry Volcano. Since the instrumental period began in 1980 with the expansion of the Pacific Northwest Seismic Network (PNSN) into Oregon, there have been only six  $M_L^{12} \geq 3.0$  earthquakes within 100 km (62 mi) of Newberry, most of which occurred in 1999 during a single swarm located 98 km (61 mi) southeast of Newberry. Wong et al. (2010) conclude that based on the instrumental record, no earthquakes have been located within 10 km (6 mi) of well NWG 55-29. Four microseismic events have been recorded at distances of 10-15 km (6-9 mi) from NWG 55-29 (see Figure 5 in ISMP Appendix F) in 2004 and 2005. These events all had  $M_L \leq 2.2$  and occurred at depths between 4 and 8 km (2.5-5 mi) (ANSS, 2011). Please refer to Section 3.3 of Appendix A-1 for full details on historical seismicity.

### 4.2 BACKGROUND SEISMICITY MONITORING

To improve seismic coverage around Newberry Volcano, AltaRock installed two new regional seismic stations (2 Hz, three-component sensors) in September 2010 to supplement the PNSN, one at River Meadows Home Owners Association (RMHA) in Three Rivers and another at La Pine High School (LPHS)<sup>13</sup>. AltaRock also installed a temporary surface microseismic array (MSA) in August 2010 consisting of seven seismic stations (4.5 Hz three-component sensors) surrounding NWG 55-29 that is currently

---

<sup>12</sup>  $M_L$  refers to Richter magnitude, and M refers to moment magnitude. See Appendix A-1 for detailed definitions.

<sup>13</sup> Stations RMHA and LPHS on map at [http://www.pnsn.org/WEBICORDER/BETTER/pnsn\\_staweb/index.html](http://www.pnsn.org/WEBICORDER/BETTER/pnsn_staweb/index.html)

collecting background seismicity to determine whether any natural microseismicity is occurring under the Demonstration area.

In addition to collecting background seismicity, the initial MSA array was installed to provide information needed for developing a velocity and attenuation model of the site, and designing the array that will operate during creation and circulation testing of the EGS reservoir. In cooperation with the U.S. Geological Survey (USGS), a calibration survey of the surface stations was performed in August 2010. Figure 4-1 illustrates which of the 12 shots were recorded at each of the seven MSA stations. Analysis of 36 arrival time measurements on seven AltaRock seismometers and 182 arrivals on 25 USGS seismometers, all at the surface, yielded a robust 5-layer velocity model down to a depth of 900 m (2953 ft) (Table 4-1; Appendix D-1). In addition, the surface MSA minimum magnitude threshold was estimated to be M 0.5 based on analysis of the signal from the explosive shot compared to the noise level (Appendix D-1).

Table 4-1. 1-D velocity model derived by Foulger Consulting (2010).

Depth Interval (m)	Depth Interval (ft)	Velocity (km/s)
0 – 150	0 – 492	2.0
150 – 300	492 – 984	2.0
300 – 450	984 – 1476	3.4
450 – 600	1476 – 1969	3.5
600 – 750	1969 – 2461	3.7
750 – 900	2461 – 2953	3.8
> 900	> 2953	unresolved

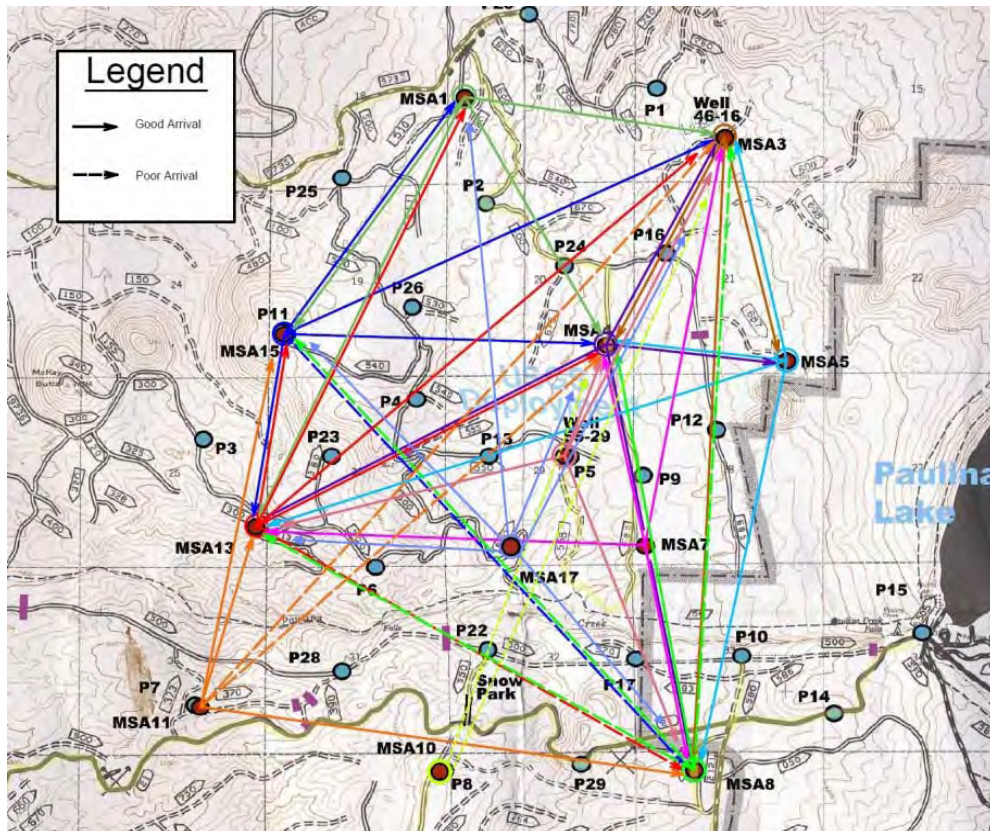


Figure 4-1. Calibration shot arrivals. Stations with colored circles represent shot points, and the associated colored arrows show which stations recorded the arrivals from that calibration shot.



After the calibration survey, the surface MSA was left to record natural background seismicity to determine whether any natural microseismicity is occurring under the Demonstration area at magnitudes too low to be detected by the regional network ( $M < 2.0$ ), but large enough to be detected by surface seismometers ( $M > 0.5$ ). To date, the local MSA has not detected any local events in the data that have been downloaded and processed. Although the network was designed to detect local microseismicity, not regional and teleseismic earthquakes, the network did trigger on an M 5.4 event that occurred offshore of Oregon on 8 February 2011 (Figure 4-2). An examination of time windows in which global earthquakes with  $M > 7.0$  occurred revealed long period seismic energy arriving at the network from at least six global events (Table 4-2) including the 11 March 2011 M 9.0 earthquake in Japan, and two major aftershocks. Please refer to Section 3.3 of Appendix A-1 for full details on background seismicity monitoring.

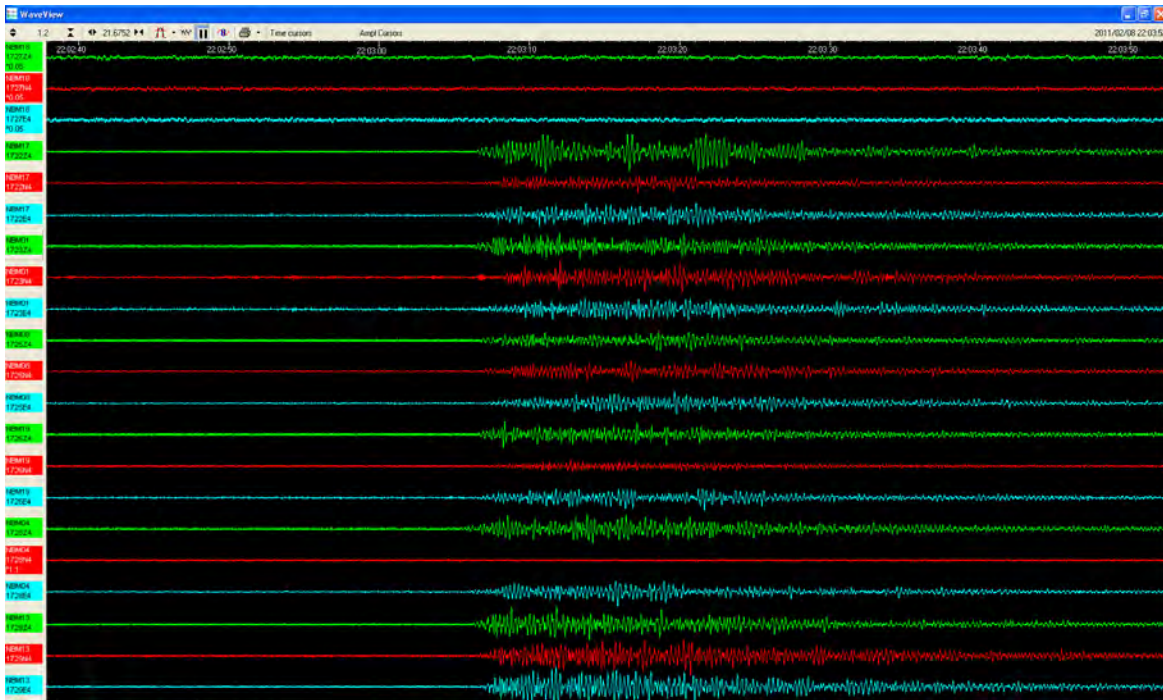


Figure 4-2. Seismic energy recorded on 16 of 21 components of the local MSA (7 stations, 3 components each) from M 5.4 regional event that occurred ~230 km (143 mi) off the Oregon coast at a depth of 34 km (21 mi) at 22:02:05 UTC on 8 February 2011.

Table 4-2. One regional and six global earthquakes identified on the local MSA network.

Date – Origin Time	Magnitude	Location
12/25/2010 – 13:16:37	7.3	Vanuatu Region
01/01/2011 – 09:56:58	7.0	Argentina
01/13/2011 – 16:16:41	7.0	Loyalty Island
02/08/2011 – 22:02:05	5.4	Oregon (triggered)
03/11/2011 – 5:46:24.62	9.0	Japan
03/11/2011 – 6:15:40.88	7.9	Japan
03/11/2011 – 6:25:50.79	7.1	Japan

### 4.3 EVALUATION OF PROXIMAL FAULTS

As previously mentioned, Wong et al. (2010) determined that no earthquakes have been detected within 10 km (6 mi) of NWG 55-29 during the instrumental period. However, nearby faults and structural features have been studied to assess their potential for experiencing movement due to induced seismicity. Four caldera ring fractures have been mapped on the northwest flank of Newberry (Sherrod et al., 2004). NWG 55-29 is located within 3.2 km (2 mi) of the caldera rim and near the projection of ring fractures, and these ring fractures could potentially have been intersected during drilling. However, detailed review of drilling logs, mud logs, BHTV data, and cuttings analysis reveals no evidence of ring fractures or faults in the NWG 55-29 well bore (Letvin, 2011).

AltaRock joined the Oregon LiDAR consortium to add La Pine, the community nearest the Demonstration, to the 2010 LiDAR survey of Newberry Volcano and Deschutes National Forest. In particular, we were interested in better characterizing the La Pine Graben faults shown in the USGS Quaternary fault and fold database west of La Pine (Personius, 2002a), the ring fractures (Personius, 2002b), and checking for evidence of unmapped faults or fractures in the Demonstration area. Our analysis of the 880 km<sup>2</sup> (340 mi<sup>2</sup>) of new LiDAR data is shown in Figure 5-3 and Figure 5-4, and is discussed in detail in [Cladouhos et al. \(2011a\)](#).

Within the LiDAR dataset, the ring fractures mapped in the USGS database are not prominent. The ring fractures are expressed as curved lineaments defined by an alignment of vents, some of which with central fissures, that end more than 3 km (1.9 mi) from NWG 55-29. Dip-slip fault offset along the ring fractures is not observed in the LiDAR surfaces. In conclusion, based on the results of CalEnergy exploration and LiDAR, the ring fractures on the northwestern and western flank of the edifice do not appear to be active faults. Therefore, for the purpose of hydroshearing controls and mitigation presented below, the ring fractures are not considered to be at risk of slipping. Please refer to Appendix A-1 Section 3.7 for a more extensive discussion on the evaluation of proximal faults.

### 4.4 FINAL MSA DEPLOYMENT PLAN

The accuracy of earthquake hypocenters and moment tensors is a function of the number of seismic stations and geometry of the seismic network. The accuracy of seven different proposed seismic networks were modeled (Appendix D-2). All simulations with different combinations of the locations indicated on Figure 4-3 had horizontal location errors of less than 408 m (1340 ft), with an average error of all networks of 218 m (715 ft). These location errors are a worst case for real-time, single-event locations. During the actual stimulation, event locations will be iteratively improved and errors reduced by relative relocation techniques, improved velocity models, and review by seismologists. For now, we take a cautious approach and assume a horizontal accuracy of 400 m (1312 ft).

The current plan for the final MSA, based on the optimal network configuration (Figure 4-4) determined by Foulger Consulting (2011), consists of 4-7 surface seismometers and 6-10 borehole seismometers. Figure 4-3 shows the locations of the proposed stations, including some alternate sites. These locations will be evaluated as part of the permitting process and, therefore, is subject to modification. In addition to these MSA stations, a strong motion sensor (SMS) will be installed at or near the Paulina Lake Visitor Center. Please refer to Section 3.3 of Appendix A-1 for full details on the final MSA deployment plan.

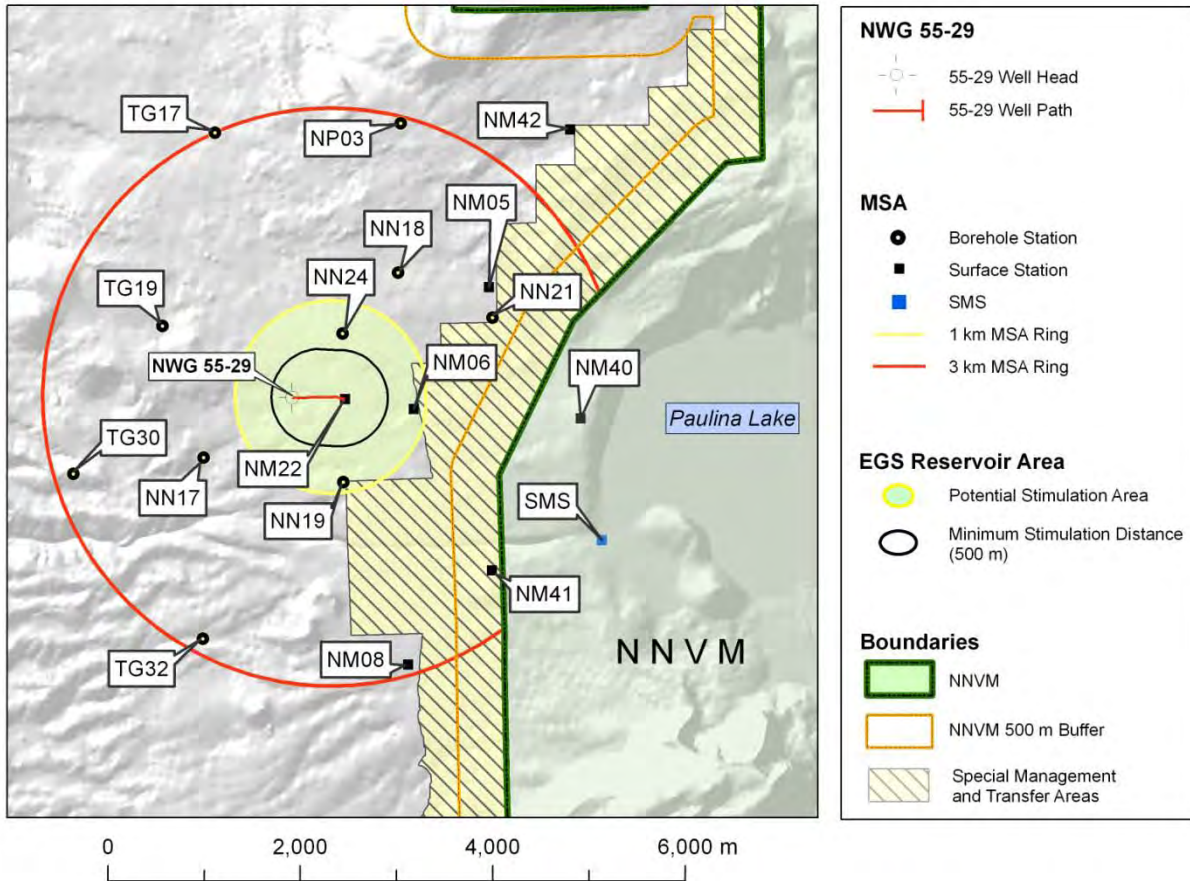


Figure 4-3. AltaRock final MSA as currently planned. Yellow and red circles represent 1 km (0.6 mi) and 3 km (1.9 mi) radii, respectively, around stimulation zone. Green region within 1 km (0.6 mi) radius is current prediction of the microseismicity cloud that will be induced, and the inner black ring the approximate extent of the EGS reservoir potential stimulation area, based on a preliminary stress model. Multiple zones will have different depths but roughly the same map view. Hatched area is a Special Management Area (no surface occupancy) adjacent to the Monument (outlined in green).

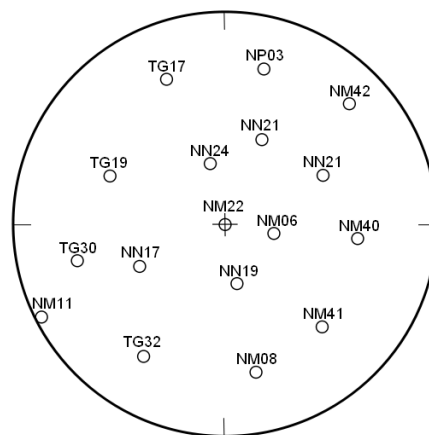


Figure 4-4. Focal coverage map showing final MSA geometry as planned, adapted from Foulger Consulting (2011).

## 4.5 SEISMICITY ANALYSIS PLAN

Each MSA station will be equipped to collect and transmit real-time, continuous data to an operational center. The raw data will also be provided in real-time via broadband internet connection to Lawrence Berkeley National Laboratory (LBNL) where the data will be archived and displayed to the public on the EGS Induced Seismicity website<sup>14</sup>. The current MSA plan calls for 16 stations with telemetry, which provides redundancy in the event a station is temporarily out of service. Field seismologists and IT specialists will be on-contract to ensure that 90% of the stations are operational at all times, and to implement station repairs as quickly as possible.

Auto-processing software will be set to auto-pick and locate events. The operational center will be staffed by seismologists that will refine seismic wave auto-picks, improve event locations, and track maximum event size and the size distribution of microseismicity (the b-value) 24 hours a day. The Project Manager will ensure that a seismicity report is transmitted daily to the DOE, BLM, FS, PNSN, and LBNL. Trigger and mitigation reports will be prepared and sent to the DOE, BLM, FS, PNSN and LBNL if any triggers are exceeded or mitigation actions taken (see Section 5 of Appendix A-1).

Locations and seismograms of identified seismic events will then be sent via Internet to LBNL. Data sharing and archiving agreements, links, and search tools will ensure that the raw seismic data will be available to the public and scientific community from LBNL<sup>14</sup>, PNSN<sup>15</sup> and the Northern California Earthquake Data Center<sup>16</sup> (NCEDEC) websites. This system will be operational before stimulation begins, and operation will continue throughout the Demonstration. Please refer to Section 3.3 of Appendix A-1 for full details on seismicity analysis plan.

## 4.6 GEOMECHANICAL PREDICTIVE MODELING

AltaRock is participating in two DOE projects, one at Pennsylvania State University and another at Texas A&M University, on modeling the geomechanical/thermal/geochemical responses to EGS reservoir creation and circulation. AltaRock is providing cost-share in the form of personnel time and the in-kind value of data provided for modeling.

The project at Pennsylvania State University, under the direction of Dr. Derek Elsworth, is titled "*THMC Modeling of EGS Reservoirs - Continuum through Discontinuum Representations*" (DOE Grant DE-EE0002761). This project is exploring the timing and magnitude of permeability evolution during and after stimulation, including the potential to manage the various factors that would control permeability in a producing EGS field.

The project at Texas A&M, under the direction of Dr. Ahmad Ghassemi, is titled "*Development of a Geological and Geomechanical Framework for the Analysis of MEQ in EGS Experiments*", (DOE grant GO18194). This project will: (1) develop a 3D model for stochastic seismicity-based reservoir characterization that considers rock failure in shear and tension based on damage mechanics; (2) analyze the rock response to injection using fully-coupled poro-thermoelasticity in a finite element model with stress dependent permeability; and (3) utilize a probabilistic description of model parameters and a geostatistically derived ensemble of rock mass permeability and criticality distributions to predict micro-seismic events. The modeling results will be compared to the reservoir seismicity response using a stochastic inversion process to estimate the reservoir permeability, in-situ stress and stimulated volume.

---

<sup>14</sup> [Lawrence Berkeley National Laboratory, Earth Sciences Division - EGS Earthquake Maps](#)

<sup>15</sup> [The Pacific Northwest Seismic Network](#)

<sup>16</sup> [Northern California Earthquake Data Center](#)



Reservoir-scale predictions are not available at this time from either of the above modeling efforts. To model and visualize EGS stimulation scenarios in advance, AltaRock has been using AltaStim, a proprietary stochastic fracture and flow model developed internally. The output from the model allows the uncertainty in the stimulation process to be assessed and some key engineering decisions to be made, such as the potential variability in the stimulation fluid volume, and the hydraulic and thermal performance of the EGS reservoir.

The AltaStim approach does not treat the stimulation as a dynamic, hydraulic process. It considers a series of static assumptions of the pressure field within the rock mass. This simplification reduces the execution time for each realization, and enables the investigation of a statistically meaningful number of realizations. The development of a preliminary Newberry EGS AltaStim model and the modeling results are discussed in Section 7.4 and Cladouhos et al. (2011b).

#### 4.7 LESSONS LEARNED FROM OTHER PROJECTS

Geoscientists from the AltaRock team have studied the history of injection-induced seismicity (IIS) (Table 4-1), including work done by Majer et al. (2007) and Wong et al. (2010). Some details of our analysis can be found in Cladouhos et al. (2010) and [Cladouhos et al. \(2011a\)](#). IIS is associated with changes in stress or fluid pressure in the Earth's crust that can accompany withdrawal or injection of fluids during both geothermal and non-geothermal operations (oil and gas development, enhanced oil recovery, waste disposal in deep wells). The most relevant lessons learned from the previous EGS projects are described below. A more extensive discussion can be found in Section 3.8 of Appendix A-1.

In previous EGS projects, the stimulated injection well was usually shut-in after hydroshearing. The excess pressure, created by water injection and thermal expansion of the injected fluid, slowly diffused into the fracture network and rock matrix, and continued to induce microseismicity. At the Basel project, the largest event occurred after pumping had stopped and the well was shut-in, possibly because a flow test was not initiated to relieve reservoir pressure. In an extensive review of induced seismicity in EGS projects, Majer et al. (2007) notes "... at Soultz, The Geysers, and other sites, the largest events tend to occur on the fringes, even outside the main 'cloud' of events and often well after injection ceases." They continue "... moreover, large, apparently triggered events are often observed after shut-in of EGS injection operations, making such events still more difficult to control." A possible solution to this problem is suggested by the two instances where the wells were flowed back to the surface rather than remaining shut-in. After Soultz GPK3/2 dual well stimulation (Charlety et al., 2007), and at Basel after the largest event occurred (Häring et al., 2008), the wells were bled-off and microseismicity rates declined faster than in the more numerous instances in which the wells were shut-in and not flowed back.

**Table 4-3. Projects involving injection-induced seismicity studied for this Demonstration.**

Project Site	Project Type	Approx. Start Date
Geysers <sup>1,2,3</sup> (USA)	Geothermal	1960
Rocky Mountain Arsenal <sup>1</sup> (USA)	Waste Disposal	1962
Rangely <sup>1</sup> (USA)	Oil Field	1967
Fenton Hill <sup>3,4</sup> (USA)	Geothermal (HDR)	1973
Soultz <sup>1,2</sup> (France)	Geothermal (EGS)	1987
Hijori <sup>3,4</sup> (Japan)	Geothermal (HDR)	1988
Ogachi <sup>3</sup> (Japan)	Geothermal (HDR)	1989
Paradox Valley <sup>1</sup> (USA)	Brine Disposal	1991
Berlin <sup>2</sup> (El Salvador)	Geothermal (EGS)	2003
Cooper Basin <sup>2</sup> (Australia)	Geothermal (EGS)	2003
Basel <sup>1,2</sup> (Switzerland)	Geothermal (EGS)	2008

<sup>1</sup> Discussed in Cladouhos et al. (2010)

<sup>2</sup> Discussed in Majer et al. (2007)

<sup>3</sup> Discussed in [Wong et al. \(2010\)](#)

<sup>4</sup> Discussed in [Cladouhos et al. \(2011a\)](#)

After hydroshearing is completed at the Newberry EGS Demonstration, we plan to flow back the injected water after a brief shut-in period of at least 3 hours, but not exceeding 24 hours, to relieve reservoir pressure and mitigate continued fracture growth and induced seismicity. Based on the Basel experience, we plan to keep sumps on two well pads empty so as to hold at least 10% of the volume injected in any stage. Accordingly, two sumps with a combined capacity of about 10600 m<sup>3</sup> (2.8 million gallons) will be available, sufficient to contain 20% of the maximum water use estimated for single-well stimulation over a 21-day period. We will be on alert for rising pressure at constant flow rates and M > 2.0 seismic events. Flow rates will not be increased without careful review of surface and downhole pressure, and microseismic event magnitudes and rates, as detailed in Appendix A-1.

## 4.8 MAXIMUM MAGNITUDE PREDICTIONS

Maximum magnitudes ( $M_{max}$ ) are one of most important inputs into seismic hazard analysis. The magnitude of an earthquake is proportional to the area of the fault that slips in an event and the amount of stress that is released (i.e., stress drop). Several conditions must be met for a potentially damaging earthquake to occur. There must be a large enough fault, stresses must be high enough to cause slip, and the fault needs to be pre-stressed and near failure. As recognized by many, the characteristics of induced seismicity are controlled by the characteristics and distribution of pre-existing fractures and faults, and the local stress field in the volume of rock surrounding the well where fluid is being introduced (Majer et al., 2007).

Two basic approaches are used to estimate the potential  $M_{max}$  for Newberry EGS activities, analogs from other EGS and geothermal projects, and theoretical models. After evaluating results from other projects and three deterministic models, an upper-bound for  $M_{max}$  for the Newberry EGS Project of M 3.5 to 4.0 is defensible. Applying the most recently developed model, the probability of an event with M > 3.0 is less than 1%, with the most likely (median)  $M_{max}$  less than M 1.0. Please refer to Section 3.4 of Appendix A-1 for full details on maximum magnitude predictions.

## 4.9 LOCAL INDUCED SEISMICITY DURING INJECTION

In an area with a known Gutenberg-Richter relationship (discussed in Section 2.3 of Appendix A-1) from either natural seismicity or induced seismicity, the distribution of future seismic events (natural or

induced) due to injection can be constrained. However, the region around the Newberry EGS Demonstration is aseismic and there is currently no geothermal development or associated anthropogenic seismicity; therefore, no a- or b-value can be determined in advance. Instead, we can assume an a- or b-value based on project goals, and consistent with analogous locations, to estimate the probability of larger events. A simple illustration of this approach is shown in Figure 4-5. For the example here, a b-value of 1.25 is assumed from the results observed during stimulation of Soutz well GPK2 (Dorbath et al., 2009). As discussed Section 5 of Appendix A-1, a project goal is to keep the magnitude of induced events below M 2.0. For this example, we set the a-value so that an M 1.7 has a probability of 100% during the one month stimulation process. As shown in Figure 4-5, this approach predicts over 2300 M -1 events, 133 M 0 events, and 7 M 1.0 events. In this example, the probability of an M 3.0 event is 2% over the same period. A robust theoretical approach has been introduced to use regionally determined a- and b-values and the volume injected to better constrain the probabilities of larger events (discussed in Sections 3.4 and 3.9 of Appendix A-1). The more robust calculations yield a probability of less than 1% for an M 3.0 event during the stimulation.

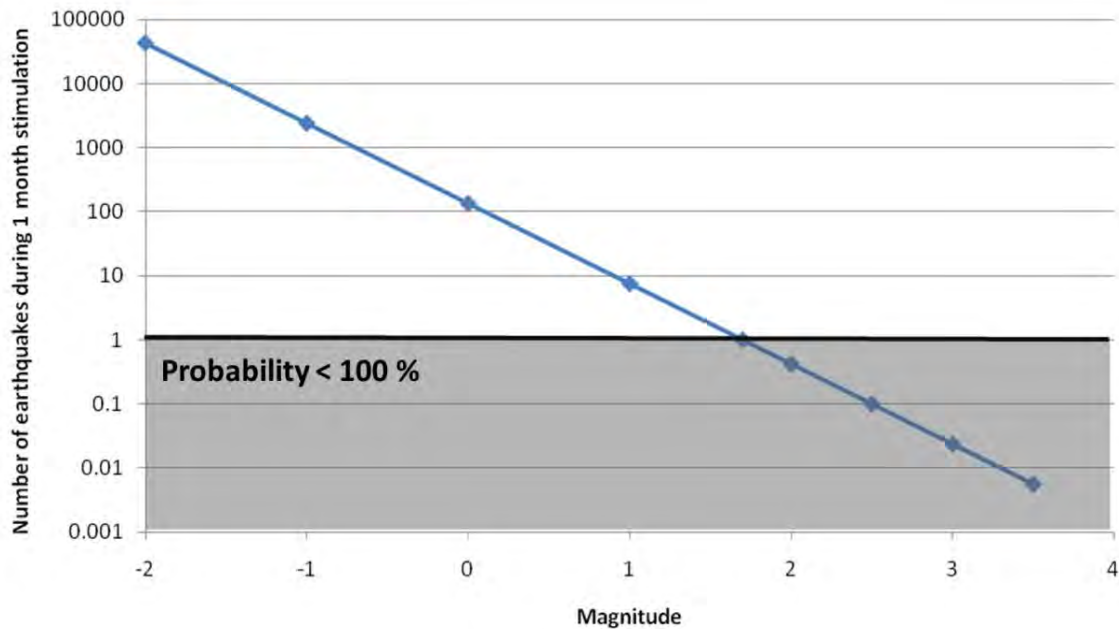


Figure 4-5. Hypothetical Gutenberg-Richter Law illustrating the probability and expected size distribution of seismicity during the Newberry EGS Demonstration. This relationship is defined by the equation:  $\log(N) = a - bM$ , where  $N$  = number of earthquakes during 1 month stimulation,  $M$  = magnitude,  $b = 1.25$  (based on Soutz GPK2), and  $a = 2.125$  (chosen so that a M 1.7 event has a 100% ( $N=1$ ) probability of occurring during the approximately 1 month injection period).

## 4.10 ASSESSMENT OF INDUCED SEISMICITY AND SEISMIC HAZARDS AND RISK

As mentioned above, AltaRock contracted URS to conduct an independent Induced Seismicity and Seismic Hazards and Risk Analysis for the Demonstration. A full discussion of this seismic hazards and risk analysis can be found in Section 3.5 of Appendix A-1, and the complete URS report is attached as Appendix F to the ISMP.

The executive summary of Appendix F to the ISMP concludes:

“The results of the probabilistic seismic hazard analysis indicate that there is no difference in hazard at La Pine, Sunriver, and the Project site (NWG 55-29) between the baseline conditions (which incorporates the hazard from both natural tectonic and volcanic seismicity) and the EGS induced seismicity. As a result, potential EGS induced seismicity poses no seismic risk to the residents in the neighboring communities.

However, potentially larger EGS earthquakes of M 3.0 and higher, should they occur, will probably be felt in La Pine and Sunriver, but not at damaging levels of ground motions (>0.10 g). Individual residents within 10 km (6.2 mi) of the Project site will feel the larger events. The strength of shaking will depend on the size of the event, and distance to and site conditions at each location. The effects of induced seismicity will be more of a nuisance than a hazard to the vast majority of local residents because of the small size of the events and distances to centers of population.”

For natural earthquakes, a peak ground acceleration (PGA) of 0.1 g is perceived by humans as strong shaking and the potential for damage is light (Wald et al., 1999). However, it has been observed that perceived shaking and damage due to EGS induced seismicity is typically lower (Majer et al., 2007).

## 4.11 INDUCED SEISMICITY MITIGATION PROTOCOL AND PROPOSED CONTROLS

The DOE-approved ISMP for the Newberry EGS Demonstration includes detailed plans for mitigation of induced seismicity, and defines limits (or ‘triggers’) that, if activated, will initiate mitigation actions up to and including stopping injection and immediately flowing the well to reduce reservoir pressure. The triggers will be monitored during hydroshearing and EGS reservoir creation, and throughout the remainder of the Demonstration. These triggers are based on real-time measurement of seismic activity on the PNSN regional network, the AltaRock MSA, and the Paulina Lake SMS.

## 4.12 SUMMARY

To allay concerns that the Newberry EGS Demonstration may result in excessive induced seismicity and unacceptable seismic risk, AltaRock has conducted a series of investigations prior to any stimulation activity. Based on the results of these investigations, AltaRock has developed an extensive ISMP, including detailed discussions regarding induced seismicity, and the robust safeguards and mitigation controls that will be applied during the Demonstration. The safeguards are built on a foundation of local geologic conditions and monitoring, lessons learned from previous EGS projects, and geomechanical theory. We are confident the ISMP will serve as an effective safeguard for the Newberry EGS Demonstration.



## 5 IN SITU STRESS

The *in situ* stress tensor is a primary control on the design and creation of an EGS reservoir. Stress orientations and relative magnitudes control which fractures are most likely to slip and, consequently, the orientation and overall shape of the resulting EGS reservoir (e.g., Hickman and Davatzes, 2010). Stress magnitudes determine the fluid pressure required to initiate hydroshearing, the effectiveness of that shearing in enhancing permeability (depending also on rock mechanical properties; see Lutz et al., 2010), and the volume of the EGS reservoir. At the outset of any EGS project, tectonic studies, well tests and geophysical logs must be used to constrain the stress state.

### 5.1 REGIONAL STRESS INDICATORS

South of Newberry, Crider (2001) inverted for stress directions using focal mechanisms from earthquakes with moment magnitude ( $M$ ) greater than 4.0 (Figure 5-1). The solution yields a stress tensor with: (1) the least compressive stress sub-horizontal ( $S_{\text{hmin}} = \sigma_3$ ) and oriented E-W or slightly ENE-WSW ( $264^\circ \pm 29^\circ$ ); (2) the greatest compressive stress near vertical ( $S_v = \sigma_1$ ); and (3) the intermediate stress approximately N-S ( $S_{\text{Hmax}} = \sigma_2$ ). Other geologic stress indicators including dikes, cinder cones, and normal faults yield stress directions within the study area shown in Figure 5-1 that are consistent with the results of this focal mechanism stress inversion (Figure 5-2).

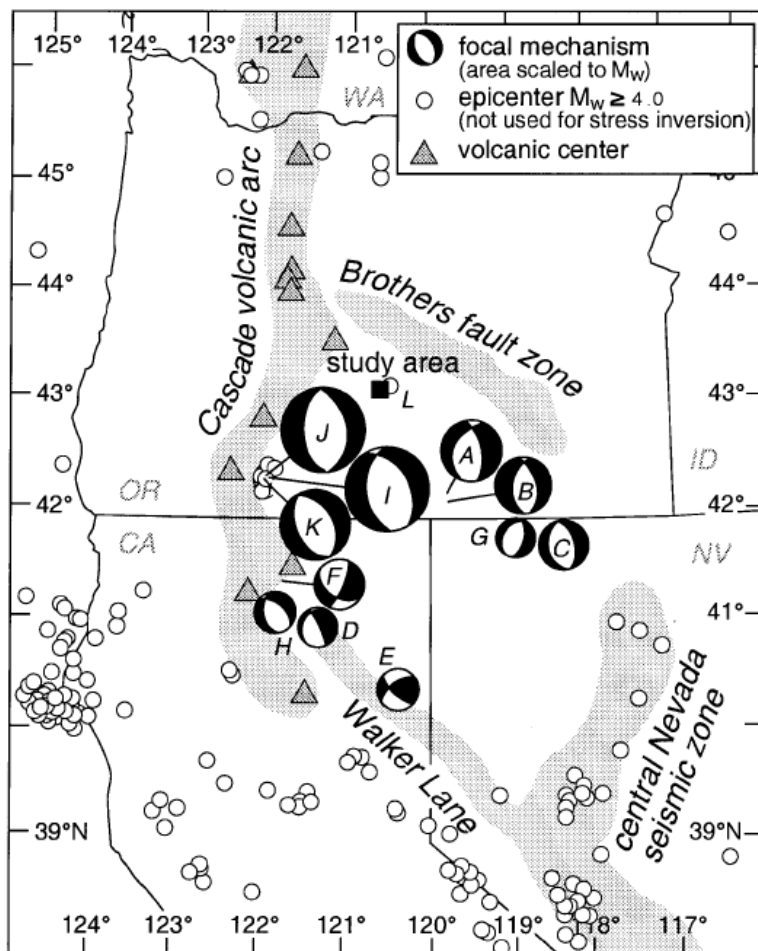


Figure 5-1. Earthquake focal mechanisms used to invert for principal stress directions (from Crider, 2001, Figure 5). Shaded areas represent boundaries of tectonophysiographic regions. References for focal mechanisms are given in Table 1 in Crider (2001). Other earthquakes are from the National Earthquake Information Center (2000). Base map is adapted from Pezzopane and Weldon (1993). Gray triangle immediately above the "study area" of Crider (2001) represents Newberry Volcano.

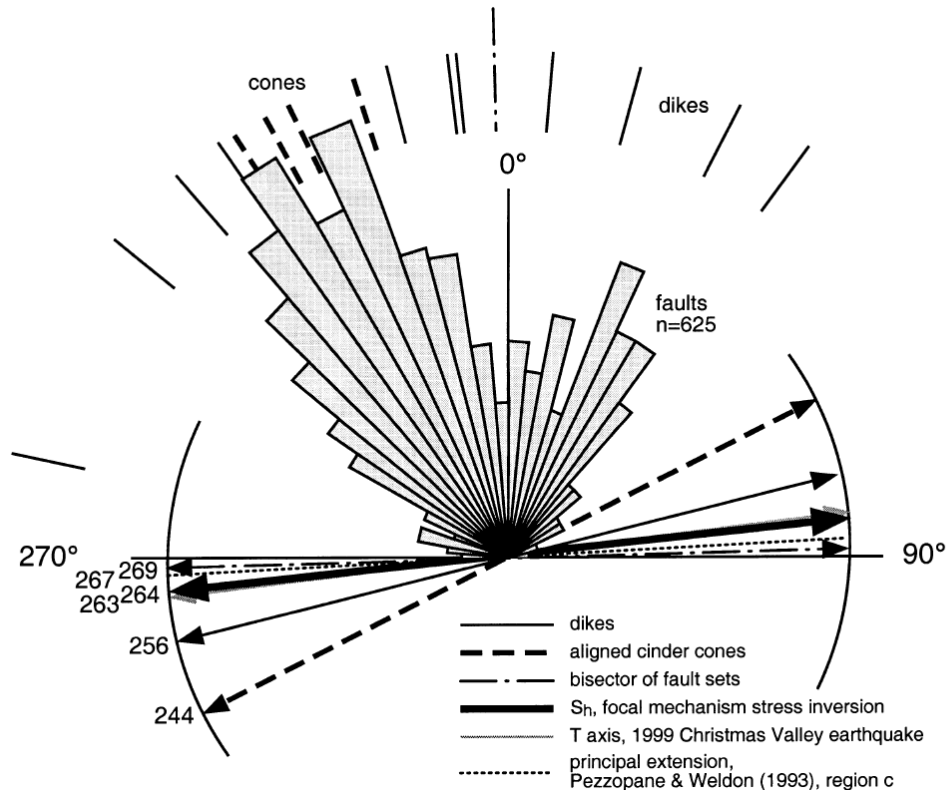


Figure 5-2. Rose diagram summarizing the strike of mapped normal fault scarps and other geologic structures in the Crider study area that were used to infer stress directions (reproduced from Crider, 2001, Figure 4). Fault data (Donath, 1958) are divided into 5° sectors; the length of each sector is proportional to the number of scarps. Two clusters of fault strikes are evident, centered at azimuths of 025° and 332°. The bisector of the two clusters is shown at the perimeter of the diagram, along with the strikes of 11 dikes and the direction of alignments of three or more cinder cones (Walker et al., 1967). Arrows show associated directions of regional extension. The geologic least-compressive stress is interpreted to be perpendicular to the mean strike of dikes or cone alignments and horizontal, and is thus equivalent to the least horizontal principal stress,  $S_{hmin}$ . These geologic extensional stress directions are consistent with the current direction of  $S_{hmin}$  (heavy black arrow) as determined by Crider (2001) from inversion of earthquake focal mechanisms, with the uncertainty in this inversion depicted by the associated arcs. For reference, the extension direction shown is a mean value obtained from the bisector to the Donath (1958) data and moment tensors summation (Pezzopane and Weldon, 1993).

Closer to Newberry, the strike of normal faults and extensional vents or fissures mapped with LiDAR provide a first approximation of the local  $S_{hmin}$  direction that will control the orientation of the EGS Reservoir. The fault scarps on the west side of the La Pine Valley cut modern alluvial sediments and are considered to be younger than 130 ka (Personius, 2002a). The youngest vents and fissures are part of the Northwest Rift and must be younger than 7 ka because they were conduits for basalts flows which overlie the Mazama ash erupted between 6600 and 6700 carbon-14 years BP (MacLeod et al., 1981).

The average normal fault strike on the west side of the LiDAR compilation and the average fissure strike on the east side of the data set differ by only about 10° (Figure 5-3 and Figure 5-4). The sense of offset and attitude of these features suggest a normal faulting stress regime with roughly E-W extension across the area shown in Figure 5-3. The fault scarps show only minor variation in strike, suggesting that these structures reflect the geologically recent direction of the least compressive principal stress,  $S_{hmin}$ , near the Newberry EGS site. This local stress orientation is more uniform than might be expected for the Newberry region based on the juxtaposition of three different structural trends evident in Figure 2-3.

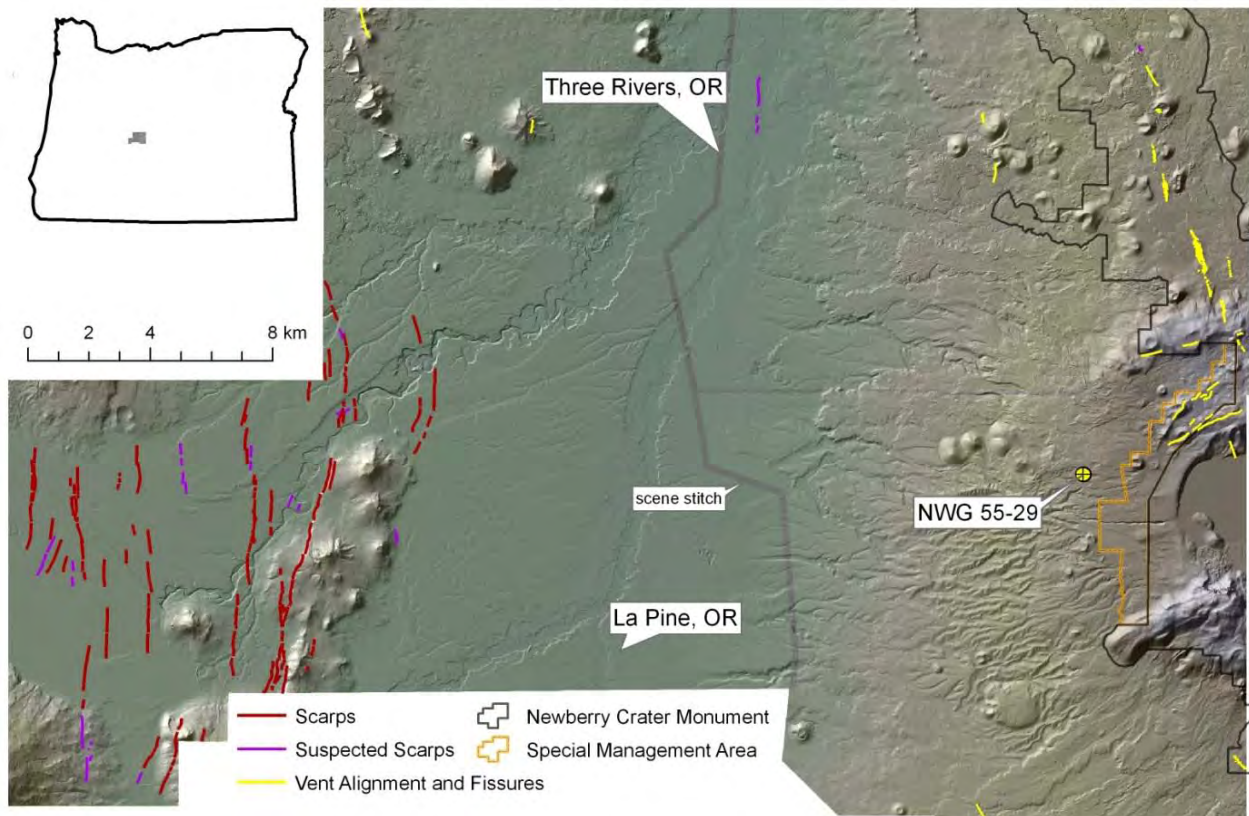


Figure 5-3. LiDAR image from the west flank of Newberry Volcano. Image from Oregon LiDAR Consortium. Lineament interpretations by AltaRock (Cladouhos et al., 2011a).

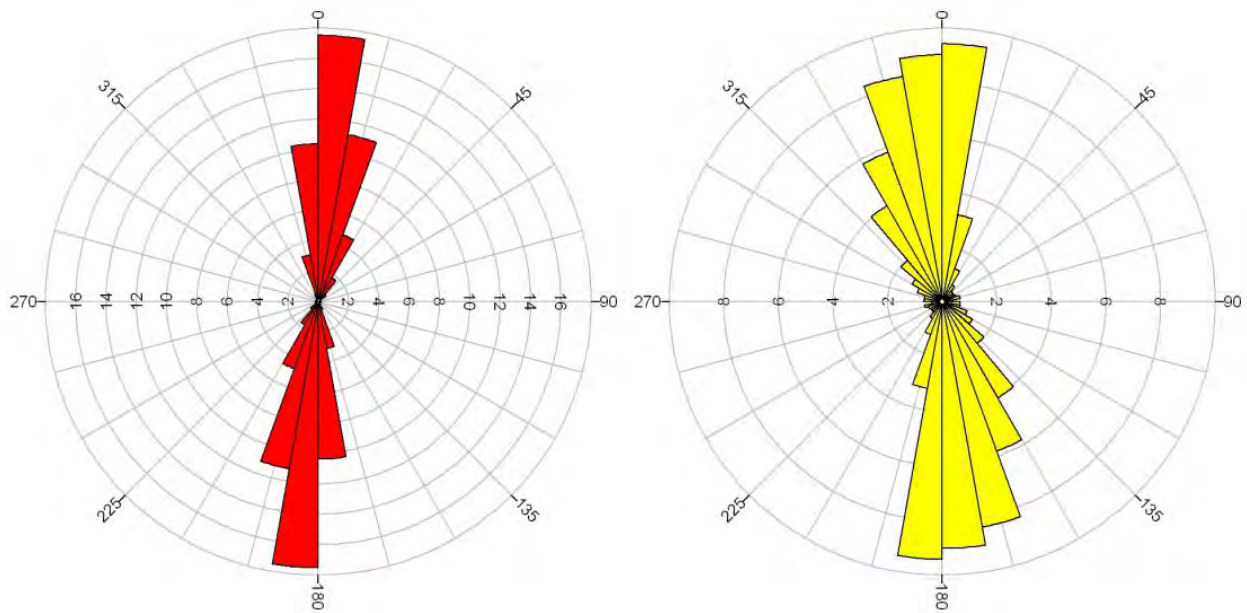


Figure 5-4. Rose diagrams of LiDAR scarps (left) and fissures (right) mapped in Figure 5-3 (from Cladouhos et al., 2011a). Concentric circles are in percent of total data.

In a normal faulting stress regime with  $S_{\text{hmin}}$  oriented approximately E-W, we expect that the EGS reservoir will grow in a north-south direction due to activation of steeply dipping, N-S striking fractures as seen in similar stress regimes (e.g., Heffer, 2002; Cornet et al., 2007). This conclusion is further supported by the analysis of BHTV data acquired in Newberry EGS Well 55-29 (Section 5.4) that shows similar stress directions and fracture populations.

## 5.2 STRESS INDICATORS FROM NEARBY WELLS AND TEMPERATURE COREHOLES

A review of past work conducted on the western flank of the Newberry volcanic edifice reveals limited information from two CalEnergy holes related to the flow banding, fracturing and stress conditions (Figure 5-5). CalEnergy temperature core hole CEE 76-15 TCH was logged with the Sandia televiewer in October, 1995. Fracture and flow band attitudes were picked from the interval 838 to 1108 m (2748-3636 ft). The best data are limited to a depth range of 838 to 945 m (2748-3100 ft), providing images in only about 7% of the hole.

The flow bands dip, on average,  $56^\circ$  to the west-northwest (Figures 5-6 left) indicating that, at least in the 107 m-thick (352-ft) block where most of the attitudes were measured, the volcanic rocks were deposited on a very steep slope or they have been tilted since deposition. The steep dips are similar to NWG 55-29, as discussed in Section 3.2.8 and shown in Figure 3-45, although the dips of layers in NWG 55-29 are both to the west and east. The dominant fracture orientation dips  $69^\circ$  to the northwest, with lesser fracture sets dipping  $70^\circ$  to  $80^\circ$  from E-NE to E-SE (Figures 5-6 right). The report discussing these data (Pulka, 1995) does not mention borehole breakouts. However, it does state that a maximum horizontal principal stress direction of  $229^\circ$  was “deciphered from televiewer response in the elliptical borehole” without a clear explanation of what these features looked like or the methodology used to interpret them. Thus, the three elements measured by the televiewer run, flow bands, fracture orientations, and maximum horizontal principal stress, all seem to be broadly subparallel to the local ring fracture attitudes, which have NE-SW azimuths in the area (Figure 5-5).

Taken at face value, the Pulka (1995) analysis requires a roughly  $45^\circ$  clockwise rotation of the maximum horizontal principal stress axis at hole CEE 76-15 TCH compared to the regional stress indicators discussed in the previous section, which both independently indicate a roughly E-W minimum horizontal principal stress. If real, this stress rotation could be related to the position of the hole near the ring fractures and on the northern flank of the edifice. However, it is difficult to ascertain the quality of the data and interpretations with the limited information available.

CEE 23-22, one of the two CalEnergy production-sized exploration holes, was logged with the Halliburton CAST (circumferential acoustic scanning tool) from 244-1306 m (800-4285 ft). The CAST log was not available, but AltaRock did examine the fracture and bedding plane orientation interpretation from this log. There is a great deal of scatter in this data set, and no accompanying interpretation or data quality annotations. Therefore, the CEE 23-22 data is not considered to be a reliable indicator of fracture or flow attitudes.



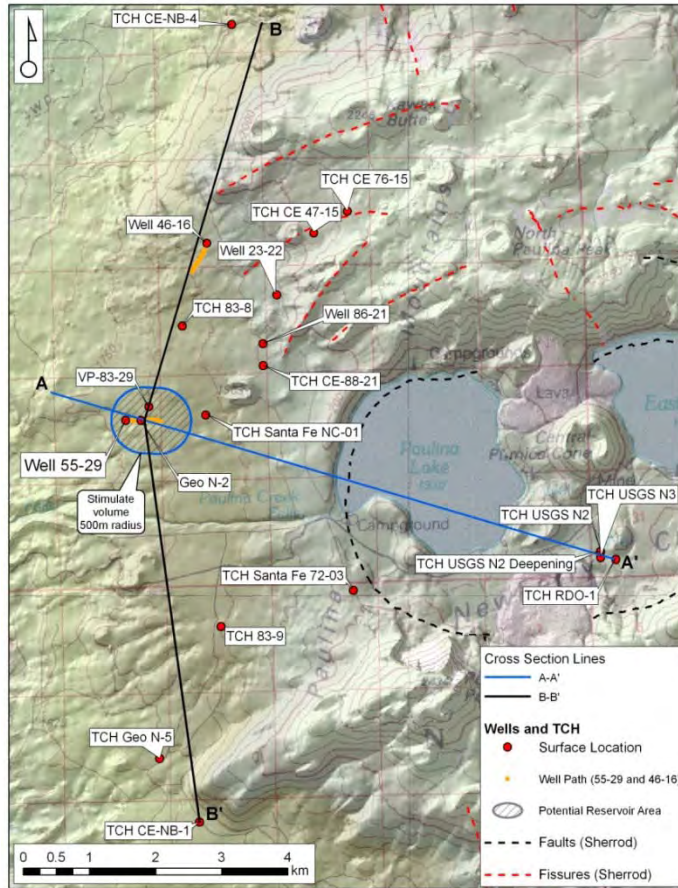
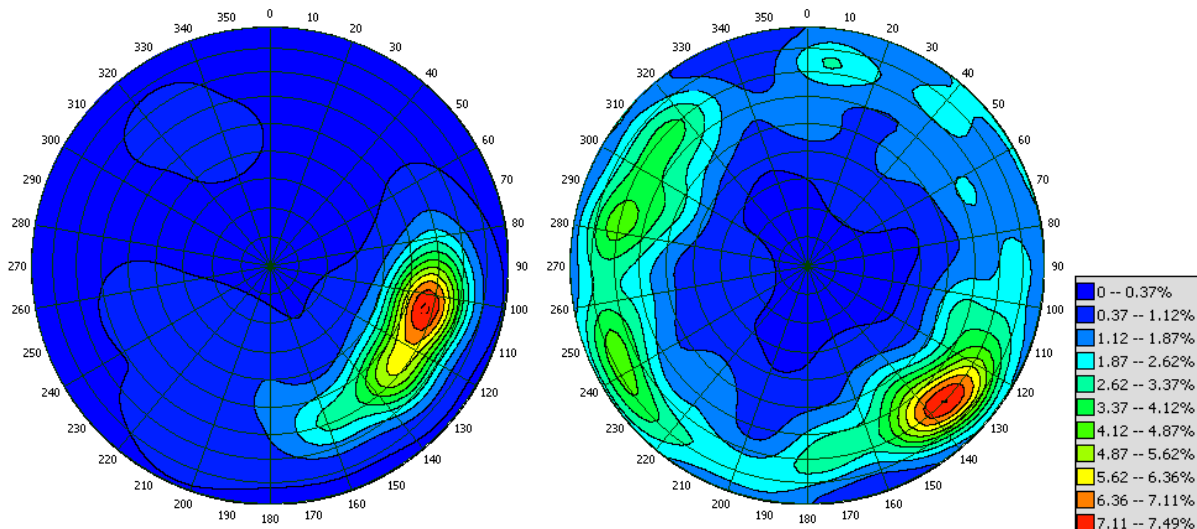


Figure 5-5. Locations of exploratory holes on western flank of Newberry, including CEE 23-22, CEE 76-15 TCH and NWG 55-29, discussed in this section.



Figures 5-6. Contoured stereonet plots of interpretations from borehole televiewer logs acquired by Sandia in hole CEE 76-15 TCH (from Pulka, 1995). Contoured poles of flow bands (mean dip angle/direction: 56°/105°; left). Contoured poles to fractures (mean dip angle/direction: 69°/134°; right).

### 5.3 STRESS FROM LOCAL BACKGROUND SEISMICITY

The nearest earthquakes for which focal mechanisms have been derived are located approximately 165 km (103 miles) south and 175 km (109 miles) north of Newberry Volcano (Section 5.1). The few events detected on the periphery of the Newberry edifice (Section 4.1) are much too small to be used for focal mechanism determinations. Thus, it is not possible to determine stress from local seismicity.

### 5.4 BOREHOLE STRESS INDICATORS IN NWG 55-29

#### 5.4.1 BOREHOLE BREAKOUT - BACKGROUND

One of the primary goals of conducting a BHTV survey is to determine the azimuth of the principal horizontal stresses from drilling-induced structures. Concentration of tectonic stress around the free surface of a borehole induces failure of the rock both adjacent to the borehole wall and immediately ahead of the drill bit. Field studies have demonstrated that these induced structures reliably record the orientations of the horizontal principal stresses in near-vertical boreholes where one principal stress is parallel to the borehole (see discussion below; Plumb and Hickman, 1985; Davatzes and Hickman, 2005; Moos and Zoback, 1990; Peska and Zoback, 1995; Zoback et al., 2003).

Three types of drilling-induced structures are recognized: (1) breakouts; (2) tensile fractures; and (3) petal-centerline fractures (see Davatzes and Hickman, 2010a for details). Breakouts are opposite areas of the borehole wall that undergo compressive failure due to the elastic concentration of effective stresses around a circular borehole. In a near-vertical hole, breakouts are oriented along the minimum horizontal principal stress ( $S_{hmin}$ ) azimuth. Breakouts are distinguished in BHTV logs as irregular patches of low amplitude and increased travel time that occur in pairs on diametrically opposed sides of the borehole. In NWG 55-29, breakouts were identified in the BHTV log acquired using the Advanced Logic Technologies (ALT) ABI85 high-temperature borehole televiewer. These results are discussed in Section 5.4 below.

In contrast, in a near-vertical hole, tensile failure of the borehole wall or ahead of the drill bit produces pairs of tensile fractures and petal-centerline fractures, respectively, that strike along the maximum horizontal principal stress ( $S_{Hmax}$ ) direction. Neither of these structures was observed in the BHTV logs obtained from NWG 55-29 and the potential implications of the lack of these structures are a matter of continuing investigation. However, it should be noted that tensile borehole wall failure, especially as a result of large tensile thermal stress accompanying cooling immediately adjacent to the borehole, are narrow and best imaged with resistivity-based image logs, which could not be used here due to temperature limitations.

#### 5.4.2 PRINCIPAL HORIZONTAL STRESS AZIMUTH

The borehole deviation, as determined from the BHTV and single-shot borehole directional surveys acquired during drilling, ranges from 10.5° to 15.1° over the logged interval, and is sufficiently low to eliminate the need for corrections required for highly deviated boreholes (Peska and Zoback, 1995). In this case, the vertical stress,  $S_v$ , is taken as a principal stress (Anderson, 1951; Hubbert, 1951) and is approximately aligned with the borehole axis. Following the method of Davatzes and Hickman (2010a and b), the orientation of  $S_{hmin}$  was determined from the breakouts weighted by their vertical extent in the borehole.

Clearly defined breakouts are distributed throughout the image log in the volcanic materials above 2624 m (8610 ft) MD (Figure 5-7 and Figure 5-8), but are absent in the underlying granodiorite. These breakouts show a consistent azimuth independent of borehole deviation and indicate that  $S_{hmin}$  is

oriented at  $092^\circ \pm 17.6^\circ$  relative to true north (Figure 5-9). As discussed in detail below, the azimuth of  $S_{hmin}$  is consistent with normal faulting of the majority of natural fractures revealed in the BHTV log (Figure 3-45). However, the uniform breakout azimuth, with minimal localized rotations as might be expected if slip were occurring on active faults penetrating the hole, taken in combination with the extremely low rate of seismicity in the region and the weak expression of natural fractures in the image log, suggests that there is little recent or active slip on fractures in the vicinity of the well.

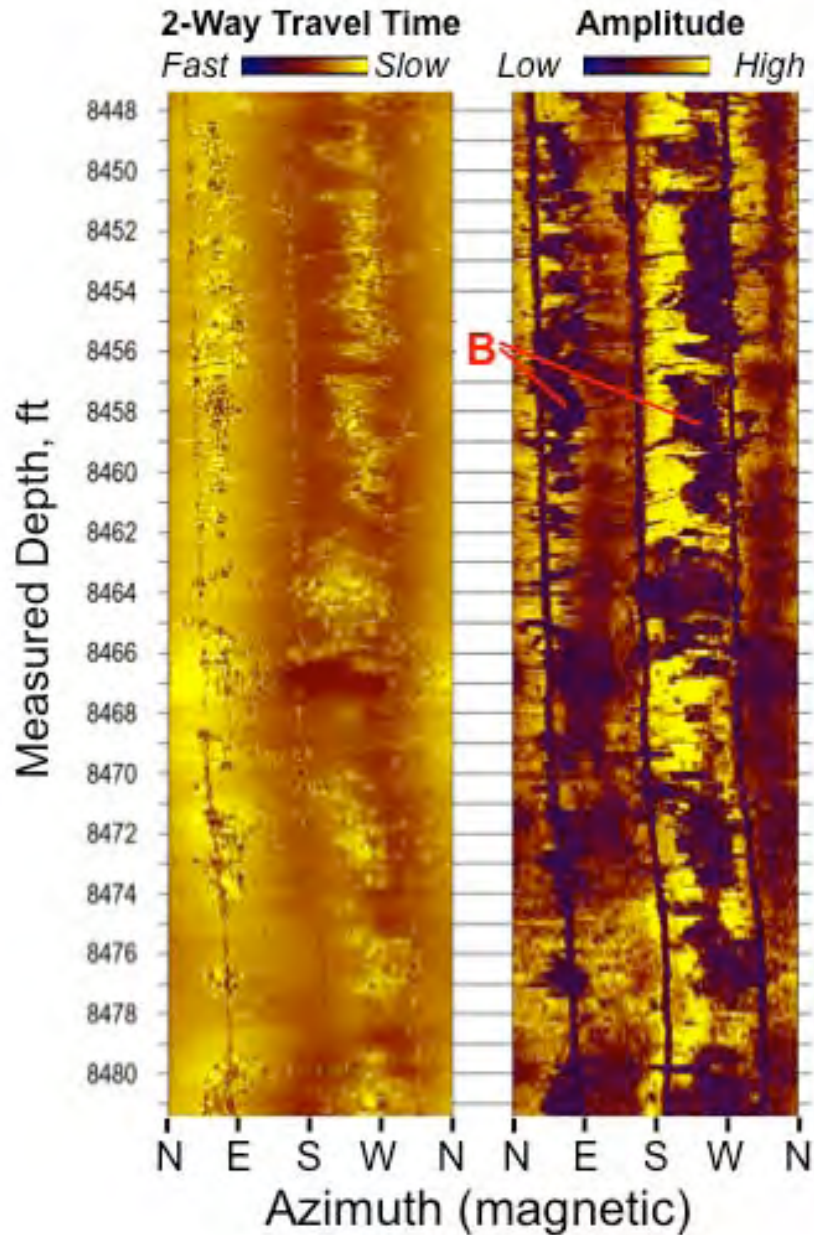


Figure 5-7. Unwrapped images of the travel time and amplitude signals recovered from NWG 55-29 showing the geometry of breakouts (B) as patches of low amplitude, increased travel time and variable width. Here, and in subsequent figures, bright yellow indicates long travel times and high amplitude, respectively. The three dark bands at  $120^\circ$  increments are from the harness that helps secure the piston assembly at the bottom of the instrument below the acoustic window to the rest of the tool. These images are in a magnetic north reference frame and depth is relative to the original BHTV log depths, which are 1.2 m (4 ft) above ground level.



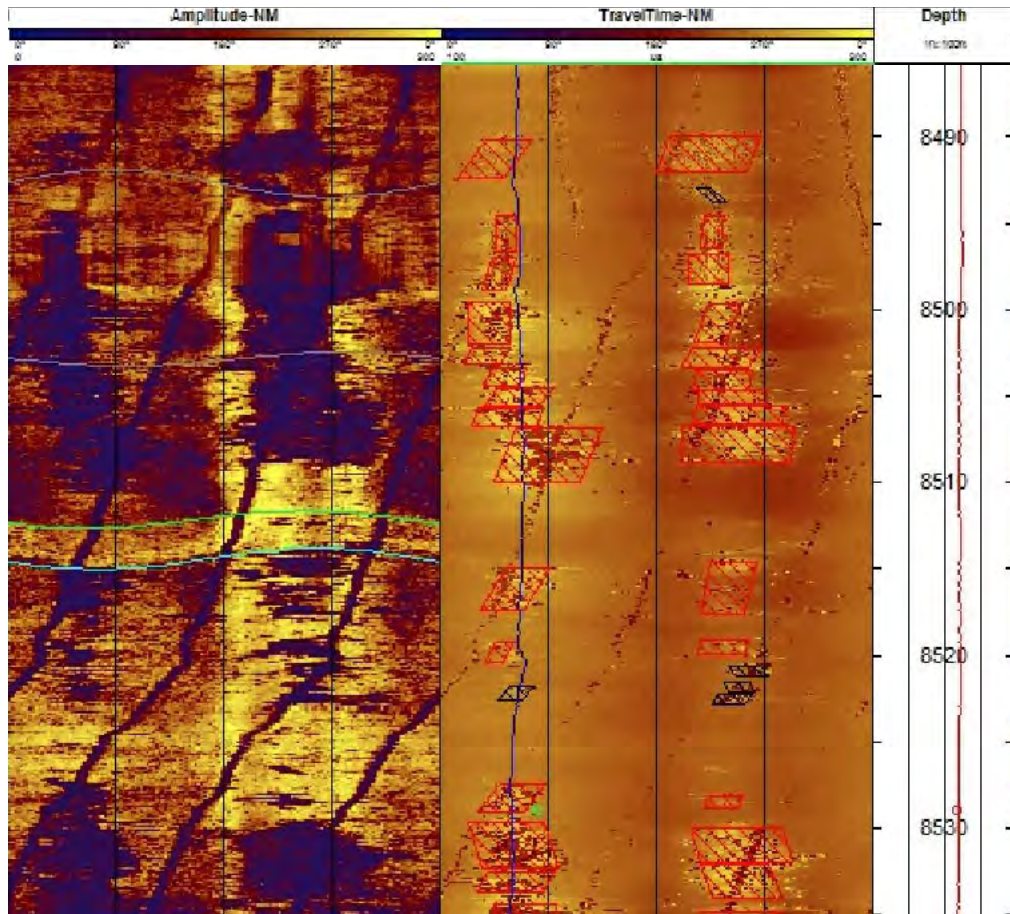


Figure 5-8. Amplitude and two-way travel time images from the NWG 55-29 BHTV log, with breakouts indicated in the travel time image as red parallelograms. Breakouts are absent in intervals of high amplitude corresponding to a change in rock type (indicated by green lines like at 2595 m [8513 ft]). The localized lack of breakouts in these intervals is most easily explained by increased rock strength. These images are in a magnetic north reference frame (given at the top of the figure) and measured depth is relative to the original BHTV log depths, which are 1.2 m (4 ft) above ground level.



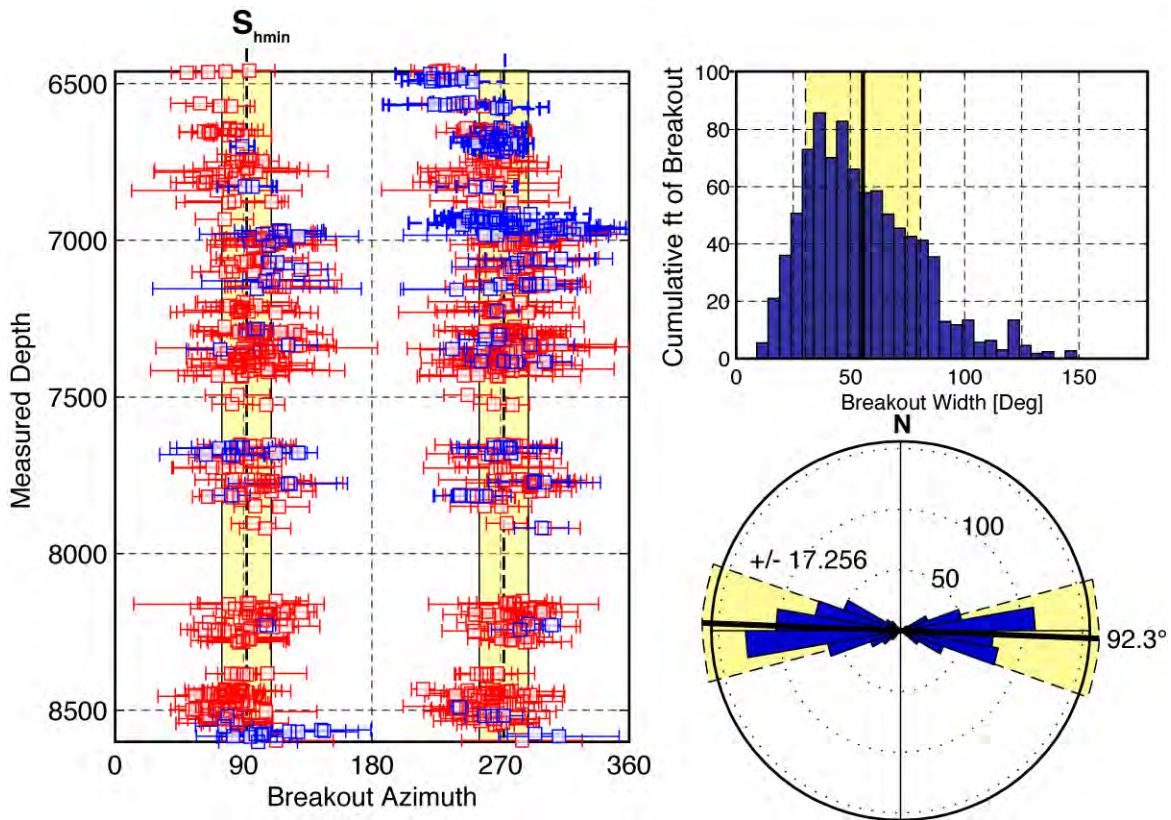


Figure 5-9. Statistics of breakout occurrence in NWG 55-29. Left panel shows the vertical distribution of breakouts versus measured depth (ft), where horizontal bars indicate breakout width, red breakouts correspond to high quality picks of paired breakouts, and blue breakouts are lower quality picks of single breakouts, typically in areas of poor image quality. Vertical yellow-filled boxes show the mean  $S_{hmin}$  azimuth  $\pm$  one standard deviation as calculated using circular statistics and weighted by the vertical extent of individual breakouts. The upper right histogram shows the distribution of breakout widths. The lower right rose diagram summarizes the cumulative height (ft) of breakouts in  $10^\circ$  azimuthal bins.

## 5.5 STRESS MAGNITUDE MODEL FOR OPEN HOLE OF NWG 55-29

Breakouts span portions of the borehole wall where the compressive normal stress tangential to the borehole wall exceeds the compressive strength of the rock (Zoback et al., 2003; Haimson, 2007). Since the borehole wall is in contact with the borehole fluid and the pore pressure in rock immediately outside the borehole during breakout formation is assumed approximately equal to the borehole fluid pressure, the appropriate strength criterion for breakout formation is the uniaxial compressive strength (UCS; Zoback et al., 2003, Zoback, 2007, and Haimson, 2007). If the UCS is known at the depth where the breakouts occur, then the width of breakouts can be used to estimate the maximum differential stress at the borehole wall, which, in turn, provides constraints on the magnitudes of the remote principal stresses

In this simple case of a borehole aligned within  $12^\circ$ - $15^\circ$  of one of the three principal stresses (Peska and Zoback, 1995), the variation of the stress components along the borehole wall is described by the 2D plane strain boundary value problem solved by the Kirsch equation (Kirsch, 1898). Additional sources of effective stress at the borehole wall include formation pore fluid pressure ( $P_f$ ), the pressure difference between  $P_f$  and the fluid pressure in the borehole ( $P_m$ ), and thermal stresses induced at the borehole wall by circulation of hot or cold fluids (e.g., during drilling). Following Zoback et al. (2003), the Kirsch equation is modified to include all of these contributions to the stresses causing breakout formation:

**Equation 5-1**  $\sigma_{\theta\theta} = S_{Hmax} + S_{hmin} - 2(S_{Hmax} - S_{hmin})\cos(2\theta) - 2P_f - \Delta P + \sigma^{thermal}$ ,

where  $\sigma_{\theta\theta}$  is the tangential circumferential normal stress at the borehole wall,  $\theta$  is the angle measured from the  $S_{Hmax}$  azimuth, and  $\Delta P$  is the difference between the mud pressure and the formation fluid pressure, such that  $\Delta P = P_m - P_f$ . In this formulation, positive  $\Delta P$  adds a component of tensile circumferential stress at the borehole wall. The term  $\sigma^{thermal}$  refers to thermal circumferential stresses induced by heating or cooling the borehole wall (e.g., by fluid circulation during drilling). Here and throughout the text we conform to the geological sign convention for stress, in which compression is positive.

For breakout formation, the maximum value of circumferential stress is aligned with the  $S_{hmin}$  azimuth, (Figure 5-10), where  $\theta$  in Equation 5-1 is either  $90^\circ$  or  $270^\circ$ . Breakout width (wBO) is defined as the angle subtended by the breakout at the borehole wall and corresponds to the condition at which  $\sigma_{\theta\theta} \geq UCS$ . In addition to the remote principal stresses, breakout formation is promoted by the combination of the lowest (most negative) magnitude of  $\Delta P$  and the most compressive  $\sigma^{thermal}$ , with the latter corresponding to heating of the borehole wall above the ambient temperature. Breakouts might form at any time between the time of drilling and logging, so the most favorable conditions for breakout formation within that time period should be evaluated in relating breakout occurrence and width to the magnitudes of  $S_{hmin}$  and  $S_{Hmax}$ .

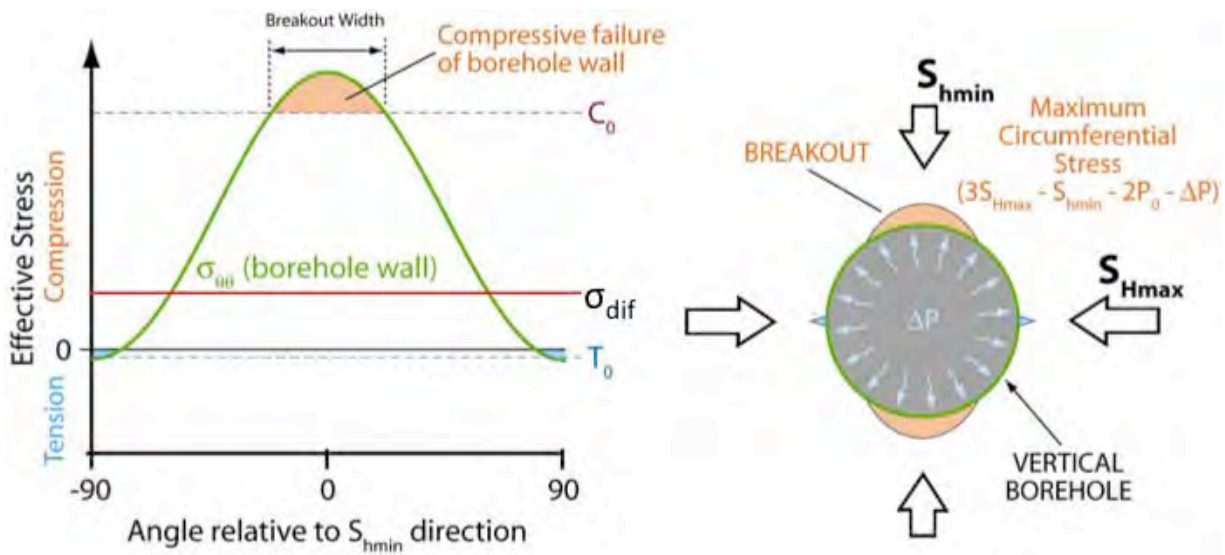


**Figure 5-10.** Circumferential variation of tangential normal stress,  $\sigma_{\theta\theta}$ , along the wall of a vertical borehole relative to the directions of the principal horizontal stresses,  $S_{Hmax}$  and  $S_{hmin}$ . Here,  $C_0$  refers to the uniaxial compressive strength (UCS) and  $P_0$  to the formation fluid pressure.

Tensile fractures were not observed in the logged interval of the NWG 55-29 borehole. Equation 5-1 suggests that circumferential tension, and thus borehole wall tensile fractures, can be induced by the combined impact of the remote principal stresses, large positive  $\Delta P$  (i.e., high  $P_m$  relative to  $P_f$ ) and negative  $\sigma^{thermal}$  (i.e., borehole wall cooling). In principle, the absence of these structures could then be used to constrain the principal horizontal stresses. However, previous attempts to apply simple thermoelastic models in geothermal boreholes that sustain very large cooling have been problematic (pers. comm., S. Hickman, April 2011), and overpredict the occurrence of thermal cooling (tensile) cracks for realistic stress conditions, rock properties and cooling histories. This constraint is not implemented at this time, but is a matter of continuing research.

Thus, in order to estimate the relative magnitudes of  $S_{Hmin}$  and  $S_{Hmax}$  at depth from the occurrence and width of breakouts, several parameters must be determined, including: (1) the distribution of breakouts with depth and their corresponding widths; (2) the UCS of the rock forming the borehole wall; (3) the formation fluid pressure,  $P_f$ ; (4) the minimum borehole fluid (mud) pressure,  $P_m$ ; and (5) the maximum (compressive) magnitude of  $\sigma^{thermal}$ . As noted above, since breakouts can form at any time between when the borehole is drilled and when it is logged, these parameters are evaluated when the quantity  $\sigma_{\theta\theta}$  given by Equation 5-1 is at a maximum. These constraints are derived and applied in the construction of an *in situ* rock strength and stress model in the following sections.

### 5.5.1 IN SITU STRENGTH MODEL

As discussed above, the azimuthal width of breakouts depends on a minimum of two independent parameters, the magnitudes of the principal stresses and the UCS, a property of the borehole wall rock that must be overcome for breakouts to form. The magnitude of the differential stress driving breakout formation can be constrained from the width of the breakout if the UCS at the depth of the breakout is known. Since UCS typically varies by at least three orders of magnitude, and as many as six orders of magnitude in volcanic rock (Price et al., 1993; Li and Abertson, 2003; Ma and Daemen, 2004; Entwisle et al., 2005; Frolova et al., 2005), large variations in breakout width can occur at constant differential stress.

In NWG 55-29, the borehole compensated neutron porosity and litho-density logs are strongly impacted by the total porosity. The neutron porosity log measures the total porosity of the rock by direct interaction of neutrons with hydrogen atoms primarily associated with water molecules between a source and a detector. It is insensitive to the shape of the pore containing the fluid and to whether the water is structured in minerals such as clays or zeolites, or present as a free fluid. The log underestimates porosity in steam zones and overestimates porosity in the presence of hydrated minerals. We note that mineralogical analysis indicates a paucity of clays and only a small weight percent of zeolites in rocks encountered by the NWG 55-29 borehole. Litho-density tools measure the bulk density of the rock mass by the interaction of gamma rays with the electrons orbiting atoms between a source and a detector. This measurement is highly sensitive to both the number of atoms in the path of the gamma rays and the atomic number of those atoms. Figure 5-11 shows a comparison of these parameters within the interval logged by the BHTV in NWG 55-29 where breakout width has been measured. Neutron porosity and litho-density logs have depth resolutions ranging from ~8-40 cm (3-16 in) along the borehole, depending on borehole wall rugosity, rock type and other factors (Hearst et al., 2000), which is at a fine enough scale for correlation with the depth variations in wBO observed in NWG 55-29. Although mineralogy is available from X-ray diffraction and thin section analysis of cuttings, the vertical resolution of these measurements is limited by the cuttings sample interval of 3 m (10 ft), making it less suitable for application to a detailed breakout analysis.



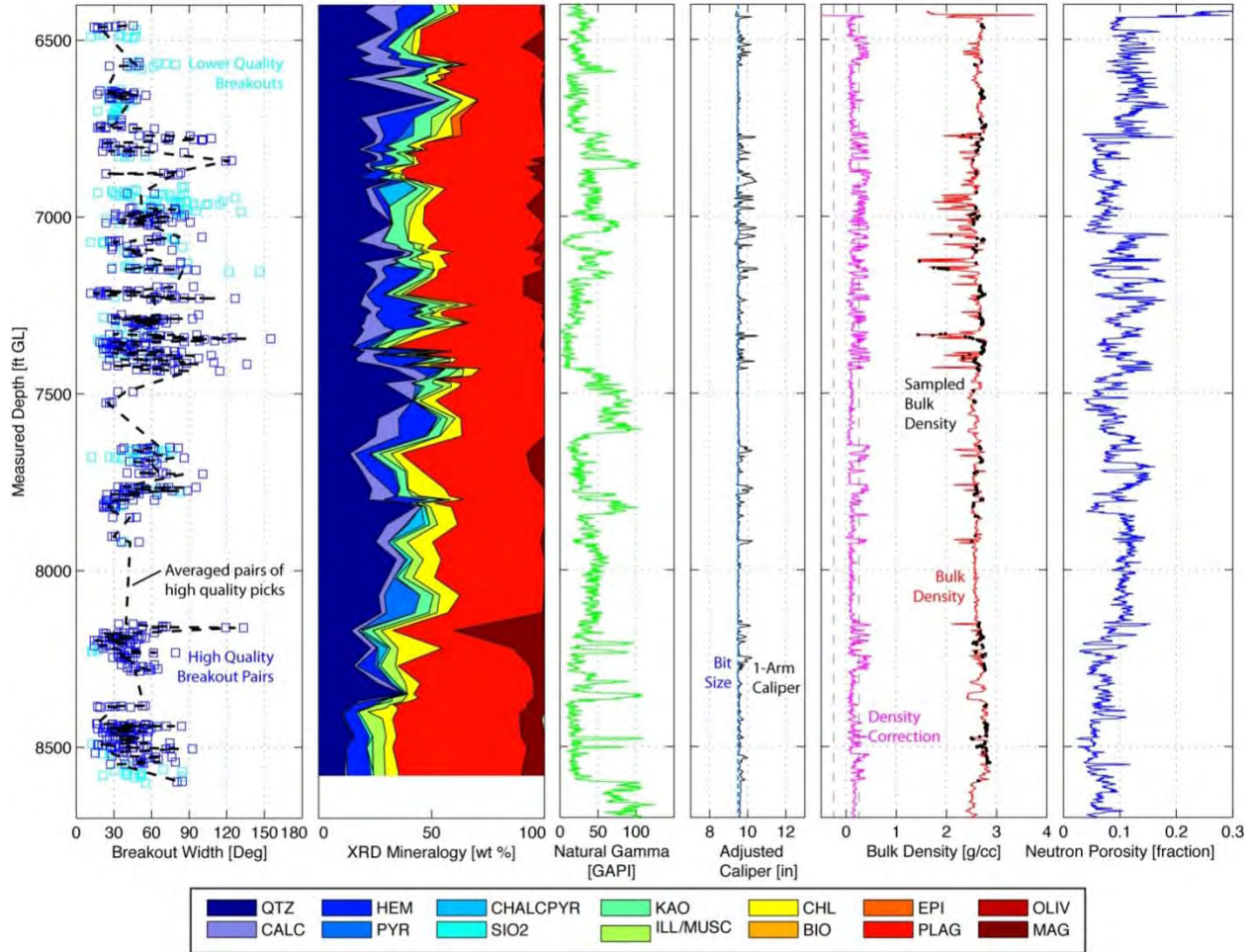


Figure 5-11. Initial evaluation of the correspondence of breakout width and geologic and geophysical constraints on rock composition, properties and strength in NWG 55-29. Measured depth is relative to ground level (GL). From left to right: (1) measured breakout width (wBO); (2) weight percent of minerals in cuttings from XRD; (3) natural gamma; (4) adjusted caliper; (5) bulk density; and (6) neutron porosity. Sampled bulk density (black dots) is shown in comparison to log-derived bulk density and was calculated from XRD analyses on cuttings (see text). The depth interval plotted represents the extent of the BHTV log. Dark blue breakouts correspond to high quality picks of paired breakouts and light blue breakouts are lower quality picks of single breakouts, typically in areas of poor image quality. Note that QTZ = quartz, CALC = calcite, HEM = hematite, PYR = pyrite, CHALCPYR = chalcopryrite, SIO<sub>2</sub> = silica, KAO = kaolinite, ILL/MUSC = illite/muscovite, CHL = chlorite, BIO = biotite, EPI = epidote, PLAG = plagioclase, OLIV= olivine, MAG = magnetite.

Examination of Figure 5-11 shows first-order correlations between breakout width and the key rock properties of mineralogy, density, and porosity. Regions characterized by low quartz content and high kaolinite, chlorite, and illite/muscovite content tend to show larger breakout width. The relative natural radioactivity of the rock measured in the gamma ray log shows no clear general correlation to breakout width, although in a few intervals of high natural gamma count breakouts are relatively scarce (e.g., ~2271-2332 m, 7450-7650 ft). Depth intervals in which the borehole is enlarged by breakouts are also revealed in the caliper log and as intervals of anomalously low bulk density and relatively high neutron porosity.

The locations in which there are no measurements of breakout width correspond to intervals in which no breakouts occur, since image log quality is generally good throughout the entire logged interval. At



the base of the borehole this corresponds to the crystalline intrusives that tend to lack significant chlorite, kaolinite, or illite/muscovite alteration. This abrupt absence of breakouts suggests that there is a large strength contrast between the relatively weak overlying volcanics, which have experienced alteration into the greenschist facies, and relatively strong unaltered intrusives. As shown below, this observation provides an inequality constraint in which the strength of the rock exceeds the stress causing breakout formation, thus providing an upper limit on stress causing breakout formation.

Depth de-correlation of as much as 1 ft per 1000 ft is within the typical range of error for borehole geophysical logging due to cumulative error at the depth encoder and, more importantly, cable stretch (Hearst et al., 2000). This latter effect is likely exacerbated by high temperatures in borehole NWG 55-29 and the use of different cable types among the various logging runs. To address this possible inconsistency in the comparisons among logs, two quality assurance steps were performed: (1) checking for correlation among logs and to independent depth ties (including the casing shoe) and adjusting depths as needed within reasonable offsets; and (2) smoothing the geophysical logs with a non-recursive moving average filter, approximately 1.8 m (6 ft) wide, so the data was sampled at common intervals and potential offsets due to variations in sampling were partially suppressed. This latter approach will tend to underestimate extreme variations in these properties in this analysis.

Finally, although acquired by borehole compensated tools, both the litho-density and neutron porosity are sensitive to stand-off (separation) of the tool from the borehole wall. In general, density is clearly low at depths where the 1-arm caliper does not match the bit size, which is consistent with anomalously low measured density (or high porosity) due to increased separation between the tool and the borehole wall. To address this systematic error, where the borehole was extremely out of gauge or where the correction to the density log exceeded 0.2 g/cc, that data was excluded from the analysis. It is also apparent that increased caliper and decreased density, or highly variable density, coincide with regions of highest breakout frequency and widest breakout occurrence, such as at 2057-2271 m (6750-7450 ft) MD below ground level.

UCS depends strongly on the internal structure of materials and, in particular, on the mineralogy and distribution of flaws that can locally concentrate stress and initiate failure (Griffith, 1921; Lawn, 1993; Quane and Russel, 2003; Li and Albertson, 2003; Hudyma et al., 2004; Paterson and Wong, 2005). Total porosity, pore shape and, to a lesser degree, pore size impact the magnitude of the stress concentration and, thus, have the strongest impact on the strength of the rock. In volcanic rocks, there can be a high degree of variability in pore size and shape due to the presence of two distinct pore populations: (1) small, sharp micro-cracks resulting from cooling stress, burial, and tectonic activity; and (2) potentially large, rounded vesicles that form during cooling from a melt and exsolution of volatiles (Figure 5-12A). There is also a high potential for mineral alteration or mineral infilling of pores (Figure 5-12B) due to interaction with volcanic gases, steam and hydrothermal fluids.

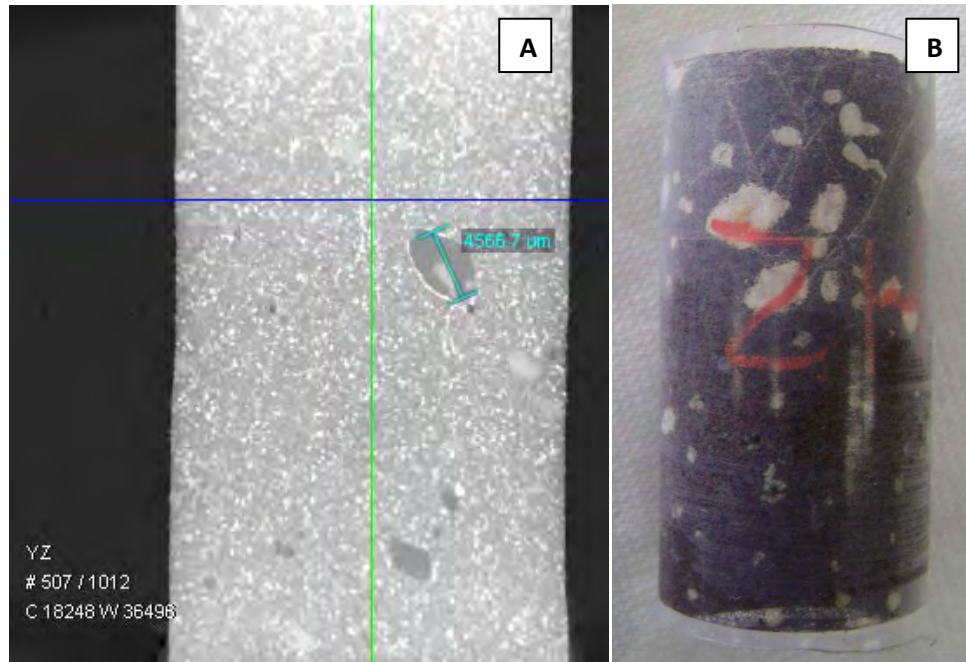


Figure 5-12. A) High resolution X-ray computed tomography (CT) scan of core sample from Newberry well GEO N-2 at a depth of 1305 m (4281 ft) MD, revealing a wide distribution of pore sizes and aspect ratios, including vesicles associated with volcanic extrusive rocks common to the geologic section imaged by BHTV log. B) Photograph of sample from same well at a depth of 1305 m (4281 ft) MD after conducting multiple-cycle testing to derive preliminary estimates of the coefficient of internal friction, cohesion, and uniaxial compressive strength. Sample is approximately 4.4 cm (1.75 in) tall. (See the Rock Mechanics discussion for details.) (Images courtesy of Dr. Ahmad Ghassemi)

The control of porosity on strength has been experimentally investigated for many volcanic rocks, providing a reference database for estimating the UCS of rock types relevant to NWG 55-29. In Appendix E-1, the reference data is used to develop an empirical relationship between porosity and UCS, which is then used to estimate the *in situ* UCS appropriate to NWG 55-29 from the filtered neutron porosity (NPHI) data (Figure 5-13). The model suggests that UCS increases with depth, reflecting the overall reduction in porosity with increasing depth. This systematic increase in strength is also reflected in a similar, though smaller, tendency for breakout width to decrease with depth (although with considerable scatter). At the base of the imaged interval, the average UCS is high, consistent with the lack of breakouts. The widest breakouts are generally associated with low UCS. These consistencies among the two data sets suggest that the *in situ* strength model explains at least some of the variations in breakout width observed in the BHTV log. However, there remains considerable scatter, which would require either independent variations in the differential stress or may indicate that some variability in strength is not captured by the neutron porosity log. Notably, the current model based on NPHI does not take into account expected variation in UCS due to variations in pore geometry, including the presence of oversized pores such as vugs or vesicles, nor due to the potential impact of compositional variations (Price, 1966; Olson et al., 1991).

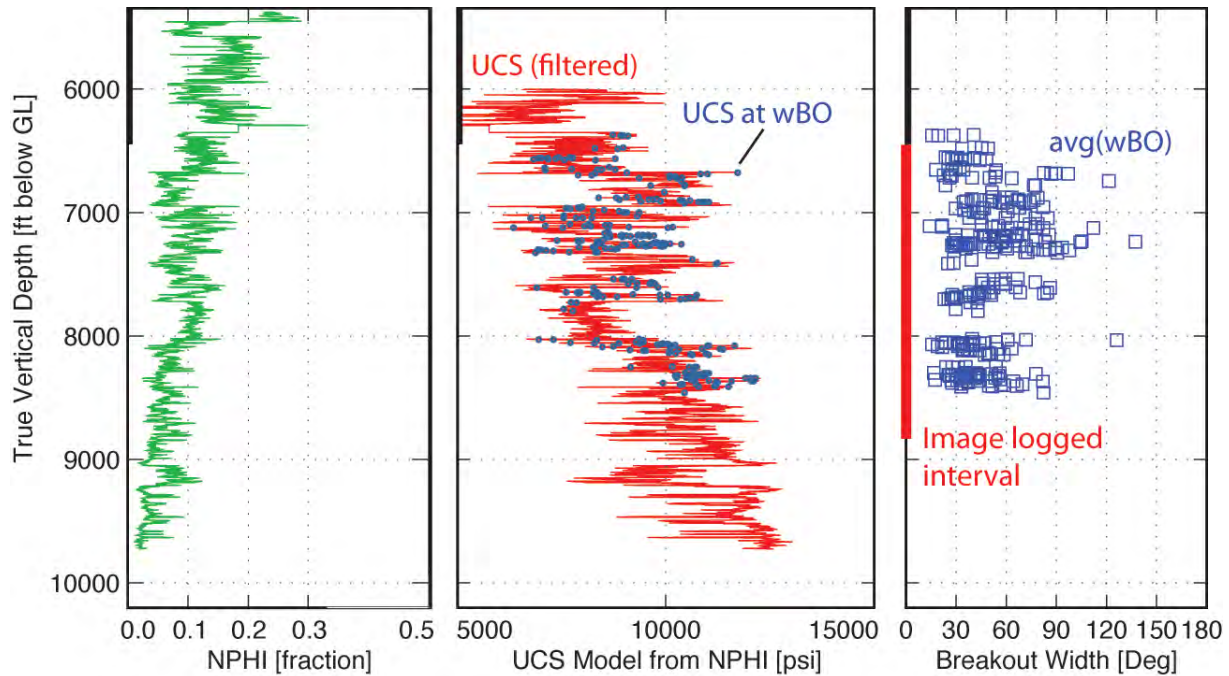


Figure 5-13. *In situ* model showing estimates of the uniaxial compressive strength (UCS) derived from exponential model and the NPHI log data in the open hole interval of NWG 55-29. See Equation 5-3 and associated discussion (below), and Appendix E-1 for details. Black and red vertical lines depict the lowermost cased section of the hole and the open-hole interval logged with the BHTV, respectively. Values depicted by UCS at wBO represent strength values used in creation of the variable-UCS stress model, discussed below.

An additional limit on *in situ* stress magnitude is imposed by the frictional strength of the fractures and faults found throughout the rock volume. Several studies have shown that crustal stresses are limited by the frictional strength of pre-existing, optimally oriented faults (e.g., Townend and Zoback, 2000), in accord with laboratory measurements of the frictional strength of pre-fractured rock (also known as Byerlee's Law, after Byerlee, 1978). A first-order control on frictional strength is mineralogy (Lockner and Beeler, 2002), which has been carefully documented by the cuttings analysis of NWG 55-29 (Figure 5-11). The major rock forming minerals in the NWG 55-29 borehole are quartz and plagioclase, which have coefficients of static friction,  $\mu_s$ , of approximately 0.7. Also relevant is the strength of whole rocks such as tuffs, which in systematic studies such as performed on the Yucca Mountain Tuff (Morrow and Byerlee, 1984) tend to have  $\mu_s$  consistent with Byerlee's Law (Byerlee, 1978). These provide an upper bound on the frictional strength of the rock and thus an upper bound on the differential stress the rock can sustain before slip occurs to relieve elastic strain. However, vein fillings and fault rocks can have distinct mineralogy that diverges from the host rock and may reduce the frictional strength of the rock mass. At Newberry, the analysis of core (see discussion of fault rock types at Newberry in Section 3.2.6) and cuttings (Section 3.2.5) suggests that such minerals in the NWG 55-29 borehole might include: (1) calcite, which has a frictional strength similar to the host rock; and (2) illite, muscovite, or chlorite, which have a frictional strength from about 0.38 to 0.46 (Figure 5-14), and would allow for only a relatively small differential stress.

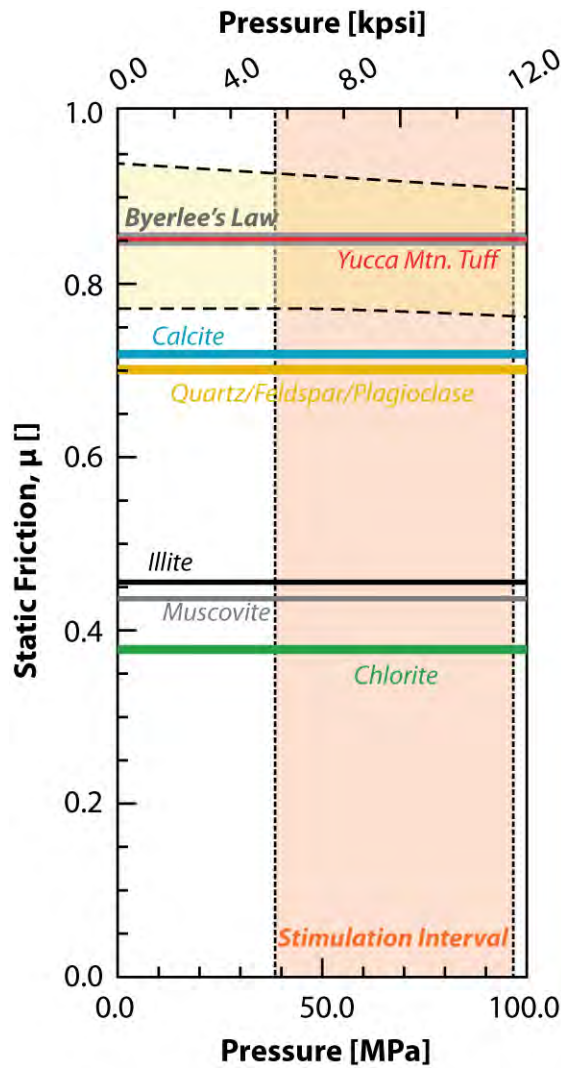


Figure 5-14. Static coefficient of friction of key mineral phases (modified from Lockner and Beeler, 2002) known to occur in NWG 55-39 from analysis of cuttings, as a function of effective confining pressure (roughly comparable to mean stress,  $P_f$ ). Also shown in yellow bounded by dashed black lines is the range of friction coefficients for typical crustal rocks defined by Byerlee's Law (Byerlee, 1978) and for tuff from Yucca Mountain (Morrow and Byerlee, 1984), Topah Spring Member of the Paintbrush Tuff, and the Bullfrog Member of the Crater Flat Tuff, which are welded, devitrified tuffs (without zeolites) similar to the tuffs at the top of the open hole interval in NWG 55-29.

### 5.5.2 VERTICAL PRINCIPAL STRESS

The stress tensor acting on the volume containing NWG 55-29 should be completely characterized by the vertical principal stress and two horizontal principal stresses, all of which are counteracted by the formation fluid pressure through the effective stress principle. Starting with the vertical principal stress in this section, we model each of these four components to determine the effective stress tensor. This includes constraints on the magnitudes of horizontal principal stresses derived from the injection history, borehole deformation, and strength limits of the rock that the borehole penetrates.



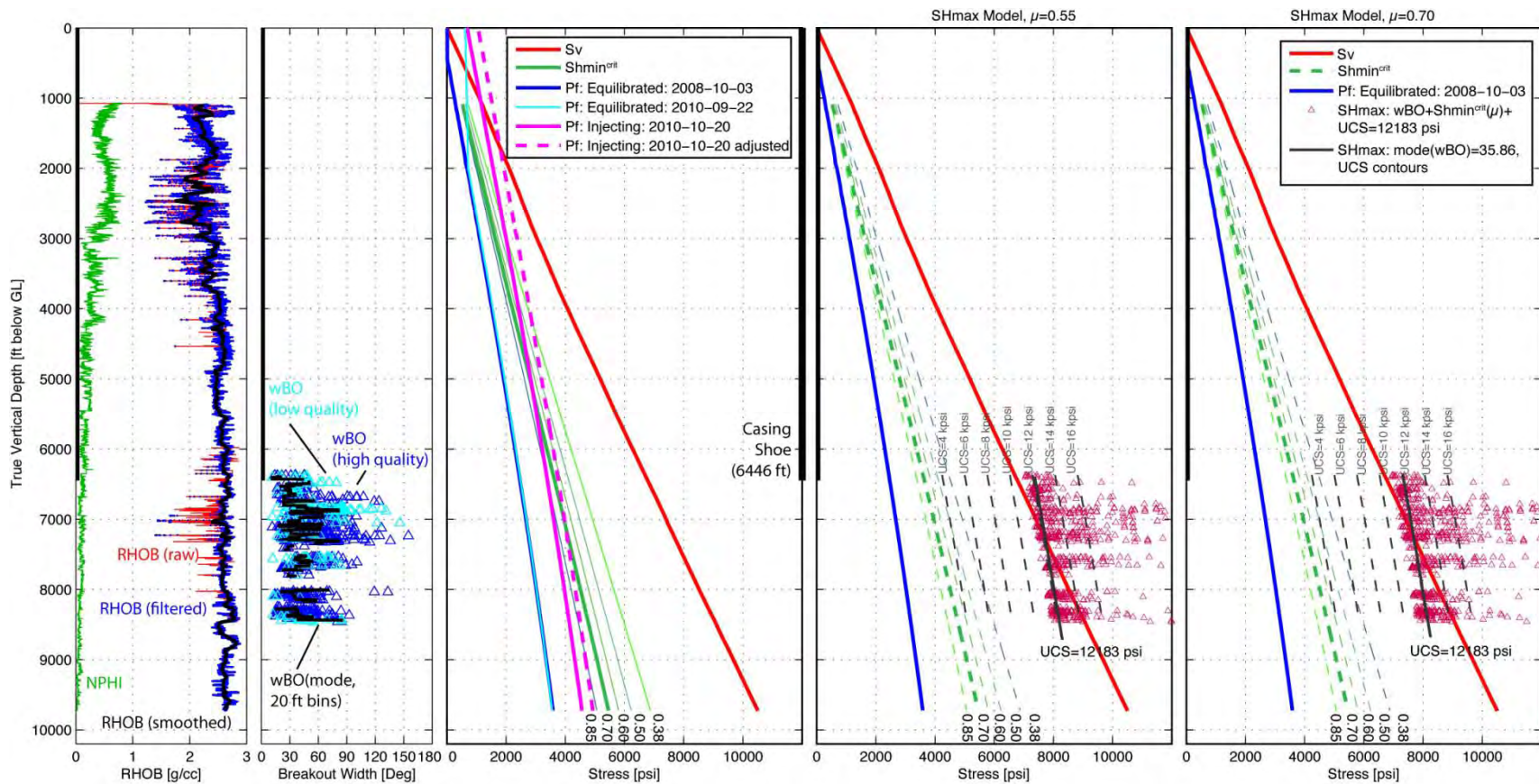


Figure 5-15. Analysis of stresses versus depth for NWG 55-29, assuming a constant UCS. From left to right: *Panel (1)* fractional porosity (green), raw bulk density (red), filtered bulk density (blue) and smoothed bulk density (black) from the litho-density log; *Panel (2)* measured breakout width from the BHTV log (color code as in Figure 5-11); *Panel (3)* vertical stress profile including: (1) the vertical stress ( $S_v$ ) integrated from the filtered bulk density; (2) the *in situ* fluid pressure ( $P_f$ ) estimated from equilibrated static pressure logs conducted on 3 October 2008 and 22 September 2010; (3) critical values of the minimum horizontal principal stress ( $S_{hmin}^{crit}$ ) for frictional failure on optimally oriented normal faults derived from Equation 5-2 for coefficients of friction of 0.38 to 0.85; and (4) the maximum fluid pressure profiles achieved in the borehole to date (“ $P_f$ : injecting”); *Panel (4)* estimated magnitudes of the maximum horizontal compressive stress ( $S_{Hmax}$ , red triangles) from  $S_{hmin}^{crit}$  for  $\mu_s = 0.55$ , the observed breakout width as a function of depth, and an assumed uniform UCS = 84 MPa (12183 psi; consistent with a laboratory measurement on welded tuff from nearby well GEO N-2 by Texas A&M University, Ahmad Ghassemi, pers. comm., 2011). Also shown as a solid black line is the estimated depth variation in  $S_{Hmax}$  using a statistical mode of  $wBO = 35.86^\circ$  with UCS = 12183 psi. For reference, dashed black lines show  $S_{Hmax}$  for various other constant UCS models. *Panel 5*: estimate of  $S_{Hmax}$  similar to Panel 4, but using  $S_{hmin}^{crit}$  for  $\mu_s = 0.70$ . The solid black vertical lines along the edges of each panel denote the depth extent of casing, with the open-hole interval below this.

We calculate the vertical stress ( $S_v$ ) using a geophysical litho-density log spanning 333 m (1091 ft) below GL to a depth of 3066 m (10040 ft) MD below GL, and an estimated average density for the overlying interval. The log data were filtered to remove spurious bulk density measurements in cases where the bulk density correction exceeds 0.2 g/cc (Asquith and Krygowski, 2004) or where one-arm caliper logging showed extensive washouts (Figure 5-11). Geophysical measurements of bulk density are consistent with the bulk density estimated from the weighted average of the mineralogy measured through Rietveld refinement of cuttings XRD analysis corrected for water-filled porosity using the neutron porosity log data (Figure 5-11). The litho-density log data and the variation in  $S_v$  with depth calculated from these data are shown in Figure 5-15.

The estimate of the undisturbed formation fluid pressure was derived from two equilibrated pressure logs, one conducted 3 October 2008, approximately 2.5 months after the borehole was completed, and the second conducted 22 September 2010, prior to the inject-to-cool preparations for borehole televiewer logging (Table 5-1). As shown in Figure 5-16 (below), the first of these logs was conducted when the borehole was open to the atmosphere, and reflects a static water table at 128 m (420 ft) TVD GL.

**Table 5-1. Injectivity in NWG 55-29 measured immediately before borehole televiewer logging.**

Log Date	Wellhead Pressure (psig)	Injection Rate (gpm)	Pressure Log	Duration	Apparent Injectivity (gpm/psi)
24-27 Sept 2010	751	10	No	3 days	0.013
27 Sept 2010	619	13	Yes	Short-term	0.021
	821	17			0.021
11-20 Oct 2010	1153	22	No	9 days	0.019
20 Oct 2010	785	13	Yes	short-term (conducted during logging after 1153 psi WHP)	0.017

### 5.5.3 CONSTRAINTS ON MINIMUM HORIZONTAL PRINCIPAL STRESS

In most stress analyses carried out in geothermal systems, we measure the magnitude of  $S_{hmin}$  directly using a mini hydraulic fracturing test ('mini-frac'; see Hickman and Davatzes, 2010, and references therein for details) and then constrain the magnitude of  $S_{Hmax}$  using observations of breakout width and estimates of UCS,  $P_f$  and  $P_m$  (e.g., Davatzes and Hickman, 2006). Because reliable and safe open-hole packers do not presently exist for use at temperatures typical of geothermal wells, these mini-frac tests are usually carried out in a short (~15 m [50 ft]) and relatively impermeable section of well bore drilled just below a cemented casing shoe. This open-hole interval is then rapidly pressurized until a hydraulic fracture is formed and repeated pressurization, shut-in and flow-back cycles are applied to propagate the hydrofrac away from the borehole. Downhole pressure records from these tests are then used to determine the magnitude of  $S_{hmin}$ . Conducting a mini-frac over a short open-hole interval (usually through drill pipe with a cased-hole packer set just above the casing shoe) minimizes borehole storage effects, provides a narrow depth range over which to calculate  $S_{hmin}$ , and helps ensure that the measured pressure response is not masked by excessive leak-off into preexisting permeable fractures. Because NWG 55-29 has over 1000 m (>3000 ft) of open hole, and isolating a short section of the hole (e.g., through sanding and cement plug-back procedures) would require a drilling rig, it is not feasible to conduct a mini-frac to determine  $S_{hmin}$  prior to stimulation due to budgetary and well bore risk constraints. However, we will be using step-rate injection tests during the early stages of the stimulation of NWG 55-29, with downhole pressure and temperature profile monitoring to provide direct constraints on the magnitude of  $S_{hmin}$  and depth of hydrofrac initiation, if it occurs (see Section 7 of this

report). In addition, we will be carrying out mini-frac tests during drilling of the production wells later in Phase II, employing the procedures outlined above.

Although we currently lack a direct measurement of  $S_{hmin}$ , previous injection tests do provide constraints on  $S_{hmin}$ . During the inject-to-cool operation carried out prior to BHTV logging (Table 5-1), PT logs were conducted at wellhead pressures (WHP) of 4.4 MPa (640 psi) and 5.4 MPa (785 psi), providing complete records of pressure and temperature variation with depth (Figure 5-16). Later in the inject-to-cool operation, although no PT log was obtained, maximum WHP reached 7.95 MPa (1153 psi). This WHP was achieved over three days prior to running the temperature-pressure log at 785 psi, so the downhole pressures corresponding to a WHP of 1153 psi are estimated by shifting the measured pressure profile during the 785 psi WHP survey to bring it into alignment with the maximum WHP of 1153 psi. This adjusted injecting  $P_f$  profile is plotted in Figure 5-15 (Panel 3). In spite of the high borehole fluid pressures attained, these injection tests did not result in hydrofracture, as indicated by a lack of change in injectivity (Table 5-1), a lack of either pressure or temperature signatures in concurrent PT logs (Figure 5-16), and the lack of tensile fractures visible anywhere in the BHTV log. In addition, the apparent injectivities during this operation are similar to those measured in other un-stimulated boreholes at Newberry, including CEE 76-15 TCH, CEE 86-21 and CEE 23-22 (Spielman and Finger, 1998). Because hydrofractures form in response to borehole fluid pressure in excess of  $S_{hmin}$ , the failure to create a hydrofracture during this inject-to-cool operation provides a lower bound to the magnitude of  $S_{hmin}$ . In particular,  $S_{hmin}$  within the open-hole interval of NWG 55-29, must lie to the right of the dashed magenta line in Panel 3 of Figure 5-15, otherwise hydraulic fracturing would have occurred.

Another approach is to explore additional limits on  $S_{hmin}$  derived from a combination of the assumption of the tectonic environment and the frictional strength of the crust. As discussed above, it is reasonable to assume a normal faulting environment at Newberry based upon the attitude of the preponderance of natural fractures seen in the BHTV log, mapped faults at the surface, and the similarity of the  $S_{hmin}$  azimuth to the dip direction of these structures. In such a normal faulting environment, the maximum differential stress a rock can sustain is given by the difference between  $S_v$  and  $S_{hmin}$ , assuming there is a population of optimally oriented cohesionless fractures available. In accordance with the Coulomb failure criterion, frictional failure (i.e., normal faulting) would then occur at a critical magnitude of  $S_{hmin}$  given by (after Jaeger and Cook, 1979):

$$\text{Equation 5-2} \quad S_{hmin}^{crit} = (S_v - P_f) / [(\mu_s^2 + 1)^{1/2} + \mu_s] + P_f$$

where  $\mu_s$  is the static coefficient of friction of preexisting faults. As discussed above and shown in Figure 5-14), it is assumed here that  $\mu_s$  ranges from an extreme of 0.38, consistent with the coefficient of friction of chlorite (Lockner and Beeler, 2002), to 0.85, consistent with a representative rhyolite tuff from another locality (i.e., the paintbrush tuff in the vicinity of Yucca Mountain, NV, Morrow and Byerlee, 1984). In general, laboratory sliding experiments on a variety of rock types and mixtures show average behavior  $\mu_s \sim 0.75-0.90$  (Byerlee, 1978), but lower  $\mu_s$  of 0.55 to 0.6 is also common (Jaeger and Cook, 1979; Paterson and Wong, 2005). Similar constraints on frictional strength have been derived from extensive *in situ* stress measurements in a wide range of tectonic environments (e.g., Townend and Zoback, 2000) as well as in other geothermal fields (Barton et al., 1998; Hickman et al., 1998, 2010; Davatzes and Hickman, 2006, 2010b; Cornet et al., 2007; Valley and Evans, 2007; Hickman and Davatzes, 2010) and support the idea that differential stress levels in the crust are generally limited by  $\mu_s$  of about 0.6 to 1.0. To provide frictional bounds on  $S_{hmin}$  in the vicinity of hole NWG 55-29, we use Equation 5-2 to calculate  $S_{hmin}^{crit}$  corresponding to  $\mu_s$  ranging from 0.38 to 0.85 (Figure 5-15).

The frictional limits on differential stress can also be visualized as a polygon on a plot of  $S_{hmin}$  versus  $S_{Hmax}$  normalized to  $S_v$  (Jaeger and Cook, 1979; Moos and Zoback, 2000; Zoback, 2007), which is illustrated at a depth corresponding to the bottom of casing in NWG 55-29 (Figure 5-17). The edges of the polygon are



determined from Equation 5-2 for a given fluid pressure and coefficient of static friction assuming optimally oriented fractures are present in the stressed volume. Combinations of the principal stresses contained within the polygon can be supported by the frictional strength of the surrounding crust. The relative magnitudes of  $S_{hmin}$  and  $S_{Hmax}$  to  $S_v$  also determine the type of fault slip that should predominate: (1) normal; (2) strike slip; or (3) reverse. The polygon derived from  $\mu_s = 0.85$  provides a range of stress magnitudes supportable by the maximum estimated strength of welded tuff, based upon measurements made on comparable samples from Yucca Mountain, NV (Morrow and Byerlee, 1984). It is important to note, however, that the lower limit for  $S_{hmin}$  corresponding to  $\mu_s = 0.85 S_v$  is not permissible based on the maximum borehole fluid pressure constraint discussed above. Smaller polygons in Figure 5-17 are associated with lower frictional strengths.

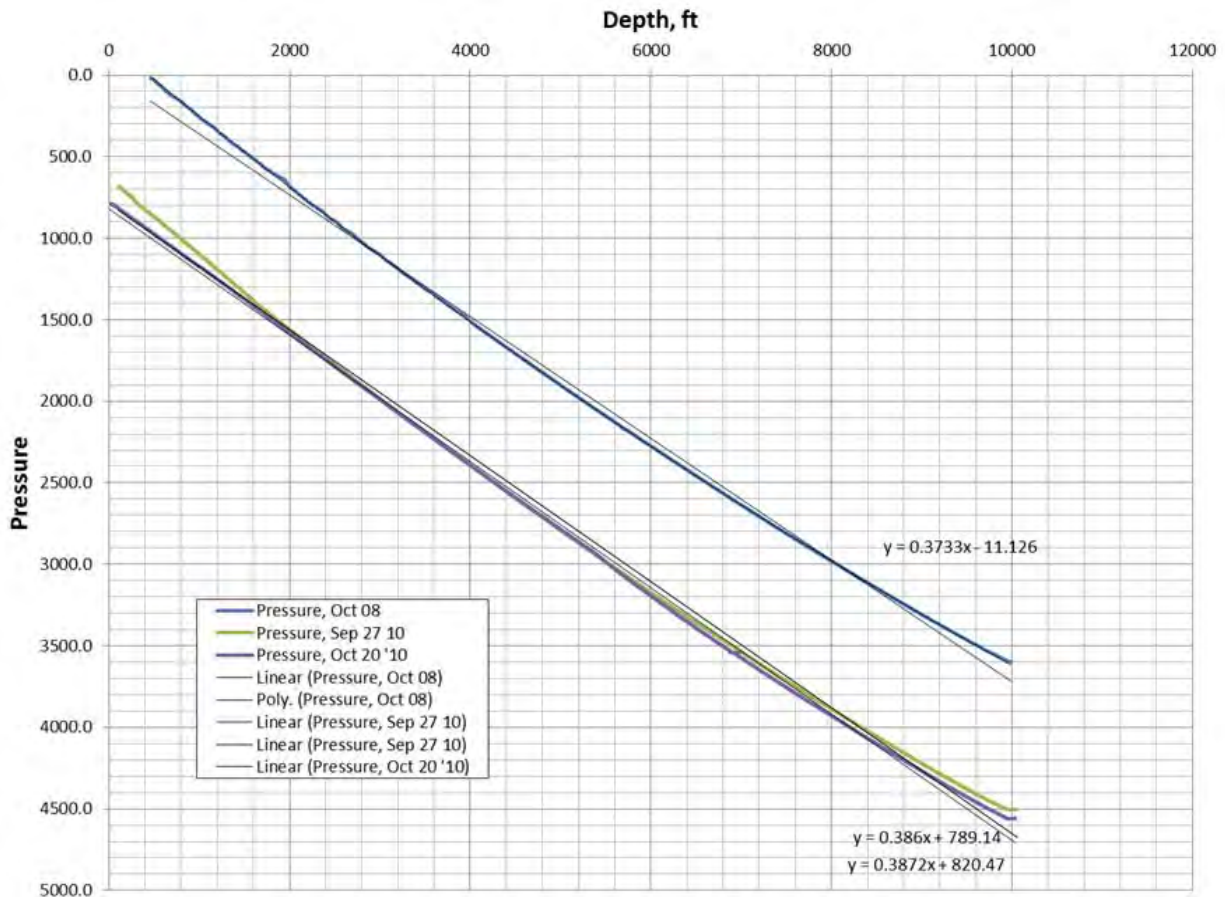


Figure 5-16. Summary of minimum and maximum fluid pressures measured in NWG 55-29. The minimum fluid pressure is used in the modeling of frictional strength of the crust and breakout formation. The maximum fluid pressure is used as a lower bound on  $S_{hmin}$ , because hydraulic fracture should result when borehole fluid pressure exceeds  $S_{hmin}$ , and no tensile fractures have been detected. Note that the pressure log from 20 October 2010 (purple curve) was recorded at 5.4 MPa (785 psi) wellhead pressure due to wireline lubricator pressure limitations, significantly below the maximum injection pressure of 7.95 MPa (1153 psi) (see text). Despite differences in injection rate, the pressure gradients for the equilibrated static logs and the two injecting pressure logs are very similar in both the casing and in the open hole.



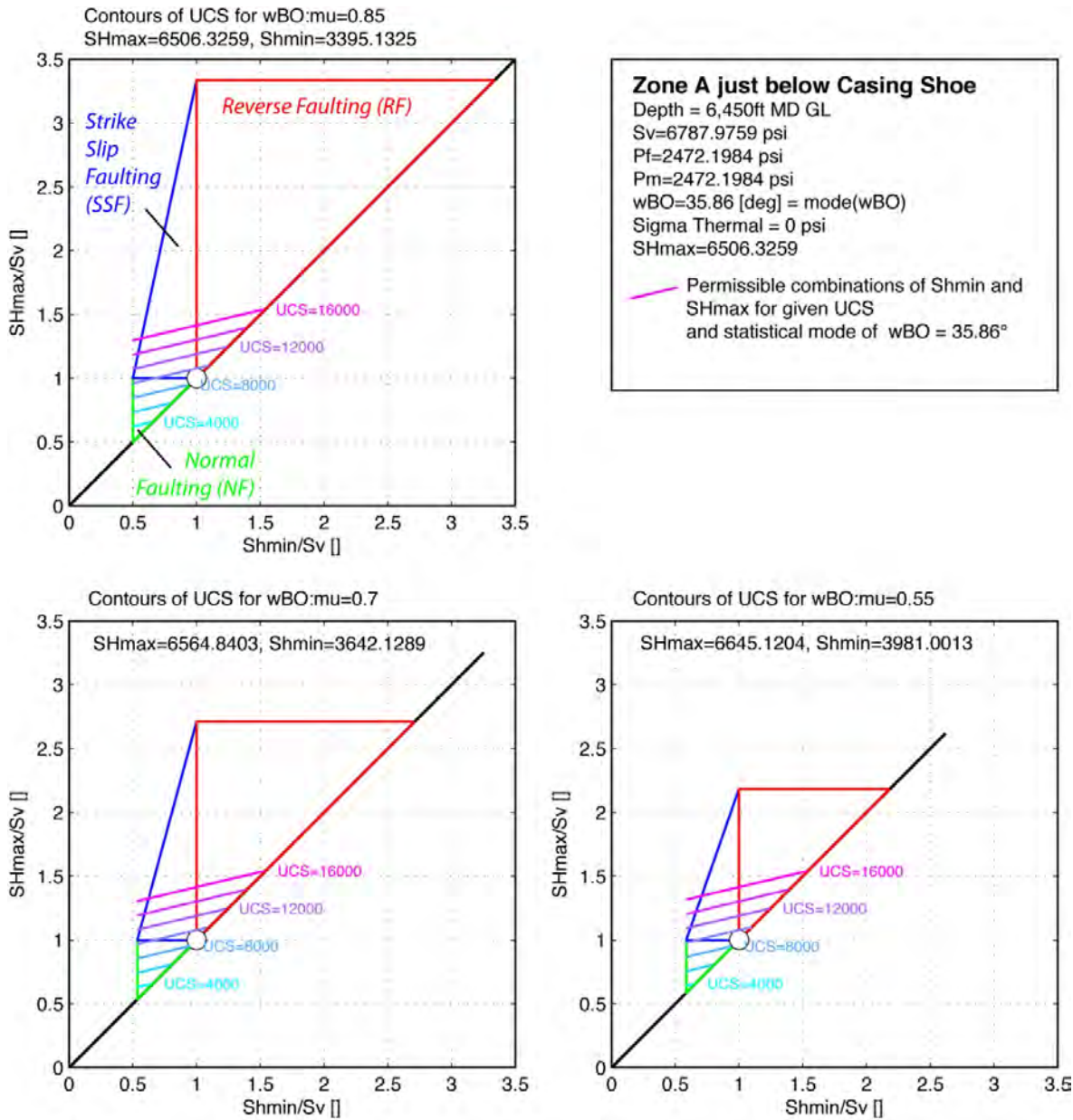


Figure 5-17. Example of stress polygons mapping the range of principal stress ratios permitted by the frictional strength of the crust, illustrated here at the depth of the casing shoe in NWG 55-29. The stress regimes corresponding to these discrete polygons are labeled in the upper left panel. These polygons are drawn for the following assumed frictional strengths: *Upper Left*: a coefficient of static friction,  $\mu_s = 0.85$ , corresponding to lab measurements on welded tuff from Yucca Mountain, NV (Morrow and Byerlee, 1984). *Bottom Left*:  $\mu_s = 0.70$ , corresponding to the expected friction for quartz, plagioclase, and calcite mixtures. *Bottom Right*:  $\mu_s = 0.55$ . Sloping colored lines correspond to combinations of  $S_{hmin}$  and  $S_{Hmax}$  that can reproduce the statistical mode of breakout widths observed in the logged interval of NWG 55-29 ( $wBO = 35.86^\circ$ ) for the specified magnitudes of UCS.

The injecting fluid pressure and frictional constraints on  $S_{hmin}$  are compared in the Panel 3 of Figure 5-15. The constraint from the maximum fluid pressures achieved during injection suggests that if the  $S_{hmin}$  profile was in frictional equilibrium with  $\mu_s = 0.7$ , then a hydrofrac would have been likely just below the casing shoe. In the absence of such a hydrofrac,  $S_{hmin}$  must be larger than predicted by this frictional

failure envelope. A larger magnitude of  $S_{hmin}$  at this depth suggests one of two currently indistinguishable possibilities: (1) the volume is in frictional equilibrium with a lower  $\mu_s$  (i.e.,  $\mu_s < 0.6$ ), requiring one of the phyllosilicate phases present in the borehole (Figure 5-14) to control fault strength, thus reducing the difference between  $S_{hmin}$  and  $S_v$ ; or (2) the volume is not critically stressed. Given the generally low seismicity in this region (Wong et al., 2010, 2011) and lack of seismicity detected during the observation period of the Demonstration, the latter scenario seems most likely.

#### 5.5.4 CONSTRAINTS ON MAXIMUM HORIZONTAL PRINCIPAL STRESS, $S_{HMAX}$

As discussed above, the presence or absence of breakouts and their widths constrain the stress state along the borehole if UCS is known and  $S_{hmin}$  can be estimated. Breakouts occur extensively throughout the logged interval of NWG 55-29 in all units except the crystalline intrusive rocks at the base of the imaged interval. To model breakouts, we use the conditions most favorable to their formation, which in the NWG 55-29 borehole includes: (1) minimum borehole fluid pressures given by the equilibrated fluid pressure profile (because excess borehole fluid pressure contributes tension to  $\sigma_{\theta\theta}$  that inhibits breakout formation); and (2) zero stress due to cooling, in effect neglecting the thermal stress term in Equation 5-1 (which would contribute a tension to  $\sigma_{\theta\theta}$  that would also inhibit breakout formation).

In the simplest case, we explored two models for the magnitude of  $S_{Hmax}$  derived from individually measured breakout widths assuming a constant UCS throughout the borehole, as derived from a single complete failure envelope for welded tuff from nearby well GEO N-2 (Section 3.2.6 and Figure 3-22), and assuming that the magnitude of  $S_{hmin}$  was controlled by optimally oriented, critically stressed faults with coefficients of friction of 0.55 and 0.70 (Figure 5-15). Under these assumptions,  $S_{Hmax}$  has a similar magnitude to  $S_v$  in the interval logged with the BHTV for the preponderance of breakout widths (red triangles in Figure 5-15), with  $S_{Hmax} > S_v$  at the casing shoe decreasing to  $S_{Hmax} < S_v$  midway through the logged interval. As noted earlier, in the context of borehole fluid pressures during injection, the model of  $S_{hmin}$  in frictional equilibrium with  $\mu_s=0.7$  represents the lower bound. For either  $S_{hmin}$  profile, magnitudes of  $S_{Hmax}$  that exceed  $S_v$  in this model lie outside the frictional bounds on stress in the crust and likely reflect variations in rock strength that are not accounted for in the uniform strength model. In other words, low UCS can account for wide breakouts without invoking excessive  $S_{Hmax}$  magnitudes. Alternatively, the crust could be under-stressed with respect to  $S_{hmin}$ , in which case  $S_{hmin}$  would be greater than expected from Equation 5-2, allowing the magnitude of  $S_{Hmax}$  to lie within the strike-slip faulting regime (i.e.,  $S_{Hmax} > S_v$ ) while still not exceeding the frictional strength of the crust (Figure 5-17).

In addition to the model of  $S_{Hmax}$  derived from constant UCS for each individual breakout, we solved Equation 5-1 to define contours of  $S_{Hmax}$  as a function of UCS for a single breakout width representative of the entire population, using a statistical mode for wBO of  $35.86^\circ$ . This provides alternate models for variations in  $S_{Hmax}$  magnitude with depth, which exhibit the same vertical gradient as in the variable wBO case, but with distinct stress-magnitude intercepts (Figure 5-15). These contours can also be projected onto the stress polygons defining the limits of differential stress for a given rock friction (Figure 5-17), where they define distinct combinations of  $S_{hmin}$  and  $S_{Hmax}$  consistent with the statistical mode of the mapped breakout width. Smaller UCS magnitudes reduce the  $S_{Hmax}$  necessary to yield this representative breakout width and allow more potential combinations of  $S_{hmin}$  and  $S_{Hmax}$  within the normal faulting stress regime (Figure 5-17). Since the circumferential compressive stress leading to breakout formation ( $\sigma_{\theta\theta}$ ) increases rapidly with increasing  $S_{Hmax}$ , whereas increases in  $S_{hmin}$  cause a relatively small reduction in  $\sigma_{\theta\theta}$  (Figure 5-10 and Equation 5-1), the slope of these contours is only at a small positive angle to the  $S_{hmin}/S_v$  axis (Figure 5-17). Thus, for a given rock strength and breakout width, relatively small increases in  $S_{Hmax}$  are required to counteract large increases in  $S_{hmin}$ . This explains the small differences in calculated  $S_{Hmax}$  magnitudes corresponding to  $S_{hmin}$  models in which  $\mu_s = 0.55$  versus  $\mu_s = 0.7$  (Figure 5-15).]

Numerous studies have demonstrated a good empirical correlation between porosity and UCS for a variety of rock types (Ryshkewitch, 1953; Duckworth, 1953; Rzevsky and Novick, 1971; Novik, 1978; Dunn et al., 1993; Price et al., 1993; Moos and Pezard, 1996; Li and Aubertin, 2003; Kleb and Vasarhelyi, 2003; Ma and Daemen, 2004; Entwisle et al., 2005; Ma et al., 2006; Zoback, 2007; details are extensively discussed in Appendix E-1). To allow for variations in UCS within the open-hole interval of NWG 55-29, we refined our constraints on  $S_{Hmax}$  using breakout width to account for variable UCS using porosity determined from the litho-density log (NPHI; see Figure 5-18) as follows:

**Equation 5-3**      $UCS = 13800 \exp(-0.04744\phi)$ ,

where porosity,  $\phi$ , is in percent. The fitting constant in the exponential term was derived from laboratory determinations of UCS versus porosity for numerous rocks with lithologies similar to those encountered in NWG 55-29 and the pre-exponential term was chosen to pass through the UCS value determined from triaxial testing of welded tuff from hole GEO N-2 (see Figure 5-12). For a detailed derivation of Equation 5-3, see Appendix E-1. In creating this variable-UCS stress model, we filtered the more complete breakout data set to base the model solely on the average width of breakouts that occur in distinct pairs and UCS estimates based on filtered porosity values, as previously discussed. The resulting model (Figure 5-13) suggests that the UCS of rock within the open-hole interval of NWG 55-29 ranges from about 41-83 MPa (6000-12000 psi). This is actually somewhat lower than obtained from the laboratory testing on core from GEO N-2, which is consistent with the relatively low porosity of the GEO N-2 sample tested in the lab compared to the rock penetrated by NWG 55-29 and the tendency for strength to reduce as porosity increases (Figure 5-13 and Figure 5-18).

As in our previous (constant UCS) stress model, in this variable-UCS model we computed two estimates of  $S_{Hmax}$  for each breakout pair based on the assumption that  $S_{Hmin}$  is at frictional equilibrium for  $\mu_s = 0.55$  and 0.7 in a normal faulting setting. Consistent with the lower UCS values, the majority of breakouts suggest that  $S_{Hmax}$  is less than  $S_v$  throughout the open-hole interval of the NWG 55-29 (Figure 5-18), which is consistent with geologic evidence (discussed above) suggesting that this site is in a predominately normal faulting stress regime. Although these results from a variable-UCS stress model conform to geologic expectations, it is important to note that there are a range of stress states capable of producing breakouts of the observed depth distribution and width if the crust is severely under-stressed for frictional failure (i.e., the magnitude of  $S_{Hmin}$  is larger than assumed here) or if UCS is significantly higher than expected. In particular, since  $S_{Hmax}$  in this model is only slightly less than  $S_v$  (Figure 5-18), increases in UCS of several hundred psi would move this site into a transitional normal faulting to strike-slip faulting stress state in which  $S_{Hmax} \sim S_v$ , as inferred, for example, from the constant-UCS stress model discussed above (Figure 5-15).

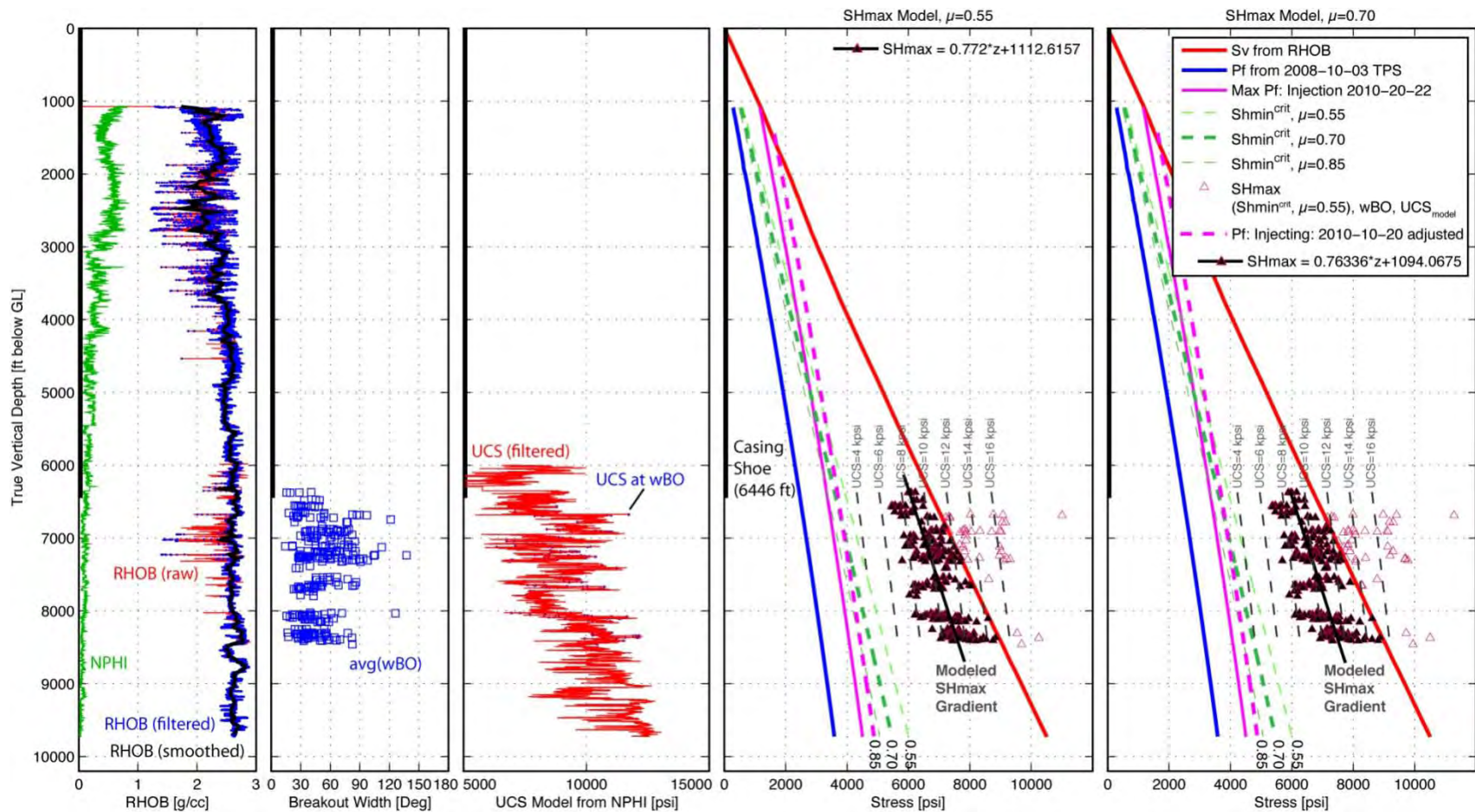


Figure 5-18. Analysis of stresses versus depth for borehole NWG 55-29, assuming a variable UCS. From left to right: *Panel 1*: Fractional porosity (green), raw bulk density (red), filtered bulk density (blue) and filtered and then smoothed bulk density (black) from the litho-density log. *Panel 2*: Average width of pairs of high-quality breakouts. *Panel 3*: UCS modeled from filtered neutron porosity (red) and UCS values used to model  $S_{Hmax}$  from breakout width (blue dots). *Panel 4*: Vertical stress profile as in Figure 5-15, but with estimates of  $S_{Hmax}$  assuming  $S_{hmin}$  corresponds to the critical magnitude for normal faulting for  $\mu_s = 0.55$  and allowing for variable UCS as derived from panel to the left (blue dots). For comparison, dashed black lines show  $S_{Hmax}$  for a variety of constant UCS models. *Panel 5*: vertical stress profile assuming  $S_{hmin}$  corresponds to the critical magnitude for normal faulting at  $\mu_s = 0.70$  using variable UCS as in the panel to the left. The thick vertical line indicates the extent of casing. In Panels 4 and 5, the black triangles correspond to the subset of  $S_{Hmax}$  magnitudes derived from breakout width consistent the assumption of a volume critically stressed for normal faulting. This subset is used to estimate a gradient in  $S_{Hmax}$  in the image logged interval.



### 5.5.5 COMPLETE STRESS MODEL

A stress polygon (Figure 5-19) provides a means to summarize the analysis of stress magnitudes in the open-hole interval of NWG 55-29 and review combinations of horizontal principal stress magnitudes consistent with the constraints derived from borehole fluid pressure, rock strength, and breakouts. This preliminary model is derived for the middle of Zone C at a depth of 2566 m (8420 ft) MD, using a variety of approaches outlined in the caption to Figure 5-19. See Section 3.2.8 for a discussion of fracture analysis and definition of fracture zones. From this analysis, three distinct stress states can be distinguished within the current constraints: (1) the volume is critically stressed for normal faulting; (2) the volume is critically stressed for strike slip faulting; and (3) the volume is under-stressed. In the normal faulting case, the  $S_{hmin}$  profile lies above the maximum injection pressures and in the range consistent with frictional failure at 0.6 to 0.4, below the transition to strike slip faulting consistent with the most common fault orientations mapped regionally and with fractures identified in the borehole, and consistent with breakout occurrence using the typical range of porosity-dependent UCS. The strike slip faulting case requires high average UCS to explain the most common breakout widths and is not consistent with most mapped faults and fractures, but is otherwise similar to the normal faulting case. In the case of an under-stressed volume, the stresses are insufficient to cause slip on normal strength rocks under ambient fluid pressure conditions. This case is consistent with an overall lack of seismicity (see caveats below) and the absence of distinct stress rotations in the BHTV log (which would indicate localized stress rotations due to fault slip) and potentially with low permeability related to high proportions of healed (sealed) fractures. Regarding this latter possibility, previous studies at the fault-hosted geothermal field at Dixie Valley, NV, showed that permeability in wells was low when individual fractures, as well as the overall fault zone hosting the geothermal field, were not critically stressed for frictional failure (Hickman et al., 1998; Barton et al., 1998). However, the extent of this under-stressing was small, and mini-frac tests still showed significant differential stresses, even in very low permeability wells.

Most of the potential combinations of horizontal principal stresses lie within the normal faulting stress regime (Figure 5-19), especially when considering the probable magnitudes of UCS, which range from 41-83 MPa (6000-12000 psi) in the open hole interval and average about 69 MPa (10000 psi) near the center of Zone C, where this stress constraint was obtained (Figure 5-13). Although the three possible stress states listed in Table 5-2 are not distinguishable without additional constraint provided by a direct measurement of  $S_{hmin}$  from a mini-frac, the under-stressed (or slightly under-stressed) NF case is probably the most likely. However, although a lack of seismicity may be consistent with an under-stressed crust at this location, it is important to note that areas known to be critically stressed from extensive mini-frac tests can be seismically quiescent, especially in areas of low tectonic stressing rates (e.g., Stock et al., 1985; Hickman et al., 1998). Furthermore, the majority of sites where *in situ* stresses have been measured directly are critically stressed or near-critically stressed, even in stable continental interiors (Townend and Zoback, 2000). Thus, the horizontal differential stresses at this site might be as large as indicated in our critically stressed NF stress model (for  $\mu_s \sim 0.55$ ), which would promote shear reactivation along well-oriented faults with modest increases in fluid pressure. Finally, relatively high horizontal differential stresses are consistent with the observation that breakouts in well NWG 55-29 are strongly developed and uniformly oriented (e.g., Figure 5-7 and Figure 5-8), in spite of localized variations in rock fabric, fracturing or structure (e.g., dikes), which might otherwise be expected to lead to local scatter in breakout azimuths.

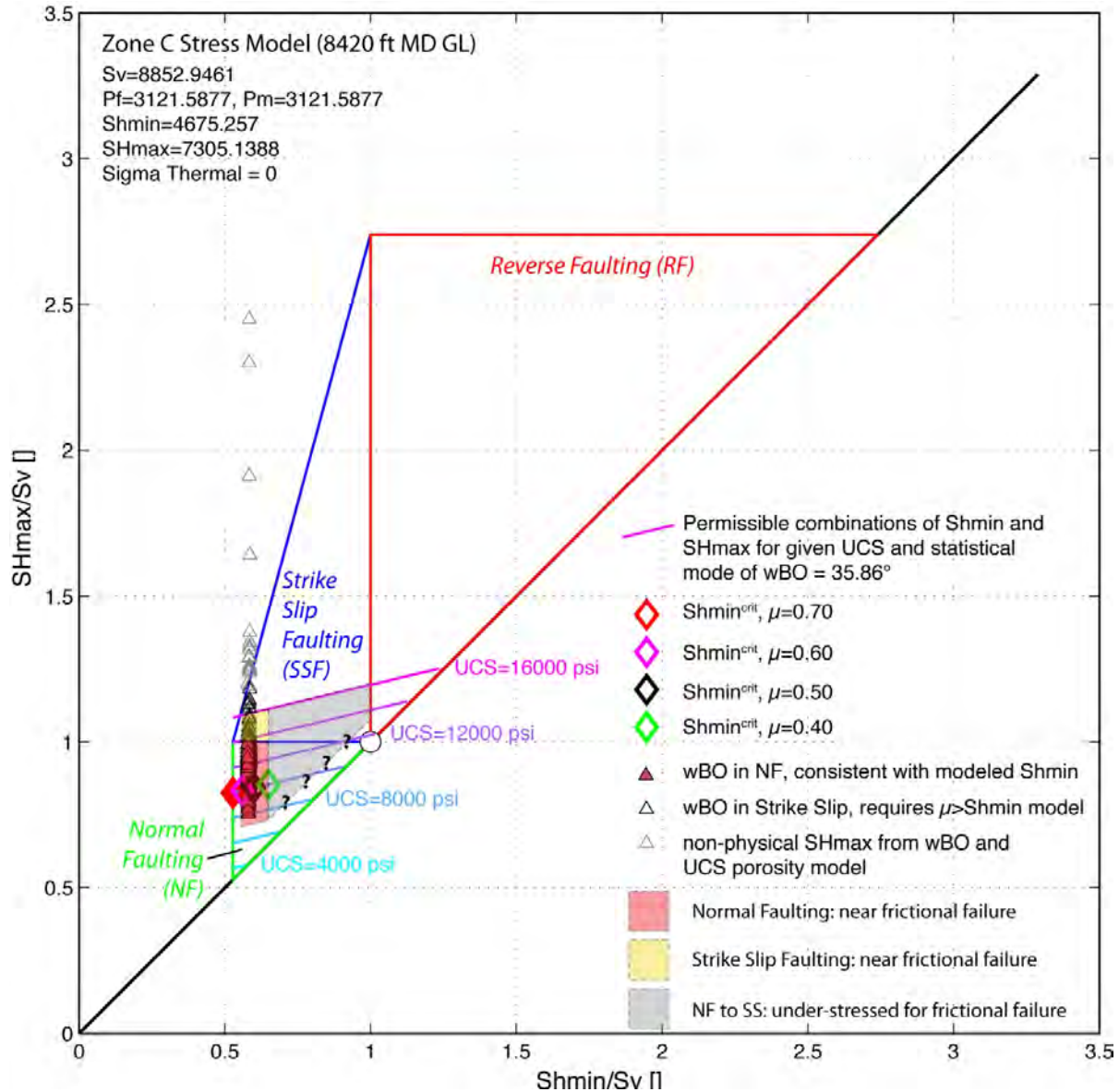


Figure 5-19. Stress polygon showing bounds on principal stress ratios for normal faulting, strike-slip and reverse faulting stress regimes permitted by a coefficient of static friction,  $\mu_s$  of 0.7, at a depth of 2566 m (8420 ft) MD GL of EGS stimulation Zone C which extends from a depth of 2438 to 2633 m (8000 to 8640 ft) MD. The best estimate of stress magnitudes at this depth is for  $S_{Hmin}^{crit}$  in frictional equilibrium with  $\mu_s = 0.55$  and corresponding estimates of  $S_{Hmax}$  from individual measurements of breakout width and a porosity-dependent UCS. Combinations of  $S_{Hmin}$  and  $S_{Hmax}$  consistent with the statistical mode of measured breakout widths can be traced for specified magnitudes of UCS along the colored sloping lines. Three potential ranges of horizontal principal stress are distinguished: (1) normal faulting (red); (2) strike slip faulting (yellow); and (3) a system that is either normal or strike slip, but is under-stressed even for coefficient of friction,  $\mu_s < 0.4$  (gray). Diamonds show possible stress states when  $S_{Hmin}$  is at frictional equilibrium with the coefficients of friction shown, with  $S_{Hmax}$  derived from the statistical mode of wBO and using the porosity-dependent UCS appropriate to this depth (~69 MPa [10000 psi]; see Figure 5-13). Triangles indicate stress constraints for breakouts, assuming  $S_{Hmin}$  in equilibrium with  $\mu_s = 0.55$  and with  $S_{Hmax}$  determined using individual measurements of wBO and porosity-dependent UCS. These stress states either lie within the stress polygons for normal or strike-slip faulting (as indicated) or exceed the frictional strength of the crust in a strike-slip faulting stress regime (non-physical case).

**Table 5-2. Characteristics of permissible stress regimes.**

Stress Case	Pros	Cons
Characteristics common to all stress cases	<ul style="list-style-type: none"> <li>• <math>P_i/S_v \approx 0.34</math> in the open hole.</li> <li>• <math>S_{hmin}</math> profile lies above greatest injection pressure profile.</li> <li>• Reverse faulting is incompatible with regional tectonics.</li> </ul>	<ul style="list-style-type: none"> <li>• No unique constraints on horizontal principal stresses (especially <math>S_{hmin}</math>).</li> </ul>
NF (critically stressed)	<ul style="list-style-type: none"> <li>• Frictional failure occurs in the range <math>\mu_s = 0.4</math> to <math>0.6</math>.</li> <li>• Compatible with the majority of mapped regional faults and fractures revealed in the BHTV log.</li> <li>• Compatible with the most common (statistical mode) wBO measurements and variable-UCS stress model.</li> </ul>	<ul style="list-style-type: none"> <li>• Requires relatively low static friction compared to mineralogy, Byerlee's Law or Yucca Mtn. Tuff to be currently active.</li> </ul>
SSF (critically stressed)	<ul style="list-style-type: none"> <li>• Frictional failure occurs in the range of <math>\mu_s = 0.4</math> to <math>0.6</math>.</li> <li>• Compatible with high magnitudes of <math>S_{Hmax}</math> predicted from some wBO measurements and variable-UCS stress model.</li> </ul>	<ul style="list-style-type: none"> <li>• Requires high average UCS to explain predominately low wBO if <math>S_{Hmax} &gt; S_v</math>.</li> <li>• Not consistent with most faults mapped at surface or seen in BHTV log.</li> </ul>
Stable (Under-stressed)	<ul style="list-style-type: none"> <li>• Consistent with lack of seismicity.</li> <li>• Allows for expected ranges of rock <math>\mu_s = 0.65</math>-<math>0.85</math>, without violating lower bound on <math>S_{hmin}</math> imposed by inject-to-cool operations.</li> <li>• Average UCS to explain individual wBO measurements most consistent with a NF or transitional NF-SSF stress state.</li> <li>• NF stress state consistent with range of regional fault and borehole fracture attitudes.</li> </ul>	<ul style="list-style-type: none"> <li>• None. This is the most likely stress case, although the crust could be only slightly removed from criticality (see text).</li> <li>• Consistent breakout azimuth requires <math>S_{hmin}</math> cannot approach the magnitude of <math>S_v</math>.</li> <li>• Note that the most likely range of UCS is from 55-83 MPa (8000-12000 psi).</li> </ul>

### 5.5.6 SLIP TENDENCY

Despite uncertainties in the stress models, we can assess which fractures will first slip based on the attitude of the fractures mapped by the image log, the direction of  $S_{hmin}$ , and reasonable models for the principal stress magnitudes and fluid pressure. A simple comparison of the dip direction and dips of natural fractures with the azimuth of  $S_{hmin}$  (Figure 3-45) suggests that many fractures throughout the logged interval should be well-oriented for frictional failure. Although we cannot distinguish exactly how close the system is to failure, we can establish a minimum possible hydrofracture gradient from the maximum borehole fluid pressure exerted to date (Figure 5-15) and hypothesize which fractures would fail first, should they be invaded by borehole fluids during hydraulic stimulation. We modeled two cases that conform to the normal faulting stress regime for which the tendency for slip primarily depends on the difference between  $S_v$  and  $S_{hmin}$ . As in Figure 5-7 and Figure 5-18, the first case is for a critically stressed volume in which the  $S_{hmin}$  profile is at the limit for  $\mu_s=0.70$  (Figure 5-20) and the second case for a volume in which the  $S_{hmin}$  profile is at the limit for  $\mu_s =0.55$  (Figure 5-21), but is under-stressed if  $\mu_s$  is higher. In both cases,  $S_{Hmax}$  is derived from individual measurements of breakout width and the variable-UCS model for appropriate magnitudes of  $S_v$ ,  $S_{hmin}$ , and  $P_p$  (Figure 5-18).

In each model, we use 3-D Mohr circles to represent the ratio of shear to the effective normal stress as a measure of the proximity of a particular fracture to frictional failure at a particular depth. The analysis was performed for each of the four stimulation zones distinguished by their geology and fracture population in Section 3.2.8 (see summary in Table 3-15. Zone summary. Table 3-15) that overlap the BHTV log, including Zone A from 1966-2057 m (6450-6750 ft) MD, Zone B from 2057-2438 m (6750-8000 ft) MD, Zone C from 2438-2633 m (8000-8640 ft) MD, and Zone D from 2633-2908 m (8640-9540 ft) MD. For the first model (Figure 5-20), the 3-D Mohr circle is tangent to a failure envelope for  $\mu_s=0.70$ , and in this critically stressed model we see that each interval contains pre-existing natural fractures likely to slip under ambient conditions, whereas the majority of bedding and dike attitudes are not well-oriented for slip. In addition, this model allows for stress profiles that do not pass through the origin, which better honors the stress models throughout the open-hole interval. This analysis reveals that well-oriented fractures are distributed throughout the open-hole interval. However, most of the thickest fractures are poorly oriented for frictional failure in the inferred stress field, having dips that are either too steep or too shallow to experience slip resulting from increases in fluid pressure induced by hydraulic stimulation. That is, most of the large red diamonds on Figure 5-20(b) plot at low slip tendency values. The current model predicts that a distributed population of natural fractures (smaller red and gray diamonds) will slip well before all but one of the thick fractures.

Figure 5-21 presents the case of a slightly under-stressed fault system, wherein we have assumed that  $S_{hmin}$  is given by  $S_{hmin}^{crit}$  for  $\mu_s=0.55$ , taking into account the necessary changes in both the  $S_{hmin}$  and  $S_{Hmax}$  profiles necessary to remain consistent with UCS and breakout width data. Assuming a rock strength given by  $\mu_s=0.70$ , this system would require positive borehole fluid pressure to induce slip. Because the stress magnitude models show that a significant difference between  $S_{hmin}$  and  $S_{Hmax}$  is required (Figure 5-18), there is still a strong preference for fractures that are well-oriented for normal faulting to slip, and thus little change is seen in the population of fractures likely to slip during stimulation relative to the critically stressed case (Figure 5-20). In general, the stress models coupled with variability in the fracture orientations should allow a range from pure normal slip to oblique slip and limited strike slip during hydraulic stimulation.

In Section 7.4, AltaStim, a stochastic fracture and flow software model developed by AltaRock, is used to model and visualize EGS stimulation scenarios and provide guidance for stimulation planning. The Newberry-specific AltaStim model further illustrates the relationship between principal stress orientation, stress magnitudes, fracture attitudes and slip tendency.



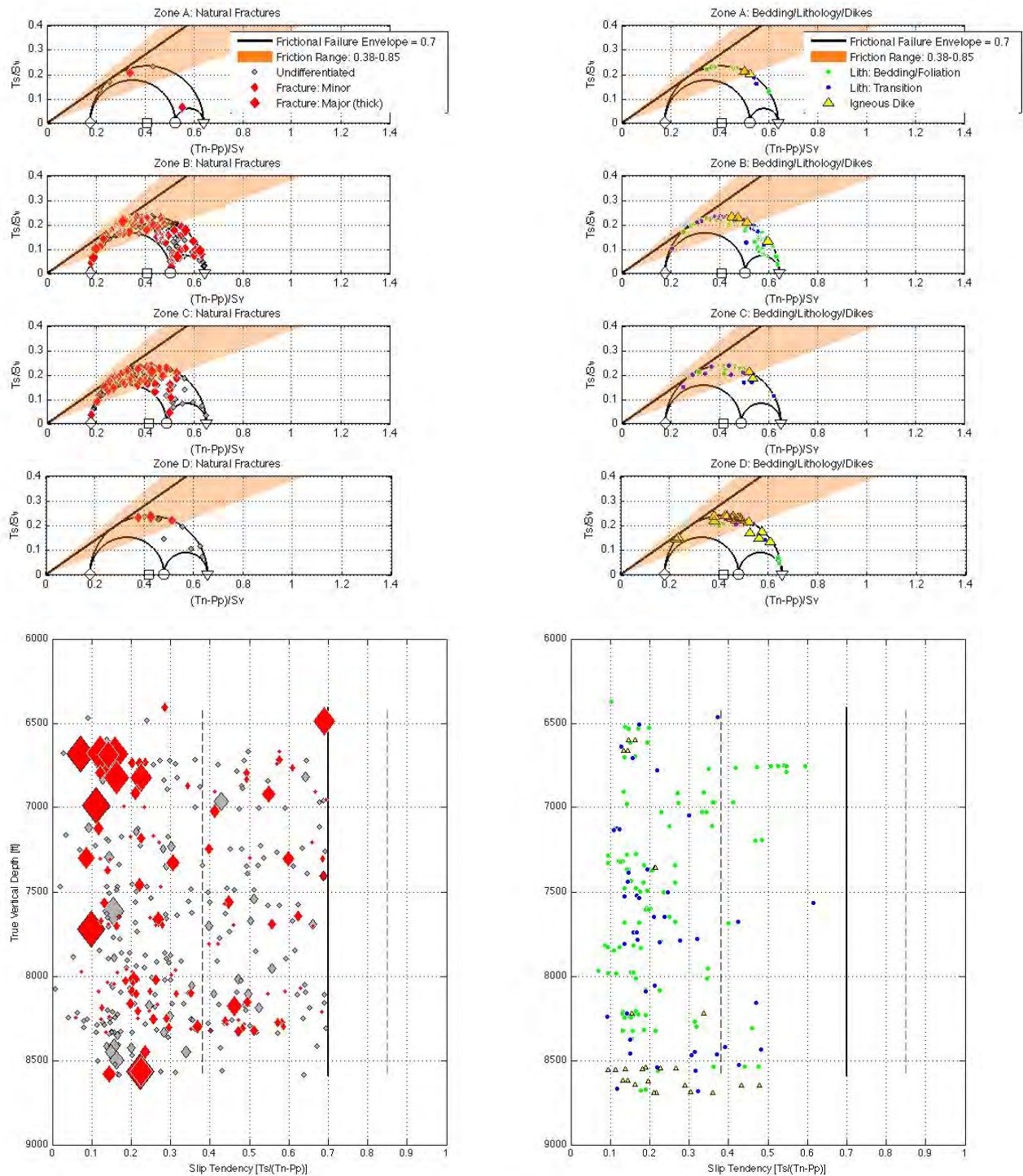


Figure 5-20. (a) Mohr Circle analysis of ambient stress and fluid pressures assuming  $S_{hmin}$  in frictional equilibrium with  $\mu_s = 0.7$ , with the same frictional strength assumed along fractures and other features seen in the BHTV log. This corresponds to a critically stressed model, and assumes uniform principal stress and fluid pressure magnitudes within each zone. (b) Slip tendency plot versus depth based on a constant vertical gradient in  $P_p$ ,  $S_{hmin}$ ,  $S_v$ ,  $S_{Hmax}$  derived from our preceding stress models. Note that in this case the depth profiles of principal stresses and fluid pressure are not forced through the origin and thus honor the stress magnitude model.

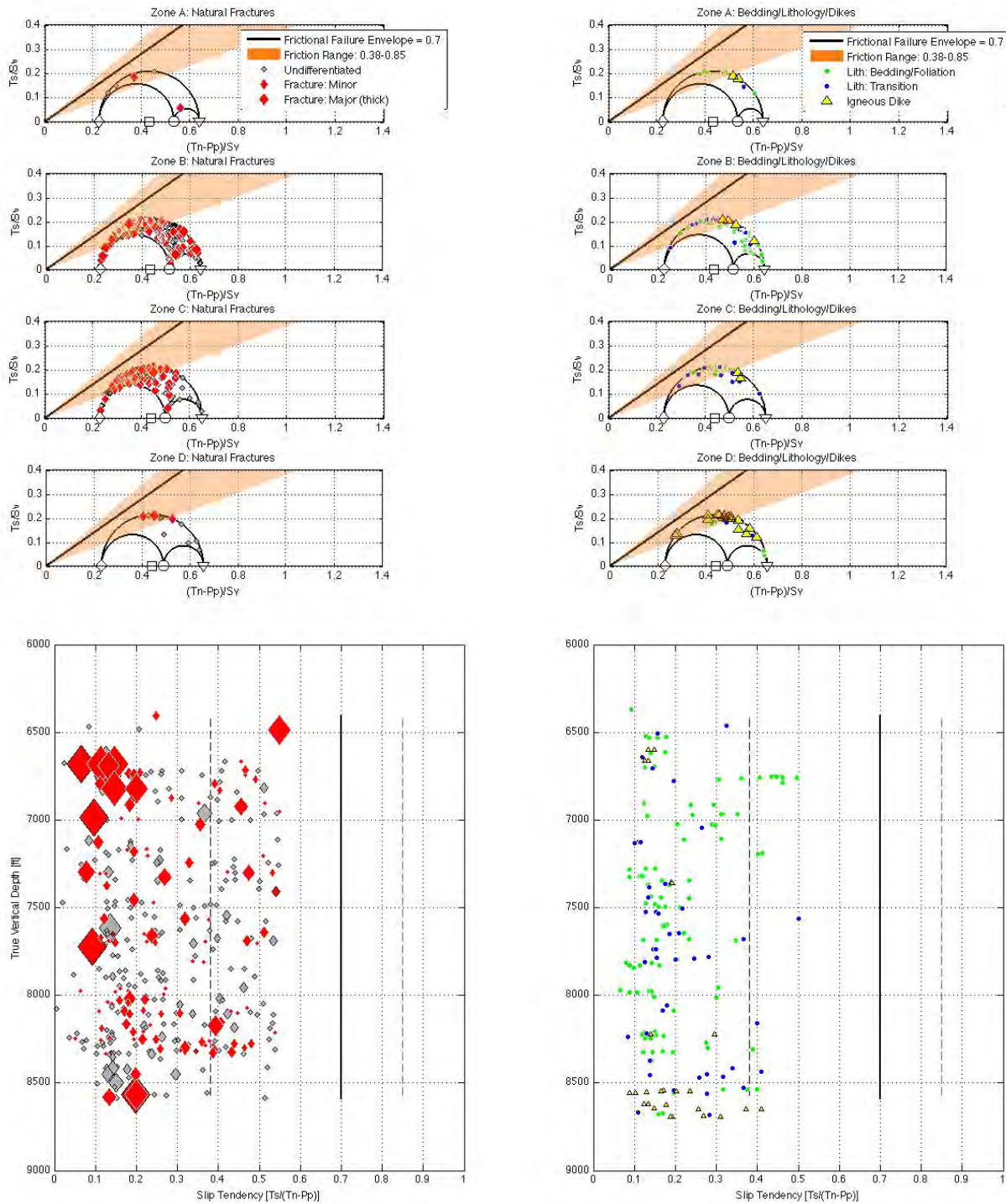


Figure 5-21. (a) Mohr Circle analysis of ambient stress and fluid pressures assuming  $Sh_{min} = Sh_{mincrit}$  as predicted for  $\mu_s = 0.55$ , but with higher friction (as shown) along fractures and other features seen in the BHTV log. This case corresponds to an under-stressed model, and assumes uniform principal stress and fluid pressure magnitudes within each zone. (b) Slip tendency plot versus depth based on a constant gradient in PP,  $Sh_{min}$ , SV,  $SH_{max}$  based on earlier plots. Note that in this case the profiles of the principal stresses and fluid pressure are not forced through the origin and thus honor the stress magnitude model.

### **5.5.7 POTENTIAL FOR STIMULATION AND DILATANCY DURING SLIP**

The potential for dilation of a fracture during slip strongly depends on three independent parameters: (1) mineralogy; (2) initial porosity; and (3) stress state. In the former case, fractures containing smectite, or that can incorporate smectite from the host rock during slip, are prone to pore collapse, pore clogging, and loss of permeability during slip (e.g., Davatzes and Hickman, 2005, 2010b; Hickman and Davatzes, 2010; Lutz et al., 2010). In addition, excessive porosity promotes localized grain crushing that clogs pores, whereas low porosity rock is susceptible to ‘self-propping’ dilatation and permeability enhancement during fluid injection and shearing (Brown, 1987; Teufel, 1987; Willis-Richards, 1996). In the latter case, the differential stress that drives slip and the average effective stress (which reflects the magnitude of the normal stress that presses the surfaces of a fracture together) can be used to visualize the role of the stress state in controlling dilatancy (Figure 5-22). At low average effective stress, differential stress is sufficient to cause dilatancy when the rock fails above the critical state line. As mean stress increases, dilation due to shearing is inhibited, and at the initial yield cap pore collapse initiates.

The cuttings analysis from NWG 55-29 demonstrates a lack of clay in the open-hole interval. Examination of cuttings and core from the nearby GEO N-2 borehole indicate a bimodal distribution of pore geometries, including early-formed cracks due to cooling stresses in volcanic flows and igneous intrusive rocks, and the presence of vesicles in the volcanic flows. Pores are also introduced along large macroscopic fractures, such as those revealed by the image log. Examination of the core from GEO N-2 in a related study (Fetterman, 2011) suggests extensive porosity production in clay-poor fractures that in the past facilitated fluid flow, including porosity recovery during fault reactivation and the creation of open pores. Overall, porosity is moderate to low in NWG 55-29, as indicated by the borehole compensated neutron porosity log. Our previous analysis and discussion suggests significant horizontal differential stress within the system (Figure 5-19), in addition to the likely large difference in stress magnitudes between  $S_v$  and  $S_{hmin}$ . Assuming that pre-existing cohesionless fractures exist near the borehole, these differential stresses will promote shearing (as opposed to tensile failure) during hydraulic stimulation. Overall, a normal faulting environment tends to minimize mean stress, and thus the potential magnitude of normal stress, facilitating dilation during hydraulic stimulation (Figure 5-22). This combination of material properties and the stress state driving deformation should promote dilatancy during hydraulic reactivation of the well-oriented natural fractures intersected by the NWG 55-29 borehole.



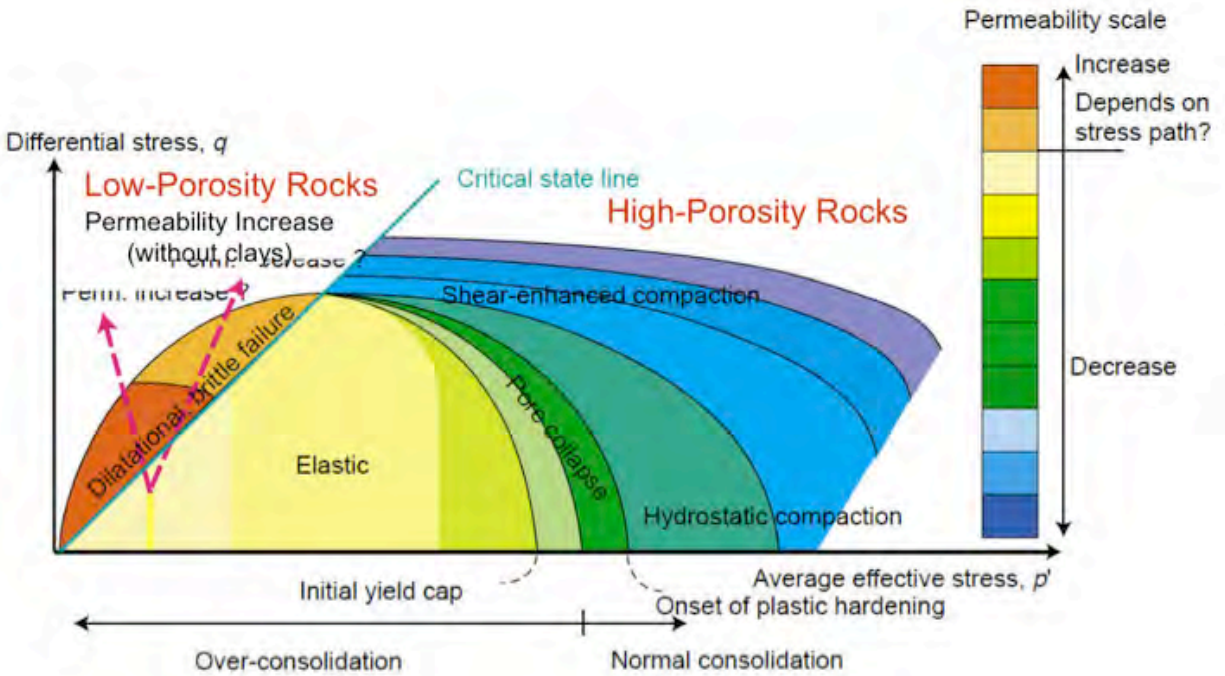


Figure 5-22. End cap model illustrating dependence of fracture dilatancy on ratio of mean effective stress,  $p'$ , to differential stress, and related changes in permeability expected during deformation. Comparisons of lab and *in situ* permeability show 'hard' rocks with low porosity undergo greatest permeability increases upon shearing (Brace 1980, 1984; Zhu and Wong, 1997; Wong and Zhu, 1999; Crawford et al., 2003; Crawford and Yale, 2002) whereas high porosity rocks can undergo pore collapse. Figure reproduced from Heffer, 2002.

In addition, during the fall 2010 inject-to-cool operation prior to BHTV logging, repeat temperature logs revealed localized temperature anomalies (Figure 5-23) consistent with flow into relatively permeable fractures (Davatzes and Hickman, 2010b). Although the overall permeability of the open-hole interval is very low, the existence of these fluid loss zones suggests that the effective normal stresses that stabilize the natural fractures intersected by the NWG 55-29 borehole can be reduced during hydraulic stimulation and, thus, induce slip. These and other temperature data will be analyzed in regions of borehole televiewer coverage to identify fracture characteristics and slip tendency, and lithologies associated with these fluid loss zones.

Thus, the current conditions of NWG 55-29 are consistent with the local geologic criteria identified by Davatzes and Hickman (2009), Hickman and Davatzes (2010), and Lutz et al. (2010) for successful hydraulic stimulation, including: (1) the stimulation interval is well below the zone of smectite alteration; (2) the interval exhibits high formation temperatures; (3) the interval intersects fractures well-oriented for shear failure and includes intervals of slight permeability, as indicated by mud losses and slight temperature anomalies (Figure 5-23); and (4) the mechanical properties of the rocks are conducive to dilation and self-propping if sheared.



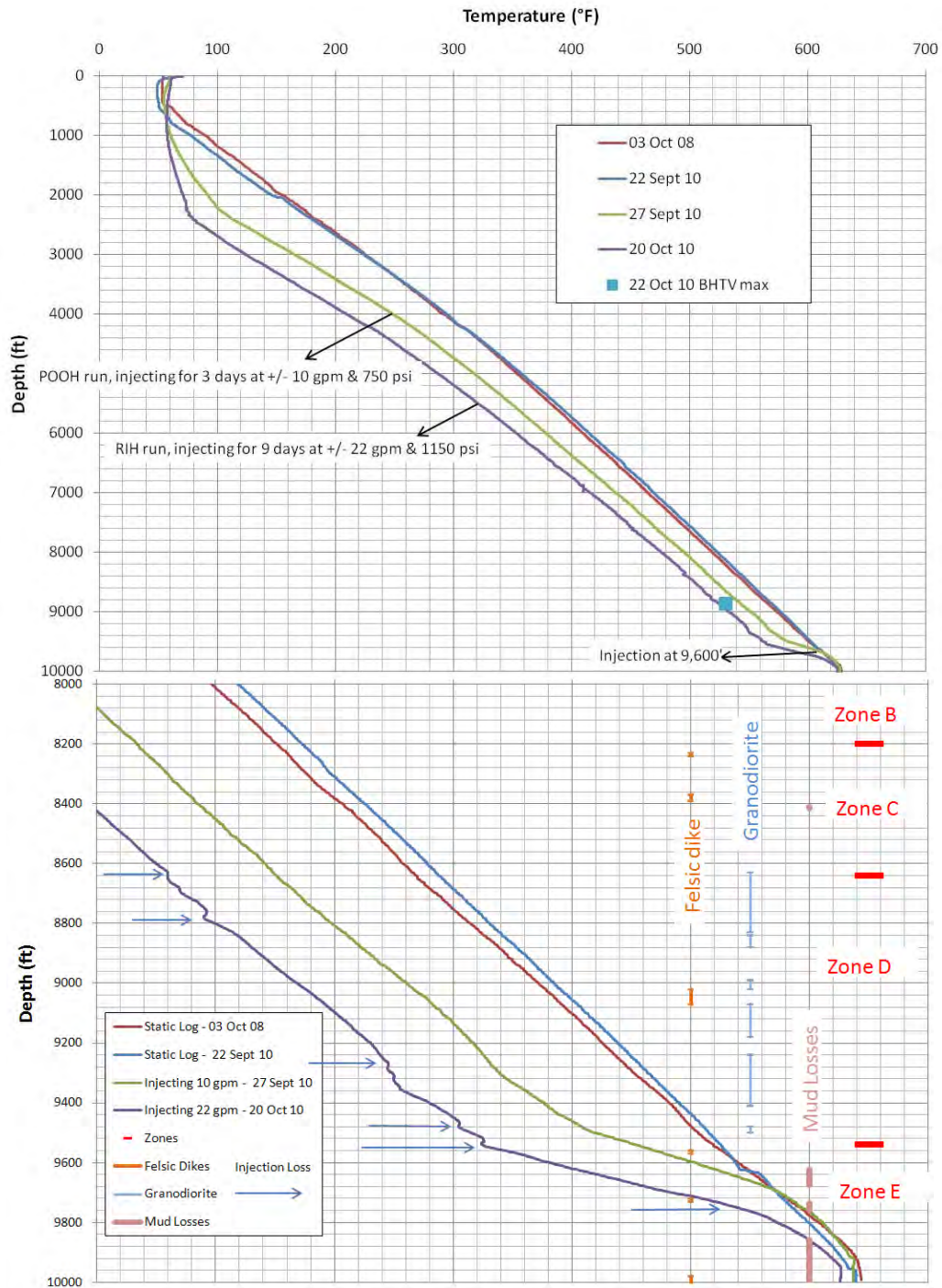


Figure 5-23. Temperature logs acquired during the inject-to-cool operation in Sept.-Oct. 2010, compared to earlier data. Red data acquired 3 October 2008, several months after well was drilled; blue data acquired 22 September 2010, prior to inject-to-cool; green data acquired 3 days after start of inject-to-cool. Injecting was discontinued 30 September and resumed 13 October 2010. Purple data taken 7 days after injection resumed. Repeated logging throughout the low WHP injection period from 22 September to 20 October 2010 records cooling of borehole. Lower graph shows localized anomalies indicative of fluid exit points from 8640-8800 ft (2633-2682 m) and 9280-9560 ft (2829-2914 m), as expected from flow into permeable fractures (see Davatzes and Hickman, 2010b). Also shown are data from the mud log. Depth is measured depth from KB (32 feet above GL).

Analysis of regional seismicity and geological structures (Crider, 2001; Cladouhos et al., 2011a) indicates that the minimum horizontal stress ( $S_{hmin}$ ) in the region is roughly east-west and the maximum principal stress is vertical, indicative of a normal faulting regime. The maximum horizontal stress ( $S_{hmax}$ ), necessarily perpendicular to  $S_{hmin}$ , is roughly north-south. The BHTV image log from NWG 55-29 shows clear borehole breakouts distributed throughout, indicating a consistent minimum horizontal stress azimuth,  $S_{hmin}$ , of  $92.0^\circ \pm 16.6^\circ$ . The azimuth of  $S_{hmin}$  determined from borehole breakouts in NWG 55-29 is consistent with the regional stress directions inferred from seismicity and regional structures.

A mini-frac is currently not possible in NWG 55-29 due to the large open-hole section and high formation temperatures, precluding the reasonable use of packers. Instead, stress magnitudes are estimated from modeling of breakout widths, models of *in situ* strength from the mineralogy of cuttings, and porosities from geophysical well logs and rock mechanics tests. Analysis of the vertical stress from the litho-density log of formation fluid pressure from the equilibrium fluid pressure logs, and of breakouts visible in the BHTV image suggest a tendency for a normal faulting stress regime consistent with the attitude of natural fractures and faults seen in the image log and mapped at the surface. Strike-slip faulting is also possible, but consideration of the measured distribution of breakout widths generally requires a UCS much larger than currently estimated from the preliminary model of *in situ* rock strength derived from the single laboratory measurement of UCS on welded tuffs from Newberry, a fit to UCS versus porosity data available in the literature, and neutron porosity and litho-density logs from the well. The occurrence of well-developed and consistently oriented breakouts also requires a significant difference between  $S_{hmin}$  and  $S_{hmax}$ , which suggests fractures that slip during stimulation will have a strong tendency to strike nearly north-south. This could impact the shape of the stimulated volume, because previous studies in normal faulting regimes have shown a strong tendency for stimulation to extend in the direction of  $S_{hmax}$  by following the strike of highly stressed fractures (e.g., Willis-Richards et al., 1996; Heffer, 2002; Rahman et al., 2002; Valley and Evans, 2007). In the absence of a mini-frac, current constraints on stress magnitude do not definitively determine the proximity of the volume penetrated by NWG 55-29 to frictional failure, but do limit the potential range of stress states.

Analysis of cuttings from the open-hole interval shows a distinct lack of weak, expandable clays and the common occurrence of calcite and quartz veins. The characteristics of fractures in shallow core suggest that natural fractures with this mineralogy commonly dilate if reactivated (Fetterman, 2011; Fetterman and Davatzes, in press). Given the likely relatively low stress magnitudes and this brittle mineralogy, there should be a strong tendency for fractures intersected by NWG 55-29 to dilate once reactivated.

Detailed analysis of temperature logs to further refine the hydrology of the borehole and additional analyses of the potential stress tensor are ongoing. In addition, we note that a related study on the dilation potential and history of natural fracturing of core from Newberry borehole GEO N-2 is ongoing as an independent, DOE-funded project (DOE grant DE-EE0002757).

## 5.6 CONTINGENCY AND RISK MITIGATION

As introduced in this section, the *in situ* stress tensor is a primary control on the design and creation of an EGS reservoir. Stress orientations and relative magnitudes control the fractures most likely to slip and, consequently, the orientation and overall shape of the resulting EGS reservoir. Stress magnitudes determine the fluid pressure required to initiate hydroshearing, the effectiveness of that shearing in enhancing permeability, and the volume of the EGS reservoir. In general, it remains a challenge to model the stress tensor in the EGS volume due to the potential effect of local stress variations caused by weak fault zones, recent fault slip, density variations, natural fluid pressures, volcanic activity, and variability in the mechanical properties of the rock mass.

Tectonic studies, well tests and geophysical logs have been used to constrain the stress state. Given the data available, the stress state in the rock mass surrounding NWG 55-29 is as well-constrained and modeled as is currently technically feasible. The stress orientation model was initially determined from tectonic studies at multiple scales and confirmed by the consistent orientation of borehole breakouts observed in the BHTV images. A unique stress magnitude model cannot be determined at this time with the available data. However, a range of plausible magnitudes of the three principle stress magnitudes at the target stimulation depths have been determined based on mechanical testing of core, borehole breakouts widths, geophysical logs, and well-developed geomechanical precepts. In addition, by comparing the stress state, the orientation of the fractures observed in the BHTV and the mineralogy of drill cuttings, the tendency for fractures to slip and dilate during EGS stimulation was determined.

We have followed the best practices developed over the last 20 years for determining the stress and fracture models in boreholes, particularly the methodologies developed by geoscientists working in geothermal sciences and EGS. Still, uncertainties remain concerning the stress and fracture models in NWG 55-29. In Section 7, the described stimulation plan for NWG 55-29 is designed to be flexible to account for the remaining uncertainty.

## 6 PERMITTING

Geothermal exploration and development activities have been conducted at Newberry periodically since the 1970s, including efforts by CalEnergy that included the completion of an Environmental Impact Statement (EIS) for development and operations, up to and including installation of a power generating station. This EIS was approved by the BLM and FS in 1994, and serves as a basis for identifying many potential activities and impacts that might occur as part of the Newberry EGS Demonstration. Davenport has been conducting geothermal exploration activities at Newberry since 2007 and, therefore, has already secured necessary permits for various activities that will occur as part of the Demonstration. Additional permits will be obtained for activities specifically related to EGS stimulation and testing. These requirements are described below.

### 6.1 EXISTING PERMITS

#### 6.1.1 SURFACE PERMITS

The following four surface permits have been obtained (Appendix F-1):

1. **Oregon Department of Environmental Quality (DEQ) Simple Air Contaminant Discharge Permit**  
Air emissions from the diesel-generator sets used during stimulation and production well drilling.
2. **Oregon Department of Environmental Quality (DEQ) Letter Permit of Authorization**  
Sump design for Pads S-16 and S-29.
3. **U.S. Forest Service Temporary Special Use Permit**  
Surface microseismic stations.
4. **U.S. Forest Service Road Use Permit**  
Use of Forest Service roads to access project site.

#### 6.1.2 SUBSURFACE PERMITS

The following four subsurface permits have been obtained (Appendix F-2):

1. **BLM Geothermal Drilling Permit (GDP)**  
Geothermal well permit for NWG 55-29.
2. **Oregon Department of Geology and Mineral Industries (DOGAMI) Geothermal Well Permit**  
Geothermal well permit for NWG 55-29.
3. **Oregon Department of Environmental Quality (DEQ) Underground Injection Control (UIC) Permit**  
Temporary UIC permit for the injection of groundwater into NWG 55-29.
4. **Oregon Water Resources Department (OWRD) Limited Use License**  
Groundwater use permit for water supply wells at Pads S-16 and S-29.

### 6.2 OUTSTANDING PERMITS

As an initial step in conducting the Newberry EGS Demonstration, AltaRock convened a meeting on 21 September 2010 in the Portland office of DOGAMI to discuss the project scope and identify permitting requirements. The meeting included representatives from DOGAMI, DEQ, OWRD, BLM, FS and DOE. The discussion included an overview of each agency's permitting process, application requirements, permitting timeframes, and associated fees. This and numerous subsequent discussions with these representatives have identified the permit requirements described below.



### 6.2.1 SURFACE PERMITS

Two additional surface permits will be required prior to stimulation activities at the site:

1. **BLM Authorization of Notice of Intent to Conduct Geothermal Resource Exploration Operations** (Form 3200-9)
2. **Deschutes County Building Permit**  
For modular office units at Pad S-29 during stimulation and drilling.

### 6.2.2 SUBSURFACE PERMITS

Two additional subsurface permits are required in advance of stimulation activities, and two additional permits are required prior to drilling additional production wells:

1. **BLM Geothermal Sundry Notice (GSN)**  
Geothermal Sundry Notice allowing stimulation of NWG 55-29.
2. **DEQ UIC Permit**  
Injection of diverter products into NWG 55-29.
3. **BLM Geothermal Drilling Permit (GDP)**  
Geothermal well permits for the drilling of production wells NWG 55A-29 and 55B-29.
4. **DOGAMI Geothermal Well Permit**  
Geothermal well permits for the drilling of production wells NWG 55A-29 and 55B-29.

## 6.3 NEPA-RELATED ITEMS AND DETERMINATION

On 8 June 2010 AltaRock and Davenport submitted a Notice of Intent (NOI) to Conduct Geothermal Resource Exploration Operations (Form 3200-9) to the BLM. To authorize this NOI, BLM is conducting an environmental review in accordance with NEPA regulations.

The primary regulatory agencies are the BLM, FS and DOE. All three agencies have responsibilities under NEPA to conduct environmental analysis and make a determination and decision based on the findings of that analysis. Because three federal agencies are involved, lead and cooperating agencies were designated, and each has its own specific purposes for involvement. The BLM, acting as the lead agency for NEPA review, is in the process of preparing an Environmental Assessment (EA) for the project. USFS and DOE are cooperating agencies on the EA.

The specific roles, responsibilities, and timelines of each agency are outlined in separate Memorandums of Understanding (MOUs) between BLM and FS, and BLM and DOE. Because DOE has the most expertise and has issued specific guidance for managing induced seismicity, BLM will rely on the DOE for their technical expertise and support in the area of induced seismicity.

BLM has responsibility for subsurface activities and management of geothermal operations. BLM also ensures that operations are conducted in accordance with NEPA decisions and mitigation measures defined in the EA to minimize resource impacts. Eight independent studies, and one report prepared by AltaRock, were prepared to support the EA. Those reports are summarized below.

After the EA is completed, the three agencies will either issue a Finding of No Significant Impact (FONSI) or require an Environmental Impact Statement (EIS). If the agencies conclude their environmental review with a FONSI, the NOI would be authorized and the demonstration project could proceed. Any mitigation measures or monitoring requirements would be added to the NOI as conditions of approval.

### **6.3.1 HYDROLOGY**

An independent review that considered the existing hydrologic resources and environment within the upper Deschutes Basin of central Oregon was conducted by Kleinfelder (2011) and is included as Appendix B-5. The Newberry EGS Demonstration will require up to 538000 m<sup>3</sup> (142 million gallons or 436 acre-feet) of water from the shallow groundwater aquifer on the west flank of Newberry Volcano. This volume of water, used intermittently over about two years, represents approximately 0.3% of the estimated annual recharge to the Deschutes Basin aquifer from the western flank of Newberry Volcano.

The nearest domestic wells and local beneficial use aquifers (Newberry Caldera and La Pine) are not in hydraulic connection with the shallow aquifer at the EGS Demonstration site and, as such, no impact is expected to these areas. A monitoring well completed in the groundwater aquifer will be located down-gradient of NWG 55-29 to detect the escape of any fluid from the EGS reservoir. In addition, turbidity and metals concentrations will be monitored in the two closest existing groundwater wells near La Pine to compare to pretest conditions. Water levels will be monitored during testing to determine the footprint and extent of any potential impacts, if any, to the shallow groundwater. Other than expected temporary drawdowns near each of the water supply wells, no direct, indirect, or cumulative effects to surface water bodies, local groundwater, or regional aquifers are expected as a result of groundwater pumping or injection.

### **6.3.2 VISUAL IMPACT**

A scenic resource assessment was conducted by Robert Scott Environmental Services (2011; Appendix F-3). In compliance with the FS Scenery Management System, it considered effects of visual contrast from six key Visual Observation Points in terms of Scenic Attractiveness Classes, Visibility and Scenic Concern, Seen Areas and Distance Zones, Visual Absorption Capability, and Existing Scenic Condition.

Most of the EGS activities are located at sites previously used for geothermal exploration. However, three new seismic monitoring borehole sites will be constructed. One of these sites will be located within the Scenic Views Management Area (MA-9), as is existing well pad S-29. The other two new seismic monitoring boreholes will be located in the General Forest Management Area (MA-8). The Project will be in compliance with Forest Plan direction and will meet objectives for Scenic Condition Levels.

Impacts to scenic resources will be short-term and primarily associated with road dust from traffic, equipment at well pad S-29, site preparation at the three new seismic borehole sites, and a steam plume during venting periods. Most project facilities and activities would not be visible from any of the six key viewing points, primarily due to topography, distance, and the small scale of the Demonstration relative to the features of the viewed landscape. Impacts to scenic resources will be minimal and Demonstration activities are not expected to draw attention or adversely affect the viewing experience.

### **6.3.3 INDUCED SEISMICITY MITIGATION PLAN**

The International Energy Agency (IEA) developed a protocol for addressing induced seismicity during geothermal projects that was adopted by the U.S. Department of Energy (DOE) for EGS demonstration projects ([Majer et al., 2008](#)) and is currently being updated in draft form (Majer et al., 2011). Although the DOE considers the induced seismicity protocol a guideline rather than a permitting requirement, it is an essential component of documents that will be reviewed as part of the EA process. AltaRock prepared an *Induced Seismicity Mitigation Plan* (ISMP) specifically for its Newberry EGS Demonstration. The ISMP is adapted to the local geologic and environmental conditions and includes site-specific

controls and mitigation procedures. The complete ISMP, including its 14 appendices is attached as Appendix A-1.

The ISMP includes five appendices, prepared by independent consultants, which assess EGS induced seismicity, and seismic hazards and risks. These assessments, summarized below, include:

In ISMP Appendix F, prepared by URS Corporation, the authors study case histories in similar settings, to determine that, although unlikely, seismic events could be induced to an upper range of moment magnitude M 3.5 to 4.0. They concluded that the Demonstration presents no increase in risk at the Demonstration site or nearest communities relative to baseline conditions. EGS induced seismicity poses no risk to residents, and although unlikely, if events of M 3.0 and higher were to occur, they may be felt but would not be damaging. In ISMP Appendix E, Fugro Consultants compared four independent methods for determination of the maximum magnitude of induced seismicity, concluding that the probability of an event with  $M > 3.0$  is less than 1% over a 50-day period, and that, at a 95% probability, that the maximum induced event magnitude will be less than M 2.2.

Using the best available ground motion prediction models, ISMP Appendix G, presents shake maps showing that a peak ground acceleration (PGA) of 0.1 g (light shaking) might be felt at distances up to 5-12 km (3-7 miles) from the stimulation area surrounding NWG 55-29. They concluded that the highest estimated PGA of 0.25 g would be localized around the injection well, and that this is expected to be predominantly high-frequency and short duration and, therefore, unlikely to be damaging. In appendix F-4 (of this section) the potential for damage to structures located within and near NNVM is evaluated, and it is concluded that structural damage is not expected as the buildings are in reasonably good structural condition. He also evaluated potential impacts at the Lava River Cave, located 19 km (12 mi) from NWG 55-29, concluding that visitors would probably not detect any ground shaking from an M 3.5 seismic event, and that it was very unlikely that the cave itself would suffer even minor damage. He evaluated the potential for snow avalanches resulting from induced seismicity, concluding that avalanches could be triggered in low levels of ground shaking. Mitigation measures for snow avalanche are addressed in the ISMP (Appendix A-1).

Seismic events could be detectable by wildlife in the form of short-duration sound frequencies and ground shaking; however, these stimuli may be mistaken for natural environmental conditions and not generate a response. The magnitude and intensity of the events are anticipated to cause minimal temporary disturbance to large mammals or nesting birds.

As a follow-up study to the studies presented in ISMP Appendix F, engineers from Treadwell & Rollo evaluated potential impacts to the Paulina Lake dam, and to talus slopes located along Road 500 to Paulina Peak and the north sides of Paulina and East Lake. They concluded that there is no risk of damage to the Paulina Lake dam at  $PGA \leq 0.028$  g. They note that the dam already shows signs of cracking and evidence of crack monitoring, and conclude that additional cracking could occur at PGA up to 0.10 g, and that continued crack monitoring of the dam should be conducted as a mitigation measure. This mitigation is included in the ISMP. Regarding the talus slope along Road 500, they concluded that because this road with slopes up to 70 degrees already experiences rocks on the roadway and that this is likely to continue with induced seismicity, the mitigation should include preparations to promptly remove rocks from the roadway, but that the probability of a landslide is low. Their evaluation of the slopes on the north sides of Paulina Lake and East Lake conclude that the risk of a deep-seated landslide was low to very low, and that this should not create a seiche hazard in the lakes.

Similarly, engineers from Simpson, Gumpertz & Heger provided a follow-up study to the stability of structures (small building and bridges), identified by FS, located in and adjacent to NNVM. With respect to buildings, they found that the PGA required to reach a 10% probability of collapse was no less than

0.25 g, which is not expected to occur anywhere in NNVM based on the results presented in the ISMP. Furthermore, they found that even cosmetic damage is not likely to occur at  $\text{PGA} \leq 0.025 \text{ g}$ . Regarding the bridges over the Paulina Lake dam, they concluded that the collapse rating of these structures is well above any expected PGA, and that even cosmetic damage is not expected at  $\text{PGA} \leq 0.15 \text{ g}$ , far higher than mitigation triggers. They do recommend that crack monitoring of the bridge be performed as a mitigation measure and, thus, this is included in the ISMP.



## 7 STIMULATION PLAN

### 7.1 INTRODUCTION

An EGS reservoir will be created and characterized in Phase II by completing several primary tasks: (1) installation of a permanent microseismic array; (2) hydroshearing stimulation of an existing injection well; (3) drilling and hydroshearing stimulation of two new production wells; and (4) confirmation of connectivity and reservoir performance during a 30-60 day circulation test. The goal of Phase II is to establish a three-well, hydraulically-connected EGS reservoir that efficiently extracts heat from the geothermal resource at economically viable flow rates.

The injection well and, if necessary, the production wells, will be stimulated using a process termed 'hydroshearing'. The goal of hydroshearing stimulation is to create multiple zones of enhanced permeability in low permeability rock to optimize the heat exchange area of an EGS system. Hydroshearing is the process of hydraulically inducing shear failure in subsurface rock formations along existing natural fractures. Hydroshearing requires that stimulation pressure be maintained at levels less than formation breakdown pressure, unlike traditional oil and gas fracturing techniques. Exceeding the formation breakdown pressure can induce tensile failure, which can lead to short-circuiting. A short-circuit is defined as a fast path of high permeability within the rock matrix. Fluid travel times would be too swift along a short circuit to allow for sufficient heat to be transferred from the rock to the injectate during EGS circulation, thus, causing thermal breakthrough and lower system enthalpy. Inducing shear failure offers the greatest potential for creating an EGS reservoir that will provide sufficient surface area and residence time for injected fluids to reach optimum production temperature and maximize reservoir life by minimizing short-circuiting and premature injection fluid breakthrough. In shear failure, the opposite fractures walls slip past one another and asperities or irregularities on the fracture walls prop open the fractures, maintaining the enhanced fracture permeability once hydraulic pressure is removed. A tensile failure, on the other hand, does not cause slippage and will collapse upon itself once hydraulic pressure is removed. Hence, tensile fracturing, the goal of most oil and gas fracturing, requires an artificial proppant, like sand, to remain open.

To create a network of optimum fracture width, density and overall dimension, hydroshearing stimulation is conducted at multiple levels in the target well. The advantages of multiple stimulations include:

- Creation of a larger reservoir volume, thereby doubling or tripling available heat exchange area.
- Enhancing system permeability and connectivity to allow for higher production rates and lower injection pressures; thereby, increasing the economic viability of the project.
- Establishing a single-well production total mass flow rate of 75 kg/s (approximately 1200 gpm).
- Forming a fracture network 'half-length' of at least 500 m (1640 ft) (Jupe et al., 1995)
- Reducing effective costs (near-wellbore skin, frictional losses and water losses) to increase system profitability.
- Expanding knowledge base to grow demonstration project to commercial scale.

NWG 55-29, due to temperature over 315°C (600°F) and lack of permeability, is an ideal candidate for EGS stimulation. After the necessary permits are in place and the risk of induced seismicity determined to be acceptable, water will be injected using surface pumps to shear the shallowest set of pre-existing fractures. The water will be tagged with thermally reactive and conservative chemical tracers to aid in determination of reservoir surface area, average temperature and fluid travel time. These tracer compounds, used widely throughout the geothermal and groundwater industries, are not radioactive

and are environmentally safe. Microseismicity, measured with a permanently installed seismic array, will be continuously monitored along with surface injection rates and pressures. A fiber optic monitoring system will be deployed in the wellbore to provide real-time distributed temperature information and bottomhole pressure. The orientation and shape of the fractured reservoir created by stimulation is controlled by the in-situ stress regime at any given depth.

Once fracture geometry with a long axis radius of about 500 m (1640 ft) is achieved, a high-temperature, diverter (Section 7.6) will be pumped to redirect the hydraulic treatment to the next set of natural fractures. To create multiple fracture sets in a single well requires hydraulic isolation of each fracture network after it has been stimulated. To provide hydraulic isolation for the creation of multiple fractures a diverter material (a temporary sealant) can be used. After stimulation of the first fracture zone, a diverter material is added to the injected water to temporarily seal off that zone at the borehole.

Additional pressure is then applied to the injected water and a second fracture zone is stimulated. After multiple fracture zones are stimulated, injection is discontinued and the well bore is allowed to reheat to the original well temperature. This causes the diverter material to dissolve, leaving all fractures open for circulation and flow during the operation of the EGS system. AltaRock is a pioneer in the use of diverters in geothermal applications. AltaRock has developed, lab-tested, and patented a portfolio of materials designed for the moderate to high temperatures encountered in geothermal wells.

The distributed temperature, microseismic and pressure data will be analyzed to determine if the diversion has been successful. The creation of three separate, stacked fracture networks is the primary objective of the treatment. The project budget provides for up to 21 days of stimulation by pressurized water injection to achieve this target. If the diverter does not provide sufficient zonal isolation to allow creation of multiple fracture networks, a rig will be mobilized and a mechanical isolation device, such as a scab liner, will be installed in the well to ensure that at least two separate fracture networks are created.

## **7.2 HISTORICAL DATA – REVIEW OF WORLDWIDE EGS STIMULATION**

The Newberry EGS Demonstration will draw on experience gained in other EGS developments conducted around the world since the 1970s. This section provides a brief review of other EGS stimulations around the world, and their key findings relevant to Newberry. The following paragraphs include excerpts from the ISMP (Appendix A-1), which discusses these findings in more detail, particularly with respect to seismic mitigation controls.

Table 7-1 summarizes pertinent data from six previous EGS developments for which data was publically available. Figure 7-1 plots the rates and pressures that were utilized during stimulation treatments at two EGS projects (Basel and Soultz) that employed stimulation approaches similar to what will be used at Newberry. As the graph illustrates, Basel, Soultz and Newberry all begin at relatively similar pre-stimulation injectivity values. The stimulation rates and pressures of the three Soultz wells is most similar to what is planned at NWG 55-29. It is neither possible, nor desirable, to achieve the high pressures and rates that were used in the stimulation of DHM-1 at Basel.

Table 7-1. Summary parameters of other EGS development efforts. NA= information not available.

Well	Stimulation Duration (day)	Maximum Injection Rate (gpm)	Injected Volume (gal)	Maximum Wellhead Pressure (psi)	Pre-Stimulation Injectivity (gpm/psi)	Post-Stimulation Injectivity (gpm/psi)
EE-2 Fenton Hill	3	1585	5,706,000	6960	NA	NA
Basel DHM-1	6	871	3,056,500	4293	0.01	0.31
Habanero 1 Cooper Basin	9	760	5,283,500	10875	0.05	0.2
Groß Schönebeck	4.4	2376	3,479,000	8499	NA	NA
Landau GtLa2	1	3000	2,900,000	1885	NA	NA
GPK2 Saultz	5.9	792	5,991,500	2103	0.02	0.49
GPK3 Saultz	10.6	792	9,853,600	2321	0.22-0.38	0.58
GPK4 + GPK3 Saultz	3.5 + 3.9	712	2,456,800 + 3,249,300	2466 + 2030	0.01	0.36

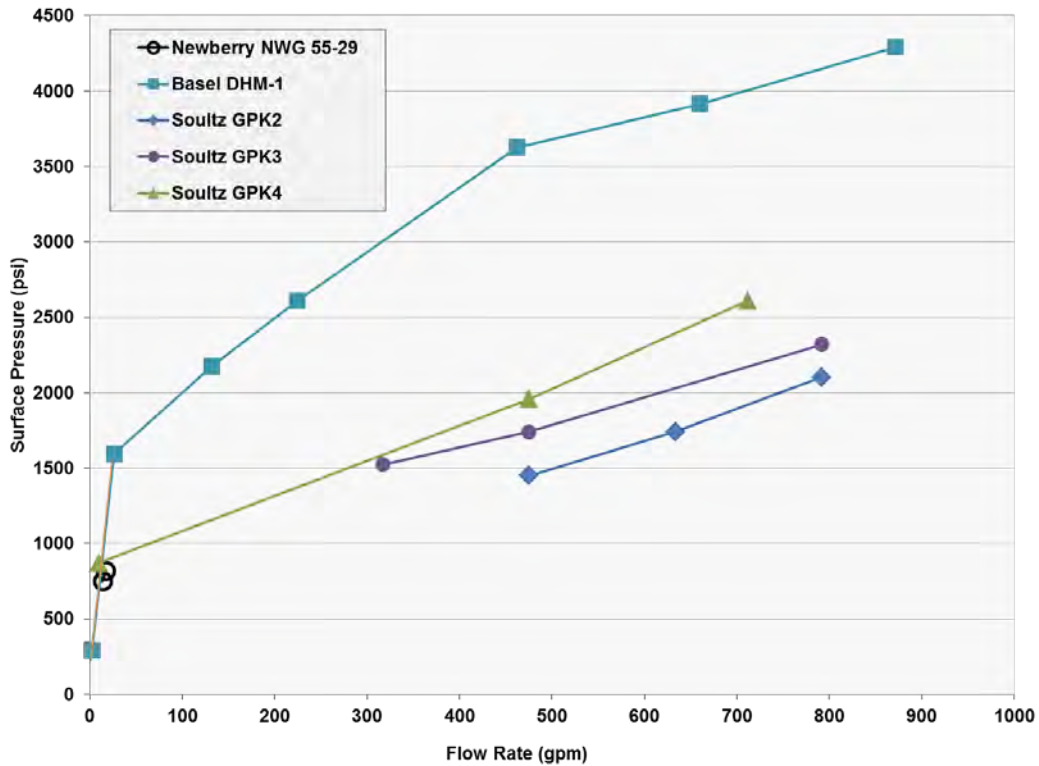


Figure 7-1. Injectivity comparison for several EGS projects worldwide, including the pre-stimulation injection test data from NWG 55-29.

### **7.2.1 FENTON HILL, NEW MEXICO**

The first EGS demonstration, then referred to as ‘hot dry rock’ or HDR, was begun at Fenton Hill, New Mexico in 1974. This was the first attempt to use hydraulic stimulation to create an artificial geothermal reservoir. The geologic setting of Fenton Hill is similar to that of Newberry. Fenton Hill is located on the western flank of Valles Caldera, just outside the ring fractures which define this large (20 km, 12 mi diameter) caldera. During a December 1983 experiment, 850 microseismic events ranging in magnitude from  $M_L -3$  to  $M_L 0$  were reliably located by borehole seismometers (House et al., 1985). Given the similar tectonic setting, a low seismic response is also likely at Newberry. Thus, the Newberry MSA network is being designed to detect events lower than  $M 0.0$ . Traditional oilfield stimulation was implemented at Fenton Hill, which created a large, induced tensile fracture in the reservoir. We now know that tensile fractures are undesirable in EGS reservoirs for two main reasons: (1) tensile fractures will likely close after wellhead pressure is released because the fractures have been ‘jacked’ open and have not slipped past each other as they do in shear failure; and (2) when wellhead pressure is applied, tensile cracks create a short-circuit between the injection and production wells, potentially resulting in rapid thermal breakthrough.

### **7.2.2 BASEL, SWITZERLAND**

In 2006, a deep well was drilled for the purpose of creating an EGS reservoir as part of the Deep Heat Mining (DHM) project in Basel, Switzerland. Basel DHM hydraulically stimulated with approximately  $11000 \text{ m}^3$  (3 million gallons) of water at a maximum rate of 55 L/s (871 gpm) and a maximum wellhead pressure of 29.6 MPa (4293 psi) over a six day period in December 2006 (Table 7-1). An  $M_L 3.4$  event on the sixth day of stimulation caused the project to be permanently shut down (Baisch et al., 2009). Careful study of the injection rate, wellhead pressure, event magnitudes, and event rate reveals important information about the behavior of the DHM hydraulic system and possible warning signs for future EGS operations. Stimulation started with a flow rate of 1.7 L/s (27 gpm), enough to increase the wellhead pressure to 11 MPa (1600 psi) and initiate seismicity. Over the next six days the flow rate was increased five times. After the first two flow rate increases, the pressure eventually dropped, indicating a beneficial improvement in injectivity. At the median (third) flow rate (28 L/s [450 gpm]), the pressure and seismicity rates continued to climb for a day, indicating a build-up of pressure in the EGS reservoir. Despite this now-apparent warning sign, the rate was again increased to 41 L/s (650 gpm) and within 8 hours the first  $M_L > 2.0$  seismic event occurred. After the increase to the final and maximum flow rate of 55 L/s (870 gpm) and wellhead pressure of 29.7 MPa (4300 psi), four  $M_L > 2.0$  events occurred, so injection was stopped and the well shut. However, induced seismicity did not decline immediately due to the high reservoir pressure that had accumulated. Before the pressure could be relieved at the wellhead the  $M_L 3.4$  event occurred. Once implemented, bleed-off did significantly reduce the rate of seismicity. At Newberry, we will be on alert for rising pressure at constant flow rates and  $M > 2.0$  seismic events. If either condition arises at Newberry, flow rates will not be increased without careful review of surface and downhole pressure, and microseismic event magnitudes and rates. The stimulation methods used at Basel are not analogous for design purposes at Newberry. The stimulation of NWG 55-29 will be conducted at much lower pressures, well within the shear failure envelope. One goal of the stimulation treatment is to avoid creation of tensile fractures that could lead to short-circuiting during the circulation phase. Therefore, the Basel stimulation was used primarily for mitigation planning for NWG 55-29.

### **7.2.3 COOPER BASIN, AUSTRALIA**

The EGS project at Cooper Basin (Australia) has successfully stimulated two deep, hot wells, Habanero 1 and Jolokia 2. The stress regime in Cooper Basin, being compressional and requiring very high surface



injection pressures for stimulation, is not analogous to the Newberry site and is, therefore, not useful in determining expected wellhead rates and pressures during the stimulation of NWG 55-29. Nevertheless, the project is part of the worldwide EGS stimulation knowledge base. Habanero 1 was stimulated over a 9-day period with over 20000 m<sup>3</sup> (5.2 million gallons) of water at a maximum injection rate of 48 L/s (760 gpm) and maximum wellhead pressure of 75 MPa (10875 psi; see Table 7-1). The results from Jolokia 2 have not yet been made public.

#### **7.2.4 GROß-SCHÖNEBECK, GERMANY**

An EGS doublet was created in 2007 at Groß Schönebeck field on the Northern German Plain. Unlike the planned stimulation at Newberry, a 'slickwater' fracture treatment was designed and implemented in well GtGrSk4/05 at a high rate and pressure (Zimmerman et al., 2008). The fluid consisted of water, friction-reducing chemicals, acetic acid, and low concentrations of 20/40 mesh sand to serve as a proppant. A maximum injection rate of 150 L/s (2376 gpm) at a maximum surface pressure of 58.6 MPa (8500 psi) was applied to the well to induce rock failure and create enough velocity to transport the sand in the low-viscosity fluid (Table 7-1). At these rates and pressures, the stimulation pressure was most likely above the shear-failure envelope. The fracture treatment lasted 4.4 days and pumped nearly 13000 m<sup>3</sup> (3.5 million gallons) of fluid. At Newberry, only fresh water with fluid tracers and periodic use of diverter products will be used to stimulate NWG 55-29. No proppants, gelling agents, acids or friction-reducing chemicals are planned, and the goal is to remain well below the pressure required to induce tensile rock failure. Thus, the fracture treatment at Groß Schönebeck did not provide guidance regarding the effects of a freshwater stimulation at sub-tensile pressures.

#### **7.2.5 LANDAU, GERMANY**

The Landau, Germany geothermal project consists of a well doublet, GtLa1 and GtLa2, which are now generating power at an operating facility (Schindler et al., 2010). The wells at Landau differ from NWG 55-29 and do not provide a good analogy for stimulation planning. The wells targeted a known, existing fault zone, which was so productive in GtLa1 that it did not require stimulation. GtLa2 was not as naturally productive as GtLa1, so it was stimulated at much higher injection rates than is expected to be required at Newberry. The treatment consisted of approximately 5000 m<sup>3</sup> (1.3 million gallons) of water at 187 L/s (2960 gpm) and 13 MPa (1890 psi) surface pressure. High flow rates were necessary at Landau in order to build up enough pressure in this already permeable well for stimulation and injectivity improvement to occur. This historical information is not particularly useful for stimulation planning at Newberry because of the significant permeability differences between the two sites. As indicated previously the NWG 55-29 wellbore does not intersect a known fault, nor does it contain significant permeability.

#### **7.2.6 SOULTZ-SOUS-FORÊTS, FRANCE**

Soultz-sous-Forêts, France (Soultz) provides the best example for stimulation planning at Newberry. Over two decades of research and development in EGS has been carried out at Soultz, resulting in a pilot program that currently includes a 200°C (392°F) EGS reservoir, an injection well, two production wells, two downhole pumps and a 1.5 MW<sub>e</sub> binary power plant (Genter et al., 2009). Dorbath et al., (2009) and Cladouhos et al. (2010) compared the stimulation of three different wells at Soultz (GPK2, GPK3, and GPK4) and found that the induced seismicity characteristics (maximum magnitude and event rate) and stimulation efficacy (improvement of injectivity and reservoir volume) are a function of the characteristics of the preexisting natural fractures and faults in the well bore. To stimulate the GPK2 well, about 23000 m<sup>3</sup> (6 million gallons) of water was injected over a six day period. The largest induced seismic event recorded was M 2.5. A maximum injection rate of 50 L/s (790 gpm), coupled with a

maximum surface pressure of 14.5 MPa (2100 psi), resulted in a 25-fold injectivity increase from a natural injectivity of 0.18 L/s per MPa (0.02 gpm/psi) to a post-treatment injectivity of 4.48 L/s per MPa (0.49 gpm/psi; see Table 7-1). The seismicity induced by stimulation of GPK2 was characterized by a few events in the range of M 2.0-2.5 and numerous smaller events, resulting in a dense network of medium-sized fractures (Dorbath et al., 2009). In contrast, the GPK3 stimulation used about 38000 m<sup>3</sup> (10 million gallons) over a 10.6 day time period, and the largest induced event recorded was M 2.9. A maximum injection rate of 50 L/s (790 gpm) and a maximum wellhead pressure of 16.0 MPa (2320 psi) resulted in a 1.5- to 3-fold increase in injectivity, from 2.01-3.48 L/s per MPa to 5.31 L/s per MPa (0.22-0.38 gpm/psi to 0.58 gpm/psi). Although wellhead injection rates and pressures were similar, the stimulation of the GPK3 borehole resulted in several seismic events in the range of M-2.9, less permeability improvement, and 70% of the fluid flow occurring in the one existing major fracture or fault zone (which corresponded to a single widely opened fracture found in image logs at a measured depth of 4705 m (15440 ft; Dorbath et al., 2009). The lesson learned in comparing GPK2 and GPK3 is that to maximize the effectiveness of hydroshearing, stimulation plans need to account for the features encountered by the well. At the Newberry EGS Demonstration, AltaRock diverter technology (Section 7.6) will allow a change in stimulation depth if a single zone is producing larger seismic events (e.g., the 4705 m fracture in GPK3), if the microseismic signature is indicating reservoir growth along a linear feature and not through a dispersed network of fractures, or if fracture growth has reached the target radius and depth.

### **7.2.7 IMPLICATIONS FOR NEWBERRY NWG 55-29**

To develop the stimulation plan for NWG 55-29, the EGS project in Soultz, France was used as an analogy, specifically GPK2. Soultz was the first EGS project to successfully demonstrate hydraulic connection between an injection and production well couplet. The stimulation treatments conducted at Soultz on wells GPK2, GPK3 and GPK4 are summarized in Table 7-1. A fracture network of just over one kilometer (3281 ft) in length, measured along the long axis (estimated from the dimensions of the microseismic cloud), was created during the GPK2 stimulation treatment (Figure 7-2). Hydrothermal experience and reservoir modeling have taught the industry that a well separation of at least 500 m (1640 ft) is desirable to avoid excessive thermal breakthrough and ensure a project life of at least 20 years. Well spacing greater than 1000 m (3280 ft), though leading to a longer reservoir thermal life, is generally not desirable due to the relatively low rate of heat extraction. Additionally, decreased flow rates due to friction in a larger circulating system will require more pumping horsepower to overcome, which will add more cost to the project and could lead to continued reservoir growth during circulation. During the stimulation NWG 55-29, the microseismic cloud will need to extend to approximately 550 m (1804 ft) to ensure that a network of fractures, and not just a few fractures, has been extended to 500 m (1640 ft). It is worth noting that each of the Soultz stimulations utilized millions of gallons of water to create a large fracture area. The average injection pressures were above the critical shear failure pressure, but below the tensile failure envelope. By pumping above the critical pressure, the Soultz team ensured that more, less ideally-oriented fractures slipped. This practice allowed for the creation of a more diffuse fracture network (Figure 7-2). Hence, another goal of the Newberry stimulation will be to pump close to the tensile failure pressure than without crossing over into a tensile failure regime. Additionally, to create a reservoir of the desired shape and size, other EGS projects have illustrated that an injection volume on the order of 19000 to 34000 m<sup>3</sup> (five to nine million gallons) per stimulation stage is required. Thus, we expect to pump between 57000 to 102000 m<sup>3</sup> (15 and 27 million gallons) of water to create a multi-zoned reservoir of sufficient size, surface area and transmissivity at Newberry.

For project planning purposes, we estimate that the hydroshearing treatment of NWG 55-29 will require up to 21 days of stimulation treatment to create three separate fracture networks at a injection rate of

50 L/s (800 gpm). The Soultz project never exceeded 50 L/s (800 gpm) during the GPK2 stimulation (Figure 7-3), so our assumption of a maximum rate of 800 gpm ensures that enough hydraulic horsepower and water resources are dedicated to the stimulation treatment to accomplish the objective of creating three separate fracture networks with a long axis radius of 500 m (1640 ft). Additionally, a goal of the Demonstration is to produce 75 kg/s (595 kph, or 1200 gpm) from each production well. Hence, NWG 55-29, being the injection well, must be capable of accepting a minimum of 150 kg/s (1191 kph, or 2400 gpm) at reasonable injection pressures. During the stimulation of NWG 55-29, we will ensure that each discrete fracture network, of which three are anticipated, is capable of accepting 75 kg/s (800 gpm) to ensure the goal is achieved. It would be impractical to assume that an injection rate of 800 gpm through each fracture network could be achieved at a reasonable surface pressure during the circulation test if the fractures were created at a much lower rate and had never been exposed to 75 kg/s during stimulation. Therefore, at the end of each of the three fracture stages, we will inject at 75 kg/s, as long as we can do so safely, for three to six hours to ensure that system permeability allows for this amount of flow at a reasonable pressure drop.

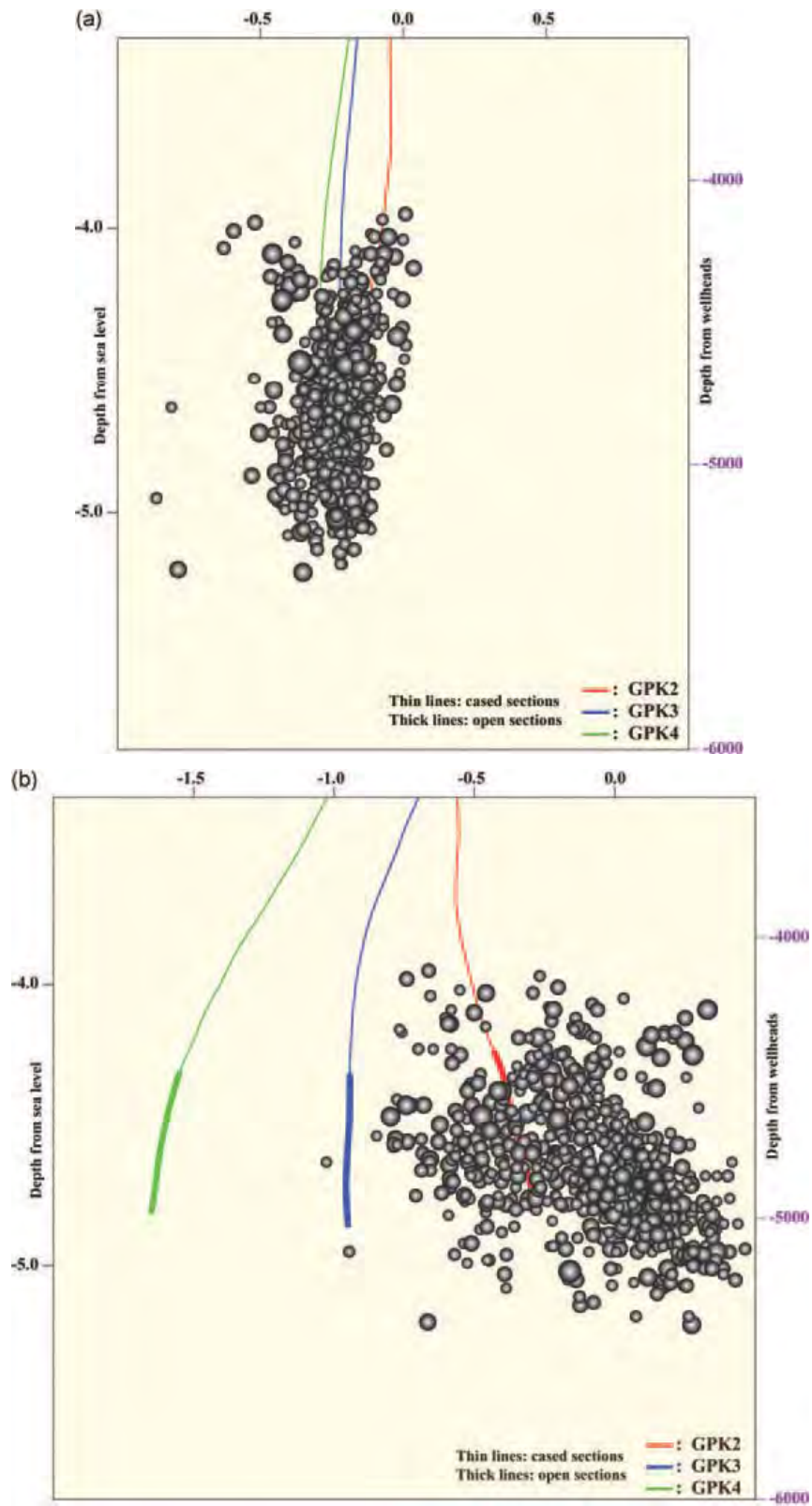


Figure 7-2. The 2000 stimulation of GPK2: (a) vertical cross-section through the cloud of induced seismic events ( $M > 1$ ) along a line N20°W; and (b) vertical cross-section through the cloud of induced seismic events ( $M > 1$ ) along a line N70°E. Units are in km and m. Long axis of seismic cloud is approximately 1 km (3280 ft).



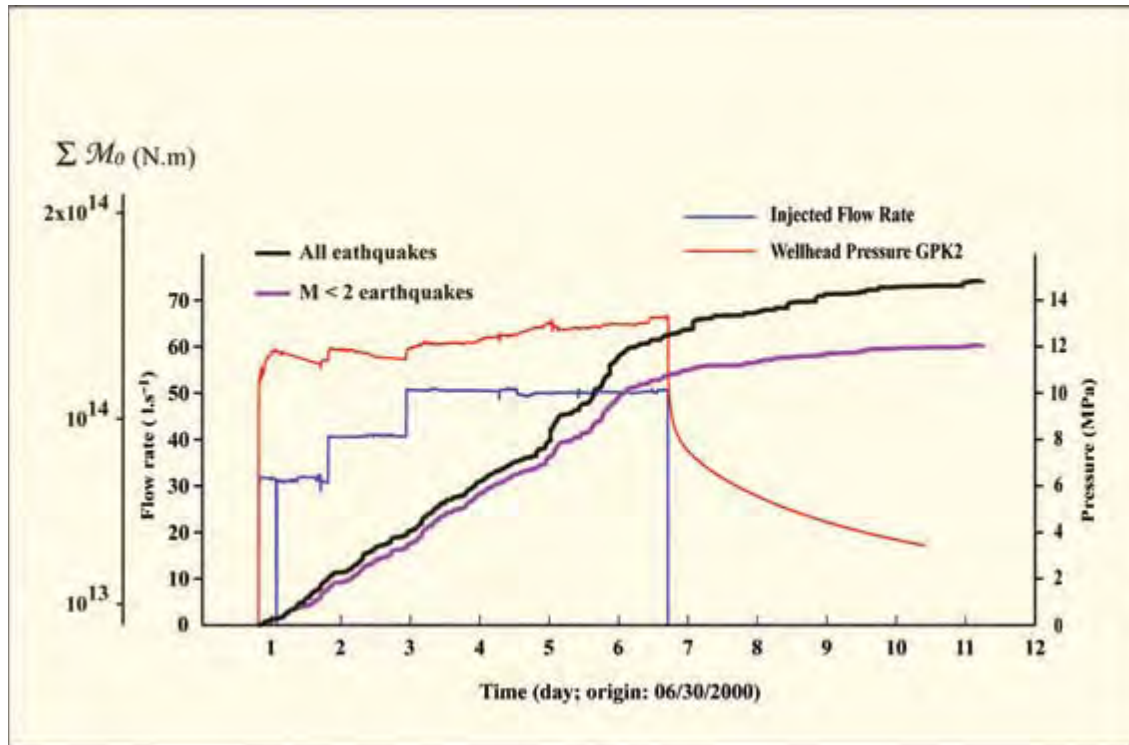


Figure 7-3. GPK2 hydraulic stimulation parameters: pressure (red); and flow rate (blue). Cumulative seismic moment: all earthquakes (black); and M < 2 earthquakes (violet) (Dorbath et al., 2009).

## 7.3 PRE-STIMULATION CONDITIONS AT NWG 55-29

### 7.3.1 *IN SITU* STRESS MAGNITUDES AND PATTERNS

A high-resolution borehole televiewer (BHTV) log was conducted in NWG 55-29 well on 25 October 2010. Prior to logging, an ‘inject-to-cool’ program was successfully completed to extend the depth of the logged interval. The resulting log spans the upper 739 m (2425 ft) portion of the 1106 m (3629 ft) open-hole interval from the casing shoe at a measured depth (MD) of 1961 m (6435 ft) below ground level (GL) to 2701 m (8860 ft) MD below GL and an injecting temperature range from 199.7°-277.0°C (391.5°-530.6°F). The image log and the subsequent detailed interpretation is thoroughly discussed in Sections 3.2.8 and 5.4.

### 7.3.2 *ROCK PERMEABILITY*

The *in situ* permeability of the open hole section of NWG 55-29 is very low, on the order of microdarcies. The exact permeability has not been quantified because existing pressure tools cannot withstand bottom-hole temperatures in NWG 55-29 long enough to collect build-up data so that a Horner analysis can be conducted. The drilling history, mud log, open-hole logs, temperature surveys, production flow and injection testing all point to a lack of permeability across the open-hole, which extends from 6462 ft to 10060 ft (1970 m to 3066 m) MD.

A review of the mud logs does not give evidence of any distinct drilling breaks encountered when NWG 55-29 was drilled. Drilling breaks in geothermal wells are often associated with zones of high permeability. The mud log was analyzed from a stimulation target perspective, assuming that altered intervals or dike zones would contain the highest concentration of natural fractures (Table 7-2).

Table 7-2. Analysis of mud log for possible stimulation targets.

Depth	Peak ROP (ft/hr)	Altered/Transition Zone	Dikes/Intrusives	Loss/Gain Zones
6870	70			Lost 22 bbls 6868-6880 ft
6900	30	Altered crystal ash tuff		
7030	20	Altered crystal ash tuff		
7200	60	Chloritized dacite tuff		
7265	60	Chloritized crystal lithic tuff		
7300	20	Chloritized crystal lithic tuff		Lost 25 bbls 7295-7297 ft
7350	35	Chloritized Rhyodacite tuff		
7400	25	Chloritized crystal tuff		Lost 30 bbls 7400-7425 ft
7420	30	Altered zone at 7420		Gain 27 bbls 7428-7431 ft
7450	25	Altered zone		Lost 26 bbls 7432-7454 ft
7660	55			
7760	55			
8005	75			
8280	60			
8375	45		Felsic dike	Lose 15 bbls 8411-8415 ft
8470	20		Felsic dikelets	
8635	65	Chloritized microxln granodiorite		
8750	60	Microcrystalline granodiorite		
8940	20		Chloritized intrusive	
9020	35		Felsic intrusive	
9090	25	Microcrystalline granodiorite		
9120	60			
9175	80			
9230	50	Microcrystalline granodiorite		
9310	25	Microcrystalline granodiorite		
9480	20	Microcrystalline granodiorite		
9630	10			Lost 91 bbls 9628-9676 ft
9670	5		Microcrystalline felsic dike	
9750	10			Lost 98 bbls, breaking circulation
9800				Losing 12 bbl/hr 9736-9760 ft
9845	5		Altered intrusive/basalt	
9900	5			Losing 12 bbl/hr 9860-10060 ft due to seepage
9990	5		Aplite/felsic dike	
10030	5		microcrystalline granodiorite/dacite	

Prior to AltaRock's involvement, Davenport Power attempted to flow test and inject into NWG 55-29. The well produced the equivalent of roughly one wellbore volume of fluid, and then died. Multiple attempts to induce flow by injecting compressed air through coiled tubing were unsuccessful in producing sustained flow due to the lack of permeability in the well. The injection testing results also pointed toward the lack of a hydrothermal resource connected to the well. Davenport pressurized the wellhead to 970 psig with drilling rig pumps but was unable to record any injection rate with the rig instrumentation.

A zone at approximately 9500 ft (2896 m) exhibited cooling during drilling and injection testing, as indicated by temperature surveys (Figure 5-23), but was not productive. This zone is associated with a 91 bbl/hr fluid loss, and a felsic dike as indicated on the mud log, when the well was drilled. However, later surveys reveal the temperature in this zone to be essentially linear, indicating a conductive thermal regime and a lack of permeability. This contrasts with a typical hydrothermal reservoir, which should exhibit an isothermal temperature profile due to a convective flow regime.

AltaRock sought to establish baseline injectivity utilizing low rate, high pressure pumping equipment and more sensitive flow measurement instrumentation prior to stimulation treatment. The well also had to be cooled in order to conduct the BHTV survey. On 22 September 2010, AltaRock Energy conducted a static memory tool PT survey in NWG 55-29 to record the temperature profile, identify fluid level and ensure that the well was open to total depth (Figure 5-23). Subsequently, untreated groundwater produced from the onsite water well was injected. Water was injected at approximately 10 gpm at a surface pressure of 750 psig for three days, followed by an injecting pressure-temperature survey to determine if injection was cooling the well bore.

From 18-20 October, a higher injection rate of 22 gpm at a surface pressure of 1150 psig was achieved. Pre-stimulation injectivity was determined to be between 0.01 and 0.05 gpm/psi. These results are consistent with measurements in nearby wells (Spielman and Finger, 1998). Productive hydrothermal reservoirs consist of a network of highly permeable, naturally-occurring fractures that allow for injectivities three to four magnitudes higher than the pre-stimulation injectivity of NWG 55-29. On 20 October, a third PT survey was conducted just prior to BHTV logging to ensure that the well was cool enough for tool deployment. The injection pressure was reduced during the PT survey to accommodate the wireline lubricator limitations. The fluid was found to be exiting from 8640-8800 ft (2633-2682 m) and from 9280-9560 ft (2829-2914 m; Figure 5-23). Also shown in Figure 5-23 are dikes and an altered zone containing "abundant epidote", as well as several transitions between basalt bodies and granodiorite identified in mud logs. These contact surfaces all represent prime stimulation targets because these are areas of likely high natural fracture density.

It is intriguing that the zone from 8640-8800 ft (2633-2682 m) does not appear to be open during the September survey when water was injected at 750 psi and 10 gpm, but that higher pressures resulted in changes in the temperature profile. We can assume that 750 psig was not enough pressure to shear and dilate existing fractures in this interval of open-hole because the zone from 8640-8800 ft (2633-2682 m) did not show any cooling during the September injection. On the other hand, cooling in the same interval at 1153 psig revealed in the October survey indicates that the higher pressure may have initiated shear failure.

The borehole televiewer log identified 351 fractures in the open-hole section of NWG 55-29 from 6462-8882 ft (1970-2707 m), most of which have an apparent aperture greater than zero at the wellbore interface. These fractures represent stimulation targets because they are weak points in the rock matrix, but, as indicated by all previous logging and testing, they lack significant permeability and are currently not productive. The felsic dike boundaries from 8375-8468 ft (2553-2581 m) were found to contain the highest fracture density in the BHTV survey. The image log data is being analyzed in conjunction with the

mud log, the open-hole logs and production log data to identify zones of weakness and high fracture concentration.

## 7.4 ALTASTIM MODELING

In this section, the fracture and stress models developed for NWG 55-29 in Section 3 and Section 5, respectively, provide the necessary inputs to AltaStim, a stochastic fracture and stimulation software model developed by AltaRock to plan and predict EGS reservoir creation and productivity. AltaStim is used to model and visualize EGS stimulation scenarios and provide guidance for final planning. The process of creating an AltaStim model requires synthesis of geologic observations at the well, the modeled stress conditions, and the stimulation plan. Any geomechanical model of an EGS stimulation will require many assumptions. Thus, the model developed here should not be considered a definitive prediction, but a plausible outcome given reasonable assumptions. AltaStim is a tool for understanding the effect of known constraints, assumptions, and conceptual models on plausible outcomes.

### 7.4.1 THEORETICAL OVERVIEW

AltaStim is a software implementation of the 2D equations developed in Willis-Richards et al. (1995, 1996), and then extended into 3D by Jing et al. (2000). Previous software implementations based on the approach have been used to model geothermal reservoirs in Europe, Australia and the U.S (Kohl and Megel, 2005; Narayan et al., 1998). At the heart of the model is: (1) a rule for determining when hydroshearing occurs; (2) an equation to adjust the aperture of a hydrosheared fracture; and (3) a summation to calculate the directional fracture permeability that controls the overall growth of the stimulation volume.

Hydroshearing on a pre-existing fault plane occurs when the fluid pressure,  $P_f$ , reduces the effective normal stress,  $\sigma_{eff}$ , such that the shear stress on the plane,  $\tau$ , is exceeded,

**Equation 7-1**      $\sigma_{eff} = \sigma_n - P_f$

**Equation 7-2**      $\tau < \sigma_{eff} \mu$

where  $\sigma_n$  is the stress normal to the fault plane and  $\mu$  is the coefficient of static friction on the fault plane.

The aperture of a hydrosheared fracture ( $a$ ) is determined from Equation 14 of Willis-Richards et al. (1996),

**Equation 7-3**     \_\_\_\_\_,

where  $U$  is shear displacement,  $a_0$  is initial aperture,  $\phi_{dil}$  is shear dilation angle, and  $\sigma_{nref}$  is the closure stress.

The increase in directional permeability ( $\Delta K_i$ ) due to the  $i^{th}$  hydrosheared fracture is proportional to the aperture ( $a_i$ ) and the angle ( $\theta$ ) between the fracture and the direction in which permeability is being calculated.

**Equation 7-4**      $\Delta K_i \sim a_i^3 \cos 2\theta$

To calculate the relative bulk fracture permeability of a part of the model, Equation 7-4 is summed over all fractures in that part of the model.

The reader is referred to the technical papers for more details of these governing equations for the AltaStim model. Modeling runs involve the following steps:



1. The user inputs a fracture model, rock mechanics parameters, native state stress conditions for three principle magnitudes and directions, and the initial hydrostatic fluid pressure.
2. A network of circular fractures is generated by starting with a random center, determining fracture orientation, aperture and length parameters from either a statistical model or a list of actual fractures observed in the bore hole (bootstrapping). The shear stress and normal stress is calculated for each fracture. Fracture generation continues until the goal of fracture porosity or fractures intersected in a simulated well is achieved.
3. The user inputs the wellhead pressure to be applied to the modeled well. This overpressure within the open-hole section is assumed to be constant during the entire stimulation operation.
4. The stimulation proceeds in a series of discrete spatial steps, through which the boundary of the stimulation propagates out through the fracture network. These steps are analogous to increasing injection time, but there is no explicit consideration of the dynamics of fluid flow. It is assumed that the overpressure in the stimulation volume decreases linearly from the injection borehole to the current stimulation boundary.
5. The initial stimulation boundary is considered to be a cylinder with two spherical caps, where the axis of the cylinder is parallel to the borehole.
6. At each stimulation step the mechanical deformation is calculated for each fracture within the current stimulation volume. By comparing the coefficient of sliding friction, normal stress, shear stress, and fluid pressure (Equation 7-1 and Equation 7-2), each fracture is tested to determine whether it will hydroshear. If a fracture does hydroshear, then a seismic event is recorded and the fracture aperture increases (Equation 7-3).
7. An apparent permeability tensor is updated after every stimulation step (Equation 7-4). This describes the relative improvement in conductivity in all directions within the 3D reference frame. The permeability tensor is then used to define the stimulation boundary for the next stimulation step. This means that the extent of the stimulation boundary in any direction is directly proportional to the relative permeability. In this way the growth of the AltaStim stimulation mimics the way in which actual stimulations are controlled by the interaction of the fracture network and stresses.
8. The model continues testing fractures for hydroshearing and increasing the dimensions of the EGS reservoir until the long dimension of the reservoir reaches the reservoir length goal, plus 10%, or after a set number of cycles with no reservoir growth (a stalled stimulation).
9. AltaStim outputs include total fracture volume, a 3D image of the seismic events and vectors, and the status of each of the tested fractures (resolved shear stress, normal stress, fluid pressure, aperture, number of seismic events, etc).

## **7.4.2 NEWBERRY EGS MODEL**

### **7.4.2.1 MODEL DIMENSIONS AND ZONES**

For the Newberry EGS AltaStim model, the horizontal dimensions are 700 m (2300 ft) east-to-west and 1100 m (3610 ft) north-to-south. A rectangular shape was used because the EGS reservoir is expected to grow in a north-south orientation due to the fracture and stress orientations.

In Section 3.2.8, the open hole was divided into five zones based on BHTV fracture density, lithology, mud losses while drilling, and water losses during the injection tests. The characteristics of these zones are summarized below in Table 7-3. Each of these zones requires different inputs for fracture

orientations and density. The thickness of the modeled zones depends on the depth range being modeled.

Additional observations help constrain the AltaStim parameter settings for each zone:

**Zone A** – During the September and October 2010 injection tests there was no evidence of water exiting the borehole in Zone A; the temperature profile remained linear across the zone. This is not surprising because Zone A has a very low fracture density; just five fractures were identified in the 91 m (300 ft) interval, and the welded tuffs of this zone are not likely to have an significant matrix permeability.

**Zone B** – There was no evidence of water exiting the well borehole in Zone B during the injection tests. Like Zone A, this zone's primary rock type is volcanic tuff, however, this zone has a higher fracture density than Zone A and more open fractures. The fractures in this zone must be sealed and have coefficients of sliding friction high enough to prevent hydroshearing at about 8 MPa (1153 psi) WHP, the maximum pressure reached in the preliminary injection tests.

**Zone C** – Despite having the highest fracture density in the BHTV log, the injection test showed no evidence of water exiting the well bore in this zone. This zone is characterized by basalts (rather than the tuffs on the upper two zones) and two thin felsic dikes described in the mud log. Like Zone B, observations indicate that the fractures in this zone must be sealed and have relatively high coefficients of sliding friction.

**Zone D** – This zone may have begun to hydroshear between 5.2 and 7.9 MPa (750 and 1153 psi) WHP. Zones at 2637 m (8650 ft) and 2682 m (8800 ft), roughly correlated with the top and bottom of the first 61 m (200 ft) of a thick granodiorite intrusion, began to take fluid during higher pressure injection (Figure 3-49). The mud logs indicate chloritized granodiorite at 2630 m (8630 ft), chloritized intrusive at 2728 m (8950 ft), and abundant epidote, minor pyrite and other sulfides at 2868 m (9410 ft). Altered zones associated with the contacts between granodiorite intrusions and basalt may be more likely to hydroshear due to the low coefficient of sliding friction of chlorite and other alteration minerals (Lockner and Beeler, 2002).

Zone D provides special complications for modeling. The BHTV images of this zone are of a lower quality than shallower zones because the images were collected at a higher rate of descent in order to log as deeply as possible before the tool reached its maximum temperature and stopped working. The higher logging speeds greatly reduce vertical resolution. The top 61 m (200 ft) of Zone D is within microcrystalline granodiorite, a unique rock type in the BHTV image log. In the BHTV images, the granodiorite contains no borehole breakouts and low fracture density, indicating that the granodiorite is relatively strong.

In contrast to the observations of greater strength and sparse fracturing in the top 61 m (200 ft) of Zone D, this zone appears to be the depth in which most of the water loss occurred during the injection test. One explanation for the apparent contradiction is that the intrusive contacts between the granodiorite and the country rock (basalts) are commonly altered or chloritized, and may represent fluid exit points.

Thus, an AltaStim model of Zone D was built to account for the potential role that the intrusive contacts may play during EGS stimulation. Unlike the fractures modeled in the other zones, which have stochastic locations, the depths of these contacts are known from the mud logs (Table 7-4). The contacts are likely to extend far from the well bore; therefore, the intrusive contacts were input to the model as deterministic features. Two orientations were measured on the BHTV image at the top of the first granodiorite dike, the only large dike contact that was reached by the BHTV. These orientations are

alternated for all the dikes in the model (Table 7-4). The dikes are considered to be major features that will extend outside of the Zone D model volume; therefore, they are given a radius of 200 m (656 ft).

**Zone E** – The BHTV did not reach the depth of Zone E, so no fracture data is available for this zone. However, Zone E has many things in common with Zone C. Both zones are adjacent to large granodiorite intrusions. Both zones are predominantly basalt, with some felsic dikes described in mud logs. Zone E has the most significant mud losses in the well, while Zone C had one minor mud loss. Because Zone C is considered the best analogue for Zone E, the Zone C fracture model was used for Zone E.

**Table 7-3. Summary of AltaStim modeled zones based on parameters observed in NWG 55-29.**

Zone	Depth to Center (m)	Zone Thickness (m)	Fracture Count	Fracture Density Per Meter	Lithology	Mud Losses During Drilling
A	1978	86	5	0.06	Primary: Welded Lithic Tuff Secondary: Other Tuff	None
B	2201	360	173	0.4	Primary: Tuffs Secondary: Basalt, Dacite, and Andesite	< 50 bbl
C	2481	200	157	0.8	Primary: Basalt and Basaltic Andesite Secondary: Two Felsic Dikes,	< 20 bbl
D	2712	262	16	0.06	Primary: Microcrystalline Granodiorite (5 dikes, 174 m total) Secondary: Basalt, one 15 m felsic dike	None
E	2922	200	No data		Primary: Basalt Secondary: Three felsic Dikes	>100 bbl

**Table 7-4. Inputs for deterministic dikes.**

Measured Depth KB (ft)	Vertical Depth GL (ft)	Vertical Depth GL (m)	Strike	Dip	Radius (m)
8640	8466	2581	212	62	200
8830	8662	2641	206	76	200
9240	9064	2763	212	62	200
9400	9219	2811	206	76	200
9580	9391	2863	212	62	200

#### 7.4.2.2 ORIENTATIONS, APERTURES, DENSITY AND SIZE

One approach for generating model fractures is to determine statistical models for fracture orientation, apertures, and sizes based on the analysis of the data, and then use those statistics to generate fractures. A simpler approach, commonly called *bootstrapping*, is to draw attributes from a list of the actual fractures identified in the BHTV image. For the Newberry model, the 351 fractures identified in the BHTV images are divided into separate lists, by zone, and using those lists to populate the fracture orientations and apertures in the model for each zone. Fractures are added to a model zone until fracture intersections in a modeled well reaches the same count as the real well in the same zone.

The initial fracture apertures were assigned to account for the very low fracture permeability currently observed. After hydroshearing, the maximum fracture aperture in the models was about 5 mm (0.20 in), with an average aperture of about 1.5 mm (0.06 in). Fracture radius is a very difficult parameter to

determine from well data because all that is known for certain is that the fracture is bigger than the well bore. For the purpose of the AltaStim models, fractures were randomly assigned a uniform distribution of radii between 33 m (108 ft) and 120 m (394 ft). The lower limit keeps the total number of fractures in the model to a computationally acceptable number and the upper limit prevents any fractures from cutting fully across the model space.

#### 7.4.2.3 COEFFICIENTS OF SLIDING FRICTION

The fluid pressure at which hydroshearing initiates will depend on the coefficient of sliding friction,  $\mu$  (Equation 7-2), which is also expressed as the angle of sliding friction  $\theta_f$ , where  $\mu = \tan \theta_f$ . The constraints on friction are related to the rock types described in the mud logs. Zones A and B are dominated by silica-rich extrusives (tuff, rhyolite and dacite). Mechanical testing of a similar suite of rocks from Yucca Mountain indicates that these rocks are likely to have a relatively high coefficient of sliding friction ( $\mu=0.85$ ,  $\theta_f=40^\circ$ ; Morrow and Byerlee, 1984). Therefore a coefficient of sliding friction of 0.85 was used in these two zones.

Zone C and E are dominated by basalts, with more plagioclase and less quartz than the overlying extrusive rocks. There is evidence for localized contact metamorphism and alteration in these zones, which may have created weaker minerals, like chlorite, along fractures and contacts. Therefore, a moderate sliding friction of  $\mu=0.70$  ( $\theta_f=35^\circ$ ) is used in Zones C and E (Lockner and Beeler, 2002).

Zone D has the most evidence for localized contact metamorphism along the margins of the granodiorite dikes. Therefore, a relatively low sliding friction of  $\mu=0.64$  ( $\theta_f=32.5^\circ$ ) is set in Zone D (Lockner and Beeler, 2002).

The coefficients of sliding friction chosen above are consistent with the hypothesis that: (1) Zones A and B are far from failure and were unaffected by the pressure increase to 7.9 MPa (1153 psi) during injection testing; (2) Zones C and E are closer to failure, as indicated by drilling mud losses and fluid loss during injection; and (3) Zone D was in incipient failure at a WHP of 7.9 MPa (1153 psi) as indicated by the change in temperature logs between two injection tests conducted at 5.2 MPa (750 psi) and 7.9 MPa (1153 psi) WHP.

#### 7.4.2.4 STRESS

A detailed discussion of the state of stress around NWG 55-29 is presented in Section 5. Relevant conclusions pertaining to the stimulation model are presented below.

Stress orientation in boreholes can be determined from breakouts caused by compressional failure of the borehole walls. In NWG 55-29, the breakouts show a consistent azimuth indicating that the minimum horizontal stress,  $S_{hmin}$ , is oriented at  $092 \pm 17^\circ$  relative to true north. This azimuth of  $S_{hmin}$ , in combination with the attitude of the majority of natural fractures revealed in the image log, is consistent with a normal faulting stress regime. The consistency of breakout azimuth, without localized rotations, taken in combination with the extremely low rate of seismicity in the region, and the weak expression of natural fractures in the image log, suggests that there is little recent or active slip on fractures in the vicinity of the well.

Determining the stress magnitudes of the three principle stresses is more difficult. In a normal faulting regime, the maximum principle stress,  $S_v$ , is vertical, with a magnitude related to the weight of the lithostatic overburden. The minimum horizontal stress,  $S_{hmin}$ , at a given depth, is best determined from a mini-frac, a well test in which  $S_{hmin}$  is determined from the fluid pressure at which tensile fracturing is initiated. As discussed in more detail in Section 5.5.3, an accurate mini-frac requires a short (~15 m, 50 ft) section of relatively unfractured well bore to be isolated. Isolation allows for sufficient pressure build-

up to cause tensile fracturing, provides a narrow depth range over which to calculate  $S_{hmin}$ , and ensures that the measured pressure response is due to a tensile failure and not hydroshearing. Because NWG 55-29 has over >1000 m (3281 ft) of open hole and isolating a short section would require a drilling rig, it is not feasible to conduct a mini-frac to determine  $S_{hmin}$ . Instead,  $S_{hmin}$  must be constrained based on reasonable geomechanical assumptions. The magnitude of the maximum horizontal stress,  $S_{Hmax}$ , is also difficult to determine, but is constrained to lie between  $S_v$  and  $S_{hmin}$ . The wide borehole breakout widths over most depths in NWG 55-29 indicate that the horizontal stress difference ( $S_{Hmax} - S_{hmin}$ ) is relatively large, with the preferred stress state based on breakout width and rock strength analyses, corresponding to  $S_{Hmax}$  equal to or slightly less than  $S_v$ .

In Section 5, the stress profile for each of the principle stresses in NWG 55-29 is derived from the average rock density, borehole breakout widths, rock strength, assumed coefficient of frictional sliding, and tectonic environment (Figure 7-4). The stress gradients assumed for the AltaStim models (Table 7-5) were determined as explained below. The vertical stress,  $S_v$ , and fluid pressure,  $P_f$ , assumed for the AltaStim model match the gradients shown in Figure 7-4 (red and blue lines, respectively). For the maximum horizontal stress,  $S_{Hmax}$ , Figure 7-4 shows a profile, labeled “Modeled  $S_{Hmax}$  Gradient”, that does not have a zero intercept. For the AltaStim models, all stress gradients were assumed to be linear to the origin with a zero intercept at GL. Therefore, for use in the AltaStim model, the  $S_{Hmax}$  profile was simplified by assuming a linear gradient of 1.04 psi/ft (23.5 MPa/km). In practice, the intermediate stress does not have a large impact on the AltaStim models. In this case, a higher intermediate stress gradient will promote more fractures to slip with a strike-slip sense of movement, but not affect the pressures required to hydroshear.

In the AltaStim modeling, the minimum principle stress profile has the largest effect. Two different gradients were used, with each case representing a different assumption regarding the deformation that occurred during the injection test that produced 7.9 MPa (1153 psi) WHP. In the first case, wherein a gradient of 14.9 MPa/km (0.66 psi/ft) for  $S_{hmin}$  is used, the model predicts that a few ideally oriented fractures would hydroshear at 1153 psi WHP, which accounts for changes observed in temperature logs during the injection test. In Figure 7-4, this gradient corresponds to the dashed line labeled “ $S_{hmin}^{crit}$ ,  $\mu=0.55$ ”, which predicts that only the weakest ( $\mu=0.55$  being a relatively low coefficient of sliding friction) ideally-oriented fractures would reach critical stress (slip) at 1153 psi WHP. In the second case, an  $S_{hmin}$  gradient of 15.8 MPa/km (0.7 psi/ft) is used, and no hydroshearing is predicted by the model at 1153 psi WHP. In Figure 7-4, this gradient is shown by the orange line, which results in a lower differential stress and would not predict any critically stressed fractures for realistic sliding friction coefficients.

**Table 7-5. Stress inputs to AltaStim models.**

Component	Gradient <sup>1</sup> (MPa/km)	Gradient <sup>1</sup> (psi/ft)	Direction	Principle Stress
$S_v$ gradient	24.1	1.07	vertical	Maximum
$S_{Hmax}$ gradient	23.5	1.04	2 (N-S)	Intermediate
$S_{hmin}$ gradient	14.9 - 15.8	0.66 - 0.70	92 (E-W)	Minimum
$P_h$ gradient	8.8	0.39	-	-

<sup>1</sup> All stresses magnitudes are assumed to be linear to the origin, with a zero intercept at GL.



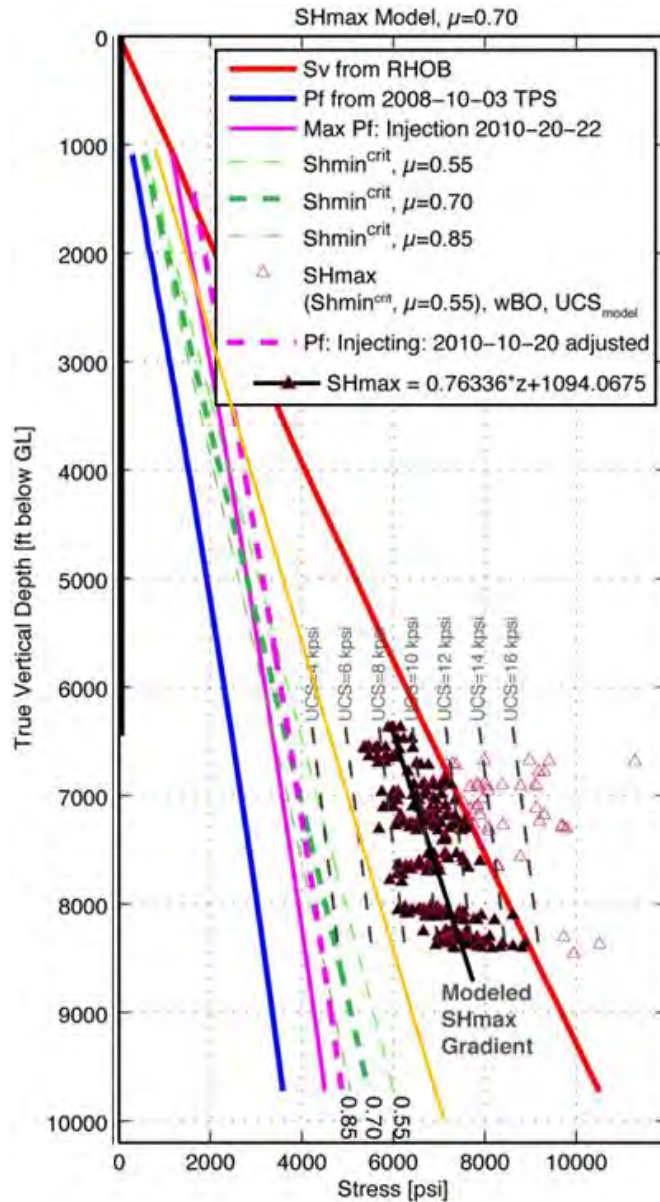


Figure 7-4. Stress profile for NWG 55-29 based on average rock density, borehole breakout widths, rock strength, assumed coefficient of frictional sliding, and tectonic environment. See Figure 5-18 for more information about the derivation of the profiles here.

#### 7.4.2.5 STOCHASTIC REALIZATIONS

AltaStim generates random locations for fractures. Each run of the AltaStim model with the same parameters, but different random seeds, called realizations, have different initial conditions that will control how details of the stimulation process proceeds. Even separate runs of the Zone D model, which contains five deterministic fractures, turn out different due to the background fractures also in the model.

In well-constrained, mature models it is preferable to run sufficient realizations (10-100) to develop statistics, standard deviations, and confidence intervals. The modeling effort reported here focuses on developing the initial model inputs. Therefore, the number of realizations was kept to a minimum. The

results below are based on three realizations for each model scenario. Even with the limited number of realizations, a wide range of results were produced.

#### 7.4.2.6 MODEL OUTPUTS

An AltaStim model run produces synthetic outputs for each fracture (shear slip, final aperture, and resolved stress components) and model-wide outputs (total fractures tested, hydrosheared, and distance of stimulation from well bore). The following parameters are tracked and reported below:

**Total fracture volume** – The fluid volume for an individual fracture is simply calculated by multiplying the sheared aperture by the fracture area ( $a\pi r^2$ ). The total fracture volume is calculated by summing across all the fractures that have been stimulated. It is assumed that in impermeable rocks, all injected fluid volume goes into filling the hydrosheared fractures. This *parallel plate assumption* for fractures is a simplification between two possible end-members. First, the assumption underestimates the volume injected because some fluid will leak off into secondary features, non-sheared fractures, and even the rock matrix. Second, the assumption overestimates the volume injected because real sheared fractures won't be circular or have the same aperture everywhere on the fracture surface. Theoretically, the maximum aperture will be at the center and decrease to zero at the fracture tips. Observationally, natural fracture surfaces tend to be rough with variable apertures on a short length scale. The natural roughness of a fracture surface means that fluid will likely flow along channels on the fracture surface, rather than between parallel plates.

**Reservoir shape** – The reservoir shape is tracked by plotting the 'seismicity' generated each time a fracture is hydrosheared. Each seismic event has a location that can be displayed in a 3D plotting program. Reservoir shape is also tracked by the set of vectors whose growth in each cycle is determined from its relative fracture permeability. When the longest vector reaches 550 m (1804 ft) in long dimension from the center of the model region, the model run is over.

**Mohr Circle** – Stress is not easy to visualize because, in the 3D case, it is a 3x3 tensor that can only be simplified to three principal stress magnitudes and directions. The Mohr Circle for 2D stress is one method used to visualize a state of stress. It is used here to show the relationship between the effective (fluid-weakened) stress state and the frictional failure envelope. Hydroshearing of a fracture of a given orientation is indicated when the shear stress and effective normal stress coordinates for that fracture plot to the left of the friction sliding failure envelope. As fluid pressure increases and lowers the effective normal stress on all fractures, more fractures orientations will cross the failure envelope and become favorably oriented for hydroshear.

**Wellhead Pressure** – Wellhead pressure was the primary input that was varied in the model runs. The modeled stimulations began at the injection test pressure of 7.9 MPa (1153 psi) WHP and continued to a pressure sufficient to reach the EGS reservoir length goal (13.4 to 16.2 MPa or 1950-2350 psi, depending on the stress case). To remain in the hydroshearing regime, wellhead pressure in the models was kept low enough to prevent exceeding the minimum principle stress in almost all model runs.

#### 7.4.3 RESULTS

The average results for three model realizations for each of the five model Zones A-E, at seven different wellhead pressures (7.9 to 16.2 MPa or 1153-2350 psi), and using two different stress models, are shown in Table 7-6. The overall results of the modeling are summarized graphically by plotting wellhead pressure versus the total volume of the fractured reservoir (Figure 7-5). The average aperture of the hydrosheared fractures in all the models is 1-1.5 mm (0.04-0.06 in). Therefore, the differences in fracture volumes are simply related to the total number of hydrosheared fractures in each model run.

Overall, the modeling indicates that Zones C, D, and E have sufficient fracturing to reach the volume goal of over 19000 m<sup>3</sup> (5 million gallons). In the 14.9 MPa/km (0.66 psi/ft)  $S_{hmin}$  stress case, significant hydroshearing begins at 9.3 MPa (1350 psi) WHP, while over 13.4 MPa (1950 psi) WHP is required to consistently reach the volume goal. In the 15.8 MPa/km (0.70 psi/ft)  $S_{hmin}$  stress case, hydroshearing begins at 9.3 MPa (1350 psi) WHP, and 15.2 MPa (2200 psi) WHP is required to meet the volume goal. Zone D is consistently the zone that accepts the most fluid at the lowest pressure. This is a result of the model being populated with deterministic dikes and an assumed lower coefficient of sliding friction. The deterministic features were added to Zone D in order to satisfy the observation that the interval may have been in incipient failure during the injection tests at 7.9 MPa (1153 psi).

The results for each zone and their implications are discussed in more detail below. In particular, graphical results for Zone C are more thoroughly investigated because this the high fracture density and variety of fracture orientations in this zone most clearly elucidate model results.

#### 7.4.3.1 ZONE A

The low fracture density in the Zone A models limited the average number of hydrosheared fractures to less than 10 out of an average of 1266 fractures in the model space, even at the highest wellhead pressure, in both stress cases. The average volume injected in this zone was less than about 130 m<sup>3</sup> (35000 gallons) in every case.

#### 7.4.3.2 ZONE B

The moderate fracture density in the Zone B model allowed for significantly more stimulated volume in Zone B than Zone A. However, the volume goal was not met for this zone at any pressure. One reason for this is that the Zone B models were often asymmetric. That is, the EGS reservoir would grow in only one direction from the well. The stimulation may stall for lack of connectivity due to the low fracture density in Zone B.

#### 7.4.3.3 ZONE C

A wide range of fracture orientations and high fracture density make Zone C the most instructive for understanding the impact of increased fluid pressure in an AltaStim model and the hydroshearing process. At 7.9 MPa (1153 psi) WHP, a few fractures are in contact with the failure envelope (Figure 7-6), but too few to propagate away from the well bore. At 9.3 MPa (1350 psi) WHP, less than 20% of the tested fractures were found to hydroshear, resulting in a narrow simulated fracture network that reached the length goal of 550 m (1804 ft), but not the volume goal of >19000 m<sup>3</sup> (>5 million gallons; Figure 7-7). At the maximum WHP of 13.4 MPa (1950 psi) for the 14.9 MPa/km (0.66 psi/ft)  $S_{hmin}$  stress case, about half of the fractures cross the frictional failure envelope (green triangles in Figure 7-6). On average, a 21000 m<sup>3</sup> (5.5 million gallons) reservoir is created at 13.4 MPa (1950 psi) that is wider than the reservoir created at a pressure closer to the critical hydroshearing pressure (Figure 7-8).

#### 7.4.3.4 ZONE D

As indicated on Table 7-6, Zone D consistently produces the best fracture network at all wellhead pressures. This result is partly due to the five dike margins included in the model that are ideally oriented for shear failure with respect to the minimum principle stress direction. The role of the dike margins is apparent in an image of the induced microseismicity (Figure 7-8), where these features produce steeply dipping seismic streaks. The Zone D model also includes background fractures that account for most of the horizontal growth of the EGS reservoir in this zone.

#### *7.4.3.5 ZONE E*

The results for Zone E closely track the results for Zone C because these two zones share a fracture model (same fracture density, orientations, and sliding frictions). This assumption was made because no fracture data exists for Zone E because the BHTV did not function at the high temperatures at this depth. Like Zone C, Zone E is adjacent to granodiorite dikes and dominated by basalt with minor felsic dikes.

#### *7.4.3.6 ALL ZONES*

To visualize the complete stimulation, the simulated microseismicity for all zones was combined into a single 3D visualization (Figure 7-9). For both stress cases (Table 7-7), the total volumes are about 83000 m<sup>3</sup> (22 million gallons), so this could be considered an end result after a 21-day stimulation at about 44 L/s (1 million gallons per day, 694 gpm). Fracturing multiple zones in a single open-hole interval, as has been modeled using AltaStim, will require the use of AltaRock's proprietary diverters.

Table 7-6. AltaStim model realizations. Average results by Zone and WHP. Values shown *italic gray* where length goal was not met (>550 m, 1804 ft), and **bold blue** where volume goal was met (>19000 m<sup>3</sup>[>5.0 million gal]).

Zone	WHP (psi)	Stress Model 1 ( $\Delta S_h = 0.66$ psi/ft)			Stress Model 1 ( $\Delta S_h = 0.7$ psi/ft)		
		Average Volume (Mgal)	Average # Fractures Tested	Average Number Hydrosheared	Average Volume (Mgal)	Average # Fractures Tested	Average Number Hydrosheared
A (avg 1266 fractures)	1153	<i>0.004</i>	19.7	1.3	<i>0</i>	10.3	0
	1350	<i>0.012</i>	34.3	4.3	<i>0.002</i>	10.3	0.3
	1550	<i>0.013</i>	23.3	5.0	-	-	-
	1750	<i>0.022</i>	23.3	7.7	<i>0.010</i>	25.3	4.0
	1950	<i>0.035</i>	22.7	10.3	-	-	-
	2150	-	-	-	<i>0.020</i>	14.0	5.3
	2350	-	-	-	<i>0.024</i>	15.0	6.7
B (avg 12866 fractures)	1153	<i>0.035</i>	143.0	2.7	<i>0</i>	129.0	0
	1350	0.349	331.0	42.0	<i>0.002</i>	129.0	1.0
	1550	0.758	407.0	83.3	0.243	302.3	34.0
	1750	1.981	594.3	175.3	0.645	357.3	76.3
	1950	2.722	618.0	225.7	2.047	631.0	183.0
	2150	-	-	-	2.367	571.7	202.3
	2350	-	-	-	3.145	585.0	239.0
C (avg 946 fractures)	1153	0.182	358.0	34.3	<i>0</i>	82.3	0
	1350	1.000	606.0	118.0	<i>0.022</i>	82.3	4.0
	1550	1.549	562.3	167.7	0.221	378.0	57.3
	1750	3.233	700.3	302.3	1.716	620.0	197.3
	1950	<b>5.584</b>	845.3	462.3	3.018	562.0	247.0
	2150	-	-	-	4.040	604.3	314.3
	2350	-	-	-	<b>5.992</b>	726.0	436.3
D (avg 5966 fractures)	1153	0.193	380.3	50.0	<i>0.000</i>	207.3	0.0
	1350	<b>3.501</b>	899.7	476.0	0.140	427.7	61.7
	1550	<b>6.169</b>	922.3	661.3	2.723	785.7	418.3
	1750	<b>6.691</b>	861.0	709.3	4.789	788.7	534.0
	1950	<b>8.092</b>	861.3	734.7	4.627	706.3	561.0
	2150	-	-	-	<b>7.982</b>	863.0	691.7
	2350	-	-	-	<b>5.768</b>	646.0	537.7
E (avg 14632 fractures)	1153	<i>0.035</i>	273.0	15.3	<i>0.000</i>	106.3	0.0
	1350	0.673	704.3	102.0	<i>0.000</i>	106.3	0.0
	1550	1.670	976.0	201.3	<i>0.009</i>	193.3	5.7
	1750	3.625	1542.0	446.3	0.299	409.7	48.3
	1950	<b>5.664</b>	1687.3	643.3	1.599	846.0	184.3
	2150	-	-	-	4.722	1497.7	466.0
	2350	-	-	-	<b>7.585</b>	1583.0	644.7



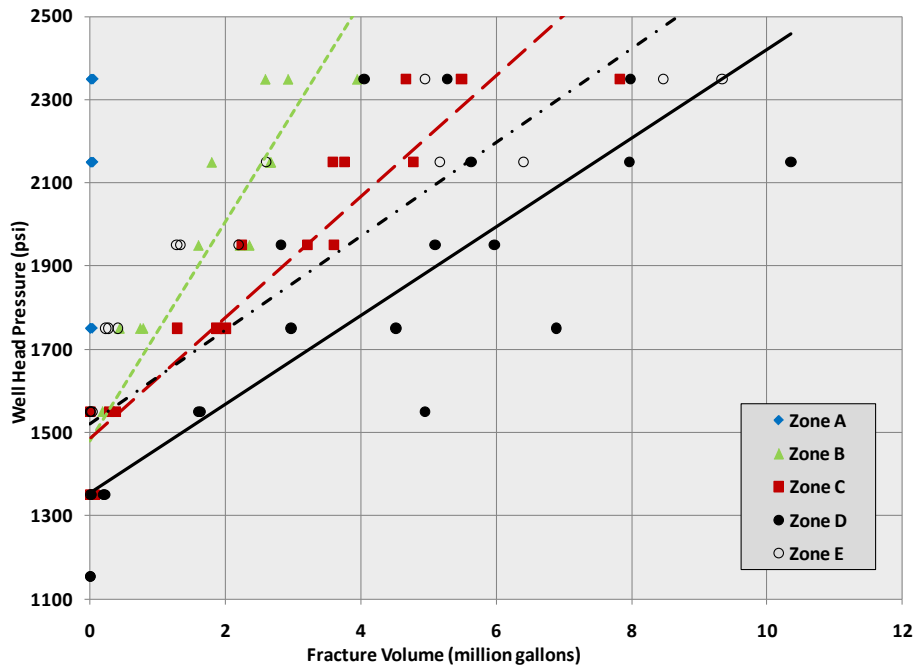
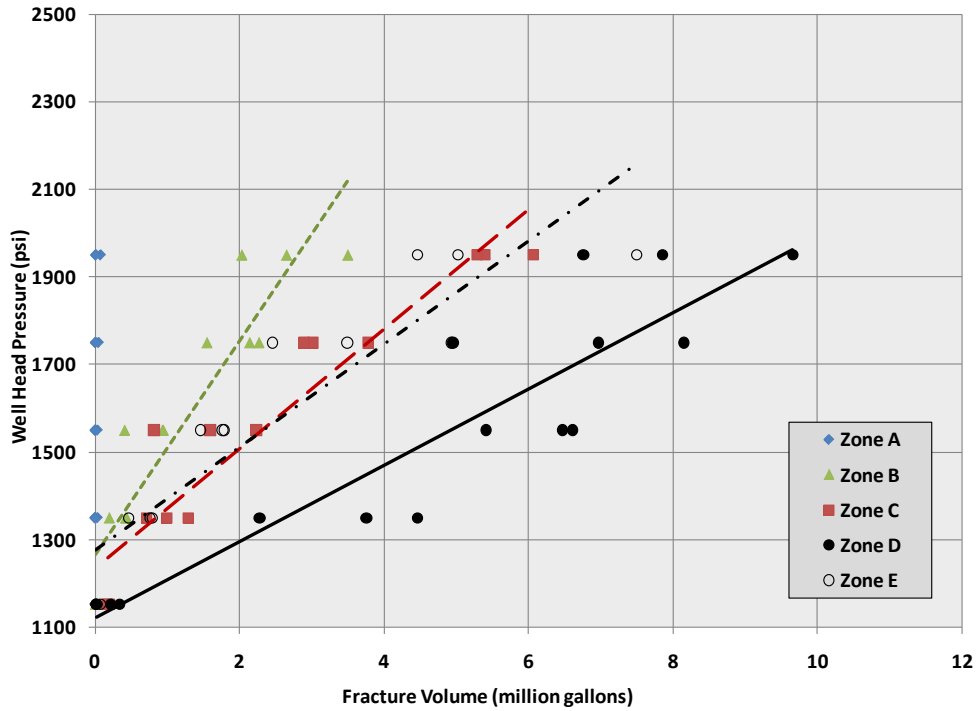


Figure 7-5. Total (injected) fracture volume for five different wellhead pressures in each of the different Zones A-E. Top graph is for 14.9 MPa/km (0.66 psi/ft)  $S_{hmin}$  stress case and bottom graph is for 15.8 MPa/km (0.70 psi/ft)  $S_{hmin}$  stress case. Three points at each pressure for each zone represent the different stochastic realizations. The slope of the linear fit is a measure of the efficacy of stimulation in each zone, with a lower slope indicating more effective stimulation. The zero volume intercept shows the pressure where, on average, hydroshearing initiates for that zone.

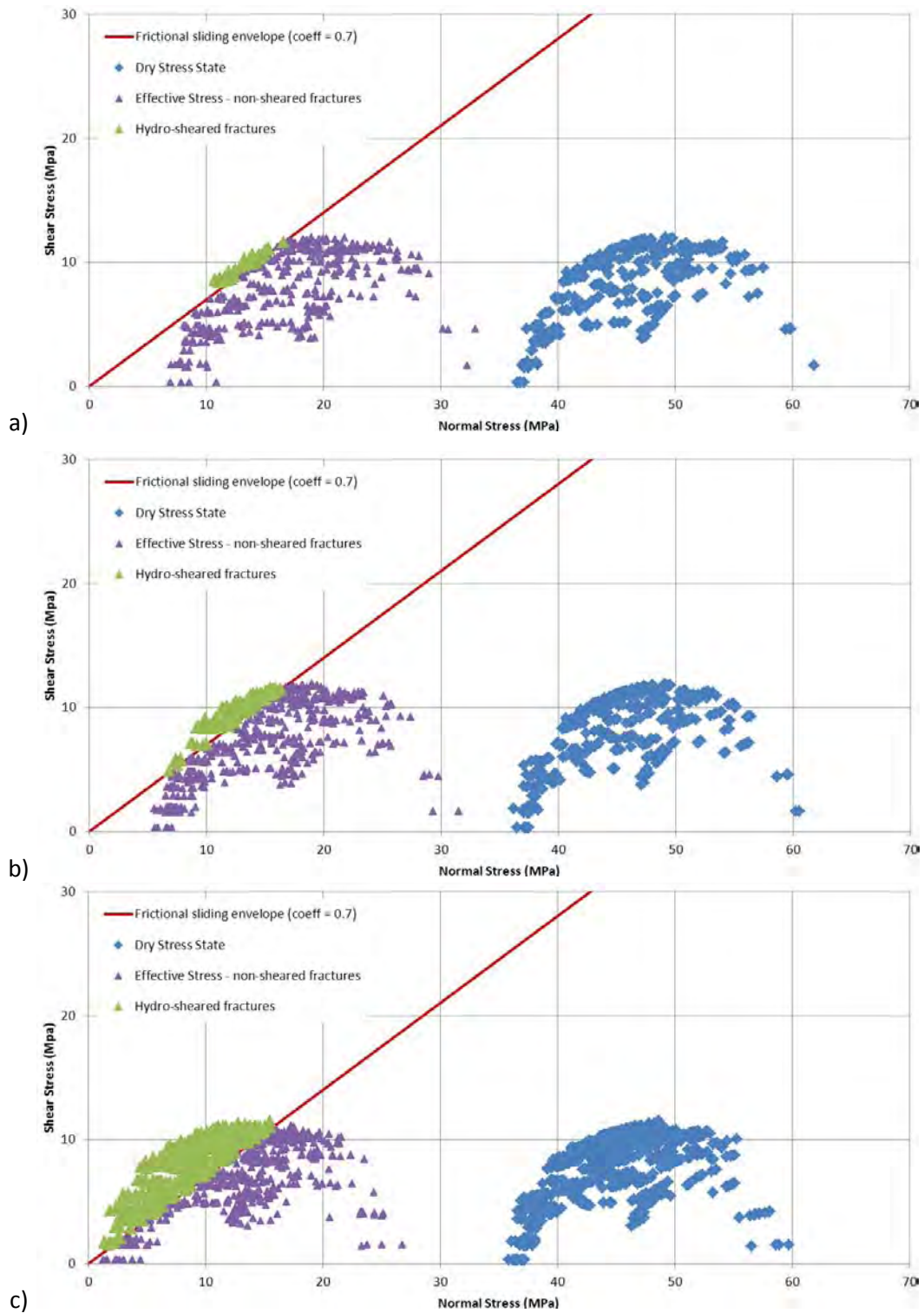


Figure 7-6. Mohr circle plots for Zone C, stress case 14.9 MPa/km (0.66 psi/ft)  $S_{hmin}$  at a) 7.9 MPa (1153 psi) WHP, b) 9.3 MPa (1350 psi) WHP and c) 13.4 MPa (1950 psi) WHP.

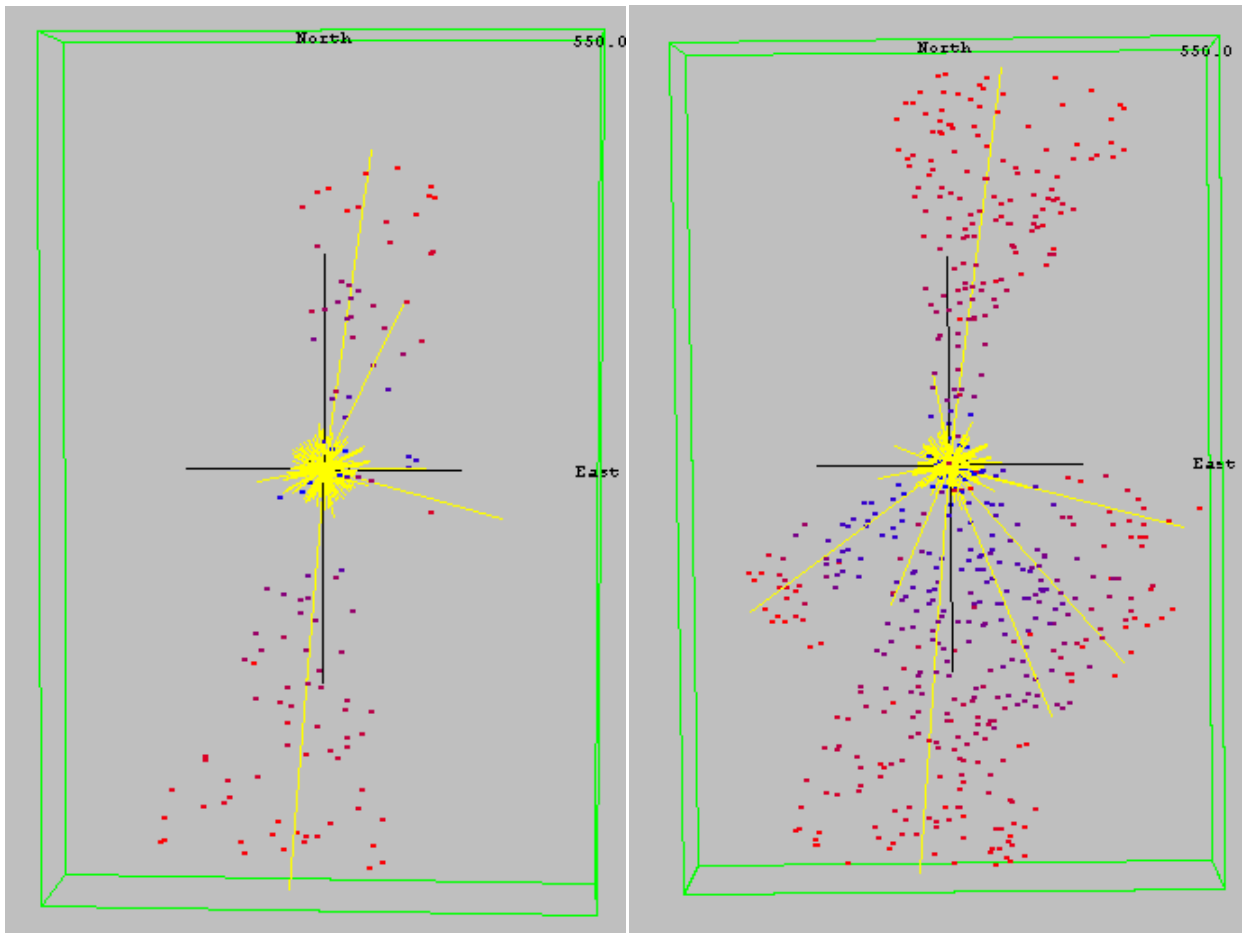


Figure 7-7. Modeled cloud of microseismicity for one model realization of Zone C at 9.3 MPa (1350 psi) WHP (left) and 13.4 MPa (1950 psi) WHP (right). Fracture volume for model on left is 2700 m<sup>3</sup> (710 thousand gallons). Fracture volume for model on right is 23000 m<sup>3</sup> (6.0 million gallons).

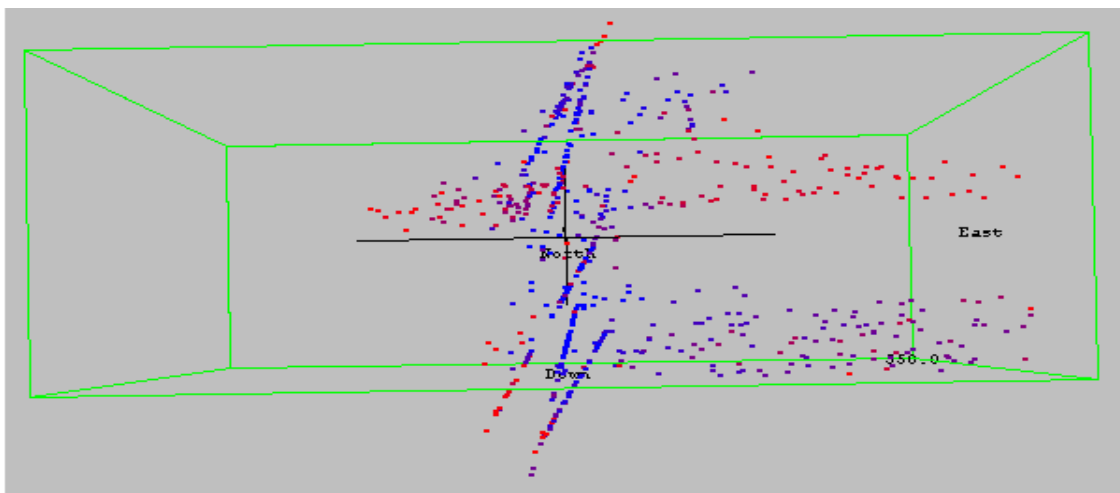


Figure 7-8. View looking north through modeled microseismicity for Zone D at 13.4 MPa (1950 psi) WHP at the end of model run. Deterministic dike margins can be seen as seismic streaks.

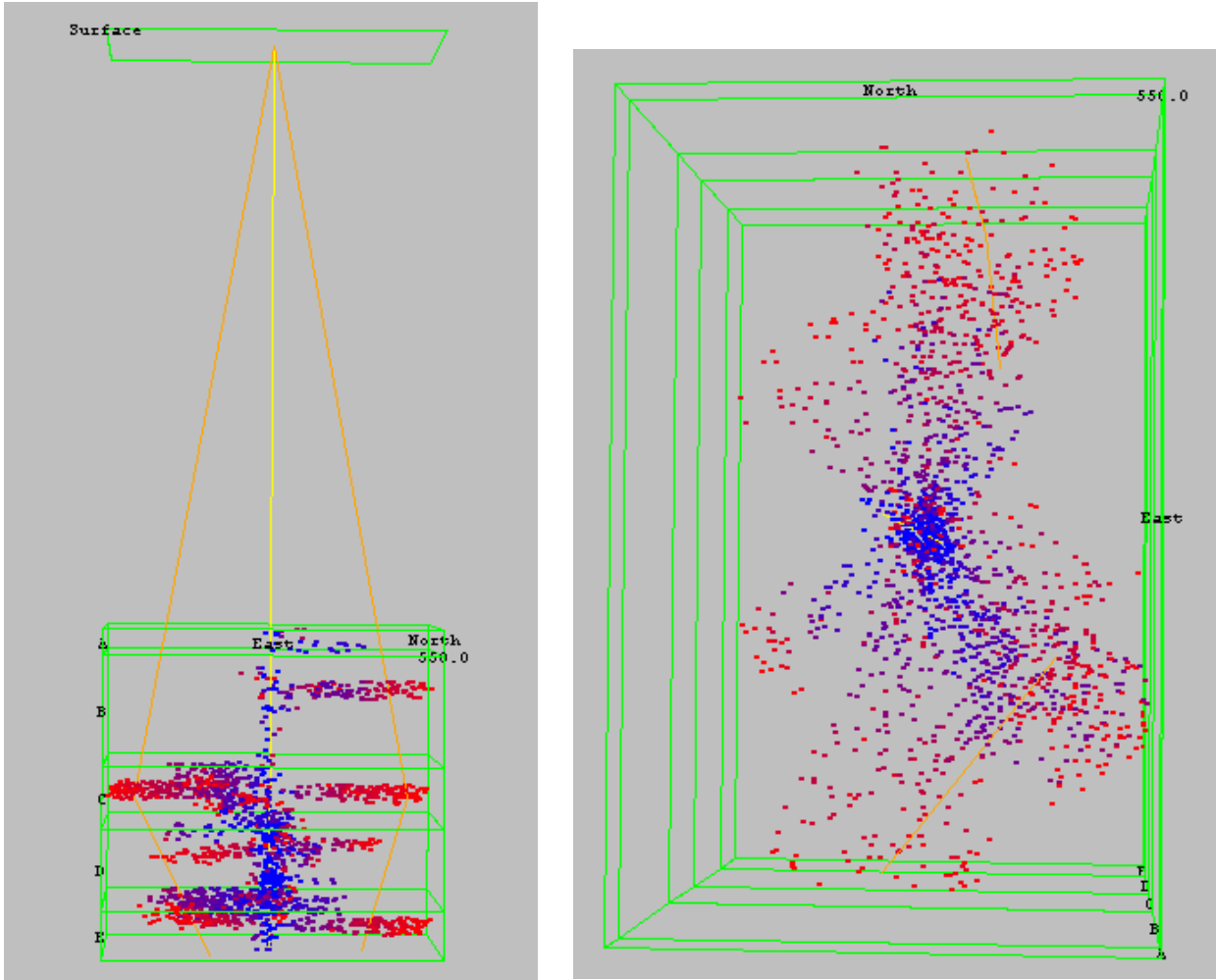


Figure 7-9. Combined microseismicity for all five zones. Scaled view (left) looking west includes well courses of NWG 55-29 (yellow) and proposed production wells (orange). Map view (right) shows combined microseismicity.

Table 7-7. AltaStim total volume for combined model of all zones.

WHP (psi)	Stress Case 1 (0.66 psi/ft $S_{hmin}$ )	Stress Case 2 (0.70 psi/ft $S_{hmin}$ )
	Total Volume (million gallons)	Total Volume (million gallons)
1153	0.4	0.0
1350	5.5	0.2
1550	10.2	3.2
1750	15.6	7.5
1950	22.1	11.3
2150	---	19.1
2350	---	22.5

#### 7.4.4 CONCLUSIONS

With a native state stress close to failure (14.9 MPa/km, 0.66 psi/ft  $S_{hmin}$ ), 9.3 KPa (1350 psi) WHP will initiate hydroshearing in all model zones except Zone A, the least fractured portion of the well bore. A WHP of 13.4 MPa (1950 psi) can create individual EGS fracture networks to meet the goals of each stimulation stage, (>19000 m<sup>3</sup> or 5 million gallons) injected per stage and 550 m (1804 ft) half-length. With a native state further from failure 15.8 MPa/km (0.70 psi/ft  $S_{hmin}$ ), 10.7 MPa (1550 psi) WHP will initiate hydroshearing in all zones except Zone A. At this stress case, a WHP of 14.8 MPa (2150 psi) can create individual EGS fracture networks to meet the goals of each stimulation stage.

In the model, it is possible to reach the EGS reservoir length goal (550 m, 1804 ft) without reaching the volume goal (>19000 m<sup>3</sup> or 5 million gallons). This result occurs when the wellhead pressure is high enough to initiate hydroshearing, but the orientation range of the stimulated fractures is narrow, resulting in a thin, low-volume reservoir. The best model results are realized when the pressures are well into the hydroshearing regime and just below the tensile failure regime.

Relatively low fracture density and high coefficient of sliding friction ( $\mu=0.85$ ) of silicic extrusive volcanic rocks (tuff, rhyolite, and dacite) may suppress hydroshearing in Zones A and B. Zone D, populated with ideally oriented, weak dike margins, produces the highest volume fracture network and requires the lowest pressures. Zones C and E, with the highest modeled fracture densities, also produce high volume fracture networks. The modeling effort presented here is not complete. Additional AltaStim models will be developed in prior to stimulation as further data and research results become available.

#### 7.5 TEMPERATURE MODELING

NWG 55-29 has a static temperature of 232°C (450°F) at the 9-5/8 in casing shoe at 1970 m (6462 ft), and 332°C (630°F) at the total depth of 3066 m (10060 ft). The ability to predict downhole temperature and flow conditions under various operating scenarios is crucial for the Newberry project. The Petris DrillNET temperature modeling module enables accurate predictions of wellbore temperature profiles during injection, production and static operations.

DrillNET was used during Phase I to predict the amount of cooling that would occur during the injectivity testing in September 2010. Temperature modeling was also used to determine the temperature profile of NWG 55-29 under various injection stimulation scenarios to aid in the diverter selection process. Depending on the depth and temperature of the created fractures, and their relationship to the next stimulation zone, a specific diverter material will be selected to ensure proper sealing of the existing fracture zone.

In setting up the model, it was assumed that the water injection temperature is 10°C (50°F). For simplification, it was also assumed that there was no water lost to the surrounding rock and that the surrounding rock exhibits the same thermo-mechanical properties throughout. For the open-hole section of the well bore, the temperature at the water-rock interface was assumed to be the same as the water temperature. For the open-hole sections, the friction term was neglected because this has a negligible impact on the results. Lastly, steady state heat transfer was assumed, meaning that the rate of heat gain by the water is equal to the rate of heat transferred to the surrounding rock.

AltaRock modeled several injection cooling (Figure 7-10) and thermal recovery scenarios (Figure 7-11) prior to the injectivity testing and logging in September 2010. These results were independently confirmed by modeling at West Virginia University by Dr. Brian Anderson. The team at West Virginia University examined two flow rates, 40 gpm and 120 gpm, assuming injection at the 2926 m (9600 ft) loss zone for 0, 1, 2, 3, and 8 days (Figure 7-12 and Figure 7-13). Two geothermal gradients were modeled, the first a constant gradient of 95.4 °C/km, and the second using two gradients, assuming 23.9



°C/km from surface to 1100 m (3609 ft), and 142.3 °C/km from 1100 m to the injection zone at 2926 m (9600 ft). The second proved to be more accurate when compared to the measured static temperature (Figure 7-14). Model outputs were then compared to the actual data to verify software validity for future modeling purposes. Figure 7-15 shows demonstrates excellent correlation between the modeled temperature for injection of water at 9.8 gpm with temperatures measured during the September 2010 inject test at the same rate.

Temperature modeling is also helpful when estimating the duration of diverter degradation, modeling the expected temperature profile during the drilling and stimulation of the two production wells, cementing design, and to predict flowing temperatures during the long term circulation test. The results for the temperature recovery (heat-up) are provided in Table 7-8. In preparation for the stimulation of NWG 55-29, this modeling information will allow AltaRock to estimate the amount of time that each diverter material will remain intact without sufficient cooling by sustained injection.

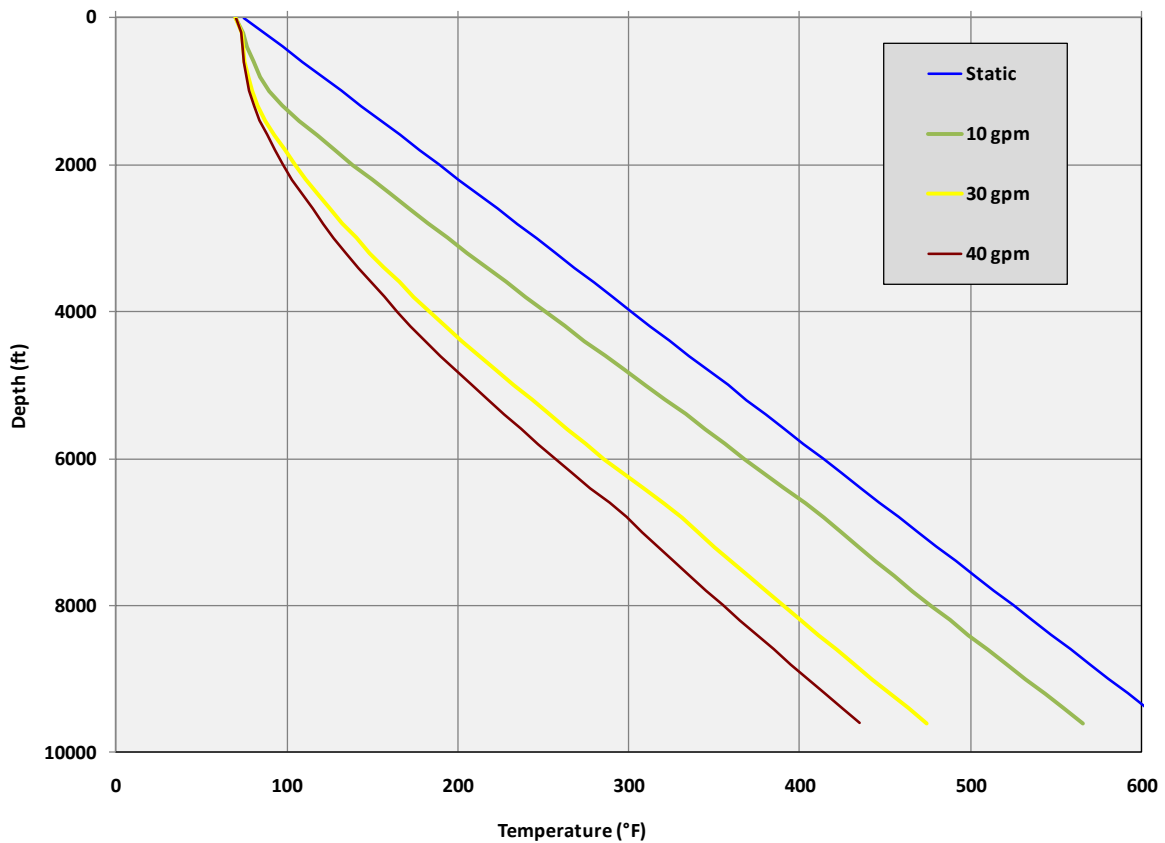


Figure 7-10. Modeled cooling after injecting at 9600 ft for one month at 10, 30 and 40 gpm.

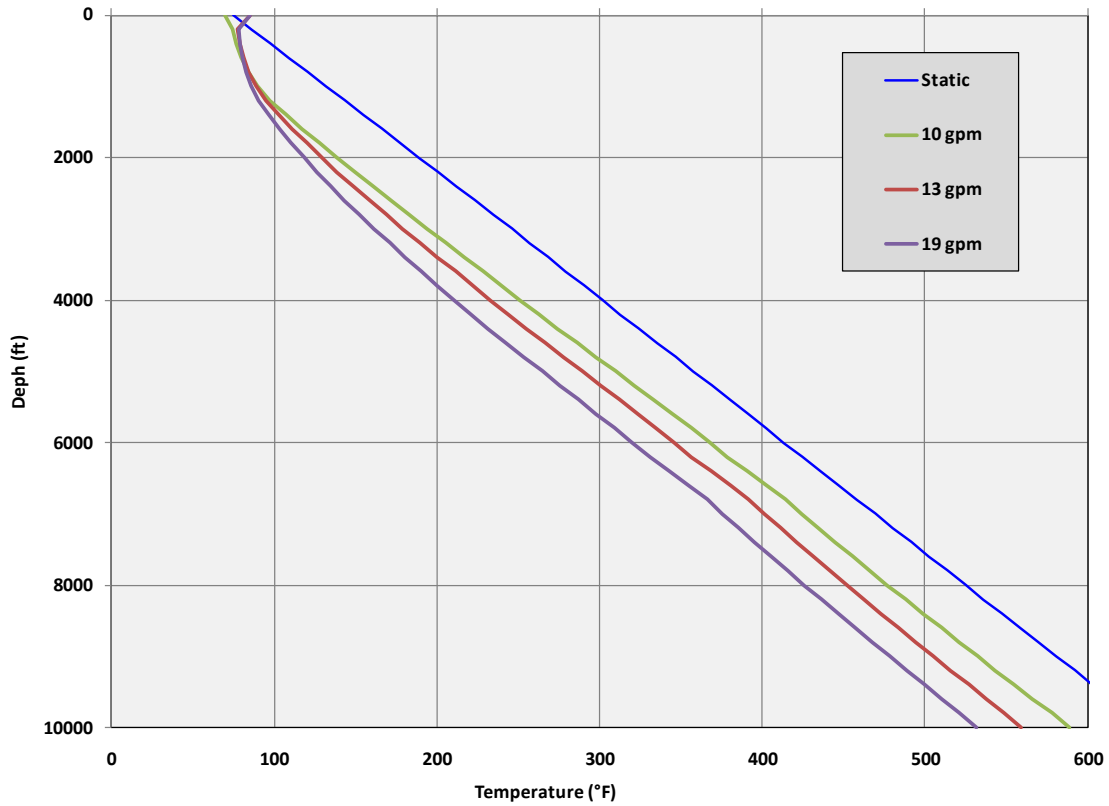


Figure 7-11. Modeled thermal recovery after injecting at 9600 ft for one month at 10, 13 and 19 gpm.

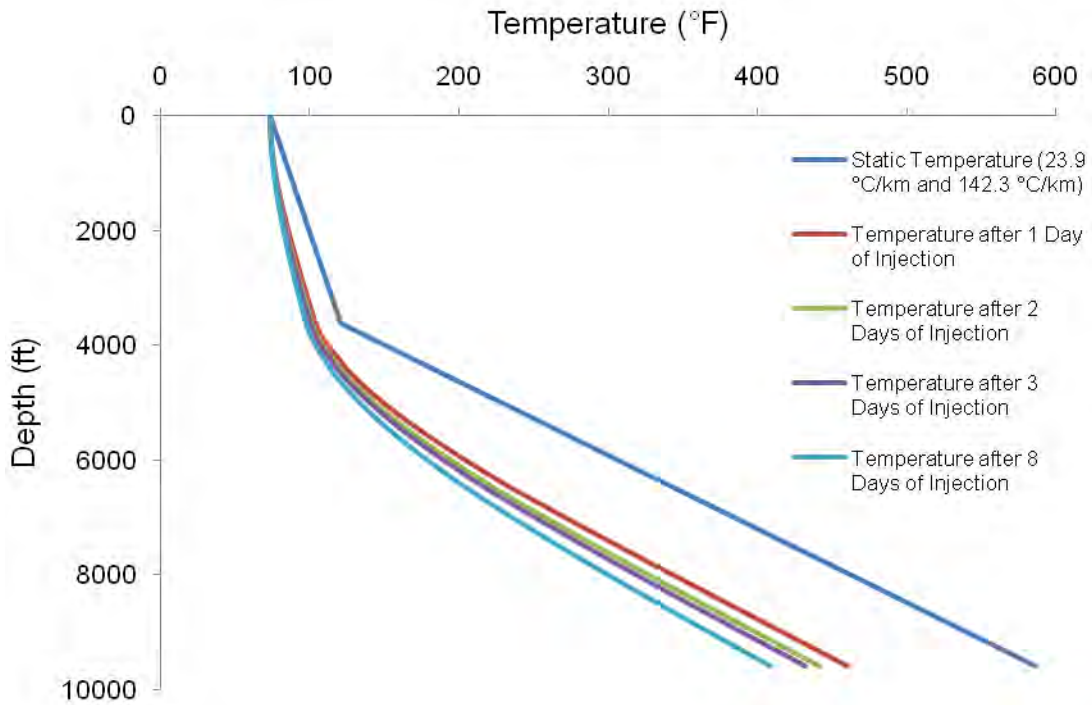


Figure 7-12. Modeled temperature profiles after injecting 40 gpm for 0 (static), 1, 2, 3 and 8 days, assuming thermal gradients of 23.9°C/km and 142.3°C/km.

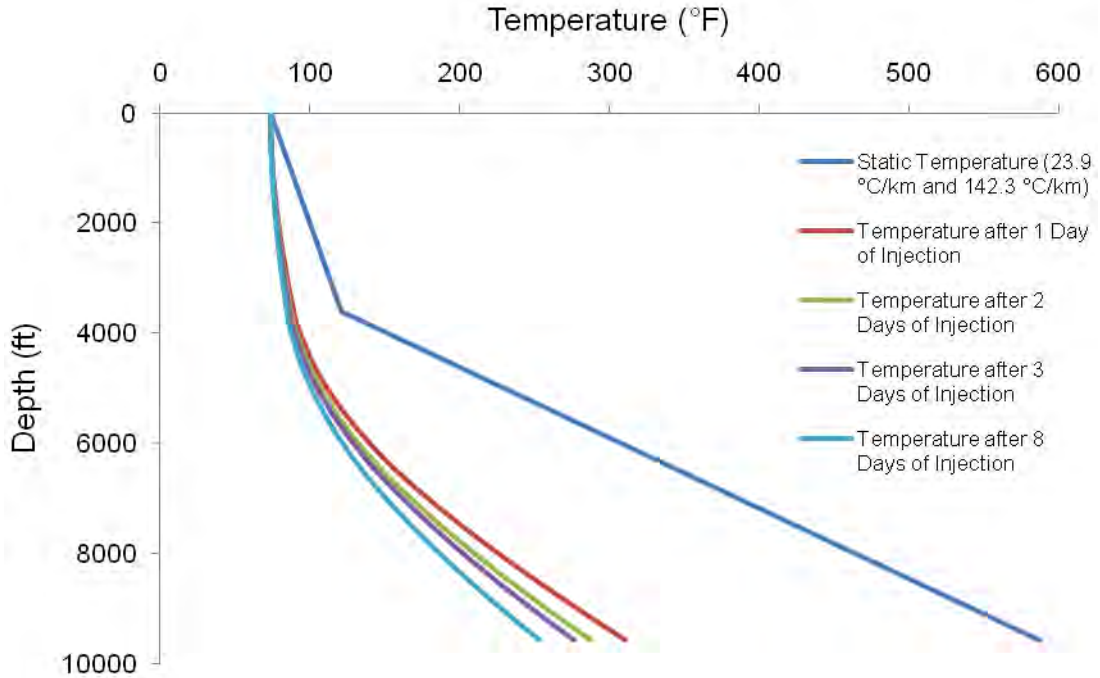


Figure 7-13. Modeled temperature profiles after injecting 120 gpm for 0 (static), 1, 2, 3 and 8 days, assuming thermal gradients of 23.9°C/km and 142.3°C/km.

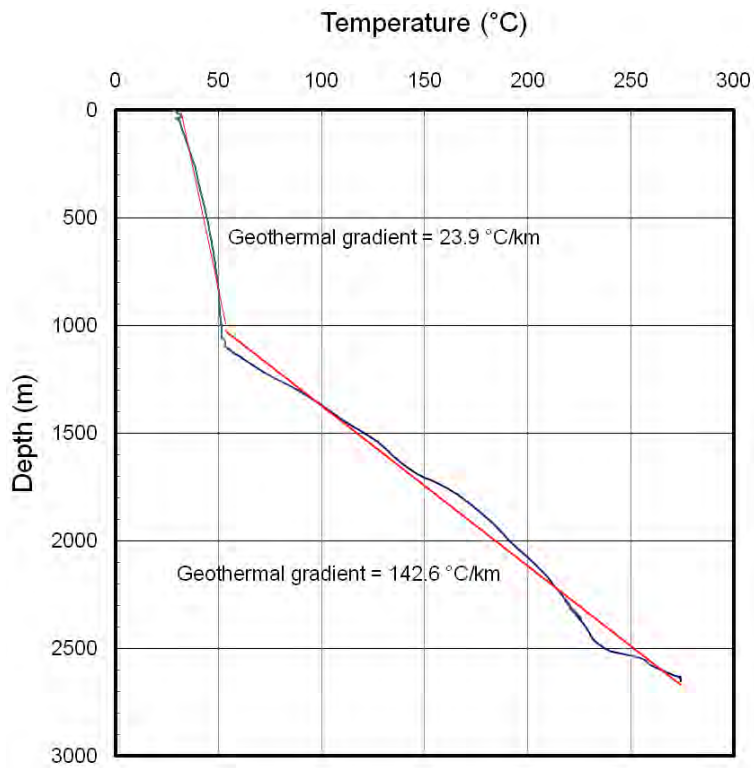


Figure 7-14. Comparison of measured and modeled downhole temperatures in NWG 55-29, assuming thermal gradients of 23.9°C/km and 142.3°C/km.

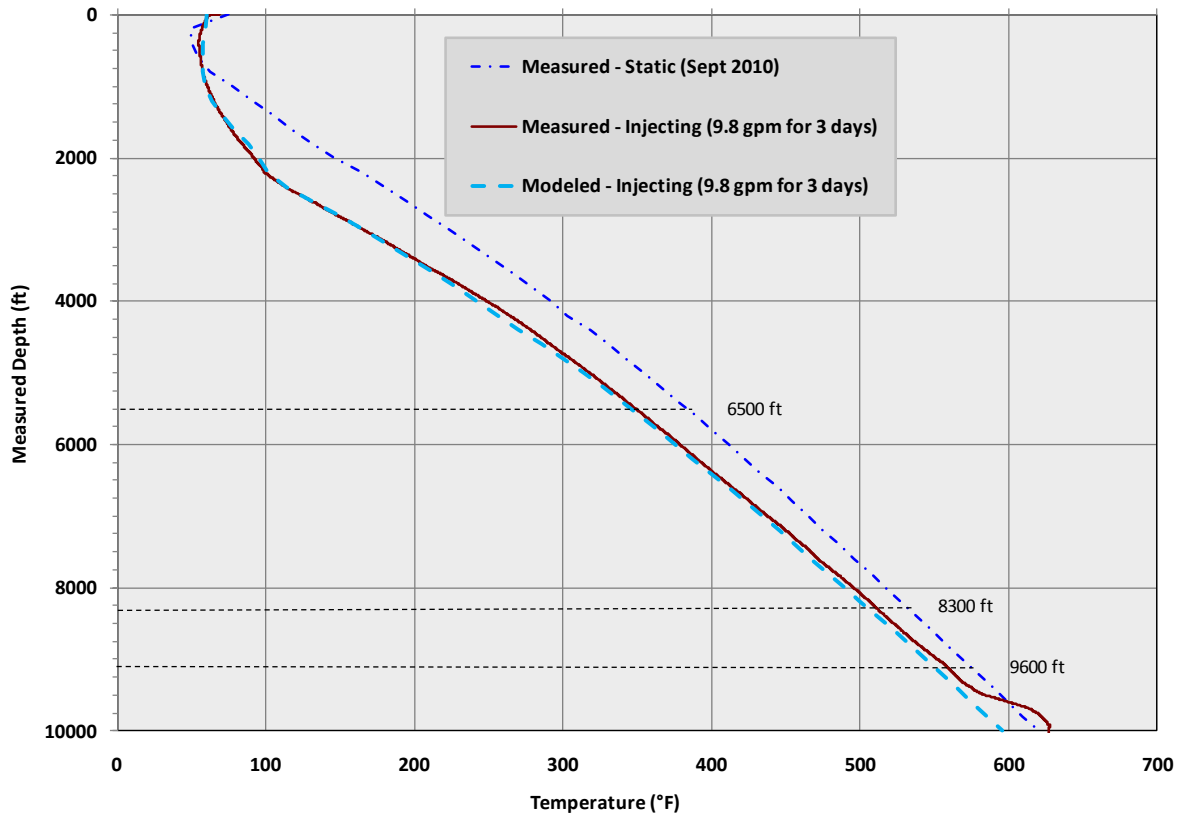


Figure 7-15. Comparison of measured and modeled downhole temperatures in NWG 55-29 after 3 days of injection at 9.8 gpm rate.

Table 7-8. Temperature recovery after 120 gpm injection at 2530 m (8300 ft), as illustrated in Figure 7-13.

Days Injecting	1	2	3	8
Recovery Time (hours)	Temperature During Recovery (°F)	Temperature During Recovery (°F)	Temperature During Recovery (°F)	Temperature During Recovery (°F)
0	301	281	271	250
3	409	380	375	333
6	437	411	403	361
8	446	429	421	378
11	446	439	431	390
14	466	444	438	400
17	479	446	443	408
19	487	446	445	414
22	493	446	446	420
25	497	458	446	424

## 7.6 DIVERTER TECHNOLOGY

### 7.6.1 INTRODUCTION

The creation of EGS reservoirs has historically involved the stimulation of a single fracture set around an existing well bore. This is due to the fact that during stimulation the existing fracture with the lowest hydroshearing pressure will open when water is pumped from the surface and pressure is applied in the injection well, and other existing fractures that require a higher shear pressure are not affected.

The stimulation of multiple fracture sets in a single injection well will increase EGS efficiency. To stimulate multiple fracture sets in a single well requires hydraulic isolation of each fracture network after it has been stimulated. To provide hydraulic isolation for the stimulation of multiple fractures a diverter product can be used (Petty et al., 2011). After the stimulation of the first fracture set (Figure 7-16A), a diverter pill is mixed and pumped to temporarily seal the fracture network from accepting additional fluid (Figure 7-16B). Additional pressure is then applied to the well and a second set of fractures (Fracture B), which had a higher minimum hydroshearing pressure than Fracture A, will be stimulated (Figure 7-16C). After multiple fractures are stimulated injection is discontinued and the well bore is allowed to reheat to the original well temperature. This causes the diverter material to thermally degrade, leaving all fractures open for circulation and flow during the operation of the EGS reservoir (Figure 7-16C).

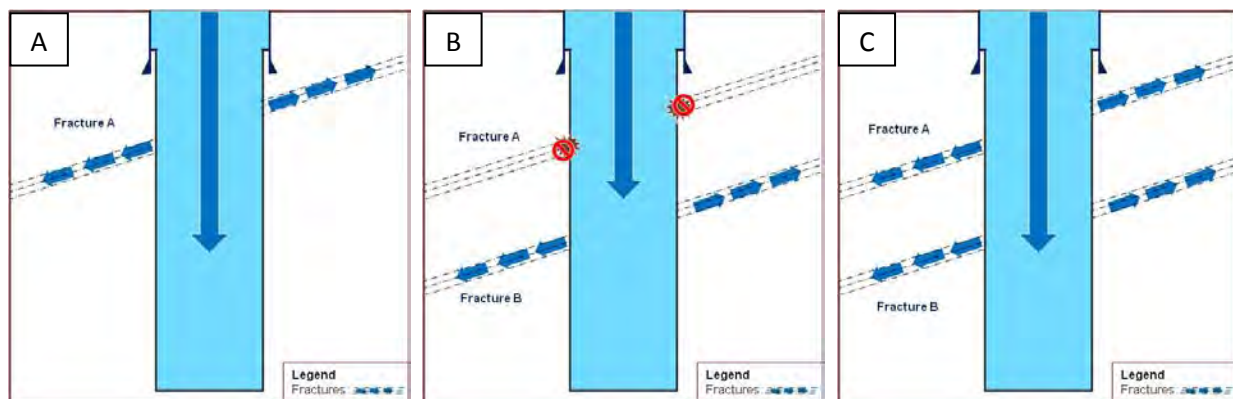


Figure 7-16. Stimulation of a single fracture set (A), stimulation of second fracture set after diverter application in first fracture set (B), and an EGS well with multiple fracture sets after diverter degradation (C).

### 7.6.2 DIFFERENCES BETWEEN EGS STIMULATION AND OIL AND GAS HYDRAULIC FRACTURING

In theory, hydraulic fracturing ('fracking') of oil and gas (O&G) wells is significantly different than EGS hydroshearing. There are two major differences that should be understood. The first is that O&G fracking typically involves applying enough pressure on the formation rock to cause tensile failure and the creation of new fractures. In EGS hydroshearing stimulation, pump pressure is maintained in the shear failure pressure envelope and is carefully controlled and limited to prevent tensile failure. EGS hydroshearing stimulation results in the 'opening' of existing fractures and limits the creation of new fractures. Once the fracture is opened, the rock faces can then slip past each other. When the fractures close slightly after stimulation pressure is relieved, the asperities on the shifted rock faces do not allow the fractures to close completely, leaving a path for water flow. A significant advantage of the hydroshearing approach over tensile failure is that hydroshearing tends to create a more diffuse 'cloud' of newly permeable fractures, maximizing heat exchange area per unit volume and minimizing the likelihood of thermal breakthrough between injection and production wells. In practice, both shearing



and tensile failure is occurring simultaneously in both types of stimulation treatments. The goal of EGS stimulation is to minimize tensile failure and maximize shear failure.

Another major difference is that sand and chemicals are purposefully pumped into the open fractures in O&G fracking operations to hold the fractures open and to aid in the stimulation treatment. A typical O&G fracking treatment may contain the materials listed in Table 7-9. In EGS hydroshearing, only water with small quantities of fluid tracers is pumped into the injection well and fractures. Diverter products<sup>17</sup> are pumped into the well between stimulation treatments. Diverter materials are designed to pack off at the fracture face inside the wellbore. After EGS hydroshearing, the stimulated well is allowed to reheat. As the well, fluids and diverter begins to reheat, the diverter materials degrade and dissolve into the wellbore fluid, and are then produced back to the surface when the well is allowed to flow. Diverter materials are selected to be benign and to have benign breakdown products. More information regarding AltaRock diverter products is included in the proprietary Appendix G-1.

**Table 7-9. Typical stimulation treatment for O&G application (SPE Monograph 12, *Recent Advances in Hydraulic Fracturing*).**

Material	Amount
Sand	136078 kg (300000 lb)
Potassium chloride (KCl)	6350 kg (14000 lb)
Guar	1143 kg (2520 lb)
Borate	318 L (84 gal)
pH buffer (NaOH or acetic acid)	318 L (84 gal)
Surfactant	318 L (84 gal)
Sodium persulfate (Na <sub>2</sub> S <sub>2</sub> O <sub>8</sub> )	38 kg (84 lb)

### 7.6.3 USE AND APPLICATION OF DIVERTERS FOR NEWBERRY EGS DEMONSTRATION

Proprietary diverter products developed by AltaRock will be used in the Newberry EGS Demonstration between stimulation treatments of each fracture network. Water will be pumped for about seven (7) days to stimulate each fracture set. Stimulation of at least three fracture sets is planned, for a maximum total of twenty-one (21) days of pump time. When the desired water volume has been pumped and the target fracture volume has been stimulated (Section 7.7), a suspension of diverter particles will be mixed with stimulation water and pumped into the well. The amount of diverter material is expected to be between 45 and 113 kg (100-250 lbs) per diverter treatment. The particles will be carried down to the fractures that are currently accepting water. The particles will pack off in the fractures at the well bore face and seal off additional flow into the fractures (Figure 7-16B, Fracture A). The diverter material will contain a distribution of various particle sizes to aid in the sealing capability of the diverter material. Once the diverter pill is mixed and ready to be pumped, the injection rate will be slowed down by one third until the diverter has sealed the fractures to allow for better system control. Effective sealing is determined by real-time monitoring of the downhole temperature profile using a fiber optic distributed temperature sensing system that will be in place during stimulation. Cooling of the wellbore down to the fractures being stimulated is expected to occur during the stimulation treatment. When fractures are sealed by the diverter material and flow is diverted elsewhere in the wellbore, a change in the temperature profile will occur (e.g., if flow is diverted deeper in the well then cooling should occur deeper in the well). Additional pump pressure will be applied and a new set of fractures, typically below the first set of fractures, will be stimulated by hydroshearing. Pumping at full rate will resume until the

<sup>17</sup> AltaRock holds a portfolio of patents, patent applications, licenses and related proprietary intellectual property regarding its diverter and stimulation technology, materials and methods.

second fracture set grows to the target volume. This process will be repeated to stimulate a third fracture set. Rates of injection will be adjusted as per the specifications of the written stimulation plan. Fracture growth will also be continuously monitored with the MSA by mapping microseismic events during the stimulation process. The injection rate and duration will be adjusted based on formation response and the seismic event trigger mitigation steps as described in the ISMP (Appendix A-1).

The procedure and contingencies for diverter application that will be followed for stimulation will be as follows:

- Stimulate first fracture set.
- Follow stimulation plan and grow fractures to target length from wellbore.
- Pump diverter to seal off given fractured zone.
  - If the first fractures to open are at or near 2926 m (9600 ft), the diverter selected will be a high temperature material with thermal stability at >260°C (>500°F) for at least 7 days because, in this case, the second fractured zone to be stimulated will likely be shallower than 2926 m (9600 ft). If the second stimulated zone is above the first fracture set, the well bore around the deeper fractured zone will heat up rapidly and cause degradation of any diverter material that will not hold up to temperatures that will occur within 24 hours after diversion.
  - If the first fracture set to open is significantly shallower than 2926 m (9600 ft), the diverter selected will be suitable for lower temperatures because cooling of the first fracture set sealed by the diverter will continue during injection and stimulation of the deeper fracture sets. One factor that will affect the selection of the diverter used in this case is the geostatic temperature of the well at the depth of the sealed fractures. It is important that the selected diverter degrades in a reasonably short period of time at the measured geostatic temperature.
- Continue pumping according to stimulation plan to grow second fracture set to target distance from wellbore.
- Pump diverter to seal second stimulated fracture network.
- Continue pumping according to stimulation plan to grow third fracture set to target distance from wellbore.
- Contingencies -
  - If a given fracture does not seal completely (a fractured interval that is completely sealed will show nearly complete diversion based on real-time DTS temperature data that is gathered during the stimulation treatment):
    - A second diverter treatment with the same or adjusted size distribution and/or volume will be applied. Volume may be increased or decreased depending on well response to previous treatment. If nearly all of the first fracture set is effectively sealed with the first treatment, the size of the second diverter treatment volume will be decreased by at least half. Conversely, if very little of the original fracture set is sealed by the first diverter treatment, the volume of diverter material will be increased to minimize the number of treatments needed to completely seal the fractures. The volume of subsequent treatments will be based on actual well response during the treatment.
    - The well may be sanded back to above a particular fracture set if it is deemed that the next set of fractures to be stimulated will be above the existing first stimulated fracture.

'Sanding back' refers to the process of filling part of the well bore with clean silica sand, from the bottom of the well to some higher level.

- If well is sanded back, the sand will be removed with a coiled tubing unit after stimulation operations are complete. Coiled tubing units are commonly used in well applications and can be mobilized to the site. The size and pump rates of the coiled tubing will be determined if and when this operation is needed. The best method to remove sand after stimulation is to reverse circulate the water and flow the sand and water up the coiled tubing as it is slowly lowered into the area of the hole containing the sand. The critical flow velocity will easily be high enough to move the sand up the coiled tubing.
- Stimulation will have to be temporarily terminated if well is sanded back to allow for sand to settle to depth.
- If two or more fracture sets open at the same time and take injection fluid:
  - If it is determined that all fractures are taking fluid and that they grow away from the wellbore at relatively the same rate, pumping will continue and multiple fractures will be stimulated at the same time.
  - If one or more fractures take the majority of the fluid and grows in a linear fashion, such that a short-circuit is likely developing, diverter will be pumped to seal off the fractures, or the well will be sanded back to seal up the fractures that are taking some of the injection fluid.
- If one of or more of the fractures is sealed by a diverter but the diverter seal fails part way through a subsequent stimulation treatment:
  - If the majority of the stimulation fluid continues to flow into and stimulate the second fracture set, the stimulation operation can continue and additional water might be needed to complete this stimulation treatment. If the first, reopened, fracture set begins taking a large portion of the stimulation fluid it will need to be sealed off again.
    - The re-opened fractured zone will be sealed off by sanding back the well to above the depth of this fracture set or,
    - The re-opened fractured zone will be sealed off with another treatment of diverter. Re-sealing with diverter will work most effectively if the re-opened fracture set is shallower than the second fracture set.
- If a single linear feature develops that is taking the majority of the stimulation fluid (i.e., a short circuit), one of the two options can be applied:
  - Pump diverter to seal off fractured zone in which short circuit has occurred, or
  - Sand back the zone of short-circuiting and stimulate new fractures above.

After the stimulation treatment, the well will be left static for a minimum of 72 hours at >121°C (>250°F) to allow for degradation of low temperature diverters. High temperature diverters may need to be exposed to temperatures above 260°C (500°F) for up to several weeks; the exact time will be dependent on the degradation characteristics of the specific diverter material that is used and the depth and temperature at which the diverter was emplaced.

#### **7.6.4 HANDLING AND STORAGE OF DIVERTER MATERIALS**

All diverter materials will be approved by BLM before shipment, storage and use at the Demonstration site. Diverter materials are stable, non-toxic, granular solids of various particle sizes. Materials will be stored on location in 23-45 kg (50-100 lb) sacks, 208 L (55-gal) drums or 1 m<sup>3</sup> (~35 ft<sup>3</sup>) polyethylene

sacks. Material will be protected from the weather with plastic wrap, covering, or storage in an enclosed and protected area. A total of 460 to 900 kg (1000-2000 lb) of each selected diverter will be on hand at the well location. A Material Safety Data Sheet (MSDS) will be included with the diverter material during shipment to and from storage at the site for inspection by appropriate regulatory agencies.

### **7.6.5 CHEMICAL COMPOSITION OF POTENTIAL DIVERTERS AND THEIR DEGRADATION PRODUCTS**

Appendix G-1 contains a list of proprietary diverter materials that might be used in the Newberry EGS Demonstration. One or more of these proprietary products may be used during the Demonstration based on the results of ongoing field investigations and laboratory testing of diverter performance. We expect to pump three stimulation stages. If a low temperature diverter with a density of 1.25 g/cc is used then 57 kg (125 lb) of diverter will be used between each stage. One diverter treatment will be pumped between the first and second stimulation, and another treatment pumped between the second and third stimulation. Thus, we expect to use a total of about 114 kg (250 lb) of diverter material if the low temperature diverter material is used.

It should be noted that the decomposition products of the planned diverters are either benign materials, like lactic acid, or minerals that are commonly found in drinking water. The exact compositions of the various potential diverter materials are proprietary. Details of the breakdown products of potential diverter materials are also listed in Appendix G-1. It should also be noted that the diverter materials are designed to stay inside the well bore or well skin by either bridging off at the fracture face, or falling to the bottom of the well bore. Little to no material will actually flow any appreciable depth into the fractures. When the material degrades it will dissolve into the water inside the well bore and be produced back to the surface during the flow-back test. Therefore, because of the benign nature of the material and the fact that no significant amount of the degradation products will flow into the fractures, there should be no detrimental impact from the diverters to the environment.

## **7.7 FIELD OPERATIONS AND MONITORING**

### **7.7.1 STIMULATION OF NWG 55-29**

As discussed in the ISMP (Appendix A-1), a goal of the project is create a sustainable EGS reservoir. Initial modeling suggests that 500 m (1640 ft) spacing between the injection and production wells at the EGS zone will provide sufficient surface area for sustainable heat exchange (Jupe et al., 1995)). Therefore, injection in each zone will continue until microseismicity indicates that the fracture cloud has extended to a long axis diameter of at least 1000 m (3280 ft) to accommodate one injector and two producers. An assessment of geosciences (Section 3) and stress conditions (Section 5) indicate that the fracture networks and main cloud of microseismicity will elongate in the north-south direction. The fracture networks will be allowed to grow horizontally to a long dimension of 1000 m (3280 ft; Appendix A-1 Figures 3-2 and 4-2). Note that EGS reservoir growth may be not be symmetric around the well and could grow further in one direction than the other. Also note that there is no adverse risk of EGS reservoir growth in an unpredicted direction as there is sufficient space at the Demonstration site for growth in any direction The two production wells, to be drilled after the EGS reservoir creation phase, will be targeted to intersect the outer edges of the stimulated zone.

As shown in Figure 10 in the ISMP (Appendix A-1), all of the microseismicity at both Sultz GPK2 and Basel DHM-1 occurred within a 500 m (1640 ft) radius of the wells, although it was more tightly clustered at GPK2 than DHM1. We expect the microseismicity at Newberry to be simi larly clustered, growing outward as the injected fluid opens connected fractures. Some event locations may be outliers

and thus are not representative of the main EGS reservoir. For a sustainable reservoir, it is important to maximize the temperature of the stimulated rock. Because intersecting reservoir rock cooler than 200°C (392°F) will not be desirable, an upper vertical limit for reservoir growth will be set at a depth of approximately 1830 m (6000 ft) or about 58 m (189 ft) below sea level, the approximate depth of the 200°C (392°F) temperature contour.

As discussed in the water monitoring document (Appendix B-4) and the independent consultant's hydrology review (Appendix B-5), the base of the local groundwater resource is generally shallower than 1000 feet on the western flank of Newberry Volcano. NWG 55-29 penetrated volcanic rocks correlated to the Newberry, Deschutes, John Day Formations and, below about 8500 feet total vertical depth (TVD), subvolcanic intrusives presumed to be related to the Newberry volcano (AltaRock, 2010). In temperature profiles of NWG 55-29 and other deep wells, the base of permeability is characterized by a transition from isothermal temperatures above to conductive thermal gradients below, indicating limited groundwater flow below a depth of 1000 feet (Dames and Moore, 1994). Thus, setting a vertical growth boundary at 6000 feet TVD in NWG 55-29 will provide a buffer of 5000 feet (1.5 km) of impermeable rock between the EGS reservoir and local groundwater resources and ensure that producing temperatures in the EGS triplet will be optimized. The vertical growth boundary will be monitored by both microseismicity and by real-time fiber optic temperature and pressure monitoring in the wellbore. AltaRock will use a fiber optic distributed temperature sensing (DTS) system with an optical pressure sensor to constantly monitor downhole pressure and temperature throughout the wellbore. Not only will the DTS system allow AltaRock to monitor the success of the diversion in realtime, it will also show the depth of injection at any point during the treatment. Selected injection rates and diverter products will depend on where the injection is occurring in the open-hole interval and the temperature at that depth.

Because the minimum hydroshearing pressure is not known, the stimulation will begin with a step-rate injection test. Previous injection tests reached a flow rate of 1.4 L/s (21 gpm) at a wellhead pressure of 7.9 MPa (1153 psi), with no change in injectivity or evidence of hydroshearing (Table 7-10). Yet, evidence of slight cooling in the lower portion of the open-hole during the inject-to-cool operations may be indicating that 7.9 MPa (1153 psi) is near the lower limit of the shear failure envelope. Due to the large open-hole interval length in NWG 55-29 (~1100 m or 3500 ft), it may prove difficult to stimulate these lower zones, below 2621 m (8600 ft), without inducing tensile failure near the casing shoe at 1970 m (6462 ft). Because these lower zones represent the highest enthalpy target, it is important that the stimulation procedure attempt to first enhance these deeper zones before tensile failure at the casing shoe occurs. To that end, the initial step rate test will progress in very small rate steps while monitoring the DTS system for indications of fluid exit depths (Table 7-11). The flow rate will be held at each rate for a minimum of two hours or until the pressure stabilizes (whichever is longer). The results of the step-rate testing will allow an optimal injection rate to be determined for initial hydroshearing.

If significant fluid losses occur at the casing shoe, wellhead pressure will be held constant to fully exploit the potential for shear stimulation at greater depth. Significant fluid losses in the shallow open-hole interval, before sufficient permeability enhancement occurs in the lower zones, could indicate tensile failure near the shoe, which would be detrimental to the project goal of stimulating at least three distinct fractures networks along the open hole. The rate will only be increased as the lower zone stimulates, deep permeability enhancement occurs and the pressures decline.

Because it will be difficult to determine whether the rock is failing in shear or tension, several data streams and possible outcomes will be explored to guide the stimulation procedure:

1. If DTS monitoring indicates fluid exiting shallow, within the first 152 m (500 ft) of the open-hole interval, a tensile fracture may be developing. NWG 55-29 stress analysis indicates that rising



borehole fluid pressures are most likely to exceed the magnitude of  $S_{hmin}$  at these depths (Section 5.5, Figure 5-18). Also, the BHTV survey indicated very low fracture density in the rock formations near the casing shoe. Hence, the rock is fairly competent and may only fail in tension in this zone.

2. Since tensile rock failure is a relatively inefficient generator of radiated seismic energy (Bame and Fehler, 1986; Ferrazzini et al., 1990), a large cooling event in the temperature curve near the casing shoe, coupled with minimal detectable microseismic activity, may indicate that a tensile fracture has been created. There are other characteristics of the radiated seismic wavefield that may help discriminate between tensile and shear failure, such as observations of non-double couple mechanisms from moment tensor solutions (Julian et al., 2009). However, these approaches are computationally intensive and may not be applicable in real-time, as is required to guide EGS stimulation in the field.
3. The fracture gradient at certain fluid exit points will be recalculated throughout the stimulation process. Fractures propagating at gradients above 13.6 MPa/km (0.6 psi/ft) could be tensile fractures, because the range of likely magnitudes for  $S_{hmin}$  derived from stress models for NWG 55-29 (Section 5.5, Figure 5-18) indicate that  $S_{hmin}$  should be exceeded above this level. Fractures that are propagating at gradients between 11.3 and 13.6 MPa/km (0.5-0.6 psi/ft) (which is below the pressure already experienced by the well during the inject-to-cool operation, as discussed in Section 5) could be failing in shear.

Without a mini-frac to identify  $S_{hmin}$  magnitude, the shear failure envelope cannot be well-defined in advance of stimulation, but can be determined during the stimulation process. Thus, the stimulation will have to proceed cautiously while interpreting all data streams to avoid tensile fracturing. Therefore, a step-rate injection test at higher rates and pressures will be reserved for the second stage of stimulation, after stimulation of the lowest zones is completed successfully (Table 7-11).

**Table 7-10. Baseline injection test flow rates and pressures.**

Injection Rate (gpm)	WHP (psi)	Measured Injectivity Index (gpm/psi)
10	751	0.03
21	1153	0.03

**Table 7-11. Step-Rate<sup>1</sup> test flow rates and estimated pressures.**

Injection Rate (gpm)	Estimated WHP (psi)	Estimated Injectivity Index (gpm/psi)
25	1275	0.03
50	2000	0.03
75	2050	0.50
150	2200	0.50
225	2350	0.50

<sup>1</sup>Injection rate will be held constant at each step for 2 hours or until pressure stabilizes, whichever is longer. Flow rates will not be increased if surface pressure will exceed 3000 psi or if microseismic response exceeds specified triggers. The estimated onset of hydroshearing shown here, as noted by increased injectivity, is hypothetical for illustration purposes.

### 7.7.1.1 PUMPING EQUIPMENT

Typically, trailer-mounted injection pumps are used in conjunction with water tanks, high pressure pipelines, valves and instrumentation to stimulate geothermal wells. The water well on Pad S-29 will tie directly to the tanks and supply water for the treatment. Water management during stimulation will be

important because a large volume of groundwater is required to create three distinct fracture networks with a long-axis radius of 500 m (1640 m). Water will be supplied by two existing, on-site groundwater wells and stored in the tanks on Pad S-29 before being pumped into NWG 55-29 during stimulation treatment. For the stimulation of NWG 55-29, at least eighteen water storage tanks, each with 83 m<sup>3</sup> (22000 gallons) of capacity, will be assembled in parallel. This will provide at least 1500 m<sup>3</sup> (396000 gallons) of surge capacity. A temporary, above-ground pipeline will transfer water from the Pad S-16 water well to the tanks on Pad S-29. Water well flow rates and cumulative volumes will be continuously recorded by in-line, digital paddle wheel flow meters. Aquifer water levels will be continuously recorded by downhole, digital pressure transducers that are currently installed in each well. The tanks will be piped to a batch mixer that feeds the suction side of the injection pumps. The batch mixer will be used to add diverter materials as necessary. The diverter equipment is described in detail in Section 7.7.1.5. The injection pumps will be manifolded together to allow flexibility in pumping rate and pressure. See Appendix G-2 for process flow, piping and instrumentation diagrams of the water gathering and stimulation equipment.

In the September and October of 2010 NWG 55-29 injection test and temperature surveys, the baseline injectivity did not increase after injecting into at 1.4 L/s (22 gpm) and 7.9 MPa (1153 psi). Yet, the October 2010 injecting PT survey showed slight cooling from 2633-2682 m (8640-8800 ft), where no cooling had occurred previously at lower injection pressures. This suggests that a surface pressure of 7.9 MPa (1153 psi) may be approaching hydroshearing pressure. Based on this observation and stimulation pressures observed at other EGS sites (Figure 7-1), we expect that the hydroshearing pressure for NWG 55-29 will be between 8.3 and 16.5 MPa (1200 and 2400 psi).

The surface pressure must always remain below 24.6 MPa (3566 psi) to ensure that the integrity of the surface casing is not compromised. The 13-3/8 in, 72 lb/ft, L-80 surface casing is cemented from the surface to 1338 m (4391 ft) to separate the geothermal reservoir from the surface and to protect local groundwater resources. While stimulating down the casing, the weakest part of the well is located at 1277 m (4189 ft), which is the deepest section of 13-3/8 in casing exposed to the wellbore fluid pressure. The 13-3/8 in casing has a burst pressure of 5380 psi. At a depth of 1277 m (4189 ft), and assuming a stimulation water gradient of 9.8 MPa/km (0.433 psi/ft), only 24.6 MPa (3566 psi) of additional surface pressure can be applied before the burst pressure of the 13-3/8 in casing is exceeded. The burst pressures for casing are calculated using 87.5% minimum yield strength for steel according to API standards, and, hence, incorporate a 1.14 safety margin. Burst pressure testing is conducted on uncemented, free-hanging pipe, so the cement sheath also provides additional, but unquantifiable, strength to the wellbore.

Maximum wellhead pressure will be limited to 20.7 MPa (3000 psi). Stimulation equipment specification will include multiple pumps, with 50% horsepower redundancy, capable of injecting 0.6-50 L/s (10-800 gpm) at pressures ranging from 5.2-24.6 MPa (750-3000 psi) (Figure 7-17). Typical triplex pumps have a minimum output of 2.0-2.6 L/s (32-42 gpm). Because the initial stimulation rate will be 1.6 L/s (25 gpm), we will require two different types of pumps to span the expected range of rates and pressures. If a third-party is hired to perform the stimulation treatment, we can expect three to four of their truck-mounted triplex pumping units to be on site (Figure 7-18), along with a cementing truck to provide lower injection rates.

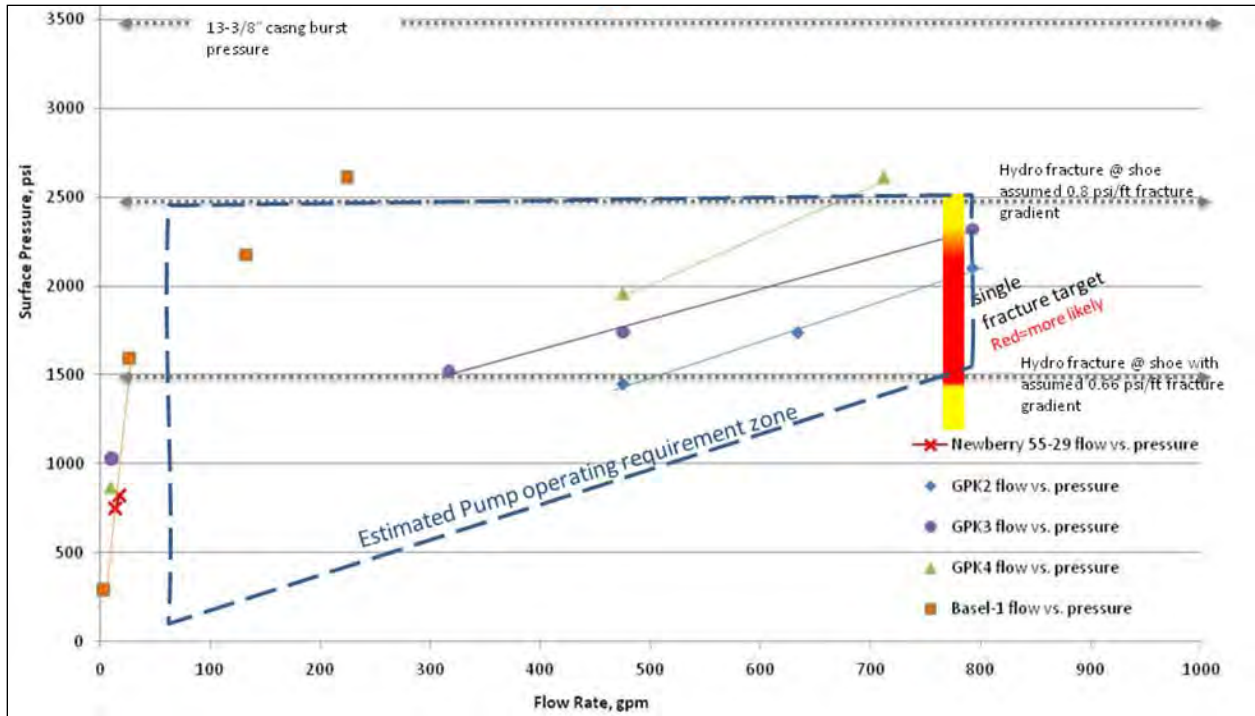


Figure 7-17. Estimated stimulation pump output pressure and flow rate for NWG 55-29, showing analogous data from previous EGS developments.

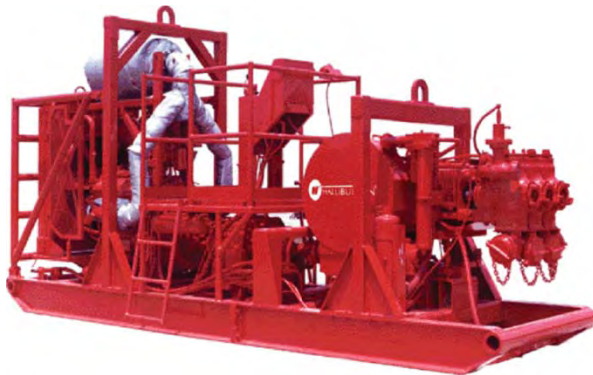


Figure 7-18. Picture of skid-mounted triplex injection pump.

The discharge from the injection pumps will flow through 10 cm (4 in) high-pressure, hammer-union pipe into a high pressure wellhead that will be installed on top of the 13 3/8 in casing head (Figure 7-19). The pipe is rated to 41.4 MPa (6000 psi) at 84.8 L/s (1344 gpm). All equipment on the discharge side of the injection pump will be rated to at least 24.1 MPa (3500 psi), 3.4 MPa (500 psi) greater than maximum stimulation pressure. The injection water will be at or near ambient temperature, so no high-temperature equipment is necessary in the upstream equipment. The stimulation procedure will require all piping and equipment to be pressure-tested to 3.4 MPa (500 psi) above maximum stimulation pressure prior to the start of the stimulation job. The injection treatment will be conducted rig-less, without drill pipe in the hole, such that the casing will be exposed to the injection pressure and fluids. An in-line magnetic flow meter, pressure transducer and dial indicators, and temperature transducer and dial indicators, on the discharge side of the pumps will provide continuous information to the onsite data trailer. The trailer will house the computers and data loggers that will record information from all of the surface instrumentation, as well as from the microseismic system and the fiber optic DTS

monitoring cable. AltaRock personnel will staff the data trailer 24 hours a day on a 12-hour rotation. If a third-party contractor is used, a stimulation monitoring van may also be on-site. These highly sophisticated trucks allow the engineers to control and monitor the equipment on-the-fly. The van computers record the entire treatment, including total discharge rate and per pump discharge rate, pressures, temperature, fluid viscosities, trouble time, and maintenance logs and are used to generate job reports.



**Figure 7-19. Existing wellhead on NWG 55-29. Everything above and including the gray, 12 in master valve will be replaced with a high-pressure wellhead suitable for stimulation.**

#### **7.7.1.2 SURFACE INSTRUMENTATION**

The surface injection rate will be monitored through an in-line flow meter on the discharge side of the pumps that is connected to a data logger in the data trailer. If a stimulation monitoring van is on site, the discharge rate will be monitored and controlled from the van. The injection rate is our main tool in controlling well bore pressure and treatment duration. The surface pressure will be monitored via a pressure transmitter and data logger. Temperature transducers will be utilized to monitor injection fluid temperature through the data logger. Dial thermometers and pressure gauges will also be in place for redundancy, with readings recorded manually on a periodic basis. Spare indicators will also be on-site in case of instrument failure.

The water wells on Pad 29 and Pad 16 will also be monitored through surface instrumentation. Each well has an AG-2000 magnetic flow meter with data output capability installed in the discharge line to measure flow rate. The flow meters record rate and total volume pumped. Downhole pressure transducers are currently installed in both water wells. Flow meter output will be transmitted to the

data logger in the trailer so that water level and rate can be continuously monitored and recorded. A downhole pressure transmitter is also recording pressure and water level in Water Well #2, which will remain shut in throughout Phase II operations.

#### *7.7.1.3 FIBER OPTIC MONITORING*

Downhole temperature during stimulation will be monitored using a Schlumberger WellWatcher BriteBlue HT – Gen2 distributed temperature sensing (DTS) system. This DTS is a multi-mode, high-temperature, 50/125 fiber with a carbon polyimide coating. The DTS surface unit laser shoots the line with 1064 nanometer waveband, and stokes/anti-stokes reflections are measured in the 1014-1114 nm waveband. The 3810 m (12500 ft) DTS fiber is installed in 316L stainless steel 0.64 cm (¼ in) capillary tubing that has been temperature-hardened. It has a yield strength of 827 MPa (120000 psi). A Fabry-Perot pressure gauge will be installed at the bottom of the DTS line to measure pressure at the end of the tubing. A surface acquisition unit will be connected to the downhole sensors. The Schlumberger Sensa Sensor Manager software unit stores and visualizes the fiber optic data. A Schlumberger technician will be on-site during stimulation to provide technical support and data interpretation support. Downhole pressure and temperature monitoring via DTS will allow us to identify open fracture paths at the borehole face in real-time. This data provides essential information about the depth of fracture initiation and the success or failure of the diverter materials in sealing open fractures. The fluid initiation point and the corresponding temperature at that depth is a controlling factor on the type of diverter to be used. Additionally, the temperature and pressure at a given depth is the data that will be relied upon to determine whether or not the diverter has successfully sealed off open fractures at the wellbore face. The real-time fiber optic data will enable us to make these types of decisions in the field.

#### *7.7.1.4 OFFSET WELL MONITORING*

There are no plans to monitor pressure in well NWG 46-16. The well has a blockage, likely due to formation collapse, at the top of the open-hole section around 1452 m (4765 ft). The hole was reamed out in 2008 from 1425-2231 m (4765-7318 ft), at which point cleanout operations were abandoned. Because the well is located 3 km (1.86 mi) from NWG 55-29 at the surface, and 2.3 km (1.4 mi) away at depth, and contains a bridge at 1452 m (4765 ft) and formation collapse from at least 2231-3536 m (7318-11600 ft), pressure monitoring during stimulation would not be useful. Additionally, because the rocks at depth have very low native permeability, it is unlikely that a hydraulic connection between NWG 46-16 and NWG 55-29 will occur. No other open, deep wells exist at Newberry to provide an alternate location for offset well monitoring. See Section 7.9.5 for information about the geochemical monitoring plan for nearby water wells.

#### *7.7.1.5 DIVERTER EQUIPMENT*

The diverters that will be implemented in the stimulation operation consist of particulate material of variable sizes. The material will be injected into the stimulation water between stimulation stages. This will be done by first mixing the diverter in water in a batch mixer commonly used in the oil and gas industry for mixing and pumping spacer fluids for cement jobs. Batch mixers have two 50-bbl tanks. Each tank has an agitation paddle in the middle and an on-board recirculation pump to keep the particulate material in suspension before it is injected into the well. Some of the diverter material will have a relatively low density of about 1.2 g/cc, and can easily be suspended in water with little agitation. Other diverter materials that may be used might have a higher density (above 2.0 g/cc) and require more agitation to maintain suspension prior to being pumped into the well.



### 7.7.1.6 TRACER EQUIPMENT

Near the end of each stimulation phase (within six hours of pump shut-down or diversion), a solution containing a pair of tracer compounds will be injected as a pulse into NWG 55-29. The pair of tracers will include a sorbing and a conservative tracer, or two tracers possessing contrasting diffusivities. This tracer solution will be entrained in the stimulation fluid and flow into the near-wellbore formation. After the entire stimulation treatment is complete, the well will be shut-in temporarily to allow for heat-up. After a brief shut-in period of at least 3 hours, but not exceeding 24 hours, the well will be induced to flow and the solution sampled. The produced fluid will be sampled and analyzed for the tracers. From an analysis of the reactive and conservative tracers, the near-wellbore fracture surface area will be determined.

Ten kg (22 lbs) of each of the sorbing (e.g., safranin T or LiBr) and conservative (e.g., 2,6-naphthalene disulfonate) tracers, or 10 kg (22 lbs) of each of the contrasting-diffusivity tracers, will be added to a 208 L (55-gal) drum of water and mixed thoroughly. Then the solution will be injected over a period of 10 minutes into the injection stream of the stimulation fluid. This procedure will be repeated for each stimulation event. Each tracer will be approved in advance by BLM and an MSDS will be included with the shipped product and made available at the site.

### 7.7.2 FLOW TEST OF NWG 55-29

After stimulation is completed, the well will be shut-in to allow for reheating (a period of at least 3 hours). After sufficient recovery, a single-well flow test will be conducted to allow productivity measurement, wellbore surveys, and tracer and geochemical sampling. A model was constructed in Petris DrillNet to predict the time required for thermal recovery after 21 days of injection at a depth of 2926 m (9600 ft) and a rate of 31 L/s (500 gpm). The model predicts that only 12 to 24 hours will be required before the fluid in the bottom 610 m (2000 ft) of the well is over 260°C (500°F; Figure 7-20).

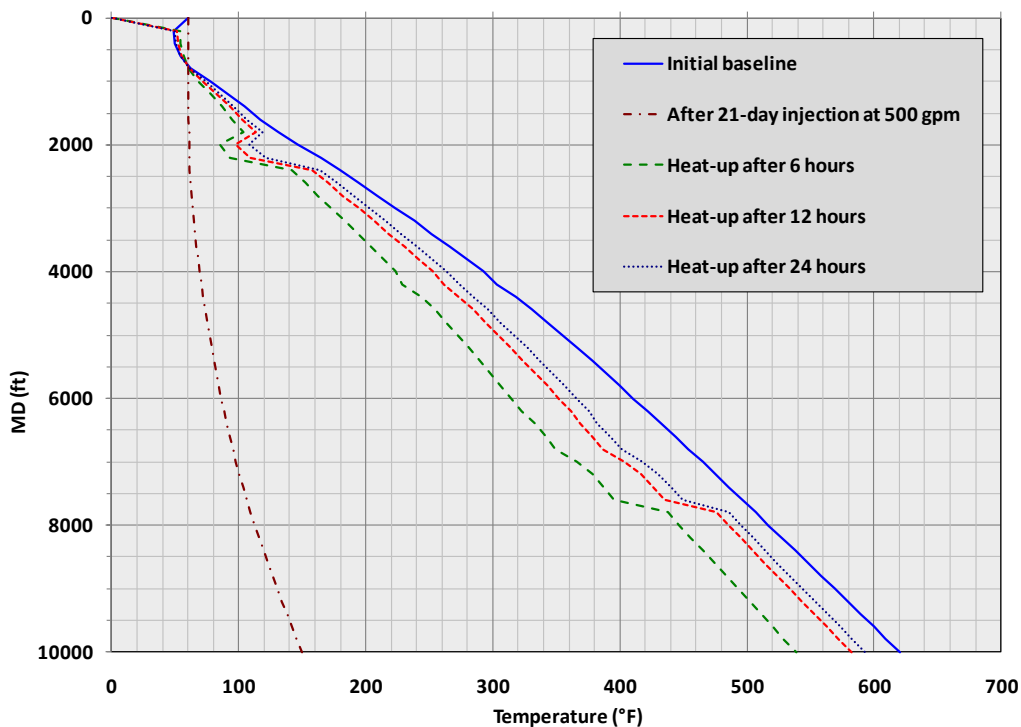
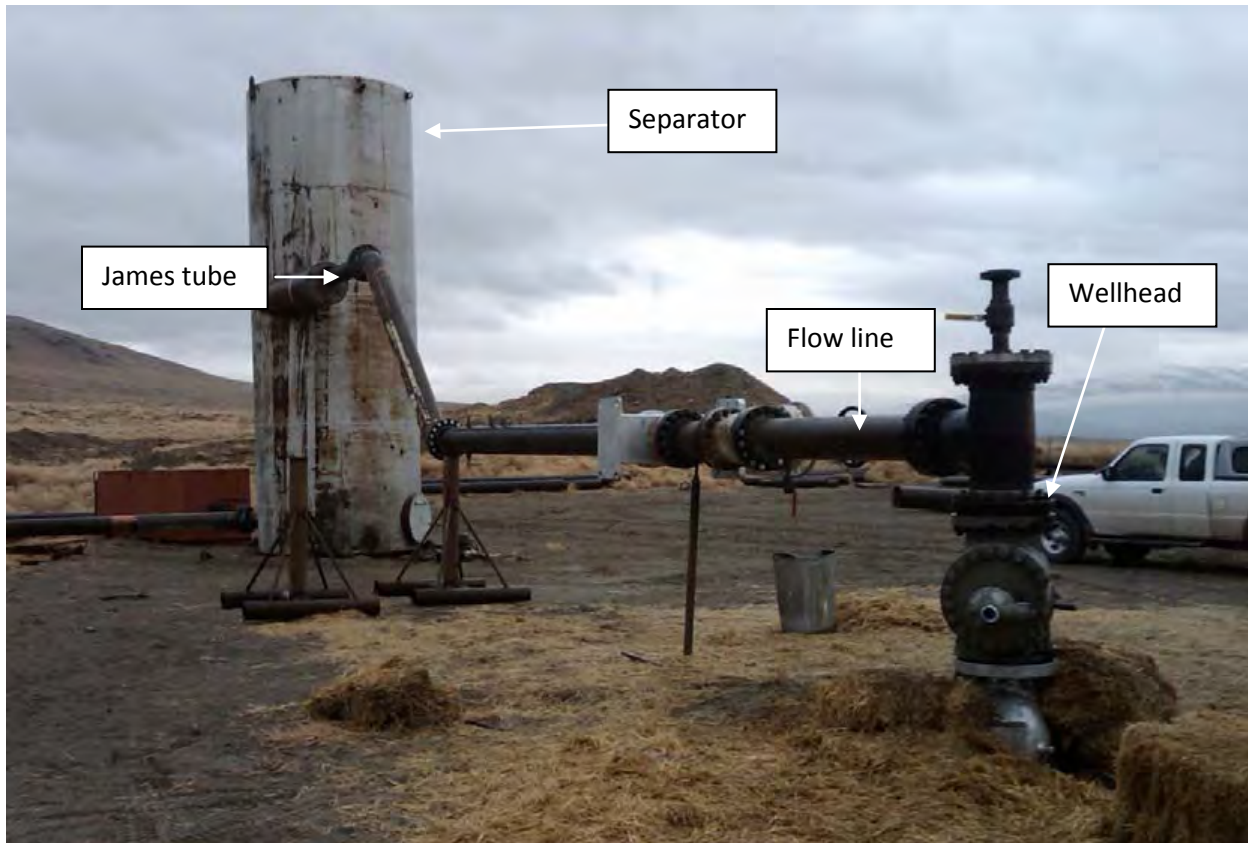


Figure 7-20. Modeled heat-up of NWG 55-29 after injecting 31 L/s (500 gpm) for 21 days.

### 7.7.2.1 FLOW TEST EQUIPMENT

The flow test configuration will include a flow tee, flow control valve, flow line with temperature and pressure monitoring instruments, a James tube with lip pressure monitoring, atmospheric separator, and weir box. Ancillary equipment will include a geochemical sampling separator and H<sub>2</sub>S monitoring and abatement equipment. The James tube and weir box assembly will be used to measure total mass flow and enthalpy. Dr. Peter Rose (Energy and Geoscience Institute at University of Utah) will supervise tracer injection, sampling and analysis. Tracer sampling will occur at a port downstream of the wing valve (see piping and instrumentation diagrams in Appendix G-2). AltaRock personnel will collect liquid and noncondensable gas samples from the sampling separator for geochemical analysis. A suite of production logs (PTS) will be run to identify flow zones and determine the relative contribution of each zone. In addition, the wellbore surveys will provide a measure of heat flow as the well warms up from the lengthy injection. After the three-day flow test, the well will be shut-in while the microseismic, hydraulic, fiber optic and flow test data is analyzed.

The flow test equipment will be connected to the wellhead on NWG 55-29 prior to and during the entire stimulation treatment. Once the well has had enough time to thermally recover (12-24 hours, see Section 7.7.2), the master valve and flow line valve will be opened, and the well will be allowed to flow through the separator and weir box and into the empty sump on Pad S-29. The water will travel from the wellhead through the flow line and control valve into the James tube assembly. Steam flow is calculated utilizing the lip pressure method and the James tube assembly (James, 1970). Three different sizes of assemblies, most likely 10 cm (4 in), 15 cm (6 in) and 20 cm (8 in), will be on site to ensure that the steam flow can be calculated accurately at different fluid flow rates. The fluid will then be separated into two phases, liquid water and steam, with an atmospheric separator (Figure 7-21). The planned separator for Newberry is 3.7 m (12 ft) in diameter. The steam discharges vertically and the water is funneled into an outlet at the bottom of the separator. From that point, the liquid flows through the weir box where the flow rate is determined by measurement of the height of the liquid flowing through a V-notch weir. Hence, the liquid and steam flow rates will be measured and calculated separately so that total fluid flow and twophase enthalpy can be calculated. The weir box discharges into the sump on Pad S-29. If the Pad S-29 sump begins to approach maximum capacity of 5300 m<sup>3</sup> (1.4 million gallons), redundant, high-head transfer pumps will be in position to transfer water from the sump on Pad S-29 to the sump on Pad S-16 through the temporary piping. For redundancy, each pump will be capable of pumping 63 L/s (1000 gpm) of water uphill to Pad S-16, which is 110 m (362 ft) higher in elevation than Pad S-29. Effectively, the two sumps will provide about 10600 m<sup>3</sup> (2.8 million gallons) of geofluid storage capacity during the flow-back operations. This is approximately 12% of the maximum estimated water usage for the 21-day stimulation.



**Figure 7-21. Wellhead, flow line, control valve, James tube and atmospheric separator used in geothermal well flow test in Nevada, similar to, but smaller than the separator to be used at Newberry.**

To initiate flow-back, the flow line valve will be opened completely, exposing the well to atmospheric pressure. For flow-back planning purposes, we assume that the well will produce no more than 50.4 kg/s (400 kph), or approximately 50.1 L/s (794 gpm). A total flow rate of 50.4 kg/s (400 kph) is equivalent to the maximum planned injection rate of 50 L/s (800 gpm) that will be used to stimulate well NWG 55-29. We estimate a single-phase reservoir production temperature of 177°C (350°F), such that the total mass flow will have an enthalpy of 748.5 J/g (321.8 BTU/lbm) and a flowing steam fraction of 16.3% at atmospheric pressure. With a steam fraction of 16.3%, we expect 42.0 L/s (665 gpm) of liquid flow and 8.2 kg/s (65 kph) steam flow. These assumptions are reasonable because the well will have significantly cooled during injection operations and will not have completely re-heated prior to flow-back. If the formation temperature is higher, the enthalpy and steam fraction will also be higher, so the liquid storage requirement will be lower. At a temperature of 279°C (535°F), the producing fluid stream would have a steam fraction of 37.6%, which equates to 31.2 L/s (495 gpm) of liquid flow and 18.9 kg/s (150 kph) steam flow. The atmospheric separator has a total mass flow capacity of 93.7 kg/s (743 kph) for 177°C (350°F) fluid production flow. The weir box, with a 25.4 cm (10 in) tall, 90° V-notch, has a liquid handling capacity of 126 L/s (2000 gpm). This capacity is significantly higher than the expected liquid flow rate range of 31.2 to 42.0 L/s (495-665 gpm). At this production rate, the initially empty Pad S-29 double-lined sump will have sufficient capacity for 35 hours of maximum liquid water flow, or about 6% of the total water volume used for stimulation, which is expected to be 91000 m<sup>3</sup> (24 million gallons) if an injection rate of 50 L/s (800 gpm) is applied for 21 days. If the well flow approaches the sump capacity, while still maintaining the required freeboard, additional produced liquid will be transferred to the double-lined sump on Pad S-16, which provides for a similar flow duration and capacity, increasing

total allowable flow time at maximum water production rates to about 70 hours, or 12% of the total stimulation water volume. Seventy hours is a sufficient duration to adequately characterize stimulation success. Because the newly created EGS reservoir is a closed system, and based on the results of flow testing conducted at Basel, it is highly unlikely that the reservoir will retain sufficient pressure to continue unassisted flow after production of 10% of the stimulation volume (Appendix A-1 Section 3.8). Another system safeguard is the flow control valve, which can be closed as necessary to reduce the production rate as the sumps are nearing capacity. Water discharged to sumps will be removed by one of several methods. Whenever possible, water will be reinjected into the EGS reservoir. If the injection well is unavailable, and prior chemical analysis of sump liquid indicates a hazardous composition, water will be spread over roads and well pads for dust control. Otherwise, water will be evaporated using spray systems positioned over the sumps. See Section 10.1 for more details on the flow-back test.

#### 7.7.2.2 GEOCHEMISTRY

The geochemistry of produced fluids will be determined by periodic sampling and analysis. Samples will be collected from two-phase flow conditions in the flow line downstream of the wellhead (upstream of the James tube and atmospheric separator), and single-phase liquid samples will be collected from the weir box. Sample frequency will vary depending on the stage and duration of flow testing. Weir box samples may be collected as often as every 15 minutes early in a flow test, with sampling frequency decreasing to twice daily after several days of flow. The Chief Geochemist will determine sampling frequency based on initial sampling and analysis results. Two-phase sample collection will be conducted according to ASTM Method E1675-04e1, *Standard Practice for Sampling Two-Phase Geothermal Fluid for Purposes of Chemical Analysis*. This method utilizes a Webre sampling separator to separate steam and gas from liquid at the flow line temperature and pressure. Downhole single-phase fluid composition can then be reconstructed by applying flash corrections based on enthalpy determined by the James method. Single-phase liquid samples will be collected from the weir box using simple grab methods. Some analytes will be determined by field analysis, including but not limited to pH, conductivity, redox, alkalinity and hydrogen sulfide (H<sub>2</sub>S). Gas analysis will include but not be limited to the typical geothermal analytes CO<sub>2</sub>, H<sub>2</sub>S, H<sub>2</sub>, N<sub>2</sub>, O<sub>2</sub>, Ar, CH<sub>4</sub>, Hg and He. Liquid analysis will include but not be limited to the typical geothermal analytes Na, K, Ca, Mg, SiO<sub>2</sub>, Sr, Li, As, Hg, Fe, Mn, Cl, F, B, NH<sub>4</sub>, H<sub>2</sub>S, TDS, TSS and laboratory duplication of the field analytes listed above. Date, time, location, temperature, pressure and sampler ID will be recorded for each sample. Sample analyses will be conducted according to EPA Method SW-846. Laboratory analysis will be conducted by EPA and state-certified laboratories.

#### 7.7.2.3 TRACER SAMPLING EQUIPMENT

Samples will be collected via a sampling separator that will be connected to the flow line downstream from the wellhead. Liquid phase samples will be collected from the weir box. The samples will be sent to a laboratory for analysis by either liquid or ion chromatography.

### 7.8 OPERATING PROCEDURES

The following procedure includes all well testing that will be performed during the stimulation treatments. The procedures will be posted in the control room on Pad S-29 during stimulation and testing.

#### 7.8.1 GENERAL GUIDELINES FOR WORK ON WELL PADS S-16 AND S-29

1. All visitors and personnel on site are required to wear Personal Protective Equipment including hard hats, safety glasses, ear protection and steel-toed boots. If anyone arrives on site without the appropriate equipment, that person may be asked to leave.

2. Under no circumstances should the geothermal wells (NWG 55-29 and NWG 46-16) be opened without consent from AltaRock personnel.
3. All well survey operations must be accomplished with adequate wellhead pressure control, (i.e., lubricator assembly).
4. The well pads are located on USFS land and are accessed through USFS gates. Keys must be checked out from the Davenport office in Bend, OR. Maps and directions to the site are available from their office as well. All gates are to remain closed and locked at all times.
5. Maintain safe speed on all paved and unpaved roadways.
6. All vehicles on location must be parked upwind of the wellhead, if possible, and pointing toward the exit for quick evacuation in case of emergency. A windsock is installed on both pads so that the wind direction can be known.
7. At least one representative from each company on site must have a functioning 4-gas meter or H<sub>2</sub>S alarm on their person when working on the Newberry pads.
8. In case of an emergency, all personnel must immediately make their way to a pre-designated, upwind location for evacuation (this area should be reviewed during daily safety meetings).
9. The well pads are surrounded by heavily wooded USFS land. Personnel are not authorized to venture off the roads or pads by foot or vehicle. Personnel should remain within the designated areas, unless an emergency dictates an alternate evacuation route through unmarked US Forest Service land.
10. Personnel should remain vigilant about wildlife in the area.
11. The water well pumps can only be started into an open-discharge (into a tank, permeable well or an atmospheric sump). They cannot be started against a “no-flow” barrier like a closed valve, which would cause the motors to burn-up.
12. The area around the geothermal wellheads is off-limits except to essential personnel who are actively working in the well.
13. High pressures are expected during the injection operations in well NWG 55-29. Maximum stimulation pressure is 20.7 MPa (3000 psi). After injection begins, a circle measuring 6.1 m (20 ft) in radius around well NWG 55-29 will be off-limits to all but essential personnel.
14. Remain vigilant during night operations. These sites have been frequented by vandals seeking to destroy equipment.

### ***7.8.2 EMERGENCY RESPONSE PLAN***

Call 911 for immediate aid. Vehicles should be parked upwind of the wellhead and pointed toward the pad exit for quick evacuation. All personnel should meet at the designated safe area in the event of an emergency. If an individual sustains a life-threatening injury, then 911 should be called and LifeFlight requested. The GPS coordinates below are provided for all emergency responders. All emergencies, leaks, tank or sump overflows and equipment failures should be reported IMMEDIATELY to the AltaRock Energy on-site supervisor. A contact list will be available on site (Table 7-12).

#### **GPS Coordinates for emergency vehicles and Life Flight**

43°43'34" N


121°18'57" W



**Hospital**

The closest and largest hospital in the area is St. Charles Hospital located at 2500 NE Neff Road, Bend, OR (approximately 48 km (30 miles) north of La Pine).

**Driving directions to 2500 NE Neff Rd, Bend, OR 97701 - 35.6 mi – about 1 hour 3 mins**

1. Head west on Paulina-East Lake Rd toward Nat for Dev Rd 9736 for 6.9 miles
2. Continue straight onto Nat for Dev Rd 2120 for 1.8 miles
3. Continue onto Paulina Lake Rd for 1.4 miles
4. Turn right at US-97N/The Dalles-California Hwy and travel 23.4 miles
5. Turn right at NE Greenwood Ave and travel 0.4 miles
6. Turn left at NE 8<sup>th</sup> St and travel 0.4 miles
7. Take the 3<sup>rd</sup> right onto NE Penn Ave in 0.3 miles
8. Continue on NE Neff Rd for 1.2 miles
9. Arrive at St. Charles Hospital, 2500 NE Neff Road, Bend, OR 

**Fire** - The La Pine Rural Fire Protection District, located at 51590 Huntington Road, La Pine, OR, can be contacted via phone at 541-536-2935.

**Police** - Deschutes County Sheriff’s office is located at 51340 Highway 97 #G, La Pine, OR. Their phone number is (541) 536-1758.

**HazMat** - The Hazardous Materials Response Team for Deschutes County is located at City of Redmond Fire: 341 West Dogwood, Redmond, OR.

**Potential Hazards for the Operation:**

- Vandals and unauthorized personnel
- Aerial work (boom lifts, ladders, etc.) above 1.8 m (6 ft) off the ground
- Heavy manual lifting
- Automobiles and heavy machinery
- Wireline wines
- Cranes and crane trucks
- Hydrogen sulfide and carbon monoxide gases
- High pressures (equipment will be tested to 24.1 MPa [3500 psi])
- Wildlife
- Hazardous driving conditions

**Table 7-12. Responsibilities and contact information.**

Contact Name	Telephone Number	Responsibility
Laura Nofziger	206-604-5145	AltaRock Energy, Production Engineer, contact for questions about the procedure and well operations. Onsite company representative during stimulation.
Will Osborn	760-604-0701	AltaRock Energy, Project Manager, onsite company representative during stimulation.

### 7.8.3 STIMULATION PROCEDURE

The detailed stimulation procedure as it will be provided to affected parties and associated vendors is presented below.

#### **MAXIMUM WELLHEAD PRESSURE 20.7 MPa (3000 PSIG)**

#### **INDUCED SEISMICITY MITIGATION PLAN (APPENDIX D-1) MUST BE POSTED IN THE CONTROL ROOM AND FOLLOWED THROUGHOUT THE STIMULATION PROCEDURE**

The following steps must be followed:

1. Ensure that both sumps on Pad S-29 and Pad S-16 are completely dry. If not, take samples of the water from both sumps and have it analyzed. Once the benign nature of the water has been confirmed by laboratory testing, obtain regulatory permission to remove the water as per agency approval.
2. Rent a small trash pump and sprinklers for both sites and dry out the sumps by spraying the water onto the pads.
3. Rent and install eighteen 22000 gallon<sup>18</sup> water storage tanks on Pad S-29. Manifold the tanks together with rental hoses and ensure that each tank can be isolated by a valve, if necessary.
4. The existing groundwater wells, one on Pad S-29 and one on Pad S-16, will flow directly into the tanks via above-ground, temporary piping. Rent and install temporary 6 in aluminum piping with Victaulic fittings from Pad S-16 to Pad S-29. Attach the discharge line from the Pad S-16 water well to the 6 in piping in order to transport water from that well to the storage tanks on Pad S-29. The elevation drop is 362 ft from Pad S-16 to Pad S-29. Ensure that the magnetic flow meter, downhole pressure transducer, valve and control panel are installed on the Pad S-16 water well and functioning properly.
5. Install a tee, valving and a second, open-ended discharge line that empties into the sump at Pad S-16.
6. The 6 in temporary piping should include a tee on Pad S-29. One end of the line should be connected to a transfer pump with a suction line from the sump. Install a second, redundant, transfer pump in the same location. Both pumps should be capable of transferring warm water at 1000 gpm uphill to Pad S-16 sump.
7. The second part of the 6 in piping should be installed to the suction side of the storage tank manifold.
8. Install temporary 6 in piping from the Pad S-29 water well discharge line to the suction side of the storage tank manifold. Ensure that the water well magnetic flow meter, valve, control panel and downhole pressure transducer are installed and functioning properly.
9. Rent and set two light plant generators for Pad S-16 and three for Pad S-29.
10. Rent one large generator to power the downhole pump in the Pad S-16 water well, which is 250 HP. A Caterpillar XQ300 or equivalent is required.
11. Rent generator to power the downhole pump in the Pad S-29 water well, which is 100 HP. A Caterpillar XQ100 or equivalent is required.
12. Program the variable frequency drive (VFD) on the Pad S-29 water well to 50% output. Turn on pump and fill all eighteen storage tanks with water.

---

<sup>18</sup> To prevent confusion with US vendors, only English units are used in the procedure.

13. Set and install flow-back equipment. The flow-back line should connect to one of the wing valves. Install valve, gauges, sampling ports, sampling separator, James tube assembly, atmospheric separator and weir box. Bleed off pressure from wellhead through the wing valve through the flow-back equipment and into the sump on pad S-29.
  14. Once the well is dead, remove the existing master valve (currently 12 in, 900# series) and replace with a 1200# series valve, or remove the master valve and install a frac stack from Stinger Wellhead Protection (or similar vendor) on top of the 13-3/8 in flange.
  15. Move in and rig up the pumping services company. The pumps must be manifolded together on the suction and discharge sides. Valves should be positioned to allow each pump to be isolated for maintenance and repair, when necessary. The pumps must be capable of flow rates from 10-800 gpm at discharge pressures from 750-3000 psi with at least 50% redundancy.
  16. Set and rig up a separate discharge line from the batch mixer to the suction side of one of the triplex pumps. The water line from the storage tanks should have a tee and a valve that allows flow through the batch mixer when we are mixing diverter. Otherwise, the batch mixer will be bypassed.
  17. The discharge lines and manifold must be rated to at least 3500 psi. Install the hammer union, steel pipe, in-line flow meter, pressure transmitter, pressure dial indicator, temperature transmitter and temperature dial indicator on the discharge side of the pumps. All digital instrumentation should also have a non-digital back-up instrument installed (pressure gauge, dial thermometer, etc.). Connect the discharge line to the wing valve on the wellhead or the frac stack.
  18. Connect all surface instrumentation to the data logger in the control room and set up all electrical connections to the monitoring van.
  19. Once all of the equipment is positioned and installed, ensure that the master valve on the wellhead or the stack is closed.
  20. Flag and tape off the high-pressure equipment and the wellhead.
  21. Conduct safety meeting. Safety meeting should:
    - Identify areas that are off limit to personnel.
    - Review the maximum operating pressure of 3000 psi.
    - Reiterate that personnel should continuously monitor for line leaks, equipment malfunction, operating pressure, hazardous gases and induced seismicity to ensure a safe operation.
    - Review evacuation procedures, wind sock location and request that all personnel back-in their vehicles, upwind of the equipment, if possible.
    - Designate evacuation vehicles.
    - Review 911 and nearest hospital information.
    - Review PPE requirements.
  22. Fill pumps and lines with water and pressure test to 3500 psi, 500 psi above maximum treatment pressure, for 10 minutes. Check for line leaks and failures. Replace any bad equipment and tighten all connections.
  23. Bleed off pressure. Move in and rig up Schlumberger fiber optic monitoring equipment and truck. Deploy pressure gauge and cable into well NWG 55-29 through the frac stack. Install surface data acquisition unit. Ensure that the cable is sending viable data.
  24. Prepare to begin pumping water down the casing with the high pressure, low rate pump.
- Conduct step-rate injection test as outlined in Table 7-13.

**Table 7-13. Step-Rate test flow rates and estimated pressures.**

<b>Injection Rate Steps (gpm)<sup>1</sup></b>	<b>Predicted Wellhead Pressure (psig)</b>	<b>Projected Injectivity Index (gpm/psi)</b>
25	1275	0.03
50	2000	0.03
75	2050	0.50
150	2200	0.50
225	2350	0.50
300	2500	0.50
375	2650	0.50
450	2800	0.50
500	2900	0.50

<sup>1</sup> The flow rate will be held at each rate for 2 hours or until the pressure stabilizes, whichever is longer. Flow rates will not be increased if pressures will exceed the maximum surface treating pressure of 3000 psig or if the microseismic response exceeds the triggers (see Section 5).

25. Pump the steps for a minimum of two hours each or until the pressures stabilizes, whichever is longer. Step back down at the same rates and time steps. Shut down pumps and monitor pressure decay until 80-90% of recovery. Rates to be adjusted as necessary so that pressures do not exceed formation breakdown (keep rates below necessary maximum). Calculate permeability, injectivity and skin effects from data.
26. Begin pumping Stage 1 of the stimulation treatment. The microseismic network will provide real-time data of the seismic events so the duration and rate of the treatment can be adjusted 'on-the-fly' to optimize the fracture network geometry. The fiber optic data will be monitored to identify fluid exit points.
27. Conduct daily meetings in the morning with essential staff to discuss the previous day events, current day plans and any modifications that are necessary, as well as any safety concerns. Staff will rotate on 12-hour schedules.
28. Rig up necessary tracer equipment. Within six hours before the end of each stimulation phase, inject a solution containing a pair of tracers as a pulse into NWG 55-29 (Section 7.7.1.6). This procedure will be repeated for each stimulation and diversion event.
29. As the fracture radius approaches 500 m (1640 ft), increase injection rate to 800 gpm. Inject at 800 gpm for at least two hours.
30. Decrease the injection rate to below 400 gpm, and prepare to pump diverter material. Mix diverters in batch mixer. After diverter mixing is complete, open the appropriate valves on the discharge side of the batch mixer and pump the diverter slurry down hole. Displace the diverter with fresh water. Which diverter is used, when it is used, and how much is used are decisions that will be made during the stimulation treatment based on how the well responds, how the fractures grow, at what depth the fractures are formed, etc. However, the general guiding principles for the diverter treatments will be as follows:
  - If the first stimulated fracture extends from the wellbore at a depth of 9600 ft (depth at which initial injection testing took fluid) the diverter material that will be used to seal it off will be a high temperature diverter material, like AltaVert 300 or AltaVert 301 (Appendix G-3). This is due

to the fact that the second set of fractures will most likely open above this first stimulation zone. In this scenario, cooling of the wellbore at 9600 ft will stop and the well will heat back up rapidly to the geostatic temperature of over 316°C (600°F). Only the high temperature diverter materials are designed to hold up for extended periods of time at this temperature. The lower temperature diverter materials would degrade rapidly if they were used and would not provide the needed sealing of the fracture for the remainder of the stimulation treatments. If the diverters fail to seal at these high temperatures, prepare to sand back well to top of fractured interval.

- If the first stimulated fracture zone extends from the wellbore at a depth less than 9600 ft (depth at which initial injection testing took fluid), the diverter material that will be used to seal it off will be a lower temperature diverter material, like BioVert. If this is the case, stimulation water will continue to flow past the sealed fracture, help keep the temperature of the diverter material relatively low, and prevent it from premature degradation or dissolution until after stimulation has been completed and the well is allowed to heat back up to geostatic temperatures.
  - If a given fracture set is only partially sealed by one diverter treatment, a second treatment of equal or larger volume will be pumped to seal the remainder of the fracture set.
31. Monitor fiber optic temperature for depth location of new fractures. Observe microseismic data to monitor the growth of new fractures.
  32. After diversion has been confirmed, prepare to conduct a step-rate test on the second zone. Conduct step-rate injection test on second zone. Pump the steps outlined in



33. Table 7-13 for a minimum of two hours each or until the pressures stabilizes, whichever is longer. Calculate injectivity.
34. Maintain rate at final step rate and pump Stage 2. Do NOT step-down or shut-down the pumps arbitrarily because the diverters require cold water injection to remain intact.
35. Repeat tracer procedure as outlined in Step 28 using different tracer pairs.
36. As the target fracture radius of the second zone approaches 500 m (1640 ft), increase injection rate to 800 gpm. Inject at 800 gpm for at least two hours.
37. Begin pumping water at a slower rate, approximately 400-500 gpm, and prepare to pump diverter material. Mix diverters in batch mixer. Once the diverter is mixed, open the necessary valves on the discharge side of the batch mixer and pump the diverter down hole. Displace the diverter with fresh water. The general guiding principles for the diverter treatments will follow those outlined in Step 30.
38. Monitor fiber optic temperature for depth location of new fractures. Observe microseismic data to monitor the growth of the fracture network.
39. After diversion has been confirmed, prepare to conduct a step-rate test on the third zone. Conduct step-rate injection test on second zone. Pump the steps outlined in step 25 for a minimum of two hours each or until the pressures stabilizes, whichever is longer. Calculate injectivity.
40. Maintain rate at final step rate and pump Stage 3. Do NOT step-down or shut-down the pumps arbitrarily since the diverters require cold water injection to remain intact.
41. Repeat tracer procedure as outlined in Steps 28 and 34 using different tracer pairs.
42. As the third stimulation zone approaches the target fracture radius of 500 m (1640 ft), increase injection rate to 800 gpm. Inject at 800 gpm for at least two hours.
43. After two hours at 800 gpm, begin soft shut-in by conducting another step-down test following the rates in step 25. Ensure that the tanks are drained during the final step-down testing.
44. Shut-in water wells. Monitor their recovery with downhole pressure data.
45. After the final step of 10 gpm, shut-down all pumps and monitor pressure decay/leak-off while watching the fiber-optic temperature readings for a minimum of one hour.
46. Pull out of hole with fiber optic monitoring system. Rig down, move off Schlumberger fiber optic. The control line and fiber optic cable are to be stored for AltaRock by Schlumberger in their Bakersfield warehouse.
47. Rig down, move off stimulation company and equipment. Clean eighteen water storage tanks and release. Release all temporary piping and pump equipment.
48. Prepare to flow well NWG 55-29. Once the well has heated up and has sufficient energy to flow (not less than 3 hours but not more than 24 hours), open the surface valve to absolute open flow. A compressor may be utilized to push air down the well and further energize the system, if necessary.
49. Conduct safety meeting with all personnel involved at the site. Ensure that all personnel are familiar with the safety supervisor on site, outfitted with appropriate personnel protective equipment, and are aware of safety requirements and escape routes.
50. Open wellhead valve and flow line valve. Inspect wellhead equipment for leaks upstream of flow control valve.
51. Slowly open the throttle valve. Inspect flow line equipment for leaks.
52. Allow well flow to stabilize at a low rate.
53. Record James tube lip pressure and weir box liquid level.

54. Calculate total mass flow and enthalpy. Ensure that total flow does not exceed separator design maximum flow rate.
55. Measure H<sub>2</sub>S concentration and mass rate, and initiate H<sub>2</sub>S abatement if rate exceeds 5 lb/hr.
56. Continue to slowly open throttle valve to maximum well capability or maximum separator design flow rate, whichever is less.
57. Allow well flow to stabilize.
58. On an hourly basis, record all flow test data, including wellhead pressure and temperature, throttle valve position, H<sub>2</sub>S concentration, abatement chemical injection rates, particulate scrub water rate, flow line pressure and temperature, James tube lip pressure, weir box liquid level, water tank levels, pump discharge pressure, and pump flow rate.
59. Conduct step-rate flow test. Collect data at five separate flow rates for the same time-step (at least two hours at each rate) to build a productivity curve.
60. Collect fluid samples for tracer testing and geochemical analysis according to the following schedule (Table 7-14).

**Table 7-14. Flow-back test sampling schedule.**

Sample Type	Sampling Location	Day 1	Day 2	Day 3
Tracers	Weir box	Every 15min until stable flow, every 1 hour after that	Every 6 hours	Every 8 hours
Geochemical – basic analysis	Weir box	Every 15min until stable flow, every 1 hour after that	Every 6 hours	Every 8 hours
Geochemical – full analysis	Sampling separator	Every 6 hours	Every 8 hours	Every 12 hours

61. Shut-in well after flowback period. Rig down flowback equipment.
62. Rig down frac stack, if used, and release.
63. Secure both water wells and well NWG 55-29 by placing locked containers over them.

## 7.9 EGS RESERVOIR CHARACTERIZATION

During the stimulation, data will be collected and monitored in real-time to characterize the EGS reservoir as it grows. Our data streams include microseismicity, downhole fiber optic temperature and pressure surveys, wellhead temperature, wellhead pressure, and injection and flow rates as well as geochemical analyses.

### 7.9.1 MICROSEISMIC DATA

The collection, analysis and procedures involving microseismicity are detailed in the ISMP (Appendix A-1).

### 7.9.2 DOWNHOLE TEMPERATURE AND PRESSURE

DTS will be used to continuously monitor downhole temperature during stimulation (Section 7.7.1.3). Downhole pressure and temperature monitoring via DTS will allow us to identify open fracture paths at the borehole face in realtime. This data will also provide essential information about the depth of fracture initiation and the success or failure of the diverter materials in sealing open fractures. The fluid initiation point and the corresponding temperature at that depth is a controlling factor on the type of diverter to be used. Additionally, the temperature and pressure at a given depth will provide evidence that the diverter has successfully sealed off open fractures at the wellbore face.

### **7.9.3 HYDRAULIC DATA**

The stimulation injection rate will be monitored through a continuous-reading magnetic flow meter installed in the discharge side of the pumps. The injection rate is a primary tool in controlling wellbore pressure and stimulation duration. Wellhead pressure will also be recorded continuously. Maximum wellhead pressure will be strictly limited to 20.7 MPa (3000 psi). Wellhead pressure will be closely monitored to avoid any rapid increase. If pressure is rising at an undesirable rate, a decrease in injection flow rate will be applied. Injection fluid temperature will be continuously recorded. Dial thermometers and pressure gauges will also be in place as a redundancy measure to provide data backup to digital instrumentation. These values will be manually recorded at regular intervals by site personnel. Spare indicators will also be on-site in the data trailer in case of instrument failure.

The water wells on Pad 29 and Pad 16 will also be monitored using surface instrumentation. Each well is equipped with an AG-2000 magnetic flow meter with data output capability installed in the discharge line to measure flow rate. The magmeter records rate and total volume pumped. Downhole pressure transducers are installed in both water wells. The transducers and magmeters will supply data to the logger in the trailer so that water level and rate can be continuously monitored and recorded. Additionally, the downhole pressure and water level in Water Well #2 will be monitored remotely using a pressure transmitter and data logger.

### **7.9.4 TRACERS**

Near the end of each stimulation phase (within six hours of pump shut-down or diversion), a solution containing a pair of tracer compounds will be injected as a pulse into NWG 55-29 (Section 7.7.1.6). After a brief shut-in period of at least 3 hours but not exceeding 24 hours, the well will be induced to flow. The produced fluid will be sampled and analyzed for the tracers. From an analysis of the reactive and conservative tracers, the near-wellbore fracture surface area will be determined.

### **7.9.5 GEOCHEMICAL DATA**

Numerous samples collected and analyzed from the Pad S-16 and Pad S-29 water wells prior to stimulation will provide a baseline for composition of the stimulation fluid. Additionally, a monitoring plan recommended by Kleinfelder will be implemented to monitor groundwater geochemistry at a down-gradient site (Appendix B-5). Although these analyses will not be available during the stimulation operation, the results will subsequently verify that no aquifer contamination has occurred. During the flow-back test of NWG 55-29, geofluids, including liquid, steam and noncondensable gas will be sampled and analyzed. Some samples, which are collected more frequently, will be field-tested for pH and conductivity. Other less frequent samples will be collected and shipped to a laboratory for comprehensive chemical analysis. Geofluid composition will aid in determining the type and extent of water/rock reaction occurring as the fluids reside in the geothermal reservoir. Corrosion rates will also be measured in surface piping. If elevated corrosion rates are detected, a corrosion mitigation program may be implemented in the injection or production wells, potentially including enhanced casing metallurgy or application of filming amine corrosion inhibitors. The sampling will be conducted as outlined in Table 7-14 over the three-day flow-back test.

## **7.10 PRODUCTION WELL STIMULATION**

After stimulation and testing of NWG 55-29, a second stage-gate review will be conducted. If the results of the stimulation and testing are favorable, two production wells will be drilled to intersect each side of the created fracture network (See Section 9). After the drilling of each production well, seven-day connectivity tests involving the injection well and each production well will be conducted to determine

the system productivity, circulating temperature, reservoir transmissivity, skin, and fluid loss. Tracers will be metered into the injection well for sampling at the production well. Breakthrough times will be recorded to ensure that short-circuiting is not occurring. In addition, the concentration of conservative tracers that were injected during the stimulation of the injection well will be measured to determine if the production well is in connection with each of the discrete fracture networks created during stimulation. Injecting and producing PTS surveys will be carried out in both wells to identify flow zones, the percentage contribution of each zone to the total flow, and producing and injecting wellbore temperature profiles. The production log data will be used for numerical modeling and reservoir management.

If the system is found to have too much skin damage or too little transmissivity, a stimulation treatment will be designed for the production well. Building on experience from the Soultz project, a dual stimulation or 'focused' stimulation treatment may be applied to overcome pressure barriers between the two wells and increase connectivity to achieve a single-well production rate of 75 kg/s (595 kph). At Soultz, the microseismic data identified a flow barrier between wells GPK3 and GPK4 that was not overcome during stimulation treatments of GPK4 (Baria et al., 2006). The Soultz team utilized brine, chemical treatments and a focused stimulation to enhance transmissivity (Genter et al., 2009; Nami et al., 2008). To enhance the connection between NWG 55-29 and the production well(s) at Newberry, injection pumps will be installed on the injection and production well. The water supply system will be upgraded to include storage tanks with filters and level controls, transfer pumps, piping, control valves and flow meters. Water will be injected under pressure simultaneously into NWG 55-29 and the production well in an attempt to enhance connectivity and overcome any pressure barriers. The microseismic network will continue to provide information about the size, shape and growth direction of the created reservoir during the focused stimulation. Subsequent production logging, flow testing and tracer testing, and seismicity will be used to quantify the results of this additional stimulation.

## 7.11 CONTINGENCY AND RISK MITIGATION

The following risks associated with the stimulation treatment of NWG 55-29 have been considered and mitigated.

1. MSA not sensitive enough to detect microseismic events.

RISK: MSA is not sensitive enough to detect microseismic events caused by hydroshearing, preventing visualization of the treatment.

MITIGATION: All other stimulation treatments at EGS projects worldwide have been visualized with installed seismic networks. Even at the Fenton Hill HDR project, which occurred some 30 years ago, the seismic network was able to visualize events of  $M < -0.5$ . The design of our network was recommended by Foulger Consulting, who has extensive expertise in visualizing induced seismicity from hydroshearing treatments. Calibration of the Phase I surface-deployed MSA suggests a detection limit of  $M 0.5$ . The Phase II MSA will include numerous borehole seismometer installations, which are expected to significantly enhance detection compared to the Phase I MSA (only surface sensors).

2. Stress model has underestimated coefficient of sliding friction.

RISK: Underestimation of rock strength prevents results in failure to induce shear at  $\leq 20.7$  MPa ( $\leq 3000$  psi) WHP. This outcome is highly unlikely because 20.7 MPa (3000 psi) WHP and a warm column of fresh water at 9.0 MPa/km (0.40 psi/ft) will exert 35.1 MPa (5085 psi) of pressure at a depth of 1970 m (6462 ft) (the top of the open-hole interval). This amount of pressure equates

to a gradient of 17.8 MPa/km (0.79 psi/ft). Most intact rock fails well below 17.0 MPa/km (0.75 psi/ft), so a maximum treatment pressure of 20.7 MPa (3000 psi) at surface should suffice.

MITIGATION: Mobilize drill rig and install a packer at the top of the 9-5/8 in production casing. Utilizing a drill string and packer combination, the 13-3/8 in casing, which is the weakest section of the wellbore, would be isolated from the stimulation fluid and pressure. The burst pressure of 9-5/8 in, 53.5 lb/ft, L-80 casing is 54.7 MPa (7930 psi), which would allow much higher pressures than the currently exposed 13-3/8 in casing to initiate hydroshearing.

3. Tensile failure occurs near the casing shoe.

RISK: Temperature monitoring indicates that a fracture has opened or been created within 152 m (500 ft) of the casing shoe before deeper zones have been stimulated. As discussed above, distinguishing between tensile and shear failure during the stimulation will be difficult. Hence, any fractures forming within 152 m (500 ft) of the casing shoe will be assumed to be tensile in nature because a tensile crack is most likely to occur at the top of the open-hole interval. Fractures in this zone will also be undesirable from a producing temperature standpoint and will need to be sealed.

MITIGATION: Stimulation injection rates will be decreased in an attempt to lower bottomhole pressure and reduce further shallow fracturing. If the rate decrease does not reduce fluid flow into the fractures near the casing shoe, diverters will be used in an attempt to seal the shallow zones. The diverters have shown the capability of withstanding 12.4 MPa (1800 psi) of differential pressure in the laboratory, so they should be reliable in the field to pack off a tensile crack. Unfortunately, the diverter seal won't prevent other tensile cracks from developing near the newly sealed fracture; hence, decreases in rate may be the only way to control fracturing near the shoe if it develops. Finally, if tensile failure is occurring in the shallow sections of the open hole and we are unable to divert any significant distance away from the original fractures, the stimulation may have to be postponed until a rig can be mobilized and mechanical isolation devices such as scab liner, packers and drill pipe can be used to divide the open hole interval into separate stimulation zones.

4. Development of a 'short-circuit'.

RISK: The creation of a high permeability fracture path from injection to production well, or a 'short-circuit', is undesirable because the injected water will not have enough residence time in the reservoir to be sufficiently heated before reaching the adjacent production well, resulting in rapid thermal breakthrough and low production enthalpy. A short-circuit could be the result of the formation of tensile cracks, or they could be caused by intersecting an existing fault-like structure. If microseismic data shows that reservoir growth is following a linear structure, as was the case in Soultz GPK3, a short-circuit may be indicated. Also, if the temperature data indicates a significant fluid path with little associated microseismicity, a tensile crack could be growing at that depth.

MITIGATION: Use diverters to seal off the flow path and divert the stimulation treatment to another zone. The fiber optic and subsequent microseismic data will indicate whether the diverter application is successful.

5. Diverters fail to effectively seal fracture network.

RISK: Diverters may fail to block fracture networks due to rapid degradation of diverter due to excessive temperature, or due to the diverter particle size being too large or too small.



MITIGATION: If premature degradation occurs, a diverter with higher temperature rating will be applied. Multiple diverters will be on-hand to handle the wide range of temperatures that we expect to encounter during the treatment. If high temperature diverters fail to effectively block fractures, the well will be sanded back so that the upper intervals can be stimulated. If the diverter particle size does not effectively block the fracture set, a diverter of a smaller or larger size will be on hand to cover a wide range of fracture apertures. Lab testing is currently underway to develop the ideal particle size distribution for the higher temperature diversion chemicals.

6. Pump or related equipment fails during stimulation.

RISK: The failure of stimulation pumps, transfer pumps, valves, piping or instrumentation could severely delay the stimulation process.

MITIGATION: The AltaRock team has extensive experience in mechanical process design and operation, and all process designs will be reviewed by a licensed mechanical engineer (Appendix G-2). Critical equipment will include appropriate levels of redundancy. Horsepower redundancy will be in place to handle any unanticipated equipment failures. At least one extra stimulation pump will be on-site as a back-up to the triplex units. Additionally, the transfer pump from the Pad S-29 sump to the Pad S-16 sump will have a back-up installed and at-the-ready in case of mechanical failure. Pumps will be rotated in and out of service for scheduled maintenance, including oil changes, to ensure that they can last the duration of the stimulation and flow-back. Mechanics will be on-call during the entire stimulation event. Spare parts, such as oil filters and fluid ends, will be on location.

7. Insufficient sump capacity.

RISK: If induced seismicity mitigation requires relief of reservoir pressure by flowing the well, or the liquid production rate is relatively high during flow-back testing, the Pad S-29 sump could be filled to capacity.

MITIGATION: The sumps on Pad S-29 and Pad S-16 will remain dry during stimulation. A battery of eighteen tanks will be used to provide storage for 1500 m<sup>3</sup> (396000 gallons) of stimulation water. NWG 55-29 will flow directly into the Pad S-29 sump, which has 5300 m<sup>3</sup> (1.4 million gallons) of storage capacity. If the S-29 sump reaches capacity, a transfer pump capable with 63 L/s (1000 gpm) capacity will be used to transfer water directly to the Pad S-16 sump. The sump at Pad S-16 will also be dry, providing the flow test with another 5300 m<sup>3</sup> (1.4 million gallons) of storage capacity. If both sumps are approaching capacity, the well can also be throttled or closed completely using the flow control and master valves. At the maximum expected liquid production rate, the initially empty Pad S-29 and Pad 16 double-lined sumps will have sufficient capacity for 70 hours of maximum liquid water flow, or about 12% of the total water volume used for stimulation. Because the newly created reservoir will have some far-field leak-off and since the intersection of a geopressured reservoir is not likely, the reservoir will not retain sufficient pressure to continue unassisted flow at high rates for very long. The system will be deflated enough after this 12% volume reduction to mitigate the risk of damaging seismicity in the far-field. Seventy hours of flow-back time is a sufficient duration to adequately characterize stimulation success. See Section 7.7.2.1 above, Appendix A-1 and Section 3.8 for more details.

8. Casing or wellbore failure.

RISK: Exceeding casing design limits could result in breach or failure of casing. The weakest point in the wellbore is at 1277 m (4189 ft), which is the deepest point at which the 13-3/8 in casing is exposed.

MITIGATION: The maximum surface pressure for the stimulation treatment will be strictly limited to 20.7 MPa (3000 psi), 3.9 MPa (566 psi) less than the API-rated burst pressure 13-3/8 in, 72 lb/ft, L-80 casing (assuming a freshwater gradient of 9.8 MPa/km [0.433 psi/ft]). The surface discharge pressure will be monitored continuously at the Demonstration site. A daily safety and data review meeting will reiterate the maximum surface pressure to all personnel.

9. Open-hole collapse or bridging.

RISK: Thermal cycling can cause the open-hole well bore to fracture and spall, causing a blockage in the well. If the open-hole has collapsed or bridged, it would not be possible to effectively continue stimulation treatment, and would prevent the removal or installation of wireline survey equipment.

MITIGATION: Depending on the depth and severity of the collapse, a coil tubing rig could be mobilized to clean out the well to total depth to resume stimulation.

10. Nearby residents are disturbed by seismicity.

RISK: Induced seismicity could result in shaking that is felt in the NNVM and surrounding communities. Shaking, though not dangerous or damaging, could disturb and cause concern to some residents in surrounding home sites.

MITIGATION: Detailed plans to educate and inform stakeholders, especially visitors and local residents, are discussed in detail in Appendix A-1.

11. Vertical reservoir growth above 1829 m (6000 ft) depth.

RISK: The reservoir grows vertically such that the top of the reservoir is shallower than 1829 m (6000 ft) below the surface, as indicated by the microseismic data. In order to maintain an approximately 1524 m (5000 ft) buffer between the top of the stimulation zone and the bottom of the groundwater-bearing intervals, the top of the reservoir will not be allowed to grow shallower than 1829 m (6000 ft).

MITIGATION: Use diverters to seal off the flow path and divert the stimulation treatment to a deeper zone. The fiber optic and subsequent microseismic data will tell us if the diverters have been successful. This mitigation is discussed in detail in Appendix A-1.

12. Horizontal reservoir growth to the east.

RISK: The reservoir grows horizontally east as indicated by the microseismic data and threatens to cross over into NNVM.

MITIGATION: Use diverters to seal off the flow path and divert the stimulation treatment to another interval. The fiber optic and subsequent microseismic data will tell us if the diverters have been successful. This mitigation is discussed in detail in Appendix A-1.

13. Safety Incident

RISK: Geothermal field operations involve the use of heavy equipment and rotating machinery, and work with very hot pipe and related materials, sometimes in adverse weather conditions. Accidents can occur without proper training and other precautions.

MITIGATION: All field operations will include detailed written procedures, including provision for health and safety. Safety meetings will be conducted every morning and at the start of each new event (e.g., stimulation, flow-back testing) to remind on-site personnel of job procedure and hazards, wind direction, evacuation plan and personal protective equipment. An emergency response plan accompanies the operating procedures for the stimulation. A copy of these procedures will be given to a representative of each vendor on-site. The emergency response plan will also be posted on-site in the data trailer. BLM will be notified immediately of any safety incident that occurs on the well pad, and BLM and FS will be immediately notified of any incident that occurs off the well pad.

#### 14. Environmental Incident.

RISK: Geothermal field operations involve work around hot water, steam, noncondensable gases and industrial chemicals. The Newberry EGS Demonstration is occurring on a geothermal lease in the Deschutes National Forest. Without adequate precautions, harm to the environment could occur due to spills or chemical release.

## 8 EGS RESERVOIR CHARACTERIZATION

During the stimulation of NWG 55-29, microseismicity data, and downhole pressure and temperature data delivered via fiber-optic distributed sensing, will provide real-time indication of the characteristics of the growing EGS reservoir (Section 7). Post-stimulation tracer and geochemical sampling, and flow test data, will provide further means of studying the newly created reservoir through modeling. In this section, we discuss the advanced techniques and studies that will use data collected during the stimulation to provide a more precise description of the EGS reservoir. The results of the advanced EGS characterization will be used to target and design the production wells. Once drilled, the production wells will test and refine the hypothesized and modeled characteristics of the EGS reservoir. These results will guide Phase III efforts to produce a conceptual model of a full EGS development, including wellfield and power plant, at this or a similar site.

### 8.1 ANALYSIS OF INDUCED MICROSEISMICITY

The MSA will collect and transmit real-time, continuous data seismic data to an operational center. The raw data will also be provided in real-time via broadband internet connection to Lawrence Berkeley National Laboratory (LBNL) where the data will be archived and displayed to the public on the EGS Induced Seismicity website. Auto-processing software will be set to auto-pick and locate events. The operational center will be staffed by seismologists that will refine seismic wave auto-picks, improve event locations, and track maximum event size and the size distribution of microseismicity (the b-value) 24 hours a day. Below we provide details on the expertise, tools and methods that will be deployed to extract as much information as possible from the microseismic data that will be collected.

#### 8.1.1 ABSOLUTE LOCATIONS

Accurate locations of microearthquakes induced by fluid injection can potentially provide the coordinates of hydrosheared volumes that can be targeted by production wells. However, in order for this to be successful, the absolute locations must be highly accurate, and the uncertainties must also be estimated correctly. Earthquake location procedures traditionally used for regional tectonic studies do not perform to the required standards for this study.

Our earthquake location process for the Newberry EGS Demonstration will include specialized elements to ensure the highest possible absolute earthquake locations:

- Seismic network design: The planned Newberry seismic network was designed using numerical modeling to optimize network geometry, number of stations, depth and design of borehole emplacements, as well as data sampling rate and recording strategies.
- Accounting for the crustal model: In a complex geological area like Newberry, the crustal model may vary by 10% or more laterally. Using a laterally invariant, one-dimensional crustal model (the only type that most location programs can use) thus introduces major biases in absolute locations. We are addressing this problem by implementing, as circumstances allow, the most advanced of the following potential approaches:
  - Developing an improved 1- or 3-dimensional crustal model, by simultaneous inversion of the earthquakes themselves, along with any shot or explosion data available (Julian and Foulger, 2010; Kissling, 1995; Thurber, 1983). Modeling results suggest that this approach may remove about 20% of absolute location errors.
  - Determining explicit station corrections for the seismic ray paths between the fluid injection stimulation zone and the individual seismic stations. This requires a calibration survey.

Modeling results suggests that this approach may remove about 70% of absolute location errors.

### 8.1.2 RELATIVE RELOCATIONS

Relative hypocenter location methods can greatly reduce the relative errors in location between individual seismic events in a cluster, thereby improving the resolution of seismically active structures. Relative location methods use, for each seismic station, the differences in arrival times of waves from closely spaced seismic events. For such events, the biases caused by imperfectly modeled geological structures along the ray paths are almost identical. They, thus nearly cancel out when arrival times are differenced, and the variations in arrival times remaining are largely a result of true, small variations in location between the events. The results of relatively relocating events in a tight cluster can be a spectacular improvement in the clarity of delineated structures (Julian et al., 2010a) (Figure 8-1).

We will calculate relative locations using the program **hypocc**. This program is based on the approach of Waldhauser and Ellsworth (2000), but is a more efficient version written in the C programming language (Julian, unpublished). This carries with it many advantages, including extreme speed. Under DOE Award No. DE-FG36-08GO18187, Foulger Consulting extended **hypocc** to include absolute location constraints. This ability is lacking in other relative relocation programs, meaning that although such programs can focus clusters of microseismicity to reveal faults, the absolute positions of those faults is poorly constrained. The new version of **hypocc** can maximize the quality of the relative locations, thereby maximizing the clarity of activated structures, while preserving the best possible estimate for the absolute location of the structure as a whole.

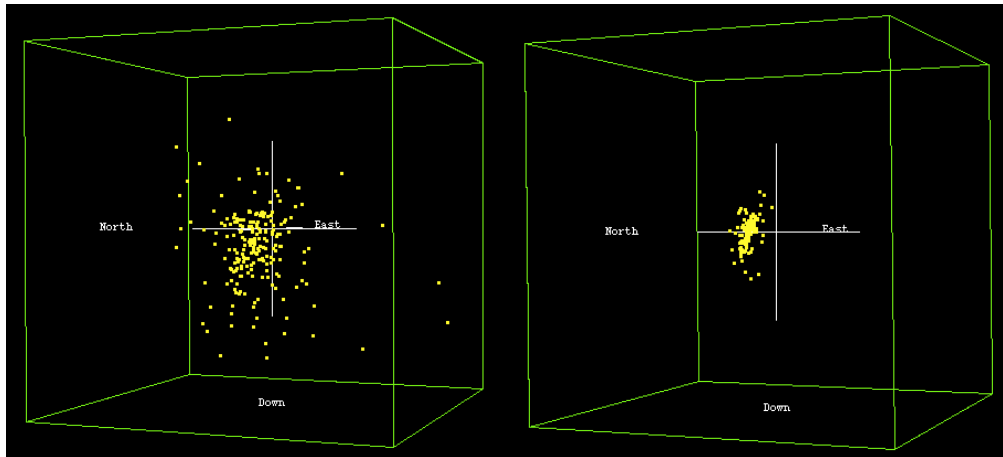


Figure 8-1. Microseismic event hypocenters determined conventionally (left) and with relative relocation (right). The new version of **hypocc** maximizes focusing of the fault without degrading its absolute location.

### 8.1.3 MOMENT TENSORS AND FAULT PLANE SOLUTIONS

Microseismicity in geothermal reservoirs can involve several different physical processes (Julian et al., 1998; Miller et al., 1998a). These include:

1. simple shear slip on planar faults
2. tensile cracking
3. rapid fluid motion

Understanding these processes is critical to understanding hydroshearing in EGS demonstrations. Traditional ‘fault-plane solutions’ assume that only Process 1 occurs, thus ignoring processes associated with opening and closing cracks, and fluid flow. For this reason, such an approach is inadequate for EGS



work. Instead, a moment-tensor approach must be used. In order to determine moment tensors, more information than simply *P*-wave polarities is needed. The most effective and readily obtained information is the amplitudes of *P*- and *S*-phases (Julian and Foulger, 1996). Using amplitude ratios in inversions causes several major error sources (e.g., anelastic attenuation and geometric spreading) to approximately cancel.

The preferred way of displaying moment tensors graphically is to use separate source-type and orientation plots (Hudson et al., 1989). This has been applied to many natural and industrially induced microseismicity sequences, including geothermal and hydrocarbon reservoirs and EGS stimulations (Julian and Foulger, 1996; Julian et al., 1997; Julian et al., 2010a; Miller et al., 1998b; Ross et al., 1996).

We will also compute uncertainties for moment tensors using a new computational method developed by Foulger Consulting under DOE Award No. DE-FG36-08GO18187. This process involves exploring the range of extreme moment tensor solutions that the data will tolerate, given reasonable estimates of errors. An example of the results of such computations is shown in Figure 8-2.

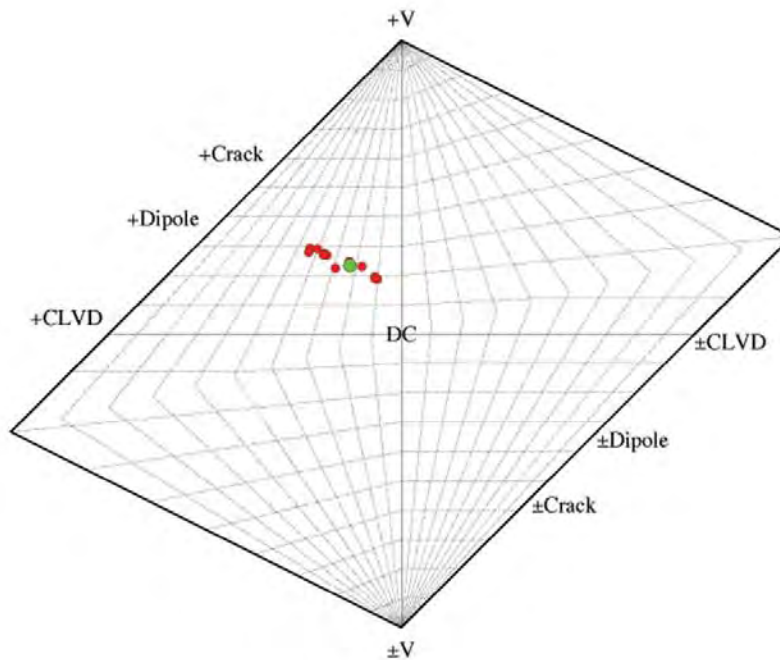


Figure 8-2. An example of the confidence region for the source type of a microearthquake at the Coso geothermal field, California. Green symbol: best-fit solution; red symbols: other acceptable solutions that fit the observations within specified errors.

#### 8.1.4 JOINT INTERPRETATION OF MOMENT TENSORS AND HYPOCENTER LOCATIONS

Interpreting moment tensors is non-unique and, in order to understand the results in terms of physical processes in the rock formation, independent information is required. An effective approach is to combine moment tensors with structural geometric information from relative seismic event locations.

An example of such a joint interpretation for a hydraulic injection in the Coso geothermal field is shown in Figure 8-3 (Julian et al., 2010b). Relative earthquake locations delineate an obvious fault plane, 600 m (1970 ft) in length, striking N20°E, and dipping at 75° to the west-northwest. Surface geology and borehole televiewer observations show that this plane coincides with a pre-existing fault. The earthquakes had non-double-couple mechanisms involving volume increases, and the fault plane bisects

the dilatational *P*-phase polarity fields. From this, it could be concluded that the source process was dominated by tensile failure.

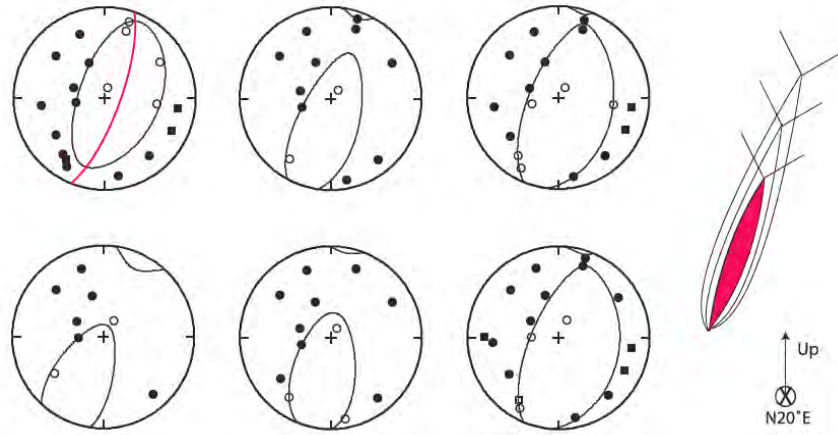


**Figure 8-3. Moment tensors for six microseismic events from a hydraulic injection at the Coso geothermal field (from Julian et al., 2010b), displayed as *P*-wave polarity plots. Black lines: nodal curves. Red line: fault plane delineated by relative hypocenter locations. Open/solid circles: dilatational/compressional arrivals; open/solid squares: dilatational/compressional arrivals, plotted at their antipodes; +: the center of the focal hemisphere. Right: a schematic illustration of a suggested interpretation, a propagating tensile crack (red) with shear wing faults.**

## 8.2 GEOMECHANICAL RESPONSE MODEL

AltaRock is participating in two other DOE-funded projects to model the thermal, hydrologic, mechanical and chemical (THMC) responses to EGS reservoir creation and circulation, one at Pennsylvania State University and another at Texas A&M University (Section 4.6). The pre-stimulation model parameters shown in Table 8-1 have already been shared with both projects. After successful stimulation, it will be possible to better constrain these input variables. For example, the depth, temperature, and fluid pressure at initial hydroshear failure will be well known.

The AltaStim models described in Section 7.4 will be validated using effective stress measurements and the geometry and volume of the actual seismicity. Modifications to the model assumptions may be necessary to fit the data.

Table 8-1. Newberry Volcano model parameters.

Parameter	Model Value
Geological Fracture spacing [m]	1.2-20
Conductive Fracture spacing [m]	12-200 m
Spacing between wells [m]	400-500
Initial permeability [m <sup>2</sup> ]	10 <sup>-17</sup> (0.01 mD)
Bulk modulus of rock without significant fracturing [GPa]	10
Poisson ratio of intact rock [unitless]	0.25
Coefficient of thermal expansion [1/°C]	10 <sup>-5</sup>
Rock mineralogy (Letvin, 2011)	Major minerals: Plagioclase 35-60% Quartz 10-40% Minor minerals: (0-10%) (Calcite, Chlorite, Magnetite, Kaolinite) Trace minerals: (0-5%) (Hematite, Pyrite, biotite, illmenite, epidote, olivine)
Injection water source	groundwater
Heat capacity [J/kg-°C]	918
Thermal conductivity [W/m-°C]	2.7
Injection rate [kg/s]	10-80
Maximum injection pressure, wellhead (0.0 km)	17.2 MPa (3000 psi)
Maximum injection pressure, mid-open hole (2.5 km)	40 MPa (5800 psi)
Maximum injection pressure, bottom-hole (3.0 km)	45 MPa (6500 psi)
Overburden density [kg/m <sup>3</sup> ]	2460
Reservoir temperature [°C]	240-330
Injection temperature [°C]	20-70
Cohesion [Pa]	10000
Friction angle (TAMU tests)	20-40
Porosity (unitless)	0.01-0.05
Initial stress gradients ( $\sigma_x, \sigma_y, \sigma_z$ ) and orientations [MPa]	$S_v$ 24-26 MPa/km $S_H$ 23.5 MPa/km $S_{hmin}$ 15-18 MPa/km $S_{hmin}$ E-W; $S_H$ N-S $S_{max} = S_v = \text{lithostatic}$
Stimulation depth [km]	a) >2.0 (casing shoe) b) 2.9 (exit zone during injection)
Current well TD [km]	3.0

### 8.3 TRACER MODELING

A reactive tracer injected in combination with a conservative tracer as part of a single-well injection and withdrawal test can be used to measure the newly created fracture surface area. The pair of tracers will include a sorbing and a conservative tracer or two tracers possessing contrasting diffusivities. This tracer solution will be entrained within the stimulation fluid and flow into the near-wellbore formation. After a brief shut-in period, the well will be induced to flow and the solution sampled. The produced fluid will be sampled and analyzed for the tracers. From an analysis of the reactive and conservative tracers, the near-wellbore fracture surface area will be determined.

The tracer, Safranin T, is an excellent candidate sorbing tracer. It possesses reasonably good thermal stability and is very detectable by fluorescence spectroscopy. Shown in Figure 8-4 is the degradation of Safranin T at various temperatures on coarse Ottawa sand relative to the conservative tracer 1,5-naphthalene disulfonate.

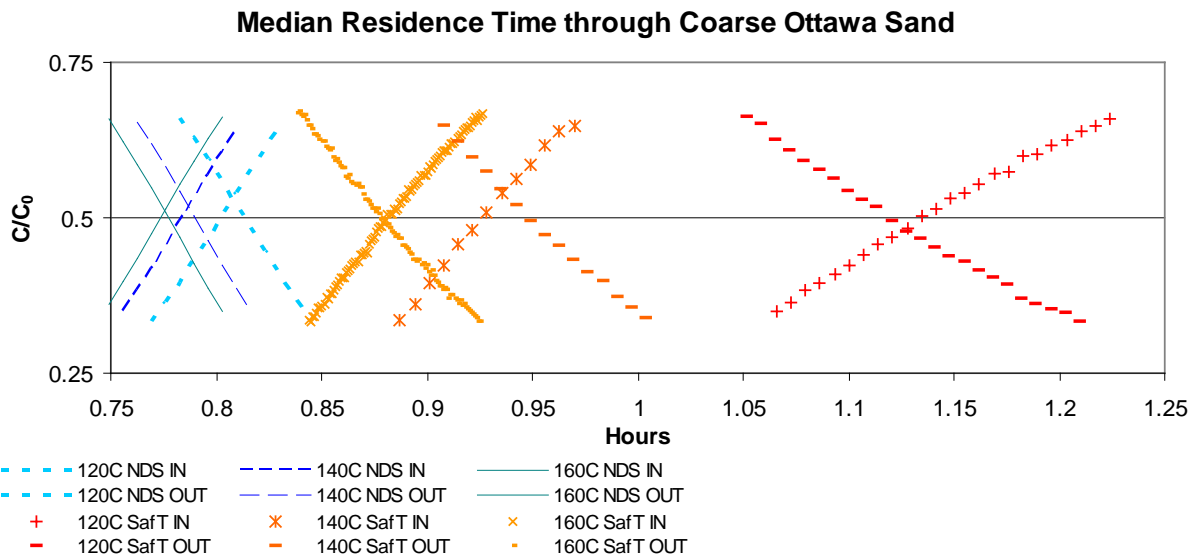


**Figure 8-4. Mean residence time of the sorbing tracer Safranin T and the conservative tracer 1,5-naphthalene disulfonate at various temperatures.**

Values for the relative retention of Safranin T, as  $R_f - 1$ , are plotted as a function of temperature in Figure 8-5. As with all sorbing compounds, relative retention decreases with temperature, but is still measurable above 250°C (482°F).

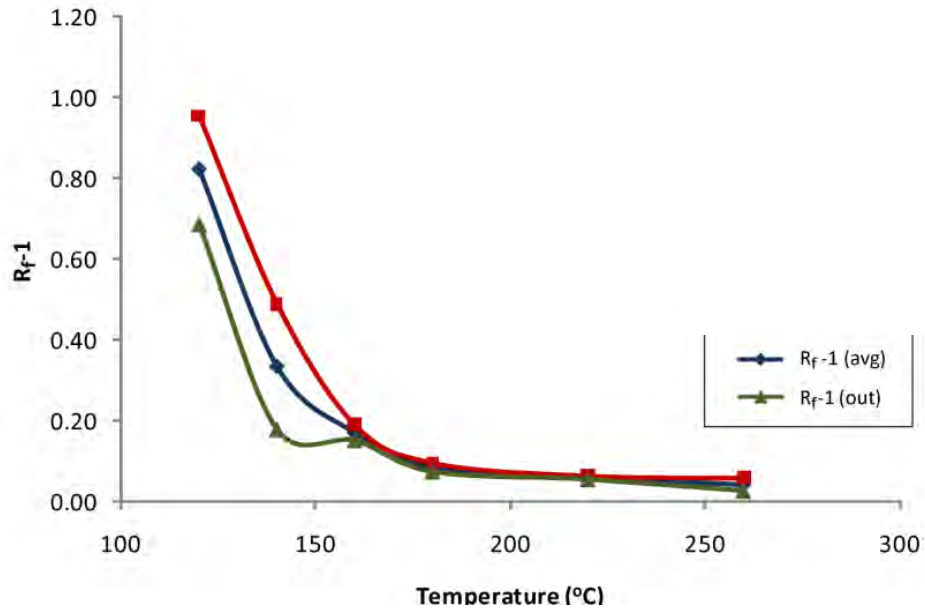


Figure 8-5.  $R_{f-1}$  for Safranin T as a function of temperature.

Adsorption equilibrium constants from flow-through experiments were determined based on instantaneous, linear adsorption and desorption from the advective diffusion equation relationship between retardation factor and distribution coefficient:

$$\text{Equation 8-1} \quad R_f = 1 + \frac{\rho_b}{n_e} K_{d,m}$$

where  $\rho_b$  is the bulk density (g/cc),  $n_e$  is the effective porosity, and  $K_{d,m}$  is the distribution coefficient (mL/g). The mass-based distribution factors from Safranin T experiments, as functions of temperature, are shown in Table 8-2.

Table 8-2. Distribution coefficients of Safranin T on fractions of Ottawa sand.

Ottawa Grade	Sand	Temperature (°C)	Adsorption $K_{d,m}$ (mL/g)	Desorption $K_{d,m}$ (mL/g)
Coarse		120	0.089	0.076
Coarse		140	0.040	0.045
Coarse		160	0.028	0.027
Medium		120	0.239	0.172
Medium		140	0.119	0.043
Medium		160	0.047	0.037
Medium		180	0.023	0.018
Medium		220	0.014	0.012
Medium		260	0.012	0.005

Adsorption and desorption equilibrium constants are used in numerical simulation experiments to fit for fracture surface area. The results of numerical flow experiments for a sorbing tracer show that sorption occurs not only on the fracture walls but also on the pore walls within the matrix (Figure 8-6). Because sorption cannot be distinguished from diffusion, both are used in fitting to the data. The figure shows that by allowing for both sorption and diffusion, an excellent match can be obtained between data and model.



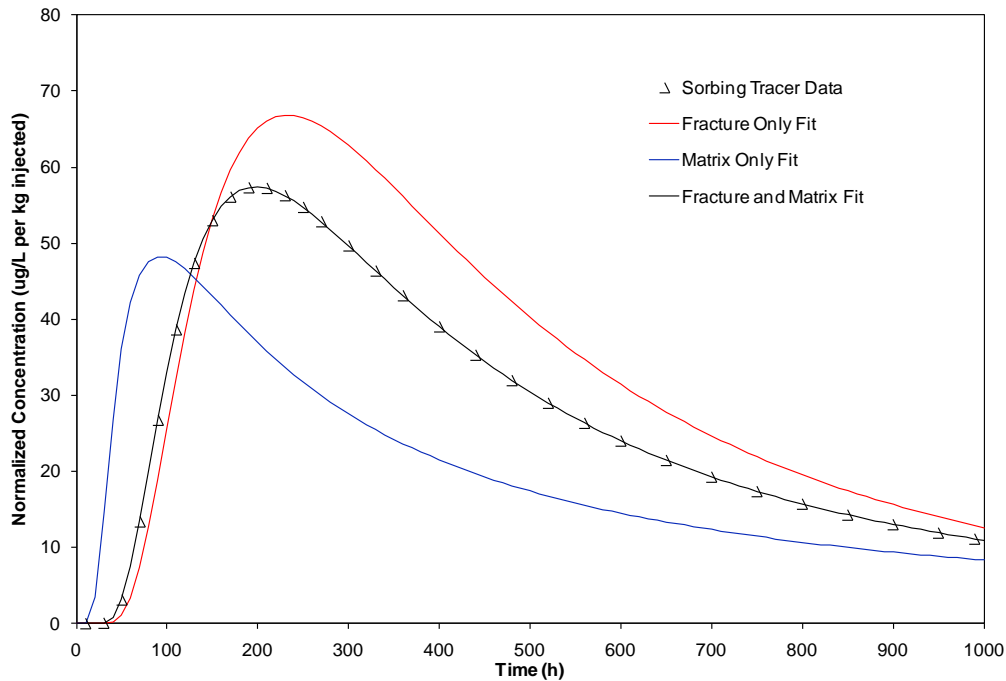


Figure 8-6. Assuming sorption only in fractures or matrix (red and blue curves) results in much poorer fits to the sorbing tracer breakthrough curve than assuming sorption occurs in both domains. The fracture surface area to volume ratio can be deduced from the best-fitting model parameters for the black curve.

## 8.4 UPDATED THMC MODEL

A team led by Dr. Eric Sonnenthal at Lawrence Berkley National Laboratory (LBNL) is developing a THMC reservoir model for the Demonstration using the TOUGH2 and TOUGHREACT software platforms. LBNL is a sub-receipient under the project's DOE grant. The THMC model uses many parameters, in most cases estimated. Many of these parameters are discussed in Sections 3.2.7 and 8.2. New data from the stimulation, flow testing, groundwater geochemistry, and other upcoming field activities will be incorporated to accommodate extensions of the model to consider current phenomena and modeling approaches. For the thermal-hydrological basis of the THMC model, dual-continuum and discrete fracture modeling approaches will be employed when a model of fracture densities and orientations become available. The model will also be extended to consider multiphase flow owing to the possible vapor-dominant character of the geothermal system. Consideration will be made to extending TOUGHREACT to consider supercritical water (as in the Croucher and O'Sullivan approach used in Section 3.2.7) if funding becomes available for this effort.

The geothermometry computations point to the need, in the future, to collect data not only on water and noncondensable gas compositions, but also on: (1) the steam (total gases including H<sub>2</sub>O) weight fraction in total discharge; (2) the amount of H<sub>2</sub>O gas in the wet gas; and (3) aluminum analyses (requiring filtration to 0.2 microns or smaller for accurate determination of soluble/ionized Al). Analyses of water that have been injected and returned to the surface will be used to estimate the effective reaction rates and fracture surface areas. Sampling of water at various times after injection with known residence times can be used to further refine reactive surface areas.

It will be important to refine the initial lithologic distribution, porosities, and mineralogical variations particularly for permeable zones and fractures. With the dual-permeability formulation, mineralogical data can then be assigned to the rock matrix, and the fracture fillings and coatings, as in Sonnenthal et

al. (2005). In concert with the improved mineralogical description, all thermodynamic and kinetic data will be reevaluated and tested against field and laboratory data. Once details of the fracture distribution are known, then apertures can be estimated and the permeability law using effective hydraulic aperture in TOUGHREACT can be utilized.

Following the extension of the flow model to multiphase water-water vapor, gas species transport will be added for the important noncondensable and reactive gases (i.e., Ar, N<sub>2</sub>, CO<sub>2</sub>, SO<sub>2</sub>, HCl, HF, and H<sub>2</sub>). For analysis of stimulation, injection, and production, other gas species, tracers, and isotopic systems will be added, such as <sup>3</sup>He/<sup>4</sup>He, <sup>18</sup>O/<sup>16</sup>O, D/H, and <sup>13</sup>C/<sup>12</sup>C (as in Dobson et al., 2006). In the aqueous phase and minerals, oxygen isotopes will be incorporated to further refine the model to use the calculated extent of reaction from Carothers et al. (1987) as another constraint to the effective reaction rates at differing temperatures, fluid compositions, and lithologies. Strontium isotopic studies of primary volcanic lithologies from Newberry Volcano (Goles & Lambert, 1990) and alteration mineralogy can also be used to provide constraints on rates of water-rock interaction, especially for stimulation predictions.

Coupled THMC effects of stimulation are being evaluated using a new mechanics module coupled to TOUGHREACT (Kim et al., in prep.) developed through another DOE GTP project entitled "*Coupled Thermal-Hydrological-Mechanical-Chemical Model And Experiments For Optimization Of Enhanced Geothermal System Development And Production*", (PI, Eric Sonnenthal). A preliminary coupled THM simulation has been performed on the flow tests conducted at NWG 55-29 in 2010 (0.6 and 1.4 L/s, 10 and 22 gpm), using estimated horizontal and vertical stresses. Fully coupled THMC model simulations are in progress and will utilize new hydrological, mechanical, chemical, and tracer data as they become available.

## 8.5 PRODUCTION WELL TARGETS

Production well targets will be determined by mapping fractures resulting from the stimulation of NWG 55-29. The directional drilling program will be designed to direct the trajectory of the well perpendicularly through the stimulated fracture planes to intersect as many of the stimulated fractures as possible. Optimization of the well path will also consider the cost and risk of directional drilling, including the limitations of directional drilling equipment in a high temperature reservoir.

Modeling by Jupe et al. (1995) indicates that a fracture length and production-injection well spacing of 500 m (1640 ft) will provide a reservoir life of 20 years before significant cooling occurs. Similar well spacing used at operating hydrothermal fields has been shown to optimize reservoir life with the time value of money. Thus, the trajectories of the wells drilling into the stimulated volume around NWG 55-29 will be designed to provide similar separation. Two production wells will be drilled into the stimulated fractures. These wells will likely be drilled on opposite flanks of the elongated EGS reservoir created around NWG 55-29. Possible well trajectories are shown in Figure 8-7. For additional discussion of potential well paths, see Section 9 and Appendices I-1 and I-2. The actual well trajectories will be adjusted based on the orientation of the fracture network mapped using seismicity.

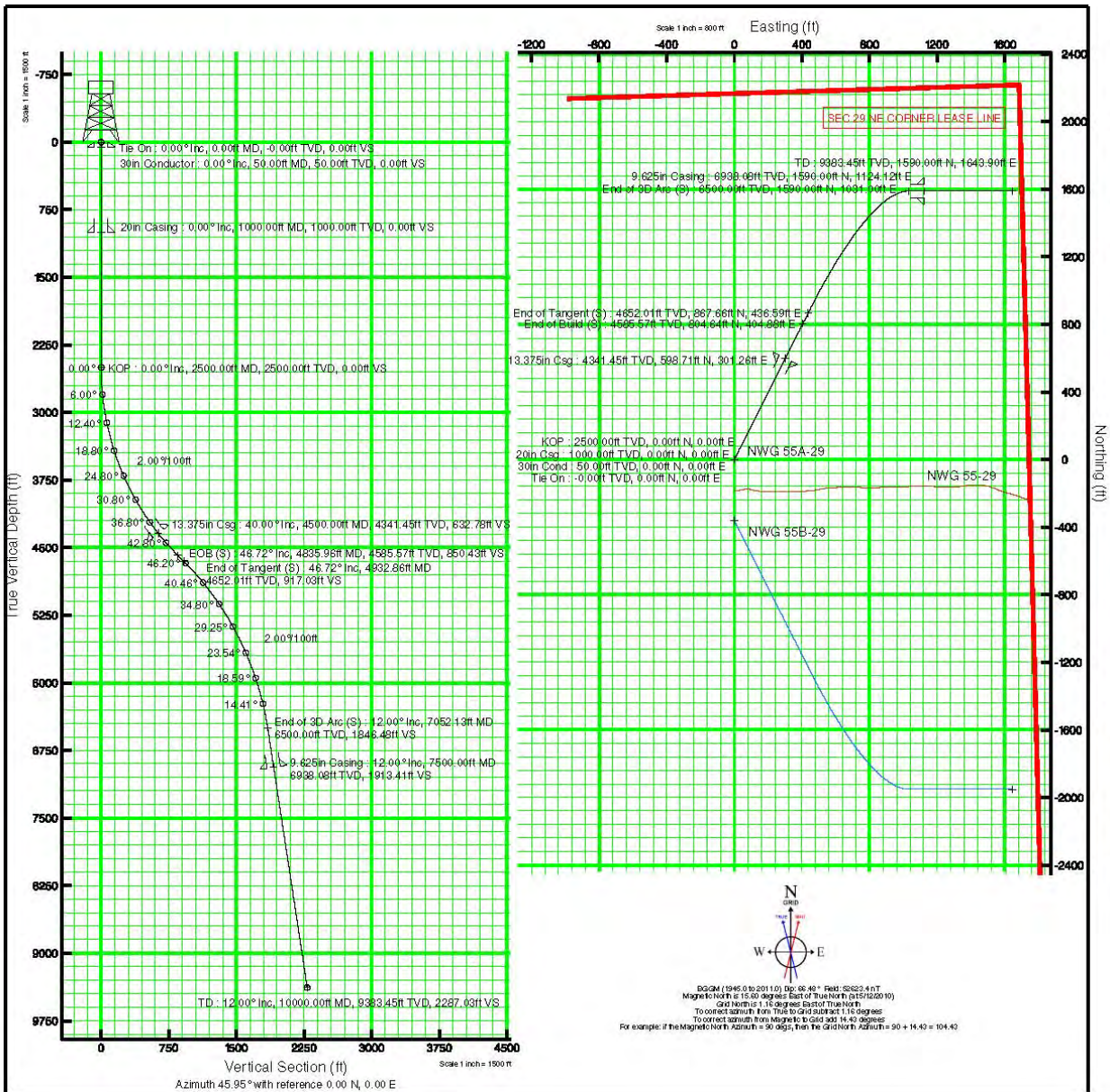


Figure 8-7. Cross-section (left) and plan view (right) of possible well trajectories for NWG 55A-29 and NWG 55B-29 to be drilled into stimulated volume around existing well NWG 55-29. NWG 55-29 is directionally drilled to the east. All three wellheads will be located on Pad S-29.

## 9 DRILLING PROGRAM

### 9.1 INTRODUCTION

This section describes preliminary plans for well drilling and completion that will occur in Phase II after the stimulation and flow-back testing of NWG 55-29. Because the results of stimulation and testing will be required to identify drilling targets and final well designs, detailed plans will be presented in the post-stimulation stage-gate review. Each rig move, drilling, casing, cementing, lost circulation, fishing, flow testing, and other drilling operations will be conducted according to detailed written procedures approved in advance by BLM and DOE.

Two production wells, tentatively designated NWG 55A-29 and NWG 55B-29, will be drilled to intersect an EGS reservoir created around the existing well NWG 55-29. Both wells will be directionally drilled from Pad S-29 (Figure 9-1). The EGS reservoir is expected to develop in the shape of an oblate spheroid with a radius of about 500 m (1640 ft), oriented in a north-south direction, and the vertical extent of the EGS fracture network is expected to range from 1829-3658 m (6000-12000 ft).

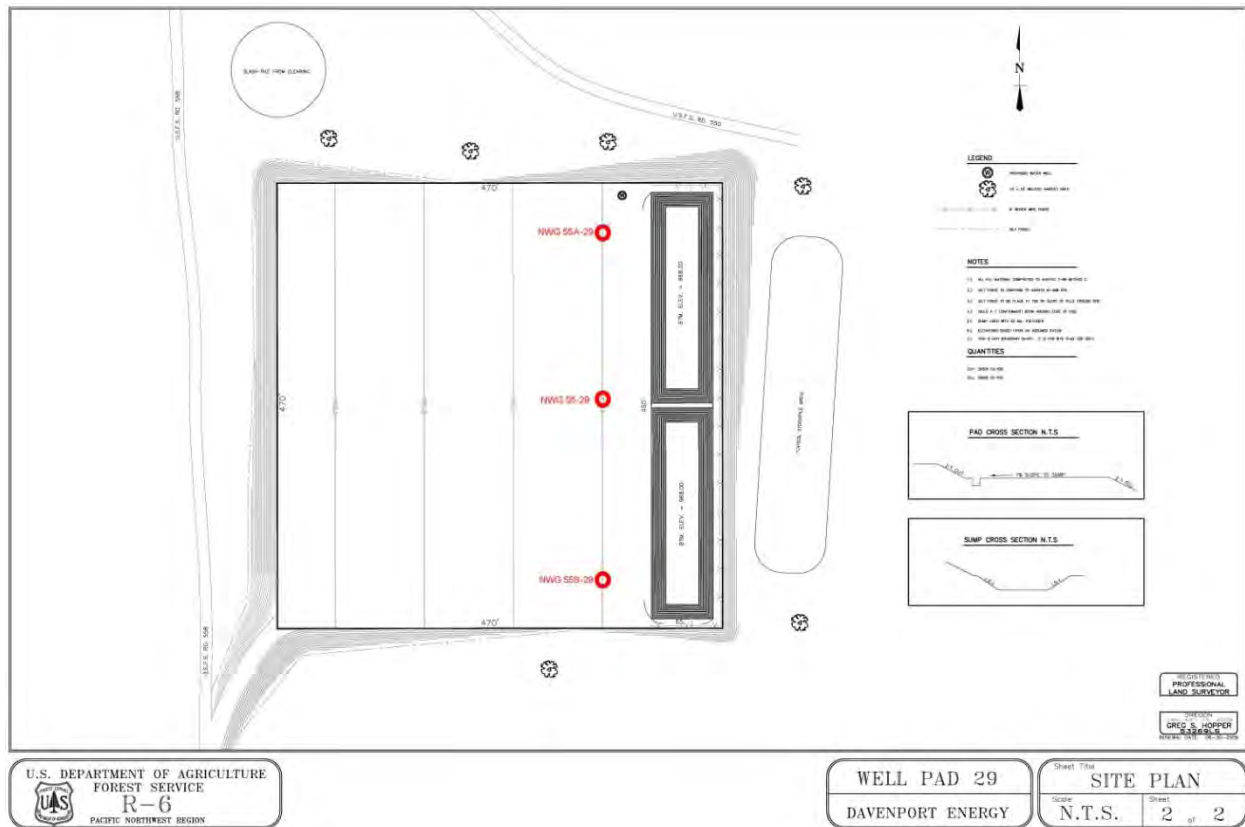


Figure 9-1. Well Pad S-29, showing existing well NWG 55-29 (middle) and locations of proposed wells NWG 55A-29 (upper middle) and NWG 55B-29 (lower middle).



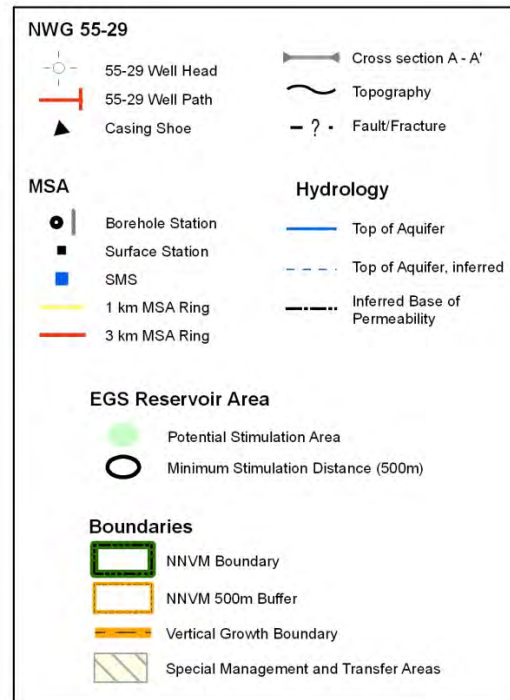
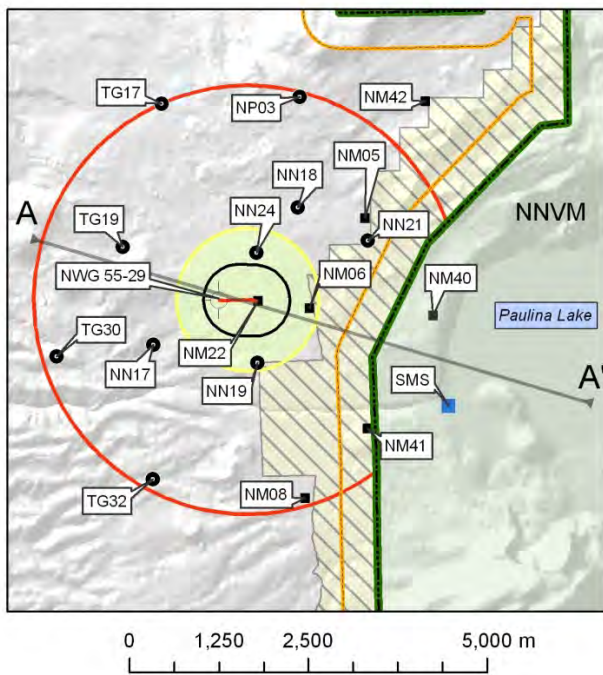
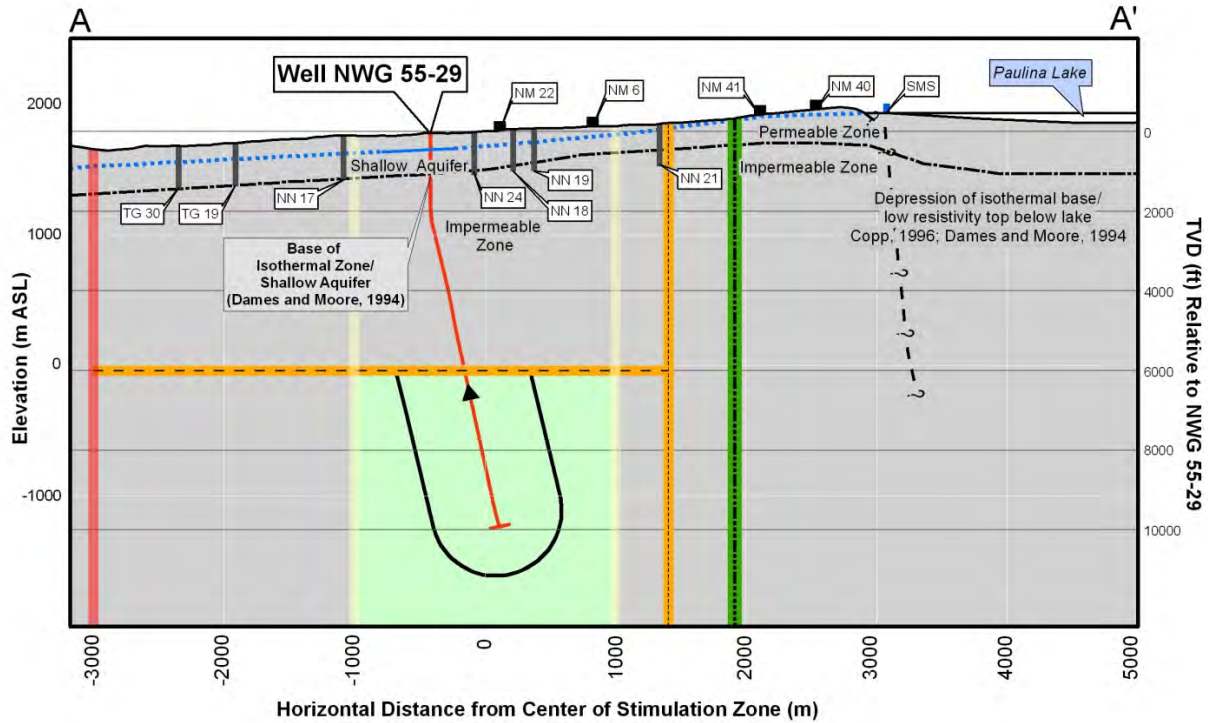


Figure 9-2. Cross-section and map showing expected EGS reservoir area, MSA and SMS station locations, horizontal and vertical growth limits, and trigger boundaries.

Drilling operations will specify a drilling rig of National 110E-class, or better, with top drive. Design ratings and experience in geothermal drilling have shown that the National 110E-class rig is capable of safely drilling to more than 3658 m (12000 ft). National 110-class rigs are rated at 1500 HP, usually with



two PZ 9 pumps, and with mast ratings of 272-363 tons (600000-800000 lb). The top drive is essential to continuously circulate drilling fluid while tripping pipe in order to prevent failure of directional drilling equipment (motor and MWD). This potential failure could occur if the directional drilling equipment is not kept cool while in the well. Higher pump flow rate and pressure capability also enhances the utility of the National Class 110-class rig. The smaller National 80-class rig has insufficient pump horsepower and mast capacity to safely install 1524 m (5000 ft) of 72 lb/ft, 13-3/8 in casing (i.e.,  $\geq 360000$  lb allowance for over-pull of 100000 lb).

Sufficient water volume for drilling fluid, cementing, and other requirements is available from the water well located on Pad S-29. The second water well, located nearby on Pad S-16, provides 100% supply redundancy. Permits for water usage have already been secured.

## 9.2 DRILLING SCHEDULE

After a final decision has been made to drill the production wells, there will be several long lead time items that must be procured before drilling can begin. These are outlined in Table 9-1. The drilling schedule for the five different production well cases is outlined in Table 9-2.

**Table 9-1. Long-lead time items prior to drilling.**

Item	Lead Time
Mobilization of rig	60 – 90 days
Special drill bits	60 days
Wellhead equipment	
<i>600 and 900 series wellheads</i>	120 days
<i>1500 series wellheads (if needed)</i>	150 days
Permits	
<i>BLM Geothermal Drilling Permit</i>	60 days
<i>DOGAMI Permit</i>	60 days
<i>Air Permit (modified existing permit)</i>	60 days

**Table 9-2. Drilling stage durations (days).**

Operation	Case No.1 Base	Case No.2 Liner	Case No.3 Shallow	Case No.4 Deep	Case No.5 Large
Pre-Spud Activities	7	7	7	7	7
Mobilization of Rig	8	8	8	8	8
Drill and complete Interval 1 – 20 in casing	10	10	10	10	11
Drill and complete Interval 2 – 13-3/8 in casing	21	21	21	21	23
Drill and complete Interval 3 – 9-5/8 in liner	17	17	14	17	18
Drill Interval 4 – 8.5 in open hole to total depth <sup>1</sup>	23	22	20	31	24
<b>Total Time</b>	<b>86</b>	<b>86</b>	<b>80</b>	<b>95</b>	<b>91</b>

<sup>1</sup> Slotted liner may be installed in Interval 4 if required to keep hole open during well operation.

## 9.3 DRILLING AND CASING PLAN

### 9.3.1 WELL DESIGN

Reservoir dimensions and drilling targets will be determined based on stimulation and testing results. Therefore, we have developed well designs, schedules and budgets for five different cases that provide for variations in top of the EGS reservoir, depth of completion, well productivity and mode of production. The casing sizes and depths of the model cases are shown in Table 9-3.

**Table 9-3. Production well casing designs.**

<b>Case No.</b>	<b>Base 1</b>	<b>Liner 2</b>	<b>Shallow 3</b>	<b>Deep 4</b>	<b>Large 5</b>
Conductor (ft)	50	50	50	50	50
Surface (ft)	1000	1000	1000	1000	1000
Intermediate (ft)	4500	5500	4500	4500	4500
Production – top (ft)	0	5200	0	0	0
Production – bottom (ft)	7500	7500	6000	7500	7500
Open Hole Diameter (in)	8.5	8.5	8.5	8.5	10.625
Total Depth (ft)	10000	10000	8000	12000	10000

The casing points were chosen in the following manner:

- Surface casing will be set at 305 m (1000 ft) to ensure that the most severe lost circulation zones are sealed behind pipe and groundwater aquifers are protected by two or three layers of casing and cement.
- Intermediate casing set at 1372 m (4500 ft), about midway between 1000 and 2286 m (7500 ft) casing points. The intermediate casing will be run just into the top of the John Day formation, estimated to occur at 4400 ft beneath Pad S-29. For Case 2, with 9-5/8 in liner, the intermediate casing will be set at 5500 ft, and the production liner hung from 5200 ft, to minimize well flow frictional losses and provide a sufficient hole diameter for installation of a production pump. Case 5 further decreases frictional losses by increasing casing diameters through the total depth of the well.
- Production casing set at 7500 ft and cemented to surface to allow production from the uppermost fracture zone, while providing for relatively high production temperature. Case 3, with production casing set at 6000 ft, allows for a shallower uppermost fracture zone. If this resulted in a relatively low mass-weight production enthalpy, a hung production liner, as in Case 2, could be utilized.
- In the Base case, the open-hole interval is drilled with 8-1/2 in bit to 10000 ft, similar to existing well NWG 55-29. This depth may be greater or less depending on the final target depth and will be determined from post-stimulation processing of the microseismic data. We expect fracture zones to be relatively steeply dipping, with zones deeper on one side of the reservoir and shallower on the other. Thus, Case 3 provides for a total depth of 8000 ft and Case 4 provides for deep completion to 12000 ft. Case 5 provides a larger open-hole diameter of 10-5/8 in to maximize productivity.

### **9.3.2 CASING PLAN**

All casing strings have been selected to accommodate the temperature, pressure and stresses that might be encountered during stimulation and production, with additional safety margin consistent with standard engineering practice and American Petroleum Institute specifications. Specific values for casing strings are given in the individual well sections below. While high stimulation pressures are not anticipated, the casing design will be planned to support higher than normal pressures. Final drilling plans, including casing configuration and engineering calculations, will be reviewed and approved by BLM as part of the drilling permit process.

**Table 9-4. Production well casing size, weight, grade and connection.**

<b>Case No.</b>	<b>Base 1</b>	<b>Liner 2</b>	<b>Shallow 3</b>	<b>Deep 4</b>	<b>Large 5</b>
Conductor	30 in, 108 lb/ft 54000 psi mild steel welded	30 in, 108 lb/ft 54000 psi mild steel welded	30 in, 108 lb/ft 54000 psi mild steel welded	30 in, 108 lb/ft 54000 psi mild steel welded	30 in, 108 lb/ft 54000 psi mild steel welded
Surface Casing	20 in, 106.5 lb/ft K-55, buttress	20 in, 106.5 lb/ft K-55, buttress	20 in, 106.5 lb/ft K-55, buttress	20 in, 106.5 lb/ft K-55, buttress	22 in, 142 lb/ft 54000 psi mild steel welded
Intermediate Casing	13-3/8 in 68 lb/ft HCL 80 buttress	13-3/ in 68 lb/ft HCL 80 premium	13-3/8 in 68 lb/ft HCL 80 buttress	13-3/8 in 68 lb/ft HCL 80 buttress	16 in 109 lb/ft L-80 buttress
Production Casing	9-5/8 in 47 lb/ft L-80 premium	9-5/8 in 47 lb/ft L-80 premium	9-5/8 in 47 lb/ft L-80 premium	9-5/8 in 47 lb/ft L-80 premium	11.75 in 71 lb/ft L-80 premium
Perforated Open Hole Liner – (contingent on hole stability)	7-5/8 in 26.4 lb/ft K-55 buttress	7-5/8 in 26.4 lb/ft K-55 buttress	7-5/8 in 26.4 lb/ft K-55 buttress	7-5/8 in 26.4 lb/ft K-55 buttress	9-5/8 in 47 lb/ft K-55 buttress

### **9.3.3 DIRECTIONAL DRILLING PLAN**

The EGS reservoir is expected to develop in the shape of an oblate spheroid with a radius of about 500 m (1640 ft), oriented in a north-south direction, and the vertical extent of the EGS fracture network is expected to range from 6000-12000 ft. The production wells will be directionally drilled to intercept this fracture network. The final directional drilling plan will not be determined until the stimulation of NWG 55-29 is complete and final fracture intercept targets are identified. Tentative directional drilling programs for NWG 55A-29 and NWG 55B-29 are provided in Appendix I-1 and I-2, respectively. The program has been discussed with a directional drilling vendor, and the approach has been verified as technically feasible.

### **9.3.4 DISPOSAL AND SPILL PROCEDURES**

#### **9.3.4.1 CUTTINGS DISPOSAL**

During drilling, cuttings will initially be placed in the existing sump on Pad S-29. After drilling, the cuttings will be disposed at a site approved by Oregon DEQ based on chemical analysis conducted at an EPA-certified laboratory. Cuttings are expected to be non-hazardous, as was the case with NWG 55-29 and NWG 46-16.

AltaRock may apply for a solid waste beneficial use permit from the Oregon DEQ. Beneficial use is a more environmentally sustainable use of drill cuttings if analysis demonstrates the absence of hazardous constituents. If a permit is obtained, the material may be used for beneficial uses such as lining of other sumps, roads, well pads, etc. This secondary disposal method may be explored after drilling operations are complete.

#### 9.3.4.2 *EXCESS CEMENT DISPOSAL*

During cementing operations it is likely that some cement slurry will be circulated out of the well at the end of cement placement. Steps will be taken to minimize the amount of excess cement that will actually be circulated out of the hole and into waste pits. The major factor that will help minimize this waste (and disposal) is the use of ‘stab-in’ drill pipe during circulation and cement placement. This procedure will be used on all cement jobs for all casing strings, whether or not the placement circulation method is conventional or ‘reverse’. Cement will be either circulated down the drill pipe and up the annulus (conventional) or down the annulus and up the drill pipe (reverse circulation). Excess cement will be minimized when pumping conventionally by pumping ‘lead’ cement slurry until returns are seen coming out of the annulus or drill pipe, thus providing a positive indication that the annulus is completely full of cement. ‘Tail’ cement slurry will then be mixed and displaced down the drill pipe.

The use of foam cement will also decrease the excess cement requiring disposal. Because foam cement is compressible, the return flow line can be shut in while displacement of tail cement occurs at the end of the job. Instead of continuing to circulate excess cement out of the well, the return flow is shut in and the foam cement in the annulus is compressed. The compression of the foam cement actually increases the density and the compressive strength of the cement while having a minimal impact on down-hole pressure. This procedure cannot be accomplished with conventional, un-foamed cement because it is not compressible.

If conventional circulation and no inner string drill pipe are used, the job procedure will involve estimating the amount of open-hole excess that exists, pumping that large volume of cement, and then displacing the cement down the casing. The displacement volume for 1000 ft of 20 in, 106.5 lb/ft casing is 350 bbls. The displacement volume for 1000 ft of 5-1/2 in drill pipe is only 18 bbls. With the drill pipe being used as an inner string during the cement job, one can readily circulate cement back to surface, mix and pump a small volume of higher density tail cement, and then displace it down the drill pipe, thereby minimizing waste cement.

If the inner string drill pipe method is not employed, there is an increased risk of not filling the entire annulus with cement. An annulus that is not completely filled with cement increases the risk of casing failure during the life of the well, potentially leading to additional remedial repair costs or total loss of the well. This is discussed in more detail in Section 9.6.1. To ensure that the annulus is completely filled without using the drill pipe method, approximately 350 bbls of cement would have to be circulated back to surface. Not only does this excess cement have a large environmental impact, but it also greatly increases the cost of the cement job.

#### 9.3.4.3 *SPILL PROCEDURES*

AltaRock will adhere to the drilling contractor’s spill prevention, control, and counter-measures program (SPCC) to mitigate spills during drilling operations. All operation personnel will be appropriately trained to handle spills. Safety procedures will be posted and copies given to local emergency people, daily safety meeting will occur each day, etc.

#### 9.3.5 *ADDITIONAL PERSONNEL ON LOCATION*

Additional personnel, beyond those needed for well drilling activities, will be on location during specific periods of the drilling operation to provide project management, supervision and assistance. Specific operations will be witnessed and supervised by additional personnel as follows:

- All Field Operations: Will Osborn – AltaRock Project Manager
- Cementing: Daniel Bour – AltaRock

- Logging: Laura Nofziger – AltaRock, Trenton Cladouhos – AltaRock
- Minifrac Test: Laura Nofziger – AltaRock, Trenton Cladouhos – AltaRock

### **9.3.6 PRE-SPUD ACTIVITIES**

#### **9.3.6.1 SITE PERMIT**

Site permits have already been obtained for this operation so there will be no delay in proceeding with site preparations.

#### **9.3.6.2 SITE PREPARATION AND CONDUCTOR INSTALLATION**

The existing well pad, S-29, is of sufficient size (5 acres) and design to easily accommodate the drilling of two or more additional wells. No additional pad preparation is necessary, and all drilling operations can be conducted on the existing location. The foot print of the rig will be considered when arranging the drill site to allow for easy access. For example, transport trucks carrying casing will require a free path to the pipe racks, so this pathway cannot be obstructed by rig equipment. Space for office trailers will be provided for the rig manager, company man, directional drilling contractor, mud logger, mud man, and shift crew operations, at a minimum.

A shallow cellar, approximately 8 x 8 x 4 feet deep, will provide for water collection and runoff through an 18 in diameter pipe pipeline installed from the cellar to the adjacent sump. A local water well driller will drill to 50 feet, then run and cement the 36 x 30 in, 3/8 in-wall, welded, line pipe conductor. The required cement volume of 108 ft<sup>3</sup> will require about 4 cubic yards of ready-mix concrete. A rat-hole driller or local water well driller will drill the relief for the mouse and rat holes as specified by the rig footprint.

#### **9.3.6.3 RIG AND TRAILER MOBILIZATION**

The drilling rig will be mobilized and installed on location. The rig equipment will include three large mud tanks (800 to 1000 bbls total) to accommodate drilling fluid. Installation of office trailers and specialized equipment onto location will also occur during the drilling rig mobilization.

#### **9.3.6.4 RIG PREPARATION**

Spud mud will be mixed. Blow-out prevention equipment (BOPE) will be installed and tested for functionality. The BOPE stack will then be pressure-tested as per BLM requirements. At the conclusion of each casing and cementing job, all well control elements of the BOPE stack will be re-tested. The BOPE stack will be tested every 7 days during drilling, as per BLM requirements, and after every major change in the drilling operation. A BLM representative will be notified before every test.

### **9.3.7 SURFACE CASING**

The surface casing interval will be drilled with a 26 in bit and bottom-hole assembly (BHA) to 1000 feet. Existing well NWG 55-29 encountered severe circulation losses in this interval. Aerated drilling fluids will be used to mitigate lost circulation. It is important to clear the hole of cuttings in order to prevent stuck pipe, as was reported in NWG 55-29 in this interval. Foam or viscous slugs will be used to frequently clear the hole. Lost circulation material (LCM) or open-hole cement plugs will also be used minimize lost circulation. Because rapid circulation losses can lead to insufficient mud volume and, thus, lost rig time, an additional mud tank will be used to store drilling fluid. This additional drilling fluid capacity will provide more flexibility in handling mud losses in the top section of the hole.



### 9.3.7.1 *WELLHEAD, BHA, AND DRILLING OF THE SURFACE HOLE*

- Rig wellhead top section to handle aerated fluid drilling
- Rig up banjo box and rotating head
- Drill out cement in the conductor, plus 15 ft, with a slick assembly, 26 in bit, 3 collars and no stabilizers
- Perform leak-off test and refresh fracture gradient determination
- With 26 in tools, drill 1000 ft to the end of surface casing interval
- Assemble 26 in BHA and tools for drilling the surface casing interval

The BHA will consist of:

- 26 in bit IADC Class 5
  - Using 4000 lb/diameter in, the required collar weight is 104000 lb
  - Considering buoyancy with a 15% margin of safety, the required drill collar weight is 119500 lb
- 26 in full gauge, near bit stabilizer, 6-pt roller reamer
- 30 ft x 10 in non-magnetic drill collar
- 26 in string stabilizer 1/8 in under-gauge
- 30 ft x 10 in non-magnetic drill collar
- 26 in string stabilizer 1/8 in under-gauge
- Drill collars
  - 5 drill collars (7 total) – 30 ft x 10 in; 10 in drill collar weight = 51000 lb
  - 21 drill collars – 30 ft x 8 in; 8 in drill collar weight = 99100 lb
  - Total collar weight in air 150100 lb: Buoyed weight 128000 lb
  - Drill collars added as depth permits
- 6 joints (5 in – 1480 lb/joint) heavy weight drill pipe
- Shock sub
- Jars

A shock sub will be used to reduce unnecessary bit cutter damage. Jars will be run to mitigate stuck pipe problems. Single shot surveys will be taken every 60 ft (every two joints) to ensure a straight hole, with a vertical deviation of no more than 2°. A mule shoe seat will be placed at the top of the 10 in collars.

### 9.3.7.2 *END OF INTERVAL ACTIVITIES – LOGGING*

No logging will be done in this open-hole interval after drilling. This interval was logged in NWG 55-29, which is immediately adjacent, making the additional data unnecessary. It is very likely that there will be severe lost circulation problems while drilling this interval and, thus, it will be important that this interval be cased off as quickly as possible after reaching the casing depth. Conducting a logging operation would increase the risk of losing portions of this hole to formation collapse, and the instruments used for logging.

### 9.3.7.3 *END OF INTERVAL ACTIVITIES – CEMENTING*

Foamed cement will be used to cement this interval to help ensure that the casing annulus is completely filled with cement. Reverse circulation placement may be used if extreme losses occur.

Prepare to run casing, including setting up floor post, pulleys, and a trapeze. Clean, inspect and measure the casing on the pipe racks in anticipation of running the casing. The casing collapse pressure, assuming 1000 feet of 9.6 lb/gal drilling fluid, will be 3.4 MPa (500 psi). The 106.5 lb/ft K55 casing has a collapse rating of 5.3 MPa (770 psi), providing a safety factor of 1.5. This rating is well in excess of the maximum

recommended API collapse safety factor of 1.125. Run 1000 ft of surface casing. The drift of 20 in 106.5 lb/ft casing is 18.812 in.

The casing string will include:

- Guide shoe
- 1 joint 20 in casing for shoe track
- Float collar with stab-in inner liner drill pipe feature
- Remainder of 20 in casing
- Appropriate centralizers will be attached to the casing to provide a minimum of 70% standoff between the casing and the open hole. The location and number of centralizers required to achieve 70% standoff will depend on the casing size and weight, hole size, drilling fluid density, hole angle, centralizer bow strength, etc. The number and location of centralizers can be calculated along with the associated standoff using a standard program that is typically available from the major cement service companies. Centralizers will be placed on the top two joints and bottom shoe joint to ensure that casing is properly centralized at the critical locations.

After the casing has been run, rig down the casing crew equipment and rig up to cement surface casing. Circulate through the casing 2 to 4 hours to clean the hole. Circulate at least two 'bottoms-up' to lower the gel strengths of the drilling fluid, if possible, and lower the progressive gel strength development. Flat versus sharply increasing progressive gel strength of the drilling fluid is optimal. Follow procedure given in Section 9.4.1 for cementing. The temperature at 305 m (1000 ft) is estimated to be 43°C (110°F). Cementing will use direct circulation foam.

Pressure test casing immediately after cement is placed and before the cement has set. By pressure-testing immediately, we will prevent damaging the cement bond, since the cement will still be liquid at this point.

Allow 4 to 6 hours for cement to firm up and check for fall back and determine if a top job is needed. Integral joint tubing (1-1/8 in) will be used to pump a top-out cement job. Determine whether the top job was successful or whether another top job is necessary.

Wait on cement at least 24 hrs total before resumption of drilling activities (i.e., drilling out the 20 in casing shoe).

### 9.3.8 INTERMEDIATE CASING INTERVAL

#### 9.3.8.1 BEGINNING OF INTERVAL – WELLHEAD, BOPE, BHA, SHOE TEST AND DRILLING AHEAD

Cut off the conductor pipe and weld on the 20 in SOW (Slip-On-Well) wellhead. Nipple up the 21-1/4 in, 14 MPa (2000 psi) BOPE stack (Figure 9-2) and pressure test as per BLM requirements.

#### 21-1/4 inch 2000 psi Annular / Dbl gate / drilling cross / wellhead

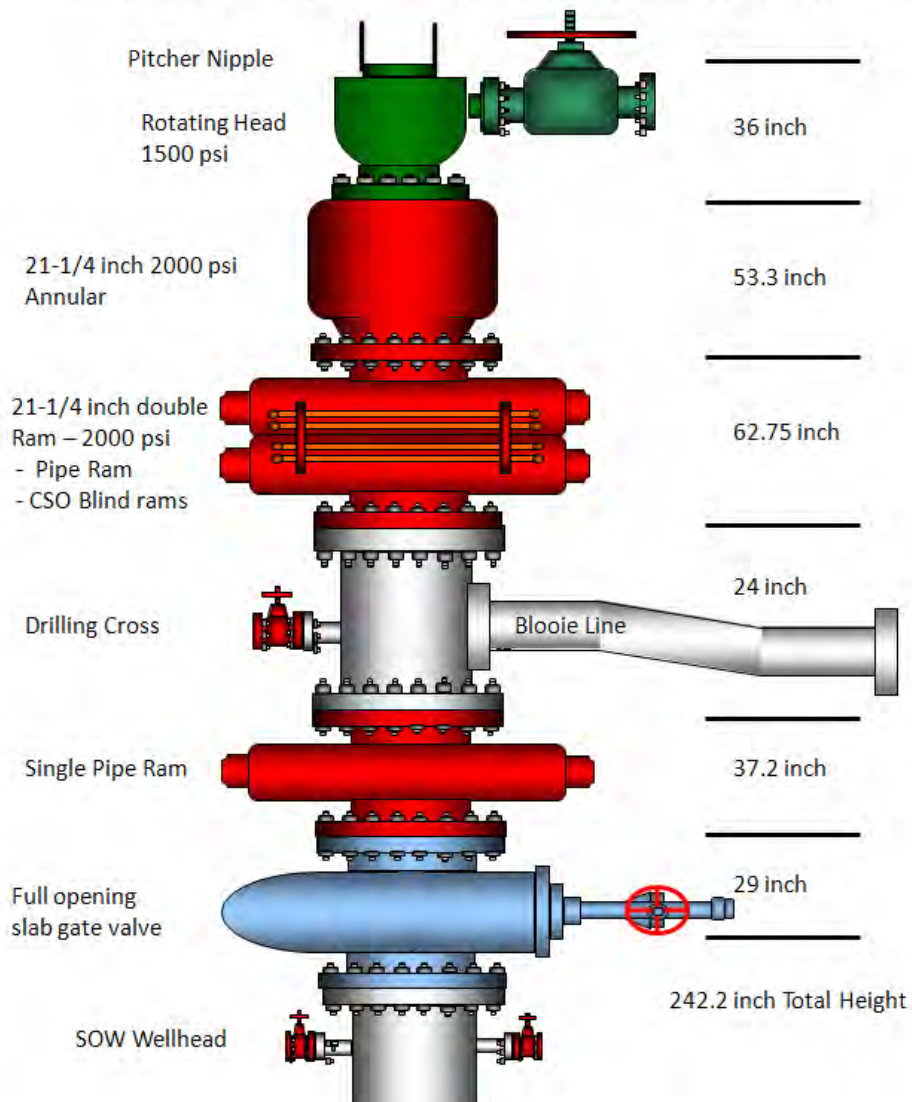


Figure 9-2. 21-1/4 in BOPE stack configuration.

The intermediate interval will be drilled from 305 to 1370 m (1000-4500 ft) with a 17-1/2 in bit. The BHA assembly will include:

- 17-1/2 in bit, (IADC class 5 TSI bit)
  - 5000 lb/diameter in = 87500 lbs
  - w/ 15% margin 100625 lbs
- Near bit stabilizer full gauge, 6 point roller reamer

- 30 ft x 10 in non-magnetic drill collar
- String stabilizer 1/8 in under gauge
- 30 ft 10 in non-magnetic drill collar
- String stabilizer 1/8 in under gauge
- Drill Collars
  - 3 drill collars (5 total) – 10 in – collar weight of 5 x 10 in drill collars 36400 lb
  - 21 drill collars – 30 ft x 8 in – collar weight of 21 x 8 in drill collars 99100 lb
  - Total collar weight 135500 lb in air: Buoyed weight 115500 lb
- Neutral point will be in the 8 in collars
- Geothermal rated shock sub
- 6 joints heavyweight drill pipe (5 in 1480 lb/joint)
- 5 in drill pipe for the remainder of the string
- Note: 9 in slow speed drilling motor may be used in this interval. If necessary, it will be placed just above the bit.

Shock subs, jars and non-magnetic directional collars will be substituted based on the directional survey instruments to be used.

High temperature, polymer-based drilling fluids will be used in this interval. The drilling fluids engineer will specify the composition and mud check frequency, and specify operating parameters for treatment in this interval. Temperature will increase significantly in this interval, so careful attention will be paid to changes in the mud properties.

Drill out the cement, plus 15 feet, by entering the hole with a 17-1/2 in bit and slick assembly of six 9 in drill collars. Perform a formation injection test to determine the fracture gradient.

### *9.3.8.2 END OF INTERVAL ACTIVITIES – LOGGING*

The logging program will be determined by the reservoir engineer. Equipment will be set up for running logs if required. The rig will use drilling fluid to circulate 4 to 8 hrs to clean the hole; at least 2 bottoms-up. Log the well interval and then rig down the logging company. Currently, only a sonic log is planned for this interval.

### *9.3.8.3 END OF INTERVAL ACTIVITIES – CEMENTING*

Run and cement the 13-3/8 in casing. The 13-3/8 in casing pressure, assuming 4500 feet of 9.6 lb/gal drilling fluid, will be 3.4 MPa (500 psi). The use of 72 lb/ft HC L80 casing, with a collapse rating of 23.9 MPa (3470 psi), provides a safety factor of 1.5, well in excess of the maximum recommended API collapse safety factor of 1.125. A contract casing crew will be used to run the intermediate casing string. The casing string will include:

- Guide shoe
- 2 joints 13-3/8 in casing for shoe track
- Float collar with stab-in inner liner drill pipe feature
- Remainder 13-3/8 in casing (4500 ft, 72 lb/ft, HC L80, buttress thread)
- Appropriate centralizers will be attached to the casing to provide a minimum of 70% standoff between the casing and the open hole or the last casing string. The location and number of centralizers required to achieve 70% standoff will depend on the casing size and weight, hole size, drilling fluid density, hole angle, centralizer bow strength, etc. The number and location of centralizers can be calculated along with the associated standoff using a standard program that is typically available from the major cement service companies. Centralizers will be placed on

the top two joints and bottom shoe joint to ensure that the casing is properly centralized at these critical locations.

Set up equipment to run casing. A casing crew will be employed to rig up the floor post and pulleys and trapeze for running casing. Clean, inspect and measure the casing on the pipe racks in anticipation of running the casing. Run 4500 ft of 13-3/8 in, 72 lb/ft, K55 buttress thread casing. Remove equipment used by the casing crew equipment. Set up rig to cement casing.

Circulate drilling fluid through the casing 2 to 4 hrs to clean the hole; at least 2 bottoms-up. Lower the gel strengths of the drilling fluid if possible and lower the progressive gel strength development. Flat versus sharply increasing progressive gel strength of the drilling fluid is optimal for displacement efficiency during the cement job.

Follow procedure in Section 9.4.2 for cementing. Cement job placement method will be reverse circulation to minimize circulation pressure during placement, aid in minimizing retarder loading in upper-hole interval, and reduce cement set time. Pressure test of casing will be conducted immediately after cement is placed before the cement has set. This will be done to minimize damage to the cement bond, since the cement will still be liquid at this point. Allow 8-12 hours for the cement to set before performing a top job, if needed. Use Tremmie tubes to ensure that the top job cement is placed directly on the cement top. Allow 8 hours for the top job cement to set completely. Drill out the cement in the shoe track a minimum of 24 hours after the primary cement job.

Allow 4 to 6 hours for cement to firm up and check for fall back and the need for a top job. Integral joint tubing (1-1/8 in) will be used to pump top out cement job. Determine whether the top job was successful or if another is necessary.

Wait on cement at least 24 hrs total before resumption of drilling activities (i.e., drilling out the 13-3/8 in casing shoe).



### 9.3.9 PRODUCTION CASING INTERVAL

#### 9.3.9.1 OPTION A: LONG STRING

##### 9.3.9.1.1 BEGINNING OF INTERVAL ACTIVITIES – WELLHEAD, BOPE AND FORMATION INJECTION TEST

Cut off the intermediate casing and weld on the 13-3/8 in SOW wellhead. Nipple up the 13-5/8 in 20.7 MPa (3000 psi) BOPE stack. Pressure test BOPE stack as per BLM requirements. Stack diagrams are provided in Figures 9-3 and 9-4 below for the various cases.

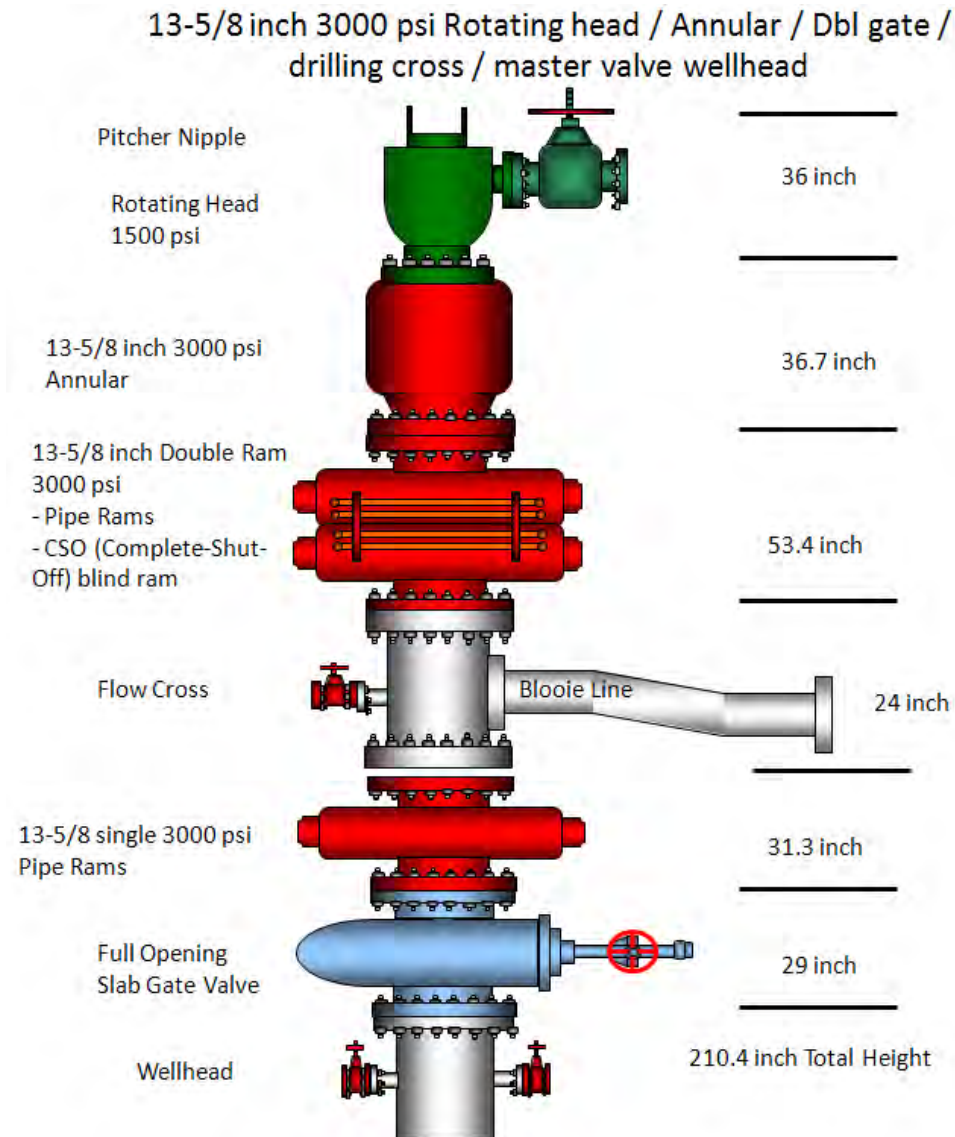


Figure 9-3. 13-5/8 in BOPE stack configuration (Cases 1 – 4).

16-3/4 inch 3000 psi Rotating head / Annular / Dbl gate / drilling cross / master valve / wellhead

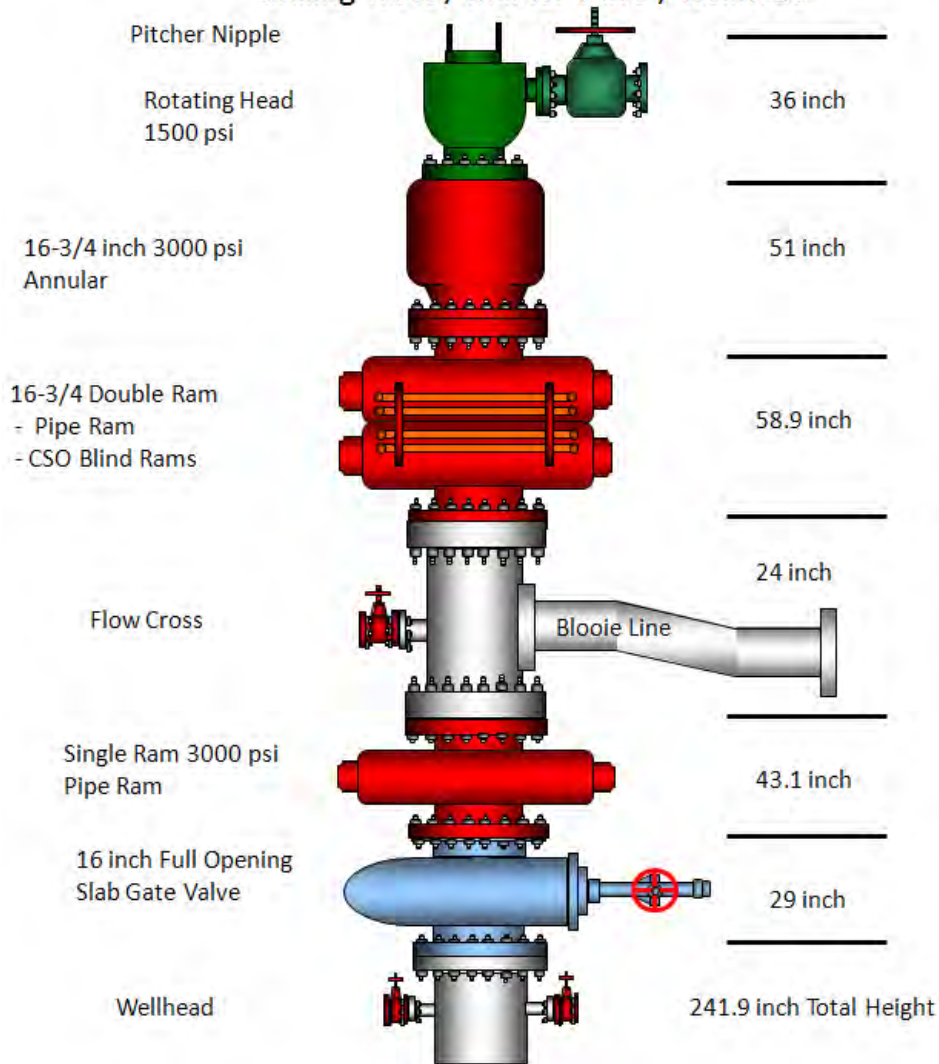


Figure 9-4. 16-3/4 in BOPE stack for Case 5 (“Large”).

Drill 6 m (20 ft) below the last joint of casing using the following assembly:

- 12-1/4 in bit
- 6 – 8 in x 2-3/4 in drill collars

Perform a formation leak-off injection test to determine the fracture gradient.

9.3.9.1.2 INTERVAL ACTIVITIES – BHA AND DRILLING

Enter the hole with a 12-1/4 in bit and BHA and drill to 2290 m (7500 ft). The BHA will include:

- 12-1/4 in bit IADC Class 5
  - 6000 lb/diameter in = 73500 lb
  - With 15% margin = 84500 lb
- 12-1/4 in near bit 6 pt roller reamer stabilizer full gauge
- 30 ft 9 in non-magnetic drill collar with mule shoe seat

- 12-1/4 string stabilizer 1/8 in under gauge (non-magnetic recommended)
- 30 ft 9 in non-magnetic drill collar
- 12-1/4 string stabilizer 1/8 under gauge
- Drill Collars
  - 3 drill collars (5 total) – 30 ft x 9 in – Drill collar weight 9 in collars 28830 lb buoyed
  - 21 drill collars – 7-1/4 in (x 2-1/2 in bore) drill collars – drill collar weight 7-1/4 in collars 71800 lb
  - Total collar weight 100630 lb in air, buoyed weight 85800 lb
- 6 joints of (5 in 1480 lb) heavy-weight drill pipe
- Enough 5 in drill pipe to complete the string
- Shock sub and jars will be integrated into the string.
- An 8 in, slow speed mud motor may be used depending on drilling progress.

#### *9.3.9.1.3 END OF INTERVAL ACTIVITIES – LOGGING*

The logging program will be determined by the reservoir engineer. Set up equipment for running logs, if required. Circulate 4 to 8 hrs to clean the hole; at least 2 bottoms-up. Log the well interval. Remove the logging equipment after logging operations. Currently, only a sonic log is planned.

#### *9.3.9.1.4 END OF INTERVAL ACTIVITIES – CEMENTING*

Run and cement the 9-5/8 in, 47 lb/ft, L-80 premium thread casing. Premium casing threads are used on the production string to reduce the risk of joint casing failure due to excessive compressive stress loading that can occur during cyclic stress due to thermal expansion. The casing pressure, assuming 7500 feet of 9.6 lb/gal drilling fluid, will be 25.8 MPa (3744 psi). The use of 47 lb/ft, L80 casing, with a collapse rating of 33.0 MPa (4780 psi), provides a safety factor of 1.28, greater than the maximum recommended API collapse safety factor of 1.125.

The casing will be installed by a casing service company. The 9-5/8 in casing will be stacked as follows:

- Guide shoe
- 2 joints 9-5/8 in casing
- Float collar with stab in if long string casing is used; conventional float collar if liner is used
- Remainder of the casing string
- Appropriate centralizers will be attached to the casing to provide a minimum of 70% standoff between the casing and the open hole. The location and number of centralizers required to achieve 70% standoff will depend on the casing size and weight, hole size, drilling fluid density, hole angle, centralizer bow strength, etc. The number and location of centralizers can be calculated along with the associated standoff using a standard program that is typically available from the major cement service companies. Centralizers will be placed on the top two joints (if long string casing) and the bottom shoe joint to ensure that the casing is properly centralized at these critical locations.
- If a liner is run, an expandable liner hanger will be utilized to ensure positive seal at the top of the liner lap
- Liner lap will be a minimum of 91 m (300 ft) if liner is run

A casing crew will be employed to rig up the floor post, pulleys, and trapeze for running casing. Clean, inspect and measure the casing on the pipe racks in anticipation of running the casing. Run the casing. Take down the casing crew equipment. Set up necessary equipment to cement casing. Circulate 4 to 8 hrs to clean the hole; at least 2 bottoms up. Lower the gel strengths of the drilling fluid if possible and

lower the progressive gel strength development. Flat versus sharply increasing progressive gel strength of the drilling fluid is optimal.

Follow procedure given in Section 9.4-3 for cementing. An inner string (stab-in drill pipe) reverse circulation foam cement job will be used to provide cement that has a reduced modulus of elasticity. The foam cement will accommodate thermal variations better than standard cement. It also reduces circulation pressure during placement, which, in turn, reduces the risk of lost circulation. Reverse circulation also provides a means of reducing retarder loading in upper stages of the cement, which results in a faster setting time for cement at the surface. Pressure test of the casing will be conducted immediately after cement is placed before the cement has set. This will be done to minimize the damage to the cement bond, since the cement will still be liquid at this point. Allow 4 to 6 hours for cement to firm up and check for fall back and the need for a top job. Integral joint tubing (1-1/8 in) will be used to pump top out cement job. Determine whether the top job was successful. Repeat a top job, if necessary. Drill out the cement in the shoe track a minimum of 24 hours after the primary cement job.

#### *9.3.9.2 PRODUCTION CASING INTERVAL – LINER OPTION*

The production casing for this interval will be the same as Option A with the exception that a shorter 'liner' string will be run and cemented in place. The circulation method will be conventional, down through the drill pipe and up the annulus (Cementing Procedures 9.3.2B). Other changes will include:

- An expandable liner hanger will be used along with necessary cement dart and plugs.
- The cement at the top of the liner will be drilled out 24 hours after the cementing operation.
- There will be no "top jobs" because cement will not be circulated back to the surface.

#### *9.3.10 OPEN-HOLE INTERVAL OR PERFORATED LINER*

##### *9.3.10.1 BEGINNING OF INTERVAL ACTIVITIES – WELLHEAD, BOPE AND FORMATION INJECTION TEST*

Pressure test and check out the 13-5/8 in BOPE tests before drilling out the cement at the shoe of the 9-5/8 in casing. Wait on cement at least 24 hours before resumption of drilling activities (i.e., drilling out the 9-5/8 in casing shoe).

Drill out the shoe cement plus an additional 15 m (50 ft) with 8-1/2 in slick drilling assembly. Perform a minifrac test (Appendix I-3 for procedure) to determine the maximum in-situ stress. Determine minimum horizontal stress magnitude by inducing tensile failure of the rock through high pressure, low rate and low volume injection.

##### *9.3.10.2 INTERVAL ACTIVITIES – BHA AND DRILLING*

Enter the hole with an 8-1/2 in bit and BHA and drill to 3050 m (10000 ft) or until permeable fractures are intersected. In this drilling interval the directional program will initially determine the BHA. For conventional 8-1/2 in drilling, which may occur once the direction is set, the following BHA will be used:

- 8-1/2 in IADC Class 5 TCI bit
  - Using 5000 lb/diameter in = 42500 lb
  - With a 15% margin a drill collar weight of 48900 lb is needed
- 8-1/2 in full gauge roller reamer
- 30 ft x 7-1/4 in non-magnetic drill collar
- 8-1/2 in x 1/8 in under gauge string stabilizer
- 30 ft x 7-1/4 in non-magnetic drill collar

- 8-1/2 in x 1/8 in under gauge string stabilizer
- Drill Collars
  - 6 drill collars (8 total drill collars) – 7-1/4 in – Total 7-1/4 in collar weight is 27300 lb
  - 12 drill collars – 6-1/2 in – Total 6-1/2 in collar weight is 35700 lb
  - Total collar weight in air – 63000 lb, buoyed weight 53700 lb
- 6 x 4-1/2 in heavy-weight drill pipe
- 5 in or 4-1/2 in drill pipe to complete the string

The drilling fluid condition will be monitored closely and the viscosity reduced in this interval. It is most desirable to drill into the fractured void with clear water to prevent formation damage from cuttings and clay-laden drilling fluids. Aerated drilling fluids can be used to drill into the fractured volumes to mitigate contamination.

No cemented casing is planned in this interval. This zone will either be an open-hole completion or a perforated liner will be installed. The decision about whether or not to use the perforated liner will be based on borehole stability encountered while drilling the interval.

### *9.3.10.3 INTERVAL ACTIVITIES – DRILLING THROUGH FRACTURE ZONES*

The goal of drilling this well is to intersect the stimulated fractures so that fluid can be circulated from NWG 55-29 to the adjacent production wells. It is therefore critical that the well path intersect as much of the stimulated fractures as possible. To help detect when the fractures are intersected the fluid level of the drilling fluid tanks will be monitored while drilling in the open-hole interval. Adjustments will be made to the drilling program to drill this interval in an underbalanced pressure condition to minimize damage from drill cuttings and drill solids entering the stimulated fractures and plugging them off to flow. As a result, increased fluid levels are expected to occur. These changes in fluid levels will be recorded regularly to help determine when a given fracture network is intersected and when the intersection has ended. To aid in this process water will be injected into NWG 55-29 to maintain pressure in the fractures and help with drilling underbalanced in the open-hole section of these production wells.

### *9.3.10.4 END OF INTERVAL ACTIVITIES – DUAL STIMULATION PREPARATION AND LOGGING*

To prepare the well for possible dual stimulation, the hole will be circulated with viscous sweeps and drilling fluid after drilling has reached the target depth. Drill pipe will be removed from the well, the drilling assembly removed, and the drill pipe with no drilling assembly attached to bottom will be run to the bottom of the well. The hole will then be circulated with viscous sweeps and then fresh water to remove all solids from the hole in preparation for stimulation. The hole will be circulated with fresh water for 12 hours to cool the well (Figure 9-5). The drill pipe will again be tripped out of the hole and the Bore Hole Televiewer (BHTV) will be immediately run into the well. An attempt will be made to run the BHTV as deep as possible in the well without exceeding the instrument temperature capability.

Because of the relative importance of the data, the BHTV will be run first. The other logs will be run after the BHTV. To cool the hole for the second logging run, it is likely that an additional trip to bottom with drill pipe followed by circulation of the well will be required. An open-hole log suite containing sonic, density, neutron porosity, gamma ray, and induction logs will be a part of the second logging run. For the third logging run, with the pressure and temperature surveying instruments, no additional cooling will be required because high temperature memory tools can withstand bottom hole, static temperatures in excess of 316°C (600°F).



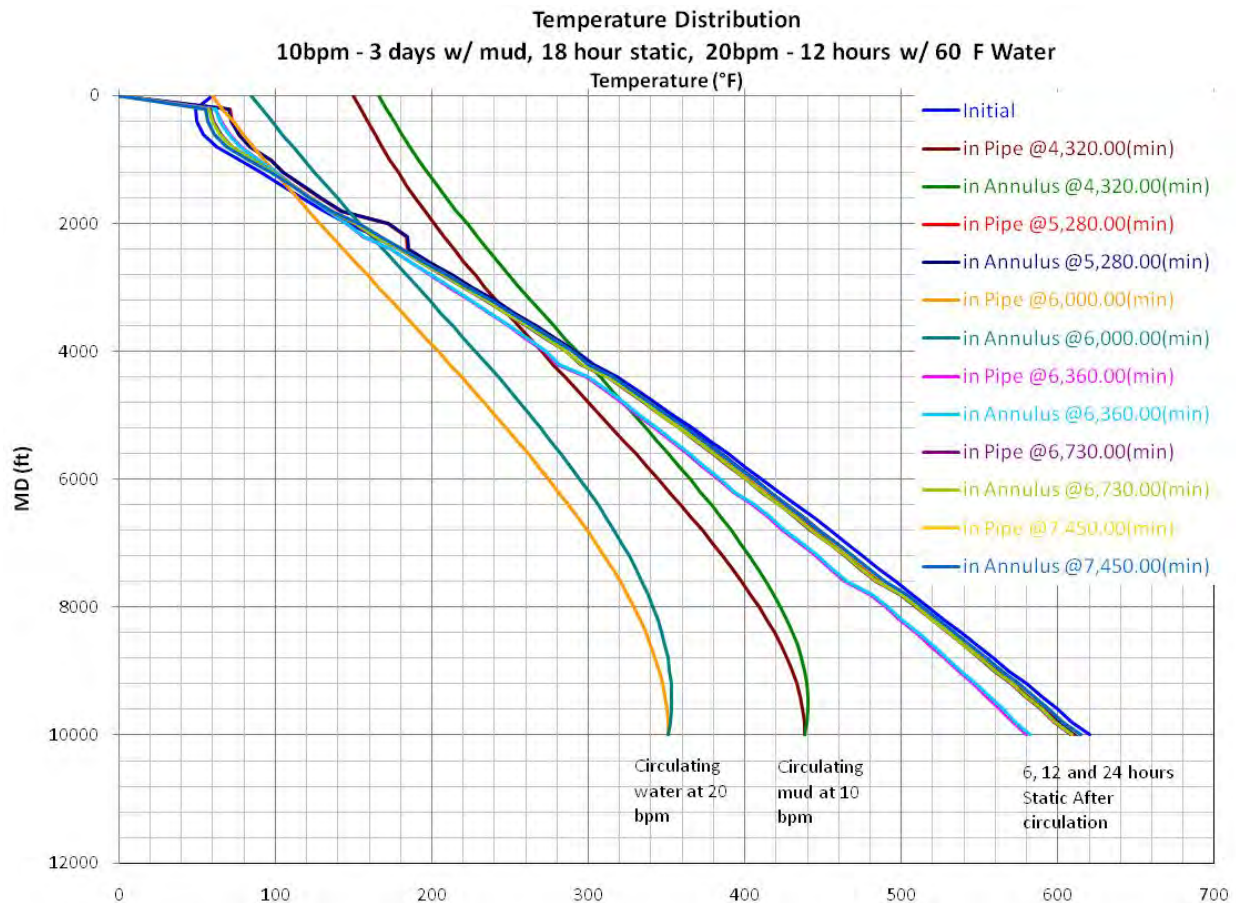


**Figure 9-5. Temperature simulation of cooling and thermal recovery prior to and during logging operations. The inputs include the circulation of 66°C (150°F) mud for 3 days, followed by 18 hours of shut-in and by 12 hours circulation of 16°C (60°F) water. The bottom-hole temperature is modeled after 6, 12 and 24 hours of static time based on injectivity test results.**

Log the well interval. Remove the logging equipment after logging operations. A portion of the logging program may involve flow testing with logging equipment to monitor results. A complete suite of logs will be run in this interval, including:

- First Logging Run
  - Ultrasonic Bore-Hole Viewer (BHTV)
- Second Logging Run
  - Fullwave Sonic
  - Neutron porosity
  - Density
  - Natural Gamma Ray
  - Induction
- Third Logging run
  - Pressure-Temperature-Spinner Survey

### 9.3.10.5 *END OF INTERVAL ACTIVITIES – RUN PERFORATED LINER*

If a perforated liner is necessary due to the instability of the open-hole formation, a casing crew will be employed to rig up the floor post, pulleys and trapeze for running casing. The casing will be cleaned,

inspected and measured on the pipe racks prior to being run in the well. The casing will be run and released at the bottom of the hole. The casing crew equipment will then be removed.

#### 9.3.10.6 *END OF RIG ACTIVITIES*

- Put rig on standby
- Perform rig-on injection and production test
  - Rig up for flow test
  - Flow well for 7 days
  - Stimulate well (if necessary)
- Move the rig to the second production location or release rig

## 9.4 CEMENTING PLAN

The goals of the cementing operation will be to:

- Fill the annulus between the casing and open hole of a given interval completely with the given cementing system during the primary cementing operation
- Place a cement material that, when set, will support the casing and provide zonal isolation during the life of the well
- Minimize waste cement
- Minimize risk by following operational procedures and risk mitigation plans

### 9.4.1 *SURFACE CASING CEMENTING PLAN*

**Well Conditions:** The 20 in surface casing will be set at 305 m (1000 ft) with a bottom-hole static temperature (BHST) of 32°C (90°F) and an expected bottom hole circulation temperature (BHCT) of 27°C (80°F) (Figure 3-2). Lost circulation will most likely be a significant risk during placement of the cement (Appendix I-3).

**Circulation Method:** The circulation method will be conventional with the use of stab-in drill pipe. This will require a stab-in float collar for the 20 in casing that will be placed one joint above the bottom of the 1000 ft-long casing string.

**Cement Design:** The density will be 15.6 lb/gal with 40% silica flour (fine crystalline silicon dioxide), 6.73 gallons per sack (gal/sk, where sk = 94 lb sack) mixing fluid, and 1.63 ft<sup>3</sup>/sk. An equivalent of 1% calcium chloride will be added to the mix water to accelerate the compressive strength of the cement after placement due to the relatively low BHST across this interval. Additional calcium chloride may be added to the un-foamed cap, shoe, and shoe track cement to further accelerate the set and strength development of the cement at the top and bottom of the casing string. Foaming surfactants will be injected into the cement slurry to provide foam stability after placement while the cement sets. Foam cement has been chosen to allow for circulation of lightweight cement that has acceptable compressive strength. This will help ensure that a full column of cement will be placed even with the potential lost circulation problems. The foam cement will also have the added advantage of improved mechanical properties and long term durability over the life of the well.

**Job Procedure:**

- Pump 16 m<sup>3</sup> (100 bbls) of water
- Pump 8 m<sup>3</sup> (50 bbls) of chemical flush (foamed if significant lost circulation occurs during circulation).
- Pump 50 bbls of foamed water

- Pump open-hole volume of cement, plus 50% excess for wash-outs. Foam base slurry down to 11 lb/gal
- Take returns and foamed fluid returns to holding tank after all drilling fluid has been circulated out of hole
- Once foamed cement is seen at surface, indicating that the entire annulus has been filled with cement, turn off nitrogen and pump base cement (un-foamed) to provide a 61 m (200 ft) of shoe cement
- Shut in back side while mixing and pumping shoe cement
- Displace shoe cement with latch-down dart
- Pump  $\pm$  20 bbls of accelerated un-foamed cap cement down backside
- Pressure test casing
- Allow cement to cure 24 hours before resumption of drilling operations

#### 9.4.2 INTERMEDIATE CASING CEMENTING PLAN

**Well Conditions:** The intermediate 13-3/8 in casing will be set at 1370 m (4500 ft) with a bottom-hole static temperature (BHST) of 165°C (328°F) (Figure 3-2) and an expected bottom-hole circulation temperature (BHCT) of  $\pm$  93°C (200°F). Lost circulation may be a minor risk during placement of the cement.

**Circulation Method:** The circulation method will be reverse with the use of a stab-in drill pipe. This will require the use of a stab-in float collar for the 13-3/8 in casing that will be placed 1 joint above the bottom of the 4500 ft long casing string. Reverse circulation will allow for the staging of cement retarder as the slurry is pumped in the hole, with higher levels of retarder injected into the slurry that is placed near the bottom of the casing, and less or no retarder in the cement closer to the surface at lower well temperature. This will help minimize the set time for the cement. This method will also help minimize the amount of excess cement that will need to be mixed and pumped, which will reduce the cost of the job, and reduced waste cement disposal.

**Cement Design:** The density of the base cement slurry will be 15.4 lb/gal with 50% silica flour (fine crystalline silicon dioxide), 7.46 gal/sk mixing fluid, and 1.76 ft<sup>3</sup>/sk. A retarder will be injected in stages as needed to keep the cement slurry liquid during placement. Foaming surfactants will be injected into the mixed based cement slurry to provide foam stability after placement while the cement sets. The base slurry will be foamed to a density of 12 lb/gal. Foam cement has been chosen because of its superior mechanical properties, which will help prevent brittle failure of the cement during cyclic loading due to pressure and temperature changes over the life of the well. The foam cement will also provide a lightweight cement to mitigate potential lost circulation. The foam cement strategy will help ensure that a full column of cement will be placed.

#### **Job Procedure:**

- Pump 100 bbls of water.
- Pump 50 bbls of chemical flush (foamed if significant lost circulation occurs during circulation).
- Pump 50 bbls of foamed water.
- Pump open-hole volume of cement plus 35% excess for wash-outs. Foam base slurry down to 12 lb/gal.
- Take returns and foamed fluid returns from the drill pipe to a holding tank after all drilling fluid has been circulated out of hole.
- Once foamed cement is seen at surface, indicating that the entire annulus has been filled with cement, turn off nitrogen and pump an un-foamed shoe and shoe track cement down the drill-

pipe while holding the annulus closed. The shoe track will be 12 m (40 ft) long and the shoe cement in the annulus will be 91 to 152 m (300-500 ft) in length.

- Displace foam cement down the drill pipe with a latch down dart. The dart provides positive surface indication when cement is completely displaced down the drill pipe. The dart also provides a means of preventing reverse flow of cement into the casing from the annulus after the job is completed. Land dart with 3.4 MPa (500 psi) and then un-stab drill pipe and check that the flapper valve is holding.
- Pump (accelerated) base cement down the annulus to provide 100 ft cap cement.
- Pressure test casing.
- Allow cement to cure 24 hours before resumption of drilling operations.

### 9.4.3 DEEP LINER AND LONG STRING CEMENTING PLAN

**Well Conditions:** The deep 9-5/8 in liner or long string will be set at 2290 m (7500 ft) with a BHST of 260°C (500°F) (Figure 3-2) and BHCT of  $\pm 120^\circ\text{C}$  (250°F). Lost circulation will be a minor risk during placement of the cement.

**Circulation Method:** If a liner is used, the circulation method will be conventional. An expandable liner hanger will be used to hold the cement in place and hold the liner in place after cementing. If a long string of casing is used, a reverse circulation cement job will be done. Reverse circulation will allow for the staging of cement retarder as the slurry is pumped in the hole, with higher levels of retarder injected into the slurry that is placed near the bottom of the casing, and less or no retarder in the cement closer to the surface at lower well temperature. This method will help minimize the set time for the cement. This method will also help minimize the amount of excess cement that will need to be mixed and pumped, which will reduce the cost of the job and need to dispose of waste cement.

**Cement Design:** The density of the base cement slurry will be 15.4 lb/gal with 50% silica flour (fine crystalline silicon dioxide), 7.46 gal/sk mixing fluid, and 1.76 ft<sup>3</sup>/sk. A retarder will be injected in stages as needed to keep the cement slurry liquid during placement. Foaming surfactants will be injected into the mixed based cement slurry to provide foam stability after placement while the cement sets. The base slurry will be foamed to a density of 12 lb/gal. Foam cement has been chosen because of the superior mechanical properties which will help prevent brittle failure of the cement during cyclic loading due to pressure and temperature changes over the life of the well. The light-weight foam cement will minimize potential lost circulation. This strategy will help ensure that a full column of cement will be placed.

#### **Job Procedure:**

- Pump 100 bbls of water.
- Pump 50 bbls of chemical flush (foamed if significant lost circulation occurs during circulation).
- Pump 50 bbls of foamed water.
- Pump open-hole volume of cement plus 25% excess for wash-outs. Foam base slurry down to 12 lb/gal. Un-foamed tail cement slurry will be pumped at the end of the job to cover between 91 and 152 m (300 and 500 ft) of annulus at the bottom of the 9-5/8 in liner.
- Place diverter packer at surface between the drill pipe and the 13-3/8 in last casing string to hold back pressure in case the foamed fluids return to surface during the job.
- Displace shoe cement down the dart that latches into the 9-5/8 in top plug. Continue to displace the top plug until it lands on 9-5/8 in casing shoe and apply an additional 500 psi.
- Set expandable liner hanger, un-set drill pipe from top of liner and circulate out any cement on top of the liner.

- Pull drill pipe out of the hole.
- Pressure test casing.
- Allow cement to cure 24 hours before resumption of drilling operations.

#### 9.4.4 OPEN HOLE CEMENT PLUGS

##### 9.4.4.1 LOST CIRCULATION PLUGS

In situations where extreme lost circulation is encountered and an open-hole cement plug is necessary the following guidelines should be followed:

- Use base cement slurry consisting of Class G cement with 35% silica flour. Additional material such as Perlite may be added to the blend to help solve lost circulation.
- Estimate or measure the temperature of the drilling fluid while circulating drilling fluid through drill pipe (Bottom Hole Circulation Temperature, BHCT)
- Test the cement slurry for thickening time at estimated BHCT. The cement slurry should have a minimum of 2 hours of thickening time.
- Calculate the hole volume and do not use more than 100% excess above bit size to account for wash-outs. Use a plug length of  $\pm 61$  m (200 ft) of open hole.
- The drill pipe should be run in the hole, open-ended, with no check valves or other tools in the work string that would hinder pulling DP after the cement has been emplaced.
- After a balanced plug has been placed, the drill pipe should immediately be pulled out of the plug to 1.5 plug lengths above the estimated top of cement.

##### 9.4.4.2 KICK-OFF PLUGS

In the event that an open-hole kick-off plug must be set to side-track around a fish, the following guidelines will apply:

- Use no more than 50% open-hole excess for volume calculations.
- Use densified, high strength cement slurry.
- Test cement at estimated BHCT. Use static temperature gradient, return fluid temperature while circulating at depth, and possibly temperature simulation to estimate BHCT.
- Design cement to have  $\pm 3$  hours of thickening time to allow for safe placement of the slurry.
- Use open-ended drill pipe with no check valves or other attachments that would impede pulling drill pipe out of the hole after cement plug placement.
- After placement of cement, pull completely out of cement plug and at least one plug length above estimated plug top before stopping to circulate hole.

## 9.5 LOGGING PLAN

Each new production well will be immediately logged after total depth is reached while the drilling rig is still onsite. To prepare the well for possible stimulation the hole will be circulated with viscous sweeps and drilling fluid after drilling operations have reached the target depth. The drill pipe will then be removed from the well, the bottom-hole assembly will be laid down, and the drill pipe will be run open-ended to the bottom of the well. The hole will be circulated with viscous sweeps, then fresh water to remove all solids from the hole in preparation for a possible stimulation. The hole will be circulated with fresh water for 12 hours to cool the well (Figure 9.3-4). The drill pipe will again be tripped out of the hole and the BHTV will be immediately run into the well. An attempt will be made to run the BHTV as deep as possible without exceeding the temperature capabilities of this logging tool.



Because of the relative importance of the data, the BHTV will be run first. The other logs will be run after the BHTV. The second logging suite includes an induction log to measure resistivity, a sonic log to measure interval transit time, lithodensity or spectral density logs to measure electron density, and natural gamma ray log to measure the presence of uranium, thorium and potassium in the rock formations. A static and injecting PTS survey will also be performed along with a caliper survey. The static PTS survey will be run immediately following the open-hole logging run. A second static pressure-temperature survey will be conducted approximately three to seven days after the first, so that a comparison between the two surveys can be made and the well heat-up rate can be determined. Table 9-5 summarizes the available high temperature logging tools and their temperature limitations.

**Table 9-5. High temperature tool options for open-hole logging and their temperature limitations.**

<b>High-Temperature Tool Options</b>	<b>Temperature Rating</b>
Halliburton HEAT suite (GR, spectral density, full-wave sonic, induction, neutron density)	260°C (500°F)
Schlumberger Xtreme suite (GR, neutron density, full-wave sonic, induction, lithodensity)	260°C (500°F)
Baker Atlas Nautilus suite (GR, neutron density, full-wave sonic, induction, lithodensity)	260°C (500°F)
Tiger Energy Services Acoustic Formation Imaging Technology tool	300°C (572°F)
USGS ALT acoustic televiewer, non-commercial tool	268°C (514°F)
Tiger PTS data-relay tool	260°C (500°F)
Tiger PT memory tool	350°C (662°F)
Welaco PTS data-relay tool	260°C (500°F)
Pacific Process Systems PT memory tool	316°C (600°F)

## 9.6 RISK MITIGATION AND CONTINGENCIES

### 9.6.1 SAFETY

- General - Daily safety meetings will be held wherein pending operations are reviewed, safety hazards and incidents are discussed and the emergency plan and evacuation route are reviewed.
- Safety Training - Safety training will be required for all personnel who come to location during drilling operations. This will be monitored and overseen by drilling rig contractor personnel.
- PPE - All personnel on location during drilling operations will be required to wear appropriate personal protection equipment (PPE) while working on site. This will include leather gloves, hard hat, safety glasses and steel-toed footwear, at a minimum.
- H<sub>2</sub>S Monitoring - H<sub>2</sub>S monitoring equipment and contractors certified in their proper use will be utilized on site during stimulation, drilling and flow test operations. During active rig operations, the drilling contractor will be responsible for H<sub>2</sub>S monitoring. Windssocks are installed on location to aid in wind direction determination in case of an emergency.
- Driving – All personnel visiting or working at the site will be informed of the 25 mph speed limit on FS roads, lease roads and well pads. There are no speed limit signs posted so the rig operator will be required to inform all staff and contractors to observe these speed limits on all FS roads.
- Parking - All passenger vehicles will be required to park in designated parking areas. In addition, all passenger vehicles will be required to follow the first-out-forward rule. That is, all vehicles will be required to be parked in such a way that their first movement when leaving location will be forward. The drilling contractor or site supervisor will be responsible for monitoring and enforcing this rule.
- Personnel Access to Rig Site - Personnel on location will be required to first register when they arrive on location. They will also be required to sign out when leaving location. The drilling contractor will be required to monitor and enforce this policy.

## 9.6.2 DRILLING RISK MITIGATION

Drilling risks are outlined below, along with the plans and procedures that will be implemented to mitigate these risks.

### 9.6.2.1 LOST CIRCULATION

Lost circulation is a known risk for wells drilled at Newberry, especially in the top 305 m (1000 ft) of the well. To mitigate this risk the following steps will be taken.

- Conventional lost circulation materials in the drilling fluid will be used while drilling the top 1000 ft interval. If this does not stop major losses, the drilling fluid will be lightened by aeration. This should allow for drilling of this interval to the target depth.
- In cases of severe lost circulation, an open-hole cement plug will be set to seal off the zone. The optimal cement design is a slurry with low to moderate compressive strength to help minimize the chance of kicking off the plug and starting a new hole. To achieve this outcome, the density of the cement should be 13.0 lb/gal or less. Another more effective method would be to spot an open-hole foam cement plug. This strategy would lower the compressive strength of the resulting plug. It would also provide a means of lowering the cement density to as low as 9 lb/gal or less while still providing a competent cement to seal the lost circulation zone. Finally, the foam cement would expand into the lost circulation zone after placement to fill large voids.

This same general procedure will be used to address the problem of lost circulation while drilling the remainder of the well except in the open-hole interval, where the use of conventional lost circulation materials will be avoided. LCM will be avoided in order to minimize formation/fracture damage, which could ultimately impede flow into the wellbore during the long term circulation test.

### 9.6.2.2 STUCK PIPE

Getting the drill pipe stuck during drilling is a significant risk. To minimize the risk of stuck pipe, the hole must be kept clean of cuttings. This will be accomplished by pumping viscous sweeps periodically while drilling to help clean drill cuttings from the well. Also, minimizing lost circulation with aeration and/or lost circulation material will greatly reduce the possibility of getting stuck from cuttings falling out of the drilling fluid around the bit.

To aid in reducing the risk of stuck pipe extra mud pumps or high capacity pumps will be on location to aid in achieving increased pump rates to help reduce the risk of stuck pipe. In addition, air compressors will be on site to aid in lightening the drilling fluid as needed to both reduce the risk of stuck pipe and aid with potential lost circulation problems.

Another rule that must be followed during drilling operations to prevent cuttings from falling out around the drill bit is to never stop circulation while the bit is on the bottom of the hole.

Another operational practice to reduce the risk of getting the drill pipe stuck is to never by-pass the shale shakers in the mud pits when circulating the drilling fluid in the well. This practice is sometimes employed when circulation losses occur. The thinking is that the additional solids that remain in the drilling fluid will help seal off the lost circulation zones. The problem is that these same solids can fall out of the drilling fluid and stick the drill pipe and the drilling assembly. In addition, the solids can cause significant damage to the mud pumps at surface leading to equipment failure and rig down-time.

If the drill pipe does get stuck the following guidelines will be followed:

- Attempt to get loose
  - Jarring with pipe lubricant

- Attempt to pump hole clean, using aeration and/or viscous sweeps as needed
- If cannot get loose
  - Do free point
  - Back off drill pipe
  - Drill over with wash pipe
  - Jar casing loose
- If the drill pipe is still stuck after a total of 3 days, a cement plug will be placed on top of the fish (follow best practices for plug cementing) and the drilling rig will either be skidded over and a new hole started (if total depth of the well is still shallow) or the well will be side-tracked.

### 9.6.2.3 *LOSS OF DRILLING EQUIPMENT IN OPEN HOLE*

The loss of expensive mud motors and drilling assemblies not only poses a significant cost risk to the operation but could also significantly delay the completion of the well. AltaRock will mitigate this risk by addressing the issue of stuck pipe as discussed above. We will also use mud coolers to minimize temperature at the bottom of the hole and thus minimize risk of exceeding temperature limits of mud motors and down-hole equipment. We will also monitor drilling fluid return temperatures and use temperature simulation software to estimate BHCT to ensure that existing temperature limitations of the equipment are not exceeded.

### 9.6.2.4 *INCOMPLETE ANNULAR FILL*

A major risk in drilling of geothermal well completion is having a cementing operation result in incomplete annular fill. Inadequate cement coverage can lead to casing collapse or other forms of casing damage if the casing is not supported over its entire length. To mitigate this risk a number of practices will be followed including:

- Use of lost circulation materials while drilling: If lost circulation can be reduced by treating the formations while drilling, it will reduce the risk of an incomplete annular fill.
- Use of light weight foam cement: A major cause of incomplete annular fill is loss circulation occurring during placement. This complication often results in incomplete annular fill. To reduce this risk, it is helpful to reduce the density of the cement system. Normal lightweight cements are limited to around 11 lb/gal and have very poor mechanical properties when set. Foam cement has improved mechanical properties (better than conventional normal weight cement) and can reduce the density of the cement during placement to as low as 9 lb/gal or less, while still providing an effective seal.
- Use of reverse circulation placement method: Another method of reducing the risk of loss circulation during cement placement is to pump in ‘reverse’, rather than conventionally (down the casing and up the annulus). This technique greatly reduces the pressure at the bottom of the hole during placement of the cement, thus minimizing the risk of lost circulation. A number of other associated advantages are achieved with this method as well, including reduction of the amount of excess waste cement that must be disposed of and shortening the waiting time for the cement to set.

### 9.6.2.5 *DAMAGE TO STIMULATED FRACTURES*

Another major risk while drilling is plugging or otherwise damaging permeability in the stimulated fractures due to the migration of drill cuttings and other drill solids into the stimulated fractures. To mitigate this risk the following procedures will be implemented:

- Underbalanced drilling: While drilling the open-hole section, an attempt will be made to drill underbalanced with respect to the pressure in the stimulated fractures. This method should prevent loss of drilling fluid and associated solids into the stimulated fractures. The pit levels will be monitored closely during this portion of the drilling operation for net fluid gain. It should not pose any significant drilling risk when this occurs, as the fluid is only hot water.
- Injection into NWG 55-29: Water will be injected into NWG 55-29 to maintain the pressure in the stimulated fractures. As the wellbore intersects the stimulated fractures a net flow of (hot) production fluid should occur into the wellbore preventing the infusion of drilling fluid, and associated solids, into the stimulated fractures.
- Non-damaging drilling fluid: The drilling fluid used while drilling the open-hole interval will contain a minimum of solids to reduce the risk of fracture damage. A minimum amount of bentonite clay will be used. High temperature polymers will be substituted as much as possible to add required viscosity to the drilling fluid. If lost circulation material is used, it will be a material like calcium carbonate, which can be readily removed with a mild acid or other treatment fluid. Other potential lost circulation materials could include proprietary diverter materials that can temporarily seal the fractures but will then degrade and dissolve over time in the presence of water and elevated temperature.
- Aeration: Aeration of the drilling fluid will also be used to reduce the density of the drilling fluid and aid in getting the well in an underbalanced pressure condition. Also, the aeration will aid in carrying drill solids and cuttings out of the well.
- Viscous Sweeps: Pump viscous sweeps (volume of highly viscous fluid) while drilling this hole section to help clean out excess drill solids and cuttings that may not be circulating out of the hole.

#### 9.6.2.6 *GENERAL OPERATIONS*

All major operations that occur during the drilling operation will have written procedures. These procedures will be made available to both the operator and all vendors and personnel that will be involved in that given operation. In addition, safety meetings will be held prior to all major operations where the given procedure will be reviewed prior to the actual operation being performed.

#### 9.6.2.7 *WINTER DRILLING*

Another major risk is the possibility of having to do a portion of the drilling during winter with freezing temperatures and deep snow. Drilling in severe winter conditions will not slow drilling if the following mitigation is applied:

- Retain drilling supervisor(s) with experience in winter operations
- Provide road clearing and transportation to the site from Highway 70
- Winterize drilling rig and associated equipment, including coverings for rig and floor
- Utilize boilers, fuel heaters and pipeline insulation to prevent fluids from freezing
- Supply heaters for mud tanks
- Add heaters to water meter cabinet and electric heat rap on all water lines

#### 9.6.2.8 *CORROSION OF PRODUCTION CASING*

Another risk is the possibility of the produced geofluid causing corrosion of the production casing string. To address this risk the following steps will be taken:

- Sample and analyze produced fluids during flow testing to identify the corrosion potential.

- If the production fluid is determined to prevent a substantial corrosion risk, one or more of the following steps can be taken:
  - Apply appropriate chemical treatment, such as commonly used geothermal filming amines, to protect metallurgy from geofluid attack.
  - Change casing grade to increase corrosion resistance.

### **9.6.3 LOGGING CONTINGENCIES AND RISK MITIGATION**

Concerns have been raised about the risks associated with open-hole logging and whether or not these risks outweigh the benefits of the data collection. Certain risk is inherent in all down-hole survey operations. Any time a tool is run in the open-hole, there is a risk that the tool will be lost or damaged. The logging risks associated with the Newberry demonstration site are outlined below:

1. Temperature – The wells will be exceptionally hot at depth, with temperatures exceeding 316°C at 3050 m (600°F at 10000 ft). The high temperature environment creates the greatest potential for internal tool damage. If the well has not been cooled by drilling operations, the open-hole ‘triple combo’ logging suite will not be utilized because these tools are rated to a maximum internal temperature of 260°C (500°F).
2. Thermal contraction – The pumping and circulation of cold water can cause volcanic formations to spall at the wellbore face and fall into the open-hole. During logging operations, the well remains static and begins to heat up, so spalling should not be a significant risk because the formation will be expanding and not contracting. The greatest potential for spalling occurs during circulation and injection.
3. Stuck tools from swelling clays – Swelling clays (e.g., illite, smectite) are only present in small quantities in this area, thus posing negligible risk.
4. Stuck tool due to well bore obstruction – Tools can become stuck if they hit a liner top or an unanticipated bottom or ledge at high speed. Written operating procedures will require that safe logging practices, including wireline speeds below 0.77 m/s (150 ft/min), are always followed. The wireline operators will be made aware of the wellbore configuration and will be required to slow down to 0.15 m/s (30 ft/min) when approaching liner tops and any other known obstruction or constriction.

The logging companies have a vested interest in ensuring the safe operation of their tools, so many safety nets have been added to logging operations to decrease the likelihood of tool damage. The open-hole logging suites and BHTV tools will be run in conjunction with temperature and tension measuring devices. Temperature is monitored continuously to ensure that the maximum tool and wireline ratings are not exceeded. The temperature readings must be watched vigilantly to ensure that damage does not occur. Operating procedures will clearly communicate to the logging company that the limitations of the tool are not to be exceeded under any circumstances. In addition to temperature monitoring, the logging trucks also have built-in tension measurement. Halliburton and Schlumberger, for example, require a tension survey to be run in conjunction with their high-temperature tools, while other companies rely on weight indicators to determine if the wireline tension is increasing. Finally, weak points are intentionally built into all wireline assemblies in case a tool becomes stuck or is lost in the hole. In the case of a stuck tool, the line will break at the weak point where an engineered fishing neck is then exposed to aid in tool recovery.

Along with these built-in risk mitigation practices, relatively inexpensive tool insurance is available from each company. The details of each insurance plan differ and are summarized below. Each plan requires at least three attempts to recover the tool through competent fishing operations. Although down-hole wireline work is risky, it is a risk we must accept to collect the required data for a successful demonstration project.



Lost-in-hole charges in logging contracts are a standard everyday occurrence in the wireline business. Although we won't be able to completely mitigate the threat of damaging or losing a piece of equipment, the risk can be lessened by common sense logging practices, experienced logging personnel, built-in temperature and tension measurements and tool insurance.

**Table 9-6. High-temperature tools and insurance availability.**

<b>Company and Tool</b>	<b>Insurance Available?</b>	<b>Cost of Insurance</b>	<b>Coverage</b>	<b>Lost-in-Hole Charges</b>
Schlumberger Xtreme logs	Yes	\$2670 per tool (there are 5 tools)	Covers 50% of the tools' costs if lost in hole	\$712000 for five tools
Halliburton HEAT logs	Yes	\$792 per tool (there are 5 tools)	Covers complete loss only, not repairs	Information requested
Tiger Energy AFIT tool	No	N/A	N/A	\$460,000
Welaco PTS tool	Yes	\$950 per well	Covers 50% of the tools' costs if lost in hole	\$430,000 and additional costs for lost wireline
Tiger Energy PTS tool	No	N/A	N/A	Information requested, usually don't offer tool insurance
Pacific Process PTS tool	Yes	\$500 per well	Covers 50% of the tools' costs if lost in hole	\$200,000 and additional costs for lost wireline

## 10 WELL TESTING

Well testing in Phase II will include: (1) a 3-day single-well test after stimulation of NWG 55-29; (2) a nominal 7-day connectivity test after the drilling of each of the two production wells; and (3) a 30-to 60-day, 3-well connectivity test.

### 10.1 SINGLE-WELL TEST

In the single-well flow test, NWG 55-29 will be flowed to preinstalled surface test equipment immediately after hydroshearing is completed to relieve reservoir pressure and quantify the success of the stimulation. Reducing reservoir pressure is expected to decrease the fluid pressure in the EGS reservoir and reduce post-hydroshearing induced seismicity. The test duration will be three days (Figure 10-1).

Prior to stimulation of NWG 55-29, at least eighteen water storage tanks will be installed on Pad S-29, with each tank holding 83 m<sup>3</sup> (22000 gallons) of water. The existing groundwater wells, one on Pad S-29 and one on Pad S-16, will flow directly into the tanks via above-ground, temporary piping. Thus, the tanks will provide a 1500 m<sup>3</sup> (396000 gallon) volume buffer and allow the doublelined sumps on both pads to remain empty until stimulation is complete, thereby making the sump available as a seismic mitigation tool (Section 4.11). Flow test equipment will be installed on the well pad prior to the commencement of stimulation operations. The flow test configuration will include a flow tee, flow control valve, flow line with temperature and pressure monitoring instruments, a James tube with lip pressure monitoring, atmospheric separator, and weir box (Appendix G-2 – Well Testing Equipment Diagrams). Ancillary equipment will include geochemical sampling, H<sub>2</sub>S monitoring and abatement equipment.

After stimulation is complete, the well will be shut-in to allow for reheating. After a brief thermal recovery period of at least 3 hours, but probably not exceeding 24 hours, the well will be induced to flow. To initiate flow, the flow line valve will be opened completely, exposing the well to atmospheric pressure. The well will flow up the casing, unassisted, and will most likely flash somewhere between the 9-5/8 in casing shoe at 1970 m and 1220 m (6462 ft and 4000 ft). If the well does not flow, a compressor will be used to depress the water column to provide additional flowing pressure. The geofluid will travel from the wellhead through the flow line and control valve into the James tube assembly. Steam flow is calculated utilizing the lip pressure method and the James tube assembly (James, 1970). Three different sizes of assemblies, most likely 4 in, 6 in and 8 in, will be on-site to ensure that the steam flow (4.4-17.4 kg/s or 35-138 kph) can be calculated accurately at different fluid flow rates. The fluid will then be separated into two phases, liquid water and steam, with an atmospheric separator. The steam will discharge vertically to the atmosphere and the water will be funneled into the outlet near the bottom of the separator. From that point, the liquid will flow through the weir box where the flow rate is determined by measurement of the height of the liquid flowing through a notch weir. Hence, the liquid and steam flow rates will be measured and calculated separately so that total fluid flow and two-phase enthalpy can be calculated. The weir box will discharge into the sump on Pad S-29.

If the Pad S-29 sump begins to approach capacity (5300 m<sup>3</sup> or 1.4 million gallons), redundant, high-head transfer pumps will be in position to transfer water from the sump on Pad S-29 to the sump on Pad S-16 through temporary piping. For redundancy, each pump will be capable of pumping 63 L/s (1000 gpm) of water uphill to Pad S-16, which is 110 m (362 ft) higher in elevation than Pad S-29. Effectively, the two sumps will provide about 10600 m<sup>3</sup> (2.8 million gallons) of geofluid storage capacity during the flow back operations. This is approximately 12% of the maximum estimated water usage for the 2-day stimulation, which should be more than enough capacity for three days of flow back. Depending on the

liquid flow rate during the test, the well may have to be throttled back to ensure that the flow back test can be completed. A five step rate test is planned during the flow-back test to build a productivity curve for NWG 55-29. Hence, the well will not be flowed at maximum open flow for the entire three-day period.

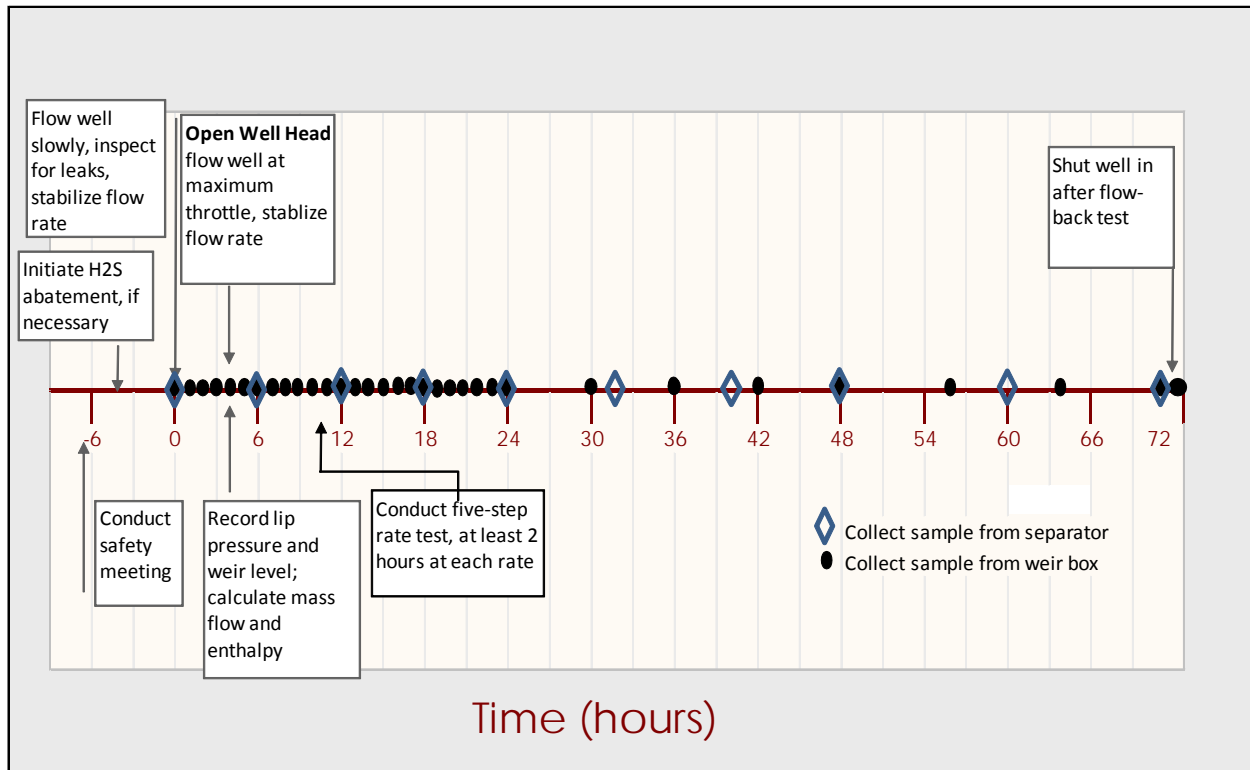


Figure 10-1. Approximate timeline of a 3-day flow test showing important test activities. The recommended tracer and geochemical sampling schedule is included below in Table 10-1. Instrument data, including pressure, temperature and level, will be recorded continuously through a digital data logger, and manually every two hours. The timing of the individual activities as depicted above is approximate and may change slightly depending on how the test progresses.

For flow test planning purposes, we assume that the well will produce no more than 50 kg/s (400 kph) total mass flow, or approximately 50.1 L/s (794 gpm) as liquid water. A total flow rate of 400 kph is equivalent to the maximum planned injection rate of 50.5 L/s (800 gpm) that will be used to stimulate well NWG 55-29. We estimate a single-phase reservoir production temperature of 177°C (350°F), such that the total mass flow will have an enthalpy of 748.5 J/g (321.8 BTU/lbm) and a flowing steam fraction of 16.3% at atmospheric pressure. With a steam fraction of 16.3%, we expect 42.0 L/s (665 gpm) of liquid flow and 8.2 kg/s (65 kph) steam flow. These assumptions are reasonable because the well will have significantly cooled during injection operations and will not have sufficient time to reheat prior to flow back. If the formation temperature is higher, the enthalpy and steam fraction will also be higher, so the liquid storage requirement will be lower. At a single-phase reservoir production temperature of 279°C (535°F), the producing fluid stream would have a steam fraction of 37.6%, which equates to 31.2 L/s (495 gpm) of liquid flow and 19 kg/s (150 kph) steam flow. The atmospheric separator has a total mass flow capacity of 93.7 kg/s (743 kph) for 177°C (350°F) fluid production flow. The weir box, with a 10 in tall, 90° V-notch, has a liquid handling capacity of 130 L/s (2000 gpm). This capacity is significantly higher than the expected liquid flow rate range of 495 to 665 gpm. At this production rate, the initially empty Pad S-29 double-lined sump will have sufficient capacity for about 70 hours of maximum liquid

water flow, representing 12% of the injection stimulation water, which is expected to be 91577 m<sup>3</sup> (24,192,000 gallons) if an injection rate of 50 L/s (800 gpm) is applied for 21 days. If the well flow approaches the sump capacity, while still allowing an adequate freeboard of three feet, additional produced liquid will be transferred to the double-lined sump on Pad S-16, which provides for a similar flow duration and capacity. Another system safeguard is the flow control valve, which can also be partially closed to reduce the production rate if the atmospheric separator, weir box or sumps are approaching design capacity.

Water discharged to sumps will be removed by one of several methods. Whenever possible, water will be re-injected into the EGS reservoir. If the injection well is unavailable, and prior chemical analysis of sump liquid indicates nonhazardous composition, water will be spread over roads and well pads for dust control. Otherwise, water will be evaporated using spray systems positioned over the sumps.

Within six hours before the end of each stimulation phase, a solution containing a pair of tracer compounds will be injected as a pulse into NWG 55-29. The pair of tracers will include ten kg (22 lbs) of each of sorbing (e.g., safranin T or LiBr) and conservative (e.g., 2,6-naphthalene disulfonate) tracers, or ten kg of each of the contrasting-diffusivity tracers. The tracers will be added to a 55-gal drum of water and mixed thoroughly. The tracer solution will be injected over a period of 10 minutes into the injection stream of the stimulation fluid. This procedure will be repeated for each stimulation and diversion event.

Dr. Peter Rose (Energy and Geoscience Institute at University of Utah) will supervise tracer injection, sampling and analysis. During flow-back testing, the produced fluid will be sampled and analyzed to determine tracer concentrations. Tracer sampling will occur downstream of the wellhead from a sampling port in the flow line, using a Webre sampling separator, or from the weir box. Dilution of the conservative tracer allows calculation of the dilution of the injected water by native geofluid. A large measured dilution indicates the system is open and contains a large volume of natural water. Minor dilution indicates the system is closed, with a small volume of native geofluid. An example of tracer data from a single-well injection and backflow test showing an open system signature is shown in Figure 10-2. The behavior of the thermally-reactive tracer(s) will provide for calculation of the weighted average temperature of the mixture of the stimulation fluid with the native geofluid. The effective temperature will be governed by the initial temperatures and volumes of the injection and formation fluids, the contact time, and the rate of heat transfer between the reservoir rock and the fracture-filling fluids. The heat transfer rate is itself governed by the fracture surface area. Given contact time, dilution volumes, initial reservoir rock temperature, and the thermal decay kinetics of the reactive tracers, a calculation of the heat transfer area will be made using an appropriate numerical model. The model will be inverted to solve for the fracture surface area that gives the best fit to the thermally-reactive-tracer data. See Section 8.5 for an in-depth discussion of tracer application and modeling.

AltaRock personnel will collect liquid and noncondensable gas samples from the sampling separator and weir box for geochemical analysis. A suite of production logs will be run to identify flow zones and calculate the thermal and mass contribution of each. In addition, the wellbore surveys will provide a measure of thermal recovery as the well warms up from the lengthy injection. After the three-day flow test, the well will be shut-in while the microseismic, hydraulic, fiber optic and flow test data is analyzed.

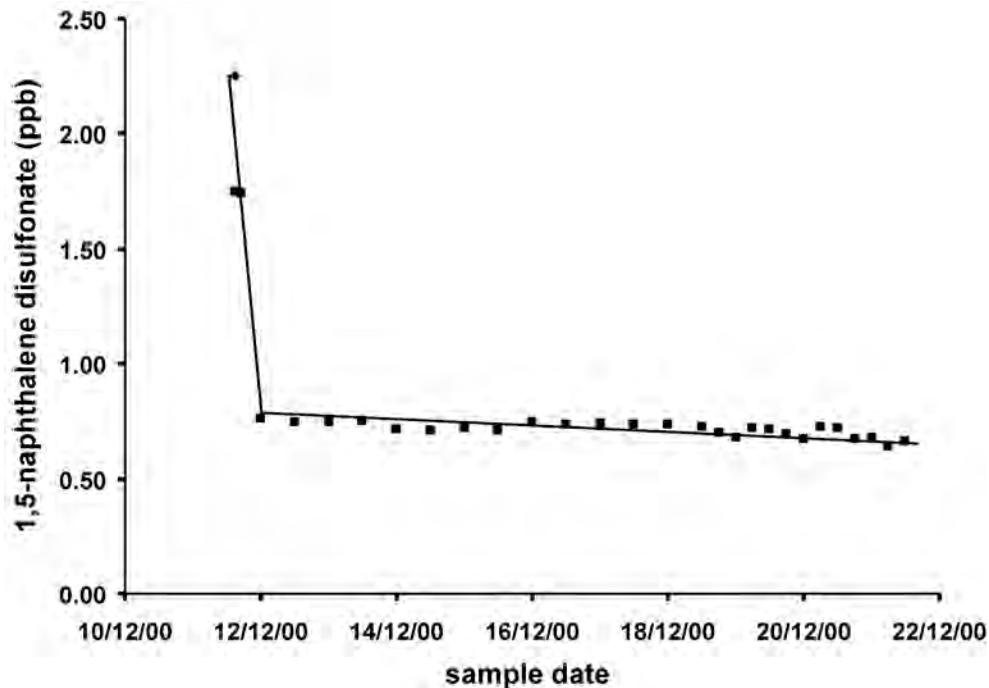


Figure 10-2. Tracer data showing the results of a typical injection and backflow experiment. Each point represents the concentration of tracer from water sampled during backflow. The early, steeply dipping line represents the concentration of tracer within the wellbore. The points along the nearly horizontal line show the concentration within the formation.

## 10.2 CONNECTIVITY TESTING

After well drilling reaches the total planned depth in each of the production wells, NWG 55A-29 and NWG 55B-29, a series of wireline surveys will be conducted, including BHTV, sonic, gamma ray, induction, neutron porosity, density, and pressure and temperature. After logging operations, the connection between the injection well and the each production well will be evaluated by conducting separate connectivity tests, for up to seven days each, to determine the system productivity, circulating temperature, reservoir permeability, skin, and fluid loss (Figure 10-3). The flow test equipment that was used on the injection well will be installed on each production well. A horizontal, surface injection pump will be installed on the injection well. Tracers, both conservative (e.g., 2,6-naphthalene disulfonate) and sorbing (e.g., Safranin T), similar to those used during the stimulation of NWG 55-29, will be injected in NWG 55-29 for sampling at the production well. Breakthrough times will be determined by evaluation of tracer return concentrations. In addition, the concentration of conservative tracers that were injected during the stimulation of the injection well will be measured to determine if the production well is in communication with the discrete fracture networks created during stimulation. Injecting and producing pressure-temperature surveys will be conducted in both wells to identify flow zones, the contribution of each zone to the total flow, and producing and injecting wellbore temperature profiles. This production log data provides essential data for numerical modeling and reservoir characterization. If the system is found to have too much skin damage or too little transmissivity, a stimulation treatment may be required. A dual stimulation, or 'focused' stimulation treatment, will be applied to overcome pressure barriers between the two wells and increase connectivity to achieve a single-well production rate of 75 kg/s (9900 lb/min).



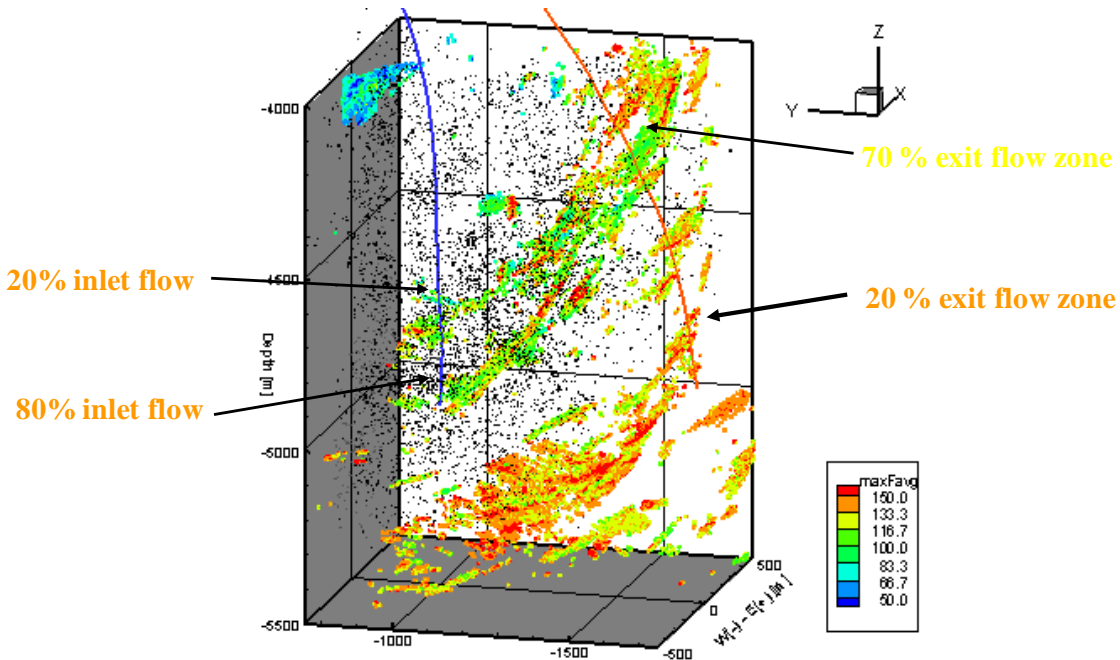


Figure 10-3. Example of connectivity test data between an injector and a producer and the relative contributions of flow contributed to each zone.

### 10.3 CIRCULATION TESTING

After drilling, testing and contingent stimulation of both production wells is completed, a 30- to 60-day circulation test will be conducted, involving the injection well and both production wells. During the circulation test, the system will be optimized mechanically with respect to injection rates, hydraulic horsepower requirements, and well productivity. Tracer analysis is particularly important during the circulation test. Conservative and sorbing tracers will be injected into NWG 55-29 and sampled at the production wells. Measured tracer concentrations will be analyzed to determine breakthrough time and heat exchange area. A weighted fiber optic temperature monitoring system will be deployed in the production wells to identify flow paths, quantify flow rate percentages, and determine production temperatures along the borehole during the entire circulation test period. If flow rates are too high or too unstable to safely deploy the fiber optic DTS equipment, then a pressure, temperature and spinner survey will be conducted with high-temperature, memory tools. The surveys will be performed several times over the duration of the test in all three wells to collect the same data that a DTS string would provide. The flash depth in both production wells will be identified by temperature instrumentation.

The connectivity test will utilize the flow test equipment described above for the single-well flow tests. Identical test equipment will be installed on both production wells. The liquid discharge from the weir boxes will be circulated through the Pad S-29 sump prior to reinjection. Existing water wells will provide the necessary make-up water. Because up to 30% of the circulating water will be lost to the atmosphere through evaporation, significant make-up water will be required to maintain circulating flow rates. Surface pressure, temperature and flow will be measured and recorded continuously. Production well fluids will be sampled and analyzed to determine the need for H<sub>2</sub>S abatement, and to assess mineral dissolution and precipitation reactions that could lead to future scaling or corrosion problems, reservoir skin damage and increased surface equipment requirements and maintenance.

A principal objective of EGS system operation is to circulate water through the reservoir at rates sufficiently high to allow economic power generation, but at low enough fluid velocity to prevent

thermal breakthrough, and low enough pressure to prevent continued reservoir growth that would allow breakthrough of injected fluid to peripheral fracture networks, resulting in water loss. Hence, the microseismic network will be constantly monitored to ensure that the generated fracture network is not continuing to expand. After the circulation test and any additional stimulation effort, the well bores will be shut-in. An injecting PTS survey in the injection well and producing PTS surveys in the production wells will be carried out to compare to the pre-stimulation baseline injectivity and productivity profiles that were measured. The net gain on each well will be calculated.

## 10.4 HYDROGEN SULFIDE ABATEMENT

A hydrogen sulfide (H<sub>2</sub>S) monitoring, warning and abatement program will be implemented as an integral part of the flow testing equipment, and will be in place during all stimulation, flow-back, connectivity and circulation testing operations. A contractor with extensive geothermal H<sub>2</sub>S abatement expertise will install and supervise all H<sub>2</sub>S monitoring and abatement. Abatement will be applied when H<sub>2</sub>S emissions are 2.3 kg/hr (5 lb/hr) or greater. An abatement record and equipment will be available for inspection by regulatory personnel at any time. A copy of the abatement log and plan will be posted in the control trailer. Multiple four-gas hand-held meters will be on-site to ensure personnel safety. At least one representative from each vendor on-site will be responsible for having a functional hand-held meter on their person. A windsock has been installed on Pad S-29 to provide a visual indication of wind direction. Daily safety meetings will emphasize H<sub>2</sub>S protocols, evacuation procedures and wind direction.

The H<sub>2</sub>S abatement system will consist, at a minimum, of the following equipment: two to four positive displacement chemical metering pumps, chemical storage tanks or drums (also called totes; 345-gallon capacity each), water storage tank, shower, eyewash, hoses and fittings. The output of the pumps is linear and proportional to stroke length. Because the output is linear, a single factor is sufficient for calculating the correct stroke length based on the desired injection rate. The pumps are serviced and calibrated periodically. The abatement plan and most recent pump calibration will be posted at the site. To apply H<sub>2</sub>S abatement, caustic (i.e., sodium hydroxide or NaOH) and hydrogen peroxide (H<sub>2</sub>O<sub>2</sub>) will be injected into the flow line downstream of the flow control valve and downstream of the orifice flange. H<sub>2</sub>S is dissolved into the sodium hydroxide, forming hydrosulfide and sulfide ions. Hydrogen sulfide oxidizes these intermediate products to sulfate, which will not revert to H<sub>2</sub>S. Steam samples are withdrawn from the flow line upstream of the James tube. For two-phase flow, the pressure at the lip of the James tube will be used to calculate the steam flow rate and the weir volume will be used to estimate liquid flow rate. The caustic injection mole ratio will be 4:1 to 8:1 to assure sufficient sodium hydroxide is applied.

## 10.5 SCHEDULE

Phase II of the Newberry EGS Demonstration will occur over about a two-year time period, including installation of the final MSA, stimulation of the injection well, production well drilling and the flow tests described in this section. An estimated timeline for the occurrence of major events in Phase II is outlined in Figure 10-4. The project begins after regulatory approval with installation of the final MSA and stimulation equipment, then the stimulation of well NWG 55-29, which will occur over a 21-day period. Following the stimulation, a three-day flow-back test of 55-29 will occur. After a stage-gate review by the DOE, the drilling of the first of two production wells will begin. We expect that each well will require approximately 90 days to complete. Following the completion of each production well, the connection between the injector and the producer will be tested for up to 7 days. Depending on the results of this test, a 5-day dual-well stimulation to enhance that connection may be conducted. Finally, a three-well

circulation test between the injection well and newly-drilled production wells will commence. The circulation test is scheduled to last 30 to 60 days.

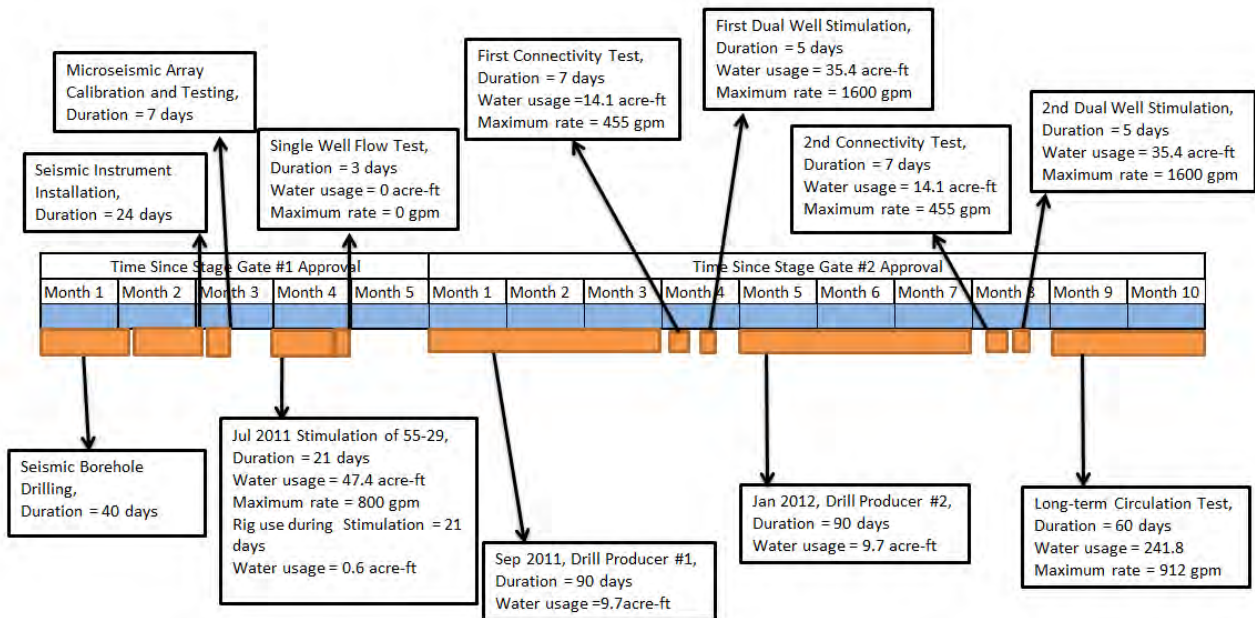


Figure 10-4. Newberry NWG 55-29 Phase II stimulation, drilling and well testing timeline.

## 10.6 DATA COLLECTION

### 10.6.1 TRACER DATA

Both sorbing and conservative tracers will be used throughout Phase II operations to characterize the EGS reservoir surface area, connectivity and transmissivity. Samples will be collected from either the Webre sampling separator, which will be attached to a sample port in the flow line, or from the weir box. Sample bottles capable of holding 60-ml (2 oz) will be used for sampling of the produced fluids every hour during the flow-back test. The samples will be analyzed for the two tracers using UPLC with fluorescence detection. Data obtained in this manner will be subjected to a modeling exercise similar to the one discussed in Section 8.5. In addition to inter-well connectivity data, the numerical analysis will serve to constrain the inter-well fracture surface area in the newly created EGS reservoir. Tentative schedules for tracer and geochemical sampling are included below for three different Phase II activities, the flow-back test, the connectivity tests and the long-term circulation test (Tables 10-1, 10-2, and 10-3). Sampling frequency may be modified based upon actual field response.

**Table 10-1. Flow-back test (duration 3 days) sampling schedule.**

Sample Type	Sampling Location	Day 1	Day 2	Day 3
Tracers	Weir box	Every 15 min until stable flow, every 1 hour after that	Every 6 hours	Every 8 hours
Geochemical – basic analysis	Weir box	Every 15 min until stable flow, every 1 hour after that	Every 6 hours	Every 8 hours
Geochemical – full analysis	Sampling separator	Every 6 hours	Every 8 hours	Every 12 hours

**Table 10-2. Connectivity test (duration 7 days) sampling schedule.**

Sample Type	Sampling Location	Day 1	Day 2	Day 3	Days 4-7
Tracers	Weir box	Every 1 hr until stable flow, then every 6 hrs	Every 8 hours	Every 8 hours	Every 12 hours
Geochemical – basic analysis	Weir box	Every 1 hr until stable flow, then every 6 hrs	Every 8 hours	Every 8 hours	Every 12 hours
Geochemical – full analysis	Sampling separator	Every 8 hours	Every 12 hours	Every 24 hours	Every 24 hours

**Table 10-3. Circulation test (duration 30-60 days) sampling schedule.**

Sample Type	Sampling Location	Day 1	Day 2-10	Day 11-30	Day 31-60
Tracers	Weir box	Every 1 hr until stable flow, then every 6 hrs	Every 12 hours	Every 24 hours	Once every other day
Geochemical – basic analysis	Weir box	Every 1 hr until stable flow, then every 6 hrs	Every 12 hours	Every 24 hours	Once every other day
Geochemical – full analysis	Sampling separator	Every 8 hours	Every 12 to 24 hrs	Once every other day	Once per week

### 10.6.2 GEOCHEMICAL DATA

The geochemistry of produced fluids will be determined by periodic sampling and analysis. Samples will be collected from two-phase flow in the line downstream of the wellhead (upstream of the James tube and atmospheric separator), and single-phase liquid samples will be collected from the weir box. Sample frequency will vary depending on the stage and duration of flow testing. Weir box samples may be collected as often as every 15 minutes early in a flow test for basic geochemical analyses like pH and conductivity, with sampling frequency decreasing to twice daily after several days of flow. The Project Manager will determine sampling frequency based on initial analytical results. Two-phase sample collection will be conducted according to ASTM Method E1675-04e1, *Standard Practice for Sampling Two-Phase Geothermal Fluid for Purposes of Chemical Analysis*. This method utilizes a Webre sampling separator to separate steam and gas from liquid at the flow line temperature and pressure. Samples taken from the sampling separator for full geochemical analysis will be collected less frequently than the weir box samples. Downhole single-phase fluid composition can then be reconstructed by applying flash corrections based on enthalpy determined by the James method. Single-phase liquid samples will be collected from the weir box using simple grab methods. Some analytes will be determined by field analysis, including but not limited to pH, conductivity, redox, alkalinity and hydrogen sulfide (H<sub>2</sub>S). Gas



analysis will include but not be limited to the typical geothermal analytes CO<sub>2</sub>, H<sub>2</sub>S, H<sub>2</sub>, N<sub>2</sub>, O<sub>2</sub>, Ar, CH<sub>4</sub>, Hg and He. Liquid analysis will include but not be limited to the typical geothermal analytes Na, K, Ca, Mg, SiO<sub>2</sub>, Sr, Li, As, Hg, Fe, Mn, Cl, F, B, NH<sub>4</sub>, H<sub>2</sub>S, TDS, TSS, and laboratory duplication of the field-measured analytes listed above. Date, time, location, temperature, pressure and sampler ID will be recorded for each sample. Sample analyses will be conducted according to EPA Method SW-846. Laboratory analysis will be conducted by EPA and state-certified laboratories.

The composition of fluids produced from NWG 55-29, offset water wells and springs will be monitored to ensure that contamination did not occur during the stimulation event. The geochemical sampling plan calls for a purpose-dedicated, water quality and level monitoring well to be constructed at a location down-gradient from Pad S-29 where the pumping and stimulation will occur. An MSA borehole directly west of NWG 55-29, site NN17, will be designed and completed for this purpose. A second monitoring well, Water Well #2, will also be equipped with a transducer for continuous monitoring of the water level and will be sampled using low flow or passive methods (Figure 10-5). The ground water wells located on Pads S-16 and S-29 will also be sampled before, during and after the stimulation event. Two groundwater wells at Newberry Estates will be used to monitor turbidity due to its down-gradient groundwater usage location. In addition, monthly samples will be collected from Paulina Hot Spring, East Lake Hot Spring, and Paulina Lake campground. For more information about the project area's local hydrology, an Independent Hydrologist Review provided by Kleinfelder is included as Appendix B-5 of this document.

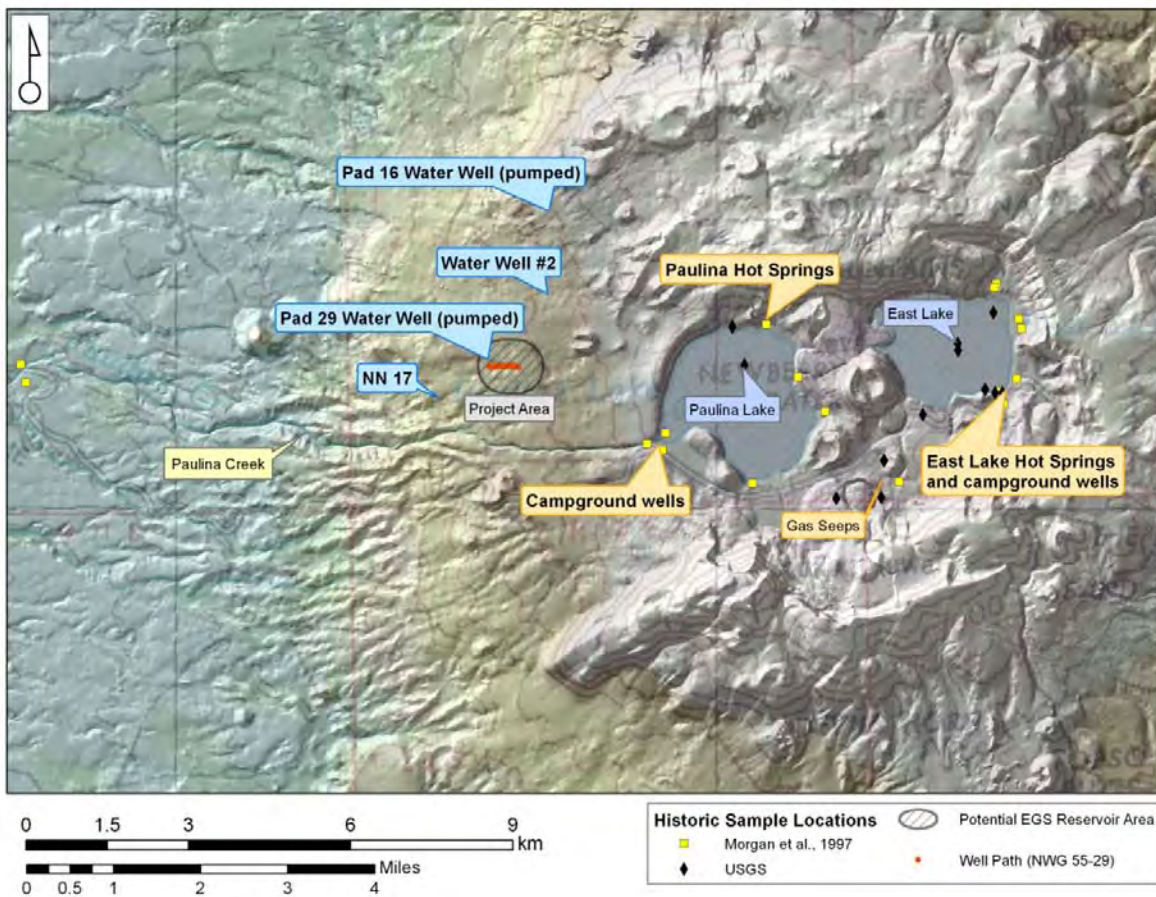


Figure 10-5. Sampling and monitoring sites around the Newberry project area. Sampling sites are shown in bold.



### **10.6.3 FLOW, TEMPERATURE AND PRESSURE DATA**

During flow testing of NWG 55-29, a post-stimulation production log will be run to assess the relative depths and contributions of each flow zone. This log will be compared to the pre-stimulation survey that was conducted in October 2010, during the baseline injection test, to determine the new flowing temperature profile, flowing pressure profile, flow zone depths, relative contributions and injectivity increase resulting from stimulation. The James tube and weir box assembly will allow for steam and liquid water flow rates to be determined during all flow tests. Digital transducers and thermocouples will be used to record flowing pressure and temperature. The same equipment will be also be used during connectivity and circulation testing to determine liquid mass flow and steam fraction. A fiber optic DTS monitoring cable with a Fabry-Perot pressure gauge will be used in each production well during connectivity and circulation testing to measure real-time temperature and pressure data. The fiber optic cable allows continuous measurement of temperature over the entire open-hole interval for the duration of the testing period.

### **10.6.4 SEISMICITY**

A principal objective of EGS system operation is to circulate water through the reservoir at rates sufficiently high to allow economic power generation, but at low enough pressure to prevent continued reservoir growth that would allow breakthrough of injected fluid to peripheral fracture networks and water loss. Hence, the MSA will be constantly monitored to ensure that the EGS fracture network is not continuing to expand. Because the surface pressure required to induce shear failure will have been determined by this time, continued reservoir growth can be mitigated by maintaining an injection rate and pressure lower than the shear pressure. Hydraulic data will be analyzed to determine the injectivity and productivity indices of the respective wells. A qualitative assessment of system permeability and skin damage will be completed after extended system operation. If injection pressure increases over several days while maintaining a constant rate, or if undesirable microseismicity is occurring, skin damage in the form of scaling or near-wellbore tortuosity may be indicated. Additional stimulation methods, including near-wellbore acid treatment, may be employed. If necessary, pressure build-up testing on the injection well can be conducted to provide quantitative information on reservoir pressure, temperature, permeability and skin in order to design the most effective post-stimulation treatment. Additionally, the Induced Seismicity Mitigation Plan will remain in effect through all stages of Phase II.

## **10.7 CONTINGENCY AND MITIGATION PLAN**

Environmental and safety risks as well as risks relating to wellbore damage associated with post-stimulation well testing are listed below:

Risk: The diverter material does not degrade.

Mitigation: The chemical diverters planned for use at Newberry are thermally degradable. The well has to be shut-in to allow “heat-up”, during which time the diverter will eventually degrade to an organic acid. Section 7.6 provides an in-depth discussion on the use and nature of the diverter materials.

Risk: The logging tool could potentially be lost in the hole during planned logging operations. This risk is low, but should be discussed. The PT tool assembly has a weak point in the cable head and would likely separate at this point, allowing the tool to fall to bottom.

Mitigation: Strict logging procedures and speed regulation will be followed. A dummy run will be conducted before every new suite of logs. The tool will not be run faster than 0.77 m/s (150 fpm) and will slow down to 0.25 m/s (50 fpm) when going through liner laps or junctions in the well. All logging

tools will be equipped with a fishing head. AltaRock will either contract for tool insurance with the service provider selected or self-insure.

Risk: Damaging the casing or the causing an open-hole collapse due to thermal cycling.

Mitigation: Injection and flow back will begin at low rates and be ramped up progressively to gradually cool or heat the well, as appropriate. The casing in NWG 55 29 has Sealock Boss premium threads, which are designed to better withstand thermal cycling than a typical buttress thread. The new production wells will also be completed with premium thread casing to minimize the potential for wellbore damage. Rocks can spall into the open-hole due to cycles of thermal contraction and expansion. This will not be an issue in the injection well because there is no instrumentation in the well during injection that could be damaged. The rocks will likely fall to the bottom of the well and not create any issue to the operation. In the production wells, the rocks will be expanding during all connectivity and circulation testing. The fiber optic DTS monitoring system will not be installed in the production wells until the wells have heated up, so that any rock spallation has already occurred and will not damage the sensitive equipment.

Risk: Increased seismicity due to injection during connectivity testing or circulation testing.

Mitigation: Existing MSA stations will be monitored during the stimulation and flow back operations. The data are available in real-time and if increasing seismic activity is observed, actions will be taken to change the flow or injection rates and pressures accordingly to prevent any major seismic events. A seismic risk hazard mitigation protocol is in place. Refer to the protocol outlined in the *Hydroshearing Controls and Mitigation of Induced Seismicity at the Newberry EGS Demonstration* document (AltaRock, 2011).

Risk: Well won't flow during single well flow testing: There is a risk that the well won't have enough energy to flow unassisted during the single well flow back test.

Mitigation: Use an air compressor to push the water column down and out into the formation or use a nitrogen unit to lift water in the wellbore out of the well, thereby reducing the hydrostatic pressure on top of the hot reservoir. By reducing the hydrostatic pressure, the hot water will flash and be induced to flow.

Risk: Sump on Pad S-29 fills to capacity.

Mitigation: A second sump on Pad S-16 of identical size, 5300 m<sup>3</sup> (1.4 million gallons) of capacity, will be empty and available for use during all testing operations. A transfer pump capable of transporting water through above-ground temporary piping at a rate of 63 L/s (1000 gpm) uphill to Pad S-16 from the sump on Pad S-29 will be in place prior to all flow testing operations. A redundant transfer pump will also be installed as a back-up measure in case of mechanical failure. If the second sump nears capacity, the well(s) can always be throttled back or shut-in by manipulating their wellhead valves, if necessary.

Risk: Flow test equipment is too small to contain total flow and significant liquid carryover is occurring.

Mitigation: The flowing well can be throttled back by partially closing the flow control valve to reduce total flow and better accommodate testing equipment. AltaRock's atmospheric separator is 3.7 m (12 ft) in diameter, which is capable of handling the expected range of flow rates and steam fractions.

Risk: A seismic station's equipment malfunctions or the data stream is lost.

Mitigation: Additional stations will be installed to provide equipment redundancy. The seismic network will be monitored continuously and can be accessed on foot, if necessary, during testing

operations if maintenance is required. A data systems contractor will be on call to implement repairs within 24 hours.

Risk: A mechanical failure of critical equipment, such as the injection pump, during testing.

Mitigation: Wherever possible, critical equipment will be backed-up by a redundant unit. For example, the transfer pumps from Pad S-29 to Pad S-16 will be installed with 100% redundancy. For the larger pieces of equipment, like the injection pump used on NWG 55-29 during connectivity and circulation testing, a strict maintenance schedule will be followed to ensure that the unit is properly maintained for optimum run-times. Additionally, a local mechanic will be on-call during the operations in case of failure. Finally, frequently used spare parts, such as fluid ends and oil filters, will be on-site to facilitate quick repairs.

Risk: Native geofluids, capable of self-induced flow and potentially hazardous concentration of H<sub>2</sub>S, are encountered during stimulation or drilling.

Mitigation: Flow test equipment, including H<sub>2</sub>S monitoring and mitigation, will be installed in for stimulation activities. During drilling, blowout prevention equipment will be installed, allowing rapid closing of the well bore, if necessary.

Risk: Mechanical failure may occur.

Mitigation: AltaRock personnel will be in the field and on site for all field activities. AltaRock personnel have extensive experience in all aspects of geothermal exploration, development and operations, and can rapidly respond to unusual field conditions. Drilling contractors will also have extensive geothermal experience.

## 11 RISK MITIGATION

Risk mitigation in a geothermal technology demonstration project involves issues that can be broadly categorized as business and technology. Business risks include financing and liability, budget and scheduling, and permitting and stakeholder concerns. Technical risks vary widely due to the array of science and engineering challenges faced in any geothermal development, but in this case generally include drilling, stimulation and flow testing.

### 11.1 FINANCING AND LIABILITY

AltaRock and Davenport will fund Phase II project costs in the amount of \$19,624,684 with a combination of equity financing and construction financing. AltaRock is funded by its principal shareholders, which are some of the most renowned and successful technology venture capital firms in the world, including, Kleiner Perkins Caufield & Byers, Khosla Ventures, Google, Advanced Technology Ventures, and Vulcan Capital. Similarly, Davenport's investors include private equity groups U.S. Renewables Group and Riverstone Holdings, LLC.

As part of AltaRock's prudent risk management practices, it has obtained both general liability and umbrella liability insurance under which a third party may collect if AltaRock is found liable for damage caused by induced seismicity. AltaRock's Commercial General Liability Insurance with the Federal Insurance Company, a subsidiary of the Chubb Group of Insurance with an A.M. Best Rating of A++, has a general aggregate limit of \$2 million and a \$1 million limit for each occurrence. The General Liability Policy covers bodily injury or property damage that AltaRock becomes legally obligated to pay by reason of liability. The General Liability Policy does not include an exclusion for "subsidence" which is defined as bodily injury or property damage arising directly or indirectly out of, caused by, resulting from, contributing to or aggravated by "subsidence, settling, sinking, slipping, falling away, caving in, shifting, eroding, mudflow, rising, tilting or any other movement of land or earth." AltaRock also has Umbrella Liability Insurance with the Federal Insurance Company with a general aggregate limit and occurrence limit of \$5 million.

### 11.2 SCHEDULE AND BUDGET

The *Project Management Plan*, dated 29 July 2009 and submitted as part of the original demonstration application, includes a detailed schedule and budget. The demonstration schedule was designed with sufficient flexibility to allow Phase II activities to begin as soon as stage-gate approval is received. The *Project Management Plan* also includes a detailed project schedule. Stimulation and testing of NWG 55-29 will be completed in about 6 months, and completion of all Phase II activities, including production well drilling and testing, will be completed in 16 months. This budget and schedule will allow successful project completion.

### 11.3 PERMITTING

A significant risk of any demonstration project conducted in the environment involves the ability of the operator to garner public acceptance and to secure all necessary permits. During the FOA application process, AltaRock concluded permitting risks were low, and that the necessary permits for an EGS demonstration could be secured in a reasonable period of time. In 1990, federal legislation created the NNVM and defined geothermal leaseholds for development on the northwest flank of Newberry. CalEnergy successfully completed the EIS process for a complete wellfield and power plant development in 1994. An EA completed in August 2007 by the BLM for the Proposed Newberry Geothermal Exploration Project resulted in a Finding of No Significant Impact (FONSI) and a Record of Decision (ROD)

involving three (3) well pads with up to nine (9) exploration wells. These legislative and successful permitting efforts indicated that no significant conditions existed that would prevent permitting of an EGS demonstration.

This project plan minimizes potential environmental risks and liabilities by thoroughly addressing all regulatory and permitting requirements, and anticipating public concerns regarding implementation of a significant new energy production technology. AltaRock and Davenport have demonstrated experience in project development and permitting, and have identified all permits and approvals necessary for project completion. The demonstration is of limited duration, with Phase II occurring over a period of no more than two years, and physical impacts are minor, with almost all activities occurring on one previously developed site location. Public outreach meetings and a comprehensive multimedia effort have informed stakeholders about project plans, and will continue to be conducted prior to and throughout Phase II activities.

## 11.4 TECHNICAL RISKS

AltaRock has assembled a team comprising the best available industry and academic experts in the field of EGS to maximize the potential for a successful project completion. Susan Petty, founder of AltaRock and the Principal Investigator for this project, is one of the world's leading experts in EGS development. She has extensive experience in field operations and has successfully participated in numerous DOE-sponsored funding programs. The AltaRock team will use an expert Technical Advisory Committee, also highly experienced in geothermal and EGS development projects, to review progress and recommend best possible practices. The AltaRock senior management team has a successful history of developing geothermal and other renewable energy projects, with the capability to ensure rigorous scheduling and timely completion, full regulatory compliance, and the ability to secure funding to bring the project to completion with the construction and operation of a power generation facility.

Risks and approaches to mitigation for specific technical issues are discussed in detail in previous sections of this report.

- Induced Seismicity – Seismicity and associated risks are thoroughly discussed in Section 4 and in the ISMP (Appendix A-1). The ISMP presents our comprehensive evaluation and risk mitigation for induced seismicity, and was evaluated, deemed technically adequate and approved by DOE on 10 August 2010.
- Stress Orientation and Magnitude – Stress orientation and magnitude are important considerations for fracture stimulation. In Section 5, we evaluate all available data to quantify stress, including regional geology, nearby wells and core holes, and NWG 55-29, including an extensive evaluation of the BHTV survey. Although the resulting stress model is non-unique due to physical limitations of data collection, possible variations have been incorporated into the stimulation planning discussed below and in Section 7.
- Stimulation – Stimulation represents the core of EGS technology and presents the widest array of technology risks in this demonstration. These risks, mitigation strategies and contingencies, discussed in Section 7.11, include:
  - Detection of microseismicity
  - Stress magnitude
  - Tensile failure and fracture growth
  - Injection breakthrough
  - Diverter performance
  - Equipment failure and sump capacity



- Casing integrity and open-hole collapse
  - Safety and environmental impacts
- Drilling – Drilling of production well will occur subsequent to successful stimulation and flow testing, including a stage-gate review. Nonetheless, for completeness we provide a preliminary drilling plan and related procedures in Section 9, including various risks and mitigation measures in Section 9.6.
- Flow Testing – Flow testing of NWG 55-29 will occur after stimulation, and testing of production wells after new well drilling is complete. Risks associated with flow testing are discussed in Section 10.7. Some of these risks are typical of any geothermal well flow test, including initiating well flow, the potential for casing damage or survey tool loss, equipment sizing and reliability, sump capacity and H<sub>2</sub>S abatement. Other risks particular to EGS are also addressed, including diverter degradation, and induced seismicity and seismic system reliability.

## 12 REPORTING

### 12.1 ONGOING ACTIVITIES

AltaRock conducts a weekly teleconference that includes members of our in-house project team. We also conduct a weekly teleconference including management personnel from AltaRock and Davenport to coordinate project activities. We conduct a separate weekly teleconference that includes members of the Newberry EGS project team, including representatives from each of the project subrecipients.

AltaRock conducts or participates in a weekly teleconference that includes invited personnel from AltaRock, Davenport, DOE, FS and BLM. In this call we discuss ongoing activities, planned activities, critical path items, and permitting and project operations schedules. Participation is not mandatory, and regulatory agencies often do not attend, but AltaRock makes every effort to keep these stakeholders fully informed of completed, ongoing and planned activities.

Although not strictly a reporting requirement, we frequently submit Sundry Notices to BLM for activities that are performed at the project site. These Notices provide BLM with a description of activities to be performed, provide BLM opportunity to modify the planned activity to safeguard various resources, and provide AltaRock and Davenport written authorization to perform such activities.

### 12.2 STIMULATION AND FLOW TEST REPORTS

In accordance with the ISMP approved by DOE, various forms of reporting will be conducted during well stimulation and flow testing activities, as detailed in Sections 4.5, 5.2 and 5.3 of Appendix A-1. These reporting procedures include:

1. Seismicity Data – Data output from the MSA will be transmitted continuously throughout Phase II and in real-time to LBNL, where software will automatically determine preliminary locations (epicenters) and magnitudes without review by a seismologist. This data will be visible, also in real-time, on the LBNL web site.
2. Daily Activity Report – Transmitted to DOE, BLM, FS, PNSN and LBNL by 11:00 am each day during active stimulation and flow testing operations, describing completed, current and planned field operations. The daily report will be accompanied by several graphs including surface pressure, bottomhole pressure and flow rate versus time, and temperature versus depth.
3. Exception Reports – In addition to the daily activity report, exception reports will be issued when a seismic event exceeds certain criteria or triggers detailed in the ISMP.
  - a. Outlier Report – An outlier report will document the location of any seismic event located outside of the expected stimulation zone. The report will be transmitted to the DOE, BLM, FS and LBNL within 2 hours after the outlier has been initially identified and the mitigation action initiated.
  - a. Trigger Report – A trigger report will document that a magnitude or shaking trigger has been exceeded, including information about the event, such as location, size, time, stimulation conditions, whether the event was felt by anyone, and what mitigation action was initiated. The report will be transmitted to the DOE, BLM, FS and LBNL within 2 hours after the trigger occurs.
  - a. Seismic Event – For higher magnitude and shaking levels, initial notification will be made by phone to inform key personnel as soon as the event is reviewed by a seismologist, in no case more than two hours after the event. This reporting level will also include

criteria to notify NNVM and Paulina Peak visitors, and owners and users of private facilities within NNVM.

- b. Mitigation Report – A mitigation report will be issued subsequent to a mitigation action to summarize the event and the results of mitigation applied in response to the event.

### **12.3 DRILLING REPORTS**

Drilling of new production wells in Phase II will include the issuance of a typical daily report describing completed, current and planned activities, cost information, mud and drilling tools in use, geology, equipment inventory, safety performance and weather (Appendix L-1). These reports can be modified as necessary to accommodate additional data needs. Daily drilling reports will be transmitted to DOE and BLM every morning by 11:00 a.m. when a rig is active.

### **12.4 DOE REPORTING**

We provide a wide variety of reports to DOE in accordance with the Federal Assistance Reporting Checklist and Instructions included with this grant award.

#### **12.4.1 MANAGEMENT**

1. Progress report – quarterly and annually, describing technical and management aspects of the project.
2. Special status report – within 5 days after event, or as specified, providing notice of problems, delays, or adverse conditions that materially impair our ability to meet the objectives of the award or developments that have a significant impact on the project, include the remedial action to be taken to correct or resolve any problems or adverse action.
3. Induced seismicity report - completed, approved by DOE, and issued before the Phase 1 report.

#### **12.4.2 SCIENTIFIC/TECHNICAL REPORTING**

Scientific/technical reports submitted under this award will be disseminated on the Internet via the DOE Information Bridge ([www.osti.gov/bridge](http://www.osti.gov/bridge)), unless the report contains patentable material, protected data or SBIR/STTR data. Citations for journal articles produced under the award will appear on the DOE Energy Citations Database ([www.osti.gov/energycitations](http://www.osti.gov/energycitations)). Reports submitted to the DOE Information Bridge will not contain any Protected Personal Identifiable Information (PII), limited rights data (proprietary data), classified information, information subject to export control classification, or other information not subject to release.

4. Final Scientific Report – 90 calendar days after expiration or termination of the award.
5. Scientific and technical conference papers/proceedings – materials or information presented at a conference, in a public meeting, or other means of public communication will be submitted to the DOE Project Officer for review and approval at least 15 days prior to the event or publication date.
6. Software/Manual – within 5 days after event or as specified.

#### **12.4.3 FINANCIAL REPORTING**

7. SF-425, Federal Financial Report – quarterly and final.

#### **12.4.4 CLOSEOUT REPORTING**

8. Patent Certification – 90 calendar days after expiration or termination of the award.
9. Property Certification – 90 calendar days after expiration or termination of the award.

#### **12.4.5 OTHER REPORTING**

10. Indirect Cost Proposal – annually, In accordance with the applicable cost principles, the recipient must submit an annual indirect cost proposal, reconciled to its financial statements, within six months after the close of the fiscal year.
11. Inventory of Federally Owned Property, If Any – annually. We do not anticipate the use of any federally owned property.
12. Phase report – prior to all go/no-go decision points. We expect this to include: (1) Phase I prior to Phase II; (2) Phase II after stimulation and testing, and prior to drilling first production well; (3) Phase II prior to drilling second production well; (4) Phase II prior to conducting long term circulation test; and (5) prior to Phase III.
13. Peer review report and presentation – annually. AltaRock has provided peer review reports and presentations for 2010 and 2011.
14. American Recovery And Reinvestment Act – no later than ten calendar days after each calendar quarter.

#### **12.5 DOE NATIONAL GEOTHERMAL DATABASE REPOSITORY**

All non-confidential data will be published in various geothermal industry and scientific forums, as appropriate, and submitted to the National Geothermal Database System (NGDS).

#### **12.6 RELATED PROJECTS**

Davenport, as part of other ongoing activities, provides additional reports to various agencies, including:

1. Oregon Department of Water Resources – In accordance with the Limited Water Usage Permit, an annual report of water use from two existing groundwater wells, listing total hours of pumping and quantity of water pumped.
2. Oregon Department of Environmental Quality – In accordance with a Simple Air Contaminant Discharge Permit, an annual report listing operations and emissions.
3. BLM – Davenport conducts an Annual Weed Monitoring survey of pads and roads, and submits a report of findings and weed removal.

## 13 REFERENCES

- Ake, J., R. LaForge, and F. Hawkins (2001). Probabilistic seismic hazard analysis for Wickiup Dam - Deschutes project, central Oregon. U.S. Bureau of Reclamation Seismotectonic Report 2000-04, 71 p.
- AltaRock (2009). Newberry Volcano EGS Demonstration – Project Narrative. Prepared for FOA DE-PS36-09GO099019, Enhanced Geothermal Systems Demonstration, 20 p.
- Anderson, E.M. (1951). *The Dynamics of Faulting and Dyke Formation* (2<sup>nd</sup> Edition). Oliver & Boyd, Edinburgh.
- ANSS (2011). Advanced National Seismic System Catalog. <http://quake.geo.berkeley.edu/anss/catalog-search.html>, last accessed 01/19/2011.
- Asquith, G. and D. Krygowski (2004). *Basic Well Log Analysis* (2<sup>nd</sup> Edition). AAPG Methods in Exploration Series 16, The American Association of Petroleum Geologists, Tulsa, OK, 244 p.
- Baisch S., D. Carbon, U. Dannwolf, B. Delacou, M. Devaux, F. Dunand, R. Jung, M. Koller, C. Martin, M. Sartori, R. Secanell, and R. Vörös (2009). Deep Heat Mining Basel – Seismic Risk Analysis. SERIANEX Group, [http://www.wsu.bs.ch/serianex\\_teil\\_1\\_english.pdf](http://www.wsu.bs.ch/serianex_teil_1_english.pdf), last accessed 08/18/2011.
- Bame, D. and M.C. Fehler (1986). Observations of Long-period Earthquakes Accompanying Hydraulic Fracturing. *Geophys. Res. Lett.* v. 13, 149-152.
- Baria, R., R. Jung, T. Tischner, J. Nicholls, S. Michelet, B. Sanjuan, N. Soma, H. Asanuma, B. Dyers, and J. Garnish (2006). Creation of an HDR Reservoir at 5000 M Depth at the European HDR Project. *Proceedings: Thirty-First Workshop on Geothermal Reservoir Engineering*, Stanford University, Stanford, CA, Jan 30-Feb 1, 2006, SGP-TR-179.
- Bargar, K.E. and T.E.C. Keith (1999). Hydrothermal Mineralogy of Core from Geothermal Drill Holes at Newberry Volcano, Oregon. *USGS Professional Paper 1578*, 92 p.
- Barton, C., S. Hickman, R. Morin, M.D. Zoback, and R. Benoit (1998). Reservoir-scale fracture permeability in the Dixie Valley, Nevada, geothermal field. In R.M. Holt (Ed.), *Rock Mechanics in Petroleum Engineering*, v. 2, Society of Petroleum Engineers, SPE 47371, 315-322.
- Basin and Range Province (2011). Wikipedia, The Free Encyclopedia. [http://en.wikipedia.org/w/index.php?title=Basin\\_and\\_Range\\_Province&oldid=420400760](http://en.wikipedia.org/w/index.php?title=Basin_and_Range_Province&oldid=420400760), last accessed 4/14/2011.
- Bauer, H.H. and J.J. Vaccarro (1987). Documentation of a deep percolation model for estimation groundwater recharge. *USGS Open-File Report 86-536*, 180 p.
- Bend, Oregon (2011). Wikipedia, The Free Encyclopedia. [http://en.wikipedia.org/w/index.php?title=Bend,\\_Oregon&oldid=424069590](http://en.wikipedia.org/w/index.php?title=Bend,_Oregon&oldid=424069590), last accessed 4/14/2011.
- Blanc, P., A. Lassin, and P. Piantone (2007). Thermoddem - A Thermodynamic Database for Modelling the Alteration of Waste Minerals. BRGM (Orléans, France). <http://thermoddem.brgm.fr>, last accessed 8/18/2011.
- Brace, W.F. and D. L. Kohlstedt (1980). Limits on lithospheric stress imposed by laboratory experiments. *J. Geophys. Res.*, v. 85, 6248-6252.
- Brace, W.F. (1984). Permeability of crystalline rocks: new *in situ* measurements. *J. Geophys. Res.*, v. 89, 4327–4330.
- Brown, S.R. (1987). Fluid flow through rock joints: Effects of surface roughness. *J. Geophys. Res.*, v. 99, 9373-9390.



- Byerlee, J. (1978). Friction of rocks. *Pure and Applied Geophysics*, v. 116, 615-626.
- Carothers, W. and R. Mariner (1987). Isotope geochemistry of minerals and fluids from Newberry volcano, Oregon. *J. Volcanol. Geotherm. Res.*, v. 31, 47-63.
- Cascadia Subduction Zone (2009). USGS Website.  
<http://earthquake.usgs.gov/research/structure/crust/cascadia.php>, last accessed 04/12/2011.
- Cathelineau, M. and D. Nieva (1985). A chlorite solid solution geothermometer: The Los Azufres (Mexico) geothermal system. *Contribution to Mineralogy and Petrology*, v. 91, 235-244.
- Cathelineau, M. (1988). Cation site occupancy in chlorites and illites as a function of temperature. *Clay Minerals*, v. 23, 471-485.
- Charley, J., N. Cuneot, L. Dorbath, C. Dorbath, H. Haessler, and M. Frogneux (2007). Large earthquakes during hydraulic stimulations at the geothermal site of Soultz-sous-Forêts. *Int. J. Rock Mech. & Mining Sci.*, v. 44, 1091-1105.
- Cladouhos, T., S. Petty, G. Foulger, B. Julian, and M. Fehler (2010). Injection Induced Seismicity and Geothermal Energy. *GRC Transactions*, v. 32, 1213-1220.
- Cladouhos, T., S. Petty, O. Callahan, W. Osborn, S. Hickman, and N. Davatzes (2011a). The Role of Stress Modeling in Stimulation Planning at the Newberry Volcano EGS Demonstration Project. *Proceedings: Thirty-Sixth Workshop on Geothermal Reservoir Engineering*, Stanford University, Stanford, CA, Jan 31-Feb 2, 2011, SGP-TR-191.
- Cladouhos, T., M. Clyne, M. Nichols, S. Petty, W. Osborn, and L. Nofziger (2011b). Newberry Volcano EGS Demonstration Stimulation Modeling. *GRC Transactions*, pre-print by request.
- Cole, D.L. (2006). Groundwater Quality Report for the Deschutes Basin, Oregon. DEQ Laboratory and Water Quality Divisions, Portland, OR., 59 p.
- Columbia Plateau (2011). Wikipedia, The Free Encyclopedia.  
[http://en.wikipedia.org/w/index.php?title=Columbia\\_Plateau&oldid=419898498](http://en.wikipedia.org/w/index.php?title=Columbia_Plateau&oldid=419898498), last accessed 4/14/2011.
- Cornet, F.H., T. Berard, and S. Bourouis (2007). How close to failure is a granite rock mass at a 5 km depth. *Int. J. Rock Mech. & Mining Sci.*, v. 44, 47-66.
- Crawford, B.R., D.R. Faulkner, and E.H. Rutter (2008). Strength, porosity, and permeability development during hydrostatic and shear loading of synthetic quartz-clay fault gouge. *J. Geophys. Res.*, v. 113, 14 p.
- Crawford, B.R., and D.P. Yale (2002). Constitutive modeling of deformation and permeability: relationships between critical state and micromechanics. Society of Petroleum Engineers, SPE 78189, 10 p.
- Crider, J.G. (2001). Oblique slip and the geometry of normal-fault linkage: mechanics and a case study from the Basin and Range in Oregon. *J. Struct. Geo.*, v. 23, 1997-2009.
- Croucher, A. E. and M. J. O'Sullivan (2008). Application of the computer code TOUGH2 to the simulation of supercritical conditions in geothermal systems. *Geothermics*, v. 37(6), 622-634.
- Crumrine, M.D. and Morgan, D.S. (1994). Hydrologic, water-quality, and meteorologic data for Newberry Volcano and vicinity, Deschutes county, Oregon, 1991-1993. *USGS Open-File Report 94-122*, 70 p.
- Dames and Moore (1994). Revised Report Newberry Geothermal Project Hydrology Baseline Study Newberry Volcano, Oregon for CE Exploration Company, Portland, OR, 268 p.
- Davatzes, N.C., M. Swyer, D. Lockner, and S. Solum (2010). Mechanisms of fault gouge evolution and physical properties. American Geophysical Union, Fall Meeting 2010, abstract #T41B-2119.

- Davatzes, N.C. and S. Hickman (2005). Controls on fault-hosted fluid flow: Preliminary results from the Coso Geothermal Field, CA. *GRC Transactions*, v. 29, 343-348.
- Davatzes, N.C. and S. Hickman (2006). Stress and faulting in the Coso Geothermal Field: Update and recent results from the East Flank and Coso Wash. *Proceedings: Thirty-First Workshop on Geothermal Reservoir Engineering*, Stanford University, Stanford, CA, Jan 30-Feb 1, 2006, SGP-TR-179.
- Davatzes, N.C. and S. Hickman (2009). Fractures, stress, and fluid flow prior to stimulation of Well 27-15, Desert Peak, Nevada, EGS Project. *Proceedings: Thirty-Fourth Workshop on Geothermal Reservoir Engineering*, Stanford University, Stanford, CA, Feb 9-11, 2009, SGP-TR-187.
- Davatzes, N.C. and S. Hickman (2010a). Stress, fracture and fluid-flow analysis using acoustic and electrical image logs in hot fractured granites of the Coso Geothermal Field, California, U.S.A., in *Dipmeter and Borehole Image Log Technology*, M. Pöppelreiter, C. Garcia-Carballido and M.A. Kraaijveld (eds.), *Amer. Assoc. Petroleum Geologists Memoir 92*, Tulsa, OK, 259-294.
- Davatzes, N.C. and S. Hickman (2010b). The feedback between stress faulting and fluid flow: Lessons from the Coso Geothermal Field, CA. *Proceedings: World Geothermal Congress*, Bali, Indonesia, April 25-29, 2010, 15 p.
- Dershowitz, W. S. and H. H. Einstein (1988). Characterizing rock joint geometry with joint system models. *Rock Mechanics and Rock Engineering*, v. 21(1), 21-51
- Dobson, P., E. Sonnenthal, M. Kennedy, T. Van Soest, and J. Lewicki (2006). Temporal changes in noble gas compositions within the Aidlin sector of The Geysers geothermal system. Lawrence Berkeley National Laboratory Paper, LBML-60159.
- Donath, F.A. (1962). Analysis of Basin and Range structure. *GSA Bulletin*, v. 71, 1-15.
- Donnelly-Nolan and Jenson (2009). Ice and water on Newberry Volcano, central Oregon, in *Volcanoes to Vineyards: Geologic Field Trips through the Dynamic Landscape of the Pacific Northwest*, J.E. O'Connor, R.J. Dorsey, and I.P. Madin (eds.), *GSA Field Guide 15*, 81-90.
- Dorbath, L., N. Cuenot, A. Genter, and M. Frogneux (2009). Seismic response of the fractured and faulted granite to massive water injection at 5 km depth at Soultz-sous-Forêts (France). *Geophys. J. Int.*, 177(2), 653-675.
- Draus, E. (2002). Magnetic Stratigraphy of the Middle Miocene (Early Barstovian) Mascall Formation, Central Oregon. *GSA Abstracts with Programs*, Annual Meeting, Denver, CO.
- Duchane, D. and D. Brown (2002). Hot dry rock (HDR) geothermal energy research and development at Fenton Hill, New Mexico. *Geo-Heat Center Quarterly Bulletin*, Oregon Institute of Technology, v. 23, 13-19.
- Electronic Code of Federal Regulations (2011). <http://ecfr.gpoaccess.gov/cgi/t/text/text-idx?c=ecfr&sid=eb899133d73c989df34bc63e332ec810&rgn=div8&view=text&node=40:22.0.1.1.5.0.39.3&idno=40>, last accessed 1/14/2011.
- Entwisle, D.C., P.R.N. Hobbs, L.D. Jones, D. Gunn, and M.G. Raines (2005). The relationship between effective porosity, uniaxial compressive strength and sonic velocity of intact Borrowdale Volcanic Group core samples from Sellafeld. *Geotechnical and Geological Engineering*, v. 23, 793-809.
- EPA (2011). <http://water.epa.gov/drink/contaminants/index.cfm>, last accessed 1/14/ 2011.
- Epoch (2008a). NWG 55-29 mud log. Internal report to Davenport Power, LLC, 07/18/2008.
- Epoch (2008b). NWG 55-29, Newberry Crater, Deschutes County, OR, Final Well Report. Internal Report to Davenport Power, LLC, 07/18/2008.

- Ferns, M.L. and J.D. McClaughry (2006). Preliminary geologic map of the Powell Buttes 7 ½' quadrangle, Crook County, Oregon. Open-File Report O-06-24, Oregon Department of Geology and Mineral Industries, Portland, OR.
- Ferrazzini, V., B. Chouet, M.C. Fehler, and K. Aki (1990). Quantitative Analysis of Long Period Events Recorded During Hydrofracture Experiments at Fenton Hill, New Mexico. *J. Geophys. Res.*, v. 95, 21871-21884.
- Fetterman, J.A. (2011). Porosity Evolution in Newberry Volcano Geothermal System: Feedback between deformation and alteration. M.S. thesis, RES | The School for Renewable Energy Science in affiliation with the Universities of Iceland and Akureyri, 74 p.
- Fetterman, J.A. and N.C. Davatzes (2011). Fracture Generated Porosity Evolution in the Newberry Volcano Geothermal System, OR: Feedback between Deformation and Alteration. *GRC Transactions*, pre-print by request.
- Fitterman, D.V. (1988). Overview of the structure and geothermal potential of Newberry Volcano, Oregon. *J. Geophys. Res.*, v. 93(B9), 10059-10066.
- Fitterman, D.V., W.D. Stanely, and R.J. Bisdorf (1988). Electrical structure of Newberry Volcano, Oregon. *J. Geophys. Res.*, v. 93(B9), 10119-10134.
- Foulger Consulting (2010). Newberry Calibration Shot Project. Internal Report to AltaRock Energy, Inc., 10/09/2010, 104 p.
- Foulger Consulting (2011). Task 1: Moment Tensors, Task 2: Sensor Selection, Task 3: Borehole Array Geometry. Internal Report to AltaRock Energy, Inc., 2/15/2011, 67 p.
- Frolova, J., V. Ladygin, H. Franzson, O. Sigurdsson, V. Stefansson, and V. Shustrov (2005). Petrophysical Properties of Fresh to Mildly Altered Hyaloclastite Tuffs. *Proceedings: World Geothermal Congress*, Antalya, Turkey, April 24-29, 2005, 15 p.
- Gannett, M.W., K.E. Lite, D.S. Morgan, and C.A. Collins (2001). Ground-water hydrology of the upper Deschutes Basin, Oregon. *USGS Water-Resources Investigations Report 00-4162*, 78 p.
- Geologic Provinces of the United States (2004). USGS Website. <http://geomaps.wr.usgs.gov/parks/province/INDEXPacificMtnSUBS.gif>, last accessed 4/14/2011.
- Geologica (2008). Geochemical analysis of from flow testing of well 55-29, Newberry, Oregon. Letter report to Al Waibel, Newberry Geothermal Company, Bend, OR, dated 10/18/2008.
- Geologica (2010). Gas analysis of Newberry wells. Memo from Jill Robinson Haizlip to Todd Jaffe, Davenport Newberry Holdings and Al Waibel, Columbia Geoscience, dated 2/4/2010.
- Geosystem (2007). Magnetotelluric survey, Newberry Volcano, Oregon, unpublished reported prepared by Geosystem Srl for Northwest Geothermal Company, November, 2007.
- Genter A., C. Castaing, C. Dezayes, H. Tenzer, H. Traineau, and T. Villemin (1997). Comparative analysis of direct (core) and indirect (borehole imaging tools) collection of fracture data in the Hot Dry Rock Soultz reservoir (France). *J. Geophys. Res.*, v. 102(B7), 15419-15431.
- Genter, A., D. Fritsch, N. Cuenot, J. Baumgärtner, and J. Graff (2009). Overview of the Current Activities of the European EGS Soultz Project: From Exploration to Electricity Production. *Proceedings: Thirty-Fourth Workshop on Geothermal Reservoir Engineering*, Stanford University, Stanford, CA, Feb 9-11, 2009, SGP-TR-187.
- Gettings, M.E. and A. Griscom (1988). Gravity Model Studies of Newberry Volcano, Oregon. *J. Geophys. Res.*, v. 93(B9), 10109-10118, doi:10.1029/JB093iB09p10109.
- Goles, G. and R. Lambert (1990). A strontium isotopic study of Newberry volcano, central Oregon: Structural and thermal implications. *J. Volcanol. Geotherm. Res.*, v. 43(1-4), 159-174.

- Griffith, A.A. (1921). The phenomena of rupture and flow in solids. *Philosophical Transactions of the Royal Society of London, Series A* 221, 163-198.
- Griscom, A. and C.W. Roberts (1983). Gravity and magnetic interpretation of Newberry Volcano, in *Survey of Potential Geothermal Exploration Sites at Newberry Volcano, Deschutes County*, G.R Priest, B.F. Vogt, and G.L. Black (eds.), State of Oregon Department of Geology and Mineral Industries Open-File Report 0-83-3, p. 68-81.
- Hadden, R.M., N.M. Woller, and C.B. Brand (1983). Preliminary soil-mercury survey of Newberry Volcano, Deschutes County, Oregon, 1983, in *Survey of Potential Geothermal Exploration Sites at Newberry Volcano, Deschutes County, Oregon*, G.R Priest, B.F. Vogt, and G.L. Black (eds.), State of Oregon Department of Geology and Mineral Industries Open-File Report 0-83-3, 45-59.
- Jensen, R.A. (2006). Roadside guide to the geology of Newberry Volcano (4<sup>th</sup> edition). CenOreGeoPub, Bend, OR, 182 p.
- Haimson, B. (2007). Micromechanisms of borehole instability leading to breakouts in rocks. *Int. J. Rock Mech. & Mining Sci.*, v. 44, 157– 173, doi:10.1016/j.ijrmms.2006.06.002.
- Häring, M.O., U. Schanz, F. Ladner, and B. Dyer (2008). Characterization of the Basel 1 enhanced geothermal system. *Geothermics*, 37, 469-495.
- Hearst, J.R., P.H. Nelson, and F.L. Paillett (2000). Well logging for physical properties: A handbook for geo-physicists, geologists and engineers (2<sup>nd</sup> edition). John Wiley & Sons, New York, NY, 483 p.
- Heffer, K. (2002). Geomechanical Influences in Water Injection Projects: An Overview. *Oil and Gas Science and Technology*, v. 57(5), 415-422.
- Hickman, S.H. and N.C. Davatzes (2010). In-situ stress and fracture characterization for planning of an EGS stimulation in the Desert Peak geothermal field, NV. *Proceedings: Thirty-Fifth Workshop on Geothermal Reservoir Engineering*, Stanford University, Stanford, CA, Feb 1-3, 2010, SGP-TR-188.
- Hickman, S.H., M.D. Zoback, and R. Benoit. (1998). Tectonic controls on reservoir in the Dixie Valley, Nevada, Geothermal Field *Proceedings: Twenty-Third workshop on Geothermal Reservoir Engineering*, Stanford University, Stanford, CA, Jan 26-28, 1998, SGP-TR-158, 291-298.
- Hickman, S.H., M.D. Zoback, C.A. Barton, R. Benoit, J. Svitek, and R. Summers (2000). Stress and permeability heterogeneity within the Dixie Valley geothermal reservoir: recent results from well 82-5. *Proceedings: Twenty-Fifth Workshop on Geothermal Reservoir Engineering*, Stanford University, Stanford, CA, Jan 24-26, 2000, SGP-TR-165.
- Hubbert, M.K. (1951). Mechanical Basis for Certain Familiar Geological Structures. *Bull. Geol. Soc. Am.*, v. 62, 355-372.
- Hudson, J. A., R.G. Pearce, and R.M. Rogers (1989). Source type plot for inversion of the moment tensor. *J. Geophys. Res.*, v. 94(B1), 765-774.
- Hudyma, N., B.B. Avar, and M. Karakouzian (2004). Compressive strength and failure modes of lithophysae-rich Topopah Spring Tuff specimens and analog models containing cavities. *Engineering Geology*, v. 73, 179-190.
- Hurwitz, S. (2003). Groundwater flow, heat transport, and water table position within volcanic edifices: Implications for volcanic processes in the Cascade Range. *J. Geophys. Res.*, v. 108(B12), 2557, doi:10.1029/2003JB002565.
- Jaeger, J.C. and N.W. Cook (1979). Fundamentals of rock mechanics (3<sup>rd</sup> edition). Chapman and Hall, New York, NY, 28–30.

- Jing Z., J. Willis-Richards, K. Watanabe, and T. Hashida (2000). A three-dimensional stochastic rock mechanics model of engineered geothermal systems in fractured crystalline rock. *J. Geophys. Res.*, v. 105(B10), 23663-23679.
- Julian, B.R., G.R. Foulger, and F.C. Monastero (2009). Seismic monitoring of EGS stimulation tests at the Coso Geothermal Field, California, using microearthquake locations and moment tensors. *Proceedings: Thirty-Fourth Workshop on Geothermal Reservoir Engineering*, Stanford University, Stanford, CA, Feb 9-11, 2009, SGP-TR-187.
- Julian, B.R. (unpublished). Hypoc: A Program for Computing High-Resolution Relative Earthquake Locations, Foulger Consulting.
- Julian, B.R. and G.R. Foulger (1996). Earthquake mechanisms from linear-programming inversion of seismic-wave amplitude ratios. *Bull. Seismol. Soc. Am.*, v. 86(4), 972-980.
- Julian, B.R., A.D. Miller, and G.R. Foulger (1997). Non-double-couple earthquake mechanisms at the Hengill-Grensdalur volcanic complex, southwest Iceland. *Geophys. Res. Lett.*, v. 24(7), 743-746.
- Julian, B.R., A.D. Miller, and G.R. Foulger (1998). Non-double-couple earthquakes 1. Theory. *Rev. Geophys.*, v. 36, 525-549.
- Julian, B.R., and G.R. Foulger (2010). Time-dependent tomography. *Geophys. J. Int.*, v. 182, 1327-1338, doi:10.1111/j.1365-246X.2010.04668.x.
- Julian, B.R., G.R. Foulger, F.C. Monastero, and S. Bjornstad (2010a). Imaging hydraulic fractures in a geothermal reservoir. *Geophys. Res. Lett.*, v. 37(L07305), doi:10.1029/2009GL040933.
- Jung, R. (1992). Connecting a borehole to a nearby fault by means of hydraulic fracturing. *GRC Transactions*, v. 16, 433-438.
- Jupe, A.J., D. Bruel, T. Hicks, R. Hopkirk, O. Kappelmeyer, T. Kohl, O. Kolditz, N. Rodrigues, K. Smolka, J. Willis-Richards, T. Wallroth, and S. Xu (1995). Modelling of a European Prototype HDR Reservoir, *Geothermics*, v. 24(3), 403-419.
- Kaieda, H., S. Hibino, and Y. Hor (1990). Hot dry rock experiment in tuff at Akinomiya, Northern Japan. *GRC Transactions*, v. 14(1), 561-565.
- Kirsch, G. (1898). Die Theorie der Elastizität und die Bedürfnisse der Festigkeitslehre. *VDI Z*; 42:707. *Zeitschrift des Vereines deutscher Ingenieure*, 42, 797-807.
- Kissling, E. (1995). *Velast user's guide*, edited, p. 26, Institute of Geophysics, ETH, Zurich.
- Kleinfelder (2011). Report, Independent Hydrologist Review, AltaRock Energy, EGS Demonstration Project, Newberry, Oregon. Internal report to AltaRock Energy, Inc., 2/24/2011, 35 p.
- Kohl, T. and T. Mégel (2005). Coupled Hydro-Mechanical Modelling of the GPK3 Reservoir Stimulation at the European EGS Site Soultz-Sous-Forêts, *Proceedings: Thirtieth Workshop on Geothermal Reservoir Engineering*, Stanford University, Stanford California, Jan 31-Feb 2, 2005, SGP-TR-176.
- Kruger, P. (1992). The first hydrofracture experiment in the Tirniauz (Russia) geothermal resource. *GRC Transactions*, v.16, 439-445.
- La Pine, Oregon (2011). Wikipedia, The Free Encyclopedia. [http://en.wikipedia.org/w/index.php?title=La\\_Pine,\\_Oregon&oldid=422761455](http://en.wikipedia.org/w/index.php?title=La_Pine,_Oregon&oldid=422761455), last accessed 4/14/2011.
- Lawn, B. (1993). *Fracture Mechanics of Brittle Solids* (2<sup>nd</sup> edition). Cambridge University Press, Cambridge, UK, 378 p.
- Letvin, A.I. (2011). Analysis of drill cuttings mineralogy and geophysical logs to investigate alteration history at Newberry well 55-29 in preparation for EGS stimulation. Confidential M.S. thesis, RES |



The School for Renewable Energy Science in affiliation with the Universities of Iceland and Akureyri, 68 p. with appendices.

- Li, L. and M. Abertson (2003). A general relationship between porosity and uniaxial strength of engineering materials. *Canadian J. Civil Engineering*, v. 30, p. 644-658.
- Lockner, D.A. and N.M. Beeler (2002). Rock failure and earthquakes, in *International handbook of earthquake and engineering seismology*, v. 81A, W.K. Lee, H. Kanamori, P. Jennings, and C. Kisslinger (eds.), Academic Press, San Diego, CA, 505–537.
- Lutz, S.J., J.N. Moore, C.G. Jones, G. Suemnicht, and A. Robertson-Tait (2009). Geological and structural relationships in the Desert Peak geothermal system, Nevada: Implications for EGS development. *Proceedings: Thirty-Fourth Workshop on Geothermal Reservoir Engineering*, Stanford University, Stanford, CA, Feb 9-11, 2009, SGP-TR-187.
- Lutz, S.J., S. Hickman, N.C. Davatzes, E. Zemach, P. Drakos, and A. Robertson-Tait (2010). Rock Mechanical Testing and Petrologic Analysis in Support of Well Stimulation Activities at the Desert Peak Geothermal Field, Nevada. *Proceedings: Thirty-Fifth Workshop on Geothermal Reservoir Engineering*, Stanford University, Stanford, CA, Feb 1-3, 2010, SGP-TR-188.
- Ma, L. and J.J.K. Daemen (2004). Final Technical Report – Part 2, Time Dependent Mechanical Behavior of Welded Tuff, Prepared for U.S. DOE/UCCSN, Cooperative Agreement DE-FC28- 98NV12081. <http://hrcweb.lv-hrc.nevada.edu/qa/Report/TR-03-018-2.pdf>, last accessed 8/18/2011.
- MacLeod, N.S. and E.A. Sammel (1982). Newberry Volcano, Oregon: A Cascade Range geothermal prospect. *California Geology*, v. 35, m. 11, 235-244. (Published simultaneously in *Oregon Geology*, v. 44(11), 123-131).
- MacLeod, N.S., D.R. Sherrod, L.A. Chitwood, and E.H. McKee (1981). Newberry Volcano, Oregon, in *Guides to Some Volcanic Terranes in Washington, Idaho, Oregon, and Northern California*, D.A. Johnston and J. Donnelly-Nolan (eds.), *USGS Circular 838*, 85-104.
- MacLeod, N.S., D.R. Sherrod, and L.A. Chitwood (1982). Geologic map of Newberry Volcano, Deschutes, Klamath, and Lake Counties, Oregon. *USGS Open-File Report 82-847*, 27 p.
- MacLeod, N.S., D.R. Sherrod, L.A. Chitwood, and R.A. Jensen (1995). Geologic map of Newberry Volcano, Deschutes, Klamath, and Lake Counties, Oregon. *USGS Miscellaneous Geologic Investigations Map I-2455*, scales 1:62,500 and 1:24,000.
- MacLeod, N.S. and D.R. Sherrod (1988). Geologic evidence for a magma chamber beneath Newberry Volcano, Oregon, *J. Geophys. Res.*, v. 93(B9), 10067-10079.
- Majer, E.L., R. Baria, M. Stark, S. Oates, J.B. Bommer, B. Smith, and H. Asamuma (2007). Induced seismicity associated with Enhanced Geothermal Systems. *Geothermics*, v. 36, 185-222.
- Majer, E.L., R. Baria, and M. Stark (2008). Protocol for induced seismicity associated with enhanced geothermal systems. Report produced in Task D Annex I (9 April 2008), International Energy Agency-Geothermal Implementing Agreement (incorporating comments by: C. Bromley, W. Cumming, A. Jelacic and L. Rybach). Available at: <http://www.iea-gia.org/publications.asp>.
- Majer, E.L., J. Nelson, A. Robertson-Tait, J. Savy, and I. Wong (2011). (Final Draft) Protocol for Addressing Induced Seismicity Associated with Enhanced Geothermal Systems (EGS). Available at: [http://esd.lbl.gov/files/research/projects/induced\\_seismicity/egs/EGS-IS-Protocol-Final-Draft-20110531.pdf](http://esd.lbl.gov/files/research/projects/induced_seismicity/egs/EGS-IS-Protocol-Final-Draft-20110531.pdf)
- Mansure, A.J., S.J. Bauer, and B.J. Livesay (2005). Geothermal Well Cost Analyses 2005. *GRC Transactions*, v.29, 515-520.
- Mardia, K.V.M. and P.E. Jupp (2000). *Directional Statistics* (2<sup>nd</sup> edition), John Wiley and Sons Ltd.

- Miller, A.D., G.R. Foulger, and B.R. Julian (1998a). Non-double-couple earthquakes 2. Observations. *Rev. Geophys.*, v. 36, 551-568.
- Miller, A.D., B.R. Julian, and G.R. Foulger (1998b). Three-dimensional seismic structure and moment tensors of non-double-couple earthquakes at the Hengill-Grensdalur volcanic complex, Iceland. *Geophys. J. Int.*, v. 133, 309-325.
- Moore, J., M.C. Adams, T.L. Sperry, K.K. Bloomfield, and R. Kunzman (2000). Preliminary Results Of Geochemical Monitoring And Tracer Tests At The Cove Fort-Sulphurdale Geothermal System, Utah. *Proceedings: Twenty-Fifth Workshop on Geothermal Reservoir Engineering*, Stanford University, Stanford, CA, Jan 24-26, 2000, SGP-TR-165.
- Moos, D. and M.D. Zoback (1990). Utilization of observations of well bore failure to constrain the orientation and magnitude of crustal stresses: Application to continental, deep sea drilling project, and ocean drilling program boreholes. *J. Geophys. Res.*, v. 100(B), 12791–12811.
- Morgan, D.S., S.R. Hinkle, and R.J. Weick (2007). Evaluation of approaches for managing nitrate loading from on-site wastewater systems near La Pine, Oregon. *USGS Scientific Investigations Report 2007-5237*, 76 p.
- Morgan, D.S., D.Q. Tanner, and M.D. Crumrine (1997). Hydrologic, water-quality, and meteorologic data for Newberry Volcano and vicinity, Deschutes county, Oregon, 1991-1995. *USGS Open-File Report 97-4088*, 72 p.
- Morrow, C. and J. Byerlee (1984). Frictional sliding and fracture behavior of some Nevada Test Site tuffs. *Proceedings: 25<sup>th</sup> U.S. Symposium on Rock Mechanics*, 467-474.
- Nami, P., R. Schellschmidt, M. Schindler, and T. Tischner (2008). Chemical Stimulation Operations for Reservoir Development of the Deep Crystalline HDR/EGS System at Soultz-Sous- Forêts (France), *Proceedings: Thirty-Second Workshop on Geothermal Reservoir Engineering*, Stanford University, Stanford, CA, Jan 28-30, 2008, SGP-TR-185.
- Narayan, S.P., D. Naseby, Z. Yang, and S.S. Rahman (1998). Creation of HDR reservoirs under Australian in-situ stress conditions. *Proceedings: Twenty-Third Workshop on Geothermal Reservoir Engineering*, Stanford University, Stanford, CA, Jan 26-28, 1998, SGP-TR-158.
- National Earthquake Information Center (2000). USGS Earthquake Data Base. <http://neic.usgs.gov/neis/epic/database.html>, last accessed 8/18/2011
- O'Connor, J.E., R.J. Dorsey, and I. Madin (2009). Volcanoes to Vineyards: geologic field trips through the dynamic landscape of the Pacific Northwest, Geologic Society of America.
- Olsen, M.P., R.A. Plumb, and S.L. Herron (1991). Influence of composition and texture on strength variations within the Travis Peak formation. *EOS*, 72-270.
- Oregon Drinking Water Program website (2011). <http://www.oregon.gov/DHS/ph/dwp/docs/pwsrules/61-0030.pdf>, last accessed 1/19/2011.
- Palandri, J. and Y.K. Kharaka (2004). A compilation of rate parameters of water–mineral interaction kinetics for application to geochemical modeling. *USGS Open-File Report 2004-1068*, 64 pp.
- Paterson, M.S. and T.F. Wong (2005). *Experimental Rock Deformation – The Brittle Field* (2<sup>nd</sup> edition). Springer-Verlag, Berlin, Heidelberg.
- Personius, S.F., compiler (2002a). Fault number 838, La Pine graben faults. In Quaternary fault and fold database of the United States, USGS Website. <http://earthquakes.usgs.gov/regional/qfaults>, last accessed 01/13/2011.

- Personius, S.F., compiler (2002b). Fault number 1806, Newberry volcano ring faults. In Quaternary fault and fold database of the United States, USGS Website. <http://earthquakes.usgs.gov/regional/qfaults>, last accessed 01/14/2011.
- Peska, P. and M.D. Zoback (1995). Compressive and tensile failure of inclined wellbores and determination of in situ stress and rock strength. *J. Geophys. Res.*, v. 100(B7), 12791–12811.
- Petty, S., D. Bour, Y. Nordin, and L. Nofziger (2011). Submitted, Temporary Diverters for EGS Reservoir Optimization – Field Applications. *GRC Transactions*, pre-print by request.
- Pezzopane, S.K. and R.J. Weldon II (1993). Tectonic role of active faulting in central Oregon. *Tectonics* v. 12, 1140-1169.
- Plumb, R. and Hickman, S. (1985). Stress-induced borehole elongation: a comparison between the four-arm dipmeter and the borehole televiewer in the Auburn Geothermal Well. *J. Geophys. Res.*, v. 90, 5513-5521.
- Price, R.H., R.J. Martin III, and P.J. Boyd (1993). Characterization of porosity in support of mechanical property analysis, SAND—92-2153C, 15 p.
- Price, N. J. (1966). *Fault and Joint Development in Brittle and Semi-Brittle Rock*. Pergamon Press, Oxford.
- Priest, G.R. (1990). Volcanic and tectonic evolution of the Cascade volcanic arc, central Oregon. *J. Geophys. Res.*, v. 95 (B12), 19583-19599.
- Pulka, J. (1995). Interpretation of Sandia televiewer data. Internal memo, dated 11/9/95.
- Quane, S.L. and J.K. Russel (2003). Rock strength as a metric of welding intensity in pyroclastic deposits. *European J. Mineralogy*, v. 15, 855-864.
- Rahman, M.K., M.M. Hossain, and S.S. Rahman (2002). A shear-dilation-based model for evaluation of hydraulically stimulated naturally fractured reservoirs. *Int. J. Numerical & Analytical Methods in Geomech.*, v. 26, 469-497.
- Reed, M.H. and N.F. Spycher (1984). Calculation of pH and mineral equilibria in hydrothermal waters with application to geothermometry and studies of boiling and dilution. *Geochimica et Cosmochimica Acta*, v. 48, 1479–1492.
- Reed, M. and J. Palandri (2006). SOLTHERM.H06, a database of equilibrium constants for minerals and aqueous species. Available from the authors, University of Oregon, Eugene, Oregon.
- Robinson, P.T. (2007). Tectonic Significance of Ash Flow Tuffs of the John Day Formation. *GSA Abstracts with Programs*, v. 39(6), 173.
- Robinson, P.T., G.F. Brem, and E.H. McKee (1984). John Day Formation of Oregon: A Distal Record of Early Cascade Volcanism. *Geology*, v. 12(4), 229-232.
- Ross, A., G.R. Foulger, and B.R. Julian (1996). Non-double-couple earthquake mechanisms at The Geysers geothermal area, California. *Geophys. Res. Lett.*, v. 23, 877-880.
- Russell, I.C. (1905). Preliminary report on the geology and water resources of central Oregon. *USGS Bulletin 252*, 138 p.
- Sammel, E.A. (1981). Results of test drilling at Newberry Volcano, Oregon. *Bull. Geotherm. Resour. Counc.*, v. 10(11), 3-8.
- Sammel, E.A. (1983). The shallow hydrothermal system at Newberry Volcano, Oregon: A conceptual model. *GRC Transactions*, v. 7, 325-330.
- Sammel, E.A. and R.W. Craig (1983). Hydrology of the Newberry Volcano Caldera, Oregon. *USGS Water Resources Investigation Report 83-4091*.

- Sammel, E.A., S.E. Ingebritsen, and R.H. Mariner (1988). The hydrothermal system at Newberry Volcano, Oregon. *J. Geophys. Res.*, v. 93(B9), 10149-10162.
- Schindler, M., J. Baumgärtner, T. Gandy, P. Hauffe, T. Hettkamp, H. Menzel, P. Penzkofer, D. Teza, T. Tischner, and G. Wahl (2010). Successful Hydraulic Stimulation Techniques for Electric Power Production in the Upper Rhine Graben, Central Europe. *Proceedings: World Geothermal Congress*, Bali, Indonesia.
- Sherrod, D.R., E.M. Taylor, M.L. Ferns, W.E. Scott, R.M. Conrey, and G.A. Smith (2004). Geologic map of the Bend 30x60-minute quadrangle, central Oregon. *USGS Geologic Investigations Series 1-2683*.
- Smith, G.A. (1986). Stratigraphy, sedimentology, and petrology of Neogene rocks in the Deschutes basin, central Oregon: a record of continental-margin volcanism and its influence on fluvial sedimentation in an arc-adjacent basin. Ph.D. dissertation, Oregon State Univ, Corvallis, OR, 467 p.
- Sonnenthal, E., A. Ito, N. Spycher, M. Yui, J. Apps, Y. Sugita, M. Conrad, and S. Kawakami (2005). Approaches to modeling coupled thermal, hydrological, and chemical processes in the Drift Scale Heater Test at Yucca Mountain. *Int. J. Rock Mech. & Mining Sci.*, v. 42, 698-719.
- Spielman, P. and J. Finger (1998). Well Test Results of Exploration Drilling at Newberry Crater, Oregon in 1995. *Proceedings: Twenty-Third Workshop on Geothermal Reservoir Engineering*, Stanford University, Stanford, CA, Jan 26-28, 1998, SGP-TR-158.
- Spycher N., E. Sonnenthal, and B.M. Kennedy (2010). An Integrated Chemical Geothermometry System for Geothermal Exploration. Fall American Geophysical Union Meeting, San Francisco, CA., Dec 13-17, 2010, Abstract V13B-2352.
- Stock, J., J. Healy, S. Hickman, and M.D. Zoback (1985). Hydraulic fracturing stress measurements at Yucca Mountain, Nevada, and relationship to the regional stress field. *J. Geophys. Res.*, v. 90, 8691-8706.
- Tembe, S., D.A. Lockner, and T.F. Wong (2010). Effect of clay content and mineralogy on frictional sliding behavior of simulated gouges: binary and ternary mixtures of quartz, illite and montmorillonite. *J. Geophys. Res.*, v. 115, B03416, doi:10.1029/2009JB006383.
- Tester, J. W., and 17 others (2006). The Future of Geothermal Energy – Impact of Enhanced Geothermal Systems (EGS) on the United States in the 21st Century. Idaho Falls: Idaho National Laboratory [http://geothermal.inel.gov/publications/future\\_of\\_geothermal\\_energy.pdf](http://geothermal.inel.gov/publications/future_of_geothermal_energy.pdf), last accessed 8/22/2011.
- Teufel, L.W. (1987). Permeability changes during shear deformation of fractured rock, in *28th Symposium on Rock Mechanics*, A.A. Balkema (ed.), Rotterdam, Netherlands, 473-480.
- Three Rivers, Oregon. (2011). Wikipedia, The Free Encyclopedia. [http://en.wikipedia.org/w/index.php?title=Three Rivers, Oregon&oldid=406926522](http://en.wikipedia.org/w/index.php?title=Three_Rivers,_Oregon&oldid=406926522), last accessed 4/14/2011.
- Thurber, C. H. (1983). Earthquake locations and three-dimensional crustal structure in the Coyote Lake area, central California. *J. Geophys. Res.*, v. 88, 8226-8236.
- Townend, J. and M. Zoback (2000). How faulting keeps the crust strong. *Geology*, v. 28(5), 399-402. USGS, 1975,
- Ussher G., C. Harvey, R. Hohnstone, and E. Anderson (2000). Understanding the resistivities observed in geothermal systems. *Proceedings: World Geothermal Congress*, Kyushu – Tohoku, Japan, May 28 – Jun 10, 2000, 1915 – 1920.

- Valley, B. and K.F. Evans (2007). Stress state at Soultz-sous-Forêts to 5 km depth from wellbore failure and hydraulic observations. *Proceedings: Thirty-Second Workshop on Geothermal Reservoir Engineering*, Stanford University, Stanford, CA, SGP-TR-183.
- Wald, D.J., V. Quitoriano, T.H. Heaton, and H. Kanamori (1999). Relationships between peak ground acceleration, peak ground velocity, and modified Mercalli intensity in California. *Earthquake Spectr.*, v. 15, 557–564.
- Waldhauser, F. and W. L. Ellsworth (2000). A double-difference earthquake location algorithm: Method and application to the northern Hayward Fault, California. *Bull. Seismol. Soc. Am.*, v. 90, 1353-1368.
- Walker, G.W., N.V. Peterson, and R.C. Greene (1967). Reconnaissance geologic map of the east half of the Crecent Quadrangle - Lake, Deschutes, and Crook Counties, Oregon. *USGS Map I-493*.
- Wells, R.E., C.S. Weaver, and R.J. Blakely (1998). Fore arc migration in Cascadia and its neotectonic significance. *Geology*, v. 26, 759–762.
- Willis-Richards, J., K. Watanabe, and H. Takahashi (1996). Progress toward a stochastic rock mechanics model of engineered geothermal systems. *J. Geophys. Res.*, v. 101, 17481-17469.
- Wilson, D.S. (1993). Confidence intervals for motion and deformation of the Juan de Fuca plate. *J. Geophys. Res.*, v. 98, 16053–16071.
- Wong, I., S. Pezzopane, M. Dober, and F. Terra ([2010](#)). Evaluation of Induced Seismicity/Seismic Hazards and Risk, for the Newberry Volcano EGS Demonstration. Internal Report to AltaRock Energy, Inc., 10/24/2010., 106 p.
- Wong, I., S. Pezzopane, and F. Terra ([2011](#)). Development of scenario ground shaking maps and evaluations of the impacts of ground shaking on local buildings, avalanches, and the Lava River Cave, Newberry Volcano EGS Demonstration. Internal Report to AltaRock Energy, Inc., 1/28/2011, 14 p.
- Wong, T. and W. Zhu (1999). Brittle faulting and permeability evolution: Hydromechanical measurement, microstructural observation and network modeling. *AGU Geophysical Monograph*, v. 113, 83-99.
- Xie, X., G.R. Byerly, and R.E. Ferrell (1997). Ilb trioctahedral chlorite from Barberton greenstone belt: crystal structure and rock composition constraints with implications to geothermometry. *Contributions to Mineralogy and Petrology*, v. 126, 275-291.
- Xu, T., E. Sonnenthal, N. Spycher, and K. Pruess (2005). TOUGHREACT User's Guide: a simulation program for non-isothermal multiphase reactive geochemical transport in variably saturated geologic media. Tech. rep., LBNL- 55460, Lawrence Berkeley National Laboratory, CA.
- Xu, T., E. Sonnenthal, N. Spycher, and K. Pruess (2006). TOUGHREACT: A simulation program for non-isothermal multiphase reactive geochemical transport in variably saturated geologic Media: applications for geothermal injectivity and CO2 geologic sequestration. *Computers and Geosciences*, v. 32, 145-165.
- Xu, T., N. Spycher, E. Sonnenthal, G. Zhang, L. Zheng, and K. Pruess (2011). TOUGHREACT Version 2.0: A simulator for subsurface reactive transport under non-isothermal multiphase flow conditions. *Computers and Geosciences*, doi:10.1016/j.cageo.2010.10.007
- Zhu, W. and T. Wong (1997). The Transition from Brittle Faulting to Cataclastic Flow: Permeability Evolution. *J. Geophys. Res.*, v. 102(B2), 3027-3041.
- Zhu, W. and T. Wong (1999). Network modeling of the evolution of permeability and dilatancy in compact rock. *J. Geophys. Res.*, v. 104, 2963-2971.



- Zimmerman, G., A. Reinicke, W. Brandt, G. Blöcher, H. Milsch, H. Holl, I. Moeck, T. Schulte, A. Saadat, and E. Huenges (2008). Results of Stimulation Treatments at the Geothermal Research Wells in GROß SCHÖNEBECK/Germany. *Proceedings: Thirty-Third Workshop on Geothermal Reservoir Engineering*, Stanford University, Stanford, CA, SGP-TR-185.
- Zoback, M.D., C.A. Barton, M. Brudy, D.A. Castillo, T. Finkbeiner, B.R. Grollmund, D.B. Moos, P. Peska, C.D. Ward, and D.J. Wiprut (2003). Determination of stress orientation and magnitude in deep wells. *Int. J. Rock Mech. & Mining Sci.*, v. 40, 1049–1076, doi:10.1016/j.ijrmms.2003.07.001.
- Zoback, M.D. (2007). *Reservoir Geomechanics*, Cambridge University Press, Cambridge, UK, 449 pg.